



HAL
open science

Mirrorless lasing and cooperative scattering with cold atoms

William Guerin

► **To cite this version:**

William Guerin. Mirrorless lasing and cooperative scattering with cold atoms. Atomic Physics [physics.atom-ph]. Université Côte d'Azur, 2020. tel-02924393

HAL Id: tel-02924393

<https://theses.hal.science/tel-02924393v1>

Submitted on 28 Aug 2020

HAL is a multi-disciplinary open access archive for the deposit and dissemination of scientific research documents, whether they are published or not. The documents may come from teaching and research institutions in France or abroad, or from public or private research centers.

L'archive ouverte pluridisciplinaire **HAL**, est destinée au dépôt et à la diffusion de documents scientifiques de niveau recherche, publiés ou non, émanant des établissements d'enseignement et de recherche français ou étrangers, des laboratoires publics ou privés.

Habilitation à diriger des recherches

présentée par

William GUERIN

Institut de Physique de Nice

Mirrorless lasing and cooperative scattering with cold atoms

Soutenue le 18 Juin 2020 devant le jury composé de:

M. Gian Luca LIPPI	Président
M. Antoine BROWAEYS	Rapporteur
M. Arno RAUSCHENBEUTEL	Rapporteur
M. Jook WALRAVEN	Rapporteur
M. Rémi CARMINATI	Examineur
M. Robin KAISER	Examineur
Mme Hélène PERRIN	Examinatrice

Laser sans miroir et diffusion coopérative avec des atomes froids

Jury:

Président du jury:

Gian Luca Lippi, Professeur à l'Université Côte d'Azur, Institut de Physique de Nice

Rapporteurs:

Antoine Browaeys, Directeur de recherche au CNRS, Laboratoire Charles Fabry de l'Institut d'Optique

Arno Rauschenbeutel, Professeur à l'Université Humboldt de Berlin

Jook Walraven, Professeur émérite à l'Université d'Amsterdam, Van der Waals-Zeeman Institute

Examineurs:

Rémi Carminati, Professeur à l'ESPCI, Institut Langevin

Robin Kaiser, Directeur de recherche au CNRS, Institut de Physique de Nice

Hélène Perrin, Directrice de recherche au CNRS, Laboratoire de Physique des Lasers

Remerciements

Je tiens tout d'abord à remercier chaleureusement tous les membres du jury, et encore plus les rapporteurs, pour le temps qu'ils ont accepté de consacrer à l'évaluation de ce manuscrit et à la soutenance, dans des conditions techniques parfois difficiles. J'ai réussi à réunir un jury de très haut niveau et c'est évidemment un grand honneur pour moi.

Les travaux relatés dans ce manuscrit ont été effectués sur une période de quasiment treize ans, au cours de laquelle j'ai interagit avec un grand nombre d'étudiants et de collaborateurs. L'écriture des remerciements est donc un défi et je ne sais par quel bout commencer.

Alors commençons par le plus évident: une dizaine de ces années se sont déroulées dans l'équipe de Robin Kaiser, que je ne pourrai jamais assez remercier pour son soutien, son enthousiasme, sa disponibilité et son immense compétence. Nous avons des personnalités très différentes (pour tous ceux qui nous connaissent un petit peu je n'ai pas besoin de préciser lequel de nous deux est introverti et lequel est extraverti!) mais, conscients de nos propres défauts, nous nous modérons mutuellement et sommes ainsi utilement complémentaires. C'est en tout cas une grande chance de travailler avec lui.

Un grands merci également aux deux autres membres permanents de l'équipe, Guillaume Labeyrie et Mathilde Hugbart, pour toutes nos fructueuses interactions, qu'elles soient professionnelles ou amicales. L'ambiance au sein de l'équipe est excellente et je n'ai aucun doute que ça va continuer, avec encore plus de randos, de matchs de ping-pong, et d'autres activités plus ou moins sérieuses.

Pour ma période à Tübingen je remercie Claus Zimmermann, dont le soutien, grandissant au fur et à mesure du projet, m'a été extrêmement précieux, et Philippe Courteille pour son soutien et son aide au début du projet, ainsi que pour les prêts de la maison de Niolon et les séminaires en Bretagne. J'en profite pour remercier également la Fondation Humboldt dont l'efficacité, le professionnalisme et la simplicité des procédures sont tout simplement remarquables.

J'ai eu la chance de travailler avec un grand nombre de thésards, post-docs, stagiaires, visiteurs, et je n'arriverai pas à tous les citer ici. Néanmoins, je les remercie tous pour leurs contributions et, quand même, je vais mentionner un certain nombre d'entre eux (dans l'ordre chronologique). Je garde un excellent souvenir du temps passé au labo avec Franck Michaud, ainsi que de nos randos dans le Mercantour, et nous nous revoyons de temps en temps avec plaisir lors de ses visites dans la région. Davide Brivio et Eleonora Lucioni ont fortement égayé l'été 2008 avec leurs accents italiens et leur gentillesse. Nicolas Mercadier a eu une contribution absolument majeur sur le projet laser aléatoire, tout en faisant, en plus, la manip sur les vols de Lévy : chapeau! (Mais ça n'excuse pas d'être aussi nul en musique.) Avec Jean-François Schaff et Tom Bienaimé ils ont formé un sacré trio d'excellents thésards. À Tübingen j'ai travaillé avec Alexander Schilke tout du long et nous avons réussi l'exploit

de communiquer malgré les barrières linguistiques. Il a réussi à me supporter malgré mes exigences et nous garderons, comme bons souvenirs parmi d'autres, les séances de baby-foot endiablées et la couverture de Nature Photonics ! À mon retour à Nice, Louis Bellando et Quentin Baudouin m'ont non seulement aidé à déménager, mais ils m'ont aussi légué leurs manips. Plus tard j'ai travaillé avec Michelle Araújo, qui a également réussi à me supporter malgré certaines barrières, culturelles cette fois. Antoine Dussaux a partagé mon bureau dans la bonne humeur et a incroyablement bien lancé le projet astro. Patrizia Weiss a pris ensuite la manip atomes froids en main pendant trois ans et a eu une contribution essentielle aux études sur la sous-radiance. Je garderai également un excellent souvenir de nos nombreuses activités dans un cadre amical, que ce soit les randos dans l'Estérel, la Siagne et ailleurs, ou les séances de jardinage, de peinture (un grand merci !) et de visionnage de films cultes, entre autres. En parallèle, sur les autres manips, ce fut un plaisir d'interagir avec Samir Vartabi Kashanian, Aurélien Éloy et Antonin Siciak. Enfin Ana Cipris a eu la lourde tâche d'être ma première doctorante officielle et elle s'en est acquittée avec beaucoup de succès.

J'ai également eu la chance de croiser sur ma route de nombreux collaborateurs, qu'ils soient ici tous remerciés, en particulier Rémi Carminati et Sergey Skipetrov sur le laser aléatoire, Nicolas Piovella, Romain Bachelard, Johannes Schachenmayer, Mark Havey et Igor Sokolov sur la diffusion coopérative. Enfin, sur le projet astro, peu évoqué dans ce manuscrit, les collaborateurs sont nombreux et j'adresse un remerciement spécial à Farrokh Vakili et Jean-Pierre Rivet : j'ai énormément appris à leur contact et c'est un plaisir de découvrir, grâce à eux, un tout nouveau domaine de la science.

Enfin mon dernier mot est pour Simone Bux, dont les lecteurs les plus perspicaces reconnaîtront le nom dans quelques références sur la diffusion coopérative. C'est grâce à elle (ou pour elle ?) que je suis allé en Allemagne, ce qui fut une expérience à la fois enrichissante d'un point de vue personnel (comme tout séjour prolongé à l'étranger), et essentielle pour l'évolution de ma carrière. Surtout, elle a ensuite accepté de me suivre en France et, même si la Côte d'Azur est une région attirante à bien des égards, cela reste un sacrifice important de quitter la région où on a sa famille et ses amis. Les premières années furent d'ailleurs assez difficiles et je lui suis infiniment reconnaissant d'avoir tenu : un très, très grand merci pour toutes ces années à mes côtés !

Contents

CHAPTER I — General introduction	11
I.1 Overview of my research activities	11
I.1.1 PhD thesis at Institut d’Optique (2003 – 2007)	11
I.1.2 Post-doc at INLN (2007 – 2009)	13
I.1.3 Post-doc in Tübingen (2010 – 2012)	15
I.1.4 Back at INLN/INPHYNI (since Oct. 2012)	17
I.2 Content of this manuscript	21

Part One

Mirrorless lasing with cold atoms

Brief introduction on the topic of mirrorless lasing	25
---	----

CHAPTER II — Gain and lasing with cold atoms	29
II.1 Different gain mechanisms	29
II.1.1 Mollow gain	29
II.1.2 Raman gain using the Zeeman structure	30
II.1.3 Raman gain using the hyperfine structure	31
II.1.4 Degenerate four-wave mixing (FWM)	31
II.1.5 Other gain mechanisms	32

II.2	Standard lasing	32
	Article: “ <i>Mechanisms for lasing with cold atoms as the gain medium</i> ”, Phys. Rev. Lett., 2008	34
CHAPTER III — Distributed feedback laser with cold atoms.		39
III.1	Photonic band gaps in 1D lattices	39
III.1.1	Photonic band gaps with two-level atoms	40
	Article: “ <i>Photonic band gaps in one-dimensionally ordered cold atomic vapors</i> ”, Phys. Rev. Lett., 2011	41
III.1.2	Photonic band gaps with EIT	45
	Article: “ <i>Photonic properties of one-dimensionally-ordered cold atomic vapors under conditions of electromagnetically induced transparency</i> ”, Phys. Rev. A, 2012	46
III.2	Distributed feedback laser	55
III.2.1	Bragg reflection with standard gain	55
III.2.2	DFB parametric oscillation	56
	Article: “ <i>Optical parametric oscillation with distributed feedback in cold atoms</i> ”, Nature Photon., 2012	57
III.2.3	Mode structure: numerical investigations	62
CHAPTER IV — Random laser with cold atoms		71
IV.1	Light transport in disordered atomic vapors.	71
IV.1.1	Resonant scattering in cold atoms	72
IV.1.2	Light diffusion in cold atoms	72
	IV.1.2.1 Diffuse transmission and reflection	73
	IV.1.2.2 Radiation trapping	74
IV.2	The quest for the best gain mechanism	75
IV.2.1	Threshold of a random laser with cold atoms	75
	Article: “ <i>Threshold of a random laser with cold atoms</i> ”, Phys. Rev. Lett., 2009	76
IV.2.2	Comparison between incoherent and coherent models	80
	Article: “ <i>Diffusive to quasi-ballistic random laser: incoherent and coherent models</i> ”, J. Opt. Soc. Am. B, 2016	81
IV.2.3	Comparison between different gain mechanisms	90
IV.3	Experimental signature of random lasing and modeling.	93
	Article: “ <i>A cold-atom random laser</i> ”, Nature Phys., 2016	96
Conclusion on Part One		110

Part Two

Cooperative scattering in dilute cold-atom clouds in the linear-optics regime

Introduction on super- and subradiance	113
CHAPTER V — Steady-state signatures of cooperativity?	117
V.1 Discussion on collective and cooperative effects	117
Article: “ <i>Light interacting with atomic ensembles: collective, cooperative and mesoscopic effects</i> ”, J. Mod. Opt., 2017	118
V.2 Radiation pressure force?	131
V.3 Off-axis scattering?	132
Article: “ <i>Optical-depth scaling of light scattering from a dense and cold atomic ^{87}Rb gas</i> ”, Phys. Rev. A, 2020	133
CHAPTER VI — Super- and subradiance in the linear-optics regime .	143
VI.1 Observation of subradiance	143
VI.1.1 Experimental requirements	143
VI.1.2 First observation of subradiance	145
Article: “ <i>Subradiance in a large cloud of cold atoms</i> ”, Phys. Rev. Lett., 2016	146
VI.1.3 Influence of the temperature	157
Article: “ <i>Robustness of Dicke subradiance against thermal decoherence</i> ”, Phys. Rev. A, 2019	158
VI.2 Observation of superradiance off axis	164
Article: “ <i>Superradiance in a large and dilute cloud of cold atoms in the linear-optics regime</i> ”, Phys. Rev. Lett., 2016	165
VI.3 Population of the collective modes	171
Article: “ <i>Population of collective modes in light scattering by many atoms</i> ”, Phys. Rev. A, 2017	172
VI.4 Superradiance as single scattering embedded in an effective medium . . .	181

VI.5	Subradiance and multiple scattering	183
VI.5.1	Interplay of subradiance and radiation trapping	183
	Article: “ <i>Subradiance and radiation trapping in cold atoms</i> ”, New. J. Phys., 2018	185
VI.5.2	Update with recent results	199
VI.5.3	Towards a ‘photonic’ picture of subradiance?	202
VI.6	Excitation dynamics: collective Rabi oscillations	204
VI.6.1	Superradiant damping	205
VI.6.2	Shift and splitting	206
	Article: “ <i>Collective multimode vacuum Rabi splitting</i> ”, Phys. Rev. Lett., 2019	208
Conclusion on Part Two		217

Appendices

APPENDIX A	— Detailed CV	219
APPENDIX B	— List of publications and communications	225
B.1	Publications	225
B.2	Communications	229
Bibliography		233

CHAPTER I

General introduction

In a manuscript for ‘Habilitation à Diriger des Recherches’ (HDR) there is traditionally some less-scientific part to describe the person’s career. This is the purpose of this first chapter. For a busy reader who only wants to know me, this is the most (or only) interesting chapter. For the reader who wants to learn some physics, on the contrary, it can be skipped.

I thus give here only a brief overview of my research activities without giving any details on the science, especially for the parts that are presented in the five following chapters. I however explain the context of the different topics on which I worked, and that is a good opportunity to acknowledge the contributions of my co-workers. Then I introduce the content of the rest of the manuscript.

I.1. Overview of my research activities

In this section I summarize the different research projects that occupied me since the beginning of my career, with also some introduction on how all that happened. I’ve included a few illustrative pictures, without any caption, on the results that won’t be described in the following of the manuscript.

I.1.1. PhD thesis at Institut d’Optique (2003 – 2007)

Bose-Einstein condensation and atom lasers

I did my PhD thesis under the supervision of Alain Aspect and Philippe Bouyer in the ‘Optique Atomique’ group of Institut d’Optique (in Orsay at that time, now in Palaiseau). I worked on a Bose-Einstein condensation experiment (using rubidium 87) devoted to the use of the condensate (BEC) as a *coherent source* for atom optics [Guerin 2007].

Indeed, Bose-Einstein condensation is the atomic analog of the laser effect: below some threshold temperature, atoms accumulate in the ground state of the trap in which they are confined, thus building a reservoir of coherent matter wave. By extracting an atomic beam from such a condensate, one obtains an ‘atom laser’. To do so, we used a radiofrequency (RF) field inducing a transition between two Zeeman states: the initial state of the BEC, $|F = 1, m_F = -1\rangle$, and a state almost insensitive to the magnetic trapping, $|F = 1, m_F = 0\rangle$. Spin-flipped atoms can then escape the trap and fall down under gravity, forming a directed and continuous coherent atomic beam (until depletion of the BEC) [Bloch 1999].

In view of future applications of this coherent atom source, for instance to atom interferometry, it is necessary to achieve a good control over the beam properties. In particular, two effects induce striking differences between photonic lasers and atom lasers and may be strong limitations for the latter. The first is that atoms interact very easily with each other via

collisions. The second is their sensitivity to gravity, which induces a strong downward acceleration of the beam. This prevents controlling the propagation direction of the atom laser as well as its de Broglie wavelength (which decreases rapidly as the beam propagates). For metrological applications it would also limit the interrogation time. I addressed these two problems during my PhD work.

Effect of interactions: degradation of the transverse mode

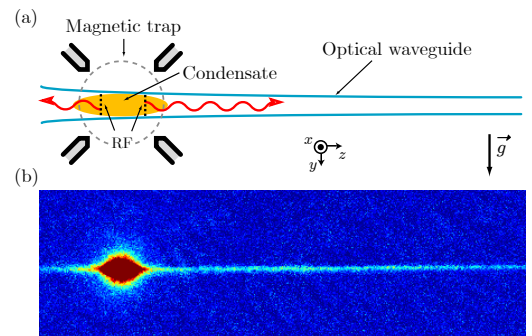
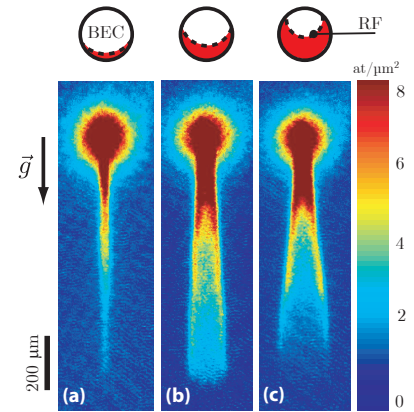
The method of RF outcoupling allows one to choose the height of the extraction of the atom laser inside the BEC, and thus the thickness that the atom laser beam must cross before reaching free space. This is perfectly adapted to study the interaction between the beam and the source condensate, which is very dense (interactions between atoms within the beam are much weaker and are neglected). These interactions can be modelled by a mean-field potential proportional to the BEC density: $V_{\text{int}} = g_{\text{coll}}|\Psi_{\text{BEC}}|^2$. The BEC density is given by the shape of the trapping potential, which gives in our case a potential V_{int} with an inverted parabola shape.

We have experimentally evidenced the harmful consequences of those strong interactions on the spatial quality of the atomic beam. We observed not only a strong divergence of the beam, consistent with previous observations [Le Coq 2001], but also an accumulation of atomic rays (like caustics) on the edges of the beam. This observation was possible thanks to the very strong confinement of our original, partly ferromagnetic, trap [Fauquembergue 2005], which induces a larger atomic density.

Following those observations, we addressed the question of a quantitative characterization of this effect. In order to model the propagation of an atom laser in the case of a non-Gaussian transverse profile, we have extended the tools developed for optics to matter waves, in particular the $ABCD$ matrices for multimode laser beams. Following the analogy with laser optics, we have also defined and measured the quality factor M^2 of the atomic beam. These results have been published in ref. [Riou 2006] and the detailed description of the theoretical tools needed for modeling the propagation of distorted atom-laser beams have been given in a follow-up paper [Riou 2008]. Since then, other teams have characterized their atom laser with the M^2 quality factor [Jeppesen 2008, Kleine Büning 2010].

Overcoming gravity: the guided atom laser

In order to overcome gravity, the solution that we have chosen consists in horizontally guiding the atomic beam. To do so we have used an optical guide made from a very anisotropic dipole trap (or ‘optical tweezers’). In order to efficiently inject the atomic beam into the guide, the source BEC is created in the hybrid trap obtained at the crossing of the optical guide and the magnetic trap. Atoms are still outcoupled via RF-induced spin flips. Since the optical guiding potential is spin-insensitive, atoms are directly coupled to the waveguide. They then propagate following an initial repulsion



due to the interaction with the condensate. This ‘pigtailed’ configuration insures an optimal coupling efficiency [Guerin 2006].

Once in the guide, atoms are transversally confined and, for the propagation direction, subjected to a weak linear potential whose slope is tunable by the combined effect of the residual curvature of the dipole trap and of the second-order Zeeman effect. By canceling this slope one can get a beam that is not accelerated. We have obtained a de Broglie wavelength of $0.5 \mu\text{m}$, constant over the propagation [Guerin 2006]. Further improvements allowed the team to reach higher values of the wavelength, until several microns [Billy 2007]. A detailed analysis of the coupling flux and limits has also been performed [Bernard 2011].

Since then, other teams have produced and studied guided atom lasers, in particular the group of David Guéry-Odelin in Toulouse [Couvert 2008, Gattobigio 2009, Gattobigio 2011], but not only [Dall 2010].

I.1.2. Post-doc at INLN (2007 – 2009)

I joined the team of Robin Kaiser at Institut Non Linéaire de Nice (INLN) in June 2007 with a post-doc funding from the ANR¹ project CAROL, meaning ‘Cold Atom RandOm Laser’ (2006 – 2010).

Two PhD students were working on the experiment when I arrived, with somewhat different PhD projects. Giovanni Luca Gattobigio had almost finished and he showed me all the tricks of the experimental setup during the first weeks before starting to write up his thesis [Gattobigio 2008]. Frank Michaud was at the end of his second year and they had started to work on gain mechanisms in cold atoms, in particular four-wave mixing (FWM) [Gattobigio 2006, Michaud 2007].

I can put here a little anecdote. Actually, during the first three weeks of my post-doc, a visitor was there in the lab, Gabriel Hétet, who was at that time a PhD student in Canberra². He had brought low-noise balanced detectors from his quantum-optics lab and the goal was to detect relative intensity squeezing in the FWM signals. This didn’t work, obviously because his stay was too short, but also because we detected a large supplementary noise in the light transmitted through the atomic cloud, which was the simplest configuration we could think of before going to FWM experiments. We had a lot of fun together in the lab trying to figure out where this noise came from. After some tests we quickly suspected that it was frequency noise of the laser converted to intensity noise by the atomic resonant transmission. The funny part of the story is that, for reasons that I’ll explain later, we did the same experiment again, in a much cleaner and more systematic way, with a thorough analysis and modeling, many years later [Vartabi Kashanian 2016b].

Then, in September 2007, I really started to work on the main topic of my post-doc project.

Towards a random laser with cold atoms

Until spring 2008, with Frank Michaud we performed an experiment on lasing with cold atoms. The goal was to study different gain mechanisms and test if they could sustain a working laser, with a standard laser cavity. This was, we thought, an interesting preliminary step towards making a random laser made of cold atoms [Michaud 2008]. I discuss the different gain mechanisms that we studied and this lasing experiment in Chapter II.

¹ This was at the very beginning of the ANR (Agence National pour la Recherche), when the success rate was not as ridiculously low as now.

² He’s now Assistant Professor in Paris.

This laser experiment, beside being successful [Guerin 2008], has been very important for us, and in particular for me, because at this occasion I discovered ‘Mollow gain’ [Mollow 1972]. The nice thing with Mollow gain is that there is a simple analytical expression for the atomic polarizability. Then I started to think that it should be possible to predict the feasibility of a random laser based on Mollow gain in cold atoms.

Briefly, a random laser is a laser in which the optical feedback is not provided by an optical cavity (with well-defined modes, etc.) but by multiple scattering in the gain medium itself. Considering the diffusion equation with a supplementary gain term, Vladilen Letokhov showed in 1968 that there is a threshold on the system size above which some runaway amplification occurs [Letokhov 1968], until gain saturation, like in a standard laser.

So, if the atomic response is analytically known, one can compute the scattering, the gain, and Letokhov’s threshold. I did this, and with the help of Rémi Carminati (partner of the ANR project), who taught me the difference between the attenuation length and the mean free path in a non-passive medium, and with his former post-doc Luis Froufe-Pérez, who did some supplementary simulations, we published the first theoretical predictions on the possibility of random lasing in cold atoms [Froufe-Pérez 2009]. This is described in Section IV.2.1.

Mollow gain is however not necessarily the best gain mechanism, and even has some serious drawbacks that made the predictions of [Froufe-Pérez 2009] not particularly realistic. The difficulty is to combine at the same time (i.e., at the same optical frequency) enough gain and scattering. We thus started a quest for the best gain mechanism, i.e. the one with the lowest threshold for random lasing with realistic parameters. This lead us, in particular, to make an experimental characterization of the atomic response with Raman gain between Zeeman sublevels, and to extrapolate the corresponding random-laser threshold [Guerin 2009]. I did this experiment with the help of Davide Brivio during his Master thesis [Brivio 2008] and then Nicolas Mercadier at the beginning of his PhD thesis. I also proposed a new configuration of non-degenerate four-wave mixing that seemed smart to us for realizing a random laser, but, after experimental and numerical investigations, it turned out to be the worst! Those results have been partly included in a review article for a special issue [Guerin 2010] and are discussed in Section IV.2.3 of the present manuscript. More details can be found in Nicolas Mercadier’s thesis [Mercadier 2011].

At this point (September 2009) my post-doc in Nice ended and I started a second post-doc at Tübingen University (Germany).

Lévy flights of light in hot vapors

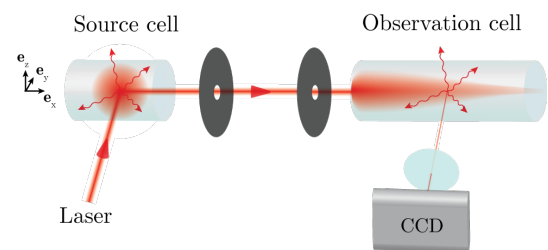
However, before leaving the (first) Nice period, I also want to mention briefly in this chapter another experiment that is not described later in this manuscript. I must say that my personal input has been quite modest: essentially, I gave technical advice at the beginning, I participated to meeting discussing the results, and I (significantly) helped write the papers [Mercadier 2009, Mercadier 2013]. Otherwise, all the real work, from the experiment to the modeling, has been done by Nicolas Mercadier during his Master thesis and the beginning of his PhD thesis [Mercadier 2011]. Our collaborator Martine Chevrollier also provided numerical simulations [Chevrollier 2010].

This experiment was on the observation of Lévy flights of light in a hot vapor cell (see [Chevrollier 2012] for a review paper). In the context of multiple scattering of light, or actually any kind of Brownian motion, the diffusion coefficient D is defined by the second moment of the step-length distribution $P(\ell)$ (the mean free path is the first moment, i.e. the

average step length). But it can happen that the second moment is undefined (or infinite) because the integral that computes the second moment doesn't converge (it can also happen with the first moment). Macroscopically, this leads to a 'superdiffusive' behavior, and the microscopic ingredients, which are the very long steps, are called 'Lévy flights'. This happens when the distribution $P(\ell)$ has a 'heavy' tail, which means that the long steps are not rare enough to be neglected, and actually dominate the large-scale properties of the transport. Mathematically, if the distribution is asymptotically a power law $P(\ell) \sim \ell^{-\alpha}$, then Lévy flights occur for $\alpha < 3$.

In hot vapors, Lévy flights are produced by Doppler broadening. Sometimes, a photon is scattered by an atom with a very large velocity, inducing a large Doppler shift. The photon makes thus a very long step before being rescattered. A precise computation of the step-length probability distribution gives $P(\ell) \sim 1/[\ell^2 \ln(\ell)]$, which is indeed heavy-tailed [Holstein 1947, Pereira 2004]. The goal of the experiment was to measure this probability distribution.

This has been done by direct imaging of the fluorescence profile in the cell in different configurations. In particular, in order to investigate the multiple-scattering regime, we have used a three-cell configuration, which was extremely demanding in term of signal-to-noise ratio. The main results have been published in Nature Physics [Mercadier 2009] and the details of the experiment and modeling have been described in a follow-up paper [Mercadier 2013]. Of course all the details are also in Nicolas Mercadier's thesis [Mercadier 2011].



Later the team performed another experiment investigating the macroscopic consequences of those Lévy flights, i.e. the superdiffusive transport [Baudouin 2014b], and much later an experiment with another broadening mechanism, collision with a buffer gas, has also shown superdiffusion with a diverging mean free path (article in preparation).

1.1.3. Post-doc in Tübingen (2010 – 2012)

Although I was happy in Nice, and there was still a lot to do to achieve a random laser, and some money had been saved on the ANR project, I had personal reasons to go to Tübingen, which had a little to do with strategic optimization of my career path in order to get a position one day, and a lot to do with consolidating a new French-German couple. There was no open position there and so I had somehow to establish myself.

Since I had a good spy in the place, I knew that Philippe Courteille (who is now Professor in São Carlos, Brazil, but was then in Tübingen) had done in the past some experiments on Bragg scattering off atomic lattices [Slama 2005b, Slama 2005a, Slama 2006] without being able to reach the photonic band gap regime [Deutsch 1995] and that he would have interest in trying again. In January 2009 I gave a seminar in Tübingen and I discussed with him and Claus Zimmermann, the head of the group, about the limitation of the previous experiments, which apparently was mainly the presence in the setup of a cavity around the atoms, which prevented from probing the system at the most appropriate angle. So I proposed to write a project with the building of a new, but simple, experiment (a simple magneto-optical trap and a 1D lattice), aiming at demonstrating a photonic band gap in cold atoms. I also added some personal touch from my previous experience: What happens if we add gain? Or something like electromagnetically-induced transparency (EIT)?

The project was submitted to the Humboldt Foundation and was accepted³. To complement my own manpower, Claus Zimmermann kindly gave me a PhD student, Alexander Schilke, who started building the experiment a few months before my arrival in January 2010. The funding lasted two years, but Claus could also complement it until August 2012, so my total stay in Tübingen lasted slightly more than 2.5 years. Since Philippe Courteille left for Brazil after two months, I was fully in charge of this project. This has been an important experience, the success of which probably contributed significantly to my getting a CNRS position in 2012.

In term of topics, it was also a good complementary experience: after studying light in disordered atoms in Nice, I was studying light in ordered atoms in Germany. Well, there is something of a cliché here...

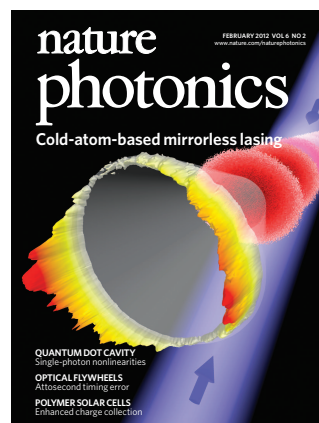
Photonic band gaps and distributed feedback lasing with cold atoms

Predictions of photonic band gaps in cold atomic lattices date from 1995 for the 1D case [Deutsch 1995] and were more recent for the 3D case [Antezza 2009, Yu 2011]. The goal of our experiment was to address the 1D case as a preliminary step before the more interesting 3D case. We trapped the atoms in a conservative lattice made by a tunable laser detuned from ~ 1 nm from the transition and loaded from a magneto-optical trap (MOT). In this system the periodic modulation of the refractive index is due to the periodic modulation of the atomic density due to the trapping potential. By a careful tuning of the lattice wavelength, which has to be precisely adapted to the angle and detuning of the probe laser, we could observe a Bragg reflection of $\sim 80\%$, much more than all previous Bragg scattering experiments so far. With the help of some theoretical modeling, in particular to compute the local density of states, this could be interpreted as the occurrence of a photonic band gap. We also discussed the intrinsic limitations of this kind of system [Schilke 2011], in particular due to the imaginary part of the atomic polarizability, which acts as losses.

Another idea was to use EIT and see if it can overcome this limitation. After working out the theory I found that this idea had already been proposed before [Petrosyan 2007]. Anyway, it does not allow overcoming this limitation, but it still is interesting, because it creates a secondary band gap, which is narrower and controllable by an external laser. We have performed this experiment and demonstrated the use of this secondary band gap as an all-optical switch [Schilke 2012b].

These results are presented in Section III.1.

Then my other original idea was to add gain, for instance Raman gain, which I was familiar with, and see what happens. My idea was that the combination of multiple Bragg reflection and gain might create a huge transmission and reflection. It actually did. The nice unexpected effect appeared when we induced four-wave mixing: then a huge signal came out of the atomic lattice, even without any probe beam. This was the first mirrorless laser (or, more precisely, an optical parametric oscillator), and the feedback mechanisms was the ‘distributed feedback’ due to the 1D periodic density modulation, like in commercial DFB laser diodes [Schilke 2012a]. The reason why it worked with FWM and not with Raman gain is quite subtle and is explained in Section III.2.



³ They have a very decent acceptance rate.

I.1.4. Back at INLN/INPHYNI (since Oct. 2012)

I got a CNRS researcher position in 2012 and I arrived back at INLN in October that year. The lab changed its name to Institut de Physique de Nice (INPHYNI⁴) in January 2017.

My project was to take in charge the ‘Rb2’ experiment, which had been set up in 2008 and on which some ‘cooperative scattering’ experiments had been performed [Bienaimé 2010, Bux 2010, Bienaimé 2011a], as well as a compression experiment in a rotating dipole trap, for producing dense atomic clouds in view of reaching Anderson localization of light [Bienaimé 2012]. Julien Chabé (post-doc, 2010 – 2012) had just left and there was one PhD student, Louis Bellando, doing partly experiments and partly theory, who was starting his third (and last) year [Bellando 2013]. On the same topic of cooperative scattering, there was also one PhD student doing a joint PhD, Mohamed-Taha Rouabah, who was starting his second half of his thesis in our group, doing theory [Rouabah 2015].

On ‘Rb1’, the random laser experiment, there was one PhD student, Quentin Baudouin, who was also starting his third and last year.

So the manpower situation was critical, because I only had a few months overlap with the two finishing PhD students before they start writing up their thesis, and then I would be alone in the lab with two cold-atom experiments! Moreover, there were some papers to be written [Mercadier 2013, Baudouin 2013b, Baudouin 2014a, Gerasimov 2014], which is always good but takes time. As a consequence, during the first year or so, I was mainly busy writing them and maintaining alive the two experiments.

On Rb1 I got some help from Djeylan Aktas, doing his Master thesis in spring 2013 under the supervision of Quentin at the beginning and myself at the end [Aktas 2013]. Then in fall 2013 a new PhD student started on Rb1, Samir Vartabi Kashanian, whom I trained on the experiment during the first two months [Vartabi Kashanian 2016a]. However, since I also had in charge the other experiment, I haven’t had the time to work closely with him. Combined with the absence of overlap with the previous student, with some important technical problems on the experiment (vacuum...), and his lack of previous experimental experience, Samir hasn’t had the best circumstances and the random laser experiment was delayed a lot. The situation really improved only in 2015 when first, Aurélien Éloy joined as a Master and then a PhD student, and second, Mathilde Hugbart (Fouché) joined as a permanent staff. She fully took in charge the experiment.

On Rb2, Michelle Araújo started her PhD thesis in fall 2014. When she arrived the experiment was running, taking systematic data, which is not a nice time to learn the experiment, so she spent the first months doing simulations. I was thus basically alone on the experiment until spring 2015.

A random laser with cold atoms

During my time in Germany, my followers on the random laser experiment (Nicolas Mercadier, PhD student 2008 – 2011, Vera Guarrera, post-doc 2009 – 2010, Quentin Baudouin, PhD student 2010 – 2013) had managed to devise a smart gain mechanism based on Raman gain between hyperfine levels, to observe a signature of a random-laser effect, and to develop some modeling (see Sections IV.3). Luckily for me they haven’t been fast enough to publish their results, and I arrived at a time still full of discussions about the possible interpretations of the data. I thus contributed to the final stage of those discussions and to the writing of the paper [Baudouin 2013b].

⁴ pronounced in French like ‘∞’.

Then I extended to the 2D case a computation that Letokhov did in 3D about the threshold of a random laser using the radiative transfer equation [Lavrinovich 1975] (Quentin had deciphered this computation in his PhD thesis [Baudouin 2013a]). In collaboration with Chong Yidong (Singapore) and Stefan Rotter (Vienna), this allowed us to make a systematic comparison with a much more complete model [Guerin 2016b]. This is presented in Section IV.2.2.

Due to the bad circumstances described above, this is all we did on the random laser. There has been some study of Raman gain done by Aurélien Éloy during his thesis [Éloy 2018a]. The idea was to be able to control the amount of gain and measure independently the gain and the scattering, which would have given the possibility of doing the first direct comparison between Letokhov's threshold predictions and experimental data. However problems with spurious magnetic fields prevented us to obtain enough gain to reach the random laser regime. Then the experiment took some other directions.

Cooperative scattering in cold atoms

Since 2013 my main research topic is the cooperative scattering of light by cold atoms in the linear-optics regime, and this is experimentally investigated on the MOT setup Rb2. The previous performed experiments, in Nice [Bux 2010, Bienaimé 2010] and in collaboration with the Tübingen group [Bender 2010], dealt with a reduction of the radiation-pressure force, interpreted as a consequence of the superradiant forward scattering predicted by Scully and coworkers [Scully 2006]: if light is more emitted in the forward direction, the net force is reduced. A lot had been done and understood on this topic of cooperative scattering during Tom Bienaimé's thesis [Bienaimé 2011a], with in particular a very fruitful network of collaborators: Philippe Courteille and Romain Bachelard at São Carlos (Brazil), Nicolas Piovela at Milan (see for instance the review [Bienaimé 2013]). However when I arrived the situation was a bit confused because recent data taken on the experiment also showed the reduction of the force in a regime where it was not expected, namely near resonance, when multiple scattering takes place. It was finally found out that this reduction could also have a more trivial explanation [Chabé 2014]. Later, I contributed to a more systematic study of the different effects that can lead to a collective reduction of the radiation-pressure force and we showed that all the experiments published so far could also be explained without invoking cooperative scattering [Bachelard 2016], except, perhaps, the results of [Bux 2010], which are still not well understood. Similarly, I contributed to the interpretation of data taken by the group of Mark Havey (Old Dominion University), showing that their steady-state light-scattering measurements could be understood without cooperativity [Kemp 2020]. Those results are presented in Chapter V.

But what is cooperative scattering anyway? This is a hard question, which I tried to partially answer in a discussion article in 2017 [Guerin 2017c], in an attempt to remove some of the confusion in the field. Basically, here, it will be synonymous for super- and subradiance, and so far, to my opinion, the only unambiguous experimental signatures of those effects are in the temporal dynamics, namely the accelerated or slowed decay of light after excitation of the sample.

This is what I extensively studied in all those years and that is the subject of the most important chapter of this manuscript, Chapter VI, which contains a number of results.

The first and probably the most important result has been the first direct observation of subradiant decay [Guerin 2016a], which was the main goal I had at the beginning, since the team had just published the corresponding theoretical prediction [Bienaimé 2012]. The success

of this experiment opened up many perspectives and the need for several complementary studies.

First, with Michelle Araújo [Araújo 2018a], we performed an experiment dedicated to the fast dynamics at the beginning of the decay, which exhibits a superradiant behavior [Araújo 2016]. This was not obvious because the recent literature on single-photon superradiance was only speaking about the *forward* superradiant lobe, and we looked at *off-axis* scattering. Then I performed a theoretical study on the population of the collective modes of the coupled-dipole model in order to understand some puzzling observations, for instance the fact that subradiance is enhanced near resonance while superradiance is suppressed [Guerin 2017b]. We also published some details on the simulation procedure with the coupled-dipole equations [Araújo 2018b].

At the end of 2016 we were joined by Patrizia Weiss as a post-doc (whom I knew from Tübingen), and she really took in charge the experiment and did most of the experimental work during the following three years, including significant upgrading of the experimental setup, as well as some numerical simulations. We performed a detailed study of the interplay between subradiance and multiple scattering [Weiss 2018] and a systematic study of the effect of thermal motion on subradiance [Weiss 2019].

With Ana Cipris, who started her PhD in October 2017, we also started an experiment on subradiance beyond the linear-optics regime, by increasing the intensity of the probe beam. This was motivated by some predictions made by the team of Romain Bachelard (São Carlos, Brazil). The motivation for increasing the saturation parameter is to go toward quantum effects. At the time of writing, data has been taken and we are at the stage of trying to understand them.

Furthermore, we studied the switch-on dynamics, in the linear-optics regime (by re-analyzing the superradiance data) and beyond linear optics. Here also the initial idea was that the Rabi oscillations visible at the switch-on are good candidates to detect quantum collective effects. We finally split this study into two papers, one focussed on the collective frequency shift of the Rabi oscillation [Guerin 2019] and containing linear-optics data only, and one focussed on the collective damping rate of those oscillations, including beyond linear-optics data [do Espirito Santo 2020]. This has been done in collaboration with Romain Bachelard's team and with Johannes Schachenmayer (Strasbourg).

Last but not least, I have recently enjoyed a fruitful collaboration with Igor Sokolov (Saint Petersburg) [Sokolov 2019], which allowed me to discover a new (at least for me) interpretation of superradiance [Kuraptsev 2017], which also provides a very computing-efficient modeling.

Revival of intensity interferometry

In the last years, I have also worked on another research topic, which has nothing to do with cold atoms. Since this topic is not developed further in the rest of the manuscript, I briefly summarize it here.

Everything started with bibliography about the random laser. We discovered that it was speculated, particularly by Johansson and Letokhov, that natural random lasers could occur in space [Johansson 2007]. How to detect them? Quantum-optics people know that to distinguish a laser from classical radiation, one must measure the intensity correlation function. Even if this hypothesis is very speculative (a brief summary of the current knowledge is given at the end of Part I), this triggered some discussions with Farrokh Vakili, who at that time was the director of the Nice Observatory (Observatoire de la Côte d'Azur, OCA).

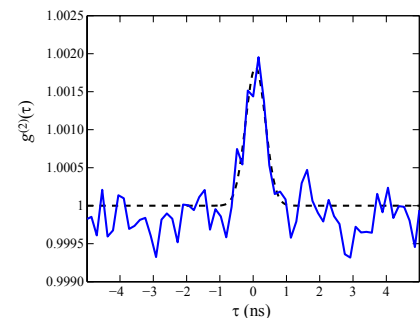
It just so happens that Farrokh Vakili is a specialist of stellar interferometry, and among this community, he is among the people who are thinking of reviving the technique of Hanbury Brown and Twiss (‘intensity interferometry’), based on the measurement of intensity correlations [Hanbury Brown 1956, Hanbury Brown 1974]. The idea has been in the air since the mid-2000s, mainly motivated by the use of the future Cherenkov Telescope Array (CTA) as a huge multi-baseline, high-resolution intensity interferometer [LeBohec 2006, Dravins 2008]. Anyway, this created a common interest and Robin and Farrokh managed to obtain from the local entities a funding for a post-doc⁵.

Antoine Dussaux arrived in January 2015 and the real work started. He learnt how to measure subnanosecond intensity correlations and found the best technique to do it (with some help of the quantum-information team of INPHYNI), he performed a test experiment using light scattered by a hot vapor [Dussaux 2016], he made a feasibility study to implement this technique at the telescopes of Calern (a site of OCA), he convinced people at Calern to embark in this effort, in particular Jean-Pierre Rivet, and with his help he finally designed and tested the instrument to be used in the telescope. During all this time I got slightly involved, essentially because Antoine shared my office and thus I naturally discussed with him and in particular I helped him a little on the hot-vapor experiment, since he had no experience in atomic physics.

Unfortunately Antoine Dussaux left the lab (and the academic world) in fall 2016, just at the most exciting time, when everything was almost ready to perform the first ‘on-sky’ tests. As a consequence, we all (i.e., Mathilde Hugbart, Guillaume Labeyrie and myself) jumped on this opportunity to have a little fun spending a few nights at the observatory. This was not the only motivation: we also thought that learning the technique of intensity correlations could also be useful for cold-atom experiments, which proved right later [Éloy 2018b].

By coincidence Antoine left exactly when Patrizia Weiss arrived on the Rb2 experiment, and as written above she has been very efficient in taking in charge the experiment, which gave me the possibility to really spend time on this astronomy project, more than my colleagues. As a consequence, since the end of 2016 approximately, I estimate that I’ve spent about half of my time on this topic, being *de facto* the main driving force on the INPHYNI side (although I insist that my colleagues did contribute, especially Mathilde).

Together we first observed photonic bunching with starlight by measuring the temporal intensity correlation function using a single telescope [Guerin 2017a]. This has been the first successful intensity correlation experiment with stars (other than the sun) since the Narrabry observatory in the 1970s [Hanbury Brown 1974] and the first ever in the photon-counting regime. Then we duplicated the instrument and performed a real spatial intensity interferometry experiment using the two telescopes of the C2PU facility at Calern⁶, separated by 15 m [Guerin 2018]. Those results have been remarked in the community, as shown by an invited paper in a special issue [Rivet 2018], an invitation to the SPIE conference on telescopes [Lai 2018], and the adhesion of OCA to the CTA consortium via its working group on intensity interferometry.



We have then been joined by Antonin Siciak, who started his PhD thesis in February 2018 on

⁵ The multi-inter-trans-disciplinary nature of the project (quantum optics and astronomy) helped.

⁶ Centre Pédagogique Planète et Univers, described at <https://www.oca.eu/fr/c2pu-accueil?sommaire>.

this project, and we have performed and/or are planning to perform a number of experiments on: intensity interferometry on a strong emission line [Rivet 2020]; polarization-resolved intensity interferometry; long-baseline interferometry with a nontrivial synchronization procedure (in collaboration with the MéO team at Calern); etc. I've also had the chance to go to Chile, with Jean-Pierre Rivet, for one observing night on the 4 m SOAR telescope⁷ in April 2019, which demonstrated the portability and reliability of our instrument. Promising discussions are underway to go back to Chile, this time on the Very Large Telescope site!

I.2. Content of this manuscript

As usual for an HDR, this manuscript describes in the following a large part of what I did after my PhD thesis, but not everything, because that would have been too much. Especially, the Lévy flight experiment and the intensity interferometry project, which I briefly summarized in this chapter, are not presented in more detail.

I organized the rest in two main parts. The first one is on ‘Mirrorless lasing with cold atoms’, which gathers the random laser project as well as what I did in Tübingen, the photonic band gap experiments being presented as a way to provide feedback for the distributed feedback laser. The different results are not presented in chronological order but instead in some more logical order (hopefully) allowing me to merge the two experiments in a consistent way. The second part will be on cooperative scattering and, to be more precise, it is entitled ‘Cooperative scattering in dilute cold-atom clouds in the linear-optics regime’, which describes more precisely what we have investigated.

Since describing about a dozen years of research would produce a huge manuscript and would have taken me an unreasonable amount of time, I (reluctantly) had to use the usual time-saving solution: including papers. All of my papers or not included, not even all those fitting the two selected topics, but most of them. Most sections are made of a short introduction before including one paper describing the main results, eventually followed by a short discussion. My text thus serves as links between the different papers in order to understand the evolution and consistency of the research. A few sections are only text, and for some of those I recycled some existing text coming from not-included papers. In particular, the review [Baudouin 2014a] has been very useful for the first part.

Finally I put in two appendices a detailed curriculum vitae and a complete list of publications and communications.

⁷ SOuthern Astrophysical Research telescope, described at <http://www.ctio.noao.edu/soar/>.

Part One

Mirrorless lasing with cold atoms

Brief introduction on the topic of mirrorless lasing

A standard laser is made of two ingredients: a gain medium, which provides amplification of light by some kind of stimulated emission; and an optical cavity, which provides feedback. The feedback has several roles. Very often, it substantially acts on the coherence properties of the laser, by introducing a mode selection. But its primary role is to re-inject light in the gain medium, such that light can be amplified many times before escaping. This creates the well-known threshold effect: when the round-trip gain is higher than the losses, a runaway amplification takes place, until gain saturation.

In the years 2000s a very strong interest started in mirrorless lasing systems [Wiersma 2010], in which the electromagnetic feedback is provided by other ingredients than a cavity. Consequently, the coherence and mode properties are also different, and that is what is interesting. The feedback can be provided either by disorder, i.e., multiple scattering in the gain medium, or by order, i.e., multiple Bragg reflections. This corresponds, respectively, to ‘random lasers’ [Wiersma 2008] and ‘photonic-crystal lasers’ or ‘nanolasers’ [Noda 2010]. The crossover regime, between order and disorder, or correlated disorder, started also to be fruitfully investigated [Conti 2008, Mahler 2010, Noh 2011].

Distributed feedback lasers

The 1D version of photonic-crystal lasers is actually a very old topic, and has become a well-known, commercially-available device, namely distributed-feedback (DFB) lasers. The principle of DFB lasers has been proposed by Kogelnik and Shank in the early 1970s [Kogelnik 1971, Kogelnik 1972] and is described in classical textbooks [Yariv 1988].

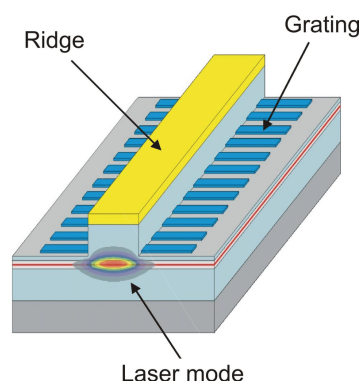


Figure 1: Illustration of the working principles of a DFB laser. Image taken from [Seufert 2008].

The basic idea of a DFB laser is to add a small modulation of the refractive index (or of the gain coefficient) along the amplification region, which is usually elongated with a transverse confinement (it is thus a waveguide, see Fig. 1). The waves propagating along the guide in the two counter-propagating directions are then coupled through Bragg reflection, which acts as a kind of optical cavity trapping the light inside the structure.

Random lasers

As early as 1968, Letokhov investigated what happens when amplification of light, or *gain*, is present in a multiple scattering medium [Letokhov 1968]. In such a situation, multiple scattering increases the length of the path of light propagating in the gain medium and thus enhances its amplification. This obvious effect can lead to a much less trivial phenomenon, which is that there is a threshold on the system size above which amplification in the medium overcomes leakage at the surface, leading to an exponential increase of the light intensity trapped in the medium (and the subsequent emitted light) [Letokhov 1968, Cao 2003]. This is very similar to the principle of a laser, which starts when gain produced by the amplifying medium overcomes the cavity losses. Here, the cavity is replaced by radiation trapping [Zemansky 1927, Holstein 1947, Molisch 1998], which provides an ‘incoherent’ feedback. Since there is no cavity axis to impose a propagation direction, the emission diagram is more or less random (like a speckle pattern), hence the name random laser. Like in a standard laser, the exponential increase of the light intensity is limited by gain saturation to a value for which gain exactly compensates losses.

After some preliminary evidence of scattering-enhanced emission of light in some gain media [Markushev 1986, Gouedard 1993, Lawandy 1994], great efforts have been made to experimentally demonstrate and study random lasing in different kinds of physical systems [Cao 1998, Cao 1999, Wiersma 2001, Strangi 2006, Gottardo 2008, Turitsyn 2010] and even in biological tissues [Polson 2004]. It has immediately appeared that Letokhov’s initial theory, which is based on the diffusion equation and thus neglects any interference effect, was not sufficient to describe random lasers, which exhibit subtle mode and coherence properties. The understanding of these properties is a theoretical challenge, as it is related to fundamental questions on the nature and properties of electromagnetic modes in open, nonlinear, disordered systems [Fallert 2009, Andreasen 2011, Wiersma 2013]. Different theoretical approaches have been developed [Wiersma 1996, Burin 2001, Vanneste 2007, Türeci 2008, Conti 2008,

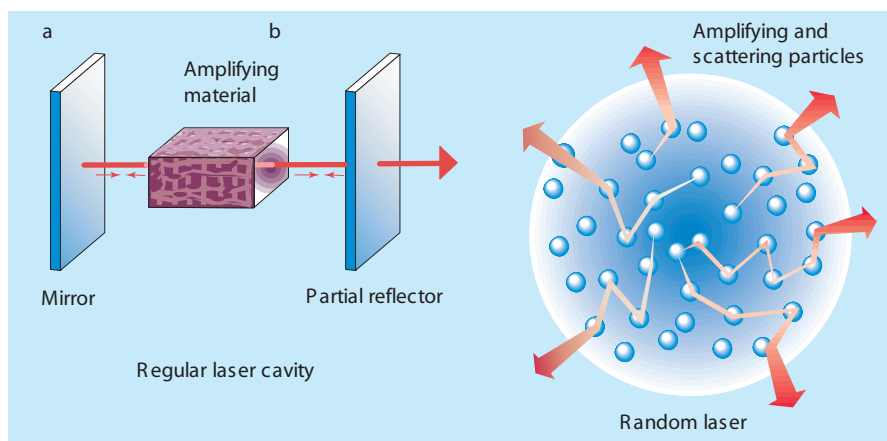


Figure 2: Illustration of the working principles of a standard laser (a) and a random laser (b). Image taken from [Wiersma 2000].

[Frank 2009, Goetschy 2011]. The connection to the fascinating subject of Anderson localization [Anderson 1958, Lagendijk 2009] also attracted a lot of attention (see, e.g., [Conti 2008]). The broad interest of random lasing was also driven by potential applications [Wiersma 2008]. For instance, the use of a random laser as a light source for speckle-free laser imaging was demonstrated [Redding 2012].

Motivations for addressing these subjects with cold atoms

Among the possible systems to produce and study mirrorless lasers, cold atoms are interesting because of their specific properties in comparison with standard photonic materials. First, they are resonant point-like scatterers, which leads to extremely narrow spectral features (gain curves, scattering cross-section), which can provide flexibility [Gottardo 2008] or give new effects. Second, their temperature is low enough to make Doppler broadening negligible in most situations but large enough to make them move substantially at the millisecond timescale, which makes disorder-configuration averaging, or dynamic evolution from order to disorder, very easy. Third, cold atoms are well isolated from the environment, which makes them good candidates to search for quantum effects.

A cloud of cold atoms constitutes a new medium to study random lasing, allowing a detailed microscopic understanding of gain and scattering. Multiple scattering of light in cold atoms had been extensively studied in the past [Labeyrie 2003, Labeyrie 2004]. Also, quasi-continuous lasing with cold atoms as gain medium, placed inside optical cavities, had already been demonstrated [Hilico 1992, McKeever 2003], illustrating the potential for a variety of gain mechanisms in a regime where optical coherence is limited by purely radiative decay channels. This is significantly different with respect to most random-lasing devices, based on pulsed excitation of condensed-matter systems, where the relaxation rates of the optical coherence are several orders of magnitude faster than the decay of the excited state population. Finally, the unique possibility to both control the experimental parameters and to model the microscopic response of our system provides an ideal test bench for better understanding random lasers.

CHAPTER II

Gain and lasing with cold atoms

Contrary to most gain media, cold atoms do not present non-radiative, fast-decaying transitions, preventing a standard 4-level scheme to produce a population inversion. Nevertheless there are many different mechanisms that allow an inversion between two different atomic states. These can either be different states of external degrees of freedom (momentum or vibrational levels in an external potential) or internal degrees of freedom (dressed states [Cohen-Tannoudji 1992] or different ground states). The atomic nonlinearity can also be used to obtain parametric gain. Finally, other, more complicated schemes using quantum interferences can provide gain without inversion [Scully 1994, Zibrov 1995, Mompart 2000].

II.1. Different gain mechanisms

The text of this section has been slightly adapted from [Baudouin 2014a].

II.1.1. Mollow gain

A very simple gain mechanism in atomic vapors was described by Mollow [Mollow 1972] and observed soon afterwards [Wu 1977] with atomic beams. It involves a two-level atom driven by one strong pumping field. The driving field induces a population inversion in the dressed-state basis [Cohen-Tannoudji 1992] and therefore a weak probe beam can be amplified. The whole process can also be described in the bare-state basis by a three-photon transition from the ground state to the excited state via two absorptions of pump photons, as sketched in Fig. II.1(a).

The main amplification feature appears for a pump-probe detuning of $\delta = \text{sign}(\Delta)\sqrt{\Delta^2 + \Omega^2}$, where $\Delta = \omega_P - \omega_{\text{at}}$ is the pump detuning from the atomic transition, $\delta = \omega_S - \omega_P$, Ω is the Rabi frequency of the pump-atom coupling, related to the pump intensity I by $\Omega^2 = \Gamma^2 I / (2I_{\text{sat}})$ (I_{sat} is the saturation intensity), and has a typical width on the order of the transition linewidth Γ . Note that another, dispersion-like feature appears around $\delta = 0$, which is associated with two-photon spontaneous emission processes [Grynberg 1993]. This contribution also induces gain with a much smaller amplitude, and can generate lasing without population inversion [Zakrzewski 1992, Mompart 2000].

In our experiment with cold ^{85}Rb atoms, we have measured single-pass gain as high as 50 %, which is more than enough to induce lasing, even with a low-finesse cavity. The gain is optimum when the probe and the pump polarization are parallel, as the driven atomic dipole is then parallel to the probe field.

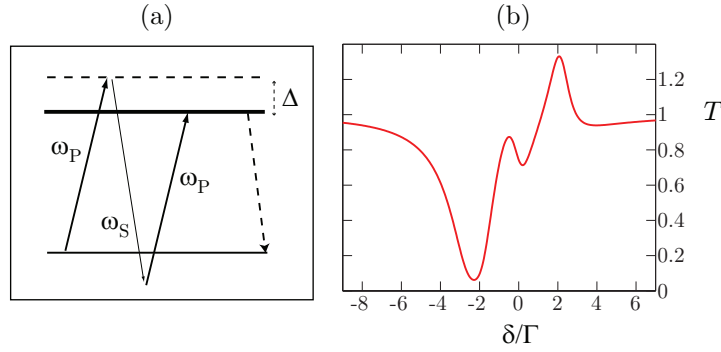


Figure II.1: (a) Principle of the Mollow gain depicted as a three-photon transition from the ground state to the excited state, with two absorptions from the pump at ω_P and one stimulated emission in the signal wave at ω_S . It can also be viewed as a population inversion in the dressed-state basis. (b) Transmission spectrum, computed for typical experimental parameters $b_0 = 10$, $\Omega = 2\Gamma$ and $\Delta = \Gamma$, with b_0 the resonant optical depth (the other parameters are defined in the text). From [Guerin 2010].

II.1.2. Raman gain using the Zeeman structure

Another gain mechanism in atomic vapors is Raman gain. Raman transitions refer in general to two-photon transitions between two non-degenerate ground states, the intermediate energy level being in the vicinity of an atomic excited states. To obtain gain, a pumping field can induce the first upward transition and a probe beam can then be amplified at the frequency of the downward transition.

A first possibility is to use the pump-induced population inversion among the different light-shifted Zeeman sublevels m_F of a given hyperfine level F , as depicted in Fig. II.2(a) [Tabosa 1991, Grison 1991]. For example, optical pumping near a closed $F = 1 \rightarrow F' = 2$ transition induced by a π -polarized laser leads to a symmetric distribution of population with respect to the $m_F = 0$ sublevel of the ground state, with this sublevel being the most populated and also the most shifted, due to a larger Clebsch-Gordan coefficient [Brzozowski 2005]. To record a transmission spectrum, atoms are probed with a linearly polarized probe beam with the polarization axis orthogonal to the pump polarization, thus inducing $\Delta m_F = \pm 1$ Raman

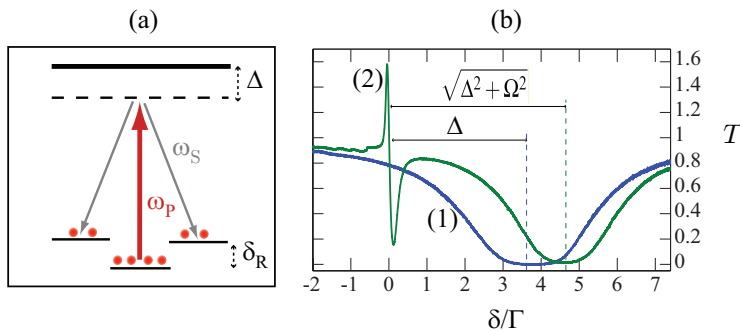


Figure II.2: (a) Principle of the Raman mechanism, depicted here for a $F = 1 \rightarrow F' = 2$ transition. (b) Experimental transmission spectra recorded with cold ^{85}Rb near the $F = 3 \rightarrow F' = 4$ transition, plotted as a function of the pump-probe detuning δ . Without pumping, spectrum (1) shows only the atomic absorption. A pump beam of detuning $\Delta = -3.8 \Gamma$ and intensity 13 mW/cm^2 , corresponding to a Rabi frequency $\Omega = 2.5 \Gamma$, is added to obtain spectrum (2), which then exhibits a Raman resonance in the vicinity of $\delta = 0$. Moreover, the atomic absorption is shifted due to the pump-induced light shift and the absorption is reduced due to saturation. From [Guerin 2010].

transitions. Depending on the sign of the pump-probe detuning δ , the population imbalance induces gain or absorption. With a larger F , each pair of neighboring sublevels contributes with a relative weight depending on the population inversion. In practice however, the contributions of different pairs are often not resolved and only two structures (with opposite signs) are visible, one corresponding to amplification for $\delta = -\delta_R$ and one to absorption for $\delta = \delta_R$. Note that this situation corresponds to a red detuning for the pump ($\Delta < 0$) and that the signs are inverted for blue-detuning ($\Delta > 0$). As δ_R comes from a differential light-shift (because of different Clebsch-Gordan coefficients), it is usually small, on the order of $\Gamma/10$, whereas Δ is a few Γ . The width γ of the resonances is related to the elastic scattering rate, also much smaller than Γ [Grison 1991]. Far from the main atomic absorption resonance, the Raman resonance is thus a narrow spectral feature, as shown in Fig. II.2(b).

This mechanism had previously been used to generate lasing with a MOT inside an optical cavity [Hilico 1992].

II.1.3. Raman gain using the hyperfine structure

The two hyperfine ground states of rubidium atoms can also be used to produce Raman gain. One advantage is that the gain and the pump frequencies are separated by several gigahertz. A drawback is that the pump laser has to be tuned close to an open transition, so that optical pumping quickly destroys any population inversion. A second laser is thus necessary to recycle the atoms (Fig. II.3), which somewhat complicates the setup.

This gain mechanism had been used in an experiment on lasing with a single atom [McKeever 2003] and our experiment on random lasing also uses this gain (Chapter IV).

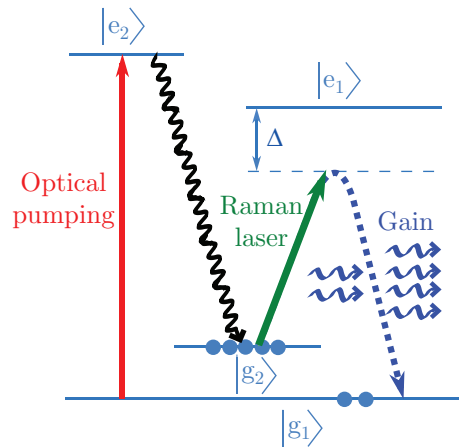


Figure II.3: Raman gain using hyperfine levels. Gain is produced by stimulated emission induced by the Raman laser (two-photon transition). The population inversion between the ground states $|g_1\rangle$ and $|g_2\rangle$ is sustained by the optical pumping laser. Adapted from [Baudouin 2014a].

II.1.4. Degenerate four-wave mixing (FWM)

By using two phase-locked pump beams, we can induce four wave mixing (FWM): the two pumps of frequencies ω_{P1} and ω_{P2} and one probe – or an initial fluctuation – of frequency ω_S generate a fourth field at frequency ω_C , called the conjugate field [Yariv 1977, Abrams 1978, Boyd 1981]. The frequencies and wave-vectors of all the fields are related by energy and momentum conservation (phase-matching condition). If we want to obtain *gain* for the probe, we have to choose a configuration where the conjugate frequency equals the probe: $\omega_C = \omega_S$. Then, the pump frequencies have to fulfill the condition $\omega_{P1} + \omega_{P2} = 2\omega_S$. From

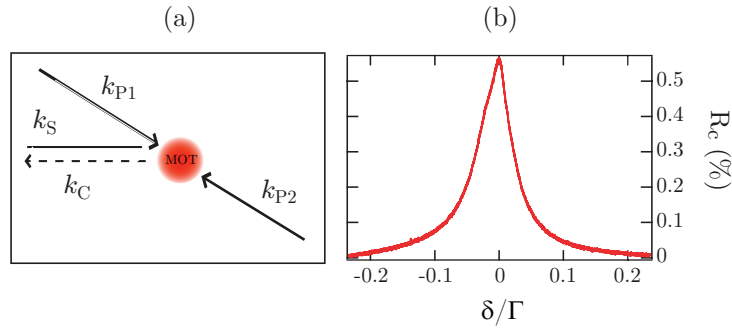


Figure II.4: (a) Principle of four-wave mixing. There are two counterpropagating pump fields P1 and P2, one probe beam (‘signal’ S) and one conjugated C field. (b) Typical experimental reflection spectrum. δ is the probe-pump detuning. From [Guerin 2010].

an experimental point of view, the most simple configuration is when all frequencies are the same (‘degenerate FWM’). This is the experimental situation with which standard lasing can be obtained. Note that this mechanism was observed a long time ago with hot atoms [Kleinmann 1985, Pinard 1986, Leite 1986].

Due to the phase-matching condition, gain is not in the forward transmission of the probe beam, but in backward reflection, provided that the two pumps are counterpropagating (Fig. II.4). The conjugate beam is actually the phase-conjugate of the probe beam. This property has a number of consequences for the cavity-laser (Section II.2) and the DFB laser (Section III.2).

II.1.5. Other gain mechanisms

The above list of the possible gain mechanisms that can be used in cold atoms is not exhaustive.

Other, more complicated, schemes involve quantum interferences to induce gain without population inversion (in any basis) [Scully 1994, Mompert 2000]. This can be realized with a Λ scheme [Padmabandu 1996] or a V scheme [Zibrov 1995, Kitching 1999].

Another possibility is to use the atomic external degrees of freedom, i.e., their kinetic energy. Transitions between different velocity classes produce recoil-induced resonances [Courtois 1994], and high gain can be achieved [Vengalattore 2005]. These resonances can ultimately lead to a ‘Collective atomic recoil laser’ [Bonifacio 1994, Berman 1999], which has been demonstrated with cold and ultra-cold atoms [Kruse 2003, Slama 2007].

Finally, one could also consider higher-order photonic processes, such as two-photon dressed-state lasers [Gauthier 1992].

II.2. Standard lasing

We have tested three of these gain mechanisms, namely Mollow gain, Raman gain between Zeeman states, and degenerate FWM, in a standard lasing configuration, by building around the MOT a low-finesse cavity.

With Mollow gain, the output intensity reaches $35 \mu\text{W}$ at most, achieved for $|\Delta| \sim 2\Gamma$. Its threshold in pump intensity is in agreement with the corresponding measured single-pass

gain and the losses of the cavity. The polarization of the emitted laser is linear, parallel to the pump polarization, because gain is maximum in that configuration.

On the contrary, with Raman gain, the output polarization is orthogonal to the pump one, and this gain produces a laser with less power ($2 \mu\text{W}$). Moreover, the sharpness of the gain curve makes the Raman gain very sensitive to any Doppler shift. Thus, the radiation pressure from the pump beam makes the laser emission stop after only $\sim 20 \mu\text{s}$. On the other hand, the narrow spectrum of the laser can be easily characterized by a beat-note experiment.

The properties of the FWM laser (or, better say, optical parametric oscillator) are quite different. First, the phase-conjugation property leads to a different threshold condition [Pinard 1986]: a reflectivity of only 1 % is enough to generate lasing, despite the much larger losses of the cavity (in our experiment, 32 % for a round trip). This is due to constructive interferences between transmitted and reflected waves, as observed in double-pass experiments [Michaud 2007]. Second, it leads to more complex transverse modes, because the phase conjugation mechanism allows any transverse pattern to be stable through the resonator [Lind 1981]. Finally, these properties lead to a much larger power than with Mollow and Raman gain, and up to $300 \mu\text{W}$ have been obtained. The phase-conjugation property is also important for the DFB laser of Tübingen, since it participates in the feedback to make it stable (section III.2).

These results have been published in the article [Guerin 2008] reproduced below.

Mechanisms for Lasing with Cold Atoms as the Gain Medium

William Guerin, Franck Michaud, and Robin Kaiser*

Institut Non Linéaire de Nice, CNRS and Université de Nice Sophia-Antipolis, 1361 route des Lucioles, 06560 Valbonne, France
(Received 31 March 2008; published 29 August 2008)

We realize a laser with a cloud of cold rubidium atoms as gain medium, placed in a low-finesse cavity. Three different regimes of laser emission are observed corresponding, respectively, to Mollow, Raman, and four-wave mixing mechanisms. We measure an output power of up to 300 μW and present the main properties of these different lasers in each regime.

DOI: [10.1103/PhysRevLett.101.093002](https://doi.org/10.1103/PhysRevLett.101.093002)

PACS numbers: 42.55.Zz, 33.20.Fb, 37.30.+i, 42.55.Ye

Since Letokhov's seminal paper [1], random lasers have received increasing interest. Random lasing occurs when the optical feedback due to multiple scattering in the gain medium itself is sufficiently strong to reach the lasing threshold. In the past decade, it has been observed in a variety of systems (see [2] for a review), but many open questions remain to be investigated, for which better characterized samples would be highly valuable. A cloud of cold atoms could provide a promising alternative medium to study random lasing, allowing for a detailed understanding of the microscopic phenomena and a precise control of essential parameters such as particle density and scattering cross section. These properties have been exploited to study coherent backscattering of light [3] and radiation trapping [4] in large clouds of cold atoms. As many different gain mechanisms have been observed with cold atoms, combining multiple scattering and gain in cold atomic clouds seems a promising path towards the realization of a new random laser. Besides the realization of a random laser, cold atoms might allow one to study additional features, such as the transition from superfluorescence [5] to amplified spontaneous emission [6] in a multiple scattering regime. One preliminary step along this research line is to use a standard cavity to trigger laser oscillation with cold atoms as gain medium. Such a laser may also be an interesting tool for quantum optics, as one can take advantage of the nonlinear response of the atoms to explore nonclassical correlations or obtain squeezing [7].

In this Letter, we present the realization of a cold-atom laser, that can rely on three different gain mechanisms, depending on the pumping scheme. By pumping near resonance, Mollow gain [8,9] is the dominant process and gives rise to a laser oscillation, whose spectrum is large (of the order of the atomic natural linewidth), whereas by pumping further from resonance, Raman gain between Zeeman sublevels [10] gives rise to a weaker, spectrally sharper laser [11]. At last, by using two counter-propagating pump beams, degenerate four-wave mixing (FWM) [12,13] produces a laser with a power up to 300 μW . By adjusting the atom-laser detuning or the pump geometry, we can continuously tune the laser from one regime to another.

Our experiment uses a cloud of cold ^{85}Rb atoms confined in a vapor-loaded magneto-optical trap (MOT) produced by six large independent trapping beams, allowing the trapping of up to 10^{10} atoms at a density of 10^{10} atoms/cm³, corresponding to an on-resonance optical thickness of about 10. A linear cavity, formed by two mirrors (a coupling mirror with curvature $RC1 = 1$ m, reflection coefficient $R1 = 0.95$, and plane end mirror with reflection coefficient $R2 \approx 0.995$) separated by a distance $L = 0.8$ m is placed outside the vacuum chamber, yielding a large round trip loss $\mathcal{L} = 32\%$ with a correspondingly low finesse $\mathcal{F} = 16$. The waist of the fundamental mode of the cavity at the MOT location is $w_{\text{cav}} \approx 500$ μm . To add gain to our system, we use either one or two counterpropagating pump beams, denoted F (forward) and B (backward), produced from the same laser with a waist $w_{\text{pump}} = 2.6$ mm, with linear parallel polarizations and a total available power of $P = 80$ mW, corresponding to a maximum pump intensity of $I = 2P/(\pi w_{\text{pump}}^2) \approx 750$ mW/cm². The pump is tuned near the $F = 3 \rightarrow F' = 4$ cycling transition of the $D2$ line of ^{85}Rb (frequency ω_A , wavelength $\lambda = 780$ nm, natural linewidth $\Gamma/2\pi = 5.9$ MHz), with an adjustable detuning $\Delta = \omega_{F,B} - \omega_A$ and has an incident angle of $\approx 20^\circ$ with the cavity axis. An additional beam P is used as a local oscillator to monitor the spectrum of the laser or as a weak probe to measure single-pass gain (insets of Figs. 2–4) with a propagation axis making an angle with the cavity axis smaller than 10° . Its frequency ω_P can be swept around the pump frequency with a detuning $\delta = \omega_P - \omega_{F,B}$. Both lasers, pump and probe, are obtained by injection-locking of a common master laser, which allows one to resolve narrow spectral features. In our experiments, we load a MOT for 29 ms, and then switch off the trapping beams and magnetic field gradient during 1 ms, when lasing or pump-probe spectroscopy are performed. In order to avoid optical pumping into the dark hyperfine $F = 2$ ground state, a repumping laser is kept on all the time. Data acquisitions are the result of an average of typically 1000 cycles.

As in a conventional laser, lasing occurs if gain exceeds losses in the cavity, which can be observed as strong directional light emission from the cavity. As we will

TABLE I. Different regimes of cold-atom laser versus pump detuning. The polarization of the lasers are either parallel (\parallel) or orthogonal (\perp) to the polarization of the pump beams.

Pump beam(s)	$\Delta < -4\Gamma$	$-4\Gamma < \Delta < +4\Gamma$	$\Delta > +4\Gamma$
F	Raman (\perp)	Mollow (\parallel)	Raman (\perp)
$F + B$	FWM (\perp)	Mollow (\parallel)	FWM (\parallel)

discuss in detail below, we are able to produce lasing with cold atoms as gain medium using three different gain mechanisms: Mollow gain, Raman gain, and four-wave mixing. We can control the different mechanisms by the pump geometry and the pump detuning Δ (see Table I). Mollow and Raman gain mechanisms only require a single pump beam (F), whereas FWM only occurs when both pump beams F and B are present and carefully aligned. With a single pump beam, we find Mollow gain to be dominating close to the atomic resonance, whereas Raman gain is more important for detunings larger than $|\Delta| \approx 4\Gamma$. Furthermore, the different gain mechanisms lead to distinct polarizations. Mollow gain generates a lasing mode with a polarization parallel to the pump polarization because the Mollow amplification is maximum for a field aligned with the driven atomic dipole [8]. On the contrary, different polarizations between the pumping and the amplified waves are necessary to induce a Raman transition between two Zeeman substates: the polarization of the Raman laser is thus orthogonal to the pump polarization. Lastly, the FWM laser has a more complex polarization behavior, as it is orthogonal for red-detuned and parallel for blue-detuned pumps. We have checked that for any pump detuning or probe power, the weak-probe FWM reflectivity is stronger for orthogonal probe polarization, as expected from previous experiments and models [14]. We speculate that pump-induced mechanical effects [15] or more complex collective coupling between the atoms and the cavity [16] might be the origin of this polarization behavior.

In Fig. 1 we show spatial (transverse) patterns of these lasers, observed by imaging the beam onto a CCD camera. Without any spatial filtering in the cavity, the different lasers (Mollow, Raman, and FWM) yield distinct transverse patterns. In Fig. 1(b) [Fig. 1(c)] we show the transverse pattern obtained with a Mollow (Raman) laser. We note that the Mollow laser typically produces transverse

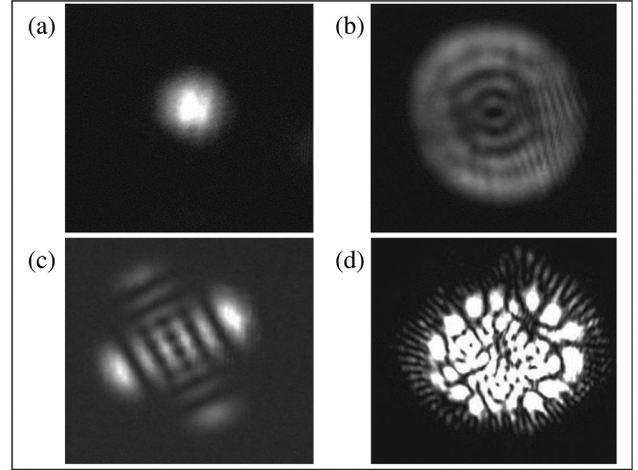


FIG. 1. Transverse modes of cold-atom lasers. (a) Gaussian TEM_{00} mode, obtained by inserting a small diaphragm in the cavity. Typical modes of (b) the Mollow laser, (c) the Raman laser, and (d) the four-wave mixing laser.

patterns with radial symmetries well described by Laguerre-Gauss modes, whereas the modes of the Raman laser are rather Hermite-Gauss modes. The origin of such radial or Cartesian symmetry may arise from the different polarization of those two lasers: the radial symmetry is preserved for the Mollow laser polarization and is broken for the Raman laser one, probably due to slightly different losses in the cavity. Figure 1(d) shows the transverse pattern of the FWM laser. As phase conjugation mechanisms are at work in such a laser, any transverse mode can easily cross the lasing threshold and complex lasing patterns are produced [17].

We now turn to a more detailed description of the gain mechanisms of the different lasers. The quantitative understanding of their behavior needs to take into account effects such as pump geometry and parameters (intensity, detuning), gain spectra, gain saturation, and mechanical effects induced by the pump beam(s).

Let us first discuss the Mollow laser. Amplification of a weak probe beam can happen when a two-level atom is excited by one strong pump beam [8,9]. The corresponding single-pass gain is $g_M = \exp[-b_0 f_M(\Omega, \Delta, \delta)]$, where b_0 is the on-resonance optical thickness (without pump) of the cold-atom cloud. The expression of $f_M(\Omega, \Delta, \delta)$ can be obtained from optical Bloch equations [8]:

$$f_M(\Omega, \Delta, \delta) = \frac{\Gamma}{2} \frac{|z|^2}{|z|^2 + \Omega^2/2} \operatorname{Re} \left[\frac{(\Gamma + i\delta)(z + i\delta) - i\Omega^2 \delta / (2z)}{(\Gamma + i\delta)(z + i\delta)(z^* + i\delta) + \Omega^2(\Gamma/2 + i\delta)} \right], \quad (1)$$

where $z = \Gamma/2 - i\Delta$ and Ω is the Rabi frequency of the atom-pump coupling, related to the pump intensity I by $\Omega^2 = \mathcal{C}^2 \Gamma^2 I / (2I_{\text{sat}})$ ($I_{\text{sat}} = 1.6 \text{ mW/cm}^2$ is the saturation intensity and \mathcal{C} is the averaged Clebsch-Gordan coefficient of the $F = 3 \rightarrow F' = 4$ transition for a linear polarization).

In our setup we observe single-pass gain higher than 50%, with a large gain curve (width $> \Gamma$). The shape of the transmission spectrum (inset of Fig. 2) is consistent with Eq. (1). From Eq. (1) we can also predict the maximum gain in respect to the pump parameters Ω, Δ . We observe

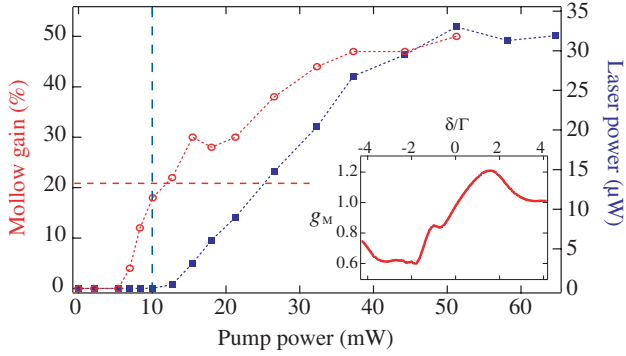


FIG. 2 (color online). Laser power (squares) and Mollow gain (open circles) versus pump power, with $b_0 = 11$ and $\Delta = +\Gamma$. Lasing threshold (vertical dashed line) is expected to appear with a gain of about 21% (horizontal dashed line), in good agreement with the experimental data. Inset: Typical weak-probe transmission spectrum.

good agreement between the behavior of the laser power and the function f_M when varying Δ : the maximum gain and laser power are achieved for $|\Delta| \sim 2\Gamma$ (the exact value depends on Ω) and $\Delta = 0$ is a local minimum. However, we measured a lower maximum gain than predicted by Eq. (1). This is due to gain-saturation induced by rescattering of spontaneous emission inside the atomic cloud [18].

As shown in Fig. 2 (squares), we observe a Mollow laser emission with an output intensity reaching $35 \mu\text{W}$. Taking into account the round trip losses \mathcal{L} , the condition for laser oscillation is $g_M^2(1 - \mathcal{L}) > 1$. This corresponds to a gain at threshold of $g_M = 1.21$ (horizontal line in Fig. 2), in good agreement with the observation.

When the pump frequency is detuned farther away from the atomic resonance, Raman gain becomes dominant. Raman gain relies on the pump-induced population inversion among the different light-shifted m_F Zeeman sublevels of the $F = 3$ hyperfine level [10,19]. Single-pass Raman gain of a weak probe can be written $g_R = e^{-b_0 f_R(\Omega, \Delta, \delta)}$. For $|\Delta| \gg \Gamma$, $f_R(\Omega, \Delta, \delta)$ is given by

$$f_R = -\frac{\Omega^2}{\Delta^2} \left(\frac{A_1}{(\delta + \delta_R)^2 + \gamma^2/4} - \frac{A_2}{(\delta - \delta_R)^2 + \gamma^2/4} \right), \quad (2)$$

where $A_{1,2}$ are the respective weights of the amplification and absorption, δ_R is the frequency difference between the Zeeman sublevels, and γ is the width of the Raman resonance [19]. We have observed the laser spectrum with a beat-note experiment, and we have checked that its frequency corresponds to the maximum gain and is related to the differential pump-induced light shift δ_R of the different Zeeman sublevels. The width of the Raman resonance γ is related to the elastic scattering rate of the pump photons and is much lower than Γ , due to the strong detuning Δ . The result is thus a much narrower gain spectrum than in the previous case (inset of Fig. 3). This leads to an im-

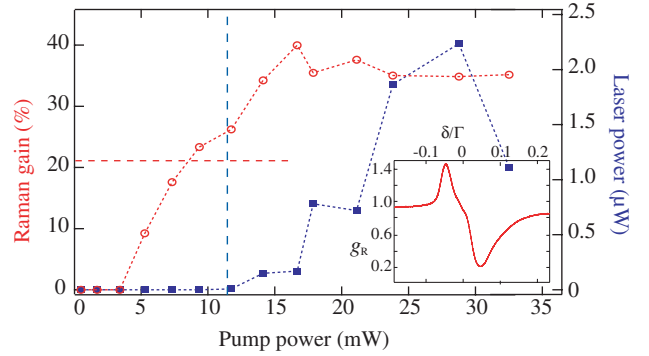


FIG. 3 (color online). Laser power (squares) and Raman gain (open circles) versus pump power, with $b_0 = 10$ and $\Delta = -7\Gamma$. Lasing threshold (vertical dashed line) is expected to appear with a gain of about 21% (horizontal dashed line), in good agreement with the experimental data. Inset: Typical weak-probe transmission spectrum.

portant practical limitation of the single-pumped Raman laser: atoms are pushed by the pump beam, acquiring a velocity v , and the subsequent Doppler shift becomes quickly larger than the width of the gain spectrum. As a consequence, the gain in the cold-atom cloud is no longer the same for a wave copropagating with the pump beam (F) and the wave running in the counterpropagating direction. For the copropagating direction, the relative Doppler shift is negligible, whereas for the counterpropagating wave, a Doppler shift of $\sim 2\omega_A v/c$, larger than the width of the gain spectrum, leads to a suppression of the corresponding gain. As a consequence, emission of our Raman laser stops after $\approx 20 \mu\text{s}$ [20].

In Fig. 3 we plot the output power of the Raman laser as a function of pump power. A comparison with the single-pass gain g_R is again in good agreement for the threshold condition $g_R^2(1 - \mathcal{L}) > 1$: for Raman gain above 21% laser emission occurs. As shown in Fig. 3 (squares), the output power of the Raman laser emission ($\approx 2 \mu\text{W}$) is much lower than the Mollow laser one. This lower output power might arise from a lower saturation intensity for Raman gain [21]. Nevertheless, with a weak signal, the Raman gain can be as high as $g_R = 2$ [21].

We have observed another lasing mechanism when a balanced pumping scheme using two counterpropagating pump beams F and B is used. In this configuration FWM appears [12,13]. The creation of photons in a reflected wave, resulting from a phase conjugation process, can also be considered as a gain mechanism. This is reminiscent of optical parametric oscillation where signal and idler photons are created under a phase matching condition. In the inset of Fig. 4 we show the FWM signal R_c (expressed as the reflection normalized to the incident probe power) illustrating the narrow spectrum of this phase conjugation signal. As expected, the maximum gain corresponds to the degenerate case $\delta = 0$ [14]. Thanks to constructive interference between transmitted and reflected waves, this

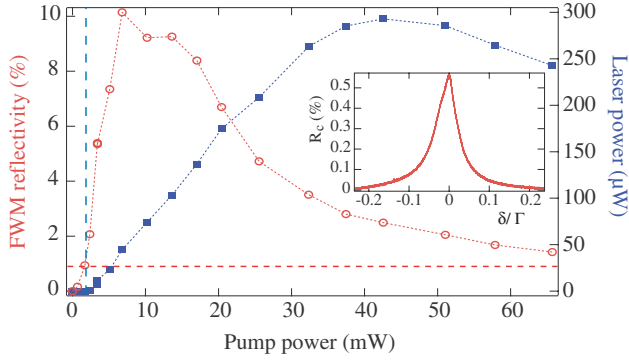


FIG. 4 (color online). Laser power (squares) and phase-conjugate reflectivity due to four-wave mixing (open circles) versus pump power, with $b_0 = 10$ and $\Delta = -8\Gamma$. Lasing threshold (vertical dashed line) is expected for a reflectivity around 1% (horizontal dashed line), in good agreement with the experimental data. Inset: Example of a weak-probe reflectivity spectrum.

mechanism produces huge double-pass gain with cold atoms [21] and it is thus an efficient mechanism to trigger laser oscillations [22]. Because of these interference effects, the threshold for laser oscillation is very different from the previous cases [21,22], and is given by

$$R_c > [(1 - \sqrt{\tilde{R}})/(1 + \sqrt{\tilde{R}})]^2 = 0.9\%, \quad (3)$$

where $\tilde{R} = 1 - \mathcal{L}$. This criterion (horizontal line in Fig. 4) is well respected for the threshold of our laser. The output power of this laser is quite strong (300 μW), with an energy conversion efficiency of 0.75% in this case. As two pump beams are used in this situation, the mechanical effects based on radiation pressure will be negligible and lasing can be sustained for a long time. However, dipole forces can induce atomic bunching and change the effective pump intensity interacting with the atoms [15].

In conclusion, we presented in this Letter three types of laser using a sample of cold atoms as gain medium. Three different gain mechanisms were demonstrated as being efficient enough to allow lasing, even with a low-finesse cavity. Comparison between Mollow and Raman laser shows that the latter has a significantly lower power, although their gain are of the same order of magnitude. These two mechanisms can produce high gain at frequencies slightly detuned from the pump, allowing one to distinguish between stimulated photons from the laser mode and scattered photons from the pump beam. Thus, they seem to be good candidates for the search of random lasing in cold atoms, and the combination of these gains with multiple scattering will be the subject of further investigations. In addition, the ability to continuously tune from a Mollow to a Raman laser (by changing the pump detuning) may allow one to study the transformation of transverse patterns from Laguerre-Gauss to Hermite-

Gauss modes [23]. The FWM laser is the most efficient in terms of power, and it should be possible to study its noise spectrum down to the shot noise level. This laser has many analogies to an optical parametric oscillator and seems to be a good candidate to explore nonclassical features of light, such as the production of twin beams [24,25]. Lastly, the coupling between the cavity mode and the atomic internal and external degrees of freedom may also reveal interesting dynamics, especially if a high-finesse cavity is used [16,26,27].

The authors thank G.-L. Gattobigio for his help at the early stages of the experiment. This work is supported by INTERCAN, DGA, and ANR-06-BLAN-0096.

*Robin.Kaiser@inln.cnrs.fr

- [1] V. S. Letokhov, Sov. Phys. JETP **26**, 835 (1968).
- [2] D. S. Wiersma, Nature Phys. **4**, 359 (2008).
- [3] G. Labeyrie *et al.*, Phys. Rev. Lett. **83**, 5266 (1999).
- [4] G. Labeyrie *et al.*, Phys. Rev. Lett. **91**, 223904 (2003).
- [5] T. Wang *et al.*, Phys. Rev. A **75**, 033802 (2007); J. O. Day, E. Brekke, and T. G. Walker, Phys. Rev. A **77**, 052712 (2008).
- [6] M. S. Malcuit *et al.*, Phys. Rev. Lett. **59**, 1189 (1987).
- [7] R. E. Slusher *et al.*, Phys. Rev. Lett. **55**, 2409 (1985).
- [8] B. R. Mollow, Phys. Rev. A **5**, 2217 (1972).
- [9] F. Y. Wu *et al.*, Phys. Rev. Lett. **38**, 1077 (1977).
- [10] D. Grison *et al.*, Europhys. Lett. **15**, 149 (1991); J. W. R. Tabosa *et al.*, Phys. Rev. Lett. **66**, 3245 (1991).
- [11] L. Hilico, C. Fabre, and E. Giacobino, Europhys. Lett. **18**, 685 (1992).
- [12] A. Yariv and D. M. Pepper, Opt. Lett. **1**, 16 (1977).
- [13] R. L. Abrams and R. C. Lind, Opt. Lett. **2**, 94 (1978); **3**, 205 (1978).
- [14] A. Lezama, G. C. Cardoso, and J. W. R. Tabosa, Phys. Rev. A **63**, 013805 (2000).
- [15] G.-L. Gattobigio *et al.*, Phys. Rev. A **74**, 043407 (2006).
- [16] D. Nagy *et al.*, Europhys. Lett. **74**, 254 (2006).
- [17] R. C. Lind and D. G. Steel, Opt. Lett. **6**, 554 (1981).
- [18] L. Khaykovich, N. Friedman, and N. Davidson, Eur. Phys. J. D **7**, 467 (1999).
- [19] T. M. Brzozowski *et al.*, Phys. Rev. A **71**, 013401 (2005).
- [20] At time scale larger than 100 μs , the single-pumped Mollow laser suffers also from mechanical effects of the pump.
- [21] F. Michaud *et al.*, J. Opt. Soc. Am. B **24**, A40 (2007).
- [22] M. Pinard, D. Grandclement, and G. Grynberg, Europhys. Lett. **2**, 755 (1986).
- [23] E. G. Abramochkin and V. G. Volostnikov, J. Opt. A Pure Appl. Opt. **6**, S157 (2004).
- [24] M. Vallet, M. Pinard, and G. Grynberg, Europhys. Lett. **11**, 739 (1990).
- [25] C. F. McCormick *et al.*, Opt. Lett. **32**, 178 (2007).
- [26] D. Kruse *et al.*, Phys. Rev. Lett. **91**, 183601 (2003).
- [27] R. Miller *et al.*, J. Phys. B **38**, S551 (2005).

Concluding remarks

The fact that the combination of gain and a cavity leads to lasing is of course not a surprise¹. The interesting point of this experiment is that several gain mechanisms are possible and that *the system chooses itself* which one works, depending on the parameters. For instance, we didn't expect Mollow gain, and it appeared by itself in some range of parameters.

It was actually a very exciting experiment, as we detected light emitted from the cavity in real time (no need for long integration time), measured its spectrum via a beat note, also almost in real time, and tried to understand what happened as we varied the parameters. Some features observed in the spectra and some polarization properties have never been understood. Some properties of the dynamics of these lasers have been reported in [Guerin 2010], along with a modeling of the Mollow laser performed by the team of Sergey Skipetrov.

Since then, several groups have produced and studied lasers using cold atoms as the gain medium [Vrijssen 2011, Bohnet 2012, Norcia 2016, Sawant 2017, Megyeri 2018, Gothe 2019].

¹ We are grateful to the referees. As an anecdote, this paper produced the most discordant reviews that I've ever seen. Referee A nicely wrote "*It is a fascinating study*", "*very well written*", "*results in a small masterpiece of text*", "*here lies the beauty of fundamental research*"..., whereas Referee B meanly wrote "*not well documented*", "*filled with rather cursory descriptions and general ideas*", "*needs to be more clearly written*", "*numerous speculative statements without solid justification*", "*the experiments seem unfinished*"... Both of them were exaggerating a lot! Fortunately, the third consulted referee agreed with Referee A. Since then, the paper has been correctly cited, and thus probably deserved its publication in a good journal.

CHAPTER III

Distributed feedback laser with cold atoms

This chapter deals with the experiments performed in Tübingen, which led to mirrorless optical parametric oscillation based on distributed feedback. The first section is thus on the distributed feedback aspect, based on a 1D elongated Bragg grating, and the second section on what happens when we add gain.

III.1. Photonic band gaps in 1D lattices

Optical lattices based on far-detuned dipole traps are nowadays standard tools in cold-atom labs. In the early days of optical lattices, people also used dissipative lattices with near-resonant lasers [Grynberg 2001] (they are still used for laser cooling of course). As early as 1995, a very interesting paper noticed that the atoms trapped in the lattice, with a periodicity of $\lambda/2$, should create a Bragg mirror that opposes to the propagation of the lattice beams themselves. To solve this apparent paradox one needs to carefully take into account the refractive index of the atoms and the precise detuning of the lattice. This led to the first prediction of photonic band gaps in cold atoms [Deutsch 1995].

These band gaps have never been observed. Indeed, with near-resonance lattice beams, many side effects may prevent such an observation. First, the dissipative nature of the lattice induces heating or cooling of the sample. Second, adding a third weak beam to probe the band gap would inevitably create four-wave mixing with the creation of a phase-conjugated beam, which would be hard to distinguish from the reflection due to the band gap. And third, the probe beam would need to be collinear with the lattice beam, and at the same wavelength, which would make its detection problematic.

Instead, it is much easier to detune the dipole beams (wavelength $\lambda_{\text{dip}} > \lambda_{\text{at}}$) and work in a conservative lattice. The periodicity of the lattice is then $\lambda_{\text{dip}}/2$, while the refractive index of the atomic sample is not negligible only close to λ_{at} . The Bragg condition can be recovered by using a small angle θ between the probe beam and the lattice axis, with

$$\cos \theta = \frac{\lambda_{\text{at}}}{\lambda_{\text{dip}}}. \quad (\text{III.1})$$

Actually, the precise Bragg condition is a bit more complicated, as one needs to take into account the atomic refractive index, which depends on the detuning of the probe beam, as detailed in the following paper.

In principle, the lattice wavelength can be largely detuned, but then the Bragg angle increases. The sample, which is very elongated since it is trapped in a 1D lattice, is then probed with an incidence that decreases the effective optical thickness of the medium. This is detrimental

because we deal with a dilute sample: the refractive index contrast is very low (on the order of 10^{-3}), which has to be compensated by a very large number of atomic layers. This problem of probing angle was the main identified limitation of the previous attempts of the Tübingen group [Slama 2006], which we overcame by building a dedicated experiment with the appropriate optical access (see [Schilke 2013] for details of the experimental setup).

We performed two experiments about these photonic band gaps. The first one only uses the atoms as two-level systems, while the second one uses electromagnetically-induced transparency (EIT). They are described in the two subsections below with the reproduction of the corresponding articles. The second paper also includes more details on the experiments and on the simulation procedure based on transfer matrices.

III.1.1. Photonic band gaps with two-level atoms

In this first experiment we achieved a Bragg reflection of about 80% and provided a detailed analysis of the reflection spectrum, whose qualitative feature can be well understood by the detailed Bragg condition and the necessary trade-off between the refractive index and the scattering losses. We also related the reflection coefficient to the local density of states inside the medium. The article [Schilke 2011] is reproduced below.

Photonic Band Gaps in One-Dimensionally Ordered Cold Atomic Vapors

Alexander Schilke,¹ Claus Zimmermann,¹ Philippe W. Courteille,² and William Guerin^{1,*}

¹Physikalisches Institut, Eberhard-Karls-Universität Tübingen, Auf der Morgenstelle 14, D-72076 Tübingen, Germany

²Institut de Física de São Carlos, Universidade de São Paulo, 13560-970 São Carlos, SP, Brazil

(Received 18 January 2011; revised manuscript received 4 April 2011; published 3 June 2011)

We experimentally investigate the Bragg reflection of light at one-dimensionally ordered atomic structures by using cold atoms trapped in a laser standing wave. By a fine-tuning of the periodicity, we reach the regime of multiple reflection due to the refractive index contrast between layers, yielding an unprecedented high reflectance efficiency of 80%. This result is explained by the occurrence of a photonic band gap in such systems, in accordance with previous predictions.

DOI: 10.1103/PhysRevLett.106.223903

PACS numbers: 42.70.Qs, 37.10.Jk, 42.25.Fx

Cold atomic vapors can be used as suitable optical media for a number of applications or fundamental studies, in particular, in the fields of nonlinear and quantum optics, but also as complex optical media to study exotic wave transport phenomena, for instance coherent multiple scattering [1], weak localization [2] or random lasing [3]. In these examples, an essential property is the *disorder* inherent to atomic vapors that are simply confined in a magneto-optical trap (MOT).

On the contrary, *ordered* clouds of cold atoms should exhibit different light-transport properties. The appearance of photonic band gaps (PBGs) has indeed been predicted in one-dimensional lattices [4,5] and recently in three-dimensional, diamond (non-Bravais) lattices [6]. The realization of PBGs in cold-atom samples would open the way to study new regimes of light transport in atomic vapors, where correlations and long-range order play a dominant role. The crossover regime, between order and disorder, or correlated disorder, is also a rich subject (see, e.g., [7]), in particular, in relation to Anderson localization [8].

However, creating efficient photonic structures is hard with cold atoms because these dilute systems have a low refractive index [Fig. 1(a)] and a limited length. So far, efficient Bragg reflection of light has only been obtained with hot vapors, using an electromagnetically induced grating [9]. Previous investigations with cold atoms trapped in optical lattices have reported Bragg scattering with low efficiency. A first series of experiments used three-dimensional quiresonant lattices [10–12], with a lattice geometry that does not create PBGs [6]. Efficiencies below 1% were reported. A second series of experiments investigated the 1D case [13–15], where a band gap is expected, but the maximum reflectance was only 5% in total power (30% corrected from the partial overlap between the probe beam and the atomic sample) [15]. The limitations came mainly from the probing angle, which limited the interaction length with the lattice, and losses, i.e., out-of-axis scattering, due to the imaginary part of the atomic polarizability near resonance.

In this Letter, we report the observation of an efficient Bragg reflection at a one-dimensional lattice, reaching the regime of multiple reflections due to the refractive index contrast between layers and an 80% efficiency in total power. This high efficiency is obtained by (1) using a small-diameter probe beam and a small probing angle to optimize the overlap with the atomic grating, and (2) adjusting the periodicity of the lattice so that the Bragg condition is fulfilled off the atomic resonance, thus strongly reducing the losses. Our experimental observations are explained by the appearance of a PBG, which we show to be robust against the system imperfections (finite length, varying density).

The experiment starts with a vapor-loaded MOT of ⁸⁷Rb containing about 6×10^8 atoms. A dipole trap is generated by a homemade titanium-sapphire laser, whose available power is 1.3 W and whose wavelength λ_{dip} is tunable. The beam is focussed on a waist ($1/e^2$ radius) $w_{\text{dip}} = 220 \mu\text{m}$ at the MOT position (Rayleigh length $z_R \approx 0.2 \text{ m}$). A 1D optical lattice is made by retroreflecting the beam, thus generating a structure whose periodicity is $\lambda_{\text{dip}}/2$.

After stages of compression and molasses, the MOT is switched off and a waiting time of a few ms allows the untrapped atoms to fall down. Then, we can characterize the trapped sample with absorption imaging or acquire transmission and reflection spectra. Typical numbers for the trapped atoms are $N = 5 \times 10^7$ atoms distributed over a length $L \sim 3 \text{ mm}$ (~ 7700 layers). The temperature, $T \sim 100 \mu\text{K}$, is related to the potential depth U_0 by a constant factor $\eta = U_0/k_B T \sim 3.5$. The transverse extension of the cloud is then $\sigma_{\perp} = w_{\text{dip}}/(2\sqrt{\eta}) \approx 60 \mu\text{m}$ and the thickness of each layer along the lattice axis z is $\sigma_z = \lambda_{\text{dip}}/(2\pi\sqrt{2\eta}) \approx 47 \text{ nm}$ (rms radii in the harmonic approximation).

To acquire spectra, we shine a weak and small (waist $w_0 = 35 \mu\text{m}$), linearly polarized probe beam onto the lattice under an angle of incidence $\theta \approx 2^\circ$. The angle is small enough so that the probe interacts with the lattice over its entire length and that the reflection is specular [14]. The transmitted and reflected beams are then recorded with

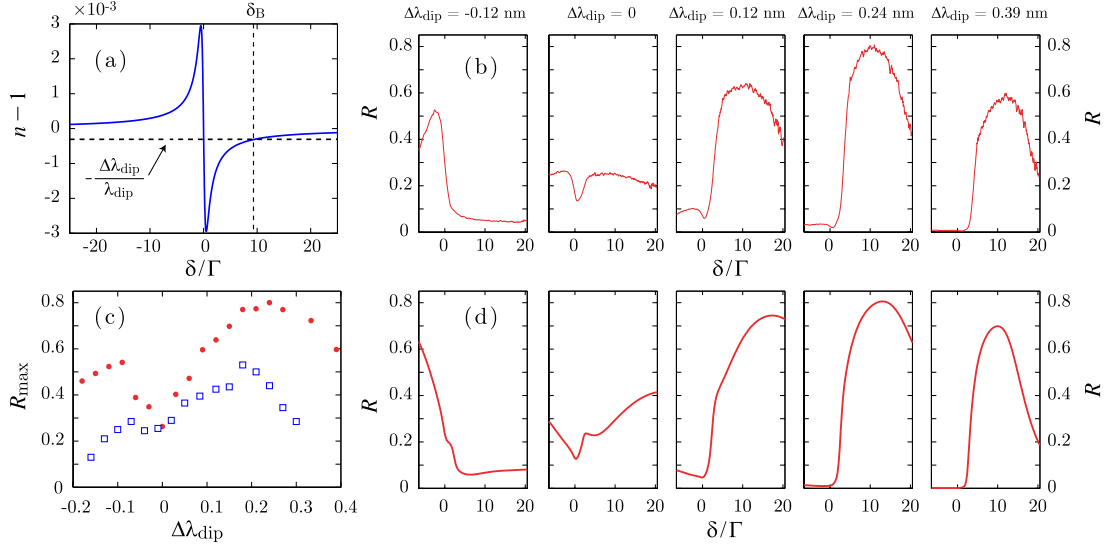


FIG. 1 (color online). (a) Refractive index n as a function of the normalized detuning δ/Γ for an averaged density $\rho = 7 \times 10^{11} \text{ cm}^{-3}$. The dashed lines represent the Bragg condition Eq. (1) with $\Delta\lambda_{\text{dip}} = 0.24 \text{ nm}$. (b) Experimental reflection spectra for different $\Delta\lambda_{\text{dip}}$. (c) Measured maximal reflectance as a function of $\Delta\lambda_{\text{dip}}$ for two different atom numbers, $N = 2 \times 10^7$ (squares) and $N = 6 \times 10^7$ (dots). The spectra of (b) are taken from the latter. (d) Simulated reflection spectra.

avalanche photodiodes. The probe frequency ω is swept in the vicinity of the atomic resonance ω_0 ($F = 2 \rightarrow F' = 3$ closed transition of the $D2$ line, $\lambda_0 = 780.24 \text{ nm}$, linewidth $\Gamma/2\pi = 6.1 \text{ MHz}$) by using an acousto-optical modulator in double-pass configuration. The other hyperfine levels are far enough to be negligible. The presented data are the result of an average of typically 100 cycles (the duration of each cycle is $\sim 1 \text{ s}$).

Reflection occurs in the vicinity of a Bragg condition: the difference between the incident probe wave vector and the reflected wave vector must equal the lattice vector, i.e. $2n(\delta)k_0 \cos\theta = K_{\text{lat}}$, where $k_0 = 2\pi/\lambda_0$ is the probe wave vector in vacuum, n is the real part of the average refractive index of the medium, $\delta = \omega - \omega_0$ is the probe detuning from the atomic resonance, and $K_{\text{lat}} = 4\pi/\lambda_{\text{dip}}$ is the lattice vector [16].

Experimentally, we keep the angle constant and adjust the Bragg condition by tuning the wavelength of the lattice beam. It is thus meaningful to rewrite the Bragg condition in the following form,

$$n(\delta) - 1 = -\frac{\Delta\lambda_{\text{dip}}}{\lambda_{\text{dip}}}, \quad (1)$$

where $\Delta\lambda_{\text{dip}} = \lambda_{\text{dip}} - \lambda_{\text{dip}0}$ is the shift from the “geometric” (with $n = 1$) Bragg condition $\lambda_{\text{dip}0} = \lambda_0/\cos\theta$. With $\theta = 2^\circ$, $\lambda_{\text{dip}0} \approx 780.7 \text{ nm}$. Then, for a given lattice wavelength, the Bragg condition is fulfilled for probe detunings δ given by Eq. (1), see Fig. 1(a). There are in general two such frequencies, but one is almost on resonance, where losses prevent any efficient reflection. The other Bragg frequency [δ_B in Fig. 1(a)] may be farther from resonance and can be tuned in order to search for an optimum.

Such an experiment is reported in Fig. 1(b), which shows a set of spectra for different $\Delta\lambda_{\text{dip}}$. As expected from

Eq. (1), the spectra display a strong asymmetry, which evolves as the lattice wavelength is changed, the maximal efficiency going from one side of the resonance to the other side while $\Delta\lambda_{\text{dip}}$ changes its sign. One can also clearly observe an optimum value of $\Delta\lambda_{\text{dip}}$ for reaching high efficiencies, namely $R_{\text{max}} \approx 80\%$ for $\Delta\lambda_{\text{dip}} \approx 0.24 \text{ nm}$ with our best atom number [Fig. 1(c)]. Note that for each $\Delta\lambda_{\text{dip}}$, we adjust the power accordingly to keep constant the potential depth and subsequently the atom number and temperature.

The existence of an optimum can easily be understood by considering the limiting cases. When $\Delta\lambda_{\text{dip}}$ is very small, the Bragg condition is fulfilled where the refractive index is almost one, in virtue of Eq. (1), very far from resonance, leading to a very small index contrast in the periodic structure and thus to an inefficient reflection. In the opposite limit, when $\Delta\lambda_{\text{dip}}$ is large, the Bragg condition is fulfilled near $\delta = \pm\Gamma/2$, where losses, due to the imaginary part of the atomic polarizability, are large and play a detrimental role. Ultimately, if $\Delta\lambda_{\text{dip}}$ is too large for the given averaged atomic density ρ , the Bragg condition cannot be fulfilled at all. The optimum $\Delta\lambda_{\text{dip}}$ depends on the average density ρ : a larger density allows us to increase $\Delta\lambda_{\text{dip}}$, and thus the index contrast, without shifting the Bragg frequency towards resonance, i.e., without increasing losses. This is illustrated in Fig. 1(c), which shows that the optimum $\Delta\lambda_{\text{dip}}$ is larger with more atoms.

We have also studied the reflection spectrum as a function of the atom number for a given $\Delta\lambda_{\text{dip}}$. In order to vary the atom number while keeping the lattice length constant, we have changed the waiting time in the lattice, before the spectra acquisition, from 5 ms to 400 ms, thus varying atom losses. The result is reported in Fig. 2. As expected

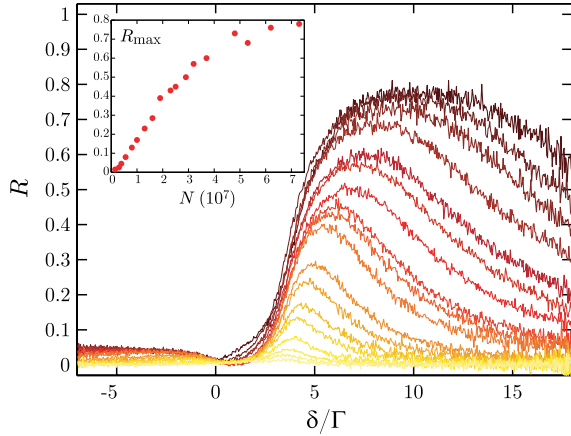


FIG. 2 (color online). Spectra for different atom numbers N in the lattice (constant length, varying density) with $\Delta\lambda_{\text{dip}} = 0.15$ nm. Inset: Maximum reflectance as a function of N .

from Eq. (1), we observe a shift farther from resonance together with a broadening for increasing densities. The evolution of the maximum reflectance as a function of the atom number (inset of Fig. 2) reveals that we almost reach saturation.

With such a high efficiency, it is natural to ask whether a photonic band gap occurs in our system and is responsible for the high reflectance. It is well-known that periodic 1D systems give rise to PBGs for any nonzero index modulation [17], so that no distinction is usually made between a 1D PBG and a Bragg reflector. However this is true only for infinite, lossless, and perfectly periodic media. As already noted, the atomic polarizability is complex so that our system has losses, and it is of course finite. Moreover, the lattice is not perfectly homogeneous but has a smooth density variation, so that the periodicity is not perfect. The situation is thus more intricate and deserves a careful analysis.

We can get a first insight with orders-of-magnitude estimations. A Bragg reflector made of repeated pairs of dielectric layers gives rise, in the stop band, to an evanescent wave whose penetration length (or Bragg length) is given by $L_{\text{ew}} = \lambda_0/(4\Delta n)$, where Δn is the refractive index difference between the two materials [18]. By approximating the Gaussian atomic distribution in each well by a single layer of constant density with the same rms width and using Eq. (1), the index contrast is $\Delta n = \pi\sqrt{\eta/6} \times \Delta\lambda_{\text{dip}}/\lambda_{\text{dip}}$. In our experiment, the maximum reflection is obtained for $\Delta\lambda_{\text{dip}} \sim 0.24$ nm and we have $\eta \sim 3.5$, which gives a penetration length $L_{\text{ew}} \sim 0.26$ mm, sensibly smaller than our optical lattice ($L \sim 3$ mm), so that we are indeed in the multiple-reflection regime. The effect of losses can also be evaluated by comparing the corresponding attenuation length L_{loss} to L_{ew} . Given our estimated averaged density $\rho \sim 7 \times 10^{11} \text{ cm}^{-3}$ and the detuning δ_B determined by the Bragg condition (1), we estimate $L_{\text{loss}} = 1/\rho\sigma_{\text{sc}}(\delta_B)$,

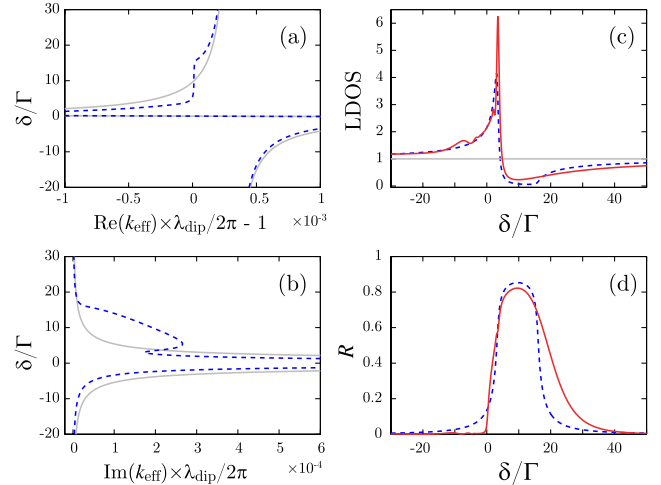


FIG. 3 (color online). Modeling of our system. (a),(b) Real (a) and imaginary (b) parts of the effective wave vector k_{eff} in the medium as a function of the probe detuning δ . The axes are reversed so that the graphs look like standard dispersion relations $\omega(k)$. (c) Normalized local density of states. (d) Reflection spectrum. In all plots, the light gray line corresponds to a homogeneous, nonperiodic medium of the same average density, the dashed line to an infinite lattice and the solid red (medium gray) line simulates the actual density distribution of our system.

where $\sigma_{\text{sc}}(\delta_B)$ is the scattering cross section, which gives $L_{\text{loss}} \sim 3.8$ mm, also much larger than L_{ew} . Thus, this simple calculation confirms that our system fulfills the conditions $L_{\text{ew}} \ll L$, L_{loss} , which are necessary for the appearance of a band gap. A number of effects are however not taken into account, in particular the actual density distribution along the lattice, so that a more precise modeling is still valuable.

We use the transfer matrix formalism to simulate the wave propagation in our system, and we refer to [4,5,15] for detailed descriptions in similar contexts. From the transfer matrix of one single period, which takes into account the Gaussian atomic distribution in each well [15], we draw the dispersion relations of the medium (effective wave vector k_{eff} vs ω), valid in the limit of an infinitely long lattice (Bloch theorem). These are shown in Figs. 3(a) and 3(b), for the typical parameters of the experiment $\rho = 7 \times 10^{11} \text{ cm}^{-3}$, $\eta = 3.5$ and $\Delta\lambda_{\text{dip}} = 0.24$ nm. The imaginary part of k_{eff} is composed of one Lorentzian of width Γ centered on resonance, which corresponds to losses, and a supplementary part, leading to an evanescent wave, corresponding to a band gap [Fig. 3(b)]. In the same frequency range, the real part of k_{eff} has a reduced variation with ω [Fig. 3(a)], corresponding to a reduced density of states (DOS) $\mathcal{D} = d(\text{Re}(k_{\text{eff}}))/d\omega$. This last formula is however not always valid, especially in anomalous dispersive media, and we use the method of [19] to compute the normalized local DOS in the middle of the lattice. By using the complex reflection coefficients r_1 , r_2 of the two surrounding, finite or infinite [4] semilattices, we obtain

$$\mathcal{D} = \text{Re} \left[\frac{2 + r_1 + r_2}{1 - r_1 r_2} - 1 \right]. \quad (2)$$

The result, shown in Fig. 3(c), exhibits clearly the band gap, with a strong reduction of the normalized local DOS, which reaches at minimum 6% for an infinite lattice. The corresponding reflection spectrum reaches 85% [Fig. 3(d)]. In both cases, the limitation (for achieving high reflectance or low DOS) is the remaining losses.

To take into account the limited length of the sample and its actual, smooth density distribution along the lattice axis, that we characterized by absorption imaging, we compute the reflection spectra through the whole structure by multiplying elementary transfer matrices computed with the corresponding local density. The local DOS then exhibits a smaller reduction, reaching at minimum 23%, but the maximum reflectance is almost as high as in the infinite limit, reaching 82% [Fig. 3(c) and 3(d)].

Finally, to simulate our experimental spectra precisely, we must also take into account the trapping-induced inhomogeneous light shift and the finite transverse size. Indeed, we only considered so far infinitely extended layers, which is a crude approximation, the atom cloud having an rms width of 60 μm . The probe beam, having also a finite size, probes a distribution of local density, which induces an inhomogeneous broadening of the spectra. There is in fact a tradeoff for the probe beam size: a small beam allows us to probe a well-defined and maximum density, but since the reflection is very sensitive to the angle of incidence, the probe divergence induces also an inhomogeneous broadening. Experimentally, we have tried several probe sizes and obtained the maximum reflectance with $w_0 = 35 \mu\text{m}$. To simulate these effects we averaged many spectra over Gaussian distributions of incident angles and densities corresponding, respectively, to the probe divergence and atomic density distribution along the transverse directions. We obtain the spectra of Fig. 1(d), in good agreement with the experiment [20].

To summarize, we have studied experimentally the Bragg reflection of light at a one-dimensional atomic quasi-periodic structure in the regime of multiple reflection, demonstrating a high efficiency, thanks to a fine-tuning of the lattice periodicity. Then, motivated by the modeling of our system, we have investigated the effects of the finite length and of the smooth density variation along the lattice on the appearance of a band gap and its quality. These imperfections, inherent to cold-atom systems, do not destroy the band gap which, even if the DOS reduction is not dramatic, still substantially modifies the transport properties of light, as demonstrated by the observed high reflectance.

Improving further the quality of the PBG requires reducing the losses by creating the band gap farther from resonance, which could be done by increasing the density or the lattice length, for example, with a larger initial MOT. Another fascinating possibility is to tailor the atomic polarizability to remove its absorptive part, while enhancing the

refractive index, following the ideas of [21,22]. Finally, the extension to more evolved lattice geometries, for example, with bichromatic lattices [23] and to three dimensions [6], has been proposed recently. This last case is of course the most appealing since a 3D band gap would profoundly modify the atom-light interaction [24,25].

We thank J.-F. Schaff and N. Mercadier for the computer-control program. We acknowledge support from the Alexander von Humboldt foundation, the DFG and the REA (program COSCALI, No. PIRSES-GA-2010-268717).

*william.guerin@pit.uni-tuebingen.de

- [1] G. Labeyrie, *Mod. Phys. Lett. B* **22**, 73 (2008).
- [2] R. Kaiser and M. Havey, *Opt. Photonics News* **16**, 38 (2005).
- [3] L. Froufe-Pérez, W. Guerin, R. Carminati, and R. Kaiser, *Phys. Rev. Lett.* **102**, 173903 (2009); W. Guerin *et al.*, *J. Opt.* **12**, 024002 (2010).
- [4] I. H. Deutsch, R. J. C. Spreeuw, S. L. Rolston, and W. D. Phillips, *Phys. Rev. A* **52**, 1394 (1995).
- [5] M. Artoni, G. La Rocca, and F. Bassani, *Phys. Rev. E* **72**, 046604 (2005).
- [6] M. Antezza and Y. Castin, *Phys. Rev. A* **80**, 013816 (2009).
- [7] M. Pasienski, D. McKay, M. White, and B. DeMarco, *Nature Phys.* **6**, 677 (2010).
- [8] A. Lagendijk, B. van Tiggelen, and D. S. Wiersma, *Phys. Today* **62**, No. 8, 24 (2009); A. Aspect and M. Inguscio, *Phys. Today* **62**, No. 8, 30 (2009).
- [9] M. Bajcsy, A. S. Zibrov, and M. D. Lukin, *Nature (London)* **426**, 638 (2003).
- [10] G. Birkel *et al.*, *Phys. Rev. Lett.* **75**, 2823 (1995).
- [11] M. Weidemüller *et al.*, *Phys. Rev. Lett.* **75**, 4583 (1995).
- [12] M. Weidemüller, A. Görlitz, T. W. Hänsch, and A. Hemmerich, *Phys. Rev. A* **58**, 4647 (1998).
- [13] S. Slama *et al.*, *Phys. Rev. Lett.* **94**, 193901 (2005).
- [14] S. Slama *et al.*, *Phys. Rev. A* **72**, 031402(R) (2005).
- [15] S. Slama *et al.*, *Phys. Rev. A* **73**, 023424 (2006).
- [16] Note that contrary to the original situation considered in [4], the refractive index for the lattice beam is negligible.
- [17] J. D. Joannopoulos *et al.*, *Photonic Crystals: Molding the Flow of Light* (Princeton University, Princeton, NJ, 2008), 2nd ed..
- [18] L. R. Brovelli and U. Keller, *Opt. Commun.* **116**, 343 (1995).
- [19] G. Boedeker and C. Henkel, *Opt. Express* **11**, 1590 (2003).
- [20] The lower efficiency for $\Delta\lambda_{\text{dip}} < 0$ might be due to heating induced by spontaneous emission, the dipole trap being closer to resonance.
- [21] M. O. Scully, *Phys. Rev. Lett.* **67**, 1855 (1991).
- [22] M. Fleischhauer *et al.*, *Phys. Rev. A* **46**, 1468 (1992).
- [23] S. Rist, P. Vignolo, and G. Morigi, *Phys. Rev. A* **79**, 053822 (2009).
- [24] E. Yablonovitch, *Phys. Rev. Lett.* **58**, 2059 (1987).
- [25] P. Lodahl *et al.*, *Nature (London)* **430**, 654 (2004).

The fact that a periodic index modulation in 1D gives rise to a photonic band gap is almost a mathematical theorem, so this is absolutely not surprising. What is often forgotten is that this well-known result is only true for an infinite, lossless, perfectly periodic medium.

In my opinion what is interesting in this work is to discuss and quantify the intrinsic limitations. The main limitations of using cold atoms for 1D photonic band gaps are the low density, which induces a low refractive index contrast between layers and the need for a large number of layers, and the scattering losses near resonance. Note although that scattering is *loss* only because we deal with 1D propagation: light is not absorbed, it is scattered off axis. The situation would be different for a 3D arrangement. Nevertheless, well understanding the 1D case is useful before turning to the 3D case, which is far less obvious, because omnidirectional photonic band gaps only occur for very specific geometries and parameters [Antezza 2009, Yu 2011, Antezza 2013].

III.1.2. Photonic band gaps with EIT

In order to try to overcome some of the above-mentioned limitations, in particular the scattering losses, it is natural to think about playing around with the atomic polarizability. One simple idea is to use EIT. It is quite easy to adapt the numerical model to add EIT as one just needs to change the atomic polarizability (which is still linear with respect to the probe field) in the transfer-matrix model. The results of such a study, which had already been performed by [Petrosyan 2007], show that the EIT response makes a second band gap appear near resonance. However, this band gap is not of better quality than the two-level-atom band gap, i.e. the scattering losses are the same. Indeed, EIT can make the imaginary part of the polarizability completely vanish in principle at a given frequency, but at that same frequency the real part also vanishes. Slightly detuned from this point one recovers some refractive index but also some scattering losses, and the ratio between the two is actually the same as for the two-level atom polarizability.

However, this new band gap is still interesting because it can be tuned by the coupling field. In the following article [Schilke 2012b] we compute and discuss this new band gap using the transfer-matrix model, then we implement EIT and experimentally demonstrate this new band gap, and we finally use it for making a two-port all-optical switch.

Photonic properties of one-dimensionally-ordered cold atomic vapors under conditions of electromagnetically induced transparency

Alexander Schilke, Claus Zimmermann, and William Guerin*

Physikalisches Institut, Eberhard-Karls-Universität Tübingen, Auf der Morgenstelle 14, D-72076 Tübingen, Germany

(Received 12 June 2012; published 6 August 2012)

We experimentally study the photonic properties of a cold-atom sample trapped in a one-dimensional optical lattice under the conditions of electromagnetically induced transparency. We show that such a medium has two photonic band gaps. One of them is in the transparency window and gives rise to a Bragg mirror, which is spectrally very narrow and dynamically tunable. We discuss the advantages and the limitations of this system. As an illustration of a possible application we demonstrate a two-port all-optical switch.

DOI: [10.1103/PhysRevA.86.023809](https://doi.org/10.1103/PhysRevA.86.023809)

PACS number(s): 42.70.Qs, 37.10.Jk, 42.25.Fx, 42.50.Gy

I. INTRODUCTION

Atomic vapors can be used for studying many original or useful optical phenomena. Based on the atomic nonlinearity, one can produce and study bistability [1], squeezing [2], various nonlinear magneto-optical effects [3], all-optical switching [4], gain and lasing [5], and four-wave mixing [6], which allows the production of twin beams [7,8] and optical parametric oscillation [9]. Another useful property is the atomic coherence, that can be used to produce electromagnetically induced transparency (EIT) [10,11], slow or fast light [12,13], and quantum memories [14]. Finally, the large atomic scattering cross section allows studying effects related to multiple scattering of light in disordered media, for example Lévy flights in hot vapors [15], radiation trapping [16,17], and coherent backscattering in cold atoms [18,19]. In the opposite regime, cold atoms can be trapped in an ordered fashion, which gives rise to Bragg scattering [20–22] and photonic band gaps (PBGs), which have been recently observed in the one-dimensional (1D) case [23] and predicted in three dimensions [24,25].

Combining a control over the atomic spatial arrangement (external degrees of freedom) and the atom polarizability (internal degrees of freedom) allows a complex engineering of the propagation properties of light. In this spirit, radiation trapping under condition of EIT has been studied in [26,27], the combination of multiple scattering and gain gives rise to random lasing [28], and it was recently demonstrated that the combination of a 1D PBG with four-wave mixing leads to distributed feedback optical parametric oscillation [29].

In this paper, we experimentally investigate the combination of EIT and a 1D PBG formed by cold atoms trapped in a 1D lattice, like in [23]. As already shown in a theoretical paper by Petrosyan [30], such a system creates a new band gap, in the transparency window, which is spectrally very narrow and which is dynamically tunable. We report measurements of the transmission and reflection spectra and their dependence with experimental parameters, and we discuss the limitations of such a system. We finally demonstrate a two-port all-optical switch as a possible application.

It should be noted that various configurations of electromagnetically induced gratings have already been discussed in

the literature with hot or cold atoms (see [31] for theoretical proposals and [32] for experiments). In all these cases, however, the grating is due to the spatial modulation of the control field. On the contrary, in our experiment, the Bragg mirror relies on the periodic spatial modulation of the atomic density. The controls over the internal and external degrees of freedom are thus decoupled.

The paper is organized as follows. The next section is devoted to the theoretical description of our system. The dispersion relations and expected reflection and transmission spectra are computed for ideal parameters. In the following part, we present our experimental setup. Then, in Sec. IV, we present our measurements. Finally, in Sec. V, we demonstrate the use of our system as an all-optical switch.

II. THEORETICAL DESCRIPTION

We consider three-level atoms, as shown in Fig. 1(a), with two low-energy levels, which we call the ground state $|g\rangle$ and the metastable state $|m\rangle$, and one excited state $|e\rangle$. The atoms are initially in the ground state, and we are interested in the photonic response of the sample at optical frequencies in the vicinity of the transition $|g\rangle \leftrightarrow |e\rangle$ (wavelength λ_0), when the states $|m\rangle$, $|e\rangle$ are coupled by an external field. We thus consider a probe beam with a detuning $\delta = \omega - \omega_{ge}$ from the atomic transition and a coupling beam with a detuning $\Delta = \omega_C - \omega_{me}$. The probe beam has a very low intensity and we consider only the atom's linear response, described by the atomic polarizability [Fig. 1(b)]

$$\alpha = \frac{2|d_{ge}|^2}{\epsilon_0 \hbar \Gamma} \frac{-\Gamma}{2\delta + i\Gamma - \Omega^2/[2(\delta - \Delta + i\gamma)]}, \quad (1)$$

where Γ is the spontaneous emission rate of the excited state, γ the dephasing rate between the two ground states (we suppose $\gamma \ll \Gamma$), $\Omega = |d_{me}|^2 E/\hbar$ is the Rabi frequency of the coupling field of amplitude E , and d_{ij} is the dipole moment of the transition $|i\rangle \leftrightarrow |j\rangle$ [30]. In this equation, EIT is induced by the last term of the denominator [33].

The atoms are trapped in a one-dimensional optical lattice formed by a red-detuned retroreflected laser beam of wavelength λ_{lat} , thus forming an atomic density grating of periodicity $\lambda_{\text{lat}}/2$ [Fig. 1(c)]. The modulation contrast depends on the temperature T of the atomic sample, which is usually related to the trapping depth U_0 of the optical potential by a

*william.guerin@pit.uni-tuebingen.de

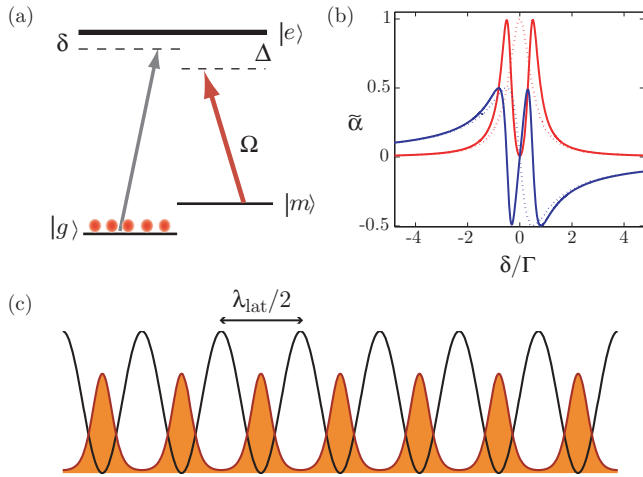


FIG. 1. (Color online) (a) Atomic levels and laser configuration. (b) Real part (blue, bottom curve) and imaginary part (red) of the dimensionless atomic polarizability $\tilde{\alpha} = \alpha \times \varepsilon_0 \hbar \Gamma / 2 |d_{ge}|^2$ for a two-level atom (dotted lines) and with EIT (solid lines), with $\Delta = 0$ and $\Omega = \Gamma$ [Eq. (1)]. (c) Scheme of the system under consideration: the atoms are trapped in a 1D optical lattice of periodicity $\lambda_{\text{lat}}/2$.

constant factor $\eta = U_0/k_B T$. We will take $\eta = 3.5$, the value observed in our experiment [23]. The density distribution of each period is then a Gaussian of rms width along the lattice axis z $\sigma_z = \lambda_{\text{lat}}/(2\pi\sqrt{2\eta})$.

Since the laser forming the lattice must have a wavelength $\lambda_{\text{lat}} > \lambda_0$ to create a dipole trap, the Bragg condition can only be fulfilled with a nonzero propagation angle θ between the probe and the lattice beams, such that $\cos\theta \sim \lambda_0/\lambda_{\text{lat}}$. In practice, it is easier in experiments to tune the lattice wavelength to adjust the Bragg condition. We can thus define $\Delta\lambda_{\text{lat}} = \lambda_{\text{lat}} - \lambda_{\text{lat}0}$ as the shift from the “geometric” Bragg condition $\lambda_{\text{lat}0} = \lambda_0/\cos\theta$. The complete Bragg condition must take into account the fact that the probe wavelength in the medium is $\lambda = \lambda_0/n$, where n is the average refractive index, which strongly depends on the probe detuning δ . The Bragg condition can then be rewritten in the simple following form:

$$n(\delta) - 1 = -\frac{\Delta\lambda_{\text{lat}}}{\lambda_{\text{lat}}}, \quad (2)$$

where the right-hand side of the equation depends only on the lattice wavelength and the left-hand side depends on the real part of the atomic polarizability and on the average atomic density ρ , with $n - 1 = \rho/2 \times \text{Re}(\alpha)$ for a dilute vapor. The imaginary part of the atomic polarizability plays also an important role since it is responsible for scattering losses [23].

Considering these losses together with Eq. (2) is sufficient to qualitatively explain the photonic properties of the system (see [23] for the simple case of two-level atoms): a band gap will appear when Eq. (2) is fulfilled at a detuning δ where the imaginary part of the atomic polarizability is small enough. With the EIT polarizability [Eq. (1) and Fig. 1(b)], one can easily see that the Bragg condition (2) can be fulfilled at four different detuning δ [crossing points between $\text{Re}(\alpha)$ and a straight horizontal line given by $-\Delta\lambda_{\text{lat}}/\lambda_{\text{lat}}$]. However, for two of these frequencies, the imaginary part of the polarizability is near its maximum, indicating a large

amount of losses and preventing any efficient Bragg reflection. Therefore, we expect two band gaps, one for a large detuning, which also appears with two-level atoms [23], and another one, narrower, in the transparency window, which is due to EIT.

A more precise description of the photonic properties of such a periodic atomic structure can efficiently be obtained by simulating light propagation in the medium with the transfer matrix method [34–36]. It is a one-dimensional model, whose use is justified when the transverse extension of the atomic layers is large compared to the probe beam size and when the incident angle is small, which is the case in our experiment (see [37] for an extended discussion on this issue). The nonzero propagation angle can be taken into account by changing the probe wave vector from $k_0 = 2\pi/\lambda_0$ to $k_0 \cos\theta$. A detailed description of this method in the context of ordered atomic samples has been given in previous papers [38–40]. In brief, the first step is to construct the transfer matrix M of one single period. To do so, one has to decompose the atomic layer in several sublayers of thickness δz . The transfer matrix of each sublayer is the product of a propagation matrix with a discontinuity matrix whose coefficients are given by the Fresnel coefficients, see [36]. Besides the density distribution, the only ingredient entering the model is the atomic polarizability. Therefore, extending the results obtained with two-level atoms [23] to driven atom under EIT conditions is simply made by replacing the atomic polarizability. Once the matrix M is obtained, we can use it to derive analytical formula that allow us to compute the dispersion relations and the reflection and transmission coefficients through N layers (see, e.g. [35,36,38]). The matrix M is related to the elementary reflection r and transmission t coefficients of one single period by

$$M = \frac{1}{t} \begin{bmatrix} t^2 - r^2 & r \\ -r & 1 \end{bmatrix}. \quad (3)$$

Then, using the property $\det(M) = 1$, the eigenvalues of M are $e^{\pm i\Theta}$ with

$$\cos(\Theta) = \cos\left(k_{\text{eff}} \frac{\lambda_{\text{lat}}}{2}\right) = \frac{\text{Tr}(M)}{2}. \quad (4)$$

This relation gives the effective wave vector (or Bloch wave vector) k_{eff} in the medium, i.e., the dispersion relation, which describes the photonic properties of the medium in the limit where it is infinite.

To compute the transmission and reflection coefficients through N periods, we first introduce the matrix A such that

$$M = e^{i\Theta A} = \cos(\Theta)I + i \sin(\Theta)A, \quad (5)$$

where I is the 2×2 identity matrix. Then, the transfer matrix of N periods writes

$$M^N = e^{iN\Theta A} = \cos(N\Theta)I + i \sin(N\Theta)A. \quad (6)$$

To get the transmission coefficient $T = |t_N|^2$ and reflection coefficient $R = |r_N|^2$ from M^N , we just need to know the coefficients of A , which are obtained by Eq. (5) and identification with Eq. (3). After some algebra, we get

$$r_N = \frac{r}{1 - t[\cos(\Theta) - \sin(\Theta) \cot(N\Theta)]}, \quad (7)$$

$$t_N = \frac{t \sin(\Theta) / \sin(N\Theta)}{1 - t[\cos(\Theta) - \sin(\Theta) \cot(N\Theta)]}. \quad (8)$$

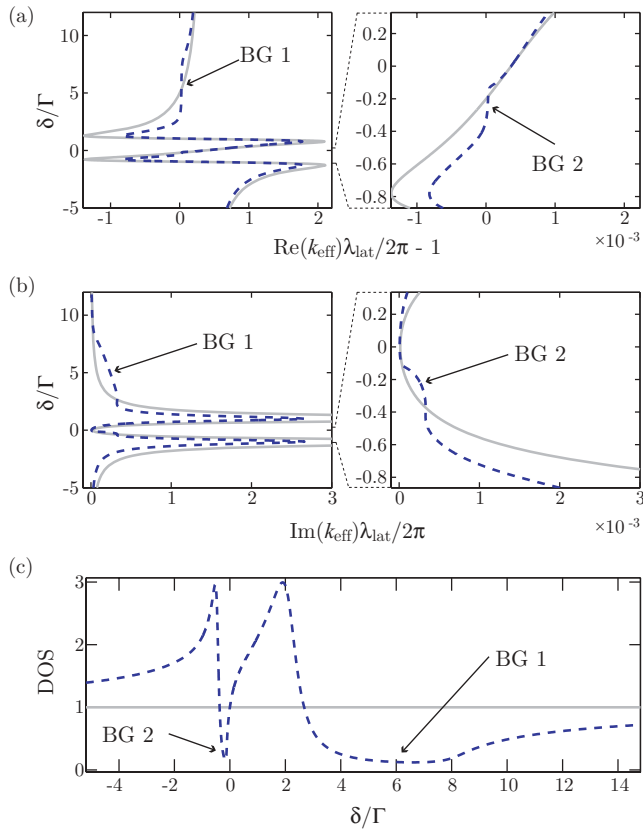


FIG. 2. (Color online) Photonic properties of the medium, valid for an infinitely long lattice. (a) Dispersion relation: the frequency (detuning δ) is plotted as a function of the effective wave vector in the medium $\text{Re}(k_{\text{eff}})$. Only the edge of the first Brillouin zone $k_{\text{eff}}\lambda_{\text{lat}}/2 = \pi$ is shown. A first band gap (BG) is visible. Right panel: zoom in the transparency window, where a second BG appears. (b) Same as (a) with the imaginary part of k_{eff} . (c) Density of states (DOS) normalized to the one in a bulk medium of the same susceptibility [Eq. (10)]. In all plots, the gray solid lines correspond to a homogeneous atomic medium of the same average density $\rho = 7 \times 10^{11} \text{ cm}^{-3}$ and the dashed blue lines correspond to atoms trapped in a lattice with $\eta = 3.5$, $\Delta\lambda_{\text{lat}} = 0.25 \text{ nm}$, and coupling-field parameters $\Omega = 2\Gamma$ and $\Delta = 0$.

For an infinite medium, and with $\text{Im}(\Theta) > 0$, we obtain

$$r_{\infty} = \frac{r}{1 - t e^{i\Theta}}. \quad (9)$$

We applied these results with the $F = 1 \rightarrow F' = 2$ transition of the D_2 line of rubidium 87 and with the optimum parameters of [23] ($\rho = 7 \times 10^{11} \text{ cm}^{-3}$, $\eta = 3.5$ [41], and $\Delta\lambda_{\text{lat}} = 0.25 \text{ nm}$) and with the coupling-beam parameters $\Delta = 0$, $\Omega = 2\Gamma$. We introduce a dephasing rate $\gamma = 0.008\Gamma$, similar to the one of the experiment [12]. We obtain the dispersion relation [ω vs $\text{Re}(k_{\text{eff}})$] shown in Fig. 2(a). As expected from the previous qualitative discussion, it exhibits two band gaps (BGs), which appear at the edge of the first Brillouin zone $k_{\text{eff}}\lambda_{\text{lat}}/2 = \pi$, i.e., where the Bragg condition (2) is fulfilled. It is characterized by a reduced variation of $\text{Re}(k_{\text{eff}})$ with ω , corresponding to a reduced density of states. One of the band gap, which we label “BG 1” in Fig. 2(a), is not influenced by EIT and is the same as the one studied in our

previous experiment [23]. The second one (“BG 2”) appears on the contrary in the electromagnetically induced transparency window. It is very much narrower and its width increases with the coupling-beam intensity.

The band gaps manifest themselves also in the imaginary part of k_{eff} . In a lossless medium, k_{eff} acquires an imaginary part only in band gaps. In our system, since the atomic polarizability is complex, the wave vector has always an imaginary part leading to the wave attenuation when it propagates in the medium. This attenuation is due to scattering losses. In this case, we see in Fig. 2(b) that the BGs add an extra component of $\text{Im}(k_{\text{eff}})$, which is responsible for the formation of an evanescent wave that leads to the reflection of the incoming light.

Finally, PBGs appear also as a reduction of the density of states (DOS), which can be computed, following [42] and considering a position in the middle of the structure, from the reflection coefficients of the two surrounding semilattices of reflection coefficients r_1 and r_2 , via

$$\mathcal{D} = \text{Re} \left[\frac{2 + r_1 + r_2}{1 - r_1 r_2} - 1 \right]. \quad (10)$$

This can be applied for a finite length lattice in order to compute the local DOS [23] or with an infinite lattice using Eq. (9). The result in that case is shown in Fig. 2(c) and demonstrates a strong DOS reduction in the two BGs. It should be noted that, despite the assumption of an infinite medium, the DOS does not completely vanish because of the scattering losses. It reaches a minimum value of 0.12 (normalized to the DOS in the bulk medium of the same susceptibility).

For a finite-size medium, the most relevant quantities are the transmission and reflection spectra, obtained from Eqs. (7) and (8). They are shown in Fig. 3, where the two band gaps appear as two reflection bands. With the above-mentioned parameters and a lattice length $L = 3 \text{ mm}$, corresponding to $N \sim 7700$ periods if $\lambda_{\text{lat}} \sim 781 \text{ nm}$, the reflection coefficient reaches $R \sim 0.73$. Note that this is slightly lower than what is reported in [23], because the considered transition strength is weaker than the closed transition used in [23], which we cannot use for EIT.

To summarize, the use of EIT makes a new PBG appear in the transparency window, in addition to the one that already appears with two-level atoms. This result was already reported in [30]. However, there is an important and natural question that has not been explicitly answered in [30] (even if the result

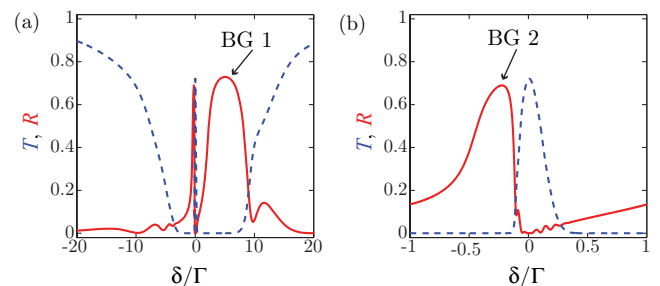


FIG. 3. (Color online) (a) Computed transmission T (dashed blue line) and reflection R (red solid line) spectra with a lattice composed of $N \sim 7700$ periods. All other parameters are the same as for Fig. 2.

is visible in Fig. 4 of that paper): is the electromagnetically induced band gap (BG 2) of better quality than the other one (BG 1)? It was shown in [23] that scattering losses were the main limitation for achieving low DOS or high reflectivity, and one could thus hope that EIT improves the band gap quality. As it can be seen in Fig. 2(c), where the DOS does not reach a lower value in the BG 2 than in the BG 1, and in Fig. 3, where the reflection coefficient is not higher in the BG 2 than in the BG 1, the answer to this question is that the EIT band gap is not of better quality. The explanation for this behavior is that even with a perfect EIT ($\gamma = 0$), where complete transparency is reached [$\text{Im}(\alpha) = 0$], it is reached precisely at a detuning δ where the real part of the atomic polarizability is also zero, thus suppressing any refractive-index grating. To build a PBG, one needs a nonzero refractive index, and the Bragg condition (2) can only be fulfilled slightly off the condition of perfect transparency. Moreover, the subsequent losses, given by $\text{Im}(\alpha)$, are exactly the same for both PBG. Taking into account an imperfect EIT ($\gamma > 0$) leads even to slightly more losses.

Nevertheless, the EIT band gap has other advantages. The most important is that it is tunable, and dynamically controllable via the coupling-beam parameters. Moreover, it is very narrow and has a very sharp transition with a good transmission band [Fig. 3(b)]. These are interesting properties for practical applications, which motivate our experimental study, described in the following.

III. EXPERIMENTAL SETUP

In this section, we present briefly our experimental apparatus, which has already been described in [23].

We trap and cool ^{87}Rb in a magneto-optical trap (MOT) loaded from a background vapor. The optical lattice is generated by a homemade titanium-sapphire laser [43] of maximum power ~ 1.3 W with a tunable wavelength λ_{lat} . The beam is focused on a waist ($1/e^2$ radius) $w_{\text{lat}} = 220 \mu\text{m}$ at the MOT position (Rayleigh length $z_{\text{R}} \simeq 0.2$ m) and then retroreflected [Fig. 4(a)]. After stages of compression and molasses, the MOT is switched off and a waiting time of a few ms allows the untrapped atoms to fall down. The sample can then be characterized by absorption imaging or used for measuring transmission and reflection spectra. In this series of experiment, the typical atom number in the lattice is $N \sim (1-2) \times 10^7$ [44].

To acquire spectra, we shine a weak ($P \sim 3$ nW) and small (waist $w_0 = 35 \mu\text{m}$) probe beam onto the lattice under an angle of incidence $\theta \simeq 1.5^\circ$, which is small enough to allow the beam to interact with the lattice over its entire length. The transmitted and reflected beams are then recorded with avalanche photodiodes (APDs). The probe detuning δ is swept in the vicinity of the atomic resonance by using an acousto-optical modulator in double-pass configuration. We use the $F = 1 \rightarrow F' = 2$ transition of the D_2 line ($\lambda_0 = 780.24$ nm, linewidth $\Gamma/2\pi = 6.1$ MHz). The other hyperfine levels are far enough to be negligible. The presented data are the result of an average of typically 250 cycles (the duration of each cycle is ~ 1 s).

EIT is induced by a coupling beam tuned in the vicinity of the $F = 2 \rightarrow F' = 2$ transition [Fig. 4(b)]. The beam has a

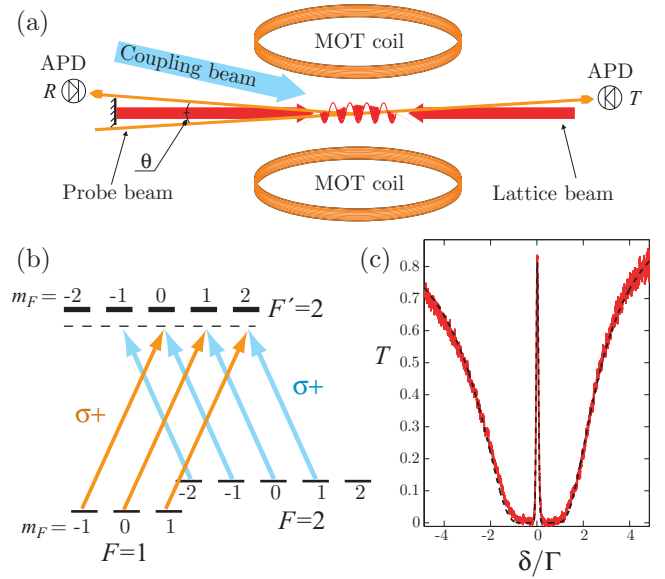


FIG. 4. (Color online) (a) Scheme of the experimental setup. (b) Atomic levels and laser configuration. The probe (orange) and coupling field (blue) drive the transition $F = 1 \rightarrow F' = 2$ and $F = 2 \rightarrow F' = 2$, respectively. (c) Transmission spectrum showing EIT with a disordered sample. The dashed black line is a fit to the data [Eqs. (1) and (11)], yielding the parameters $\gamma = 7 \times 10^{-3}\Gamma$, $\Omega = 0.8\Gamma$ and optical thickness $b_0 = 21$. The slight asymmetry is due to the cloud expansion during the sweep and is taken into account in the fit.

diameter of about 5 mm and makes an angle with the lattice axis of about 8° , small enough to ensure a homogeneous coupling strength over the whole lattice. The probe and coupling beams have both the same circular polarization, which yields to complete EIT, since all Zeeman substates of the excited states are coupled to the metastable state [45,46]. In addition, both lasers are phase-locked together via standard phase-locking techniques [47] in order to fully exploit the coherence of the EIT process. To characterize the quality of the achieved EIT, we acquire a transmission spectrum with a disordered atomic sample by suddenly switching off the optical lattice and letting the atoms expand a few microseconds before sweeping the probe frequency in $200 \mu\text{s}$. The ordered pattern has then disappeared and the transmission is given by

$$T = \exp[-b_0 \text{Im}(\tilde{\alpha})], \quad (11)$$

where b_0 is the on-resonance optical thickness ($b_0 = \sigma_0 \int \rho(z) dz$ for a medium of density ρ and with an on-resonance scattering cross section σ_0) and $\tilde{\alpha}$ is the dimensionless atomic polarizability, whose value is one at resonance (see its definition in the caption of Fig. 1). Fitting a transmission spectrum by Eqs. (11) with the polarizability (1) allows us to measure the on-resonance optical thickness, the effective dephasing rate γ and to calibrate the Rabi frequency Ω . With the recorded spectrum of Fig. 4(c), we obtain $\gamma \sim 7 \times 10^{-3}\Gamma$, giving for example a transmission of 81% with an optical thickness $b_0 = 21$ and with only $\Omega = 0.8\Gamma$ [Fig. 4(c)]. The effective decoherence rate γ mainly comes from the residual phase noise between the probe laser and the coupling lasers.

Note also that the transparency increases with the coupling strength Ω .

IV. MEASUREMENTS

We now turn to our experimental characterization of the photonic properties of the cold-atom sample trapped in the lattice under EIT conditions. From now on, all spectra are taken with the lattice beam on. To begin with, let us examine an example of transmission and reflection spectra, shown in Fig. 5(a), recorded with $\Delta\lambda_{\text{lat}} = 0.13$ nm and with the coupling-beam parameters $\Omega = 1.3\Gamma$, $\Delta = 2.5\Gamma$. The coupling field is in fact almost resonant with the atomic transition, because the lattice trapping induces a light shift. This shift is slightly inhomogeneous because of the finite extension of the atomic cloud in each well, but at the potential minimum, where most atoms are, the light-shifted atomic resonance is at $\delta \sim 2.5\Gamma$. This effect is taken into account in our simulations. Note that the light shift is the same for both transitions so that the two-photon resonance condition leading to EIT is not affected.

We clearly observe two reflection bands, as expected, corresponding to the two band gaps described in Sec. II. The wide one is the band gap already studied in [23], while the narrow one, never observed before, appears in the transparency window and is due to EIT. We observe also that the reflection of the EIT band gap is lower than the reflection of the two-level-atom band gap. This is due to the finite dephasing rate γ , which explains also why the transparency is not complete in the transmission spectrum. However, taking into account this parameter in the simulation still leads to an overestimation of the reflection coefficient [48]. Apart from this discrepancy, whose origin remains unclear, the simulated spectra are in good agreement with the experimental ones [Fig. 5(b)].

The simulations shown here and in the following are more complicated than what has been described in Sec. II because they take into account a number of experimental effects. Besides the above-mentioned light shift, the most important effect is the longitudinal atomic density distribution along the lattice, which is roughly Gaussian and can be precisely characterized by absorption imaging. This inhomogeneous distribution prevents the use of Eqs. (7) and (8). Instead, we have to compute a different elementary matrix for each position, following the measured atomic density distribution,

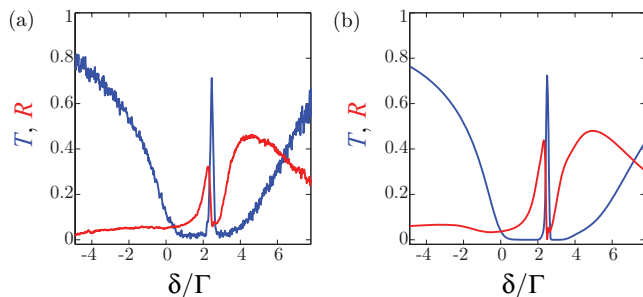


FIG. 5. (Color online) Experimental (a) and simulated (b) transmission [blue (dark grey)] and reflection [red (light grey)] spectra, with $\Delta\lambda_{\text{lat}} = 0.13$ nm, $N = 1.5 \times 10^7$ atoms, $\eta = 3.5$, and EIT parameters $\Omega = 1.3\Gamma$, $\Delta = 2.5\Gamma$, and $\gamma = 0.015\Gamma$.

and multiply them. Note that having a sample without sharp boundaries makes the usual dips and bumps at the band edges [Fig. 3(a)] disappear, inducing a kind of smoothing of the band edge. Another experimental effect that is included in the simulations is the inhomogeneous broadening due to the finite transverse sizes of the atomic sample and of the probe beam. The transfer-matrix formalism is a 1D model, but an approximate method to account for the transverse-size effects is to consider a distribution of probed densities corresponding to the overlap of the probe beam with the atomic lattice, and to average the subsequent spectra with the appropriate weighting. Since a finite probe size induces also some divergence and that the spectra are very sensitive to the incident angle, we average also over the corresponding angle distribution [49]. This procedure leads to a good agreement with the experiment (Fig. 5).

In the following, we will focus on the properties of the EIT reflection band and for clarity we will only show spectra in the corresponding, narrower spectral range. We will investigate the tunability of this reflection band, i.e., how it evolves with the coupling-beam parameters, and its dependence with the lattice wavelength via the Bragg condition (2). Both aspects are related because the Bragg condition involves the atom polarizability, which is modified by the EIT parameters. However, for simplicity, we separately present these two dependencies.

A. Dependency on the EIT parameters

To illustrate the tunability of the reflection and transmission bands, we show in Fig. 6(a) a series of spectra for different coupling-field detuning Δ with fixed intensity ($\Omega = 1.8\Gamma$) and lattice wavelength ($\Delta\lambda_{\text{lat}} = 0.11$ nm). As expected, the frequency giving the maximum transmission follows the two-photon resonance $\delta \simeq \Delta$, while the reflection band is slightly shifted on the $\delta < \Delta$ side. The corresponding simulations are in fair agreement with the experimental data, apart from the overestimated reflection in the EIT band gap [Fig. 6(b)].

The coupling field amplitude, parametrized by its Rabi frequency Ω , is also an important parameter since the transparency increases with Ω , as shown in Fig. 6(c). This increase is independent of the chosen detuning Δ . The maximum reflection coefficient increases also with Ω but this time with a strong dependency on the detuning Δ , as shown in Fig. 6(d). The interpretation for this behavior is the following. With a lattice wavelength such that $\Delta\lambda_{\text{lat}} > 0$, the Bragg condition makes the two-level-atom band gap appear on the blue-detuned side of the atomic resonance, i.e., for $\delta \gtrsim 2$ (we recall that the atomic resonance is at $\delta \sim 2$ because of the lattice-induced light shift). As a consequence, with a large Δ , like the data with $\Delta = 3$, the main effect of EIT is to create a dip in the reflection band, inducing a narrow separation between the two-level-atom band gap and the EIT band gap. Then, a small Ω makes the dip smaller but does not reduce much the reflection of the EIT band gap, and that is why the maximum reflection is almost independent of Ω . On the contrary, with a red-detuned coupling field (for example with $\Delta = 0$), the EIT band gap is farther from the other one, and has a much lower reflectance. By looking precisely at the corresponding atomic polarizability, one can see that this is due to a higher

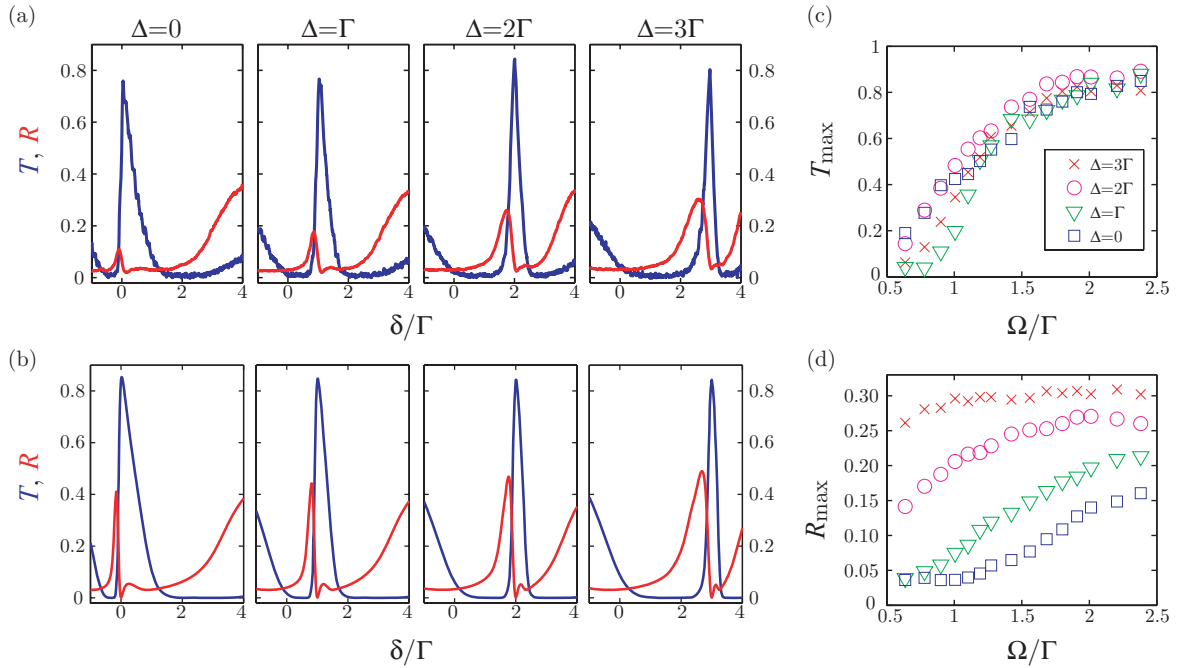


FIG. 6. (Color online) Dependency on the EIT parameters, with a fixed lattice wavelength $\Delta\lambda_{\text{lat}} = 0.11$ nm. (a) Experimental transmission [blue (dark grey)] and reflection [red (light grey)] spectra for several coupling-field detuning Δ , with $\Omega = 1.8\Gamma$. (b) Corresponding simulations. (c) Maximum transmission in the transparency window as a function of the coupling-field Rabi frequency Ω , for different detunings Δ . (d) Same as (c) with the maximum reflection in the EIT reflection band.

value of $\text{Im}(\alpha)$ at the frequency where the Bragg condition (2) is fulfilled, inducing more losses. However, increasing Ω reduces these losses.

Therefore, this is a strong limitation for practical use of the band gap tunability: changing the coupling-beam parameters changes the atomic polarizability, which leads to more or less favorable parameters via the Bragg condition.

B. Dependency on the lattice wavelength

To study the influence of the Bragg condition, we vary the lattice wavelength [50] and record transmission and reflection spectra, for different detunings Δ . First, a series of spectra obtained with the same EIT parameters is shown in Fig. 7(a) with the corresponding simulations in Fig. 7(b). The first notable feature is the qualitative behavior of the spectra, with the reflection band going from one side of the transmission band to the other side when the parameter $\Delta\lambda_{\text{lat}}$ changes its sign. This can be easily understood by looking at the graphical representation of the Bragg condition in Fig. 7(d): one can see that the frequency where the Bragg condition is fulfilled goes from one side of the maximum transparency from the other side when $\Delta\lambda_{\text{lat}}$ changes its sign. Another observation is that there is a clear optimum $\Delta\lambda_{\text{lat}}$ for maximizing the reflection coefficient; see the complete curves in Fig. 7(c). To understand this behavior, let us first take the case with the coupling beam at resonance with the atomic transition [Figs. 7(a) and 7(b) and $\Delta = 2\Gamma$ in Figs. 7(c) and 7(d)] and examine the limiting cases. When $\Delta\lambda_{\text{lat}} \sim 0$, the Bragg condition is fulfilled where the refractive index contrast is almost zero [Eq. (2)], which leads obviously to an inefficient reflection. In the opposite limit, when $\Delta\lambda_{\text{lat}}$ is large, the Bragg condition is fulfilled

where $\text{Re}(\alpha)$ is large, but $\text{Im}(\alpha)$ is also large, inducing too much scattering loss. There is thus an optimum in between, for both signs of $\Delta\lambda_{\text{lat}}$. With a nonresonant coupling field, like $\Delta = 4\Gamma$ or $\Delta = 0$ in Figs. 7(c) and 7(d), there is only one optimum lattice wavelength, for $\Delta\lambda_{\text{lat}} > 0$ ($\Delta\lambda_{\text{lat}} < 0$) with blue-detuned (red-detuned) coupling beam. This is related to the observations made in the previous paragraph: for a given $\Delta\lambda_{\text{lat}}$, there is an optimum Δ , and, conversely, for each given Δ there is a different optimum $\Delta\lambda_{\text{lat}}$. Looking very closely to a graphical representation of the Bragg condition, such as in Fig. 7(d), one can always check that the difference comes from the value of $\text{Im}(\alpha)$, giving the amount of scattering losses, where the Bragg condition is fulfilled.

V. ALL-OPTICAL SWITCHING

Finally, to illustrate a possible application of such an atom-made tunable Bragg mirror, we demonstrate its use as an all-optical switch. This is a topic of currently high interest for the processing of optical information. Standard EIT with a disordered atomic sample can also act as an all-optical switch, since the coupling beam allows switching between transmission and absorption of the probe beam. In our case, using a periodically ordered sample allows switching between transmission and reflection, i.e., between two output ports. Moreover, a small change in the coupling-field frequency is enough to induce switching so that full intensity modulation is not needed. In this case, the probe beam must have a fixed detuning and switching is obtained by changing the detuning Δ of the control beam, which induces a shift of the reflection band, so that for one value of Δ the probe frequency lies in the

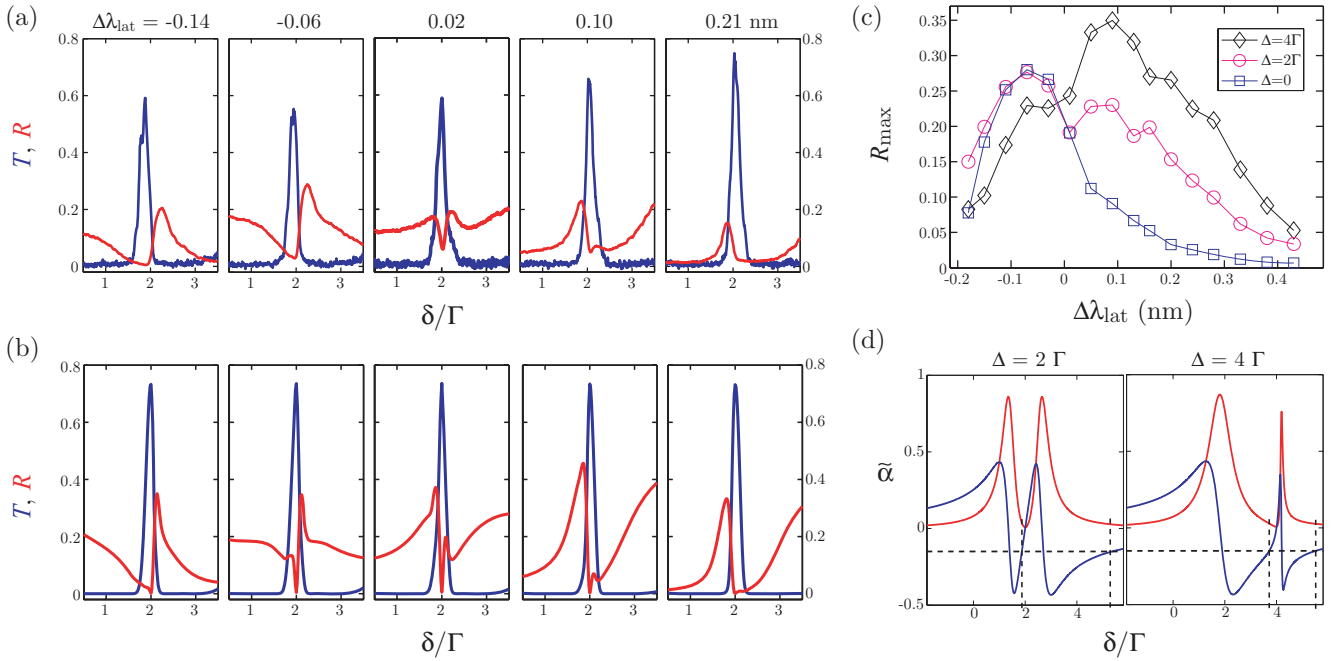


FIG. 7. (Color online) Dependency on the lattice wavelength, with a fixed coupling-beam Rabi frequency $\Omega = 1.3\Gamma$. (a) Experimental transmission [blue (dark grey)] and reflection [red (light grey)] spectra for several $\Delta\lambda_{\text{lat}}$ and with a coupling-beam detuning $\Delta = 2\Gamma$. (b) Corresponding simulations. (c) Maximum reflection in the transparency window as a function of the lattice wavelength, for different detunings Δ . (d) Illustration of the Bragg condition, which is fulfilled when the real part of the atomic polarizability (blue line) crosses the horizontal dashed black line representing $-\Delta\lambda_{\text{lat}}/\lambda_{\text{lat}}$ [Eq. (2)]. The red line is the imaginary part of the atomic polarizability, proportional to scattering losses.

reflection band and for the other value it lies in the transmission band.

We report in Fig. 8 the result of such an experiment, with a probe beam detuning $\delta = 3\Gamma$. We switch periodically the control-beam detuning between $\Delta = 3\Gamma$ and $\Delta = 3.2\Gamma$ (top panel of Fig. 8). Following the control beam, the resulting transmission and reflection are modulated with a very good

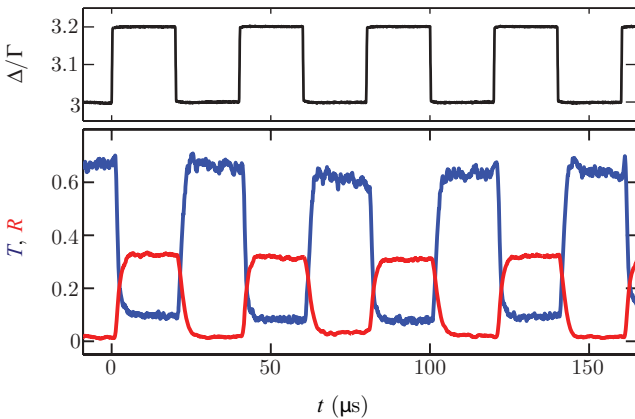


FIG. 8. (Color online) Demonstration of a two-port all-optical switch. The detuning Δ of the coupling field serves as the control parameter (top panel). The bottom panel shows the transmission [blue (dark grey)] and reflection [red (light grey)] coefficients as a function of time. The control-field Rabi frequency is $\Omega = 1.5\Gamma$, the probe detuning is $\delta = 3\Gamma$, and the lattice wavelength is such that $\Delta\lambda_{\text{lat}} = 0.15$ nm.

contrast, that we define by

$$C_T = \frac{T_H - T_L}{T_H + T_L}, \quad C_R = \frac{R_H - R_L}{R_H + R_L}, \quad (12)$$

where the subscripts H, L stand for the high and low levels. This leads, with the presented data, to $C_T = 0.76$ and $C_R = 0.88$.

Further studies are needed to better characterize the switch, in particular to determine the maximum switching rate and the minimum necessary power for the control beam. A way to achieve better performances is probably to use the four-level EIT scheme of [51], which is known to produce giant nonlinearity, with a few photons, or ultimately a single one, being enough to make the transparency appear or disappear [52]. This is required to enter the quantum regime, i.e., to make a quantum all-optical transistor, a key ingredient for quantum networks [53]. Several technologies are currently investigated for realizing quantum transistors, such as plasmonic nanostructures [54], single dye molecules embedded in crystalline matrices [55], ultrahigh quality factor whispering-gallery-mode microresonators [56], atoms or ions ensembles in hollow-core fibers [57] or in high-finesse cavities [58,59]. Since our system does not need any high-quality or microstructured mechanical elements, it might be simpler to implement.

VI. CONCLUSION

We have presented in this paper a study of the photonic properties of a sample of cold atom trapped in a one-dimensional lattice under EIT conditions. In such a system, as already predicted by Petrosyan [30], EIT creates

a supplementary band gap, in the transparency window, in addition to the one already present with two-level atoms [23]. We have experimentally observed the Bragg reflection induced by this band gap and characterized its dependency with the main experimental parameters. It allowed us to put in evidence and discuss several limitations. First, the Λ scheme necessary for EIT prevents the use of a closed transition, with an optimum transition strength, which reduces the Bragg reflection efficiency in comparison with what could be obtained with the same atomic sample by using a closed transition. In addition, the amount of scattering losses, which limit the quality of the band gaps, is at best exactly the same for the EIT band gap as for the two-level-atom band gap, and in practice slightly larger, so that the EIT band gap is of slightly lower quality. Finally, the tunability of the EIT band gap is limited by a complicated interplay between the coupling-beam parameters and the Bragg condition.

Nevertheless, it is still an interesting system, with also some advantages, like the dynamic tunability and the sharp transition between the reflection band and the transmission band. We have discussed a two-port all-optical switch as a possible application based on these properties, and we have performed a first proof-of-principle experiment. This is a promising idea that deserves further studies.

Another topic of interest is the wave propagation dynamics in this system. We have only addressed in this paper the stationary photonic properties, but it would be interesting to study pulse propagation. Both EIT and photonic band edges are known to induce slow light [12,60,61] and our system combines both ingredients. Since a short pulse is necessarily spectrally large and that, on the contrary, our system has transmission and reflection bands which are very narrow, it should induce a very large pulse distortion. This is surely not appropriate if one wants to slow down pulses without distortion, but on the contrary, a fine tuning of the parameters might allow complex and interesting pulse reshaping functions. Some proposals have recently appeared in this spirit [62–64].

Finally, the nonlinear regime, which can be investigated by using a probe beam with a larger intensity, might also reveal interesting phenomena.

ACKNOWLEDGMENTS

We acknowledge support from the Alexander von Humboldt foundation, the DFG, and the REA (program COSCALI, No. PIRSES-GA-2010-268717).

-
- [1] G. Rempe, R. J. Thompson, R. J. Brecha, W. D. Lee, and H. J. Kimble, *Phys. Rev. Lett.* **67**, 1727 (1991).
- [2] A. Lambrecht, T. Coudreau, A. M. Steinberg, and E. Giacobino, *Europhys. Lett.* **36**, 93 (1996).
- [3] D. Budker *et al.*, *Rev. Mod. Phys.* **74**, 1153 (2002).
- [4] A. M. C. Dawes, L. Illing, S. M. Clark, and D. J. Gauthier, *Science* **308**, 672 (2005).
- [5] L. Hilico, C. Fabre, and E. Giacobino, *Europhys. Lett.* **18**, 685 (1992); W. Guerin, F. Michaud, and R. Kaiser, *Phys. Rev. Lett.* **101**, 093002 (2008); G. Vrijsen, O. Hosten, J. Lee, S. Bernon, and M. A. Kasevich, *ibid.* **107**, 063904 (2011).
- [6] D. M. Bloom, P. F. Liao, and N. P. Economou, *Opt. Lett.* **2**, 58 (1978).
- [7] M. Vallet, M. Pinard, and G. Grynberg, *Europhys. Lett.* **11**, 739 (1990).
- [8] V. Boyer, A. M. Marino, R. C. Pooser, and P. D. Lett, *Science* **321**, 544 (2008).
- [9] M. Pinard, D. Grandclement, and G. Grynberg, *Europhys. Lett.* **2**, 755 (1986).
- [10] S. E. Harris, *Phys. Today* **50**, 36 (1997).
- [11] M. Fleischhauer, A. Imamoglu, and J. P. Marangos, *Rev. Mod. Phys.* **77**, 633 (2005).
- [12] L. V. Hau, S. E. Harris, Z. Dutton, and C. H. Behroozi, *Nature (London)* **397**, 594 (1999).
- [13] A. M. Akulshin and R. J. McLean, *J. Opt.* **12**, 104001 (2010).
- [14] N. Sangouard, C. Simon, H. de Riedmatten, and N. Gisin, *Rev. Mod. Phys.* **83**, 33 (2011).
- [15] N. Mercadier, W. Guerin, M. Chevrollier, and R. Kaiser, *Nature Phys.* **5**, 602 (2009).
- [16] A. Fioretti, A. F. Molisch, J. H. Mutter, P. Verkerk, and M. Allegrini, *Opt. Commun.* **149**, 415 (1998).
- [17] G. Labeyrie, E. Vaujour, C. A. Muller, D. Delande, C. Miniatura, D. Wilkowski, and R. Kaiser, *Phys. Rev. Lett.* **91**, 223904 (2003).
- [18] G. Labeyrie, F. deTomas, J. C. Bernard, C. A. Muller, C. Miniatura, and R. Kaiser, *Phys. Rev. Lett.* **83**, 5266 (1999).
- [19] Y. Bidel, B. Klappauf, J. C. Bernard, D. Delande, G. Labeyrie, C. Miniatura, D. Wilkowski, and R. Kaiser, *Phys. Rev. Lett.* **88**, 203902 (2002).
- [20] G. Birkl, M. Gatzke, I. H. Deutsch, S. L. Rolston, and W. D. Phillips, *Phys. Rev. Lett.* **75**, 2823 (1995).
- [21] M. Weidemüller, A. Hemmerich, A. Görlitz, T. Esslinger, and T. W. Hänsch, *Phys. Rev. Lett.* **75**, 4583 (1995).
- [22] S. Slama, C. vonCube, B. Deh, A. Ludewig, C. Zimmermann, P. W. Courteille, *Phys. Rev. Lett.* **94**, 193901 (2005).
- [23] A. Schilke, C. Zimmermann, P. W. Courteille, and W. Guerin, *Phys. Rev. Lett.* **106**, 223903 (2011).
- [24] M. Antezza and Y. Castin, *Phys. Rev. A* **80**, 013816 (2009).
- [25] D. Yu, *Phys. Rev. A* **84**, 043833 (2011).
- [26] A. B. Matsko, I. Novikova, M. O. Scully, and G. R. Welch, *Phys. Rev. Lett.* **87**, 133601 (2001).
- [27] V. M. Datsyuk, I. M. Sokolov, D. V. Kupriyanov, and M. D. Havey, *Phys. Rev. A* **74**, 043812 (2006).
- [28] L. S. Froufe-Pérez, W. Guerin, R. Carminati, and R. Kaiser, *Phys. Rev. Lett.* **102**, 173903 (2009); W. Guerin *et al.*, *J. Opt.* **12**, 024002 (2010); Q. Baudoin, N. Mercadier, V. Guarrera, and R. Kaiser (in preparation).
- [29] A. Schilke, C. Zimmermann, P. W. Courteille, and W. Guerin, *Nature Photon.* **6**, 101 (2012).
- [30] D. Petrosyan, *Phys. Rev. A* **76**, 053823 (2007).
- [31] A. André and M. D. Lukin, *Phys. Rev. Lett.* **89**, 143602 (2002); M. Artoni and G. C. La Rocca, *ibid.* **96**, 073905 (2006); L. E. E. de Araujo, *Opt. Lett.* **35**, 977 (2010); C. O'Brien and O. Kocharovskaya, *Phys. Rev. Lett.* **107**, 137401 (2011);

- S. Q. Kuang, C. S. Jin, and C. Li, *Phys. Rev. A* **84**, 033831 (2011).
- [32] M. Bajcsy, A. S. Zibrov, and M. D. Lukin, *Nature (London)* **426**, 638 (2003); A. W. Brown and M. Xiao, *Opt. Lett.* **30**, 699 (2005); Y.-W. Lin, W. T. Liao, T. Peters, H. C. Chou, J. S. Wang, H. W. Cho, P. C. Kuan, and I. A. Yu, *Phys. Rev. Lett.* **102**, 213601 (2009).
- [33] To be concise, we wrote a slightly simplified expression, also used in [30]. For every computation of this paper, we use the more complete equation (13) of [11].
- [34] M. Born and E. Wolf, *Principle of Optics*, 7 ed. (Cambridge University Press, New York, 1999).
- [35] J. Lekner, *J. Opt. Soc. Am. A* **11**, 2892 (1994).
- [36] J. M. Bendickson, J. P. Dowling, and M. Scalora, *Phys. Rev. E* **53**, 4107 (1996).
- [37] S. Slama, C. von Cube, A. Ludewig, M. Kohler, C. Zimmermann, and P. W. Courteille, *Phys. Rev. A* **72**, 031402(R) (2005).
- [38] I. H. Deutsch, R. J. C. Spreeuw, S. L. Rolston, and W. D. Phillips, *Phys. Rev. A* **52**, 1394 (1995).
- [39] M. Artoni, G. La Rocca, and F. Bassani, *Phys. Rev. E* **72**, 046604 (2005).
- [40] S. Slama, C. von Cube, M. Kohler, C. Zimmermann, and P. W. Courteille, *Phys. Rev. A* **73**, 023424 (2006).
- [41] With $\eta = 3.5$, the rms radius of the density distribution in each period is $\sigma_z \simeq 47$ nm and we decompose each period in 40 sublayers of thickness $\delta z \simeq 9.7$ nm.
- [42] G. Boedeker and C. Henkel, *Opt. Express* **11**, 1590 (2003).
- [43] C. Zimmermann, V. Vuletic, A. Hemmerich, L. Ricci, and T. W. Hänsch, *Opt. Lett.* **20**, 297 (1995).
- [44] For technical reasons, this atom number is sensibly lower than in our previous experiment [23], so that the measured reflection coefficient is also lower.
- [45] Y.-C. Chen, C.-W. Lin, and I. A. Yu, *Phys. Rev. A* **61**, 053805 (2000).
- [46] M. Yan, E. G. Rickey, and Y. Zhu, *J. Opt. Soc. Am. B* **18**, 1057 (2001).
- [47] M. Prevedelli, T. Freearge, and T. W. Hänsch, *Appl. Phys. B* **60**, S241 (1995); A. M. Marino and C. R. Stroud, Jr., *Rev. Sci. Instrum.* **79**, 013104 (2008); D. Höckel, M. Scholz, and O. Benson, *Appl. Phys. B* **94**, 429 (2009).
- [48] We have checked that the difference in the light shifts undergone by the two involved transitions, which induces an inhomogeneous broadening of the two-photon resonance, was indeed negligible.
- [49] For the discretizations we used the following parameters. The thickness of the sublayers in each period is $\delta z = 24$ nm, the sampling interval for the longitudinal density distribution along the lattice axis is $100 \mu\text{m}$, it is $7.5 \mu\text{m}$ for the transverse distribution of the probe-beam intensity and of the atomic sample, and 0.24° for the angle distribution that accounts for the probe beam divergence.
- [50] When we vary the lattice wavelength, we change the beam power accordingly in order to keep the same trapping depth and thus the same atom number and temperature.
- [51] S. E. Harris and Y. Yamamoto, *Phys. Rev. Lett.* **81**, 3611 (1998).
- [52] M. Yan, E. G. Rickey, and Y. Zhu, *Phys. Rev. A* **64**, 041801 (2001).
- [53] H. J. Kimble, *Nature (London)* **453**, 1023 (2008).
- [54] D. E. Chang, A. S. Sørensen, E. A. Demler, and M. D. Lukin, *Nature Phys.* **3**, 807 (2007).
- [55] J. Hwang *et al.*, *Nature (London)* **460**, 76 (2009).
- [56] D. O'Shea, C. Junge, M. Pöllinger, A. Vogler, and A. Rauschenbeutel, *Appl. Phys. B* **105**, 129 (2011).
- [57] M. Bajcsy, S. Hofferberth, V. Balic, T. Peyronel, M. Hafezi, A. S. Zibrov, V. Vuletic, and M. D. Lukin, *Phys. Rev. Lett.* **102**, 203902 (2009).
- [58] M. Albert, A. Dantan, and M. Drewsen, *Nature Photon.* **5**, 633 (2011).
- [59] A. E. B. Nielsen and J. Kerckhoff, *Phys. Rev. A* **84**, 043821 (2011).
- [60] J. P. Dowling, M. Scalora, M. J. Bloemer, and C. M. Bowden, *J. Appl. Phys.* **74**, 1896 (1994).
- [61] M. Scalora *et al.*, *Phys. Rev. E* **54**, R1078 (1996).
- [62] F. Bariani and I. Carusotto, *J. Eur. Opt. Soc. Rap. Public.* **3**, 08005 (2008).
- [63] I. Carusotto, M. Antezza, F. Bariani, S. De Liberato, and C. Ciuti, *Phys. Rev. A* **77**, 063621 (2008).
- [64] F. Bariani and I. Carusotto, *Phys. Rev. A* **81**, 013836 (2010).

III.2. Distributed feedback laser

The 1D photonic band gaps studied in the previous sections can serve as distributed feedback. The next ingredient to make a DFB laser is to add gain. We can use the gain mechanisms studied in the previous chapter.

III.2.1. Bragg reflection with standard gain

The easiest gain to implement is Raman gain between Zeeman sublevels, as it only necessitates one pump beam, which doesn't have to be very powerful. It is also quite efficient if the laser is phase-locked with the probe beam, which is straightforward to achieve by taking the two beams from the same laser and separating the frequencies with acousto-optical modulators.

The results of this experiment is summarized in Fig. III.1. One observes quite a large gain, leading to reflection and transmission coefficients above unity. One notices, however, that when the reflection is higher, the transmission is smaller.

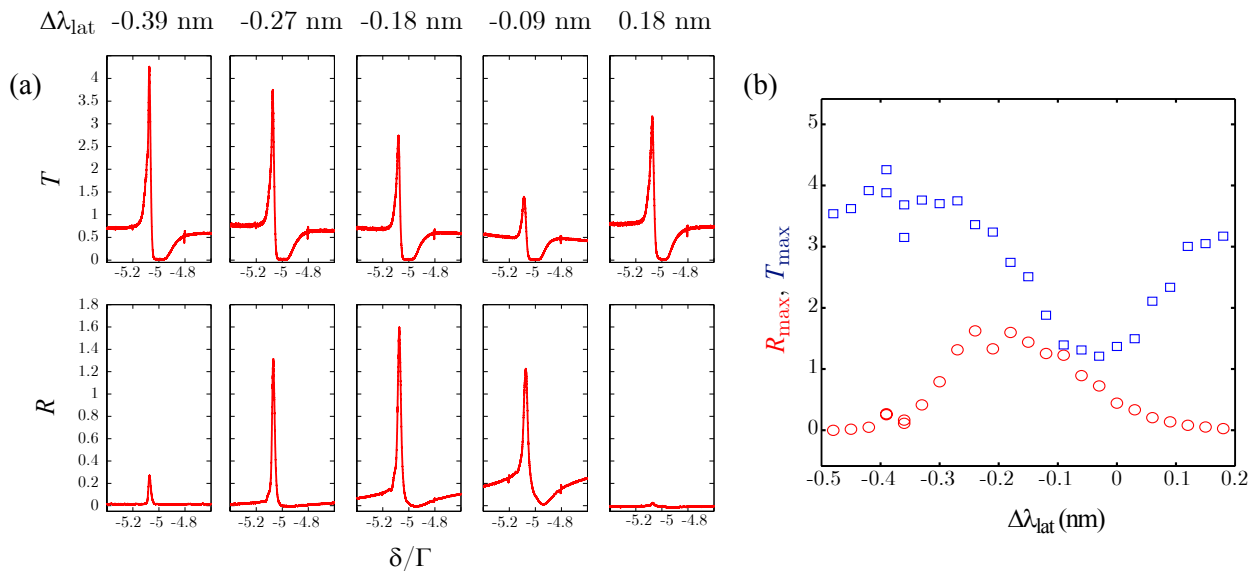
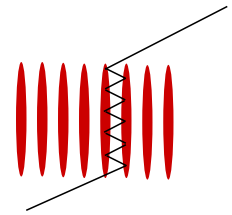


Figure III.1: (a) Experimental transmission and Bragg reflection spectra with Raman gain, which is responsible for the narrow spectral features. Here δ is the detuning between the probe beam and the atomic transition. Each panel corresponds to a different lattice detuning from the geometric Bragg condition [Eq. (III.1)] (see [Schilke 2011]). (b) The maximum transmission and reflection coefficients are reported as a function of the lattice detuning. The detuning of the Raman laser is $\Delta = -5\Gamma$ and the resonant optical depth of the sample is $b_0 \sim 30$.

By fitting a transmission curve taken without any Bragg reflection (far from the Bragg condition) one can deduce the atomic polarizability including the Raman resonance [Guerin 2009] and inject it into a 1D coupled-wave model. The corresponding (unpublished) simulations show that, with our experimental parameters, we don't have enough gain for reaching the DFB lasing threshold, but we should have seen a positive feedback effect,

i.e. having the gain in transmission and in reflection simultaneously increasing at the Bragg condition. This is not the case in the experiment and we attribute this discrepancy to an effect which does not exist in the 1D model, namely the transverse walk-off of the wave inside the medium during the multiple Bragg reflection process, because of the non-zero Bragg angle (see illustration). This prevents the buildup of a positive feedback loop.



III.2.2. DFB parametric oscillation

This problem of unstable feedback has been solved by using four-wave mixing (FWM) as the gain mechanism. To do so experimentally, we only need to carefully retroreflect the pump beam. Then we observed a huge signal appearing on the transmission and reflection detectors. We could then easily check that this signal appears above a certain threshold in pump intensity and is present without any incident probe beam. We also checked that, below threshold, we indeed observe a phase-conjugated beam, i.e., a reflected beam in the backward direction (on top of the Bragg-reflected beam visible in the specular direction).

Without any incident probe beam, the system has a cylindrical symmetry. Since the feedback is efficient only for a given angle (the Bragg condition), the light is emitted in a cone.

The question of the feedback and its stability is particularly interesting in this system. Let us consider a plane containing the symmetry axis and the four waves having an angle with the lattice axis given by the Bragg condition. Such a plane is represented in Fig. III.2, with waves labeled as E_1 , E_2 , E_3 , E_4 . The waves E_1 and E_3 are coupled by Bragg reflection, E_2 and E_4 are also coupled by Bragg reflection, while E_1 and E_4 are counterpropagating and are thus coupled by FWM, like E_2 and E_3 . The electromagnetic feedback (one wave coupled with itself) is thus obtained by combining two Bragg reflections and two phase-conjugations. The two walk-offs associated to the two Bragg reflections can then compensate each other, which produces a stable feedback loop. Note however that this description is only empirical, I have not been able to find a simple way to include the walk-off effect in a coupled-wave theory in order to prove that this interpretation is correct.

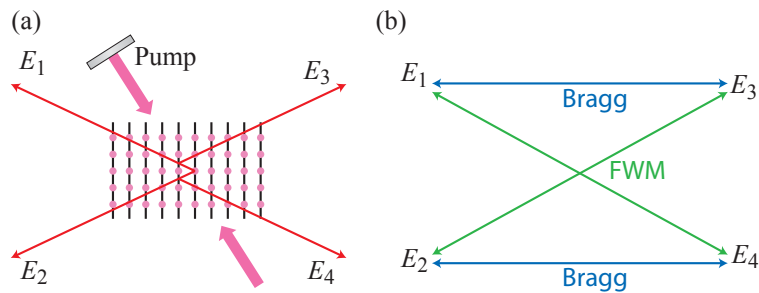


Figure III.2: Figure adapted from the *News and View* article [Rakher 2012] written about our paper [Schilke 2012a]. (a) Geometry of the experiment. The lattice axis is horizontal (beams not represented). In each vertical layer the atoms are not ordered, contrary to what is suggested. (b) The different waves and their coupling mechanisms (FWM or Bragg reflection) are represented.

The article [Schilke 2012a] on the mirrorless optical parametric oscillations with distributed feedback in cold atoms is reproduced below.

Optical parametric oscillation with distributed feedback in cold atoms

Alexander Schilke¹, Claus Zimmermann¹, Philippe W. Courteille² and William Guerin^{1*}

There is currently a strong interest in mirrorless lasing systems¹, in which the electromagnetic feedback is provided either by disorder (multiple scattering in the gain medium) or by order (multiple Bragg reflection). These mechanisms correspond, respectively, to random lasers² and photonic crystal lasers³. The crossover regime between order and disorder, or correlated disorder, has also been investigated with some success^{4–6}. Here, we report one-dimensional photonic-crystal lasing (that is, distributed feedback lasing^{7,8}) with a cold atom cloud that simultaneously provides both gain and feedback. The atoms are trapped in a one-dimensional lattice, producing a density modulation that creates a strong Bragg reflection with a small angle of incidence. Pumping the atoms with auxiliary beams induces four-wave mixing, which provides parametric gain. The combination of both ingredients generates a mirrorless parametric oscillation with a conical output emission, the apex angle of which is tunable with the lattice periodicity.

Among the possible systems that can be used to produce and study mirrorless lasers, cold atoms are interesting because of some specific properties that differ from those of standard photonic materials. First, they are resonant point-like scatterers, producing extremely narrow spectral features (gain curves, scattering cross-section), which can provide flexibility⁹ or give new effects. Second, their temperature is low enough to make Doppler broadening negligible in most situations, but large enough to make them move substantially on a millisecond timescale, which makes disorder-configuration averaging or dynamic evolution from order to disorder very easy. Third, cold atoms are well isolated from the environment, which makes them good candidates in the search for quantum effects.

Conventional lasing has already been demonstrated when cold atoms are used as the gain medium^{10,11}, as has radiation trapping due to multiple scattering¹², and efforts are under way to combine both factors to obtain random lasing^{13,14}. In the opposite regime, a one-dimensional photonic bandgap (PBG), yielding efficient Bragg reflection of light, has recently been demonstrated in a cold, ordered atomic vapour¹⁵. In this Letter, we demonstrate optical parametric oscillation (OPO) with distributed feedback (DFB) in cold atoms trapped in a one-dimensional optical lattice, by combining the PBG with four-wave mixing (FWM), which provides the gain mechanism^{10,16–18}.

We trapped cold ⁸⁷Rb atoms in a one-dimensional lattice of tunable wavelength λ_{dip} . The trapping beam was retroreflected to generate a potential of periodicity $\lambda_{\text{dip}}/2$ (Fig. 1 and Methods). Typically, $N = 5 \times 10^7$ trapped atoms were distributed over a length $L \approx 3$ mm ($\sim 7,700$ atomic layers) at a temperature $T \approx 100$ μ K, leading to a root-mean-square (r.m.s.) transverse radius of the cloud $\sigma_{\perp} \approx 60$ μ m. Such an atomic pattern gives rise to a periodic modulation of the refractive index n and we have shown recently¹⁵ that

the very small modulation amplitude $\Delta n \approx 1 \times 10^{-3}$ inherent to dilute vapours (density $\rho \approx 1 \times 10^{12}$ cm^{-3}) could be balanced by the large number of layers, provided that the Bragg condition is fulfilled for a small angle of incidence and for a frequency slightly off the atomic resonance to avoid too much scattering losses. A Bragg reflection as efficient as 80% can be obtained.

In the present experiment, we investigated the situation when gain was added to the system. Cold atoms can amplify light when pumped by auxiliary near-resonant beams, and several gain mechanisms have already been demonstrated (see ref. 10 and references therein). The combination of enough gain and multiple Bragg reflection should lead to DFB lasing.

However, in this system, the stability of the feedback mechanism is a critical issue. We trap the atoms using a lattice beam that is far red-detuned from the atomic transition (D2 line of ⁸⁷Rb, wavelength $\lambda_0 = 780.24$ nm in vacuum, linewidth $\Gamma/2\pi = 6.07$ MHz), so that the Bragg condition can only be fulfilled for a non-zero propagation angle θ , relatively to the lattice axis, given by

$$\lambda_{\text{dip}} \cos \theta = \lambda_0 / \bar{n} \quad (1)$$

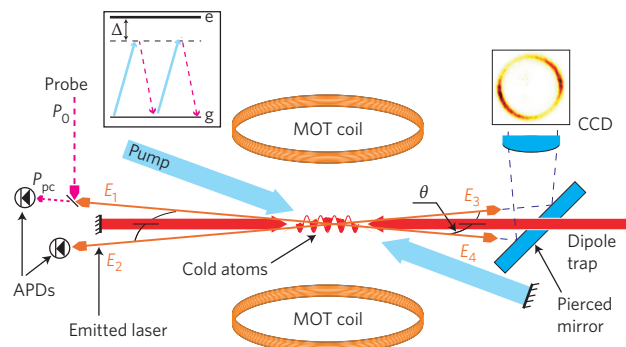


Figure 1 | Schematics of the set-up. Cold atoms are trapped in the lattice formed by a retroreflected dipole trap. The pump beam is also retroreflected and has an incident angle of $\sim 8^\circ$. Above threshold, the system emits light with an angle θ around the lattice: in any given plane including the lattice, four waves are coupled. E_1 and E_4 as well as E_2 and E_3 are coupled by the phase-conjugation process; E_1 and E_3 as well as E_2 and E_4 are coupled by the Bragg reflection. The emitted light is detected by avalanche photodiodes (APDs) and the beam cross-section is observed by a charge-coupled device (CCD) camera. Additionally, a probe beam (incident power P_0) can be used to measure the phase-conjugate reflectivity $R_{\text{pc}} = P_{\text{pc}}/P_0$, where P_{pc} is the reflected power. Inset: scheme of the four-photon transition corresponding to FWM. Upward (downward) arrows represent pump (probe and conjugate) photons. MOT, magneto-optical trap.

¹Physikalisches Institut, Eberhard-Karls-Universität Tübingen, Auf der Morgenstelle 14, D-72076 Tübingen, Germany, ²Instituto de Física de São Carlos, Universidade de São Paulo, 13560-970 São Carlos, SP, Brazil. *e-mail: william.guerin@pit.uni-tuebingen.de

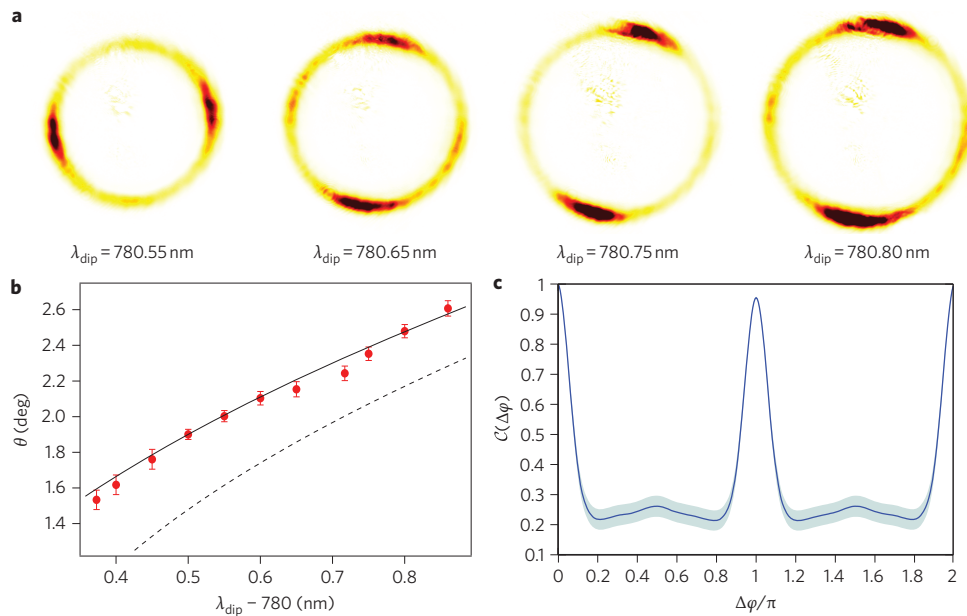


Figure 2 | Transverse mode of the emitted beam. **a**, Cross-section of the beam for different λ_{dip} . Each image is the result of an average of about 100 pictures of integration time 200 μs each. **b**, Measured emission angle θ as a function of λ_{dip} (red symbols). Errors bars indicate the uncertainty in fitting the radius on images and angle calibration (see Methods). The dashed line is the Bragg condition (equation 1) with $\bar{n} = 1$ and the solid line is a fit with \bar{n} as a free parameter. **c**, Angular correlation function $\mathcal{C}(\Delta\varphi)$ computed from the $\lambda_{\text{dip}} = 780.75$ nm data. The solid line is the average over all images and the blue area represents the statistical uncertainty.

where \bar{n} is the averaged refractive index of the atomic medium. Because of this angle, typically $\theta \approx 2^\circ$ for $\lambda_{\text{dip}} = 780.6$ nm, the light beam is not perfectly reflected onto itself such that it transversely walks off and leaves the interaction volume after a certain number of Bragg reflections.

Because this walk-off effect plays an important role, we must consider, for each plane containing the lattice, four different waves having a propagation angle θ relatively to the lattice axis (Fig. 1). In this case, a ‘standard’ gain amplifies one wave (E_4 in Fig. 1) while the Bragg reflection couples it to another one (E_2) with a walk-off. This problem can be overcome by producing gain with a phase-conjugation mechanism such as degenerate or nearly degenerate FWM^{10,16–18}. Then, each wave generates a backward phase-conjugated wave. Combined with the Bragg reflection, this leads to a global, walk-off free coupling between all four waves (Fig. 1), which favours an oscillatory behaviour.

Experimentally, inducing FWM in a phase-conjugation configuration is done by simply retroreflecting a near-resonant, linearly polarized pump beam (Fig. 1). Its typical detuning from the $F = 2 \rightarrow F' = 3$ closed transition is $\Delta = -5\Gamma$, it makes an incident angle with the lattice of $\sim 8^\circ$, and it is collimated with a waist $w \approx 2.4$ mm, thus ensuring a nearly homogeneous pumping of the whole lattice. To avoid optical pumping into the dark hyperfine $F = 1$ ground state, a repumping laser is kept on all the time. In addition, with a weak probe beam, phase-locked with the pump, can be used for pump–probe experiments or as a local oscillator.

When the pump power P overcomes a certain threshold, namely $P_{\text{th}} \approx 1$ mW for $\Delta = -5\Gamma$ (Fig. 3), we observe a strong, directional light emission that can be recorded either with avalanche photodiodes (APDs) or with a charge-coupled device (CCD) camera (Fig. 1). This radiation is due to OPO with DFB in the cold atom sample, with FWM as the gain mechanism. This interpretation is supported by many observations, as discussed in the following.

First, this radiation is obtained only with a retroreflected pump beam, the alignment of which is critical, which is a strong indication that FWM is at work (with only one pump beam, we observe a

strong Raman gain¹⁰ in pump–probe experiments but no laser). Second, the polarization of the emitted radiation is linear and orthogonal to that of the pump beam. This is also consistent with the properties of FWM, which is much more efficient for orthogonal pump and probe polarizations¹⁹. Third, we measured the frequency of the emitted light with a beat note experiment (see Supplementary Information). The emitted light is just a few kilohertz detuned from the pump frequency, which is consistent with nearly degenerate FWM²⁰ and inconsistent with Raman gain, for which the amplification line was detuned by ~ 200 kHz with similar parameters.

The role of Bragg reflection as the feedback mechanism is demonstrated by the beam shape. Emission occurs with angle θ from the lattice axis and, because of axial symmetry, forms two cone-shaped beams on each side of the lattice. From images of the beam cross-section (Fig. 2a), we extract the emission angle θ as a function of λ_{dip} . A fit with \bar{n} as a free parameter is fully consistent with the Bragg condition (equation 1) and gives $\bar{n} - 1 = (2.2 \pm 0.5) \times 10^{-4}$ (Fig. 2b), which is the expected order of magnitude given the atomic density (the refractive index depends also on the pump power).

The intensity profile $I(\varphi)$, where φ is the in-plane angle, exhibits strong shot-to-shot fluctuations. However, there is always a symmetry, that is, $I(\varphi) \approx I(\varphi + \pi)$. This can be more precisely quantified by computing from the images the angular correlation function $\mathcal{C}(\Delta\varphi) = \langle I(\varphi)I(\varphi + \Delta\varphi) \rangle / \langle I(\varphi)^2 \rangle$, which shows indeed a very strong correlation $\mathcal{C}(\pi) \approx 0.96$ (Fig. 2c). This correlation comes from the couplings, namely the Bragg reflection and the phase conjugation, that exist in any given plane between the four directions of emission (Fig. 1). In contrast, the shot-to-shot fluctuations can be understood by the random direction of the initial spontaneous emission event that triggers the laser oscillation and by the absence of coupling between waves in different planes. In addition, we note that even after averaging, the intensity is not uniformly distributed along the ring (Fig. 2a), indicating that some effects break the axial symmetry (the incident angle of the pump beam and possibly some residual astigmatism in the lattice beam).

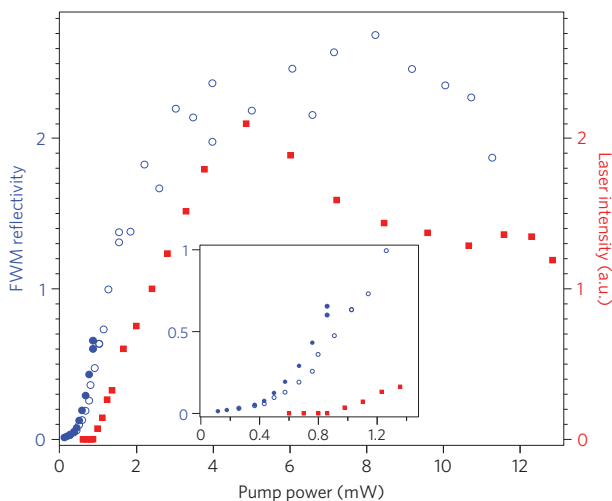


Figure 3 | Emitted laser power and maximum FWM reflectivity as a function of pump power. Red filled squares: laser intensity. Blue filled circles: FWM reflectivity below the threshold. The pump detuning is $\Delta = -5\Gamma$. Blue open circles: FWM reflectivity measured without lattice (to compensate the lattice-induced light shift, we increased the pump detuning to $\Delta = -7\Gamma$). Inset: zoom-in for low pump power. The comparison between the reflectivity measured with and without the lattice shows that the lattice increases the reflectivity when approaching the threshold, which demonstrates a positive feedback effect. Above threshold, only the reflectivity without lattice can be measured.

Finally, we measured the emitted intensity as a function of the pump parameters. We observed that the OPO is not very sensitive to the precise value of the pump detuning Δ , provided it is negative (red-detuned) and not too close to resonance: we did not observe any significant change between $\Delta = -4\Gamma$ and $\Delta = -10\Gamma$. Closer to resonance or with a positive detuning, the pump-induced heating destroys the lattice, and the laser emission is inhibited or much weaker. The dependence on pump power is much more important. Above the threshold, the emitted power increases with pump power up to an optimum at $P \approx 5$ mW, above which a decrease is observed (Fig. 3). We estimate the maximum emitted power to be $\sim 3 \mu\text{W}$ on each side. The decrease of the reflectivity past an optimum pump intensity is a known behaviour of FWM¹⁶. In our case, we also suspect a detrimental mechanical effect (heating or residual radiation pressure), which destroys the lattice. We indeed observed, in the temporal behaviour of the emitted light, that radiation is sustained for a longer time for lower pump intensities, the longest duration being ~ 0.5 ms.

In summary, it is interesting to note that the threshold condition requires $\sim 50\%$ phase-conjugate reflectivity measured with a disordered sample (Fig. 3) and $\sim 80\%$ Bragg reflectivity measured with a passive sample¹⁵, but when both ingredients are combined, these quantities are modified and we can no longer determine the amounts of feedback and gain, in contrast to standard lasers, in which the gain medium and cavity can be characterized independently of one another. This is also what makes our system original and interesting.

To conclude, let us discuss the possible applications of this DFB OPO. First, we stress that the idea of combining FWM with a red-detuned DFB grating to generate conical beams (and possibly Bessel beams²³) might also be applied in other systems, such as semiconductors^{21,22}. In contrast, on-axis feedback could be obtained by using higher-order Bragg reflection, for example, with $\lambda_{\text{dip}} = 2\lambda_0/\bar{n}$. Combining this idea with frequency up conversion schemes^{24–27}, one might be able to produce mirrorless oscillation

at λ_0 with pumps at longer wavelengths. In principle, λ_0 can be any atomic transition, possibly in the ultraviolet range. Another possible application is the generation of ‘twin beams’, that is, pairs of beams with a relative intensity noise below the standard quantum limit. It is indeed well known that FWM induces quantum correlations and it has been shown that FWM oscillators above threshold could create twin beams²⁰. We have already demonstrated strong angular classical correlations, and more work is needed to investigate, theoretically and experimentally, the question of possible quantum correlations in such systems. Here, the correlations should concern the four directions of emission in each plane. Finally, extension to a three-dimensional geometry, using the bandgap predicted in ref. 28, is an exciting open question.

Methods

Atomic sample preparation and experimental cycle. The atoms were trapped and cooled in a magneto-optical trap (MOT) loaded from a background vapour in 1 s. Stages of compression and molasses were used to increase the density and decrease the temperature, before loading the atoms in the dipole trap, which was generated by a home-made continuous-wave Ti:sapphire laser, following the design of ref. 29. The maximum available power was 1.3 W and its wavelength λ_{dip} was tunable in the range 770–820 nm. The beam was focused with a waist ($1/e^2$ radius) $w_{\text{dip}} = 220 \mu\text{m}$ at the MOT position (Rayleigh length $z_R \approx 20$ cm). The lattice was then formed by retroreflecting the beam. After loading the optical lattice, the molasses beams were switched off and a waiting time of 20 ms allowed the untrapped atoms to escape. Then, we could either characterize the trapped sample by absorption imaging, perform pump–probe spectroscopy to measure transmission, Bragg reflection and phase-conjugate reflection spectra, or shine only the pump beams to observe the emitted light. When the phase-conjugate reflectivity was measured without lattice (Fig. 3), the lattice was switched off with a mechanical shutter in 130 μs and the atoms freely expanded for 1 ms before measurements. This time of flight was large enough to completely smooth out the ordered structure and small enough to keep the optical thickness constant. All the stages following the initial MOT loading lasted only a few milliseconds, so the total cycle duration was not much longer than 1 s. The repetition rate was thus ~ 1 Hz, which allowed quick averaging over many realizations.

Detection tools. To measure the phase-conjugate reflectivity, we used APDs and obtained spectra by sweeping the probe frequency with an acousto-optic modulator in double-pass configuration. Because the probe power fluctuated during the sweep, the recorded reflected intensity was divided by a reference intensity recorded simultaneously with another APD illuminated by part of the probe beam. The relative sensitivity of both APDs was calibrated with a 10% uncertainty due to thermal drifts.

To observe the transverse mode of the OPO (cross-section images shown in Fig. 2), we used a CCD camera. The beam was first reflected off a mirror, which was pierced to allow the lattice beam to go through (Fig. 1), and then collimated and refocused 50 cm later on the camera. This allowed us to image the whole beam, and also to use several small black masks mounted on thin glass plates to get rid of stray reflections of the lattice beam on the vacuum chamber windows, which focused at intermediate distances. The angle calibration used the probe beam, which could also be imaged on the camera, as a reference. The incident angle of the probe beam was precisely determined using a series of Bragg reflection spectra off the passive lattice. When the spectra were symmetric, the probe angle fulfilled $\cos \theta = \lambda_0/\lambda_{\text{dip}}$ (ref. 15).

Received 7 July 2011; accepted 14 November 2011;
published online 18 December 2011

References

- Special issue on Nano and Random Laser. *J. Opt.* **12**, 020201–024014 (2010).
- Wiersma, D. S. The physics and applications of random lasers. *Nature Phys.* **4**, 359–367 (2008).
- Noda, S. Photonic crystal lasers – ultimate nanolasers and broad-area coherent lasers. *J. Opt. Soc. Am. B* **27**, B1–B8 (2010).
- Conti, C. & Fratallocchi, A. Dynamic light diffusion, three-dimensional Anderson localization and lasing in inverted opals. *Nature Phys.* **4**, 794–798 (2008).
- Mahler, L. *et al.* Quasi-periodic distributed feedback laser. *Nature Photon.* **4**, 165–169 (2010).
- Noh, H. *et al.* Control of lasing in biomimetic structures with short-range order. *Phys. Rev. Lett.* **106**, 183901 (2011).
- Kogelnik, H. & Shank, C. V. Stimulated emission in a periodic structure. *Appl. Phys. Lett.* **18**, 152–154 (1971).
- Yariv, A. *Quantum Electronics* 3rd edn (Wiley, 1988).
- Gottardo, S. *et al.* Resonance-driven random lasing. *Nature Photon.* **2**, 429–432 (2008).

10. Guerin, W., Michaud, F. & Kaiser, R. Mechanisms for lasing with cold atoms as the gain medium. *Phys. Rev. Lett.* **101**, 093002 (2008).
11. Vrijnsen, G., Hosten, O., Lee, J., Bernon, S. & Kasevich, M. A. Raman lasing with a cold atom gain medium in a high-finesse optical cavity. *Phys. Rev. Lett.* **107**, 063904 (2011).
12. Labeyrie, G. *et al.* Slow diffusion of light in a cold atomic cloud. *Phys. Rev. Lett.* **91**, 223904 (2003).
13. Froufe-Pérez, L. S., Guerin, W., Carminati, R. & Kaiser, R. Threshold of a random laser with cold atoms. *Phys. Rev. Lett.* **102**, 173903 (2009).
14. Guerin, W. *et al.* Towards a random laser with cold atoms. *J. Opt.* **12**, 024002 (2010).
15. Schilke, A., Zimmermann, C., Courteille, P. W. & Guerin, W. Photonic band gaps in one-dimensionally ordered cold atomic vapors. *Phys. Rev. Lett.* **106**, 223903 (2011).
16. Abrams, R. L. & Lind, R. C. Degenerate four-wave mixing in absorbing media. *Opt. Lett.* **2**, 94–96 (1978); erratum **3**, 205 (1978).
17. Leite, M. R. R., Simoneau, P., Bloch, D., Le Boiteux, D. & Ducloy, M. Continuous-wave phase-conjugate self-oscillation induced by Na-vapour degenerate four-wave mixing with gain. *Europhys. Lett.* **2**, 747–753 (1986).
18. Pinard, M., Grandclement, D. & Grynberg, G. Continuous-wave self-oscillation using pair production of photons in four-wave mixing in sodium. *Europhys. Lett.* **2**, 755–760 (1986).
19. Lezama, A., Cardoso, G. C. & Tabosa, J. W. R. Polarization dependence of four-wave mixing in a degenerate two-level system. *Phys. Rev. A* **63**, 013805 (2000).
20. Vallet, M., Pinard, M. & Grynberg, G. Generation of twin photon beams in a ring four-wave mixing oscillator. *Europhys. Lett.* **11**, 739–744 (1990).
21. Inoue, K., Mukai, T. & Saitoh, T. Nearly degenerate four-wave mixing in a traveling-wave semiconductor laser amplifier. *Appl. Phys. Lett.* **51**, 1051–1053 (1987).
22. Mecozzi, A., D'Ottavi, A. & Hui, R. Nearly degenerate four-wave mixing in distributed feedback semiconductor lasers operating above threshold. *IEEE J. Quantum. Electron.* **29**, 1477–1487 (1993).
23. McGloin M. & Dholakia, K. Bessel beams: diffraction in a new light. *Contemp. Phys.* **46**, 15–28 (2004).
24. Zibrov, A. S., Lukin, M. D., Hollberg, L. & Scully, M. O. Efficient frequency up-conversion in resonant coherent media. *Phys. Rev. A* **65**, 051801(R) (2002).
25. Schultz, J. T. *et al.* Coherent 455 nm beam production in a cesium vapor. *Opt. Lett.* **34**, 2321–2323 (2009).
26. Akulshin, A. M., McLean, R. J., Sidorov, A. I. & Hannafor, P. Coherent and collimated blue light generated by four-wave mixing in Rb vapour. *Opt. Express* **17**, 22861–22870 (2009).
27. Vernier, A., Franke-Arnold, S., Riis, E. & Arnold, A. S. Enhanced frequency up-conversion in Rb vapor. *Opt. Express* **18**, 17020–17026 (2010).
28. Antezza, M. & Castin, Y. Fano–Hopfield model and photonic band gaps for an arbitrary atomic lattice. *Phys. Rev. A* **80**, 013816 (2009).
29. Zimmermann, C., Vuletic, V., Hemmerich, A., Ricci, L. & Hänsch, T. W. Design for a compact tunable Ti:sapphire laser. *Opt. Lett.* **20**, 297–299 (1995).

Acknowledgements

The authors acknowledge support from the Alexander von Humboldt foundation, the Deutsche Forschungsgemeinschaft (DFG) and the Research Executive Agency (program COSCALI, no. PIRSES-GA-2010-268717).

Author contributions

A.S. and W.G. performed the experiment and analysed the data, W.G. supervised the project and wrote the paper. All authors discussed the results and commented on the manuscript.

Additional information

The authors declare no competing financial interests. Supplementary information accompanies this paper at www.nature.com/naturephotonics. Reprints and permission information is available online at <http://www.nature.com/reprints>. Correspondence and requests for materials should be addressed to W.G.

Optical Parametric Oscillation with Distributed Feedback in Cold Atoms (Supplementary information)

Alexander Schilke,¹ Claus Zimmermann,¹ Philippe W. Courteille,² and William Guerin^{1,*}

¹Physikalisches Institut, Eberhard-Karls-Universität Tübingen, Auf der Morgenstelle 14, D-72076 Tübingen, Germany

²Instituto de Física de São Carlos, Universidade de São Paulo, 13560-970 São Carlos, SP, Brazil

*e-mail: william.guerin@pit.uni-tuebingen.de

Beat note experiment

To determine the frequency of the emitted radiation, respectively to the pump frequency, we use our probe beam as a local oscillator and perform a beat note experiment.

Both beams are phase-locked together through an injection locking, which allows the resolution of very narrow spectral features. However, both beams pass through different double-pass acousto-optic modulators (AOMs) to allow us to sweep their frequencies. Standard AOM drivers suffer from thermal drifts and thus do not provide a kHz precision. As a consequence, for this beat-note experiment, we use two signal generators (Rohde & Schwarz SMR20) to drive the AOMs with a well-defined frequency difference of $f_0/2 = 150$ kHz (because of the double-pass configuration, the frequency difference between both laser is $f_0 = 300$ kHz).

We overlap the probe beam on one of our detection photodiodes and record the temporal trace of the emitted radiation beating with the probe. We generate the Fourier transform of this signal with a digital oscilloscope and we average this power spectrum $S(f)$ over many realizations. We observe a peak around f_0 (inset of Fig. S1), whose precise position gives the relative frequency shift δf between the pump beam and the emitted radiation. The precision of the measurement is limited by the duration of the OPO.

Even though the most efficient configuration for four-wave mixing is when all waves are degenerate, we observe a non-zero frequency difference. This can be explained by the role of the refractive index, which provides the feedback, and whose value is not necessarily maximum at the pump frequency. The resulting working frequency of the OPO comes thus from a trade-off between the gain efficiency and the feedback efficiency.

We measured the frequency difference δf for different pump powers and observe a linear drift (Fig. S1), which is consistent with a broadening of pump-induced spectral structures.

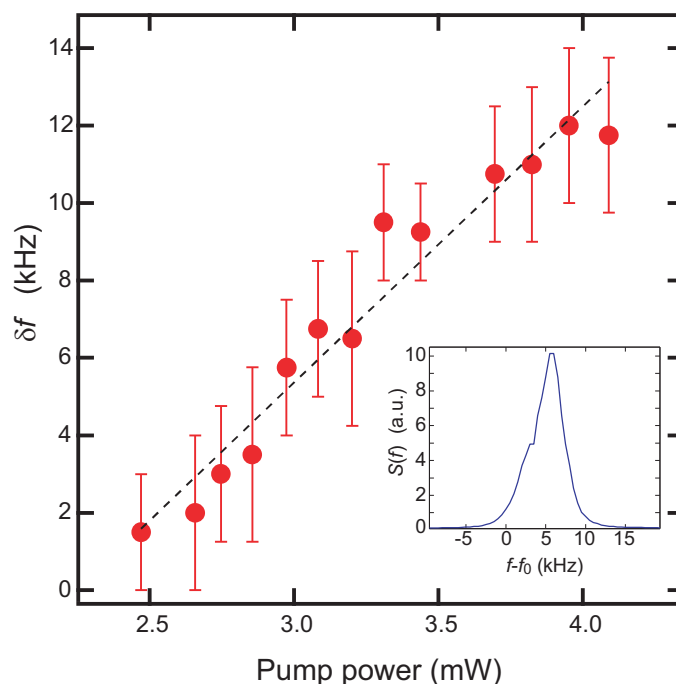


Fig. S1: Beat note experiment. Red dots: frequency difference δf between the pump and the emitted radiation, as a function of the pump power. We observe a linear frequency drift (dashed line). Inset: example of measured spectrum. The error bars of the main panel correspond to the peak width (FWHM) of the beat-note spectrum.

III.2.3. Mode structure: numerical investigations

In this section I include some unpublished calculations on the mode structure of our DFB OPO¹. DFB lasers with standard gain can be modeled by coupled-wave equations [Kogelnik 1971, Kogelnik 1972, Yariv 1988]. FWM is also usually modeled by coupled-wave equations [Abrams 1978, Nilsen 1979, Yariv 1977, Yariv 1988]. It is thus quite simple to combine the two within the same formalism. To the best of my knowledge², the combination of DFB and degenerate FWM has not been previously studied in the literature. The closest system that has been studied is a DFB OPO based on a largely-nondegenerate backward parametric gain [Huang 2005]. In this situation, the signal and idler waves have different wavelengths and only one of them is close to the Bragg condition and undergoes DFB. On the contrary, in the system considered here, both waves are Bragg-reflected by the DFB structure. Moreover, the phase-matching condition for FWM is always fulfilled. This has dramatic consequences on the mode structure, which becomes continuous.

III.2.3.1. Principle

The different waves to consider are sketched in Fig. III.3. The incident probe wave is A_1 , the Bragg reflected wave is A_2 , the phase-conjugated reflected wave, generated by FWM, is A_3 , and a fourth wave A_4 is created by the combination of FWM and Bragg reflection (we have indeed observed it when the probe had the good frequency and angle). In a pump-probe experiment, the measurable signals are

$$T = \left| \frac{A_1(L)}{A_1(0)} \right|^2, \quad R_{\text{Bragg}} = \left| \frac{A_2(0)}{A_1(0)} \right|^2, \quad R_{\text{FWM}} = \left| \frac{A_3(0)}{A_1(0)} \right|^2, \quad S = \left| \frac{A_4(L)}{A_1(0)} \right|^2. \quad (\text{III.2})$$

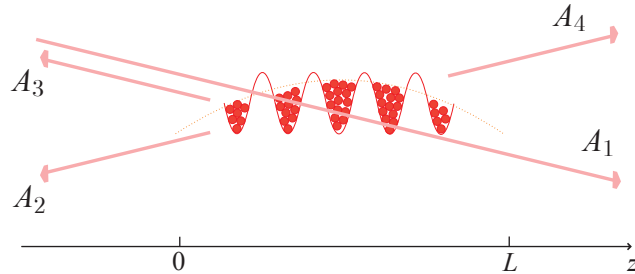


Figure III.3: Waves to consider for a theoretical modeling.

In a theoretical modeling, each wave fulfills a propagation equation with some coupling terms: A_1 and A_2 are coupled via Bragg reflection, A_3 and A_4 too, A_1 and A_3 are coupled via FWM, A_2 and A_4 too. Moreover, we have the following boundary conditions: $A_1(0) = 1$, $A_2(L) = 0$, $A_3(L) = 0$, $A_4(0) = 0$. These conditions are appropriate for a pump-probe experiment. Reaching a laser threshold means that the output signals are nonzero even with $A_1(0) = 0$. Numerically, we need a nonzero incoming wave and see a divergence of the other signals.

In the following I first investigate the situation without FWM, with only standard gain. I should recover the same results as in standard DFB lasers [Kogelnik 1971, Kogelnik 1972, Yariv 1988]. In that case, the only coupling term comes from Bragg reflection, and the

¹ I did this study in 2012 during my last months in Tübingen. I initially had the ambition of publishing it somehow, but I never took the time... I'm thus happy to put it here.

² The literature on DFB lasers is huge, with a lot of technical papers, so I cannot guarantee that I didn't miss anything.

four-wave system can be decomposed into two independent, uncoupled two-wave systems: A_1 and A_2 on one side, and A_3 and A_4 on the other side. Thus, I consider only A_1 and A_2 . Then I treat FWM only. Here also, the system simplifies to two independent two-wave systems, and I only consider A_1 and A_3 . Finally, I consider both effects together with the complete four-wave system.

III.2.3.2. Coupled-wave model of DFB

The coupled-wave theory has been first developed and used for DFB lasers by Kogelnik [Kogelnik 1972, Kogelnik 1971]. The coupled equations read:

$$\frac{dA_1}{dz} = -(\beta - i\delta)A_1 + i\kappa A_2, \quad (\text{III.3})$$

$$\frac{dA_2}{dz} = (\beta - i\delta)A_2 - i\kappa A_1. \quad (\text{III.4})$$

In these equations, A_1 and A_2 are the forward and backward propagating components of the total fields, defined with the Bragg wavevector, which means that if the actual incident wavevector do not fulfill exactly the Bragg condition, the A_1 and A_2 components undergo an additional phase-shift. This is the role of the δ parameter, which quantifies the shift from the Bragg condition. The parameter β is the gain/loss coefficients³ (negative in case of gain), and κ is the coupling constant, proportional to the index modulation amplitude. These parameters are related to the experimental ones by:

$$\delta = \text{Re}(\bar{n}) k_0 - k_{\text{lat}}, \quad (\text{III.5})$$

$$\beta = \text{Im}(\bar{n}) k_0, \quad (\text{III.6})$$

$$\kappa = \Delta n k_0 / 2, \quad (\text{III.7})$$

where \bar{n} and Δn are respectively the average and amplitude modulation of the *complex* refractive index $n(z) = \bar{n} + \Delta n \cos(2k_{\text{lat}}z)$, $k_0 = 2\pi/\lambda_0$, $k_{\text{lat}} = 2\pi/\lambda_{\text{lat}}$ and λ_0 , λ_{lat} are the wavelengths of the atomic transition and the lattice, respectively. In Eqs. (III.3-III.4), the term $(\beta - i\delta)$ could be replaced directly by $-i(\bar{n}k_0 - k_{\text{lat}})$. Taking into account a nonzero incident angle θ is done by replacing k_0 by $k_0 \cos \theta$.

It should be noted that in this model, I have to suppose that the density pattern is sinusoidal, while the experimental distribution is Gaussian. I have checked that using a sinusoidal density with the largest possible contrast, i.e. $\Delta n = \bar{n} - 1$, still slightly underestimates the Bragg reflection.

We can also rewrite the parameters with the number of layers N , the atomic polarizability α , the average density ρ and the shift from the geometric Bragg condition $\Delta\lambda_{\text{lat}} = \lambda_{\text{lat}} - \lambda_0/\cos(\theta)$:

$$\delta L = \pi N [\rho \text{Re}(\alpha) / 2 + \Delta\lambda_{\text{lat}} / \lambda_{\text{lat}}], \quad (\text{III.8})$$

$$\beta L = \pi N \rho \text{Im}(\alpha) / 2, \quad (\text{III.9})$$

$$\kappa L = \pi N \rho \alpha / 4, \quad (\text{III.10})$$

where all coefficients are now dimensionless (i.e. normalized by the lattice length L).

These equations can be numerically solved quite efficiently (using some linear algebra, especially to take into account the boundary conditions, which are not simple initial-value

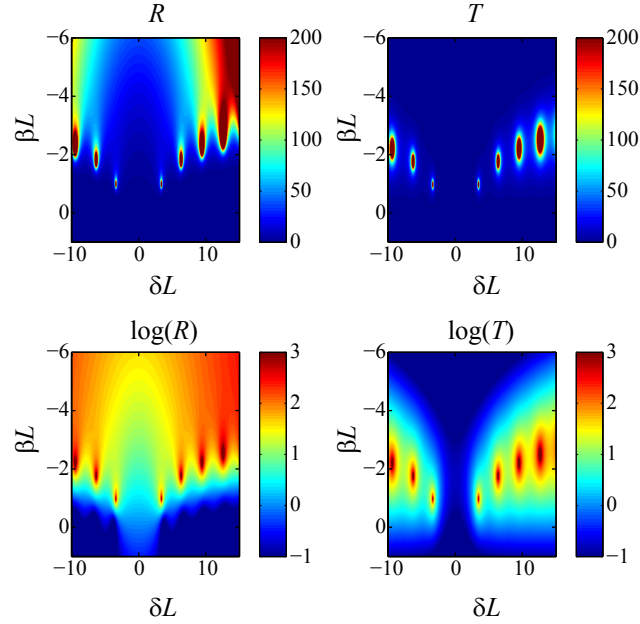


Figure III.4: Modes of a DFB laser with $\kappa L = 2$ (refractive index contrast). The parameters βL and δL quantify the gain and the Bragg condition governing the emission wavelength (in standard DFB lasers) or the emission angle (in our case).

conditions) and the results for the reflection and transmission coefficients as a function of the parameters βL and δL are shown in Fig. III.4.

One recovers the classical result for a simple DFB structure (a similar figure can be found in [Yariv 1988]). The degeneracy between the two lowest-threshold modes can be lifted by adding a $\pi/2$ phase shift in the middle of the structure or some partial reflection on the facets or by using a modulated gain instead of a modulated refractive index.

III.2.3.3. Coupled-wave model of FWM

Many papers [Abrams 1978, Nilsen 1979, Yariv 1977, Boyd 1981] and textbooks (e.g. [Yariv 1988]) treat the FWM problem. The standard approach is to start from the Helmholtz equation with the nonlinear polarization as a source term, neglect the depletion of the pump fields, then replace the electric fields $E_i = A_i e^{i(\omega_i t - \mathbf{k}_i \cdot \mathbf{r}_i)}$ by their complex amplitudes A_i , use the slowly-varying-envelope approximation and at the end, we obtain two coupled equations for the probe and conjugated waves (here, waves A_1 and A_3 , and the same for A_2 and A_4 , see Fig. III.3):

$$\frac{dA_1^*}{dz} = -\beta'^* A_1^* + i\gamma A_3 e^{i\Delta k z}, \quad (\text{III.11})$$

$$\frac{dA_3}{dz} = \beta' A_3 + i\gamma^* A_1^* e^{-i\Delta k z}. \quad (\text{III.12})$$

Here, $\beta' = -ink_0$ with n the complex refractive index, i.e. it plays the role of $(\beta - i\delta)$ previously, but there is no lattice any more. Note also that if we are only interested in the intensities (and not the phases), the results are independent of the real part of the refractive index, only the imaginary part (linear gain/absorption coefficients, like the previous β) plays a role. The γ is the coupling term due to FWM. The terms with Δk provide the phase-matching condition, and I will forget it in the following ($\Delta k = 0$), since I suppose that

³ α is used in [Kogelnik 1971] but I want to keep it for the atomic polarizability.

there is no angle between the conjugated waves (A_1 and A_3 perfectly collinear). I suppose also that the two waves are degenerate. If it were not the case, I should use different β' and γ for each wave, since these coefficients depend on the frequency.

The expression of the FWM coupling terms are [Boyd 1981]:

$$i\gamma_i^* = -\frac{k_0}{2}\rho\alpha_{\text{NL}}(\omega_i)A_{\text{P1}}A_{\text{P2}}, \quad (\text{III.13})$$

where α_{NL} is the nonlinear part of the atomic polarizability and $A_{\text{P1}}, A_{\text{P2}}$ are the amplitude of the two pump fields. I am not aware of any analytical expression for this nonlinear polarizability, which includes the effect of the polarization and Zeeman degeneracy. These effects cannot be neglected, because considering only a two-level atom would simulate the situation of parallel pump and probe polarizations. On the contrary, we use orthogonal polarizations, which leads to much more efficient FWM [Lezama 2000]. Thus, in practice, γ can be empirically determined from the FWM efficiency observed in the experiment, this is not a known *ab initio* parameter.

Here again there are simple analytical formulas for the results [Abrams 1978]. A remarkable result is that as soon as we're interested only in intensities (and not on phases), the results depend only on $|\gamma|^2$. It shows also, for example, that with $\beta' = 0$ (no gain nor losses from the linear part of the polarizability), we have $T = R + 1$, so that there is a net energy gain from FWM (and for each pump photon going in A_1 , there is another one going in A_3). Also, a very important result is that there is a self-oscillation threshold that is reached for $|\gamma|L = \pi/2$ with $\beta' = 0$. This self-oscillation, sometime called MOPO (mirrorless parametric oscillator) has been studied a long time ago with hot vapors [Grynberg 1988a, Grynberg 1988b] and recently with cold atoms [Mei 2017, Lopez 2019]. In our case, we expect to find that the addition of DFB significantly lowers the threshold condition.

III.2.3.4. Coupled-wave model of DFB and FWM together

We now combine DFB and FWM together, with the four considered waves [Fig. III.3]:

$$\frac{dA_1}{dz} = -(\beta - i\delta)A_1 + i\kappa A_2 - i\gamma^* A_3^*, \quad (\text{III.14})$$

$$\frac{dA_2}{dz} = (\beta - i\delta)A_2 - i\kappa A_1 + i\gamma^* A_4^*, \quad (\text{III.15})$$

$$\frac{dA_3}{dz} = (\beta - i\delta)A_3 - i\kappa A_4 + i\gamma^* A_1^*, \quad (\text{III.16})$$

$$\frac{dA_4}{dz} = -(\beta - i\delta)A_4 + i\kappa A_3 - i\gamma^* A_2^*. \quad (\text{III.17})$$

To solve this system, one actually has to consider a system of 8 equations for the 4 fields and their conjugate. The measurable quantities are those defined in Eq. (III.2) with the boundary conditions given below Eq. (III.2).

Results in the case $\beta = 0$, i.e. lossless and gain-less, are shown in Fig. III.5. The x -axis is δ , i.e. the detuning from the geometric Bragg condition (which gives usually the frequency of the lasing mode, for us the angle), and the y -axis is now the FWM coupling coefficient γ . Each row is for a different value of κ , the Bragg coupling coefficient. The first row ($\kappa = 0$) thus corresponds to FWM without DFB: it show the expected self-OPO at $\gamma L = \pi/2 \pm \pi$ [Abrams 1978]. Then the figure shows what happens when one progressively increases the DFB modulation κ .

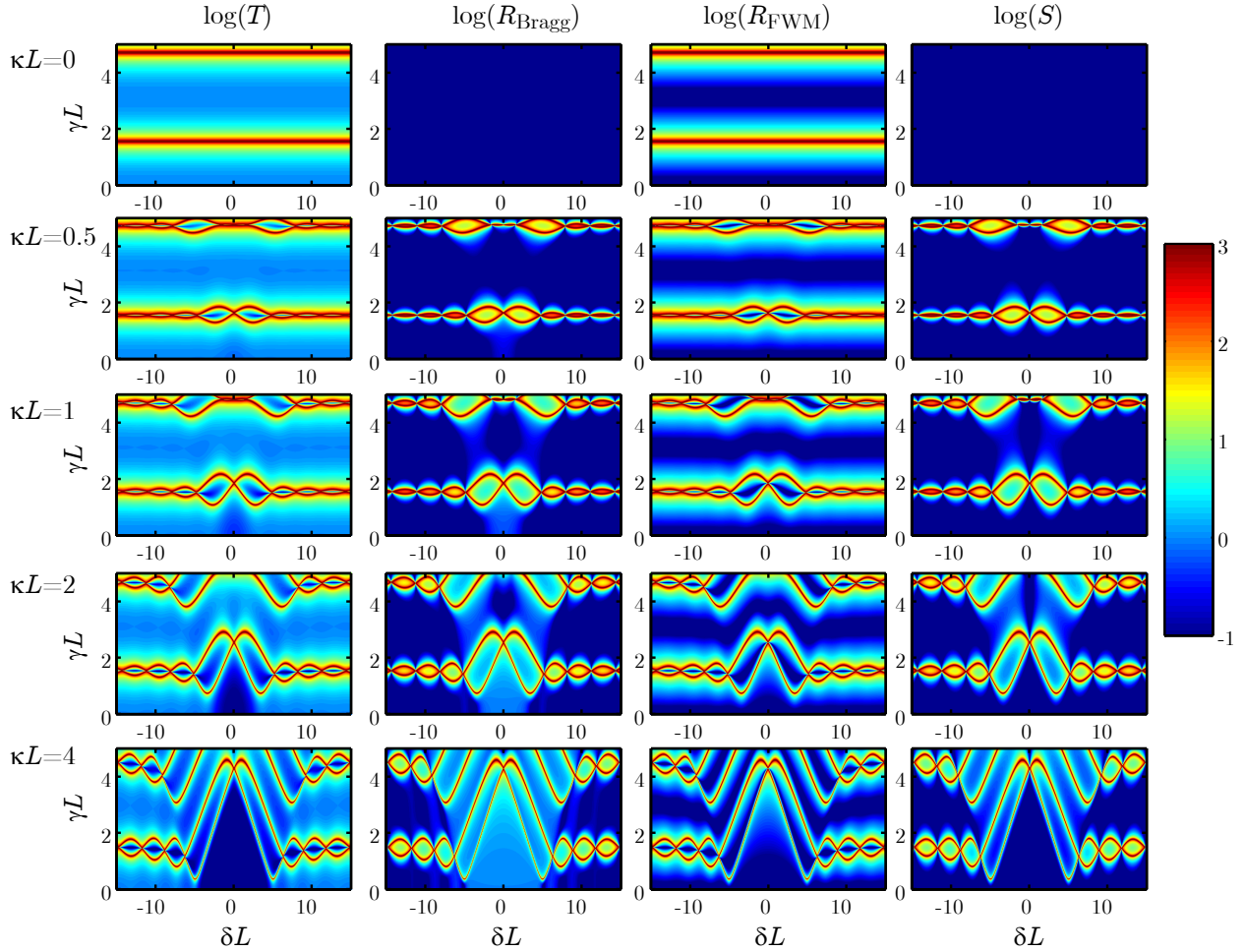


Figure III.5: Results of the system of 4 coupled-equations for $\beta = 0$ (lossless and gain-less). We scan the (δ, γ) space, for 5 different values of the Bragg coupling coefficient κ (upper row: $\kappa = 0$, no Bragg reflection). δ parameterizes the Bragg condition and γ the strength of FWM. Note the logarithmic color scale.

We observe that DFB induces a progressive deformation of the self-OPO mode, giving rise to a continuous ‘mode curve’, instead of another, disconnected supplementary discrete mode, like for a standard DFB laser.

Let us now add gain ($\beta < 0$) and see how one goes from a DFB OPO to a DFB laser with standard gain. Since all results are symmetric with respect to δ , I only show the $\delta > 0$ part. Also, since all measurable quantities (T , S , R_{Bragg} , R_{FWM}) give qualitatively similar results, I only show one of them (T).

First I show in Fig. III.6 the mode structure for a given value of the Bragg coupling coefficient $\kappa L = 2$ and for increasing gain (the first panel with $\beta = 0$ is the same as the [4th row, 1st column] panel of Fig. III.5). With gain, the ‘mode curves’ get lower, which means that the necessary threshold for the FWM coefficient is lower, and it can even reach zero, when the mode curves touch the x -axis. This happens at discrete values of δ : we recover the standard DFB laser modes.

One can also look the other way around, i.e. start from the DFB laser modes and see what happens when we progressively add FWM. This is what I show in Fig. III.7, in which the first panel, without FWM ($\gamma = 0$), is identical to the standard DFB laser modes of Fig. III.4. Then,

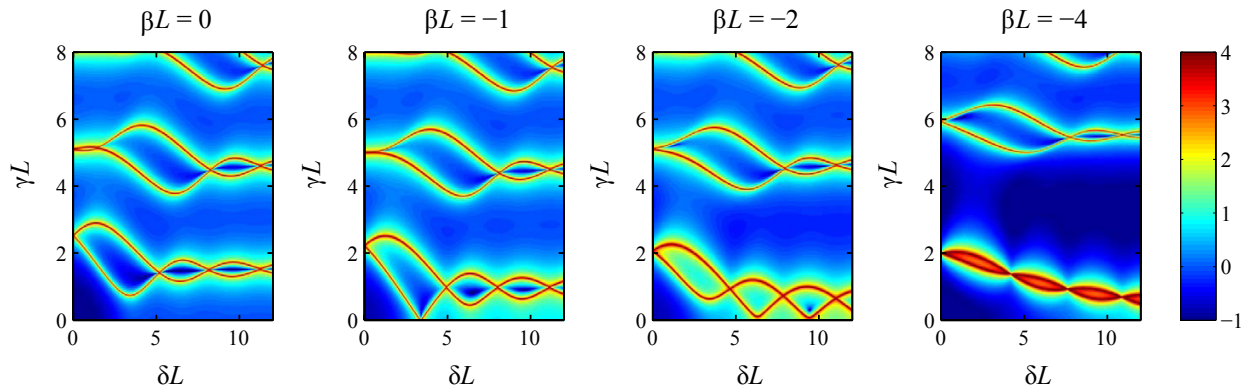


Figure III.6: Mode structure for a fixed Bragg coupling coefficient $\kappa L = 2$ and an increasing linear gain β (< 0 for gain). As in the previous figure we scan the (δ, γ) space.

the discrete modes [points in the (δ, β) space], become continuous (circles), and ultimately reach the $\beta = 0$ axis (no gain), corresponding to the DFB-OPO without linear gain.

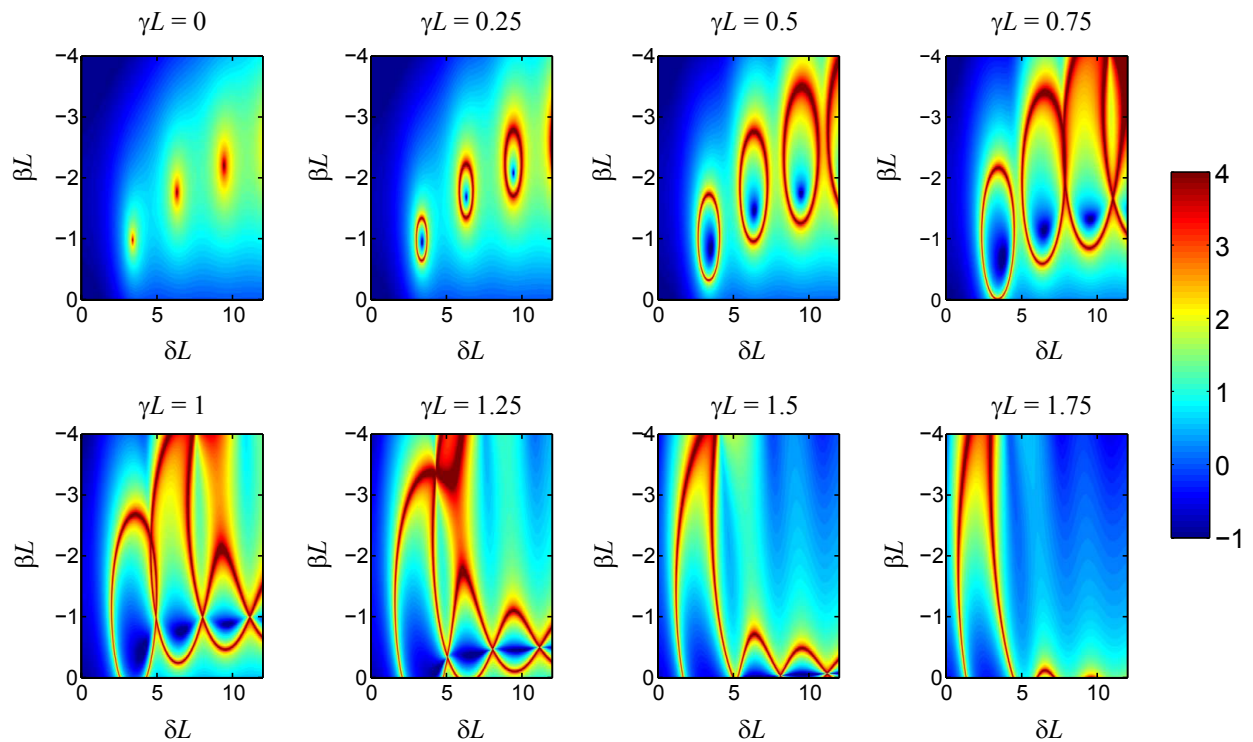


Figure III.7: Mode structure for a fixed Bragg coupling coefficient $\kappa L = 2$ and an increasing FWM coefficient γ . Unlike in the two previous figures, here we scan the (δ, β) space, like in Fig. III.4.

III.2.3.5. Discussion

The remarkable result is that the DFB OPO appears progressively as a deformation of the self-OPO and not as a disconnected supplementary mode. It doesn't give a discrete mode, but a continuous 'mode curve'. This is not obvious because the threshold condition is, like for normal DFB lasers, a complex equation (the determinant of the matrix describing the set of linear differential equations should be zero), so that we need *a priori* two variables to fulfill it. Here, once three parameters are fixed (for instance δ, κ, β), the threshold equation is fulfilled for a whole continuous range of the fourth parameter (here γ). Note that this is already the

case for the OPO self-oscillation, even with losses [Abrams 1978]. Somehow, it is the power and magic of FWM, which provides parametric gain and simultaneously an automatically resonant feedback. Similarly, it is well known that inserting a phase-conjugation mirror in an optical cavity makes it stable [Lind 1981].

In the experiment, we didn't observe the self-OPO, which means that we always had $\gamma L < \pi/2$. Actually, one can evaluate the parameter γL from the phase-conjugate reflectivity measured without the lattice, and one can evaluate κL from the Bragg reflectivity without FWM. Unfortunately, we don't have those measurements in the precise exact conditions of the DFB-OPO data, but one can still, from our experimental parameters and calibrations, give rough evaluations. We obtain that the lasing threshold is around $\gamma L \simeq 0.6$ with $\kappa L \simeq 1.4$. The experimental threshold is actually lower than predicted by the model with $\beta = 0$. This means that, either the Raman gain helps a little, or we underestimate the Bragg coupling because of the Gaussian atomic density distribution in the wells (instead of a sinusoidal modulation in the model).

Also, in the experiment, we measured the lasing frequency with a beat-note and observed that it was slightly detuned, by only a few kHz, from the pump frequency. It means that we should not consider perfectly degenerate FWM. Then, if the laser frequency is ω_1 and the pump frequency is ω_P , the conjugated wave, created by FWM, is at the frequency $\omega_2 = 2\omega_P - \omega_1$! As a consequence, we should in fact consider 8 waves, with a wave at ω_1 and a wave at ω_2 for each emission direction. But then, should not the laser be multimode? In the beat-note experiment, we observed only one frequency. It means that the threshold of both waves are different, which could be due to the very steep dispersion of the Raman gain structure. In the temporal trace, we sometimes observed oscillations, but it was not well repeatable. It might depend on the precise value of the parameters. However, I find highly non-intuitive that it can be only single-mode since the two modes are strongly coupled by FWM, and the complete 'feedback loop' of one mode passes through the other mode. It seems however that this situation was already observed in FWM experiment with hot vapors [Vallet 1990].

Finally, it would be very interesting to quantize this coupled-wave model, similarly to what has been done for other MOPO systems [Gatti 2017]. This would allow us to compute if quantum correlations are expected between the different emission directions. We already have detected strong classical correlations and it is well known that FWM can be used to produce 'twin beams' (with hot [Vallet 1990] or cold [Du 2007] atoms), so the question of quantum correlations in our system is totally open.

Concluding remarks

This mirrorless DFB parametric oscillator may have a limited practical interest, nevertheless I like this experiment very much. First it was a nice surprise that it worked so well. I had anticipated the problem of the Bragg angle making the feedback unstable, but I hadn't anticipated that FWM would solve the problem so easily. Moreover, the properties of this DFB laser is definitely different from those of standard DFB lasers, and this is due to the peculiarities of cold atoms as mentioned in the introduction of Part One.

Indeed in a standard DFB laser, tuning the periodicity allows tuning the wavelength, because the gain curve is very broad. Here the gain curve is extremely narrow and determines the emission frequency, and tuning the periodicity such that the Bragg condition can only be fulfilled with an angle creates a cone-shaped emission. This works only because of the very large nonlinearity and the versatility of cold atoms: by just adding a counterpropagating beam one completely changes the atomic response, making FWM appear, which makes the

feedback stable. So, this experiment is a very nice illustration that applying well-known concepts (DFB lasers) to new systems (cold atoms) allows discoveries.

CHAPTER IV

Random laser with cold atoms

For random lasing the idea is to combine gain and multiple scattering, which provides the necessary feedback. I'm using the opportunity of this chapter to add a first section giving some introduction about multiple scattering and light transport in disordered atomic vapors, as it is useful for understanding the rest of the manuscript. It includes the brief description of some experiments in which I was not involved [Labeyrie 2003, Labeyrie 2004]. The text is taken from [Baudouin 2014a] with little adaptation.

Then in section IV.2 I discuss our work on the threshold condition for random lasing and the subsequent quantitative comparisons to determine the best gain mechanism. Finally I present our observation of a signature of random lasing in our system (section IV.3).

IV.1. Light transport in disordered atomic vapors

A diffusion equation for the propagation of light has been used as early as 1922 by Compton to describe the transport of light in an atomic vapor [Compton 1922, Compton 1923]. Soon afterwards, however, pioneering experiments by Zemansky on the decay of the fluorescence emitted by an initially excited mercury vapor have shown a deviation from the prediction of such a diffusion model [Zemansky 1927]. It was then realized by Kenty that the frequency shift induced by scattering in a Doppler-broadened medium leads to lower excitation probabilities for photons with frequencies far from the center of the atomic resonance [Kenty 1932]. Indeed photons far from the atomic resonance can propagate over larger distances and the escape from a finite-size system cannot be described with a diffusion equation. Later, Holstein proposed an integro-differential equation to describe the transport of light taking into account the step-length distribution of the photons [Holstein 1947]. For photons at fixed frequency, this step-length distribution is an exponentially decreasing function, with well-defined mean free path and higher moments. For the diffusion model to fail, a divergence of the second moment of the step-length distribution is required. Kenty and Holstein showed that if the frequency of the photons inside the atomic vapor follows a Gaussian distribution (motivated by the Gaussian velocity distribution of the atoms) the step-length distribution of the photons has a divergent second moment, consistent with the observations of Zemansky.

In cold atoms, frequency redistribution can be neglected in most situations and light transport can be described by a diffusion equation. On the contrary, in room-temperature ('hot') vapors, frequency redistribution changes drastically the transport properties. This is what gives rise to Lévy flights and superdiffusive transport [Pereira 2004, Mercadier 2009, Baudouin 2014b].

IV.1.1. Resonant scattering in cold atoms

Some basics of multiple scattering in cold atoms can be found in [Kaiser 2000] and some more evolved theoretical concepts in [Lagendijk 1996, de Vries 1998]. For this section, we only need to consider the atoms as point-like dipoles. Then, for a two-level atom probed by a weak, monochromatic laser, the elastic scattering cross-section is given by

$$\sigma_{\text{sc}}(\delta) = \frac{\sigma_0}{1 + 4\delta^2/\Gamma^2}, \quad (\text{IV.1})$$

where δ is the detuning between the incident light and the atomic transition, Γ is the linewidth of the transition, and $\sigma_0 = 6\pi/k_0^2 = 3\lambda^2/2\pi$ is the on-resonance scattering cross-section, with $\lambda = 2\pi/k_0$ the wavelength of the transition¹. All experiments discussed in this manuscript have been performed with rubidium, with $\lambda = 780$ nm (D₂ line) and $\Gamma/2\pi = 6.1$ MHz. Another important quantity is the mean-free-path ℓ_{sc} between two scattering events, given by

$$\ell_{\text{sc}} = \frac{1}{\rho\sigma_{\text{sc}}}, \quad (\text{IV.2})$$

where ρ is the atomic density. Still considering only a weak probe beam and no external pump laser, there is no inelastic scattering nor absorption or amplification. The attenuation of the beam propagating in the medium is thus only due to elastic scattering, and the transmission T in a homogeneous sample of length L is given by

$$T = e^{-\rho\sigma_{\text{sc}}L} = e^{-L/\ell_{\text{sc}}}. \quad (\text{IV.3})$$

The quantity $b = \rho\sigma_{\text{sc}}L = L/\ell_{\text{sc}}$ is called the optical thickness (or depth) and quantifies how much the medium is opaque, or diffusive. Typically, when $b \gg 1$, i.e. $L \gg \ell_{\text{sc}}$, light is in the multiple-scattering regime. Obviously, a similar relation as Eq. (IV.1) holds also for the optical thickness, and we often use the on-resonance optical thickness $b_0 = \rho\sigma_0L$ of the atomic cloud to characterize the diffusive power or the ‘size’ of our sample. Equation (IV.1) shows immediately an important advantage of working with cold atoms, namely the ability to change the scattering cross-section by simply detuning the probe laser from a few megahertz. In particular, it allows us to measure the on-resonance optical thickness from a transmission spectrum even if the optical thickness is very high [Labeyrie 2004].

IV.1.2. Light diffusion in cold atoms

Random walk of particles in a disordered medium is often well described by a diffusion equation, characterized by a linear increase in time of the mean square displacement of the particles: $\langle r^2 \rangle = Dt$, with D the diffusion coefficient. One assumption for the diffusion equation to hold is that the size ℓ of each step of the random walk follows a probability distribution $P(\ell)$ with a finite second moment $\langle \ell^2 \rangle$, allowing the application of the central limit theorem.

Considering photons undergoing only elastic scattering off atoms at rest, the distribution of the step length between two scattering events is exponential, i.e.,

$$P(\ell) = \frac{1}{\ell_{\text{sc}}} e^{-\ell/\ell_{\text{sc}}}, \quad (\text{IV.4})$$

where ℓ_{sc} is the mean free path, as defined above. The condition to apply the central limit theorem is fulfilled and, after a large number of steps, the light-intensity (or energy density)

¹ Note that for a scalar model of light, the scattering cross section is given by $\sigma_0 = \lambda^2/\pi$.

distribution in the medium converges towards a Gaussian distribution, whose width increases linearly with the square root of time. This process is described by the diffusion equation (without source nor absorption/amplification in the medium)

$$\frac{\partial W(\mathbf{r}, t)}{\partial t} = D \nabla^2 W(\mathbf{r}, t), \quad (\text{IV.5})$$

where W is the energy density, v is the transport velocity inside the medium, and D is the diffusion coefficient given by

$$D = \frac{\ell_t^2}{3\tau} = \frac{v \ell_t}{3}, \quad (\text{IV.6})$$

with τ the transport time, ℓ_t the transport length and $v = \ell_t/\tau$ the energy transport velocity. The transport length is related to the mean free path by

$$\ell_t = \frac{\ell_{\text{sc}}}{1 - \langle \cos \theta \rangle}, \quad (\text{IV.7})$$

where $\langle \cos \theta \rangle$ is the average cosine of the scattering angle. With atoms and in the absence of longitudinal polarization or magnetic field, there is in average as much scattering in the forward direction as in the backward direction, so $\langle \cos \theta \rangle = 0$ and $\ell_t = \ell_{\text{sc}}$.

IV.1.2.1. Diffuse transmission and reflection

A first characterization of light diffusion in cold atoms can be obtained in a static experiment, by measuring the diffuse transmission and reflection [Labeyrie 2004], see Fig. IV.1. It shows in particular that the diffuse transmission decreases much more slowly than the exponential attenuation of the ballistic (or coherent) beam, as expected from the diffusion equation [van Rossum 1999]. This can have practical consequences when one needs to evaluate the light reaching the edges of the cloud. The dominant contribution can be the diffuse transmission, which thus should not be neglected. This experiment also illustrates that the amount of scattered light is not simply proportional to the atom number (except at very low b): it generally depends on b and on the detection angle. Here, the optical thickness is changed by detuning the probe laser, illustrating the advantage of having a narrow resonance.

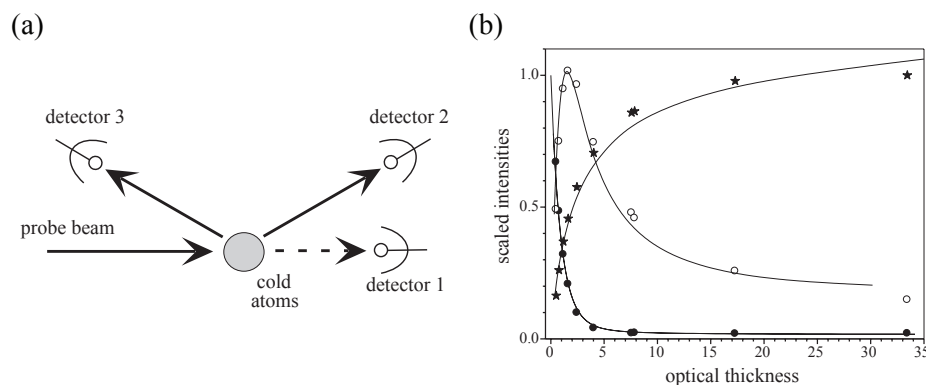


Figure IV.1: (a) Experimental scheme for measuring diffuse transmission and reflection. A small collimated laser beam is sent onto a cold-atom cloud. Three detectors measure the ballistic intensity, the diffuse reflection and the diffuse transmission. (b) The ballistic transmission (black circles) follows a Beer-Lambert law (exponential decrease). The diffused reflection (black stars) increases with the optical thickness. The diffused transmission (white circles) is not monotonic with the optical thickness. For large optical thickness b it evolves as $1/b$. Adapted from [Labeyrie 2004].

IV.1.2.2. Radiation trapping

Another experimental situation probing multiple scattering of light consists in the time-dependent detection of the scattered light (see Fig. IV.2) [Holstein 1947, Molisch 1998]. Such radiation trapping in cold atoms has been first demonstrated in [Fioretti 1998], where decay times of atomic fluorescence beyond the lifetime of the excited state for single atom scattering has been observed with increasing optical thickness.

In Ref. [Labeyrie 2003] it was shown that the transport time τ , which is the sum of the scattering time at each atom and propagation time between two scattering events, is independent of the laser detuning, as previously predicted [Lagendijk 1996] for scattering using narrow resonances (See also the Appendix of [Weiss 2018] in Section VI.5.1). Note that this result is in contrast to the result of non resonant scattering, where the energy velocity of the light is constant. For cold atoms, the time between two successive scattering events is constant, independently of the atomic density and thus of the average distance between scattering events. The transport time is equal to the lifetime of the excited states $\tau_{\text{at}} = \Gamma^{-1}$.

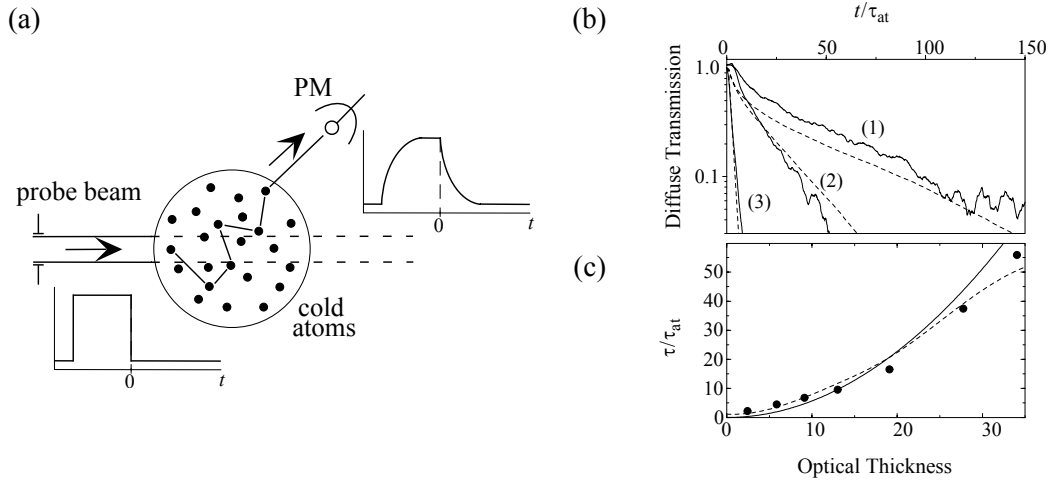


Figure IV.2: (a) Experimental scheme for observing radiation trapping. A small collimated laser beam is sent onto a cold-atom cloud. A photomultiplier (PM) records the fluorescence signal. At time $t = 0$, the laser is switched off. (b) Temporal trace of the decreasing fluorescence. (c) Corresponding time constants as a function of the optical thickness. Adapted from [Labeyrie 2003].

This result can be used to obtain scaling laws for radiation trapping in cold atomic vapors. As $|kv| \ll \Gamma$, one typically neglects frequency redistribution during multiple scattering and one can thus assume a random walk of photons before radiation escapes the atomic sample. For a Gaussian random walk in 3D, we have $\langle r^2 \rangle = 6Dt$. The average number of scattering events for escaping photons is the ratio between the time spent in the system and the scattering time:

$$\langle N_{\text{sc}} \rangle = \frac{t}{\tau} = \frac{\langle r^2 \rangle}{6D\tau}, \quad (\text{IV.8})$$

with $D = \ell_{\text{sc}}^2/(3\tau)$. When $\sqrt{\langle r^2 \rangle} \sim R = b\ell_{\text{sc}}/2$, the radiation can escape the system, leading to $\langle N_{\text{sc}} \rangle \sim b^2/8$. Radiation trapping times are thus expected to scale as b^2 . However, as shown in [Labeyrie 2005], the finite, non zero, temperature of laser-cooled atoms leads to a reduction of the trapping time, an indication that the Doppler effect is not completely negligible [Labeyrie 2005, Pierrat 2009].

IV.2. The quest for the best gain mechanism

Now that radiation trapping is well established in cold atoms [Labeyrie 2003] and gain/lasing has been demonstrated [Guerin 2008], one only has to combine the two to get a random laser. There is, however, a strong difficulty: the two ingredients have to be combined at the same time, i.e. for the same photons, i.e. at the same wavelength. Let us have a look again at, for instance, Fig. II.2 illustrating Raman gain between Zeeman sublevels. Clearly, the gain is present around the pump-probe two-photon resonance while scattering is present around the atomic resonance, so not at the same optical frequency.

It seems thus quite hard, *a priori*, to combine gain and scattering at the same time. Moreover it is not obvious to evaluate the amount of scattering in an active system. Indeed, in a transmission experiment, Beer-Lambert law gives access to the extinction (or attenuation) length, which is equal to the mean-free path only in a passive system, otherwise it is the sum of the contributions of scattering and gain.

Finally, one needs a criterion to decide which gain mechanism is better, for instance, between one with little gain and a lot of scattering, and another one with little scattering and a lot of gain. One relevant criterion is to minimize the random lasing threshold. We thus need a quantitative evaluation of this threshold.

IV.2.1. Threshold of a random laser with cold atoms

The first, and most simple model of random lasing has been introduced by Letokhov [Letokhov 1968] and consists in a diffusion equation with a gain term:

$$\frac{\partial W(\mathbf{r}, t)}{\partial t} = D\nabla^2 W(\mathbf{r}, t) + \frac{v}{\ell_g} W(\mathbf{r}, t), \quad (\text{IV.9})$$

where ℓ_g is the characteristic gain length. The procedure to solve this equation is explained in early reviews on random lasing [Cao 2003, Cao 2005] and is also in the paper [Guerin 2016b] reproduced in section IV.2.2. The result is that the threshold is given by a critical size for the medium,

$$L_{\text{cr}} \sim \sqrt{\ell_{\text{sc}} \ell_g}, \quad (\text{IV.10})$$

with a numerical prefactor that depends on the geometry.

In the following article [Froufe-Pérez 2009], we derive ‘Letokhov’s threshold’ in the case of cold atoms by writing the characteristic lengths as a function of the atomic polarizability. The critical quantity turns out to be the resonant optical depth b_0 . Then we use Mollow gain, for which the polarizability is known analytically [Mollow 1972], to evaluate the threshold quantitatively.

With this gain, the minimum threshold is obtained in a situation of high gain and very low scattering, which is not compatible with the use of the diffusion equation. Following the work of [Pierrat 2007], we compute the threshold condition from the radiative transfer equation for a slab geometry. We conclude from this study that the threshold optical thickness is of the order of 250 – 300, which is within reach of current cold-atom experiments. This is the first paper that discusses and establishes the possibility of random lasing in cold atoms.

Threshold of a Random Laser with Cold Atoms

Luis S. Froufe-Pérez,¹ William Guerin,² Rémi Carminati,³ and Robin Kaiser^{2,*}

¹*Instituto de Ciencia de Materiales de Madrid, CSIC, Sor Juana Inés de la Cruz 3, Cantoblanco, Madrid 28049, Spain*

²*Institut Non Linéaire de Nice, CNRS and Université de Nice Sophia-Antipolis, 1361 route des Lucioles, 06560 Valbonne, France*

³*Institut Langevin, ESPCI, CNRS UMR 7587, Laboratoire d'Optique Physique, 10 rue Vauquelin, 75231 Paris Cedex 05, France*

(Received 28 November 2008; published 1 May 2009)

We address the problem of achieving an optical random laser with a cloud of cold atoms, in which gain and scattering are provided by the same atoms. The lasing threshold can be defined using the on-resonance optical thickness b_0 as a single critical parameter. We predict the threshold quantitatively, as well as power and frequency of the emitted light, using two different light transport models and the atomic polarizability of a strongly pumped two-level atom. We find a critical b_0 on the order of 300, which is within reach of state-of-the-art cold-atom experiments. Interestingly, we find that random lasing can already occur in a regime of relatively low scattering.

DOI: 10.1103/PhysRevLett.102.173903

PACS numbers: 42.55.Zz, 42.25.Dd

Random lasing occurs when the optical feedback due to multiple scattering in a gain medium is strong enough so that gain in the sample volume overcomes losses through the surface. Since its theoretical prediction by Letokhov [1], great efforts have been made to experimentally demonstrate this effect in different kinds of systems [2–6], as well as to understand the fundamentals of random lasing [7,8]. The broad interest of this topic is driven by potential applications (see [9] and references therein) and by its connections to the subject of Anderson localization [10]. State-of-the-art random lasers [9] are usually based on condensed matter systems, and feedback is provided by a disordered scattering medium, while gain is provided by an active material lying in the host medium or inside the scatterers. In general, scattering and gain are related to different physical entities.

Another system that can be considered for achieving random lasing is a cold atomic vapor, using magneto-optical traps, where radiation trapping [11] as well as lasing [12,13] have been demonstrated. One advantage is the ability to easily model the microscopic response of the system components, which can be extremely valuable to fully understand the physics of random lasers. However, in such a system, the ability to combine gain and multiple scattering at the same time is not obvious, as both should be provided by the same atoms. The purpose of this Letter is to address this issue quantitatively. Note that even though new interesting features appear when coherent feedback is involved [14], we will consider only incoherent (intensity) feedback.

Following Letokhov's theory, we consider a homogeneous, disordered and active medium of size L . The random lasing threshold is governed by two characteristic lengths: the elastic scattering mean free path ℓ_{sc} [15,16] and the linear gain length ℓ_g ($\ell_g < 0$ in the cases of absorption or inelastic scattering). In the diffusive regime, defined as $L \gg \ell_{sc}$, the lasing threshold is reached when the unfolded path length, L^2/ℓ_{sc} , becomes larger than the gain length.

More precisely, the threshold is given by [1,17] $L_{\text{eff}} > \beta\pi\sqrt{\ell_{sc}\ell_g}/3$, where β is a numerical factor that depends on the geometry of the sample ($\beta = 1$ for a slab, $\beta = 2$ for a sphere), and $L_{\text{eff}} = \eta L$ is the effective length of the sample, taking into account the extrapolation length [15]. Another important length scale is the extinction length, as measured by the forward transmission of a beam through the sample, $T = e^{-L/\ell_{ex}}$. The extinction length is given by $\ell_{ex}^{-1} = \ell_{sc}^{-1} - \ell_g^{-1}$.

Let us consider now a homogeneous atomic vapor, constituted by atoms of polarizability $\alpha(\omega)$ at density ρ , submitted to a homogeneous pump field. The extinction length and the scattering mean free path are related to their corresponding cross section σ by $\ell_{ex,sc}^{-1} = \rho\sigma_{ex,sc}$, with $\sigma_{ex}(\omega) = k_0 \text{Im}[\alpha(\omega)]$ and $\sigma_{sc}(\omega) = (k_0^4/6\pi)|\alpha(\omega)|^2$ [18]. As we consider only quasiresonant light, we use only the wave vector $k_0 = \omega_0/c$ with ω_0 the atomic frequency. We also define a dimensionless atomic polarizability $\tilde{\alpha}$ such that $\alpha = (6\pi/k_0^3)\tilde{\alpha}$ (we omit the dependence on ω in the following). As it is an intrinsic parameter of the cloud, it is convenient to use the on-resonance optical thickness $b_0 = \rho\sigma_0 L$, where $\sigma_0 = 6\pi/k_0^2$ is the resonant scattering cross section (without pump laser). Using these quantities, the threshold condition writes

$$\eta b_0 > \frac{\beta\pi}{\sqrt{3}|\tilde{\alpha}|^2[|\tilde{\alpha}|^2 - \text{Im}(\tilde{\alpha})]}. \quad (1)$$

Moreover, we have $L/\ell_{sc} = b_0|\tilde{\alpha}|^2$ and $\eta = 1 + 2\xi/[L/\ell_{sc} + 2(\beta - 1)\xi]$ with $\xi \approx 0.71$ for $L > \ell_{sc}$ [19,20]. Note that deeply in the diffusive regime ($L \gg \ell_{sc}$), $\eta \sim 1$.

Equation (1) is the first result of this Letter. It shows, in the diffusive regime, the existence of a threshold of random lasing as soon as the medium exhibits gain, i.e., $|\tilde{\alpha}|^2 - \text{Im}(\tilde{\alpha}) > 0$. This threshold is given by a critical on-resonance optical thickness, expressed as a function of the atomic polarizability only. Interestingly, the condition

$\text{Im}(\tilde{\alpha}) < 0$, corresponding to single-pass amplification ($T > 1$), is not a necessary condition.

The previous result is general and does not depend on a particular pumping mechanism or atomic model. Let us now specify a gain model that will allow numerical evalu-

ations of the lasing threshold and of the features of the emitted light. We shall use the simplest case of strongly pumped two-level atoms, for which the normalized atomic polarizability at frequency ω can be written analytically (assuming a weak “probe” intensity) [21],

$$\tilde{\alpha}(\delta, \Delta, \Omega) = -\frac{1}{2} \frac{1 + 4\Delta^2}{1 + 4\Delta^2 + 2\Omega^2} \frac{(\delta + i)(\delta - \Delta + i/2) - \Omega^2\delta/(2\Delta - i)}{(\delta + i)(\delta - \Delta + i/2)(\delta + \Delta + i/2) - \Omega^2(\delta + i/2)}. \quad (2)$$

In this expression, $\Delta = (\omega_p - \omega_0)/\Gamma$ is the normalized detuning between the pump frequency ω_p and the atomic transition ω_0 of linewidth Γ , $\delta = (\omega - \omega_p)/\Gamma$ is the normalized detuning between the considered probe frequency and the pump, and Ω is the Rabi frequency, normalized by Γ , associated with the pump-atom interaction. For a strong enough pumping power, this atomic polarizability allows for single-pass gain, when $\text{Im}(\tilde{\alpha}) < 0$. This gain mechanism is referred as “Mollow gain” [13,21] and corresponds to a three-photon transition (population inversion in the dressed-state basis).

For each couple of pumping parameters $\{\Delta, \Omega\}$, the use of the polarizability (2) into the threshold condition (1) allows the calculation of the critical on-resonance optical thickness b_0 as a function of δ . Then, the minimum of b_0 and the corresponding δ determine the optical thickness $b_{0\text{cr}}$ that the cloud must overcome to allow lasing, and the frequency δ_{RL} of the random laser at threshold. The result is presented in Fig. 1 for a spherical geometry ($\beta = 2$). The result for $b_{0\text{cr}}$ is independent of the sign of Δ and we only show the region $\Delta > 0$. The minimum optical thickness that allows lasing is found to be $b_{0\text{cr}} \approx 200$ and is obtained for a large range of parameters, approximately along the line $\Omega \approx 3\Delta$. The optimum laser-pump detuning is near the gain line of the transmission spectrum, i.e., $\delta_{\text{RL}} \sim \text{sgn}(\Delta)\sqrt{\Delta^2 + \Omega^2}$ (a small shift compared to the maximum gain condition is due to the additional constraint of combined gain and scattering).

The obtained critical optical thickness is achievable with current technology [22], showing that random lasing is possible in a system of cold atoms with Mollow gain. As this result has been obtained using the diffusion approximation, the condition $L/\ell_{\text{sc}} = b_0|\tilde{\alpha}|^2 \gg 1$ must be satisfied. This is not the case in the full range of random lasing parameters that we have found. For example, with $\Delta \approx 1$ and $\Omega \approx 3$, the critical optical thickness is almost minimum, $b_{0\text{cr}} = 213$, but $L/\ell_{\text{sc}} \approx 0.44$. In this case, the threshold defined by Eq. (1) is at best unjustified, at worst wrong. In order to identify in Fig. 1 the region in which the approach should be valid, we have hatched the area corresponding to $L/\ell_{\text{sc}} < 3$. Note that random lasing is still expected in this region, but for a larger on-resonance optical thickness, that would allow fulfillment of the diffusive equation. The minimum optical thickness in the region of parameters compatible *a priori* with the diffusion

approximation is 347, and is located in the vicinity of $\{\Delta = 1, \Omega = 1.2\}$.

This first evaluation demonstrates the need for a more refined transport model. In the following, we use the approach introduced in Ref. [23], that is based on the radiative transfer equation (RTE). The RTE is a Boltzmann-type transport equation [24], that has a larger range of validity with respect to the ratio L/ℓ_{sc} than the diffusion equation [25].

Letokhov’s diffusive theory [1,17] and the RTE-based theory [23] of random lasing both rely on a modal expansion of the solution of the transport equation. In order to compare the predictions of both models, we focus on the slab geometry ($\beta = 1$) since the modal expansion of the

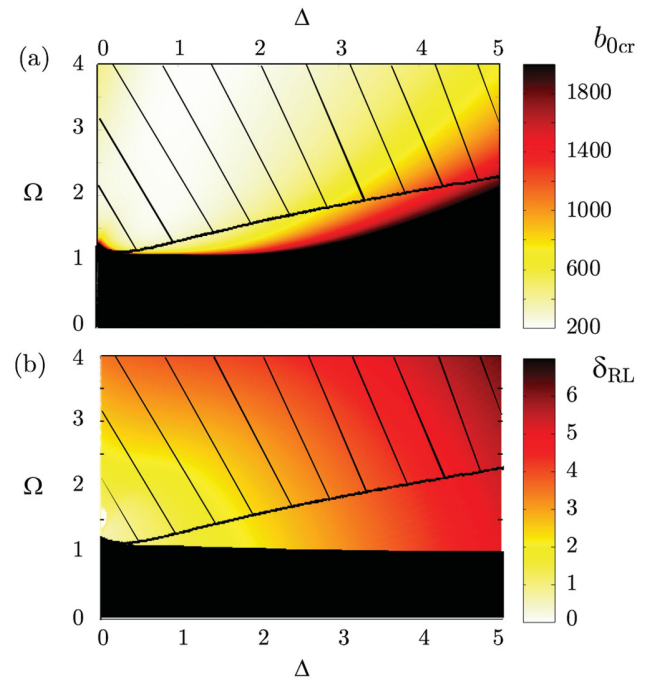


FIG. 1 (color). Threshold of random lasing based on Mollow gain [21], calculated for each pair of pumping parameters Δ (detuning) and Ω (Rabi frequency) with Eqs. (1) and (2). Only the $\Delta > 0$ part is represented. (a) Critical optical thickness $b_{0\text{cr}}$ to allow lasing. (b) Detuning δ_{RL} of the random laser from the pump frequency. The black area corresponds to a forbidden region (no gain). The hatched part corresponds to parameters for which the diffusion approximation is *a priori* not reliable.

RTE is well known in this case [19] (to our knowledge, no simple expansion is available for a sphere in the RTE approach). The modal approach consists in looking for solutions of the form $\Psi_s(z, \mathbf{u}, t) = \phi_{\kappa,s}(\mathbf{u}) \exp(i\kappa z) \times \exp(st)$, where $\Psi(z, \mathbf{u}, t)$ is the specific intensity (z is the distance from the slab surface and \mathbf{u} denotes a propagation direction). For a given real κ , $s(\kappa)$ and $\phi_{\kappa,s}$ form a set of eigenvalues and eigenfunctions of the RTE. If one denotes by $s_0(\kappa)$ the eigenvalue corresponding to the mode with the longest lifetime in the passive system, a laser instability appears when $s_0(\kappa) > 0$ in the presence of gain. The lasing threshold is defined by the condition $s_0(\kappa) = 0$. For isotropic scattering, this eigenvalue has an analytical expression valid for $\kappa \ell_{sc} < \pi/2$ [19,23]:

$$s_0(\kappa)/c = \ell_g^{-1} - [\ell_{sc}^{-1} - \kappa^2 / \tan(\kappa \ell_{sc})], \quad (3)$$

where c is the energy velocity. For a slab of width L , the dominant mode corresponds to $\kappa = \pi/L_{\text{eff}} = \pi/(L + 2\xi \ell_{sc})$. In practice, this determination of κ is meaningful as long as $\xi = 0.71$ can be taken as a constant (independent on L), which is the case for $L > \ell_{sc}$. This condition sets the limit of accuracy of the modal RTE approach.

The diffusive result is recovered from the RTE approach in the limit $\kappa \ell_{sc} \ll 1$ [25]. A first order expansion of Eq. (3) yields $s_0^{(\text{DA})}(\kappa)/c = \ell_g^{-1} - \kappa^2 \ell_{sc}/3$, where the superscript (DA) stands for diffusion approximation. The condition $s_0^{(\text{DA})}(\kappa = \pi/L_{\text{eff}}) = 0$ leads to Letokhov's threshold, with $\beta = 1$.

The comparison between the RTE and diffusive approaches deserves two comments. First, the gain contribution to $s_0(\kappa)$ [first term in Eq. (3)] is the same in both models. Second, the scattering contribution [second term in Eq. (3)] is larger in the RTE model by a factor of at most 1.13 (when $L \sim \ell_{sc}$). Thus, the correction introduced by the RTE model, compared to the diffusion approximation is relatively small, as it corresponds to an increase of $\eta b_{0\text{cr}}$ of at most a few percents. This means that the diffusive model gives accurate results down to $L \sim \ell_{sc}$, and that in cold-atom systems, random lasing can occur even in a regime of low scattering.

In Fig. 2, we compare the minimum optical thickness obtained with both models for the slab geometry and with the diffusive model for the sphere geometry. To put forward the domain of validity in each case, we plot the results as a function of L/ℓ_{sc} . As expected, in the range $L > \ell_{sc}$ the threshold predicted by the RTE for the slab geometry is only slightly larger than the one given by the diffusion approximation, so that the two curves can hardly be distinguished. For the sphere geometry, we dashed the part corresponding to the domain where the diffusive model is *a priori* not reliable, i.e., $L/\ell_{sc} < 3$. Nevertheless, by generalizing the conclusion obtained with the slab geometry, we reasonably expect the threshold to be located between 250 and 300.

Let us now turn to a first characterization of such a random laser. An important quantity to be investigated is

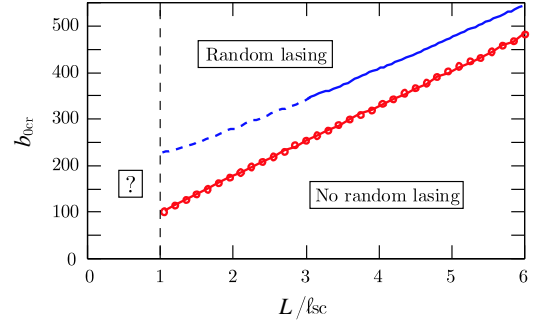


FIG. 2 (color online). Critical optical thickness for different geometries and transport models. The lower, red curve corresponds to the slab geometry (width L), with RTE model (continuous line) and diffusive model (open circle). The upper, blue curve corresponds to the sphere geometry (diameter L), with the diffusive model. The part with $L/\ell_{sc} < 3$ is dashed, as the model may not be reliable.

the emitted power as a function of the pumping power. In the stationary regime (continuous pumping) we numerically solve the optical Bloch equations for a strongly pumped two-level atom [without using the weak probe approximation that leads to Eq. (2)] to obtain the polarizability at the lasing frequency, including the gain saturation induced by the random laser intensity. Above threshold, the laser intensity *in the medium* $I_{\text{RL}}^{(\text{in})} \propto |\Omega_{\text{RL}}|^2$ is determined by the condition $s_0(\kappa, |\Omega_{\text{RL}}|^2) = 0$ (s_0 would be positive without gain saturation). The obtained intensity is analogous to the intracavity intensity of a standard laser, and thus does not correspond to the emitted power $P_{\text{RL}}^{(\text{out})}$. At equilibrium, gain compensates losses, and $P_{\text{RL}}^{(\text{out})}$ is equal to the generated power, related to the gain cross section σ_g , i.e. $P_{\text{RL}}^{(\text{out})} \propto \sigma_g |\Omega_{\text{RL}}|^2$ with $\sigma_g = \sigma_0 [|\tilde{\alpha}|^2 - \text{Im}(\tilde{\alpha})]$.

In order to know if the laser signal can be extracted from the background fluorescence, it is particularly relevant to compare the emitted laser power with the pump-induced fluorescence $P_{\text{Fluo}} \propto \sigma_0 |\Omega|^2 / (1 + 4\Delta^2 + 2|\Omega|^2)$. From this, we compute the ratio

$$\frac{P_{\text{RL}}^{(\text{out})}}{P_{\text{Fluo}}} = \frac{|\Omega_{\text{RL}}|^2}{|\Omega|^2} [|\tilde{\alpha}|^2 - \text{Im}(\tilde{\alpha})] (1 + 4\Delta^2 + 2|\Omega|^2). \quad (4)$$

We plot the result in Fig. 3 as a function of $|\Omega|^2$, for a pump detuning $\Delta = 1$. To obtain Eq. (4), we assume that both pump and laser intensities are homogeneously distributed across the whole system. We also consider only the optimum random laser frequency, thus neglecting the spectral width of the random laser or any interaction between different random laser frequencies. Hence we neglect several effects as mode competition [26] and inelastic scattering of the laser light. Nevertheless we think that the order or magnitude of the ratio laser-to-fluorescence powers can be realistic for actual experiments, at least as long as only one mode of the laser is active [26]. For the chosen set of parameters, this ratio is more than 5% and hence laser

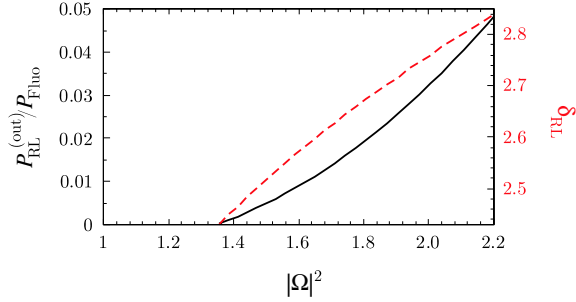


FIG. 3 (color online). Continuous line: Emitted random laser power normalized to the pump fluorescence power, as a function of the pump intensity. Dashed line: Normalized laser detuning δ_{RL} . The random medium is a spherical cloud of two-level atoms with an on-resonance optical thickness $b_0 = 650$.

emission should be measurable. Its distinction from the pump-induced fluorescence can be made by looking at the spectrum of the emitted light. Another interesting prediction of this model is that the laser emission frequency shifts as the pump intensity is increased [Fig. 3]. This corresponds to the shift of the maximum gain of the Mollow polarizability.

In summary, we have established the possibility of achieving random lasing with cold atoms. The random laser threshold is described by a single critical parameter, the on-resonance optical thickness b_0 . In the particular case of a gain mechanism based on a strongly pumped two-level atom (Mollow gain), our model predicts a critical $b_0 \sim 300$. Such an optical thickness is achievable in current cold-atoms experiments, e.g., by using crossed dipole traps [22]. We have also determined the basic features of the emitted light above threshold, showing that the random laser emission should be measurable.

Another interesting result is that, due to the large gain, lasing can be obtained with a low feedback (low amount of scattering, i.e., $L \sim \ell_{sc}$). This regime is similar to that encountered in certain semiconductor lasers with a very poor cavity, and is different from the working regime of random lasers realized to date. This new regime could be numerically investigated by RTE-based simulations [25].

Finally, let us stress that the model developed here has several limitations, so that the numbers should be considered as first-order estimates. First, we have considered monochromatic pumping, thus neglecting inelastic scattering from the pump. The inelastically-scattered photons may have a non-negligible influence on the atomic response, as shown in [27]. Second, the RTE model needs to be extended to a sphere geometry, and to a medium with inhomogeneous density and/or pumping. This would require a full numerical solution of coupled RTEs for the pump and probe beams [23]. We also outline that the case of the Mollow gain was chosen for the sake of simplicity, whereas other gain mechanisms might be more adapted for the search of random lasing, such as Raman gain or parametric gain [13]. Each gain mechanism has its advantages

and drawbacks, but the degrees of freedom they offer, together with the first estimates presented here, make us confident that the experimental realization of a cold-atom random laser is possible with current technology.

The authors thank S. Skipetrov, J. J. Sáenz, R. Pierrat, and F. Michaud for useful discussions. L. S. F. acknowledges the financial support of the Spanish Ministry of Science and Innovation through its Juan de la Cierva program. This work is supported by ANR-06-BLAN-0096.

*Robin.Kaiser@inln.cnrs.fr

- [1] V. S. Letokhov, *Sov. Phys. JETP* **26**, 835 (1968).
- [2] V. M. Markushev, V. F. Zolin, and Ch. M. Briskina, *Sov. J. Quantum Electron.* **16**, 281 (1986); C. Gouedard *et al.*, *J. Opt. Soc. Am. B* **10**, 2358 (1993).
- [3] N. M. Lawandy *et al.*, *Nature (London)* **368**, 436 (1994); D. S. Wiersma *et al.*, *Nature (London)* **373**, 203 (1995).
- [4] H. Cao *et al.*, *Phys. Rev. Lett.* **82**, 2278 (1999).
- [5] D. S. Wiersma and S. Cavaleri, *Nature (London)* **414**, 708 (2001).
- [6] S. Gottardo *et al.*, *Nat. Photon.* **2**, 429 (2008).
- [7] D. S. Wiersma and A. Lagendijk, *Phys. Rev. E* **54**, 4256 (1996).
- [8] A. L. Burin *et al.*, *Phys. Rev. Lett.* **87**, 215503 (2001).
- [9] D. S. Wiersma, *Nature Phys.* **4**, 359 (2008).
- [10] C. Conti and A. Fratalocchi, *Nature Phys.* **4**, 794 (2008).
- [11] A. Fioretti *et al.*, *Opt. Commun.* **149**, 415 (1998); G. Labeyrie *et al.*, *Phys. Rev. Lett.* **91**, 223904 (2003).
- [12] L. Hilico, C. Fabre, and E. Giacobino, *Europhys. Lett.* **18**, 685 (1992).
- [13] W. Guerin, F. Michaud, and R. Kaiser, *Phys. Rev. Lett.* **101**, 093002 (2008).
- [14] H. Cao, *J. Phys. A* **38**, 10497 (2005).
- [15] M. C. W. van Rossum and Th. M. Nieuwenhuizen, *Rev. Mod. Phys.* **71**, 313 (1999).
- [16] We consider only isotropic scattering so that the transport length equals the scattering mean free path [15].
- [17] H. Cao, *Waves Random Media* **13**, R1 (2003).
- [18] A. Lagendijk and B. A. van Tiggelen, *Phys. Rep.* **270**, 143 (1996), section 3.2.2 “Points scatterers” (pp. 164–166).
- [19] K. M. Case and P. F. Zweifel, *Linear transport theory* (Addison-Wesley, Reading, MA, 1967).
- [20] K. Drozdowicz, E. Krynicka, and J. Dąbrowska, *Appl. Radiat. Isot.* **58**, 727 (2003).
- [21] B. R. Mollow, *Phys. Rev. A* **5**, 2217 (1972); F. Y. Wu *et al.*, *Phys. Rev. Lett.* **38**, 1077 (1977).
- [22] M. D. Barrett, J. A. Sauer, and M. S. Chapman, *Phys. Rev. Lett.* **87**, 010404 (2001).
- [23] R. Pierrat and R. Carminati, *Phys. Rev. A* **76**, 023821 (2007).
- [24] S. Chandrasekhar, *Radiative Transfer* (Dover, New York, 1960).
- [25] R. Elaloufi, R. Carminati, and J.-J. Greffet, *J. Opt. Soc. Am. A* **21**, 1430 (2004).
- [26] H. E. Türeci *et al.*, *Science* **320**, 643 (2008).
- [27] L. Khaykovich, N. Friedman, and N. Davidson, *Eur. Phys. J. D* **7**, 467 (1999).

IV.2.2. Comparison between incoherent and coherent models

Letokhov's threshold is based on the diffusive description of light transport. The diffusion approximation is an 'incoherent model' in the sense that it neglects interference effects. It is usually justified to describe quantities which are averaged over the disorder configurations. However, lasing is a highly nonlinear effect, so that this kind of approximation is not justified *a priori*. In a more complete, coherent model, one should consider a speckle pattern for the light emitted outside the medium or a complicated (disordered) electromagnetic mode inside the medium. Each particular realization of the disorder gives a different set of modes and for each configuration lasing may start on the most favorable mode. One can intuitively expect that the average over the most favorable modes is better than the incoherent diffusive mode.

In the following paper [Guerin 2016b] we make a quantitative comparison between Letokhov's threshold and the model of random laser developed in the team of Douglas Stone (Yale University) [Türeci 2008, Ge 2010, Cerjan 2015]. We also generalize Letokhov's threshold with the radiative transfer equation (RTE), as in the previous paper, but going beyond the slab geometry (sphere). The results are as expected, i.e. the RTE is more accurate than the diffusive model, and the incoherent models overestimate the lasing threshold, compared to the coherent model. Nevertheless, this study also shows that the incoherent models are able to give the correct orders of magnitudes over a wide range of parameters with simple analytical expressions, and are thus extremely useful.

Diffusive to quasi-ballistic random laser: incoherent and coherent models

W. GUERIN,^{1,*} Y. D. CHONG,² Q. BAUDOUIN,¹ M. LIERTZER,³ S. ROTTER,³ AND R. KAISER¹

¹Université Côte d'Azur, CNRS, INLN, Valbonne, France

²School of Physical and Mathematical Sciences, Nanyang Technological University, Singapore 637371, Singapore

³Institute for Theoretical Physics, Vienna University of Technology (TU-Wien), A-1040 Vienna, Austria

*Corresponding author: william.guerin@inln.cnrs.fr

Received 13 June 2016; revised 19 July 2016; accepted 20 July 2016; posted 21 July 2016 (Doc. ID 268155); published 12 August 2016

We study the crossover between the diffusive and quasi-ballistic regimes of random lasers. In particular, we compare incoherent models based on the diffusion equation and the radiative transfer equation (RTE), which neglect all wave effects, with a coherent wave model for the random laser threshold. We show that both the incoherent and the coherent models predict qualitatively similar thresholds, with a smooth transition from a diffuse to a quasi-ballistic regime. The shape of the intensity distribution in the sample as predicted by the RTE model at threshold is also in good agreement with the coherent model. The approximate incoherent models thus provide useful analytical predictions for the threshold of random lasers as well as the shape of the random laser modes at threshold. © 2016 Optical Society of America

OCIS codes: (140.3430) Laser theory; (290.4210) Multiple scattering.

<http://dx.doi.org/10.1364/JOSAB.33.001888>

1. INTRODUCTION

Random lasers are probably among the most exotic sources of coherent light studied so far [1–5]. As their name already suggests, random lasers get their optical feedback not by external mirrors or through a resonator but rather by the random scattering of light in a disordered medium. Even though this operational principle makes a deliberate tuning or selection of desired laser modes and output frequencies technically rather involved [6–10], the first promising applications of random lasers are recently emerging for which these cost-efficient devices are ideally suited [11,12]. From the fundamental point of view, random lasers offer an exciting research area at the interface between mesoscopic physics, non-Hermitian optics, and laser physics [2,3,13]. Particularly exciting in this context is the hypothesis, first put forward by Lethokov [14], that random lasers also may actually be occurring on a natural basis in stellar gases because multiple scattering and amplification are present in such media [15–17]. Such hitherto unobserved “astrophysical random lasers” would have a spatial extension many orders of magnitudes larger than the micrometer-sized random lasers that are meanwhile routinely fabricated in the laboratory [18].

The vastly different length scales on which random lasing may occur, and the many different physical systems in which they have been realized, have triggered the development of different theoretical approaches to describe this phenomenon [19–26]. Whereas it might appear reasonable that a radiative transfer approach, which does not incorporate interference

effects, may be appropriate for astronomical length scales with long amplifying paths and few scattering events, and a diffusive model may be suitable to describe strongly scattering media in the diffusive limit [27], it has so far remained unexplored how to describe the crossover between such different regimes. An important aspect that is also missing in the literature is a global perspective on random lasing in which all the possible random lasing regimes are charted and properly identified.

The aim of this paper will be to take such a bird's-eye perspective on random lasing and to connect different approaches with each other. In particular, we will focus on the general question of which size a medium with a certain amount of gain and disorder needs to have such that it reaches the random lasing threshold. To address this problem, we employ approximative tools such as the radiative transfer equation (RTE) (for the low-scattering, or quasi-ballistic, limit) as well as a diffusive model (for the strongly scattering limit) and compare them with a full solution of the scalar wave equation that encompasses both of these limits just as well as the crossover region in between. While the latter model includes diffraction and interference effects and relies on heavy numerical simulations, the diffusive and radiative transfer models are “incoherent” in the sense that they neglect all wave effects. Their advantage is to provide simple analytical results.

Our paper is organized as follows. In Section 2 we first briefly recall Letokhov's seminal results on the threshold of random lasers based on the diffusion equation [19]. In Section 3

we present a theory of the random laser threshold based on the RTE. In Section 4 we introduce the employed coherent wave model. Finally, in Section 5 we compare the results from these different models and discuss the conclusions that can be drawn from them. A short summary is presented in Section 6.

2. RANDOM LASER THRESHOLD FROM THE DIFFUSION EQUATION

We summarize here the well-known results of Letokhov on the random laser threshold [19]. The presentation is inspired by the one given in the review [1]. We start from the diffusion equation for light with a gain term,

$$\frac{\partial W(\mathbf{r}, t)}{\partial t} = D\nabla^2 W(\mathbf{r}, t) + \frac{v_E}{\ell_g}, \quad (1)$$

where W is the energy density, v_E is the energy transport velocity inside the medium, ℓ_g is the gain length, and D is the diffusion coefficient. At 2D or 3D, it reads,

$$D_{2D} = \frac{v_E \ell_{sc}}{2}, \quad D_{3D} = \frac{v_E \ell_{sc}}{3}, \quad (2)$$

where ℓ_{sc} is the mean free path. For simplicity, we consider only isotropic scatterers such that the mean free path is equal to the transport length [1]. To map our results also to the case of finite-size scatterers, which scatter anisotropically, the scattering mean free path ℓ_{sc} needs to be rescaled to the transport length $\ell_{tr} = \ell_{sc}/(1 - \cos \phi)$, where ϕ is the scattering angle. The scatterers need to stay below the wavelength, though, as shape-specific resonances would otherwise destroy the universality of our analysis [28].

Using the modal decomposition

$$W(\mathbf{r}, t) = \sum_n a_n \Psi_n(\mathbf{r}) e^{(DB_1^2 - v_E/\ell_g)t}, \quad (3)$$

with appropriate boundary conditions, one can show that the threshold of a random laser is reached when

$$DB_1^2 - \frac{v_E}{\ell_g} = 0, \quad (4)$$

where B_1 is the smallest eigenvalue, corresponding with the longest-lived mode. For a 3D sphere of radius R , $B_1 = \pi/R$ and for a 2D disk of radius R , $B_1 = j_{0,0}/R$, where $j_{0,0} \simeq 2.40$ is the first root of the Bessel function J_0 .

Finally, it leads to the following critical radius:

$$R_{cr}^{3D} = \pi \sqrt{\frac{\ell_{sc} \ell_g}{3}}, \quad R_{cr}^{2D} = 2.40 \sqrt{\frac{\ell_{sc} \ell_g}{2}}. \quad (5)$$

Note that the numerical factors in front of $(\ell_{sc} \ell_g)^{1/2}$ differ from each other by only a few percents. Note also that we have neglected here the ‘‘extrapolation length’’ [29–31], which is a small correction in the diffusive limit that we consider in this section. The diffusive, or multiple-scattering regime, is reached when $R \gg \ell_{sc}$, which corresponds to the validity range of this threshold condition.

3. RANDOM LASER THRESHOLD FROM THE RADIATIVE TRANSFER EQUATION

In a regime of low scattering, transport of light is no longer governed by a diffusive equation but is well described by

the radiative transfer equation (RTE). The RTE is used in many different fields dealing with transport in complex media, such as astrophysics [32–34], neutron physics [35], or biological imaging [36]. The diffusion equation can be derived from the RTE with supplementary approximations (see, e.g., [30,36]). The RTE is thus more general and has been shown to be valid from the ballistic regime to the diffusive one [37]. It neglects, however, all wave effects such as interference and diffraction.

The basic quantity of the RTE is the ‘‘radiance’’ or ‘‘specific intensity’’ $L(\mathbf{r}, \mathbf{u}, t)$, which describes the photon density at point \mathbf{r} , propagating along direction \mathbf{u} at time t . In a system exhibiting absorption and scattering, the RTE reads,

$$\begin{aligned} \frac{1}{c} \frac{\partial L}{\partial t}(\mathbf{r}, \mathbf{u}, t) + \mathbf{u} \cdot \nabla L(\mathbf{r}, \mathbf{u}, t) \\ = -(\alpha + \chi)L(\mathbf{r}, \mathbf{u}, t) + \frac{\chi}{4\pi} \int_0^{4\pi} p(\mathbf{u}, \mathbf{v})L(\mathbf{r}, \mathbf{v}, t) d\Omega, \end{aligned} \quad (6)$$

where α is the linear absorption coefficient, $\chi = \ell_{sc}^{-1}$ and $p(\mathbf{u}, \mathbf{v})$ describes the scattering angular diagram. For a medium with gain, $\alpha < 0$, and we can also use the linear gain coefficient $g = -\alpha = \ell_g^{-1} > 0$. The RTE can be derived from Maxwell equations [38] but also can be found by simple energy conservation arguments because it is a Boltzmann-type equation.

From the specific intensity, one can define two other useful quantities: the radiative flux $\mathbf{q}(\mathbf{r}, t)$, which is identical to the Poynting vector, and the energy density $W(\mathbf{r}, t)$, which is the quantity entering into the diffusion equation:

$$\mathbf{q}(\mathbf{r}, t) = \int_{4\pi} L(\mathbf{r}, \mathbf{v}, t) \mathbf{u} d\Omega, \quad (7)$$

$$W(\mathbf{r}, t) = \int_{4\pi} \frac{L(\mathbf{r}, \mathbf{v}, t)}{c} d\Omega. \quad (8)$$

A. Random Laser Threshold

For a slab geometry, the random laser threshold was found from the RTE using a modal decomposition [22] and applied to the case of a random laser based on cold atoms [39,40]. For a sphere geometry, Letokhov and co-workers also have derived the random laser threshold from the RTE [14,41,42]. The detailed derivation can be found in [43]; we only recapitulate the result here. Moreover, for a better comparison with the data obtained from the coherent wave model (Section 4), we have extended these results to the case of a 2D disk. We also give only the result in this section; a detailed derivation is provided in Appendix A.

For a 3D sphere, one obtains a critical radius for the random laser threshold R_{cr} given by [14,41–43]

$$\tan(qR_{cr}) = \frac{2gqR_{cr}}{2g - q^2R_{cr}}, \quad (9)$$

with

$$q^2 = 3g(\chi - g) = \frac{3}{\ell_g} \left(\frac{1}{\ell_{sc}} - \frac{1}{\ell_g} \right). \quad (10)$$

For a 2D disk, the threshold condition is

$$\frac{J_0(\beta R_{cr})}{J_1(\beta R_{cr})} = \frac{\pi g}{2\beta}, \quad (11)$$

where J_0, J_1 are Bessel functions of the first kind, and with

$$\beta^2 = 2g(\chi - g) = \frac{2}{\ell_g} \left(\frac{1}{\ell_{sc}} - \frac{1}{\ell_g} \right). \quad (12)$$

These threshold equations can easily be solved numerically and give results that are very close to each other. We show in Fig. 1 the result for the 3D case. It shows a smooth transition from the diffusive regime (upper-left part) to the quasi-ballistic regime (lower-right part).

B. Limiting Cases

1. Diffusive Limit

For the 3D case, one can recover the diffusive threshold given by Eq. (5) from Eqs. (9) and (10) by supposing that there is much more scattering than gain, $\chi \gg g$, so that $q^2 \simeq 3g\chi$, and also that $\chi R_{cr} \gg 1$ (diffusive regime). One can then easily show that the r.h.s. of Eq. (9) is very small. Then Eq. (9) simplifies to $qR_{cr} \sim \pi$, which gives $R_{cr} \sim \pi/q \sim \pi(\ell_g \ell_{sc}/3)^{1/2}$ as expected.

For the 2D case, supposing also that $\chi \gg g$, then $\beta^2 \simeq 2g\chi$, and the threshold equation reduces to

$$\frac{J_0(\beta R_{cr})}{J_1(\beta R_{cr})} = \frac{\pi g}{2\beta} \simeq \frac{\pi}{2} \sqrt{\frac{g}{2\chi}} \ll 1. \quad (13)$$

We can thus take the zero of the function $J_0(z)/J_1(z)$, which is the zero of $J_0(z)$, i.e., $j_{0,0} \simeq 2.40$. Thus $\beta R_{cr} \sim 2.40$, and we recover $R_{cr} \sim 2.40(\ell_g \ell_{sc}/2)^{1/2}$.

2. Ballistic Limit

Interestingly, one also can simplify the threshold equations in the opposite limit of very low scattering and high gain.

For the 3D case, if $\chi \ll g$, we have the simplification $q \simeq \pm ig\sqrt{3}$ and $\tan(qR_{cr}) \simeq \tan(\pm i\sqrt{3}gR_{cr})$. For $gR_{cr} > 1$, it gives $\tan(qR_{cr}) \simeq \pm i$. Then Eq. (9) is easily solved to [44]

$$R_{cr} \sim \frac{1}{(\sqrt{3} - 3/2)g} \approx 4.31\ell_g. \quad (14)$$

At 2D, if $\chi \ll g$, $\beta^2 \simeq -2g^2$, $\beta \simeq \pm i\sqrt{2}g$, and the threshold equation reduces to

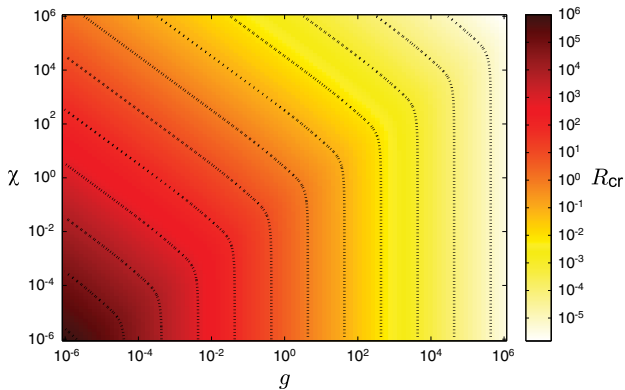


Fig. 1. Critical radius for the random laser threshold as a function of the gain coefficient $g = \ell_g^{-1}$ and the scattering coefficient $\chi = \ell_{sc}^{-1}$, as given by the numerical solution of Eq. (9). Note the log scales. The dotted lines are iso- R_{cr} contours.

$$\frac{\pm i\sqrt{2}J_0(\pm i\sqrt{2}gR_{cr})}{J_1(\pm i\sqrt{2}gR_{cr})} = \frac{\pi}{2}. \quad (15)$$

The solution is

$$R_{cr} \approx 3.76\ell_g. \quad (16)$$

In both cases, we obtain a finite critical radius that does not depend on the scattering χ , corresponding to the vertical asymptotes in Fig. 1. Surprisingly, this result suggests that a threshold exists even without scattering, a conclusion that seems clearly unphysical, suggesting that some of the approximations made to derive the RTE threshold (see Appendix A) break down in the ballistic limit. We discuss in more detail the nature of the employed approximations in Appendix B.

C. Shape of the Energy Density at Threshold

The shape of the intensity distribution at threshold can be obtained by solving Eq. (A15) (or its 3D equivalent).

In 3D one finds [43]

$$W_0(\mathbf{r}) \propto \frac{\sin(qr)}{r}, \quad (17)$$

while in 2D we obtain

$$W_0(\mathbf{r}) \propto J_0(\beta r). \quad (18)$$

In both cases, if there is more scattering than gain, $\chi > g$, β and q are real and $W_0(\mathbf{r})$ is bell-shaped with its maximum at $r = 0$. On the contrary, if $\chi < g$, β and q are purely imaginary and $W_0(\mathbf{r})$ increases from the center (Fig. 3). This is consistent with what could be expected in a quasi-ballistic regime, where photons farther from the center have been in averaged more amplified.

4. RANDOM LASER THRESHOLD FROM COHERENT WAVE CALCULATIONS

In order to compare the predictions of the RTE with a more complete model, we use coherent wave calculations of the lasing threshold, which account for the effects of finite wavelengths and wave interference. Due to the computational difficulty of performing such calculations on disordered media, we restrict the comparison study to 2D, using the scalar wave equation

$$\left[\nabla^2 + \varepsilon(\mathbf{r}, \omega) \left(\frac{\omega}{c} \right)^2 \right] \psi(\mathbf{r}) = 0. \quad (19)$$

This describes a 2D electromagnetic mode in the transverse magnetic (TM) polarization, where $\psi(\mathbf{r})$ is the complex scalar wavefunction corresponding to the out-of-plane component of the electric field, ω is the mode frequency, ∇^2 is the 2D Laplacian, and $\varepsilon(\mathbf{r}, \omega)$ is the dielectric function.

Wave equation (19) introduces an extra length scale, the wavelength $\lambda \sim 2\pi c/\omega$. For comparison with the RTE, we shall be interested in the regime where the wavelength is shorter than the other length scales, i.e., $c/\omega \ll \{R, \ell_{sc}, \ell_g\}$.

We model the random laser by uniformly distributing N delta-function scatterers at positions $\{\mathbf{r}_1, \dots, \mathbf{r}_N\}$, within a circular region of radius R . This region also contains a uniform background of gain material, with susceptibility $\chi_g \in \mathbb{C}$. Thus,

$$\varepsilon(\mathbf{r}, \omega) = \begin{cases} 1 + \chi_g + a \sum_{j=1}^N \delta^2(\mathbf{r} - \mathbf{r}_j), & r \leq R \\ 1, & r > R. \end{cases} \quad (20)$$

The parameter a , which has units of area, determines the strength of each scatterer. The use of independent delta-function scatterers allows us to relate the model parameters to the mean free path. The density of scatterers is $\rho = N/\pi R^2$, and the 2D scattering cross section of an individual scatterer in the first Born approximation is $\sigma = a^2(\omega/c)^3/4$. Thus,

$$\ell_{sc} = \frac{1}{\rho\sigma} = \frac{4\pi R^2}{Na^2(\omega/c)^3}. \quad (21)$$

From this setup, the lasing threshold calculation proceeds as follows: for a fixed lasing frequency, scatterer distribution, and scatterer strength, we find a complex value of χ_g that satisfies Eq. (19) with purely outgoing boundary conditions. The detailed procedure is described in Appendix C. Essentially, we perform a partial-wave expansion on $\psi(\mathbf{r})$, which reduces Eq. (19) to a non-Hermitian eigenproblem whose eigenvalues are the values of χ_g for which the solution is purely outgoing in the external region $r > R$. Out of these possible values of χ_g , we choose one with sufficiently small $\text{Re}[\chi_g]$ (i.e., negligible index shift), and the smallest value of $-\text{Im}[\chi_g]$ (i.e., least gain needed to reach threshold). This mode's refractive index is

$$n_g \approx 1 + \frac{i}{2}(\text{Im}[\chi_g]). \quad (22)$$

By repeating this procedure for many realizations of the scatterer distribution, we compute

$$g = \ell_g^{-1} \equiv \langle -2 \text{Im}[n_g] \omega / c \rangle = \frac{\omega}{c} \langle -\text{Im}[\chi_g] \rangle. \quad (23)$$

As in the RTE, ℓ_g represents the average path length traveled by a photon before an amplification event. By changing the individual scatterer strength a and using Eq. (21), we can find the dependence of ℓ_g on ℓ_{sc} and compare the result to the predictions of the RTE.

We perform two sets of calculations, for $\omega = 30c/R$ and $\omega = 60c/R$; as we shall see, these two frequencies give qualitatively similar results. For each case, we take $N = 250$ scatterers and tune a so that the mean free path varies over $10^{-1}R \lesssim \ell_{sc} \lesssim 10^2R$, ranging from the diffusive to the quasi-ballistic regime.

5. COMPARISON

In this section, we compare the results of the different models for the threshold and for the intensity distribution at threshold.

A. Threshold

We use the different models to plot gR at threshold as a function of $\chi R = R/\ell_{sc}$ or $1/(\chi R)$. We show in Fig. 2 the comparison between the data of the coherent wave model (previous section) and the analytical results of the diffusion (Section 2) and RTE thresholds (Section 3).

Overall, looking at Fig. 2(a), we can observe that the wave model and the RTE thresholds are quite close to each other. Moreover, the wave-model threshold becomes close to the diffusive ones for large optical thickness χR . The fact that fully incoherent models provide here very good estimates was not obvious from the outset because the incoherent models are only

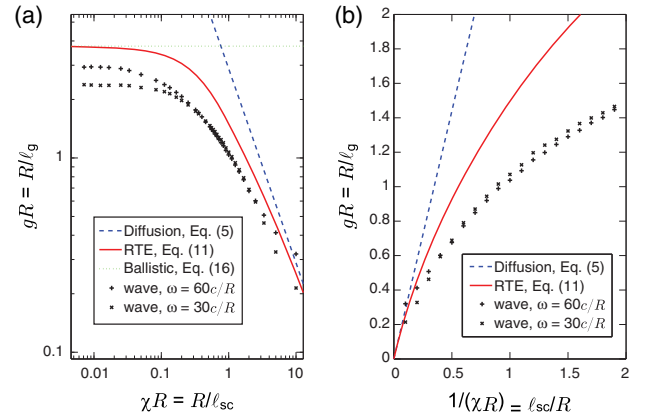


Fig. 2. (a) Comparison of the thresholds computed from the different models. Points are numerical solutions of the wave model for two different frequencies. The dashed blue line is the diffusive threshold computed from Eq. (5). The red solid line is the RTE threshold computed from Eq. (11). Its asymptotic behavior in the ballistic regime [Eq. (16)] is indicated by the green dotted line. Note the logarithmic scales. (b) Zoom into the diffusive and intermediate regimes (linear scales and inverted x axis).

expected to describe transport properties averaged over the disorder configurations. On the contrary, the coherent model selects the “best” mode at each realization (see Fig. 4). This also explains why the incoherent models predict larger gain thresholds and are thus “pessimistic.” The discrepancy between the different models increases as the optical thickness ($\alpha\chi R$) decreases [see Fig. 2(b)].

Another important observation is that the RTE threshold is significantly more accurate (closer to the wave model) than the threshold from the diffusion equation. For example, in the intermediate regime $R \approx \ell_{sc}$, the wave model predicts a gain threshold $gR \approx 1.1$, while the RTE threshold is $gR \approx 1.5$ and the diffusive one is $gR \approx 2.9$. Thus, as soon as the random laser is not deeply in the diffusive regime, the RTE theory provides a significant improvement.

However, in the limit of low scattering (ballistic or empty disk), the RTE model predicts a scattering-independent finite threshold. As already mentioned, this indicates a breakdown of the approximations used to derive the threshold in the RTE model. On the contrary, the scattering-independent threshold of the coherent model can have a clear physical interpretation: the disk boundary creates an index mismatch with the surrounding vacuum due to the gain coefficient and thus reflects some light, which induces some coherent feedback. In this regime, the laser is not “random” and is based on whispering gallery modes. The corresponding gain threshold depends on the wavelength because the index mismatch depends on the wavelength for a fixed gain coefficient. The coherent model is thus able to describe the transition from a diffusive random laser to a “ballistic,” cavity-based one. The partial reflection due to the index mismatch is not included in the incoherent models.

B. Intensity Distribution

We also can compare the averaged intensity distribution of the lasing mode at threshold obtained from the wave model and the

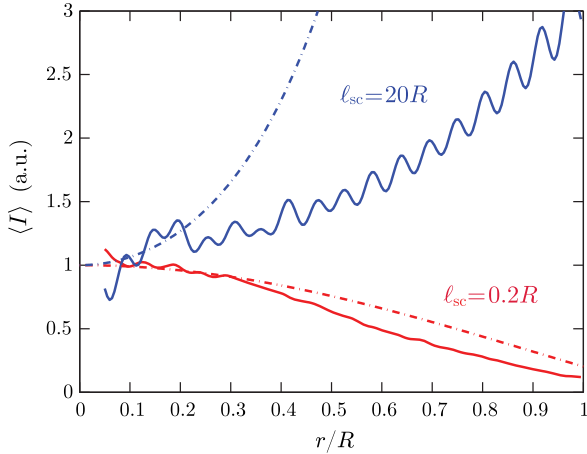


Fig. 3. Intensity distribution at threshold averaged over the disorder and over the radial angle. The solid lines are computed with the coherent wave model and the dash-dotted lines with the analytical results of the RTE model [Eq. (18)]. The vertical scale has been chosen such that $\langle I \rangle \sim 1$ at the center. In the diffusive regime ($\ell_{sc} = 0.2R$), the energy is confined near the center, while in the quasi-ballistic regime ($\ell_{sc} = 20R$) it increases from the center toward the edge.

analytical profile predicted by the RTE model [see Eq. (18)]. We show in Fig. 3 the intensity profile computed in the wave model at threshold for $\omega = 60c/R$, averaged over 100 disorder configurations and over the radial angle, for two different scatterers strengths (solid lines). For highly scattering samples ($\ell_{sc} = 0.2R$), we observe that the energy is confined near the center, as it could be expected in the diffusive regime. On the contrary, for weakly disordered samples ($\ell_{sc} = 20R$), the averaged intensity increases from the center (this also can be seen in Fig. 4 of [25]). These qualitatively different behaviors are well captured by the RTE prediction (dash-dotted lines). The agreement is even quite good in the diffusive regime. Differences are more important in the quasi-ballistic regime. First, the gain at threshold is higher in the RTE model [Fig. 2]; thus the intensity increases faster than in the wave model. Second, oscillations appear in the coherent model, which are a signature of interference effects due to the partial reflection at the boundary, creating an oscillatory pattern in the lasing mode. This partial reflection also contributes to increasing the intensity at the center, reducing the difference between the center and the edge.

6. CONCLUSION

In this paper, we have studied the threshold of random lasing in a 2D disk in the crossover from the diffusive to the quasi-ballistic regimes, and we compared different models to describe this transition. The more accurate, coherent model is able to describe this system in all regimes, at the cost of computational complexity, which, in particular, limits the size and dimensionality of the system under study. In the diffusive limit, the diffusion equation, which provides a fully incoherent description, predicts the threshold quite accurately, although interference and wave effects are neglected. Moreover, an incoherent model is also available beyond the diffusive regime. This model, based

on the radiative transfer equation, also provides analytical results, which agree with the full coherent model on a qualitative level and even show quantitative agreement in the crossover regime on a level superior to the diffusive model. The radiative transfer equation also correctly predicts the global shape of the averaged intensity distribution at threshold.

Surprisingly, even though the incoherent model is expected to break down deep in the ballistic limit because the boundary conditions cannot be treated rigorously, it predicts a random laser threshold as well as a modal intensity distribution in qualitative agreement with the coherent model. At the other extreme, the diffusion model also should break down when the mean-free path becomes comparable with the wavelength. Despite these limitations, the incoherent models are efficient in predicting the good order of magnitude for the random laser threshold in a large range of parameters.

The comparison with experimental data also would be interesting. In most experimentally accessible systems, however, the polydispersity of the samples and the complicated geometry due to the scattering of the pump [45] makes a quantitative comparison quite difficult. These problems are reduced with cold atoms, and the observed threshold reported in [46] was not far from Letokhov's diffusive threshold, showing that such simplified models can be useful guides to experimentalists.

APPENDIX A: DERIVATION OF THE RTE THRESHOLD AT 2D

We present here a detailed derivation of the random laser threshold [Eq. (11)] as well as the shape of the intensity distribution at threshold [Eq. (18)], from the radiative transfer equation for a 2D disk.

A. Threshold Condition from the RTE

We start from the RTE written at 2D:

$$\frac{1}{c} \frac{\partial L}{\partial t}(\mathbf{r}, \mathbf{u}, t) + \mathbf{u} \cdot \nabla L(\mathbf{r}, \mathbf{u}, t) = -(\alpha + \chi)L(\mathbf{r}, \mathbf{u}, t) + \frac{\chi}{2\pi} \int_0^{2\pi} p(\mathbf{u}, \mathbf{v})L(\mathbf{r}, \mathbf{v}, t)d\theta', \quad (\text{A1})$$

where $\theta' = (\mathbf{r}, \mathbf{v})$ is the plane angle between \mathbf{r} and \mathbf{v} . In the following, we suppose isotropic scattering: $p(\mathbf{u}, \mathbf{v}) = 1$. Then the last integral reads $\int L(\mathbf{r}, \theta, t)d\theta$, where θ is in the following the angle between \mathbf{r} and \mathbf{u} . In the cylindrical coordinate, the gradient is

$$\nabla L = \frac{\partial L}{\partial r} \mathbf{e}_r + \frac{1}{r} \frac{\partial L}{\partial \theta} \mathbf{e}_\theta, \quad (\text{A2})$$

and we have $\mathbf{u} \cdot \mathbf{e}_r = \cos \theta$ and $\mathbf{u} \cdot \mathbf{e}_\theta = -\sin \theta$. We thus obtain

$$\frac{1}{c} \frac{\partial L}{\partial t} + \cos \theta \frac{\partial L}{\partial r} - \frac{\sin \theta}{r} \frac{\partial L}{\partial \theta} = -(\alpha + \chi)L + \frac{\chi}{2\pi} \int_0^{2\pi} L d\theta. \quad (\text{A3})$$

We now look for a separable solution in the form

$$L(\mathbf{r}, \theta, t) = L_t(t) \times L_{sp}(\mathbf{r}, \theta), \quad (\text{A4})$$

where “sp” means “space.” Injecting Eq. (A4) into Eq. (A3) we obtain

$$\frac{1}{c} \frac{\partial L_t}{\partial t} = \frac{L_t}{L_{sp}} \times \left[-\cos \theta \frac{\partial L_{sp}}{\partial r} + \frac{\sin \theta}{r} \frac{\partial L_{sp}}{\partial \theta} - (\alpha + \chi) L_{sp} + \frac{\chi}{2\pi} \int_0^{2\pi} L_{sp} d\theta \right]. \tag{A5}$$

This is an equation in the form $\partial L_t / \partial t = c S L_t$, which induces an exponential increase when $S > 0$. The threshold condition is thus $S = 0$, i.e.,

$$\cos \theta \frac{\partial L_{sp}}{\partial r} - \frac{\sin \theta}{r} \frac{\partial L_{sp}}{\partial \theta} = -(\alpha + \chi) L_{sp} + \frac{\chi}{2\pi} \int_0^{2\pi} L_{sp} d\theta. \tag{A6}$$

B. Eddington Approximation

Unfortunately this equation is still difficult to solve, and we need an approximation. Following Letokhov and co-workers [14,41,42], we use the derivation of Sobolev [33] based on the so-called Eddington approximation [47,48]. It consists in supposing that the second moment of the luminance L_{sp} respective to the cosine of the propagation angle is proportional to the zeroth one. It is equivalent to writing

$$L_{sp}(r, \theta) = a(r) + b(r) \cos(\theta). \tag{A7}$$

We can then derive several useful relations:

$$L_0(r) = \frac{1}{2\pi} \int_0^{2\pi} L_{sp}(r, \theta) d\theta = a(r), \tag{A8}$$

$$L_1(r) = \frac{1}{2\pi} \int_0^{2\pi} L_{sp}(r, \theta) \cos \theta d\theta = \frac{b(r)}{2}, \tag{A9}$$

$$L_2(r) = \frac{1}{2\pi} \int_0^{2\pi} L_{sp}(r, \theta) \cos^2 \theta d\theta = \frac{a(r)}{2} = \frac{L_0(r)}{2}, \tag{A10}$$

$$\frac{\partial L_{sp}}{\partial \theta} = -\sin(\theta) b(r). \tag{A11}$$

We can use these relations to simplify the θ dependency in the threshold equation (A6). For this, we first integrate Eq. (A6) over θ and, using Eqs. (A9) and (A11), we obtain

$$\frac{dL_1}{dr} + \frac{L_1}{r} = -\alpha L_0. \tag{A12}$$

Then we integrate again Eq. (A6) over θ after multiplication by $\cos(\theta)$ and we obtain

$$\frac{dL_2}{dr} = -(\alpha + \chi) L_1. \tag{A13}$$

Next we multiply Eq. (A12) by $-(\alpha + \chi)$ and use Eq. (A13) to obtain

$$\frac{d^2 L_2}{dr^2} + \frac{1}{r} \frac{dL_2}{dr} = \alpha(\alpha + \chi) L_0. \tag{A14}$$

Finally, because $L_2 = L_0/2$ [Eq. (A10)],

$$\frac{d^2 L_0}{dr^2} + \frac{1}{r} \frac{dL_0}{dr} = 2\alpha(\alpha + \chi) L_0. \tag{A15}$$

At this stage, we get a single differential equation on the quantity $L_0(r)$, which is the intensity distribution, with only one variable. Note that in the derivation at 3D, small differences appear because we integrate each time over the full

solid angle, which makes a supplementary $\sin(\theta)$ appear in the integrals. We obtain at the end a very similar equation, with the factor $1/r$ replaced by $2/r$ and the 2 in the r.h.s. replaced by 3.

Another expression that will be useful in the following is obtained by combining Eqs. (A8), (A10), and (A13) into Eq. (A7):

$$L_{sp}(r, \theta) = L_0(r) - \frac{1}{\alpha + \chi} \frac{dL_0}{dr} \cos(\theta). \tag{A16}$$

C. Shape of the Mode

If we solve Eq. (A15), we get the shape of the intensity distribution $L_0(r)$ at threshold. The solution of Eq. (A15) that has no divergence at $r = 0$ is

$$L_0(r) = C J_0(\beta r), \tag{A17}$$

with $\beta^2 = -2\alpha(\alpha + \chi) = 2g(\chi - g)$, where $g = -\alpha$ is the gain coefficient, and J_0 is the Bessel function of the first kind of order 0.

D. Boundary Conditions

Because the random laser threshold obviously depends on the size of the medium, it comes from the boundary condition that should be applied to Eq. (A15).

The medium has a finite radius R . The physical boundary condition should be that there is no ingoing intensity, i.e., $L_{sp}(R, \theta) = 0$ for all θ such that $\cos \theta < 0$. However, it is not possible to fulfill this condition consistently with the Eddington approximation in Eq. (A7) (except for the trivial case of $L_{sp} = 0$ everywhere). We thus have to use an approximate boundary condition, which is that the total ingoing flux is zero:

$$\int_{\cos \theta < 0} L_{sp}(R, \theta) \cos(\theta) d\theta = 0. \tag{A18}$$

Note that the same problem appears with the use of the diffusion equation and the same approximate condition is used, leading to the extrapolation length (see, e.g., [30], p. 179).

We thus apply Eq. (A18) to Eq. (A16) to obtain $-2L_0(R) + \pi L_1(R) = 0$. Using Eqs. (A10) and (A13),

$$L_1(R) = -\frac{1}{\alpha + \chi} \frac{dL_2}{dr} \Big|_R = -\frac{1}{\alpha + \chi} \frac{1}{2} \frac{dL_0}{dr} \Big|_R, \tag{A19}$$

and we obtain the approximate boundary condition

$$L_0(R) = -\frac{\pi}{4} \frac{1}{\alpha + \chi} \frac{dL_0}{dr} \Big|_R. \tag{A20}$$

Note that the boundary condition for the 3D case is similar, the factor $\pi/4$ being replaced by $2/3$ (and is the same as in the diffusion approximation).

Using the intensity profile in Eq. (A17), we finally get a threshold condition:

$$J_0(\beta R) = \frac{\pi}{4} \frac{\beta}{\alpha + \chi} J_1(\beta R). \tag{A21}$$

We can simplify $\beta/(\chi - g) = 2g/\beta$ and, because we use quantities that are normalized to the medium size, it is better to write the threshold condition in the following way:

$$\frac{\beta R J_0(\beta R)}{J_1(\beta R)} = \frac{\pi}{2} g R \quad \text{with} \quad \beta^2 = 2g(\chi - g). \quad (\text{A22})$$

APPENDIX B: DISCUSSION ON THE APPROXIMATIONS USED IN THE INCOHERENT MODELS

From the initial RTE, there are several ways of finding a random laser threshold.

The first one is to first derive the diffusion equation and then investigate the random laser problem. This approach gives the well-known results of Section 2. The derivation of the diffusion equation from the RTE needs two approximations (see, e.g., [36] for a complete derivation, and [49] for a discussion on various possible approximations). The first one is called the P_1 approximation; it consists in decomposing the specific intensity on the basis of Legendre polynomials of $\cos \theta$ and keeping only the first order. At 3D, using the definitions of the radiative energy density and flux [Eqs. (7), (8)], it reads,

$$L(\mathbf{r}, \mathbf{u}, t) = \frac{c}{4\pi} W(\mathbf{r}, t) + \frac{3}{4\pi} \mathbf{q}(\mathbf{r}, t) \cdot \mathbf{u}. \quad (\text{B1})$$

This approximation is good if the radiation is “nearly” isotropic. For this, photons need enough scattering events to randomize their directions, i.e., one needs $R \gg \ell_{sc}$ and, in case of absorption, $\ell_a \gg \ell_{sc}$. The second approximation consists in neglecting the time derivative of the flux compared with the time scale associated with transport. This condition is usually said to be fulfilled if $\ell_a \gg \ell_{sc}$, where only absorption is considered. However, in case of gain, it adds the condition $\ell_g \gg \ell_{sc}$, which may be a limitation for the random laser problem, because it excludes the regime of parameters where there is more gain than scattering. Finally, to determine the random laser threshold from the diffusion equation, the boundary conditions due to the finite size of the medium are treated with an approximation that makes the extrapolation length appear [29–31]. Because of these approximate boundary conditions, the diffusion equation is known to be bad near the borders of the medium (meaning at a few ℓ_{sc}).

In the approach presented in Section 3, we first find a complicated threshold equation directly from the RTE, and then, on this threshold equation, we make approximations. The Eddington approximation [Eq. (A7)] is exactly the same as the P_1 approximation [note the similarity between Eqs. (B1) and (A16)], and the approximated boundary conditions [Eq. (A18)] are also exactly the same as those used with the diffusion equation [29,30]. The only condition that is relaxed is the one about the derivative of the flux. It relaxes the condition $\ell_g \gg \ell_{sc}$, which increases the validity range of the threshold condition to the case where the gain is similar or larger than the scattering. It is thus a significant improvement over the traditional Letokhov’s threshold. However, the condition $R \gg \ell_{sc}$, necessary for the isotropization of the flux, and for the approximate boundary conditions, is *a priori* not relaxed, although the RTE in itself is also valid in the ballistic regime.

However, we find in the astrophysics literature (radiative transfer in stellar or planetary atmospheres) that the Eddington approximation is good for isotropic scattering and extends to the optically thin regime [47,48]. Nevertheless, the boundary

conditions are not discussed, and, to our knowledge, there is no other method to treat the boundary conditions within the Eddington approximation. Following Letokhov and co-workers [14,41,42], we have used the method usually applied with the diffusion equation. It is known that these approximate boundary conditions lead to an extrapolation length proportional to the scattering mean-free path [29–31]. In the limit of vanishing scattering, this extrapolation length goes to infinity and so does the effective size of the medium. This may explain the appearance of a finite random laser threshold in the ballistic limit of the RTE [Eqs. (14) and (16)].

Finding a better way to treat the boundary conditions, and even including the partial reflection due to the index mismatch, as can be done with the diffusion equation [29,30,36,50–52], would certainly improve the validity range and the precision of the RTE threshold.

APPENDIX C: PARTIAL-WAVE CALCULATION OF LASING THRESHOLDS

This appendix describes the numerical method used to calculate the laser threshold of a 2D disordered system in Section 4. It relies on basis functions that are purely outgoing at infinity, called “constant flux” (CF) states [53]. CF states were originally introduced in the context of steady-state *ab initio* laser theory (SALT) [25,53–56], a method for accurately calculating above-threshold lasing solutions. In this work, however, we will not draw upon the full machinery of SALT because our interest lies in threshold statistics. The CF states we shall use are solutions to the wave equation (19), assuming (i) there are *no scatterers*, and (ii) the solutions are purely outgoing in the external region $r > R$. These wavefunctions have the form

$$u_{mp}(r, \phi) = \begin{cases} A_{mp} J_m(q_{mp} r) \Theta_m(\phi), & r \leq R \\ B_{mp} H_m^+(\omega r/c) \Theta_m(\phi), & r \geq R, \end{cases} \quad (\text{C1})$$

where (r, ϕ) are polar coordinates, (m, p) are azimuthal and radial quantum numbers, H_m^+ denotes Hankel functions of the first kind, and $\Theta_m(\phi)$ are azimuthal basis functions defined by

$$\Theta_m(\phi) = \frac{1}{2\pi} \begin{cases} \sqrt{2} \sin \phi, & m > 0 \\ 1, & m = 0 \\ \sqrt{2} \cos \phi, & m < 0, \end{cases} \quad (\text{C2})$$

which satisfy $\int_0^{2\pi} d\phi \Theta_m(\phi) \Theta_{m'}(\phi) = \delta_{mm'}$. Matching the wavefunction and its first radial derivative at $r = R$ gives

$$\frac{q_{mp} J_m'(q_{mp} R)}{J_m(q_{mp} R)} = \frac{(\omega/c) H_m^+(\omega R/c)}{H_m^+(\omega R/c)}, \quad (\text{C3})$$

which can be solved numerically to find a discrete set of q_{mp} values, corresponding to the different CF states. With appropriate normalization (choice of A_{mp}), the CF states come to satisfy a self-orthogonality condition:

$$\int_{r < R} d^2 r u_{mp} u_{m'p'} = \delta_{mm'}^{pp'}. \quad (\text{C4})$$

Note that the CF basis depends implicitly on the frequency ω , which appears in Eqs. (C1) and (C3).

We now consider the disordered system with $\varepsilon(\mathbf{r})$ given by Eq. (20). Its modes can be expanded using the CF basis states:

$$\psi(\mathbf{r}) = \sum_{mp} c_{mp} u_{mp}(\mathbf{r}). \quad (\text{C5})$$

Such a superposition automatically satisfies outgoing boundary conditions (with frequency ω), as required of lasing modes. Plugging this into Eqs. (19) and (20), and using Eq. (C5), gives

$$\sum_{m'p'} \left\{ \left[\left(\frac{q_{mp}}{\omega/c} \right)^2 - 1 \right] \delta_{mm'}^{pp'} - a \sum_j u_{mp}(r_j) u_{m'p'}(r_j) \right\} c_{m'p'} = \chi_g c_{mp}. \quad (\text{C6})$$

This is a non-Hermitian eigenproblem, whose eigenvalues are the complex susceptibilities χ_g that would allow the disordered structure to lase at frequency ω . Note that the delta-function scatterers enter in the second term in the matrix; their delta-function nature is handled “exactly” in the sense that we need not approximate them through spatial discretization.

In order to solve the eigenproblem numerically, we truncate to a finite CF basis set. For $\omega = 60c/R$ (see Section 4), we take $m \leq 75$ and $\text{Re}(q_{mp}) \leq 180/R$. Essentially, these truncations limit the resolution of the wavefunction in the azimuthal and radial directions, respectively. There are 6098 CF states in the remaining basis set. The matrix in Eq. (C6) is non-sparse, so the solution time increases with the basis size, M , as $O(M^3)$.

Figure 4 shows the computed values of χ_g for a typical disorder realization. The eigenvalues with very large $\text{Re}[\chi_g]$ are not the lasing modes we are interested in; those are modes confined because of a large real uniform background susceptibility χ_g , rather than random scattering. We filter out these solutions by truncating the eigenvalues to those with sufficiently small real parts (specifically, $|\text{Re}[1/\chi_g]| < 3|\text{Im}[1/\chi_g]|$). These remaining eigenvalues form a random distribution in $\text{Im}[\chi_g]$, i.e., the amplification provided by the gain medium. Their residual small but nonzero $\text{Re}[\chi_g]$ correspond to the index shifts necessary to make each mode lase at frequency ω . Varying ω moves these eigenvalues mostly sideways in the complex plane, without much change in $\text{Im}[\chi_g]$. As described in Section 4, we

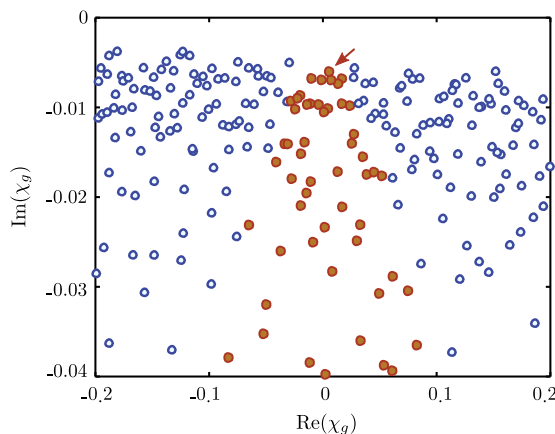


Fig. 4. Numerical values of χ_g obtained for a disorder realization with $N = 250$ scatterers and $\ell_{sc} = 0.15R$, with $\omega = 60c/R$. The susceptibility eigenvalues are truncated to those with sufficiently small real parts (solid circles); then the eigenvalue with smallest $|\text{Im}[\chi_g]|$ (indicated by an arrow) determines the laser threshold.

then pick the smallest eigenvalue with the smallest value of $|\text{Im}[\chi_g]|$, which determines the gain length ℓ_g . Shifts in the real part of χ_g due to the gain may be relevant for the study of individual laser thresholds but are neglected here, as they do not influence the overall statistics of the laser threshold we are interested in.

Funding. Agence Nationale de la Recherche (ANR) (ANR-06-BLAN-0096); Délégation Générale à l’Armement (DGA); National Research Foundation Singapore (NRF) (NRFF2012-02); Ministry of Education—Singapore (MOE) (MOE2011-T3-1-005); Austrian Science Fund (FWF) (SFB-NextLite F49-P10, I 1142-N27 GePartWave).

Acknowledgment. We acknowledge A. D. Stone for helpful discussions and guidance.

REFERENCES AND NOTES

- H. Cao, “Lasing in random media,” *Waves Random Media* **13**, R1–R39 (2003).
- H. Cao, “Random lasers: development, features and applications,” *Opt. Photon. News* **16**(1), 24–29 (2005).
- D. S. Wiersma, “The physics and applications of random lasers,” *Nat. Phys.* **4**, 359–367 (2008).
- J. Andreasen, A. A. Asatryan, L. C. Botten, M. A. Byrne, H. Cao, L. Ge, L. Labonté, P. Sebbah, A. D. Stone, H. E. Türeci, and C. Vanneste, “Modes of random lasers,” *Adv. Opt. Photon.* **3**, 88–127 (2011).
- D. S. Wiersma, “Disordered photonics,” *Nat. Photonics* **7**, 188–196 (2013).
- D. S. Wiersma and S. Cavalier, “Light emission: a temperature-tunable random laser,” *Nature* **414**, 708–709 (2001).
- R. G. S. El-Dardiry and A. Lagendijk, “Tuning random lasers by engineered absorption,” *Appl. Phys. Lett.* **98**, 161106 (2011).
- M. Leonetti and C. López, “Active subnanometer spectral control of a random laser,” *Appl. Phys. Lett.* **102**, 071105 (2013).
- T. Hisch, M. Liertzer, D. Pogany, F. Mintert, and S. Rotter, “Pump-controlled directional light emission from random lasers,” *Phys. Rev. Lett.* **111**, 023902 (2013).
- N. Bachelard, S. Gigan, X. Noblin, and P. Sebbah, “Adaptive pumping for spectral control of random lasers,” *Nat. Phys.* **10**, 426–431 (2014).
- B. Redding, M. A. Choma, and H. Cao, “Speckle-free laser imaging using random laser illumination,” *Nat. Photonics* **6**, 355–359 (2012).
- S. Schönhuber, M. Brandstetter, T. Hisch, C. Deutsch, M. Krall, H. Detz, G. Strasser, S. Rotter, and K. Unterrainer, “Random lasers for broadband directional emission,” arXiv:1605.09552 (2016).
- S. Rotter, “Random lasers: playing pinball with light,” *Nat. Phys.* **10**, 412–413 (2014).
- V. S. Letokhov and S. Johansson, *Astrophysical Lasers* (Oxford University, 2009).
- V. S. Strel'nitski, M. R. Haas, H. A. Smith, E. F. Erickson, S. W. J. Colgan, and D. J. Hallenbach, “Far-infrared hydrogen lasers in the peculiar star MWC 349A,” *Science* **272**, 1459–1461 (1996).
- S. Johansson and V. S. Letokhov, “Astrophysical lasers operating in optical Fe II lines in stellar ejecta of η Carinae,” *Astron. Astrophys.* **428**, 497–509 (2004).
- S. Johansson and V. S. Letokhov, “Astrophysical laser operating in the O I 8446-Å line in the Weigelt blobs of η Carinae,” *Mon. Not. R. Astron. Soc.* **364**, 731–737 (2005).
- H. Cao, J. Y. Xu, Y. Ling, A. L. Burin, E. W. Seeling, X. Liu, and R. P. H. Chang, “Random lasers with coherent feedback,” *IEEE J. Sel. Top. Quantum Electron.* **9**, 111–119 (2003).
- V. S. Letokhov, “Generation of light by a scattering medium with negative resonance absorption,” *Sov. Phys. J. Exp. Theor. Phys.* **26**, 835–840 (1968).
- D. S. Wiersma and A. Lagendijk, “Light diffusion with gain and random lasers,” *Phys. Rev. E* **54**, 4256–4265 (1996).

21. A. L. Burin, M. A. Ratner, H. Cao, and R. P. H. Chang, "Model for a random laser," *Phys. Rev. Lett.* **87**, 215503 (2001).
22. R. Pierrat and R. Carminati, "Threshold of random laser in the incoherent transport regime," *Phys. Rev. A* **76**, 023821 (2007).
23. C. Vanneste, P. Sebbah, and H. Cao, "Lasing with resonant feedback in weakly scattering random systems," *Phys. Rev. Lett.* **98**, 143902 (2007).
24. C. Conti and A. Fratallocchi, "Dynamic light diffusion, three-dimensional Anderson localization and lasing in inverted opals," *Nat. Phys.* **4**, 794–798 (2008).
25. H. E. Türeci, L. Ge, S. Rotter, and A. D. Stone, "Strong interactions in multimode random lasers," *Science* **320**, 643–646 (2008).
26. R. Frank, A. Lubatsch, and J. Kroha, "Light transport and localization in diffusive random lasers," *J. Opt. A* **11**, 114012 (2009).
27. F. A. Pinheiro and L. C. Sampaio, "Lasing threshold of diffusive random lasers in three dimensions," *Phys. Rev. A* **73**, 013826 (2006).
28. P. D. García, R. Sapienza, Á. Blanco, and C. López, "Photonic glass: a novel random material for light," *Adv. Mater.* **19**, 2597–2602 (2007).
29. M. C. W. van Rossum and T. M. Nieuwenhuizen, "Multiple scattering of classical waves: microscopy, mesoscopy, and diffusion," *Rev. Mod. Phys.* **71**, 313–371 (1999).
30. A. Ishimaru, *Wave Propagation and Scattering in Random Media* (IEEE, 1999).
31. The extrapolation length z_0 depends on the geometry. The well-known result is for a slab. In the diffusion approximation, one obtains $z_0 = (2/3)\ell_{sc}$, whereas the exact result for a semi-infinite slab is $z_0 \simeq 0.71\ell_{sc}$ [29,30]. For a 2D disk, the diffusion approximation gives $z_0 = (\pi/4)\ell_{sc}$, whereas numerical simulations have shown that a better value is $z_0 \simeq 0.82\ell_{sc}$ [57]. For a 3D sphere, an expression can be found in [58] and was used in previous papers [39,40]. Note that, in this case, the extrapolation length is not directly proportional to the mean-free path, it is bounded by the radius of the sphere. Finally, the extrapolation length should also depend on the gain or absorption coefficient. In [35] about neutron transport, it is stated explicitly (p. 143) that the extrapolation length depends on the number of secondary neutrons after collisions. We also see from the approximate boundary condition [Eq. (A20)] that, at 2D, we should obtain $z_0 = (\pi/4) \times (\ell_{sc}^{-1} - \ell_g^{-1})^{-1}$.
32. S. Chandrasekhar, *Radiative Transfer* (Dover, 1960).
33. V. V. Sobolev, *A Treatise on Radiative Transfer* (D. Van Nostrand Co, 1963).
34. A. Peraiah, *An Introduction to Radiative Transfer: Methods and Applications in Astrophysics* (Cambridge University, 2002).
35. K. Case and P. Zweifel, *Linear Transport Theory* (Addison-Wesley, 1967).
36. L. V. Wang and H.-I. Wu, *Biomedical Optics: Principles and Imaging* (Wiley, 2007).
37. R. Elaloufi, R. Carminati, and J.-J. Greffet, "Diffusive-to-ballistic transition in dynamic light transmission through thin scattering slabs: a radiative transfer approach," *J. Opt. Soc. Am. B* **21**, 1430–1437 (2004).
38. R. Pierrat, "Propagation et émission du rayonnement en milieu diffusant. Application à l'imagerie des milieux complexes," Ph.D. thesis (École Centrale Paris, 2007).
39. L. S. Froufe-Pérez, W. Guerin, R. Carminati, and R. Kaiser, "Threshold of a random laser with cold atoms," *Phys. Rev. Lett.* **102**, 173903 (2009).
40. W. Guerin, N. Mercadier, F. Michaud, D. Brivio, L. S. Froufe-Pérez, R. Carminati, V. Ereemeev, A. Goetschy, S. E. Skipetrov, and R. Kaiser, "Towards a random laser with cold atoms," *J. Opt.* **12**, 024002 (2010).
41. N. N. Lavrinovich and V. S. Letokhov, "The possibility of the laser effect in stellar atmospheres," *Sov. Phys. J. Exp. Theor. Phys.* **40**, 800–805 (1975).
42. S. Johansson and V. S. Letokhov, "Astrophysical lasers and nonlinear optical effects in space," *New. Astron. Rev.* **51**, 443–523 (2007).
43. Q. Baudouin, "Lumière dans des vapeurs atomiques opaques: piégeage radiatif, laser aléatoire et vols de Lévy," Ph.D. thesis (Université Nice Sophia-Antipolis, 2013).
44. Note that there is a misprint in [14,41,42].
45. M. A. Noginov, J. Novak, D. Grigsby, and L. Deych, "Applicability of the diffusion model to random lasers with non-resonant feedback," *J. Opt. A* **8**, S285–S295 (2006).
46. Q. Baudouin, N. Mercadier, V. Guarrera, W. Guerin, and R. Kaiser, "A cold-atom random laser," *Nat. Phys.* **9**, 357–360 (2013).
47. W. Unno and E. A. Spiegel, "The Eddington approximation in the radiative heat equation," *Publ. Astron. Soc. Jpn.* **18**, 85–95 (1966).
48. W. J. Wiscombe and J. H. Joseph, "The range of validity of the Eddington approximation," *Icarus* **32**, 362–377 (1977).
49. G. L. Olson, L. H. Auer, and M. L. Hall, "Diffusion, P_1 , and other approximate forms of radiation transport," *J. Quant. Spectrosc. Radiat. Transfer* **64**, 619–634 (2000).
50. J. W. Zhu, D. J. Pine, and D. A. Weitz, "Internal reflection of diffusive light in random media," *Phys. Rev. A* **44**, 3948–3959 (1991).
51. I. Freund, "Surface reflections and boundary conditions for diffusive photon transport," *Phys. Rev. A* **45**, 8854–8858 (1992).
52. R. Aronson, "Boundary conditions for diffusion of light," *J. Opt. Soc. Am. A* **12**, 2532–2539 (1995).
53. H. E. Türeci, A. D. Stone, and B. Collier, "Self-consistent multimode lasing theory for complex or random lasing media," *Phys. Rev. A* **74**, 043822 (2006).
54. L. Ge, R. J. Tandy, A. D. Stone, and H. E. Türeci, "Quantitative verification of ab initio self-consistent laser theory," *Opt. Express* **16**, 16895–16902 (2008).
55. L. Ge, Y. D. Chong, and A. D. Stone, "Steady-state ab initio laser theory: generalizations and analytic results," *Phys. Rev. A* **82**, 063824 (2010).
56. A. Cerjan, Y. D. Chong, and A. D. Stone, "Steady-state ab initio laser theory for complex gain media," *Opt. Express* **23**, 6455–6477 (2015).
57. Y. Lai, S.-K. Cheung, and Z.-Q. Zhang, "Wave transport in two-dimensional random media: the ballistic to diffusive transition and the extrapolation length," *Phys. Rev. E* **72**, 036606 (2005).
58. K. Drozdowicz, E. Krynicka, and J. Dąbrowska, "Diffusion cooling of thermal neutrons in basic rock minerals by Monte Carlo simulation of the pulsed neutron experiments," *App. Rad. Isot.* **58**, 727–733 (2003).

IV.2.3. Comparison between different gain mechanisms

Using Letokhov's threshold derived in [Froufe-Pérez 2009], we can compare the different gain mechanisms [Guerin 2010, Mercadier 2011]. The atomic polarizability (or equivalently the cross sections) can be computed, sometimes analytically (for Mollow gain), more often numerically by solving the optical Bloch equations (OBEs) [Mercadier 2011], or they can be determined experimentally from transmission spectra [Guerin 2009].

Mollow gain

As previously explained, for Mollow gain, we can use an analytical expression of the polarizability [Mollow 1972], which depends on two pumping parameters, the atom-pump detuning Δ and the pump intensity parameterized by the Rabi frequency Ω . For each couple of pump parameters, one can search for the frequency of the emitted light leading to the lowest critical b_0 , since the random laser will start lasing at the optimum frequency. This procedure allows us to determine the threshold for this gain and we obtain $b_{0cr} \sim 300$ [Froufe-Pérez 2009].

Although this is within reach of experiments, there are some problems. First, as briefly discussed in the paper, the applicability of the model to the regime of very low scattering is questionable. Second, for the optimum parameters, the pump frequency is at a lower detuning than the random laser frequency, which means that the actual optical thickness for the pump beam is large. This is in contradiction with the assumption of a homogeneous pumping, which is used for the computation, because the pump beam will be attenuated inside the sample. As a consequence we don't think that Mollow gain is appropriate for making a random laser.

Non-degenerate FWM

We have also investigated an original configuration of parametric gain, namely non-degenerate FWM, for which two different frequencies ω_F and ω_B are used for the two pump fields, and amplification occurs at frequency $\omega = (\omega_F + \omega_B)/2$. This configuration seems *a priori* promising for random lasing, since it allows one to adjust the gain frequency close to the atomic frequency ω_0 to enhance scattering, while keeping the pumps far from resonance. We have experimentally characterized this parametric gain and obtained that, although a conjugated field can indeed be produced near the atomic resonance, it cannot overcome the losses due to inelastic scattering, which means that the total net gain is negative [Mercadier 2011]. This configuration is thus not appropriate for random lasing.

Raman gain between Zeeman levels

For Raman gain between Zeeman sublevels, we have used measurements of transmission spectra to evaluate the atomic polarizability entering into the threshold condition [Guerin 2009]. The transmission spectrum gives directly access to the imaginary part of the polarizability via Beer-Lambert law. In order to determine the real part we can use Kramers-Kronig relations, which are still valid for active media. By fitting the imaginary part of the polarizability by Lorentzian functions, which turns out to be a very good approximation, the real part can be determined in a straightforward way [Fig. IV.3].

Using this procedure we can evaluate Letokhov's threshold for any couple of pumping parameter. The best critical optical thickness that we obtain is $b_{0cr} \sim 200$ [Fig. IV.4]. Note that this is also reached in a regime of high gain and low scattering.

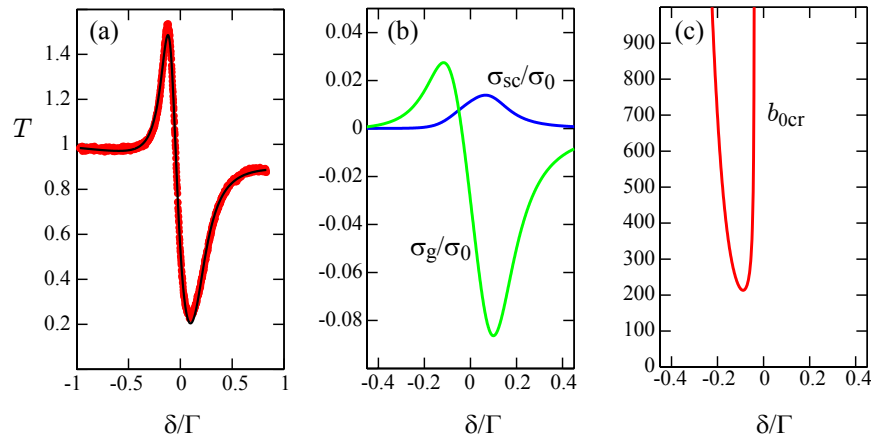


Figure IV.3: (a) Typical experimental spectrum (red dots) and its fit (black line) around the Raman resonance. (b) Gain and scattering cross sections, computed from the parameters of the Raman resonance deduced from the fit. (c) Corresponding critical optical thickness. The minimum is $b_0 \simeq 220$. This set of data corresponds to the pump parameters $\Delta = -3.4\Gamma$ and $\Omega = 3.4\Gamma$. Figure taken from [Guerin 2009].

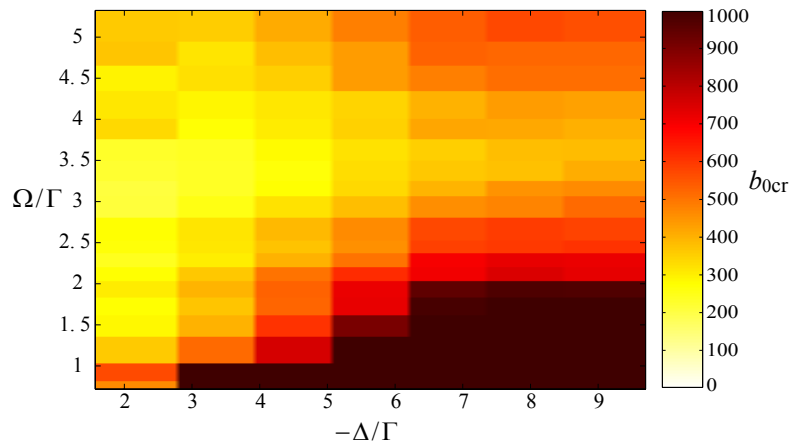


Figure IV.4: Critical optical thickness b_{0cr} as a function of the pumping parameters Δ (atom-pump detuning) and Ω (Rabi frequency of the atom-pump coupling). The minimum is around $b_{0cr} \sim 210 - 230$, for $\Delta \sim 2\Gamma$ and $\Omega \sim 2 - 3\Gamma$. Figure taken from [Guerin 2009].

Raman gain between hyperfine levels

Raman gain between hyperfine ground states is more complicated to study, as it involves more pumping parameters. Indeed, to sustain a continuous gain, a Raman laser is needed to induce the Raman two-photon transition and an optical-pumping laser is needed to maintain the population inversion (see Fig. II.3). There are thus two laser detunings and two laser intensities. Intuitively, one can expect that having more optimization parameters is favorable and should lead to a lower threshold. This is indeed what we obtain by numerically solving the OBEs and searching for the optimum parameters [Mercadier 2011]. Fig. IV.5(a) shows the critical optical thickness as a function of the detuning and intensity of the Raman laser for optical pumping parameters that have been chosen to give the lowest minimum critical optical thickness, which is $b_{0cr} \sim 100$. This is a substantial improvement in comparison with Mollow gain and Raman gain using Zeeman sublevels. However, the gain frequency is again detuned by several atomic linewidths Γ from the atomic transition that provides scattering, such that the optimum parameters correspond to a regime of low scattering compensated by a high gain.

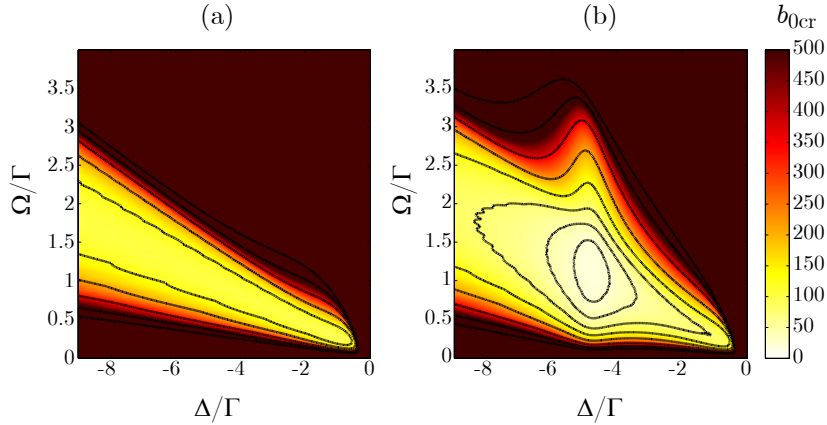


Figure IV.5: Threshold for a random laser using Raman gain between hyperfine levels, as a function of the Raman laser parameters (detuning Δ , Rabi frequency Ω). The optical pumping parameters are $\Delta_{\text{OP}} = 0$ and $\Omega_{\text{OP}} = 0.2\Gamma$. (a) Scheme with four levels. The lowest threshold is $b_{0\text{cr}} = 92$. (b) Scheme with five levels involving supplementary scattering from the $|2\rangle \rightarrow |1'\rangle$ transition (Fig. IV.6). The lowest threshold is $b_{0\text{cr}} = 20$. The contours are iso- $b_{0\text{cr}}$ lines. Figure taken from [Baudouin 2014a].

Raman gain between hyperfine level with a fifth resonant level

Fortunately, the rich atomic structure of the D_2 line of rubidium atoms (and other alkali metals) allows us to combine Raman gain between hyperfine levels with supplementary scattering provided by a supplementary closed transition. The scheme, represented in Fig. IV.6, involves five levels. As previously, two ground states ($|F = 2\rangle$ and $|F = 3\rangle$ in ^{85}Rb , noted $|2\rangle$ and $|3\rangle$) and one excited states are necessary to build Raman gain in a Λ scheme (we use $|F' = 2\rangle \equiv |2'\rangle$), and one another excited level is used for optical pumping ($|F' = 3\rangle \equiv |3'\rangle$) to sustain the population inversion. In addition, another level ($|F' = 1\rangle \equiv |1'\rangle$) can provide scattering on the gain transition if the detuning Δ of the Raman laser from the excited $|2'\rangle$ level is chosen to be equal to the frequency separation between the $|1'\rangle$ and $|2'\rangle$ levels. This supplementary level has several important features. Firstly, it is not coupled to the ground state $|3\rangle$ by any dipole-allowed transition, so that it does not interact with the Raman laser, which insures homogeneous gain. Secondly, the transition $|2\rangle \rightarrow |1'\rangle$ is closed so that it is efficient for scattering and does not change the equilibrium populations in the ground states. Finally, the separation between the $|1'\rangle$ and $|2'\rangle$ levels is only 29 MHz, which is 4.8Γ . The necessary detuning Δ is thus small enough to insure that Raman gain is efficient. Note that a similar five-level scheme is possible by using the $|F' = 4\rangle$ level for supplementary scattering but its separation from the nearest level is 20Γ and Raman gain would be much less efficient (similarly, ^{85}Rb is more favorable than ^{87}Rb because hyperfine splittings are smaller).

The relative intensity between the two external lasers allows us to adjust the relative populations, and thus to tune continuously from a sample with large gain and no scattering (with all atoms in the $|3\rangle$ state) to a situation without gain and with large scattering on the $|2\rangle \rightarrow |1'\rangle$ line (with all atoms in the $|2\rangle$ state). We can therefore search for the best trade-off between gain and scattering. With the optimum parameters, we find a critical optical thickness of $b_{0\text{cr}} \sim 20$ (Fig. IV.5(b)) with $L/\ell_{\text{sc}} \sim 6$ at the threshold², so that the diffusion approximation is justified. The model is based on the OBEs with a supplementary incoherent scattering term due to the $|2\rangle \rightarrow |1'\rangle$ transition [Mercadier 2011, Baudouin 2013b]. Note that our model neglects the Zeeman degeneracy and thus cannot use the correct relative weight of

² Here b_0 is defined as the resonant optical thickness on the $|3\rangle \rightarrow |4'\rangle$, so $b_0 = 20$ gives only $L/\ell_{\text{sc}} \sim 6$ on the $|2\rangle \rightarrow |1'\rangle$ due to a lower strength of the transition and to the partial population in $|2\rangle$.

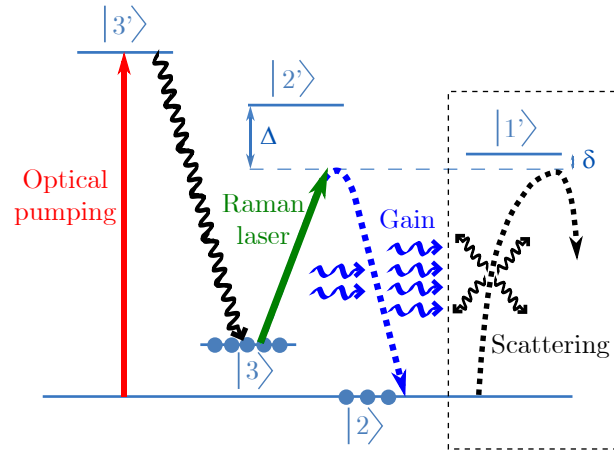


Figure IV.6: Scheme of the Raman gain used for random lasing in cold ^{85}Rb . Supplementary scattering is provided by the $|2\rangle \rightarrow |1'\rangle$ transition (dashed box). Taken from [Baudouin 2014a].

the different lines. It is thus not precise enough for quantitative predictions. Nevertheless, this gain mechanism seems by far the most appropriate to look for experimental signatures of random lasing.

IV.3. Experimental signature of random lasing and modeling

We have implemented the five-level Raman gain scheme described above. Remains the question of detecting the random laser. This is also a challenge, since the emission is not directional and is mixed with light scattered on all other lines. The different lines are also very hard to spectrally separate, even if some attempts have been done [Mercadier 2011]. Fortunately, we could find an indirect signature of the random laser threshold and emission in the total fluorescence.

The experimental procedure is described in the following paper [Baudouin 2013b] and is summarized as follows. We prepare a sample of cold atoms of ^{85}Rb with a MOT. A controlled compression period provides a variable optical thickness b_0 with a constant number of trapped atoms. We then switch off all lasers and magnetic field gradients during 1 ms before applying strong counterpropagating Raman beams. The optical-pumping laser is tuned slightly below the $|2\rangle \rightarrow |3'\rangle$ transition. Note that with the chosen detunings, the external lasers operate in the single scattering regime. The Raman laser detuning is swept slowly around $\delta = 0$, where Raman gain is on resonance with the $|2\rangle \rightarrow |1'\rangle$ transition. We measure the total emitted fluorescence, which we collect with a solid angle of $\sim 10^{-2}$ sr, and we average the detected signal over ~ 4000 cycles. We repeat the measurement for different optical thicknesses while keeping the atom number constant. Variations in the fluorescence can thus only be related to collective effects. Our observations are reported in Fig. IV.7.

Before commenting on the observations, it is important to precisely understand what we look at and why. We measure the *total emitted light* by the atomic cloud when the two external lasers are applied. This signal contains the random-laser light, but also light which is scattered from the two external lasers (and might be subsequently amplified for Raman-scattered light from the Raman laser). Moreover, in random lasers, there is not any privileged emission direction that allows one to spatially separate the random-laser light. In usual random lasers, the separation is done either spectrally or temporally (using very short pump pulses), which is very important because the light scattered from the pump is much more intense than the

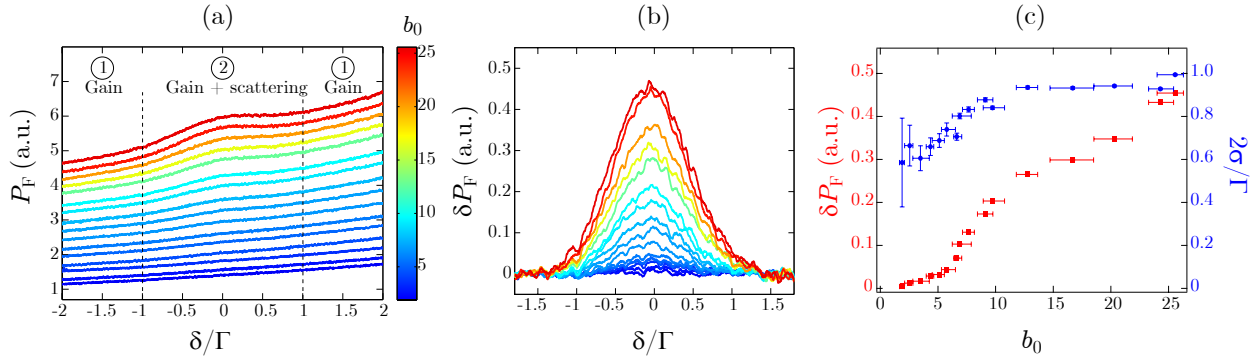


Figure IV.7: (a) Measurement of the total fluorescence emitted by the cloud as a function of the Raman laser detuning for different on-resonance optical thickness b_0 . (b) Supplementary fluorescence around $\delta = 0$ for different optical thicknesses (same color scale). The raw data are the same as in panel (a) but the wings have been subtracted and the signal has been smoothed. (c) From a Gaussian fit we extract the amplitude (red squares) and the r.m.s. width σ (blue circles) of the curves shown in (b) as a function of the optical thickness b_0 . The vertical error bars are the statistical uncertainties of the fit (not visible for the amplitude) and the horizontal error bars correspond to the fluctuations of b_0 on 5 shots. Adapted from [Baudouin 2014a].

random laser itself. In our system, however, the $|2\rangle \rightarrow |1'\rangle$ transition does not scatter light from the two external lasers. The random-laser line has thus a strength comparable to the one of the other involved transitions and that is why it is possible to detect the random laser signal in the total fluorescence. It should also be stressed that in a standard laser, the beam is well separated from the fluorescence of the gain medium, thanks to the cavity. This is not the case in our system, where both are measured together. Finally, it may be useful to have in mind that looking at the total emitted light is equivalent, due to energy conservation, to looking at the pump depletion (here the two external lasers).

A first signature of a collective behavior can be seen in a regime of negligible scattering, far from the $|2\rangle \rightarrow |1'\rangle$ transition [regions 1 in Fig. IV.7(a)]: amplified spontaneous emission (ASE) induces an overall increase of the fluorescence as a function of b_0 . Photons from the Raman beam can indeed undergo a spontaneous Raman transition. The corresponding scattered light is then amplified by Raman gain produced by the surrounding atoms while leaving the sample with a ballistic path. The efficiency of this process is directly related to the optical thickness. The ASE signal decreases as the Raman laser is detuned further away from the $|3\rangle \rightarrow |2'\rangle$ transition (located at $\delta = +4.8\Gamma$) since both the spontaneous (source contribution) and stimulated (gain contribution) Raman scattering rates decrease for larger detuning. Note that when tuning the Raman laser very close to the $|3\rangle \rightarrow |2'\rangle$ line, Rayleigh scattering dominates. Population redistribution is then responsible for the increase of fluorescence [Baudouin 2013c]. This effect is negligible for the detunings considered here, and only gain can explain the observed features.

When the Raman laser is tuned close to $\delta = 0$, the combination of gain and scattering gives rise to an enhanced fluorescence bump that emerges as the optical thickness b_0 is increased [region 2 in Fig. IV.7(a)]. This feature is due to the combined effect of gain and scattering: multiple scattering increases the path length of the photons that are amplified by Raman gain. This is exactly the mechanism at the heart of random lasing. The only remaining question to be answered before concluding that we observe random lasing is to know if the system is above the threshold or not.

To answer this question, we plot the supplementary fluorescence as a function of the on-

resonance optical thickness b_0 . To better extract this signal, we fit the wings of the curve (regions 1) by adjustable slope and curvature and remove this background. The remaining signal is a bell-shaped curve, well-centered at $\delta = 0$ [Fig. IV.7(b)]. Surprisingly, it is very well fitted by a Gaussian. We can thus use a Gaussian fit to extract its amplitude and width, as reported in Fig. IV.7(c). Although the signal consists of different emission lines, a threshold of the peak amplitude is clearly visible, with a change of slope at $b_0 = 6 \pm 1$. We interpret this threshold as the signature of the occurrence of random lasing in our sample when the Raman beams are tuned around $\delta \sim 0$ and when $b_0 > 6$. We stress that varying the optical thickness acts simultaneously on the amount of gain and feedback provided by the medium. This is unusual in laser physics, where the threshold is most-commonly defined as a critical pump power. In our case, increasing the optical-pumping intensity increases indeed the population inversion that provides gain, but simultaneously decreases the feedback, so that random lasing needs a fine tuning of the laser parameters. This extra random-laser bump was indeed seen only in a narrow range of parameters.

A cold-atom random laser

Q. Baudouin, N. Mercadier[†], V. Guarrera[†], W. Guerin and R. Kaiser[★]

In conventional lasers optical cavities are used to provide feedback to gain media. Mirrorless lasers can be built by using disordered structures to induce multiple scattering, which increases the path length in the medium, providing the necessary feedback¹. Interestingly, light or microwave amplification by stimulated emission also occurs naturally in stellar gases^{2–4} and planetary atmospheres^{5,6}. The possibility of additional scattering-induced feedback^{4,7}—random lasing^{8–14}—could explain the unusual properties of some space masers¹⁵. Here, we report experimental evidence of random lasing in a controlled, cold atomic vapour, taking advantage of Raman gain. By tuning the gain frequency in the vicinity of a scattering resonance, we observe an enhancement of the light emission due to random lasing. The unique possibility to both control the experimental parameters and to model the microscopic response of our system provides an ideal test bench for better understanding natural lasing sources, in particular the role of resonant scattering feedback in astrophysical lasers.

A cloud of cold atoms constitutes a new medium to study random lasing^{8–14}, allowing a detailed microscopic understanding of gain and scattering. Multiple scattering of light in cold atoms has been extensively studied in the past^{16,17}. Furthermore, quasi-continuous lasing with cold atoms as a gain medium, either placed inside optical cavities^{18–21} or based on distributed feedback²², has recently been demonstrated, illustrating the potential for a variety of gain mechanisms in a regime where optical coherence is limited by purely radiative decay channels. This is significantly different with respect to most random lasing devices, based on pulsed excitation of condensed-matter systems, where the relaxation rates of the optical coherence are several orders of magnitude faster than the decay of the excited state population. Long phase coherence times however allow for efficient feedback by resonant scattering, as expected in astrophysical lasers⁴.

To combine sufficient gain and scattering while using only one atomic species, we take advantage of the multilevel structure of rubidium atoms, shown in Fig. 1a (D_2 line of ⁸⁵Rb, wavelength $\lambda = 780$ nm). Two-photon Raman gain is obtained by a population inversion between the two hyperfine ground states $|2\rangle$ and $|3\rangle$ sustained by optical pumping. A Raman laser drives the $|3\rangle \rightarrow |2\rangle$ transition with a large detuning Δ , so that atoms can be transferred into the $|2\rangle$ state by stimulated emission. Scattering required for random lasing is provided by the $|2\rangle \rightarrow |1'\rangle$ line, which is a closed transition efficient for multiple scattering. Both Raman gain and scattering can occur at the same frequency (that is, for the same photons) by an appropriate choice of the Raman detuning $\Delta = -4.8\Gamma$, determined by the hyperfine splitting between the $|1'\rangle$ and $|2'\rangle$ states ($\Gamma/2\pi = 6$ MHz is the linewidth of the transition). We thus tune the Raman laser to the vicinity of this condition and define the detuning $\delta = \Delta + 4.8\Gamma$ as the relevant parameter (Fig. 1a). This scheme takes advantage of the selection rules, which forbid electric

dipole transitions between the states $|3\rangle$ and $|1'\rangle$, so that the $|1'\rangle$ level does not affect the Raman gain.

For a given amount of gain and scattering, the threshold of random lasing is determined by a critical minimum size of the sample¹. In our case, gain and scattering are provided by the same atoms and depend on the atomic density n . We have shown^{23–25} that the critical parameter defining the random-laser threshold is the on-resonance optical thickness b_0 , defined for a homogeneous cloud of radius R as $b_0 = 2n\sigma_{34'}R$, with $\sigma_{34'}$ being the on-resonance scattering cross-section for the $|3\rangle \rightarrow |4'\rangle$ transition (used to measure b_0 ; see Methods and Supplementary Fig. S1). Moreover, its critical value can be computed from the atomic polarizability alone (see Supplementary Information).

Our sample consists of a cloud of cold ⁸⁵Rb atoms collected in a magneto-optical trap. A controlled compression period provides a variable optical thickness b_0 with a constant number of trapped atoms (see Methods). We then switch off all lasers and magnetic field gradients 1 ms before applying strong counterpropagating Raman beams (intensity $I_{\text{Ra}} = 4.25$ mW cm⁻² per beam with crossed linear polarizations) tuned around $\delta \sim 0$. In addition, we use an optical-pumping laser tuned slightly below the $|2\rangle \rightarrow |3'\rangle$ transition to sustain a steady-state population inversion between the two hyperfine levels involved in our scheme. The relative intensity between the two external lasers allows us to adjust the relative populations, and thus to tune continuously from a sample with large gain and no scattering (with all atoms in the $|3\rangle$ state) to a situation without gain and with large scattering on the $|2\rangle \rightarrow |1'\rangle$ line (with all atoms in the $|2\rangle$ state). Note that with the chosen detunings, these lasers operate in the single scattering regime. The data presented here have been obtained with an optical-pumping intensity $I_{\text{OP}} = 2.9$ mW cm⁻², ensuring a small population inversion.

In random lasers, there is not any privileged emission direction that allows one to spatially separate the random-laser light from amplified spontaneous emission and scattering from the pump beam, which is usually much stronger than the random-laser emission itself. In our system, however, the $|2\rangle \rightarrow |1'\rangle$ transition does not scatter light from the two external lasers. The random-laser line thus has a strength comparable to the one of the other involved transition and the signature of random lasing can be obtained by the detection of the total emitted light from the sample, which we collect with a solid angle of 10^{-2} sr at an angle of 40° with respect to the Raman beam axes (Fig. 1b). Figure 2 shows the measured fluorescence as the Raman laser frequency is swept through the region of interest, for different values of the optical thickness b_0 of the atomic cloud (see Methods). We stress that for these measurements we vary b_0 while keeping the atom number constant. Variations in the fluorescence can thus only be related to collective features.

The first signature of such a collective behaviour can be seen in a regime of negligible scattering, far from the $|2\rangle \rightarrow |1'\rangle$

Institut Non Linéaire de Nice, CNRS, Université de Nice Sophia-Antipolis, 1361 route des Lucioles, 06560 Valbonne, France. [†]Present addresses: Saint-Gobain Recherche, 39 quai Lucien Lefranc, 93303 Aubervilliers, France (N.M.); LNE-SYRTE, Observatoire de Paris, CNRS, UPMC, 61 avenue de l'Observatoire, 75014 Paris, France (V.G.). *e-mail: robin.kaiser@inln.cnrs.fr

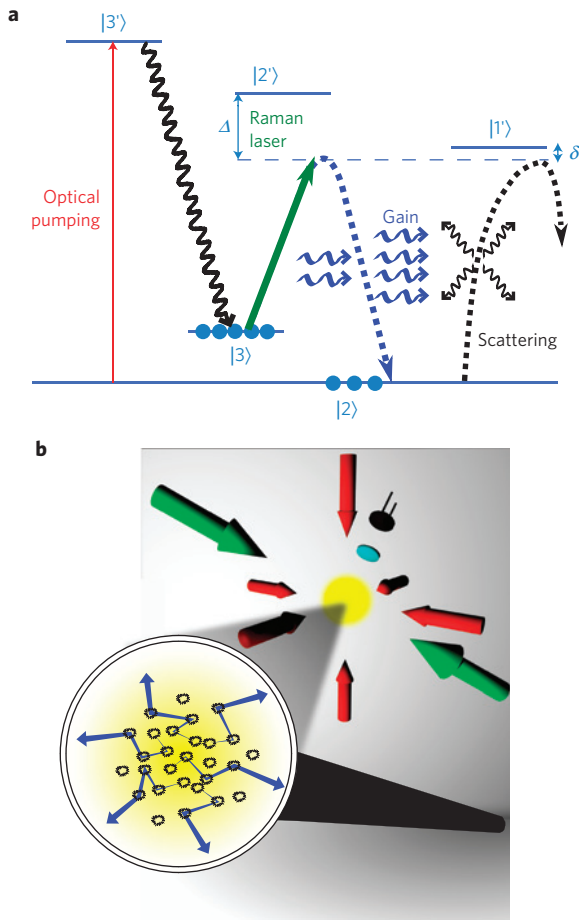


Figure 1 | Working principle of the random laser. **a**, Atomic transitions of the D_2 line of ^{85}Rb (at $\lambda = 780.24$ nm) used to create random lasing in cold atoms. The two hyperfine ground states are $|2\rangle = |F=2\rangle$ and $|3\rangle = |F=3\rangle$, separated by 3 GHz. Similarly, the involved hyperfine excited states are the states $|F'=1, 2, 3\rangle$ denoted $|1'\rangle$, $|2'\rangle$ and $|3'\rangle$ with splittings of a few tens of megahertz. Optical pumping creates a population inversion between $|2\rangle$ and $|3\rangle$. This allows us to create Raman gain by applying a laser with a detuning Δ from the $|3\rangle \rightarrow |2'\rangle$ transition. The gain frequency has a detuning δ from the closed $|2\rangle \rightarrow |1'\rangle$ transition. Around $\delta \sim 0$, this transition provides efficient scattering. Random lasing can thus occur around this frequency. **b**, Schematic of the experiment. The cold-atom cloud (yellow sphere) is exposed to two Raman-laser beams (green) and six optical-pumping beams (red). Its fluorescence is collected by a lens and detected by a photodiode. Zoom-in: light (in blue) is scattered by atoms in the $|2\rangle$ state (black) and amplified by atoms in the $|3\rangle$ state (yellow background).

transition (regions 1 of Fig. 2): amplified spontaneous emission (ASE) induces an overall increase of the fluorescence as a function of b_0 . Photons from the Raman beam can indeed undergo a spontaneous Raman transition. The subsequent scattered light is then amplified by Raman gain produced by the surrounding atoms while leaving the sample with a ballistic path. The efficiency of this process is directly related to the optical thickness (see Supplementary Information). The ASE signal decreases as the Raman laser is detuned further away from the $|3\rangle \rightarrow |2'\rangle$ transition (located at $\delta = +4.8\Gamma$) because both the spontaneous (source contribution) and stimulated (gain contribution) Raman scattering rates decrease for larger detuning. Note that when tuning the Raman laser very close to the $|3\rangle \rightarrow |2'\rangle$ line, single-photon scattering dominates. As detailed in ref. 26, population redistribution is then

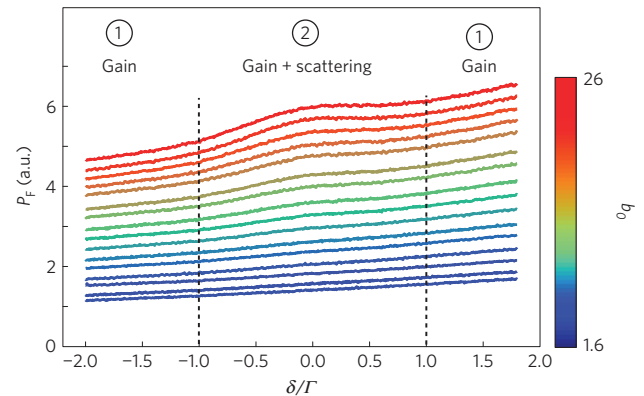


Figure 2 | Fluorescence measurement. Total fluorescence P_F as a function of the Raman laser detuning δ (in units of the linewidth Γ of the optical transition) recorded for optical thickness varying from $b_0 = 1.9$ to $b_0 = 26$. The number of atoms is kept constant at $N = 7 \times 10^8 \pm 12\%$. Two collective features are visible. In the wings (regions 1), the overall increase of the fluorescence with b_0 is due to amplified stimulated emission. Around $\delta \sim 0$ (region 2), an extra peak appears for large optical thickness. This enhanced light emission is due to the combination of Raman gain and multiple scattering provided by the $|2\rangle \rightarrow |1'\rangle$ transition and is thus a signature of random lasing.

responsible for the increase of fluorescence. This effect is negligible for the detunings considered here, and only gain can explain the observed features.

When the Raman laser is tuned close to $\delta = 0$ (region 2 of Fig. 2), the combination of gain and scattering gives rise to a random laser. It appears as an enhanced fluorescence bump that emerges as the optical thickness b_0 is increased. To better extract this signal, we fit the wings of the curves (regions 1) by adjustable slope and curvature and remove this ASE background. The remaining random-laser signal is a Gaussian peak, well centred at $\delta = 0$ (Fig. 3a), which thus comes from the scattering due to the $|2\rangle \rightarrow |1'\rangle$ transition. Therefore, the observed peak is due to the combination of gain and scattering. Moreover, although the signal consists of different emission lines, a threshold of the peak amplitude is clearly visible, with a change of slope at $b_0 = 6 \pm 1$ (Fig. 3b). This threshold is the signature of the occurrence of random lasing in our sample when the Raman beams are tuned around $\delta \sim 0$ and when $b_0 > 6$. We stress that varying the optical thickness acts simultaneously on the amount of gain and feedback provided by the medium. This is unusual in laser physics, where the threshold is most commonly defined as a critical pump power. In our case, increasing the optical-pumping intensity indeed increases the population inversion that provides gain, but simultaneously decreases the feedback, so that random lasing needs a fine tuning of the laser parameters.

Finally, we have exploited the possibility to perform *ab initio* theory by developing two simple models, one for ASE and the other for random lasing. Both are detailed in the Supplementary Information. Here, we describe briefly the random-lasing model. It consists of self-consistently coupling the atomic response, based on optical Bloch equations with additional scattering on the $|2\rangle \rightarrow |1'\rangle$ line, to a diffusion equation for the light scattered on the $|2\rangle \rightarrow |1'\rangle$ resonance. The optical Bloch equations allow us to compute the atomic polarizability and, including the additional scattering on the $|2\rangle \rightarrow |1'\rangle$ line, the mean-free path ℓ_{sc} and the gain length ℓ_g , including saturation effects due to the random laser intensity I_{RL} inside the sample. As in conventional laser theory, we look for a steady-state solution where gain exactly compensates losses. In the diffusive regime and taking into account only the diffuse mode with

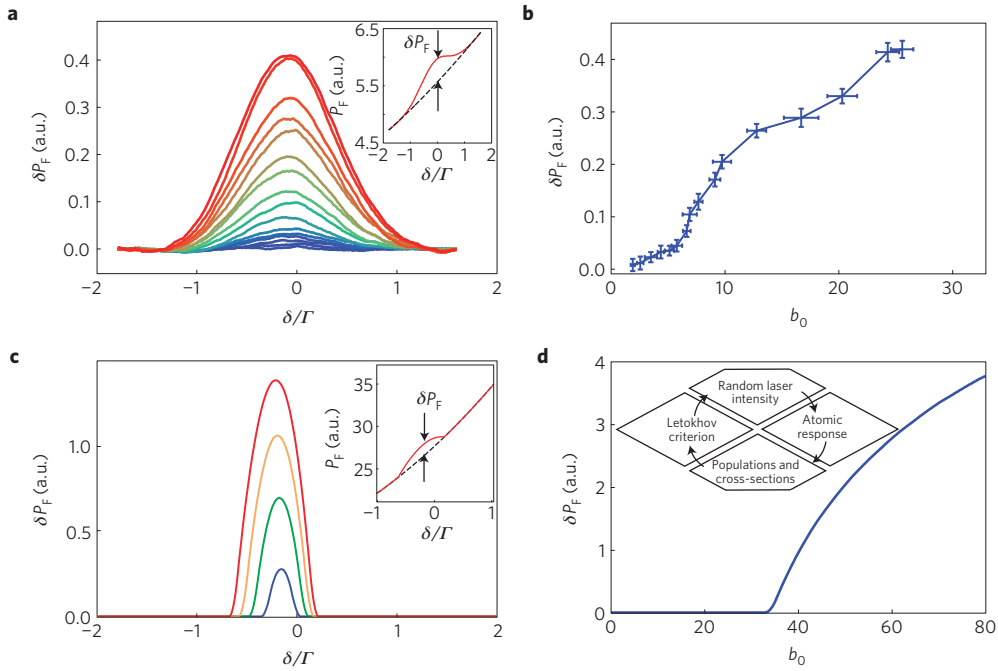


Figure 3 | Random laser emission around $\delta = 0$. **a**, Measured supplementary fluorescence δP_F due to random lasing as a function of the Raman laser detuning δ , measured for optical thickness varying from $b_0 = 1.9$ to $b_0 = 26$. The source data and the colour scale are the same as in Fig. 2, but the wings (regions 1 in Fig. 2) have been subtracted. The inset illustrates the fitting procedure. For clarity we also smoothed the data, corresponding to a detuning resolution of 0.3Γ . **b**, Measured amplitude of the peak due to random lasing. A threshold optical thickness is clearly visible at $b_0 \sim 6$. Vertical error bars correspond to the root mean squared noise on the data of Fig. 2 and horizontal error bars to shot-to-shot fluctuations of b_0 . **c**, Computed supplementary fluorescence δP_F as a function of the detuning δ , using our self-consistent model for random lasing, neglecting the contribution from ASE, for four different optical thicknesses, $b_0 = 26$ (blue), $b_0 = 30$ (green), $b_0 = 34$ (orange) and $b_0 = 38$ (red). **d**, Maximum supplementary fluorescence δP_F computed from the self-consistent model for random lasing. Inset: principle of the model. The atomic response allows the computation of the threshold optical thickness following Letokhov's criterion^{1,23}. Owing to saturation effects, this threshold depends on the random-laser intensity. Therefore, for each b_0 , we find the random-laser intensity such that the computed threshold equals b_0 , corresponding to a steady state (see Supplementary Information).

the longest lifetime, this condition is equivalent to Letokhov's result on the random-lasing threshold^{1,23},

$$R_{cr} = \pi \sqrt{\frac{\ell_{sc} \ell_g}{3}} \quad (1)$$

where R_{cr} is the critical sample size. As a consequence, for a given b_0 , we find the value of I_{RL} such that equation (1) is fulfilled. Considering the absence of any free fitting parameter and the simplicity of our model, which neglects for instance the contribution of ASE, the experimental data and the computed values for the supplementary fluorescence show satisfactory qualitative agreement (Fig. 3). The quantitative discrepancies suggest the need for more involved models. Many ingredients could play a role in our experiment and have been neglected in our models, such as the inelastic spectrum of the emitted light, interference effects on light transport, light polarization, the Zeeman degeneracy of the involved atomic levels, the finite temperature, the inhomogeneous atomic density distribution, and cooperative effects^{21,27}. The comparison between the experiment and new models including some of these effects will allow one to identify the most relevant ones and thus to better understand random-laser physics.

We have presented experimental evidence of combined gain and scattering of light in a cloud of cold atoms, demonstrating random lasing in a dilute vapour. This type of experiment, based on well-controlled atomic systems, with the possibility of *ab initio* calculations, will allow studying the role of interferences and cooperativity in random lasing^{27–29}. The combined theoretical and experimental approach described in this work can also be applied to realistic atomic structures encountered in astrophysical systems

and to test new detection schemes, based for instance on high-order photon correlations³⁰.

Methods

Sample preparation. In our experiment 6 counter-propagating trapping beams with a waist of 3.4 cm ($1/e^2$ radius of the intensity distribution) are used to load ⁸⁵Rb atoms from a background atomic vapour into a magneto-optical trap (MOT). The trapping beams are detuned by -3Γ from the $|3\rangle \rightarrow |4'\rangle$ hyperfine transition. To maintain the atomic populations in $|3\rangle$, we add 6 repumper beams tuned slightly below the $|2\rangle \rightarrow |3'\rangle$ transition. We can load between 10^8 and 10^{11} atoms by changing the background vapour pressure and the duration of the trap loading (from 10 to 500 ms). Once the atoms are trapped in the MOT, we perform a temporal dark-MOT stage by increasing the detuning of the trapping beams to -6Γ and by reducing the intensity of the repumper beams to a few per cent of their initial value. This leads to an increase of the spatial density and thus of the optical thickness b_0 of the cloud, without loss of atoms. By changing the duration of this compression stage, we are able to tune b_0 from 1.9 to 27, while keeping almost constant the total number of atoms, which, for the measurements presented here, is set to $7 \times 10^8 \pm 12\%$. The temperature is $T \sim 50 \mu\text{K}$. The optical thickness b_0 is measured by a transmission spectrum with a small and weak probe beam on the $|3\rangle \rightarrow |4'\rangle$ transition²⁴. The shot-to-shot fluctuations of b_0 (horizontal error bars in Fig. 3b) are evaluated by repeating the measurement five times.

Data acquisition. After the sample preparation, we switch off magnetic field gradients and trapping lasers and we expose the sample to two counterpropagating Raman beams with waists of 2.4 cm, intensities of 4.25 mW cm^{-2} each and linear orthogonal polarizations, and 3 pairs of counterpropagating optical pumping beams with waists of 3.4 cm, intensities of 0.48 mW cm^{-2} and σ^+/σ^- polarizations, each at a detuning of -3Γ from the $|2\rangle \rightarrow |3'\rangle$ transition. Note that the diameters of these lasers are large enough to ensure that their effective intensities on the atom cloud are independent from the chosen optical thickness. The Raman laser is obtained from a distributed-Bragg-reflector laser diode and is frequency-tuned by a double-pass acousto-optic modulator before it is amplified by two stages of saturated slave lasers. This system allows us to scan the frequency in a range up to 16Γ with intensity variations of only 0.1%.

The measuring procedure consists of scanning in 2 ms the Raman beam detuning δ from $-3, 2\Gamma$ to $4, 8\Gamma$ while a high-gain photodiode gathers the fluorescent emission of the cloud in a solid angle of $\sim 10^{-2}$ sr. The detected power is of the order of 0.4 nW. We checked that the direction of the sweep does not change the detected fluorescence, and that the duration of the sweep is short enough to avoid significant variations of b_0 during the measurements ($<5\%$) and long enough to probe a quasi-steady state (the sweep rate is $4\Gamma \text{ ms}^{-1}$). We averaged over 4,000 subsequent measurements to increase the signal-to-noise ratio, thus performing also an averaging over the disorder configurations.

Received 14 December 2012; accepted 22 March 2013;
published online 5 May 2013

References

- Letokhov, V. S. Generation of light by a scattering medium with negative resonance absorption. *Sov. Phys. JETP* **16**, 835–840 (1968).
- Weaver, H., Williams, D. R. W., Dieter, N. H. & Lum, W. T. Observations of a strong unidentified microwave line and of emission from the OH molecule. *Nature* **208**, 29–31 (1965).
- Letokhov, V. S. Laser action in stellar atmospheres. *IEEE J. Quantum Electron.* **8**, 615 (1972).
- Letokhov, V. S. & Johansson, S. *Astrophysical Lasers* (Oxford Univ. Press, 2009).
- Johnson, M. A., Betz, M. A., McLaren, R. A., Sutton, E. C. & Townes, C. H. Nonthermal 10 micron CO_2 emission lines in the atmospheres of Mars and Venus. *ApJ* **208**, L145–L148 (1976).
- Mumma, M. J. *et al.* Discovery of natural gain amplification in the 10-micrometer carbon dioxide laser bands on Mars: A natural laser. *Science* **212**, 45–49 (1981).
- Lavrinovich, N. N. & Letokhov, V. S. The possibility of the laser effect in stellar atmospheres. *Sov. Phys. JETP* **40**, 800–805 (1975).
- Markushev, V. M., Zolin, V. F. & Briskina, C. M. Luminescence and stimulated emission of neodymium in sodium lanthanum molybdate powders. *Sov. J. Quantum Electron.* **16**, 281–282 (1986).
- Lawandy, N. M., Balachandran, R. M., Gomes, A. S. L. & Sauvain, E. Laser action in strongly scattering media. *Nature* **368**, 436–438 (1994).
- Cao, H. *et al.* Random laser action in semiconductor powder. *Phys. Rev. Lett.* **82**, 2278–2281 (1999).
- Wiersma, D. S. & Cavaliere, S. A temperature-tunable random laser. *Nature* **414**, 708–709 (2001).
- Wiersma, D. S. The physics and applications of random lasers. *Nature Phys.* **4**, 359–367 (2008).
- Wiersma, D. S. & Noginov, M. A. Special issue on Nano and random laser. *J. Opt.* **12**, 020201 (2010).
- Wiersma, D. S. Disordered photonics. *Nature Photon.* **7**, 188–196 (2013).
- Truitt, P. & Strelitski, V. Transition to oscillation regime in flaring water vapour masers. *Bull. Am. Astron. Soc.* **32**, 1484 (2000).
- Labeurie, G. *et al.* Slow diffusion of light in a cold atomic cloud. *Phys. Rev. Lett.* **91**, 223904 (2003).
- Labeurie, G., Delande, D., Müller, C. A., Miniature, C. & Kaiser, R. Multiple scattering of light in a resonant medium. *Opt. Commun.* **243**, 157–164 (2004).
- McKeever, J., Boca, A., Boozer, A. D., Buck, J. R. & Kimble, H. J. Experimental realization of a one-atom laser in the regime of strong coupling. *Nature* **425**, 268–271 (2003).
- Guerin, W., Michaud, F. & Kaiser, R. Mechanisms for lasing with cold atoms as the gain medium. *Phys. Rev. Lett.* **101**, 093002 (2008).
- Vrijnsen, G., Hosten, O., Lee, J., Bernon, S. & Kasevich, M. A. Raman Lasing with a Cold Atom Gain Medium in a High-Finesse Optical Cavity. *Phys. Rev. Lett.* **107**, 063904 (2011).
- Bohnet, J. *et al.* A steady-state superradiant laser with less than one intracavity photon. *Nature* **484**, 78–81 (2012).
- Schilke, A., Zimmermann, C., Courteille, Ph. W. & Guerin, W. Optical parametric oscillation with distributed feedback in cold atoms. *Nature Photon.* **6**, 101–104 (2011).
- Froufe-Pérez, L. S., Guerin, W., Carminati, R. & Kaiser, R. Threshold of a random laser with cold atoms. *Phys. Rev. Lett.* **102**, 173903 (2009).
- Guerin, W., Mercadier, N., Brivio, D. & Kaiser, R. Threshold of a random laser based on Raman gain in cold atoms. *Opt. Express* **17**, 11236–11245 (2009).
- Guerin, W. *et al.* Towards a random laser with cold atoms. *J. Opt.* **12**, 024002 (2010).
- Baudouin, Q., Mercadier, N. & Kaiser, R. Steady-state signatures of radiation trapping by cold multilevel atoms. *Phys. Rev. A* **87**, 013412 (2013).
- Goetschy, A. & Skipetrov, S. E. Euclidean matrix theory of random lasing in a cloud of cold atoms. *Europhys. Lett.* **96**, 34005 (2011).
- Türeci, H. E., Ge, L., Rotter, S. & Stone, A. D. Strong interactions in multimode random lasers. *Science* **320**, 643–646 (2008).
- Conti, C. & Fratalocchi, A. Dynamic light diffusion, three-dimensional Anderson localization and lasing in inverted opals. *Nature Phys.* **4**, 794–798 (2008).
- Dravins, D. in *High Time Resolution Astrophysics* (eds Phelan, D., Ryan, O. & Shearer, A.) 95–132 (Astrophysics and Space Science Library, Vol. 351, Springer, 2008).

Acknowledgements

We acknowledge financial support from ANR (project ANR-06-BLAN-0096), CG06, PACA, DGA and the Research Executive Agency (programme COSCALI, No. PIRSES-GA-2010-268717). We thank R. Carminati and S. Skipetrov for fruitful discussions, and A. Aspect and S. Tanzilli for useful comments on the manuscript.

Author contributions

Q.B., N.M. and V.G. carried out the experiment and analysed the data; Q.B., N.M. and R.K. developed the theory; Q.B., W.G. and R.K. wrote the paper; R.K. supervised the project. Q.B. and N.M. contributed equally to the study. All authors discussed the results and commented on the manuscript.

Additional information

Supplementary information is available in the [online version of the paper](#). Reprints and permissions information is available online at www.nature.com/reprints. Correspondence and requests for materials should be addressed to R.K.

Competing financial interests

The authors declare no competing financial interests.

A cold-atom random laser (Supplementary Information)

Q. Baudouin, N. Mercadier, V. Guarrera, W. Guerin and R. Kaiser

Institut Non Linéaire de Nice, CNRS and Université Nice Sophia-Antipolis, 1361 route des Lucioles, 06560 Valbonne, France

In this supplementary online material, we describe the models used in this study.

I. ATOMIC MODEL

We describe the atom-light interaction by a semi-classical model based on the optical Bloch equations (OBEs). We have to consider five atomic levels: the two ground states $|F = 2, 3\rangle$ (denoted hereafter $|2\rangle$ and $|3\rangle$) and the three excited states $|F' = 1, 2, 3\rangle$ (denoted $|1'\rangle$, $|2'\rangle$ and $|3'\rangle$). They are coupled to each other by three optical fields: the external Raman laser (subscript Ra in the following), the external optical pumping (OP) and the self-generated “random-laser” (RL) around the Raman gain frequency, see Fig. S1. The Raman laser is detuned by Δ_{Ra} from the $|3\rangle \rightarrow |2'\rangle$ transition, the random laser has a detuning Δ_{RL} from the $|2\rangle \rightarrow |2'\rangle$ transition, and the optical pumping has a detuning Δ_{OP} from the $|2\rangle \rightarrow |3'\rangle$ transition. The linewidth Γ of all optical transitions is $\Gamma/2\pi = 6.07$ MHz.

In first approximation, the detunings Δ_{Ra} and Δ_{RL} are equals (and noted Δ and δ for simplicity in Fig. S1 and the main paper). However, the frequency for which the random laser starts is not exactly given by the bare-atom two-photon resonance condition. One reason for this are the various light-shifts of the atomic levels coupled to different lasers. As a consequence, it is necessary to let Δ_{Ra} and Δ_{RL} be independent parameters in the evaluation of the

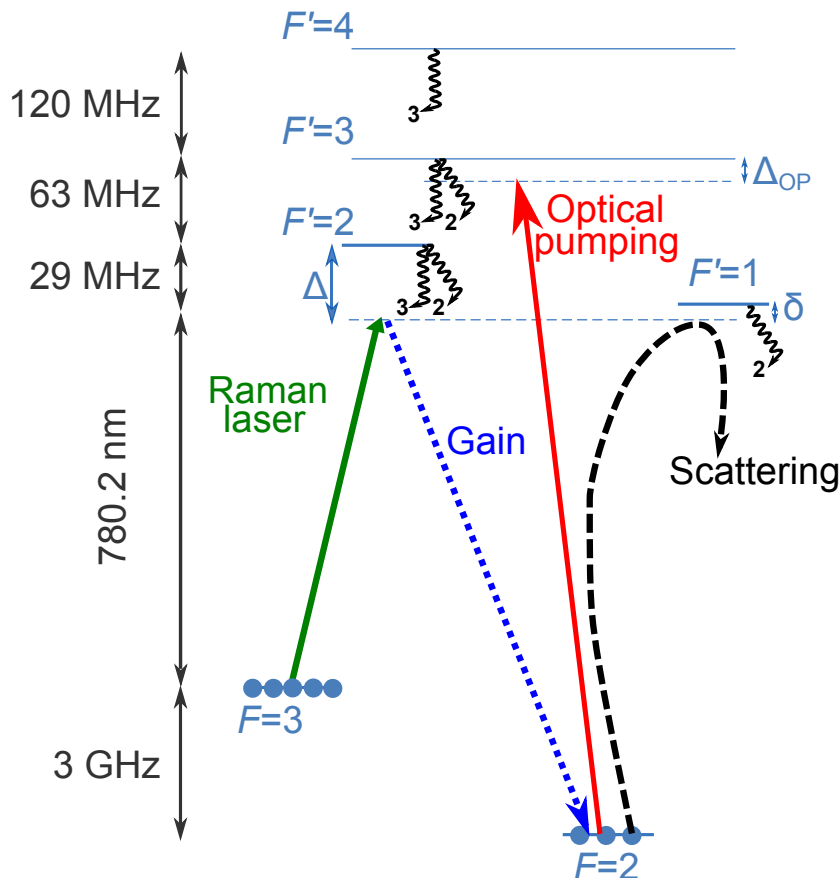


Fig. S1: **Considered atomic levels and optical fields.** The level $|4'\rangle = |F' = 4\rangle$ is only used in the laser-cooling process and is thus not included in our model. The five other levels are taken into account as well as the three optical fields: the Raman laser, the optical pumping and the “random-laser” line, where Raman gain and scattering are combined.

atomic response. Finally, we define also these detunings relatively to the $|1'\rangle$ state and note $\delta_{\text{Ra,RL}} = \Delta_{\text{Ra,RL}} + 4.8\Gamma$, where 4.8Γ is the hyperfine splitting between the $|1'\rangle$ and $|2'\rangle$ states.

A. Reduction from five to four levels

Including the $|1'\rangle$ in a fully coherent model leads to the appearance of coherence effects when we compute the scattering cross-section around the random-laser frequency: the contribution of the $|2\rangle \rightarrow |2'\rangle$ and $|2\rangle \rightarrow |1'\rangle$ transitions interfere, yielding sharp variations with the frequency [1]. We neglect these effects as we assume them to be irrelevant in the experiment because the coherence between the $|1'\rangle$ and $|2'\rangle$ states is expected to be destroyed by the multiple scattering undergone by the random-laser light.

We thus choose to describe by OBEs the coupling between the 4 levels $|F=2\rangle$, $|F=3\rangle$, $|F=2'\rangle$, $|F=3'\rangle$ and include the contribution of the $|1'\rangle$ state only as a supplementary scattering term, which adds incoherently to the off-resonant scattering provided by the $|2'\rangle$ state. We thus write for the total scattering cross-section,

$$\sigma_{\text{sc,tot}}(\delta_{\text{RL}}) = \sigma_{\text{sc}}(\delta_{\text{RL}}) + \mathcal{C}\langle\tilde{\rho}_{22}\rangle\frac{\sigma_0}{1 + 4\delta_{\text{RL}}^2/\Gamma^2}, \quad (1)$$

where σ_{sc} and $\tilde{\rho}_{22}$ are, respectively, the scattering cross-section and the population of the $|2\rangle$ state, derived from a four-level model (without the $|1'\rangle$ level) as detailed below. The resonant scattering cross-section is $\sigma_0 = 3\lambda^2/2\pi$ with $\lambda = 780.2$ nm the wavelength of the D₂ line and $\mathcal{C} = \frac{1}{3}\frac{2F'+1}{2F+1} = \frac{1}{5}$ corresponds to the average coupling of the $|2\rangle \rightarrow |1'\rangle$ transition assuming a statistical mixture of the Zeeman sublevels [2]. For $\delta_{\text{RL}} \sim 0$ and the parameters used in the experiment, the second term of Eq. (1) is the dominant contribution.

B. Optical Bloch equations for the four-level system

We derive the OBEs from the time dependent Schrödinger equation $i\hbar\frac{d\rho}{dt} = [H, \rho]$, where ρ is the density matrix and $H = H_{\text{at}} + H_{\text{int}}$ the total Hamiltonian, sum of an atomic part and of an interaction part, which reads $H_{\text{int}} = \hbar\sum_{i,j}\Omega_{ij}(|i\rangle\langle j| + |j\rangle\langle i|)$, where Ω_{ij} is the Rabi frequency of the optical field that couples the levels i and j . We choose all Ω_{ij} as real numbers and note $\Omega_{\text{Ra}} = \Omega_{32'}$, $\Omega_{\text{RL}} = \Omega_{22'}$, and $\Omega_{\text{OP}} = \Omega_{23'}$.

We add optical relaxations, use the rotating wave approximation and after making the following substitutions,

$$\begin{aligned} \tilde{\rho}_{ii} &= \rho_{ii} \quad \text{for } i = \{2, 3, 2', 3'\}, \\ \tilde{\rho}_{23'} &= \rho_{23'}e^{-i\Delta_{\text{OP}}t}, \\ \tilde{\rho}_{22'} &= \rho_{22'}e^{-i\Delta_{\text{RL}}t}, \\ \tilde{\rho}_{23} &= \rho_{23}e^{-i(\Delta_{\text{RL}}-\Delta_{\text{Ra}})t}, \\ \tilde{\rho}_{3'2'} &= \rho_{3'2'}e^{-i(\Delta_{\text{RL}}-\Delta_{\text{OP}})t}, \\ \tilde{\rho}_{3'3} &= \rho_{3'3}e^{-i(\Delta_{\text{RL}}-\Delta_{\text{Ra}}-\Delta_{\text{OP}})t}, \\ \tilde{\rho}_{2'3} &= \rho_{2'3}e^{i\Delta_{\text{Ra}}t}, \end{aligned}$$

we obtain the following equations for the populations,

$$\frac{d\tilde{\rho}_{22}}{dt} = \Gamma t_{2'2}\tilde{\rho}_{2'2'} + \Gamma t_{3'2}\tilde{\rho}_{3'3'} + i\frac{\Omega_{\text{OP}}}{2}(\tilde{\rho}_{23'} - \tilde{\rho}_{3'2}) + i\frac{\Omega_{\text{RL}}}{2}(\tilde{\rho}_{22'} - \tilde{\rho}_{2'2}), \quad (2)$$

$$\frac{d\tilde{\rho}_{2'2'}}{dt} = -\Gamma\tilde{\rho}_{2'2'} - i\frac{\Omega_{\text{Ra}}}{2}(\tilde{\rho}_{32'} - \tilde{\rho}_{2'3}) - i\frac{\Omega_{\text{RL}}}{2}(\tilde{\rho}_{22'} - \tilde{\rho}_{2'2}), \quad (3)$$

$$\frac{d\tilde{\rho}_{3'3'}}{dt} = -\Gamma\tilde{\rho}_{3'3'} - i\frac{\Omega_{\text{OP}}}{2}(\tilde{\rho}_{23'} - \tilde{\rho}_{3'2}), \quad (4)$$

$$1 = \tilde{\rho}_{22} + \tilde{\rho}_{2'2'} + \tilde{\rho}_{3'3'} + \tilde{\rho}_{33}, \quad (5)$$

where t_{ij} is the probability that an atom in state i decays into state j [2, 4]. The coherence terms are given by

$$\frac{d\tilde{\rho}_{23'}}{dt} = i\frac{\Omega_{\text{OP}}}{2}(\tilde{\rho}_{22} - \tilde{\rho}_{3'3'}) - i\frac{\Omega_{\text{RL}}}{2}\tilde{\rho}_{2'3'} - \tilde{\rho}_{23'}(\Gamma/2 + i\delta_{\text{OP}}), \quad (6)$$

$$\frac{d\tilde{\rho}_{22'}}{dt} = i\frac{\Omega_{\text{RL}}}{2}(\tilde{\rho}_{22} - \tilde{\rho}_{2'2'}) + i\frac{\Omega_{\text{Ra}}}{2}\tilde{\rho}_{23} - i\frac{\Omega_{\text{OP}}}{2}\tilde{\rho}_{3'2'} - \tilde{\rho}_{22'}(\Gamma/2 + i\Delta_{\text{RL}}), \quad (7)$$

$$\frac{d\tilde{\rho}_{23}}{dt} = -i\frac{\Omega_{\text{OP}}}{2}\tilde{\rho}_{3'3} + i\frac{\Omega_{\text{Ra}}}{2}\tilde{\rho}_{22'} - i\frac{\Omega_{\text{RL}}}{2}\tilde{\rho}_{2'3} - i\tilde{\rho}_{23}(\Delta_{\text{RL}} - \Delta_{\text{Ra}}), \quad (8)$$

$$\frac{d\tilde{\rho}_{3'2'}}{dt} = i\frac{\Omega_{\text{Ra}}}{2}\tilde{\rho}_{3'3} - i\frac{\Omega_{\text{OP}}}{2}\tilde{\rho}_{22'} + i\frac{\Omega_{\text{RL}}}{2}\tilde{\rho}_{3'2} - \tilde{\rho}_{3'2'}[\Gamma + i(\Delta_{\text{RL}} - \Delta_{\text{OP}})], \quad (9)$$

$$\frac{d\tilde{\rho}_{3'3}}{dt} = -i\frac{\Omega_{\text{OP}}}{2}\tilde{\rho}_{23} + i\frac{\Omega_{\text{Ra}}}{2}\tilde{\rho}_{3'2'} - \tilde{\rho}_{3'3}[\Gamma/2 + i(\Delta_{\text{RL}} - \Delta_{\text{Ra}} - \Delta_{\text{OP}})], \quad (10)$$

$$\frac{d\tilde{\rho}_{2'3}}{dt} = i\frac{\Omega_{\text{Ra}}}{2}(\tilde{\rho}_{2'2'} - \tilde{\rho}_{33}) - i\frac{\Omega_{\text{RL}}}{2}\tilde{\rho}_{23} - \tilde{\rho}_{2'3}(\Gamma/2 - i\Delta_{\text{Ra}}), \quad (11)$$

with $\tilde{\rho}_{ji} = \tilde{\rho}_{ij}^*$.

We find the steady-state solution of the OBEs by numerically solving the corresponding linear system. It allows us to compute all the relevant atomic quantities, in particular the atomic polarizability at the random-laser frequency,

$$\alpha = \frac{6\pi}{k_0^3} \frac{\rho_{22'}}{\Omega_{\text{RL}}/\Gamma} = \frac{6\pi}{k_0^3} \tilde{\alpha}, \quad (12)$$

where $k_0 = 2\pi/\lambda$ and $\tilde{\alpha}$ is dimensionless. The elastic scattering cross-section is then given by

$$\sigma_{\text{sc}} = \frac{k_0^4}{6\pi} |\alpha|^2 = \sigma_0 |\tilde{\alpha}|^2, \quad (13)$$

the extinction cross-section by $\sigma_{\text{ext}} = k_0 \text{Im}(\alpha) = \sigma_0 \text{Im}(\tilde{\alpha})$ and the gain cross-section by $\sigma_{\text{g}} = \sigma_{\text{sc}} - \sigma_{\text{ext}}$ [3]. The cross-sections that are relevant for the other fields are computed in the same way.

Finally, due to energy conservation, the total fluorescence emitted by the cloud is equal to the extinction of the two external beams,

$$P_{\text{F}} = \int n(\vec{r}) d\vec{r} (\sigma_{\text{ext,Ra}} I_{\text{Ra}} + \sigma_{\text{ext,OP}} I_{\text{OP}}), \quad (14)$$

where I denotes the respective incoming intensities.

Note that the OBEs allows us to compute the elements of the density matrix when all the detunings and Rabi frequencies, and in particular Ω_{RL} , are specified. To compute Ω_{RL} , we need to introduce self-consistent models that couple the EBOs with the light transport in the sample.

II. SELF-CONSISTENT MODEL WITH AMPLIFIED SPONTANEOUS EMISSION

We first consider a situation where light transport is ballistic, that is, neglecting random walk by scattering. This is relevant for the regions 1 of Fig. 2. For simplicity, we consider a spherical atomic cloud of homogeneous density n (the two external lasers have also homogeneous intensities).

Starting with $\Omega_{\text{RL}} = 0$ in the EBOs, we compute a source term corresponding to spontaneous Raman scattering, given by $P_0 = \Gamma t_{2'2} \tilde{\rho}_{3'3'}$ [second term of the right-hand-side of Eq. (2)], taken at the detuning Δ_{RL} of maximum gain. We then consider an atom at the center of the cloud (radius R) and compute the intensity at the RL frequency emitted by the other atoms. Taking into account the extinction along the ballistic path of the light, we integrate the source term P_0 described above,

$$I_{\text{RL}} = \int \frac{nP_0}{4\pi r^2} \exp(-n\sigma_{\text{ext}} r) r^2 \sin(\theta) dr d\theta d\phi = \frac{P_0}{-\sigma_{\text{ext}}} [\exp(-n\sigma_{\text{ext}} R) - 1]. \quad (15)$$

Note that $2n\sigma_{\text{ext}} R = b_0 \text{Im}(\tilde{\alpha})$ so that the dependence on the optical thickness b_0 is explicit. Note also that, in the absence of scattering, $-\sigma_{\text{ext}} = \sigma_{\text{g}}$. One can see that I_{RL} increases with b_0 only if $\sigma_{\text{ext}} < 0$, i.e., in presence of gain. This increase is smooth with b_0 , without any visible threshold [Fig. S2].

From this result we can inject $\Omega_{\text{RL}} = \Gamma \sqrt{I_{\text{RL}}/(2I_{\text{sat}})}$ in the EBOs, with $I_{\text{sat}} = 6.4 \text{ mW/cm}^2$. Since the value of Ω_{RL} changes the atomic response (due to saturation and optical pumping), the source term and the gain cross-section

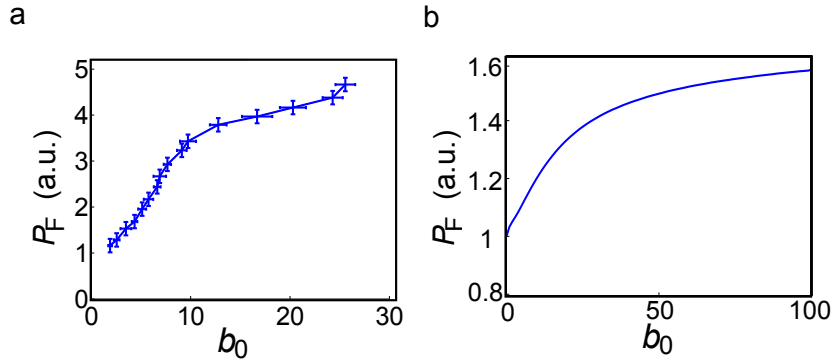


Fig. S2: **Amplified stimulated emission (ASE) due to Raman gain.** **a**, Fluorescence power at $\delta = -2\Gamma$ as a function of the optical thickness. The data are those of Fig. 2. At this detuning, scattering due to the $|1'\rangle$ excited state is small and Raman gain explains the increase of the total fluorescence as b_0 increases with a constant number of atoms. Vertical error bars correspond to the noise on the data and horizontal error bars to shot-to-shot fluctuations of b_0 . **b**, Solution of the ASE model, without any adjustable parameter.

depend on Ω_{RL} . We thus iterate this procedure until Ω_{RL} converges to a stable value corresponding to the steady-state. The total fluorescence, reported in Fig. S2b, can then be computed from Eq. (14). As mentioned above, the frequency of maximum gain is not exactly matching the two-photon resonance condition of the bare atom. We therefore scan the frequency Δ_{RL} and retain for each value of Ω_{RL} the frequency providing maximal emission.

Given the simple considered geometry, we expect this model to provide only qualitative results. Nevertheless, it has the advantage of including Raman gain and the saturation effect due to the emitted and amplified light.

Note that another effect can explain an increase of the total fluorescence with the optical thickness b_0 , when the Raman-scattered photons from the pump laser are in the regime of multiple scattering on the open $|2\rangle \rightarrow |2'\rangle$ transition. Those photons contribute to optical pumping and can increase the population of the $|F=3\rangle$ state leading to enhanced emission in some cases. This effect has been studied in detail in [4] and is the dominating effect when the Raman laser is tuned very close to resonance ($\Delta_{\text{Ra}} \sim 0$, that is, $\delta_{\text{Ra}} \sim 4.8\Gamma$). We checked that at the detunings and intensities considered in Figs. 2 and S2, this contribution is negligible. At the largest optical thicknesses that we used, a similar effect might come from inelastically scattered light [5] and slightly contribute to a change in the populations.

III. SELF-CONSISTENT MODEL WITH LETOKHOV'S CRITERION FOR THE RANDOM LASER THRESHOLD

When the Raman laser is tuned close to $\delta_{\text{Ra}} \sim 0$ (region 2 in Fig. 2), the Raman-scattered light is not in the ballistic regime but undergoes multiple scattering due to the $|2\rangle \rightarrow |1'\rangle$ transition. To describe such multiple scattering, we couple the OBEs to a diffusion equation.

We can then build on Letokhov's results on the diffusion equation with gain: above a critical size for the medium, random lasing starts [6]. With a spherical geometry, the critical radius is given by

$$R_{\text{cr}} = \pi \sqrt{\frac{\ell_{\text{sc}} \ell_{\text{g}}}{3}}, \quad (16)$$

where the mean-free-path is given by $\ell_{\text{sc}}^{-1} = n\sigma_{\text{sc,tot}}$ (Eq. 1) and the gain length by $\ell_{\text{g}}^{-1} = n\sigma_{\text{g}}$. Here we still suppose a homogeneous density n and we suppose also that the scattering is isotropic so that the transport length equals the scattering mean-free-path. As shown in [7], Letokhov's criterion can be rewritten as a critical optical thickness,

$$b_{0\text{cr}} = \frac{2\pi\sigma_0}{\sqrt{3\sigma_{\text{sc,tot}}\sigma_{\text{g}}}}, \quad (17)$$

where the cross-sections are obtained from the EBOs of the 4-level model and additional scattering at the $|2\rangle \rightarrow |1'\rangle$ line as given by Eq. (1).

Based on this threshold criterion, we can compute the emitted light on the random laser line for a given b_0 via the implicit equation $b_{0\text{cr}}(\Omega_{\text{RL}}) = b_0$, analogous to the condition that gain must exactly compensate losses at the steady

state, as in standard lasers. In practice, we start from $\Omega_{\text{RL}} = 0$, compute $b_{0\text{cr}}$ from the EBOs and Eqs. (1,17), and we increase Ω_{RL} while $b_{0\text{cr}} < b_0$. At each step we choose the random-laser detuning Δ_{RL} that induces the lowest threshold, since the laser should start with this frequency.

Then, we can use Eq. (14) to compute the total fluorescence, corresponding to the experimental signal, from which we subtract the fluorescence computed with $\Omega_{\text{RL}} = 0$ in order to compare with the measured increase of fluorescence δP_{F} [Fig. 3].

This qualitative model only allows for the computation of the random laser intensity above threshold and does not describe the emitted power below the laser threshold, for which we can use the ASE model described in the previous section. We note that this model also takes into account all saturation effects. In this system, the emitted intensity does not only change the gain, but also the scattering-induced feedback, since it changes the atomic populations.

-
- [1] Mercadier, N. *Diffusion résonante de la lumière: laser aléatoire à atomes froids et vols de Lévy des photons*, Ph.D. Thesis (Université de Nice Sophia-Antipolis, 2011), available online at <http://tel.archives-ouvertes.fr/tel-00647843>.
 - [2] Steck, D. A. *Rubidium 85 D Line Data*, available online at <http://steck.us/alkalidata>.
 - [3] Lagendijk, A. & van Tiggelen, B. A. Resonant multiple scattering of light. *Phys. Rep.* **270**, 143–215 (1996), section 3.2.2 “Points scatterers” (pp. 164–166).
 - [4] Baudouin, Q., Mercadier, N. & Kaiser, R. Steady-state signatures of radiation trapping by cold multilevel atoms. *Phys. Rev. A* **87**, 013412 (2013).
 - [5] Mollow, B. R. Power Spectrum of Light Scattered by Two-Level Systems. *Phys. Rev.* **188**, 1969 (1969).
 - [6] Letokhov, V. S. Light generation by a scattering medium with a negative resonant absorption. *Sov. Phys. JETP* **16**, 835–840 (1968).
 - [7] Froufe-Pérez, L. S., Guerin, W., Carminati, R. & Kaiser, R. Threshold of a Random Laser with Cold Atoms. *Phys. Rev. Lett.* **102**, 173903 (2009).

Concluding remarks

Our observations are in qualitative agreement with an *ab initio* model based on Letokhov's threshold, which is described in detail in the paper's Appendix. I also have adapted the same self-consistent model using the threshold computed from the RTE, with no significant difference.

There are, however, quantitative discrepancies. In particular, the measured threshold is lower than the predicted one. This might be due to interference effects, which are neglected in the diffusion model, as explained in Section IV.2.2.

Several other ingredients are neglected and might also play a role, like the polarization of light, the Zeeman degeneracy of the involved atomic levels, the finite temperature of the cloud, and the inhomogeneous density distribution. This demonstrates the need for a more evolved modeling.

Several theoretical approaches to random lasing have been developed over the years, see for instance Refs. [Wiersma 1996, Burin 2001, Vanneste 2007, Türeci 2008, Conti 2008, Frank 2009, Goetschy 2011]. To my opinion, the main interest of our experiment is to provide disorder-averaged data in a rather clean system (homogeneous pumping, monodisperse scatterers, known density profile) with perfectly known microscopic ingredients (rubidium atoms driven by two lasers with known frequencies and intensities), without any free parameters. This has triggered first collaborations with some theoreticians [Gerasimov 2014, Guerin 2016b] and we hope that more will come in the future, although unfortunately, the topic of random lasers has become a bit old-fashioned in the recent years.

Conclusion on Part One

It is interesting to note that although the different gain mechanisms had been known for a long time, the topic of gain and lasing using cold atoms was dormant for many years with very few experiments [Hilico 1992, McKeever 2003], while there have been much more experiments in the recent years [Vrijnsen 2011, Bohnet 2012, Norcia 2016, Sawant 2017, Megyeri 2018, Gothe 2019].

As far as mirrorless lasing is concerned, our two experiments [Schilke 2012b, Baudouin 2013b] are the first ones (see also the related experiment [Greenberg 2012]). Since then several MOPOs using only FWM have been demonstrated in cold atoms [Mei 2017, Lopez 2019]. None of these other experiments really use the spatial arrangement of the atoms to provide the feedback mechanism.

Although it requires some more preparation of the sample, since it has to be ordered, the DFB OPO experiment was much easier. Fundamentally, it is because the system is 1D. As a consequence, the emission is directive, which leads to very clear signatures. It is also easier to get a large optical thickness along only one direction.

For the random laser experiment, the observed signature is less striking. As already explained, what we observe is equivalent to looking at the pump depletion, which is somewhat indirect. This led us, in the following years, to work on the development of experimental methods that could provide some more direct signatures.

One effect we thought of is an increase of fluctuations at the transition. As a first preliminary experiment to learn how to deal with fluctuations and sort out technical noise from interesting fluctuations, we studied the fluctuations of quasi-resonant light transmitted through the cold-atom cloud. We indeed observed a very large extra noise introduced by the atoms and a careful analysis showed that this noise was due to the frequency noise of the probe laser converted to intensity noise by the atomic resonance [Vartabi Kashanian 2016b].

Ultimately, we would like to get a signature of random lasing on the spectral or coherence properties. One prominent signature of lasing would be a change of the intensity correlation function $g^{(2)}(\tau)$ from bunched to flat. This has been shown on a random laser too [Cao 2001]. We thus started a new research program on intensity correlations, with the idea of starting by a simple experiment and increasing the complexity step by step. The simple experiment is the measurement of intensity correlations of light scattered by cold atoms in the linear-optics regime, without any gain, in the single-scattering regime and then in the multiple-scattering regime [Éloy 2018b]. I participated to that experiment in particular by performing random-walk simulations to help interpret the data.

The next step along this program would be to add gain and see how the intensity correlation function is modified with and without multiple scattering, and then below and above the random lasing threshold. However many other interesting things can be done with such a setup, which are the subject of the current experiments performed under the leadership of

Mathilde Hugbart. In particular, before having gain, one has first inelastic scattering: a precise measurement of the Mollow triplet [Mollow 1969] has been obtained [Ortiz-Gutiérrez 2019]. How is this well-known Mollow triplet modified by collective effects? If the driving laser is out of resonance, an imbalance between the sidebands is predicted [Ott 2013, Pucci 2017], which may be interpreted by the effect of Mollow gain [Mollow 1972] that amplifies one sideband. And if the driving laser is near resonance, at large optical thickness and large saturation parameter, second-order sidebands should appear [Pucci 2017]. Those sidebands are created by two-body quantum correlations and can also be interpreted as the inelastic scattering due to atoms strongly driven by the first-order sidebands. This line of research goes towards cooperative or collective scattering effects beyond the linear-optics regime.

Finally, another experiment along this line has been performed very recently (2019) and is still at the analysis stage. It deals with a fibered random laser³ provided by the group of Anderson Gomes (Recife, Brazil). We measured the intensity correlation function below and above threshold. While we obtain bunching below threshold, we don't obtain a flat $g^{(2)}(\tau)$ function above threshold, but instead a complicated oscillatory behavior. Our current interpretation is that the random laser is coherent but multimode.

Some speculative ideas for the future

Random lasing in hot vapors?

Raman gain between hyperfine levels also works with hot vapors [Kumar 1985], so one can wonder if random lasing would be possible in hot vapors. Since the gain frequency is shifted from the pumping frequency by the hyperfine splitting, one can arrange, in a cell containing different isotopes, that the pump beam is at a frequency that is unscattered (homogeneous pumping) but not too far away from the line of one isotope (to get efficient gain), and that the gain frequency is resonant with the other isotope, to provide scattering.

With rubidium, with these qualitative criteria in mind, the most appropriate configuration would be to use the ^{85}Rb atoms for gain with a pumping detuned from ~ 500 MHz to the red of the $F = 2 \rightarrow F'$ Doppler line. Then the gain would be resonant with the $F = 1 \rightarrow F'$ Doppler line of the ^{87}Rb atoms.

Of course there are many open questions, which I didn't have the time to seriously investigate. For instance, how to sustain the gain (do we need an extra optical pumping to create and sustain a population inversion)? Even more importantly, the main problem in working with hot vapors is the Doppler broadening. First this will reduce a lot the gain efficiency. Also, scattering is inelastic and can put the photons out of the gain resonance, which would be like a kind of loss. Nevertheless, in the multiple scattering regime, the photons can come back in the right frequency range after a few scattering events. Finally, we know from our experiments on Lévy flights that light transport would be superdiffusive [Mercadier 2009, Baudouin 2014b], so we cannot use Letokhov's threshold. We can still use the RTE though, as long as the mean-free path can be defined, which is the case with Doppler broadening.

In brief, we don't know yet if that can work in reasonable conditions, but that's not *a priori* impossible. That would be a new system to study random lasing.

³ It is, actually, a random distributed feedback fiber laser [Turitsyn 2014], which provides a nice unification of the different chapters presented in Part One!

Random lasing in space?

The subject of random lasers based on atomic and molecular gases has been introduced, by Letokhov himself, in the context of astrophysical lasers. Indeed, astronomical observations in the microwave domain have led to the discovery of anomalously bright emission lines from molecules in stellar atmospheres [Weaver 1965]. It was soon understood that the only possible explanation was an amplification of the corresponding wave due to stimulated emission [Litvak 1966]. The study of these astrophysical masers, which turned out to be very common, has been an important research subject in the 1970s [Reid 1981, Elitzur 1982].

Emission lines with anomalous intensities were also known in the optical domain [Thackeray 1935, Merrill 1956] without any convincing explanation. Letokhov suggested that they could also be explained by stimulated emission, and that scattering-induced feedback could enhanced the amplification, even reaching the oscillatory regime [Letokhov 1972, Lavrinovich 1975], a phenomenon that would be called a random laser today.

Amplification by stimulated emission was indeed observed in the planetary atmospheres of Mars and Venus in the infrared (IR) domain ($\lambda \sim 10 \mu\text{m}$) [Johnson 1976, Mumma 1981] and much later in stellar atmospheres in the far IR [Strel'nitski 1996]. More recently, astrophysical lasers in the near IR was discovered by Johansson and Letokhov, based on Fe II [Johansson 2004] and O I [Johansson 2005]. In the optical domain, population inversion is much harder to obtain than in the microwave domain, and astrophysical lasers are very rare, contrary to masers [Messenger 2010].

It should be noted here that astrophysicists often call ‘lasers’ what a laser physicist would describe as amplification, or Amplified Spontaneous Emission (ASE) [Letokhov 2009]. The existence of additional feedback due to multiple scattering seems to be very speculative. In the microwave domain, there are ununderstood bursts of radiation from the water vapor maser in the Orion KL Nebula [Shimoikura 2005], and scattering-induced feedback in the oscillatory regime (i.e., random lasing above threshold) has been proposed as a possible explanation [Truitt 2000]. The latest observations, however, do not seem to confirm this idea [Hirota 2011].

Nevertheless, it seems that the ingredients necessary for a random laser, that is, multiple scattering and stimulated emission, are both present in stellar gases [Johansson 2007]. Moreover, even without feedback, ASE in a long enough medium (distances are huge in astrophysics!) might lead to saturation of the gain medium and to coherent emission. This coherence property could be detected in the intensity correlation function $g^{(2)}(\tau)$ [Chung 1980]. The most promising emission line seems to be the Fe II line at $1.68 \mu\text{m}$, which should be present in the circumstellar envelope of some spectral types of stars [Messenger 2010].

This speculative idea led us to first discussions with astrophysicists about the possibility of performing intensity-correlation measurements, which triggered a fruitful collaboration on the revival of the technique of intensity interferometry [Dussaux 2016, Guerin 2017a, Guerin 2018, Lai 2018, Rivet 2018, Rivet 2020], a project in which I have been strongly involved, as briefly mentioned in Chapter I.

Part Two

**Cooperative scattering in dilute
cold-atom clouds in the linear-optics
regime**

Introduction on super- and subradiance

“Superradiant gain is the process in which waves are amplified via their interaction with a rotating body, examples including the evaporation of a spinning black hole and electromagnetic emission from a rotating metal sphere.” This citation taken from a recent *Physical Review Letters* [Faccio 2019] shows how broad the topic of superradiance can be. Another indicator could have been the number of citations of Dicke’s seminal paper [Dicke 1954], which is about 4800 at the time of writing and is still increasing at an impressive rate.

As a consequence I will not try to do an exhaustive review, because such an attempt would fail, and I prefer to admit that I have a very limited knowledge or understanding of many experimental and theoretical works related to super- and subradiance. I will thus give a brief and very incomplete overview of the past work on the subject and a little bit more details on the more recent, so-called ‘single-photon superradiance’.

Dicke’s superradiance

In 1954 R. H. Dicke published an article entitled “*Coherence in spontaneous radiation processes*” [Dicke 1954], which introduced the concept of superradiance. It considers an ensemble of N motionless, identical, two-level atoms located in a region of space much smaller than the transition wavelength λ and addresses the question of the collective eigenmodes of the system and their radiation rates. In particular, Dicke showed that if all atoms are initially in their excited state, the deexcitation of the ensemble would follow the cascade of all symmetric states, with an acceleration of the emission rate and a coherent emission. All other, nonsymmetric states would never be populated, because they are decoupled from the ladder of the symmetric states. Among these nonsymmetric states, some have an emission rate smaller than the one of a single atom (it can even vanish) and are thus called ‘subradiant’ [Freedhoff 1967]. Note that the symmetry argument relies on hypotheses that were later revealed to be unjustified [Friedberg 1972, Gross 1982].

A hand-waving argument to describe superradiance could be the following: since all excited atoms are very close to each other, the first, spontaneously emitted photon is immediately ‘felt’ by the other atoms and triggers their stimulated emission, hence a global, collective coherent emission. What is computed in Dicke’s paper, among other things, is the dynamics of this emission, with in particular the emission rate at each level of the superradiant cascade. It should be noted that the coherence of the excitation is generated spontaneously, by the first spontaneous emission, which justifies the name of ‘quantum superradiance’ by some authors, e.g. [Berman 2010], while others have proposed ‘superfluorescence’ [Bonifacio 1975, Gibbs 1977].

The assumption of a very small size (compared to λ) may be relevant to microwave spectroscopy, but not so much in the optical domain. To go beyond this ‘Dicke limit’

one has to take into account the distance-dependent dipole-dipole interaction between atoms [Stephen 1964], as well as propagation effects. With two atoms the whole problem can be solved analytically [Lehmberg 1970b, Stroud 1972, Milonni 1974] but with many atoms in a large sample the situation is much more intricate and was addressed by many theoretical studies in the 1960s-1970s (see, e.g., [Freedhoff 1967, Ernst 1968, Ernst 1969, Lehmberg 1970a, Arecchi 1970, Friedberg 1971, Rehler 1971, Saunders 1973a, Saunders 1973b, Bonifacio 1975, Ressayre 1976, Ressayre 1977] to name a few) but experiments were not performed until the 1970s.

Experiments in the 1970s-1980s

Several groups observed and studied superradiance/superfluorescence using atomic vapors or beams, approximately between the mid-1970s and the mid-1980s. References to some of the first observations are [Skribanowitz 1973, Gross 1976, Gibbs 1977] and very interesting reviews are [Feld 1980], and, mainly for the theoretical aspects, [Gross 1982].

In almost all the works done in that period, the ideal situation of the Dicke limit is not reached: the samples are large, with often a large aspect ratio ('pencil-shaped'), and propagation/geometric effects are important (see, e.g., [MacGillivray 1976], but it is one among many theoretical and experimental studies on those aspects). In that case, the parameter of the sample which governs the superradiant decay rate is related to the optical thickness (see, e.g., [Friedberg 1976]): it is the density of excited atoms times the size along the considered propagation direction.

With this propagation picture in mind it is natural to make a link between superfluorescence and the amplified spontaneous emission (ASE) well known in laser physics [Schuurmans 1979]. In the review [Feld 1980] it is stated that "*superradiant emission and stimulated emission in a high gain medium are the transient and steady-state forms of phase-coherent amplification, respectively*", although one should distinguish the limit of a negligible dephasing rate between the dipoles (superfluorescence, with the buildup of a large macroscopic coherent dipole) from the opposite limit of a high dephasing rate, in which ASE and coherent emission can still take place [Schuurmans 1979, Malcuit 1987].

Finally, the group of Pierre Pillet investigated the possibility of observing subradiance by using a clever choice of three-level atoms [Crubellier 1980] and they succeeded in obtaining some indirect signatures of subradiant states [Pavolini 1985]. This was, to our knowledge, the only observation of subradiance in a many-atom experiment.⁴

Matter wave superradiance

A first revival of the subject took place at the beginning of the ultracold-atom era, with very nice experiments in Ketterle's group using Rayleigh scattering [Inouye 1999, Schneble 2003] and Raman scattering [Inouye 2000, Schneble 2004]. Because of the subrecoil temperature and of the coherence of the atomic sample in these experiments, there is an intricate relationship between the dynamics of the optical field and of the matter wave. In these experiments the atoms are driven by a far detuned field such that there is almost no excited atoms. The

⁴ The two-atom case has been studied experimentally with two ions, demonstrating superradiant and subradiant decay rates [DeVoe 1996]. However the change compared to the natural decay rate was only on the order of 1% because of the relatively large distance between the ions. Other signatures of subradiance in two-particle system have been reported in [Hettich 2002, Filipp 2011, McGuyer 2015].

similarity with Dicke’s superradiance comes from the *momentum* states of the atoms. The atoms in the BEC, which are initially all in the same momentum state, act like a fully inverted systems, and the superradiant dynamics takes place for the transitions between the momentum states driven by the recoil induced by light scattering. From the point of view of the light dynamics, the atomic sample acts as an amplifying media, the gain being provided by recoil-induced resonances (see Sec. II.1.5).

Several groups performed experiments in this spirit [Yoshikawa 2004, Bar-Gill 2007, Hilliard 2008], sometimes in combination with a high-finesse optical cavity enhancing the coupling between light and atoms [Slama 2007, Bux 2011, Keßler 2014]. Very recently, a form of matterwave subradiance has been observed in the Tübingen group [Wolf 2018].

Single-photon superradiance

A second revival of the topic was initiated by Marlan Scully and collaborators in 2006 with a paper that addresses what happens when one prepares an ensemble of two-level atoms by absorbing *one* photon of wave vector k_0 without any induced optical coherence: there is one excited atom but we don’t know which one. In a quantum framework, which is necessary because a single photon has been sent, the atomic sample can be described by the collective entangled state

$$|\Psi\rangle = \frac{1}{\sqrt{N}} \sum_j e^{ik_0 \cdot r_j} |g_1, g_2, \dots, e_j, \dots, g_N\rangle. \quad (1)$$

The r_j are the atoms’ random positions and $|g_j\rangle$, $|e_j\rangle$ are the ground and excited states respectively. The phase factor can be interpreted as due to the different possible arrival times of the photon on the atoms, hence the title of the article: “*Directed Spontaneous Emission from an Extended Ensemble of N Atoms: Timing is Everything*” [Scully 2006]. Then one can compute how this collective state decays by spontaneous emission, and one finds that the photon is emitted in the k_0 direction, which might seem counterintuitive for *spontaneous emission*. Note that there is no condition on the atomic density, the distance between atoms doesn’t have to be small. However, the state (1) assumes that the absorption probability was the same for all atoms, which is true only when the optical thickness of the medium is very low (no attenuation of the excitation beam during the crossing of the cloud, and no phase shift either). This paper immediately triggered a lot of discussions [Eberly 2006, Mazets 2007, Scully 2007]. The collective state (1) has been called the Timed-Dicke (TD) state and the whole subject ‘single-photon superradiance’ [Scully 2009a, Scully 2009b].

The forward emission is however not really surprising, as it is obviously due to the phase-matching condition imposed by the phase factor, which is very similar to the ‘spin wave’ picture commonly used with two-photon Raman transitions in the context of quantum memories [Hammerer 2010, Sangouard 2011]. One can also see it like an N -slit interference effect, where the atoms plays the role of the slits, like in [Grangier 1985]. These analogies are mentioned in [Scully 2006].

Since it is just, after all, an interference effect, it is the same with a continuous driving by a coherent field [Courteille 2010]. Indeed, we know that the outcome of a double-slit experiment is the same with many single photons sent one by one and with a classical field. Although it is less known, it was, actually, already mentioned in the original Dicke paper that the radiation by a coherently-illuminated large sample was in the forward direction (section “*Radiation from a gas of large extent*” in [Dicke 1954]). Of course, with a continuous illumination, the

entanglement aspect of the TD state is not relevant any more as it comes from an artificial truncation of the Hilbert space [Eberly 2006, Bienaimé 2011b]. To my knowledge, only one experiment was realized with a true single-photon source [Fröwis 2017], with the emphasis on the entanglement aspect. For all other experiments, ‘superradiance in the linear-optics regime’ is a better term than ‘single-photon superradiance’.

A less trivial aspect was predicted slightly later, it is the lifetime (or the rate of collective spontaneous emission Γ_N) of the TD state, which increases with the number of atoms according to (for N large)

$$\Gamma_N \simeq C \frac{N}{(kR)^2} \Gamma_0, \quad (2)$$

where R is the sample size, Γ_0 is the spontaneous emission rate for a single atom and C is a numerical factor depending on the geometry. It is therefore indeed a temporal superradiance effect, and not only a directional effect, with an amplification factor which is neither simply the number of atoms (as in the Dicke limit of a small sample), nor the density. In fact, for a spherical sample, $N/(kR)^2$ is proportional to the optical thickness on resonance b_0 . This calculation was carried out by several authors following the paper [Scully 2006] (see references [Mazets 2007, Svidzinsky 2008, Svidzinsky 2010, Courteille 2010, Friedberg 2010, Prasad 2010]), but we can also find this result in old papers [Arecchi 1970, Rehler 1971]. Note that the calculation involves taking into account the dipole-dipole interaction between the atoms. It has also been shown that the atoms could be treated as classical dipoles [Svidzinsky 2010], such that actually the whole problem is purely classical (see also [Ruostekoski 1997, Javanainen 1999]).

So, at this point, it appears that the relevant parameter for single-photon superradiance is the on-resonance optical thickness, actually like for superfluorescence experiments and also matterwave superradiance, so it is not very clear where the novelty is. However, it should be noted that it is much less intuitive, because the picture of a spontaneously emitted photon being amplified by other excited atoms as it propagates through the sample does not work any more. Actually the very existence of cooperative scattering in this regime of linear optics and dilute sample is not intuitive at all. I have noticed, in the last years, that most people in the cold-atom or quantum-optics community, at least those not very familiar with the topic, are convinced that superradiance needs high density/small distances between atoms, because what is known by everyone is Dicke’s paper and the two-atom case, for which it is true. Since matterwave superradiance experiments have also been realized in dense samples they sustain the confusion (although it is very explicitly written in the first of Ketterle’s papers that the relevant parameter is the optical thickness [Inouye 1999]). The confusion is also sustained by the existence of other ‘cooperative effects’ related to the density, such as all the collective shifts of the atomic resonance [Friedberg 1973]. It is the merit of [Scully 2006] to have brought this subject up to date, now that large samples of cold atoms, and even single-photon sources, are available experimentally.

Clearly, the lack of experiments on superradiance in this regime of linear-optics and large dilute samples, is, to my opinion, the reason why it is not well known. As for subradiance, predicted in this regime by our team just before my arrival [Bienaimé 2012], it had also not been seen in this regime, and even, in general, since Dicke’s paper, only one experiment had studied subradiance in the regime of a large number of excited atoms [Pavolini 1985], without however being able to directly observe the slow decay of the excitation. It is therefore with this objective that I took in charge the experiment in 2013.

CHAPTER V

Steady-state signatures of cooperativity?

Before turning to the subradiance experiment, in this chapter I will discuss some other experiments performed on steady-state observables, like the amount of scattered light or the momentum transfer to the atoms (i.E. the radiation-pressure force). Are there signatures of cooperative scattering in those experiments?

V.1. Discussion on collective and cooperative effects

The question of which kind of experimental signature can be attributed to cooperative effects is a difficult one, because it supposes first to have a clear idea of what cooperative scattering is!

At the 46th Winter Colloquium on the Physics of Quantum Electronics (PQE Conference, Snowbird, USA) in January 2016, I have assisted to a very stimulating talk by Juha Javanainen, who insisted on the fact that cooperative scattering was only high-density effects, while we were pretending the opposite. I immediately had the idea to write a ‘discussion’ paper in order to modestly try to clarify all this and to publish it in the PQE special issue of *Journal of Modern Optics* [Guerin 2017c]. To my surprise, I received several spontaneous laudatory comments about it and it has been cited quite a lot (for this journal), mainly as a kind of review article on cooperative effects, which it does not pretend to be.

I thus reproduce it here, as it is a nice introduction to the topic, or more precisely to my point of view on it.

Light interacting with atomic ensembles: collective, cooperative and mesoscopic effects

W. Guerin^a, M.T. Rouabah^{a,b} and R. Kaiser^a

^aUniversité Côte d'Azur, CNRS, INLN, France; ^bLaboratoire de Physique Mathématique et Subatomique, Université des Frères Mentouri, Constantine, Algeria

ABSTRACT

Cooperative scattering has been the subject of intense research in the last years. In this article, we discuss the concept of cooperative scattering from a broad perspective. We briefly review the various collective effects that occur when light interacts with an ensemble of atoms. We show that some effects that have been recently discussed in the context of 'single-photon superradiance', or cooperative scattering in the linear-optics regime, can also be explained by 'standard optics', i.e. using macroscopic quantities such as the susceptibility or the diffusion coefficient. We explain why some collective effects depend on the atomic density, and others on the optical depth. In particular, we show that, for a large and dilute atomic sample driven by a far-detuned laser, the decay of the fluorescence, which exhibits superradiant and subradiant dynamics, depends only on the on-resonance optical depth. We also discuss the link between concepts that are independently studied in the quantum-optics community and in the mesoscopic-physics community. We show that the coupled-dipole model predicts a departure from Ohm's law for the diffuse light, that incoherent multiple scattering can induce a saturation of fluorescence and we also show the similarity between the weak-localization correction to the diffusion coefficient and the inaccuracy of Lorentz local field correction to the susceptibility.

ARTICLE HISTORY

Received 3 May 2016
Accepted 13 July 2016

KEYWORDS

Cooperative scattering;
superradiance;
subradiance; independent
scattering approximation;
weak localization

1. Introduction

'Cooperative scattering' of light by a collection of two-level atoms has become a hot topic in the recent years, with a lot of experimental results on superradiance (1–4), subradiance (5) and 'cooperative' shifts (4, 6–10) in the 'single-photon superradiance' regime (11–13), or equivalently in the linear-optics regime. By contrast, the experiments performed in the 1970–1980s were performed in a regime where a large number of atoms are excited (14, 15). Related experiments with multi-level atoms (16) or artificial atoms (17) illustrate that the phenomena studied in two-level systems can find their application in other fields of research. Despite this recent interest, it seems that a common agreement on what should be called cooperativity is still lacking. It has recently been suggested that 'cooperativity' should be reserved to effects that could not be explained by 'the mean-field approach of traditional optics' (18), and that such effects would appear for dense atomic samples only (19). Here, 'dense' means that the atomic density ρ should not be very small compared to k^3 , where $\lambda = 2\pi/k$ is the wavelength of the atomic transition. However, our recent results on sub- and superradiance (20) show that these effects are

controlled by the resonant optical depth of the sample and not by its density (3, 5). If one agrees that Dicke sub- and superradiance in extended samples (21, 22) deserve being called 'cooperative' effects, the restriction to high spatial densities should clearly be dropped.

Although everyone certainly agrees on the physics, terminology confusion does not help in understanding this topic. It can also be a real barrier when trying to communicate with experts from other, neighboring, fields. With this problematic in mind, in this article, we would like, first, to discuss the concept of 'cooperative scattering', and, second, to point out the possible link between the so-called 'mean-field approach of standard optics' used in (18) and what is called the 'independent scattering' approximation in mesoscopy (23–25).

Unfortunately, terminology confusion has always been present in this field. For instance, Bonifacio and Lugiato proposed the term 'superfluorescence' instead of superradiance when there is no initial macroscopic dipole in the atomic system but only uncorrelated excited atoms (26). As soon as propagation effects are involved, superfluorescence can also be seen as the transient regime of 'amplified spontaneous emission' (14), a well-known,

and somewhat trivial phenomenon in laser physics, although a difference does exist and has been studied in Ref. (27). Dicke himself spoke of a mirrorless ‘coherence brightened laser’ (28). Another example is the analogy or confusion between subradiance (5, 29) and ‘radiation trapping’ (30–32). The difference and early confusion between the two phenomena was pointed out by Cummings (33).

Although we do not pretend to be able to solve all controversies, we feel that it may be instructive to tackle these questions from a broader perspective, which could be, in general, the study of all *collective* effects in light-atom interactions, or the transition from microscopic properties of light scattering by atoms to macroscopic, optical and transport properties of extended and/or dense atomic vapors. This subject is even older than Dicke’s paper, as it was investigated by Rayleigh, Lorentz, Lorenz, Ewald, Oseen, and many others (34).

We will focus on experiments in which near-resonant light from a laser is exciting a sample of N two-level atoms at rest. The experimental observables that can be measured include extensive quantities that increase with the atom number, such as the total amount of scattered light, or some intensive quantity that could *a priori* be independent of the atom number. If an extensive quantity is not simply given by the atom number times the same quantity for a single-atom, or if an intensive quantity does depend on the atom number, nontrivial collective effects probably are at work. A first example of an extensive quantity is the total amount of scattered light, which, *in some limit*, is proportional to the atom number. Another example of an extensive quantity is the dephasing accumulated by the wave crossing the sample, which is also increasing with the atom number, and the notion of refractive index, which is a macroscopic (collective) quantity provides an efficient description. Collective effects thus take place in most situations, with some effects depending on the atomic density ρ , and others on the size L of the medium, as detailed in the following. Note that as soon as propagation effects or quantities associated to transient phenomena become relevant, the size of the sample will play an important role, and the important parameter turns out to be the optical depth. On the other side, for quantities that can be defined in steady state for a bulk medium, the density is the relevant parameter.

2. Collective effects that depend on the density

Obviously, all effects or quantities that can be defined for an infinite medium depend on the atomic density ρ , which is the only parameter characterizing the medium.

2.1. At low atomic density

The most simple example is the medium susceptibility χ . At low density, it is related to the atomic polarizability α by $\chi = \rho\alpha$. For simple two-level atoms and in the linear-optics regime (low intensity), the polarizability is

$$\alpha = \frac{6\pi}{k^3} \times \frac{-1}{2\Delta/\Gamma + i} = \frac{6\pi}{k^3} \times \frac{-2\Delta/\Gamma + i}{1 + 4\Delta^2/\Gamma^2}. \quad (1)$$

The complex refractive index n is defined from the susceptibility by $n^2 = 1 + \chi$. At low density, $\chi \ll 1$ and $n \simeq 1 + \chi/2$. Inside the medium, the wavevector is changed from k to nk . The real part of the refractive index is thus responsible for the dispersive properties of the material and its imaginary part for the attenuation of the wave. One can thus define a characteristic extinction length (or linear extinction coefficient) for the intensity of the light propagating in the incident optical mode,

$$\ell_{\text{ex}}^{-1} = \rho k \text{Im}(\alpha) = \frac{\rho\sigma_0}{1 + 4\Delta^2/\Gamma^2}, \quad (2)$$

where $\sigma_0 = 6\pi/k^2 = 3\lambda^2/(2\pi)$ is the resonant scattering cross-section.

The susceptibility is not sufficient to describe the behavior of the light inside the medium. In particular, it does not make a difference if the attenuation is due to absorption, when the electromagnetic energy is transferred to the medium, or to scattering, when the energy is just removed from the incident electromagnetic mode to feed other spatial modes. Scattering is often seen as being due to impurity, or granularity of matter, and as such, it is neglected in the susceptibility, which corresponds to a continuous-medium approximation. It is often stated, in particular in the recent literature about cooperative scattering (see, e.g. Refs. (35–37)), that the continuous-medium approximation is only valid when the density is high, $\rho k^{-3} \gtrsim 1$. However, the continuous-medium approximation does actually neglect the scattered light and treats it as if it were absorbed. This can indeed be a very good approximation when one is interested in the coherent transmission and not in the scattered light. It is important to note that this approximation is not restricted to high spatial densities (as in condensed matter or very high density vapors) but also holds in the dilute limit where the interatomic distances are larger than the optical wavelength. The refractive index is thus very useful for describing light propagation in dilute atomic clouds. It has been successfully used to describe subtle experiments involving nonlinear effects (38) or photonic band gaps (39, 40).

As discussed below, it turns out that the continuous-medium approximation for atomic vapors is in fact more accurate for dilute than for dense vapors (18, 41).

In order to describe the scattered light, another approach is necessary, in which one basic quantity is the mean-free path $\ell_{sc} = 1/(\rho\sigma_{sc})$. If we only consider elastic scattering, which is valid if the incoming light has a weak intensity (42), the (elastic) scattering cross-section is related to the polarizability by (23)

$$\sigma_{sc} = \frac{k^4}{6\pi} |\alpha|^2. \quad (3)$$

In a large medium of size much larger than the mean-free path, light will be scattered many times before escaping. In this case, many observables can be very well described by a diffusion equation for the electromagnetic energy density, at the condition to perform an average over the disorder configurations. This fact is often surprising for quantum opticians, who expect that light scattered off a disordered medium produces a speckle pattern. However, it is well known to people from mesoscopic physics that after averaging over the disorder, the remaining intensity distribution, or its temporal dynamics in a pulsed experiment, fits perfectly well the prediction of the diffusion equation, although this approach neglects all interference effects¹ (44). At low density, there is one well-known exception, which corresponds to an enhanced backscattering (45–47). The diffusion coefficient is thus another, important macroscopic quantity, which is governed by the atomic density, and which allows describing the diffuse light. In three-dimensional space it reads²

$$D_0 = \frac{v_E \ell_{sc}}{3} = \frac{\ell_{sc}^2}{3\tau_{tr}}, \quad (4)$$

where $v_E = \ell_{sc}/\tau_{tr}$ is the energy transport velocity inside the medium and τ_{tr} the transport time (23, 24). Here, we considered only isotropic scattering such that the transport length equals the mean-free path. For near-resonant light, a remarkable property of cold atomic vapor is that $\tau_{tr} = \tau_{at}$, the lifetime of the excited state, independently of the detuning (23, 32).

In a nonabsorbing passive medium like an atomic vapor probed by a weak intensity laser, the attenuation of the coherent propagating wave is only due to elastic scattering. The mean-free path and the extinction length are thus equal, which leads to the relation

$$\frac{k^3}{6\pi} |\alpha|^2 = \text{Im}(\alpha), \quad (5)$$

closely related to the so-called optical theorem (23, 51). There is thus a close link between the diffusion

coefficient, or the mean-free path, governing the transport of the diffuse light, and the susceptibility, governing the transmission of the coherent light.

2.2. At high atomic density

When the typical distance between atoms becomes on the order of the wavelength, i.e. at large density $\rho k^{-3} \gtrsim 1$, several nontrivial effects must be taken into account to describe the coherent propagation and the transport of the diffuse light.

First, the relation between the susceptibility and the polarizability has to be modified to include the Lorentz local field (34),

$$\chi(\omega) = \frac{\rho\alpha(\omega)}{1 - \rho\alpha(\omega)/3}. \quad (6)$$

This leads to the famous Lorentz-Lorenz shift (52),

$$\Delta_{LL} = -\pi\rho k^{-3}\Gamma, \quad (7)$$

which depends on the density. Here $\Gamma = \tau_{at}^{-1}$ is the linewidth of the transition. Although the derivation of Equation (6) is based on mean-field arguments and uncontrolled approximations, it yields correct results in many situations (53). With hot atomic vapors, a density-dependant shift of the resonance line has indeed been observed (7, 54). With cold atoms, however, recent results suggest that correlations between scatterers at high density are not negligible and the mean-field approximation breaks down (18, 41). The difference with the hot vapor case is probably due to the absence of inhomogeneous broadening, which may suppress the correlations for hot atoms (10, 55). This argument is also consistent with the recent experiment reported in Ref. (2).

Closely related to the Lorentz-Lorenz shift is the ‘cooperative’ Lamb shift (4, 6, 7, 9, 10, 13, 52, 55). It is also a density effect but it is influenced by the finite size and the geometry of the medium. We will discuss this effect in more detail in Section 5.

On the mesoscopic side, the diffusion coefficient should also be corrected at high density, this is the so-called ‘weak localization’ (WL) correction (25),

$$D \sim D_0 \left(1 - \frac{1}{(k\ell_{sc})^2} \right). \quad (8)$$

Note that short-path diagrams not captured by the diffusion approximation are expected to yield supplementary $1/k\ell_{sc}$ corrections to the transport (56, 57). Weak localization corresponds to a slowing down of diffusion due to the constructive interference between reversed-paths of closed loops, which increases the probability of

returning to the original point. The parameter $1/(k\ell_{sc})$ quantifies the amount of ‘disorder’. On resonance, since $\sigma_{sc} = \sigma_0 = 6\pi/k^2$, $1/(k\ell_{sc}) \sim 6\pi\rho k^{-3}$.

Weak localization is thought to be a precursor of Anderson (or strong) localization (58, 59), in particular in the self-consistent theory of localization (60). Anderson localization is expected when $k\ell_{sc} \sim 1$ (Ioffe-Regel criterion (61)) and corresponds to the complete absence of diffusion. Although weak localization has been observed for light in different systems, including cold atoms using the coherent back-scattering effect (62–65), Anderson localization of light in 3D has still not been observed in any experiment (66, 67), and cold atoms may provide a route towards this goal (68).

Beyond transport properties, other subtle effects appear in the correlations and fluctuations of scattered light, such as universal conductance fluctuations (24, 25). These correlations come from common scatterers involved in different paths. If the so-called C_1 correlation is short-range and corresponds to the standard speckle grain of traditional statistical optics (69), the long-range C_2 and C_3 correlations are highly nontrivial effects, which become nonnegligible when the Thouless conductance g is small, i.e. near the strong localization regime. These effects have not been studied yet using multiple scattering of light in cold atoms.

3. Collective effects that depend on the optical depth

As soon as propagation effects are important, the macroscopic local quantities (susceptibility, diffusion coefficient) are not sufficient to describe experimental observables, but should be combined with the size of the medium. The relevant quantity then turns out to be the optical depth.

3.1. Coherent and diffuse transmission

The complex susceptibility of an atomic medium is measured by the attenuation or the dephasing of a probe wave crossing the sample. It is then obvious that the finite size L of the medium enters the problem. The phase shift induced by the sample will be

$$\varphi = [\text{Re}(n) - 1]kL = \text{Re}(\chi)kL/2, \quad (9)$$

and the transmitted intensity will be $T = \exp[-\text{Im}(\chi)kL]$. The above relation is called the Beer’s or Beer-Lambert law. The argument of the exponential is called the optical depth (or thickness) b , i.e.

$$b = -\ln(T) = \text{Im}(\chi)kL = \rho\sigma_{sc}L = L/\ell_{sc}. \quad (10)$$

Although this seems completely trivial, it is interesting to note that a consequence of this exponential attenuation is the nonlinear evolution of the total fluorescence (or ‘off-axis scattering’) with the atom number. The total fluorescence F corresponds indeed to what is not transmitted in the incident mode. We thus get $F \propto 1 - e^{-b}$, which is linear only for low b and saturates for high b . This saturation can be intuitively understood as a ‘shadow effect’: atoms at the back of the sample do not radiate because they are not illuminated by the incoming laser. For the same reason, if we sweep the detuning of the probe beam and measure the fluorescence spectrum, it will be a Lorentzian of width Γ at low optical thickness only, and deviate from a Lorentzian line shape at larger optical thickness, even though the scattering cross-section for single-atoms $\sigma_{sc} = \sigma_0/(1 + 4\Delta^2/\Gamma^2)$ is still Lorentzian. More precisely, it induces an effective broadening and a strong directional dependence of the fluorescence, as shown experimentally in (70). As a consequence, such behaviors are not unique to cooperative effects, even if they are also consistent with a full coupled-dipole model including those effects (71, 72). The shadow effect can also explain the reduction of the radiation pressure force reported in (73, 74), first interpreted as a signature of cooperativity (73). The different collective effects contributing to a modification of the radiation pressure force will be discussed in detail in a forthcoming publication (75).

To illustrate the broadening and saturation effects induced by Beer’s law, we show in Figure 1(a) the behavior of the fluorescence of an atomic cloud as a function of the detuning and the optical depth. Considering a Gaussian atomic density distribution profile, the total scattering cross-section of the cloud according to Beer-Lambert law, reads (74, 75)

$$\Sigma_{sc} = N\sigma_{sc} \times \frac{\text{Ein}(b)}{b}, \quad (11)$$

where Ein is the integer function (76)

$$\begin{aligned} \text{Ein}(b) &= \int_0^b \frac{1 - e^{-x}}{x} dx \\ &= b \left[1 + \sum_{n=1}^{\infty} \frac{(-b)^n}{(n+1)(n+1)!} \right]. \end{aligned} \quad (12)$$

Here, $b = \sqrt{2\pi}\rho_0\sigma_{sc}R_z$ is the optical depth that would be measured using a small beam crossing the cloud through its center, ρ_0 is the peak density and R_z the rms radius along the propagation axis. Although Beer’s law neglects diffraction and refraction effects inside the sample, which are *a priori* not negligible at high b and small nonzero detuning or for very small sample, it appears that such a

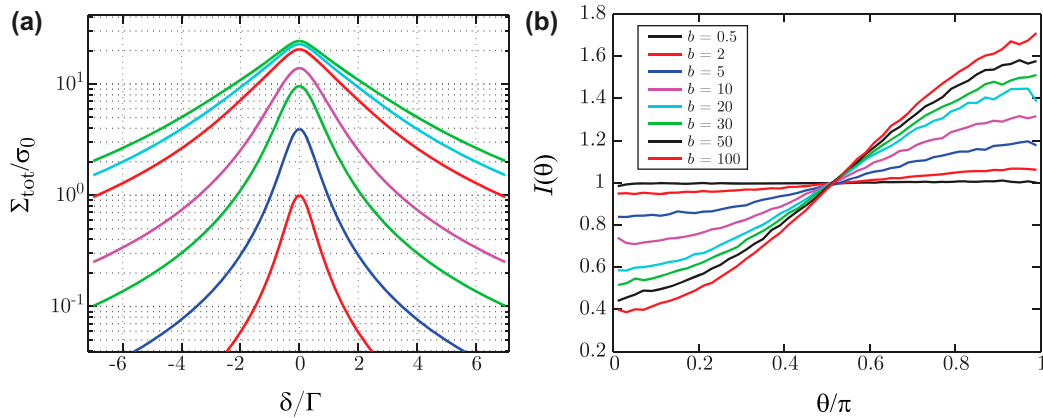


Figure 1. Collective effects in the fluorescence, which can be explained by Beer-Lambert law or by multiple scattering. (a) Total fluorescence as a function of the detuning for different atom numbers ($N = 1, 5, 20, 50, 500, 325, 450$ from the bottom to the top) and a Gaussian cloud of rms transverse size $R = 0.6\lambda$ (71). Broadening and saturation effects are well visible. (b) Emission diagram of a spherical Gaussian cloud illuminated by a plane wave, computed from random walk simulations, for several optical depths from 0.5 to 100. The emission diagram becomes more backward directed as the optical depth increases.

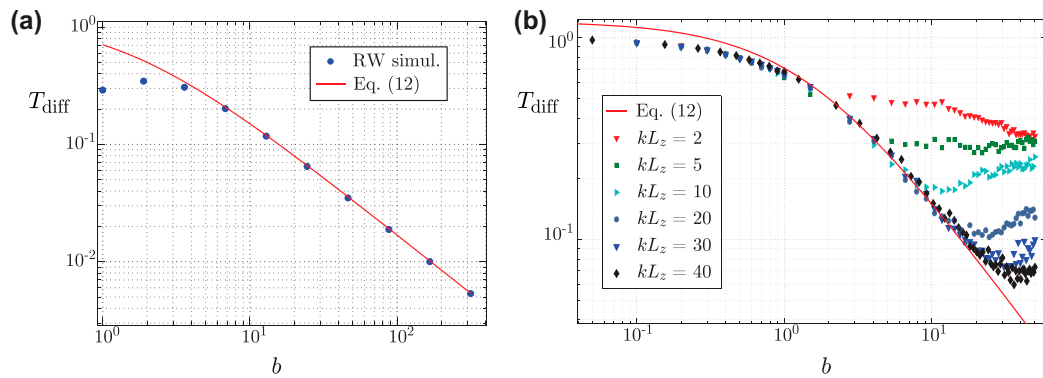


Figure 2. Diffuse transmission T_{diff} as a function of the optical depth b , compared to the asymptotic behavior predicted by the diffusion equation (Ohm’s law, solid line) (Equation (13)). (a) Dots are computed by a random walk simulation. (b) Dots are computed from the coupled-dipole equations in the scalar approximation. Each curve is computed with a given slab depth kL_z and the optical thickness is increased by changing the atom number and thus the density. The driving field is on resonance. At high density, a clear departure from Ohm’s law is observed.

simplified model is sufficient to qualitatively explain the results of (71).

The angular dependence is, however, not possible to compute analytically, and numerical simulations based on a random walk process can be used. For an isotropic cloud illuminated by a plane wave, the anisotropy of the emission diagram results from the multiple scattering of light before escaping the sample (75). We illustrate this anisotropy in Figure 1(b). It should be noted that it can lead to nonintuitive behaviors. For instance, if light is detected near the forward direction, the measured fluorescence can *decrease* as the atom number increases or as the detuning is reduced (‘self-absorption’) (70). Although a simple random walk model completely neglects all wave or coherence effects, it has been shown in Ref. (74) that, for a large and dilute cloud of two-level systems, the corresponding emission diagram agrees

very well with the emission diagram computed from a full coupled-dipole model after averaging over the disorder configurations, except in narrow angular ranges around the forward and backward directions. The forward lobe (2, 11, 20, 22), absent in an incoherent random walk model, can be explained by diffraction/refraction of light by a continuous index distribution (77). Around backward direction, a narrow cone is visible, which can be explained neither by a random walk model nor by a homogeneous index of refraction. This is a signature of interference in a disordered systems, robust against configuration average and well studied in mesoscopic physics (coherent backscattering) (45–47, 62–65). For a Gaussian cloud geometry, analytical expressions for the lobe and cone shapes have been obtained in the double scattering limit (78).

Multiple scattering obviously depends on the optical thickness. Although the diffusion coefficient depends on the density, light should first escape the sample before being detected. In steady state, the main consequence of multiple scattering is the complex emission diagram discussed above. Note that for a slab geometry (homogeneous medium of infinite transverse size and finite width L), space can be divided into two parts and we can speak of diffuse transmission and diffuse reflection. A well-known result is the asymptotic decrease of the diffuse transmission scaling as $1/L$, which corresponds to Ohm's law for photons (Figure 2),

$$T_{\text{diff}} = \frac{1 + \xi}{b + 2\xi}, \quad (13)$$

where $\xi \simeq 0.7104$ (24, 79). This result can be obtained from the diffusion equation or random walk simulations (Figure 2(a)), i.e. a model of light propagation that ignores coherence and interference effects. We have also performed numerical simulations of the diffuse transmission through a slab of atoms, using the coupled-dipole model, in the scalar approximation, where only the far-field term ($\propto 1/r$) of the dipole-dipole interaction is present. We clearly observe a departure from Ohm's law at large density (Figure 2(b)). The precise origin of the deviation is still under investigation and might be due to cooperativity. Note that the observed deviation corresponds to a relative increase compared to Ohm's law for photons and is thus not consistent with a decrease of the diffusion coefficient due to weak localization. However, it resembles recent observations made with classical scatterers (80), in which the increased transport is attributed to near-field scattering, where evanescent waves open new channels of transmission. In our model though, the near-field terms are neglected, and the physical origin of the increased transmission remains to be explained. Recent numerical studies on the distribution of excitation inside atomic samples of different geometries (72) may also be related to our observation.

The temporal dynamics of the diffuse light is also governed by the optical thickness. After some time of illumination, a sudden switch-off of the exciting laser leads to a slow decrease of the fluorescence due to multiple scattering. This 'imprisonment of radiation' (30), or 'radiation trapping' (31), has been studied in cold atoms (32, 81), taking also into account subtle effects like the frequency redistribution induced by the Doppler shift (82, 83) or the multilevel structure (84). Neglecting those effects, one can easily find the scaling of the radiation trapping time with the optical depth. For a Gaussian random walk in 3D, we have $\langle r^2 \rangle = 6Dt$. The average number of scattering events for escaping photons

is the ratio between the time spent in the system and the scattering time τ_{at} ,

$$\langle N_{\text{sc}} \rangle = \frac{t}{\tau_{\text{at}}} \sim \frac{\langle r^2 \rangle}{6D\tau_{\text{at}}}, \quad (14)$$

with $D = \ell_{\text{sc}}^2/(3\tau_{\text{at}})$. When $\sqrt{\langle r^2 \rangle} \sim R = b\ell_{\text{sc}}/2$, the radiation can escape the system, leading to $\langle N_{\text{sc}} \rangle \sim b^2/8$. Radiation trapping times are thus expected to scale as b^2 , with a precise numerical prefactor that depends on the geometry (32).

3.2. Superradiance and subradiance in extended and dilute samples

The previous effects all depend on the detuning-dependent optical depth,

$$b(\Delta) = \frac{b_0}{1 + 4\Delta^2/\Gamma^2}, \quad (15)$$

where b_0 is the on-resonance optical depth. For a cloud of size R , and using $\sigma_0 \sim 1/k^2$, we have $b_0 \sim N/(kR)^2$, with a numerical prefactor that depends on the geometry.

We now discuss why the super- and subradiant decay rates, measured at large detuning such that attenuation or incoherent multiple scattering are negligible, depend on b_0 , independently of the detuning, in the case of an extended $R \gg \lambda$ and dilute ($\rho k^{-3} \ll 1$) sample.

The physical argument to understand why the cooperativity parameter for super and subradiant decay is b_0 , is the following. Consider a sample of finite size $\sim R$ radiating in free space. Although the number of modes in free space is infinite, the boundary condition due to the sample surface ($\propto R^2$) sets limitations on the modes that are efficiently coupled to the sample. In particular, the diffraction limit ensures that no mode with a divergence smaller than $\theta \sim 1/(kR)$ can be emitted from the sample and, in 3D, the total number of modes M efficiently coupled to the sample is related to the sample surface, $M \sim (kR)^2$. It means that if we choose an arbitrary, infinite basis to express the modes in free space, a number M of those modes are enough to describe the radiation pattern of the sample. Then, if the number N of atoms in the sample is larger than the number M of modes, the emission will be cooperative because, in average, N/M atoms emit in the same modes: they are thus coupled to each other via their common coupling to the electromagnetic mode (Fano coupling). We conclude that the 'cooperativity parameter' in this problem is the ratio N/M , which turns out to be the on-resonance optical depth b_0 , up to a numerical prefactor. This argument is consistent with the Dicke limit $R \ll \lambda$, for which

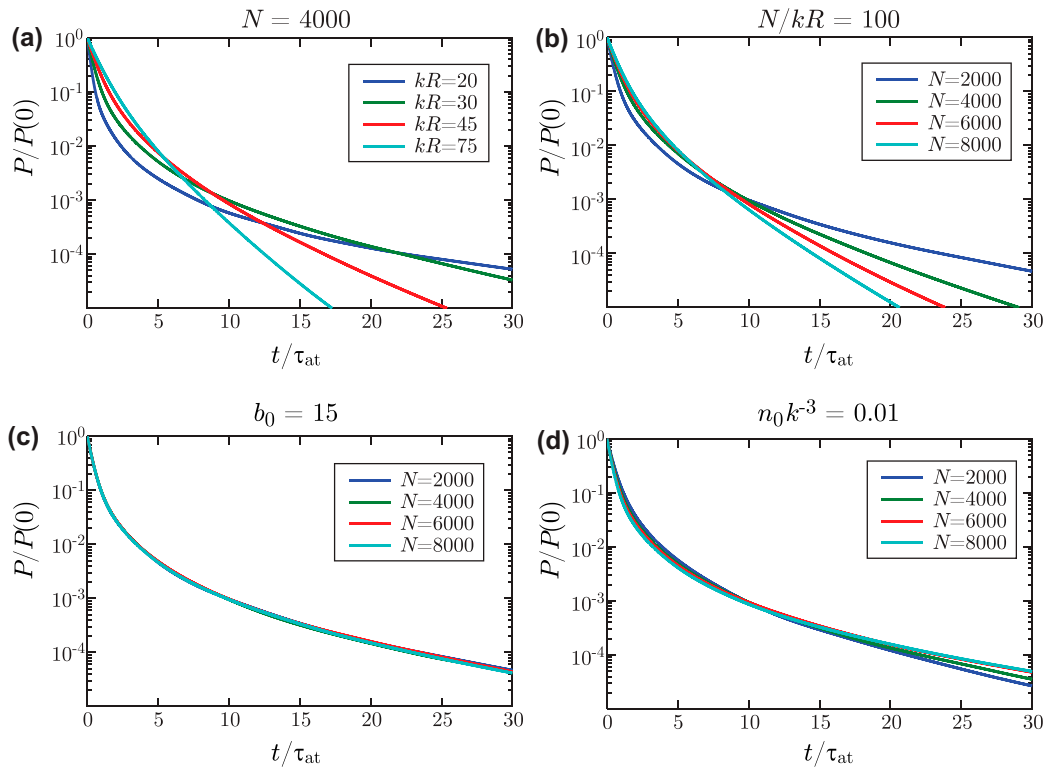


Figure 3. Decay of the total scattered power after the switch-off of the driving laser at $t = 0$ computed from the coupled-dipole model in the scalar approximation, as in (5), averaged over only two configurations. The time axis is normalized to the lifetime of the excited state τ_{at} and the vertical axis to the steady-state scattered power. The driving laser has a large detuning, $\Delta = 50\Gamma$, and has been applied for a duration of $30\tau_{\text{at}}$ so that the system reaches its steady state. In panel (a), the atom number $N = 4000$ is kept constant and the size is varied, $b_0 = 3N/(kR)^2$ is varied from 30 to 2.3. In panel (b), both N and R are varied such that N/kR is kept constant, b_0 is varied from 15 to 3.75. In panel (c), N and R are varied such that $b_0 = 15$, and in panel (d) N and R are varied such that the density is kept constant, $n_0 k^{-3} = 0.01$, and b_0 is varied from 11 to 17.5.

the only possible outgoing mode is a spherical wave, i.e. $M = 1$, and the superradiant enhancement factor is N . This reasoning was given in brief in (5, 85, 86) and is consistent with the classification of superradiance given in (87).

Let us note that super- and subradiance for $N = 2$ has a marked difference with the case of $N \gg 2$. First, in order to obtain large dipole-dipole coupling of two atoms in free space, these atoms need to be at a distance comparable to the optical wavelength. When an atomic pair is separated by many wavelengths, interferences between light emitted by these atoms can still occur (88). However a modification of the atomic lifetime requires the interatomic distance to be smaller than or comparable to the wavelength (89, 90). For small atomic distances, near-field dipole-dipole coupling, scaling as $1/r^3$, becomes dominant, while super- and subradiance obtained for many atoms in the dilute limit is relying on the far-field dipole coupling, scaling as $1/r$. This long-range behaviour of the far-field dipole-dipole coupling is essential for the collective scaling of the Dicke subradiance observed in (5). Let us also note that the

competition between the near and far-field dipole-dipole coupling has been discussed in (91, 92) and has been called ‘van der Waals dephasing’ in (15). It is interesting to note that while for $N = 2$, the eigenstates of the near-field part of the interaction Hamiltonian H_{NF} are also eigenstates of the far-field interaction H_{FF} (both being proportional to the same σ_1 Pauli matrix), for $N > 2$, H_{NF} and H_{FF} are not proportional if the distances between all atoms are not equivalent (which can be obtained in the particular case of 3 atoms equally spaced on a ring or four atoms equally spaced on a sphere). In this case H_{NF} and H_{FF} do not commute and have different eigenvectors (see Section 4 of (15)). This particular situation does not prevent the total Hamiltonian to have eigenvalues corresponding to long-lived (subradiant) and short-lived (superradiant) modes. However the symmetries of the eigenstates (and potentially their sensitivity to perturbations) will differ from those of H_{FF} .

As explained from the beginning, it is not surprising that the size of the sample is an important parameter to take into account, since the superradiant and subradiant decays are transient phenomena, which means that light

must escape the sample. However, from a mathematical point of view, when looking at the coupled-dipole model (93–97), it is not obvious which combination of the parameters yields to correct scaling laws for the different features that can be observed. In this model, once the geometry of the cloud is fixed (and spherical), there are three independent parameters: the atom number N , the size R and the detuning of the driving laser. In the limit of a very large detuning, after a long enough illumination, the system reaches a steady state given by the ‘timed-Dicke state’ (11, 95, 97). Once the laser is switched off, the decay of this state could be governed by any combination of N and R . In particular, it might be considered more intuitive that the density $\rho \sim N/R^3$ is the important parameter, in particular because the dipole-dipole coupling terms, which decay as $1/(kr)$ with the interparticle distance r , become very small as the density decreases. But even if the coupling terms are small, each atom is coupled to $N - 1$ other atoms, and N can be huge, which, somehow, balances the low density and makes $b_0 \sim N/(kR)^2$ to be the scaling parameter. Note that the $1/r$ term in the dipole-dipole interaction bears all the relevant ingredient for ‘long-range’ interaction, which, as in gravitational or Coulomb interactions, yields to well-known size-dependent effects (98). This parameter also appears in the statistical properties of the eigenvalues of non-Hermitian Euclidean random matrices such as the one involved in the couple-dipole model (99, 100) and the early (superradiant) decay of the timed-Dicke state (11), or ‘phased state’, has been computed analytically by many authors, $\Gamma_{\text{sup}} \propto b_0$ (21, 22, 35–37, 95, 101, 102). Numerical and experimental evidence have been given in (5, 86) that the long time decay is also governed by b_0 , $\Gamma_{\text{sub}} \propto 1/b_0$. Here, we show in Figure 3 that not only the short and long time limits are both depending on b_0 , but the full decay curve is in fact only dependent on b_0 . An analytical function for describing this decay curve remains to be found. We have checked that this is neither a power law, nor a stretched exponential.

4. The mean-field approach of traditional optics and the independent scattering approximation of mesoscopy

It was pointed out in recent theoretical (18) and experimental studies (41) that Equation (6), which includes Lorentz local field correction, is inaccurate for cold atoms at high density. Indeed, another term, usually not considered, has the same order of magnitude. Following (41), the more precise expression is given by

$$\chi(\omega) = \frac{\rho\alpha(\omega)}{1 - \rho\alpha(\omega)(1/3 + \beta(\omega))}, \quad (16)$$

where $\beta(\omega) \sim \alpha(\omega)k^3$ and specifically depends on the geometry. This term is neglected in the mean-field approach leading to Equation (6) even though on resonance, $\alpha(\omega) \sim k^{-3}$, and thus $\beta(\omega)$ has the same order of magnitude than the $1/3$ corresponding to the density-dependent Lorentz local-field correction. To our knowledge, this result has been first obtained by Saunders and Bullough (103, 104) (see Equation (22) of (104)) and has been later rediscovered several times (93, 105). One hypothesis for the success of Equation (6) could be that the mean-field result is recovered if some mechanism breaks the correlation between scatterers, as it could be the case, e.g. for hot vapors with the Doppler broadening (10, 55).

At this point, it is interesting to point out the close link between Equation (16) and the weak localization correction of the diffusion coefficient (Equation 8). First, we note that Equation (16) can be rewritten

$$\chi(\omega) = \frac{\rho\alpha(\omega)}{1 - \rho\alpha(\omega)/3 - \rho\alpha(\omega)\beta(\omega)}, \quad (17)$$

which isolates a correcting factor $\rho\alpha(\omega)\beta(\omega)$ in the usual Lorentz–Lorentz formula (6). Then, if $\beta(\omega) \sim \alpha(\omega)k^3$, this correcting factor is $\sim \rho k^3 \alpha(\omega)^2$, which is almost identical to

$$\frac{1}{k\ell_{\text{sc}}} = \frac{\rho\sigma_{\text{sc}}}{k} = \frac{\rho k^3 |\alpha(\omega)|^2}{6\pi}, \quad (18)$$

the disorder parameter used in mesoscopic optics. Given the close link between the diffusion coefficient and the susceptibility, there is a strong similitude between the correction of Equation (16) and the weak localization correction to the diffusion coefficient Equation (8).

This similitude is not surprising. The mean field approach of traditional optics neglects correlation between scatterers. When they exist, these correlations are due to the nonnegligible probability that a photon goes back to a previous scatterer, a process sometimes called recurrent scattering. In the mesoscopy community, neglecting this recurrent scattering and the subsequent correlations is called the ‘independent scattering approximation’ (ISA) (23–25). Weak localization effects are typical signatures of ‘dependent scattering’. The link between the ISA and the Lorentz-Lorentz local field theory has been already briefly discussed in Ref. (53) but is often not discussed in more recent works.

5. What should be called cooperative?

Based on the previous discussion, we consider that the term ‘cooperative scattering’ should not be kept for effects related to recurrent scattering only, because it is already called ‘dependent scattering’ in the mesoscopy community, and several such effects have well-established names,

like weak or strong localization. Moreover, effects related to Dicke superradiance and subradiance can appear at low density, as shown in Figure 3 and in (3–5), without recurrent scattering, and have been called ‘cooperative’ for a very long time (see, e.g. Refs. (21, 22, 26, 91, 92, 104, 106, 107)). Changing the semantics without a clear distinction of previously studied effects in different communities is therefore probably not recommendable.

However, we agree that it is questionable to call collective effects ‘cooperative’ if these effects can also be explained by conceptually more simple models, like wave propagation in a medium characterized by its susceptibility or standard multiple scattering.

In addition to the examples already mentioned (71, 73), the coherent forward emission (2, 11, 20, 22) is certainly such an effect. Even if using a single-photon *Gedankenexperiment* requires a quantum formalism to properly demonstrate that the absorbed photon will be preferentially emitted in the forward direction (11), this effect is a simple consequence of an N -wave interference, like in a multiple slit experiment, and it is well-known that slit experiments produce interference patterns even with single particles (108). The interference pattern from two atoms radiating a single photon has also been observed in (88, 109). The analogy between N -slit interference and the directionality character of superradiance has been further developed, including higher-order correlations, in Ref. (110). In the CW regime, considering the phase-matching in the forward direction is also a way to understand the index of refraction of a polarizable medium. Thus, the resulting forward lobe is actually the diffraction/refraction pattern of the sample, like a Mie scatterer (77).

The ‘cooperative’ Lamb shift is another questionable example. In the case of macroscopic samples, for which a susceptibility can be defined, Javanainen and Ruostekoski have shown (18), at least for the slab geometry that applies to the experiment of Ref. (7), that the ‘cooperative’ Lamb shift was the result of ‘standard optics’, i.e. wave propagation in a dielectric medium following the Helmholtz equation. It would be interesting to know, using wave propagation simulations, if this also holds for the cigar-shaped sample used in Ref. (4) or any other geometry (111). For example, one of the geometries studied by Manassah (111) consists of a density-modulated slab of atoms and a ‘giant cooperative Lamb shift’ was predicted when the density is modulated at the Bragg condition (112). Such an experiment has already been performed (39), and very asymmetric and shifted Bragg-reflection spectra have been indeed reported (see, e.g. Figure 2 of (39)). These feature can be explained by the coupled-dipole model (113), but they can also be very well described by a standard-optics wave-propagation

equation based on a periodic susceptibility (in that case using transfer-matrices to exploit the periodicity). Thus, it seems that in many (or most?) situations, the ‘cooperative Lamb shift’ is in fact a collective shift related to the shape and finite size of the medium, inducing refraction, reflection, lensing and waveguide effects (114), etc. which can be simulated by wave-propagation simulations.

The problem is that such wave-propagation simulations are not simple to perform. In the recent years, the coupled-dipole model has been widely used (3, 5, 9, 36, 71, 72, 93, 95–97, 115–117). It is computationally limited to a few thousand atoms, but it is otherwise very simple to use. Another strength is its completeness: it includes all collective effects we have discussed so far. But this is also a drawback: it is sometimes hard to give simple interpretation of the numerical results and, when comparing to experimental results, a good agreement does not help identifying the relevant physical ingredients of the experiment. As a consequence, it would be wise, although tedious, to systematically compare the results with simulations based on a standard-optics calculation (wave propagation in a dielectric) or with a standard multiple-scattering computation (random walk), to check if the observations do not have simple explanations. This methodology has been used in (5, 41).

It seems to us that less ambiguous signatures of cooperativity can be found in the transient response of the system, as initially envisioned by Dicke for the superradiant emission of a fully inverted system (14, 15, 20) and its subradiant counterpart (29). In the single-photon or linear-optics regime, superradiant decay rates have been observed recently in the forward direction (4) and also off-axis (3).

In the forward-direction case, the measured light is the diffracted/refracted light by the cloud. Its dynamics is thus related to the dynamics of the refractive index. The imaginary part of the refractive index is also what governs the transmission, and its dynamics at the switch-on or -off of the incident laser is what gives rise to optical precursors (118, 119) or ‘flashes’ (120–122). It has been shown experimentally and theoretically, using only Beer-Lambert law including the dephasing, that dynamics faster than Γ can appear at large on-resonance optical thickness (122). This is somehow the counterpart of the spectral broadening induced by Beer’s law at high b_0 .

Since this broadening is also present for the light scattered off-axis (see Figure 1(a)), one can wonder if similar arguments also explains off-axis superradiance. Off axis, though, the field arriving on the detector emitted by different atoms have random phases (no phase-matching). There is thus no straightforward calculation similar to the one of (122), at least to our knowledge, that could relate the spectral broadening of the system response to the

temporal dynamics observed on the fluorescence. This is, we think, the nontrivial feature of cooperativity and superradiance in the linear regime that this accelerated decay is still preserved despite the absence of any obvious phase-matching condition. Thus, the most efficient way to understand this result is to invoke the collective (cooperative) modes of the atomic excitation in the cloud, some of them decaying fast (superradiant modes), and some decaying slowly (subradiant modes). In other words, we trace over the photon degrees of freedom and look at the collective (cooperative) atomic behavior. The reverse approach, looking at the light, scattered by all atoms and interfering, is certainly possible and might provide an alternative view on the light-matter interaction for many atoms and at low intensities.

Subradiant decay, as the counterpart of superradiance, is also a good signature of cooperativity. However, a particular care is necessary to distinguish between different effects that could lead to a slow decay of the scattered light. In a dense sample with sharp boundaries, for example, long-lived cavity-like modes (or ‘polaritonic modes’ (123)) may exist, and may also give rise to high-Q Mie-like resonances (77). If the optical thickness $b(\Delta)$ is large (near resonance), multiple scattering may trap the light in the sample for a long time (radiation trapping, see Section 3.1 and Ref. (32)), and even strong localization might need to be considered (124). In that case, the qualitative difference between those various effects can be seen in their different scalings with the experimental parameters. The radiation trapping time scales as $b(\Delta)^2$ whereas the subradiant time scales as b_0 (5), independently of the detuning. Here again, Mie resonances or radiation trapping are well understood by looking at the light, whereas subradiance is well understood by looking at the collective modes of the atomic excitation. If we want to explain subradiance with a physical picture using light, we can say that coherence and interference effect modifies multiple scattering such that some ‘lucky photons’ are trapped in the sample, even at large detuning. If we neglect coherence and interference effects (diffusion or random walk model), we find, on the contrary, that multiple scattering vanishes far from resonance. The interplay between this incoherent radiation trapping and subradiance for intermediate detuning, and the way to distinguish between them, is the subject of our current investigation.

6. Conclusion

In this article, we have tried to discuss the meaning of ‘cooperative scattering’ from a broad perspective, by studying various collective effects in atom-light interaction. We conclude that what should be called cooperative is often

mainly a question of perspective. When we describe collective effects by looking at the atoms, with a microscopic modeling (based on Dicke states, coupled dipoles, etc.), most features appear to be of cooperative nature. Nevertheless, one can also understand many of these effects using the point of view of light, undergoing multiple scattering or propagating through a macroscopic sample, without using the concept of cooperativity at all.

The temporal decay of the light emitted off-axis seems to be the best example so far of a situation where a cooperative-scattering approach is the most efficient, numerically as well as conceptually, to describe the physics. We have shown that, at large detuning, the full decay curve only depends on the on-resonance optical thickness of the sample (and of its precise shape), but an analytical description of this result is still missing.

Finally, we emphasize that most, if not all, of the effects that we discussed in this article, are already known, but not always in the same fields. Superradiance and subradiance are hardly known in the mesoscopy community, and the same can be said for effects related to multiple scattering with the quantum-optics community. Establishing a bridge between those communities and their concepts seems very important to us. In particular, we have pointed out the similarity between the recurrent-scattering corrections to the susceptibility recently discussed in the quantum-optics community (18, 41) and the weak-localization corrections, which are well-known in the mesoscopy community. We have also presented new results on the deviation from Ohm’s law predicted by the coupled-dipole model. The physical origin of this deviation remains to be understood, but this is an attempt to relate cooperativity to *transport properties* (125). This connection may be fruitful for the question of Anderson localization of light in 3D (68, 124) or in relation with other topics, like superconductivity (126) or light-harvesting systems (127, 128).

Notes

1. If the medium size is not much larger than the mean free path, the radiative transfer equation should be used instead of the diffusion equation (24, 43).
2. A more general expression is $D_0 = \langle z^2 \rangle / (2d\tau)$, where d is the number of dimensions and $\langle z^2 \rangle$ is the second moment of the step-length distribution $P(z)$. For a random walk with constant step ℓ , $\langle z^2 \rangle = \ell^2$, but for the exponential distribution due to Beer’s law (Section 3.1), $P(z) = \exp(-z/\ell)/\ell$ and $\langle z^2 \rangle = 2\ell^2$, which gives Equation (4). In some special cases, like in hot vapors, the second moment can be infinite, leading to Lévy flights and superdiffusive transport (48–50).

Acknowledgements

We thank Antoine Browaeys, Yvan Sortais and Mark Havey for fruitful discussions at the PQE conference and Joachim von Zanthier for his invitation.

Disclosure statement

No potential conflict of interest was reported by the authors.

Funding

This work was supported by the Agence National pour la Recherche [grant number ANR-14-CE26-0032] (project LOVE). M.T.R. was supported by an Averoès exchange program.

References

- Goban, A.; Hung, C.L.; Hood, J.D.; Yu, S.P.; Muniz, J.A.; Painter, O.; Kimble, H.J. *Phys. Rev. Lett.* **2015**, *115*, 063601.
- Bromley, S.L.; Zhu, B.; Bishof, M.; Zhang, X.; Bothwell, T.; Schachenmayer, J.; Nicholson, T.L.; Kaiser, R.; Yelin, S.F.; Lukin, M.D.; Rey, A.M.; Ye, J. *Nat. Commun.* **2016**, *7*, 11039.
- Araújo, M.O.; Krešić, I.; Kaiser, R.; Guerin, W. *Phys. Rev. Lett.*, **2016**, arXiv:1603.07204.
- Roof, S.J.; Kemp, K.J.; Havey, M.D. *Phys. Rev. Lett.* **2016**, arXiv:1603.07268.
- Guerin, W.; Araújo, M.O.; Kaiser, R. *Phys. Rev. Lett.* **2016**, *116*, 083601.
- Röhlsberger, R.; Schlage, K.; Sahoo, B.; Couet, S.; Ruffer, R. *Science* **2010**, *328*, 1248–1251.
- Keaveney, J.; Sargsyan, A.; Krohn, U.; Hughes, I.G.; Sarkisyan, D.; Adams, C.S. *Phys. Rev. Lett.* **2012**, *108*, 173601.
- Okaba, S.; Takano, T.; Benabid, F.; Bradley, T.; Vincetti, L.; Maizelis, Z.; Yampol'skii, V.; Nori, F.; Katori, H. *Nat. Commun.* **2014**, *5*, 4096.
- Meir, Z.; Schwart, O.; Shahmoon, E.; Oron, D.; Ozeri, R. *Phys. Rev. Lett.* **2014**, *113*, 193002.
- Jenkins, S.D.; Ruostekoski, J.; Javanainen, J.; Bourgain, R.; Jennewein, S.; Sortais, Y.R.P.; Browaeys, A. *Phys. Rev. Lett.* **2016**, *116*, 183601.
- Scully, M.O.; Fry, E.S.; Raymond Ooi, C.H.; Wódkiewicz, K. *Phys. Rev. Lett.* **2006**, *96*, 010501.
- Scully, M.O.; Svidzinsky, A.A. *Science* **2009**, *325*, 1510–1511.
- Scully, M.O. *Phys. Rev. Lett.* **2009**, *102*, 143601.
- Feld, M.S.; MacGillivray, J.C. *Superradiance, Coherent Nonlinear Optics*. In Recent Advances; Topics in Current Physics 21; Springer: Berlin, **1980**; pp. 7–57.
- Gross, M.; Haroche, S. *Phys. Rep.* **1982**, *93*, 301–396.
- de Oliveira, R.A.; Mendes, M.S.; Martins, W.S.; Saldanha, P.L.; Tabosa, J.W.R.; Felinto, D. *Phys. Rev. A* **2014**, *90*, 023848.
- Tighineanu, P.; Daveau, R.S.; Lehmann, T.B.; Beere, H.E.; Ritchie, D.A.; Lodahl, P.; Stobbe, S. *Phys. Rev. Lett.* **2016**, *116*, 163604.
- Javanainen, J.; Ruostekoski, J. *Opt. Express* **2016**, *24*, 993–1001.
- Javanainen, J. *Talk at the 46th Winter Colloquium on the Physics of Quantum Electronics (PQE)*; Snowbird (UT), **2016**.
- Dicke, R.H. *Phys. Rev.* **1954**, *93*, 99–110.
- Arecchi, F.T.; Courtens, E. *Phys. Rev. A* **1970**, *2*, 1730–1737.
- Rehler, N.E.; Eberly, J.H. *Phys. Rev. A* **1971**, *3*, 1735–1751.
- Lagendijk, A.; van Tiggelen, B.A. *Phys. Rep.* **1996**, *270*, 143–215.
- van Rossum, M.C.W.; Nieuwenhuizen, T.M. *Rev. Mod. Phys.* **1999**, *71*, 313–371.
- Akkermans, E.; Montambaux, G. *Mesoscopic Physics of Electrons and Photons*; Cambridge University Press, Cambridge, **2007**.
- Bonifacio, R.; Lugiato, L.A. *Phys. Rev. A* **1975**, *11*, 1507–1521.
- Malcuit, M.S.; Maki, J.J.; Simkin, D.J.; Boyd, R.W. *Phys. Rev. Lett.* **1987**, *59*, 1189–1192.
- Dicke, R.H. The coherence brightened laser. In *Proceedings of the third international congress on Quantum Electronics*; Grivet, P. and Bloembergen, N., Eds.; Columbia University Press, New York, **1964**; pp. 35–53.
- Pavolini, D.; Crubellier, A.; Pillet, P.; Cabaret, L.; Liberman, S. *Phys. Rev. Lett.* **1985**, *54*, 1917–1920.
- Holstein, T. *Phys. Rev.* **1947**, *72*, 1212–1233.
- Molisch, A.; Oehry, B. *Radiation Trapping in Atomic Vapours*; Oxford University Press, Oxford, **1998**.
- Labeyrie, G.; Vaujour, E.; Müller, C.A.; Delande, D.; Miniatura, C.; Wilkowski, D.; Kaiser, R. *Phys. Rev. Lett.* **2003**, *91*, 223904.
- Cummings, F.W. *Phys. Rev. A* **1986**, *33*, 1683–1687.
- Born, M.; Wolf, E. *Principle of Optics*, 7th ed.; Cambridge University Press: New York, **1999**.
- Svidzinsky, A.A.; Chang, J.T.; Scully, M.O. *Phys. Rev. Lett.* **2008**, *100*, 160504.
- Svidzinsky, A.; Chang, J.T. *Phys. Rev. A* **2008**, *77*, 043833.
- Prasad, S.; Glauber, R.J. *Phys. Rev. A* **2010**, *82*, 063805.
- Labeyrie, G.; Tesio, E.; Gomes, P.M.; Oppo, G.; Firth, W.J.; Robb, G.R.M.; Arnold, A.S.; Kaiser, R.; Ackemann, T. *Nature Photon.* **2014**, *8*, 321–325.
- Schilke, A.; Zimmermann, C.; Courteille, P.W.; Guerin, W. *Phys. Rev. Lett.* **2011**, *106*, 223903.
- Schilke, A.; Zimmermann, C.; Guerin, W. *Phys. Rev. A* **2012**, *86*, 023809.
- Jennewein, S.; Besbes, M.; Schilder, N.J.; Jenkins, S.D.; Sauvan, C.; Ruostekoski, J.; Greffet, J.-J.; Sortais, Y.R.P.; Browaeys, A. *Phys. Rev. Lett.* **2016**, *116*, 233601.
- Cohen-Tannoudji, C.; Dupont-Roc, J.; Grynberg, G. *Atom-Photon Interactions: Basic Processes and Applications*; Wiley, New York, **1992**.
- Ishimaru, A. *Wave Propagation and scattering in random media*; IEEE Press, New York, **1999**.
- Johnson, P.; Imhof, A.; Bret, B.P.J.; Rivas, J.G.; Lagendijk, A. *Phys. Rev. E* **2003**, *68*, 016604.
- Kuga, Y.; Ishimaru, A. *J. Opt. Soc. Am. A* **1984**, *1*, 831–835.
- van Albada, M.P.; Lagendijk, A. *Phys. Rev. Lett.* **1985**, *55*, 2692–2695.
- Wolf, P.; Maret, G. *Phys. Rev. Lett.* **1985**, *55*, 2696–2699.

- (48) Mercadier, N.; Guerin, W.; Chevrollier, M.; Kaiser, R. *Nature Phys.* **2009**, *5*, 602.
- (49) Mercadier, N.; Chevrollier, M.; Guerin, W.; Kaiser, R. *Phys. Rev. A* **2013**, *87*, 063837.
- (50) Baudouin, Q.; Pierrat, R.; Eloy, A.; Nunes-Pereira, E.J.; Cuniasse, P.; Mercadier, N.; Kaiser, R. *Phys. Rev. A* **2014**, *90*, 052114.
- (51) Newton, R.G. *Am. J. Phys.* **1976**, *44*, 639–642.
- (52) Friedberg, R.; Hartmann, S.R.; Manassah, J.T. *Phys. Rep.* **1973**, *3*, 101–179.
- (53) Lagendijk, A.; Nienhuis, B.; van Tiggelen, B.A.; de Vries, P. *Phys. Rev. Lett.* **1997**, *79*, 657–660.
- (54) Maki, J.J.; Malcuit, M.S.; Sipe, J.E.; Boyd, R.W. *Phys. Rev. Lett.* **1991**, *67*, 972–975.
- (55) Javanainen, J.; Ruostekoski, J.; Li, Y.; Yoo, S.-M. *Phys. Rev. Lett.* **2014**, *112*, 113603.
- (56) Kirkpatrick, T.R.; Belitz, D. *Phys. Rev. B* **1986**, *34*, 2168–2175.
- (57) Eckert, F.; Buchleitner, A.; Wellens, T. *J. Phys. A: Math. Theor.* **2012**, *45*, 395101.
- (58) Anderson, P.W. *Phys. Rev.* **1958**, *109*, 1492–1505.
- (59) Lagendijk, A.; van Tiggelen, B.; Wiersma, D.S. *Phys. Today* **2009**, *62*, 24–29.
- (60) Vollhardt, D.; Wölfle, P. *Self-consistent theory of Anderson localization*. Electronic Phase Transition; Elsevier, North-Holland, **1992**; pp 1–78.
- (61) Ioffe, A.F.; Regel, A.R. *Prog. Semicond.* **1960**, *4*, 237–291.
- (62) Labeyrie, G.; de Tomasi, F.; Bernard, J.C.; Müller, C.A.; Miniatura, C.; Kaiser, R. *Phys. Rev. Lett.* **1999**, *83*, 5266–5269.
- (63) Bidel, Y.; Klappauf, B.; Bernard, J.C.; Delande, D.; Labeyrie, G.; Miniatura, C.; Wilkowski, D.; Kaiser, R. *Phys. Rev. Lett.* **2002**, *88*, 203902.
- (64) Kaiser, R.; Havey, M.D. *Opt. Photon. News* **2005**, *16*, 38–43.
- (65) Labeyrie, G. *Mod. Phys. Lett. B* **2008**, *22*, 73–99.
- (66) van der Beek, T.; Barthelemy, P.; Johnson, P.M.; Wiersma, D.S.; Lagendijk, A. *Phys. Rev. B* **2012**, *85*, 115401.
- (67) Sperling, T.; Schertel, L.; Ackermann, M.; Aubry, G.J.; Aegerter, C.M.; Maret, G. *New J. Phys.* **2016**, *18*, 013039.
- (68) Skipetrov, S.E.; Sokolov, I.M.; Havey, M.D. arXiv:1603.02968, **2016**.
- (69) Goodman, J.W. *Speckle Phenomena in Optics: Theory and applications*, 3rd ed., Roberts & Company Publishers: Greenwood Village, **2009**.
- (70) Labeyrie, G.; Delande, D.; Müller, C.A.; Miniatura, C.; Kaiser, R. *Opt. Commun.* **2004**, *243*, 157–164.
- (71) Pellegrino, J.; Bourgain, R.; Jennewein, S.; Sortais, Y.R.P.; Browaeys, A.; Jenkins, S.D.; Ruostekoski, J. *Phys. Rev. Lett.* **2014**, *113*, 133602.
- (72) Sutherland, R.T.; Robicheaux, F. *Phys. Rev. A* **2016**, *93*, 023407.
- (73) Bienaimé, T.; Bux, S.; Lucioni, E.; Courteille, P.W.; Piovella, N.; Kaiser, R. *Phys. Rev. Lett.* **2010**, *104*, 183602.
- (74) Chabé, J.; Rouabah, M.T.; Bellando, L.; Bienaimé, T.; Piovella, N.; Bachelard, R.; Kaiser, R. *Phys. Rev. A* **2014**, *89*, 043833.
- (75) Bachelard, R.; Piovella, N.; Guerin, W. arXiv:1607.01157, **2016**.
- (76) Weisstein, E.W. Ein Function, From MathWorld – A Wolfram Web Resource. <https://protect-us.mimecast.com/s/6RQOBqhzL0bVFb?domain=mathworld.wolfram.com>.
- (77) Bachelard, R.; Courteille, P.W.; Kaiser, R.; Piovella, N. *Europhys. Lett.* **2012**, *97*, 14004.
- (78) Rouabah, M.; Samoylova, M.; Bachelard, R.; Courteille, P.W.; Kaiser, R.; Piovella, N. *J. Opt. Soc. Am. A* **2014**, *31*, 1031–1039.
- (79) Garcia, N.; Genack, A.Z.; Lisyansky, A.A. *Phys. Rev. B* **1992**, *46*, 14475–14479.
- (80) Naraghi, R.R.; Sukhov, S.; Sáenz, J.J.; Dogariu, A. *Phys. Rev. Lett.* **2015**, *115*, 203903.
- (81) Fioretti, A.; Molisch, A.F.; Mütter, J.H.; Verkerk, P.; Allegrini, M. *Opt. Commun.* **1998**, *149*, 415–422.
- (82) Labeyrie, G.; Kaiser, R.; Delande, D. *Appl. Phys. B* **2005**, *81*, 1001–1008.
- (83) Pierrat, R.; Grémaud, B.; Delande, D. *Phys. Rev. A* **2009**, *80*, 013831.
- (84) Baudouin, Q.; Mercadier, N.; Kaiser, R. *Phys. Rev. A* **2013**, *87*, 013412.
- (85) Akkermans, E.; Gero, A.; Kaiser, R. *Phys. Rev. Lett.* **2008**, *101*, 103602.
- (86) Bienaimé, T.; Piovella, N.; Kaiser, R. *Phys. Rev. Lett.* **2012**, *108*, 123602.
- (87) Longo, P.; Keitel, C.H.; Evers, J. *Sci. Rep.* **2016**, *6*, 23628.
- (88) Grangier, P.; Aspect, A.; Vigué, J. *Phys. Rev. Lett.* **1985**, *54*, 418–421.
- (89) DeVoe, R.G.; Brewer, R.G. *Phys. Rev. Lett.* **1996**, *76*, 2049–2052.
- (90) Barnes, M.D.; Krstic, P.S.; Kumar, P.; Mehta, A.; Wells, J.C. *Phys. Rev. B* **2005**, *71*, 241303.
- (91) Friedberg, R.; Hartmann, S.R. *Phys. Rev. A* **1974**, *10*, 1728–1739.
- (92) Milonni, P.W.; Knight, P.L. *Phys. Rev. A* **1974**, *10*, 1096–1108.
- (93) Ruostekoski, J.; Javanainen, J. *Phys. Rev. A* **1997**, *55*, 513–526.
- (94) Javanainen, J.; Ruostekoski, J.; Vestergaard, B.; Francis, M.R. *Phys. Rev. A* **1999**, *59*, 649–666.
- (95) Courteille, P.W.; Bux, S.; Lucioni, E.; Lauber, K.; Bienaimé, T.; Kaiser, R.; Piovella, N. *Eur. Phys. J. D.* **2010**, *58*, 69–73.
- (96) Svidzinsky, A.A.; Chang, J.T.; Scully, M.O. *Phys. Rev. A* **2010**, *81*, 053821.
- (97) Bienaimé, T.; Petruzzo, M.; Bigerni, D.; Piovella, N.; Kaiser, R. *J. Mod. Opt.* **2011**, *58*, 1942–1950.
- (98) Dauxois, T.; Ruffo, S.; Cugliandolo, L.F., Eds. *Long-Range Interacting Systems*; Lecture Notes of the Les Houches Summer School 90, **2010**. Oxford University Press, Oxford.
- (99) Skipetrov, S.E.; Goetschy, A. *J. Phys. A: Math. Theor.* **2011**, *44*, 065102.
- (100) Goetschy, A.; Skipetrov, S.E. *Phys. Rev. E* **2011**, *84*, 011150.
- (101) Mazets, I.E.; Kurizki, G. *J. Phys. B: At. Mol. Opt. Phys.* **2007**, *40*, F105–F112.
- (102) Friedberg, R.; Manassah, J.T. *Phys. Lett. A* **2010**, *374*, 1648–1659.
- (103) Saunders, R.; Bullough, R.K. *J. Phys. A: Math., Nucl. Gen.* **1973**, *6*, 1348–1359.
- (104) Saunders, R.; Bullough, R.K. *J. Phys. A: Math., Nucl. Gen.* **1973**, *6*, 1360–1374.

- (105) Morice, O.; Castin, Y.; Dalibard, J. *Phys. Rev. A* **1995**, *51*, 3896–3901.
- (106) Haake, F.; Glauber, R.J. *Phys. Rev. A* **1972**, *5*, 1457–1466.
- (107) Stroud, C.R., Jr; Eberly, J.H.; Lama, W.L.; Mandel, L., *Phys. Rev. A* **1972**, *5*, 1094–1104.
- (108) Tonomura, A.; Endo, J.; Matsuda, T.; Kawasaki, T.; Ezawa, H. *Am. J. Phys.* **1989**, *57*, 117–120.
- (109) Eichmann, U.; Bergquist, J.C.; Bollinger, J.J.; Gilligan, J.M.; Itano, W.M.; Wineland, D.J.; Raizen, M.G. *Phys. Rev. Lett.* **1993**, *70*, 2359–2362.
- (110) Oppel, S.; Wiegner, R.; Agarwal, G.S.; von Zanthier, J. *Phys. Rev. Lett.* **2014**, *113*, 263606.
- (111) Manassah, J.T. *Adv. Opt. Photon.* **2012**, *4*, 108–156.
- (112) Manassah, J.T. *Phys. Lett. A* **2010**, *374*, 1985–1988.
- (113) Samoylova, M.; Piovella, N.; Bachelard, R.; Courteille, P.W. *Opt. Commun.* **2014**, *312*, 94–98.
- (114) Roof, S.; Kemp, K.; Havey, M.; Sokolov, I.M.; Kupriyanov, D.V. *Opt. Lett.* **2015**, *40*, 1137–1140.
- (115) Chomaz, L.; Corman, L.; Yefsah, T.; Desbuquois, R.; Dalibard, J. *New. J. Phys.* **2012**, *14*, 055001.
- (116) Miroshnychenko, Y.; Poulsen, U.V.; Mølmer, K. *Phys. Rev. A* **2013**, *87*, 023821.
- (117) Feng, W.; Li, Y.; Zhu, S.Y. *Phys. Rev. A* **2014**, *89*, 013816.
- (118) Jeong, H.; Dawes, A.M.C.; Gauthier, D.J. *Phys. Rev. Lett.* **2006**, *96*, 143901.
- (119) Chen, J.F.; Wang, S.; Wei, D.; Loy, M.M.T.; Wong, G.K.L.; Du, S. *Phys. Rev. A* **2010**, *81*, 033844.
- (120) Chalony, M.; Pierrat, R.; Delande, D.; Wilkowski, D. *Phys. Rev. A* **2011**, *84*, 011401(R).
- (121) Kwong, C.C.; Yang, T.; Pramod, M.S.; Pandey, K.; Delande, D.; Pierrat, R.; Wilkowski, D. *Phys. Rev. Lett.* **2014**, *113*, 223601.
- (122) Kwong, C.C.; Yang, T.; Delande, D.; Pierrat, R.; Wilkowski, D. *Phys. Rev. Lett.* **2015**, *115*, 223601.
- (123) Schilder, N.J.; Sauvan, C.; Hugonin, J.; Jennewein, S.; Sortais, Y.R.P.; Browaeys, A.; Greffet, J. *Phys. Rev. A* **2016**, *93*, 063835.
- (124) Skipetrov, S.E.; Page, J.H. *New. J. Phys.* **2016**, *18*, 021001.
- (125) Gero, A.; Akkermans, E. *Phys. Rev. Lett.* **2006**, *96*, 093601.
- (126) Baskaran, G. Superradiant superconductivity, arXiv:1211.4567, **2012**.
- (127) Monshouwer, R.; Abrahamsson, M.; van Mourik, F.; van Grondelle, R. *J. Phys. Chem. B* **1997**, *101*, 7241–7248.
- (128) Celardo, G.L.; Giusteri, G.G.; Borgonovi, F. *Phys. Rev. B* **2014**, *90*, 075113.

I must say, however, that since the writing of this article four years ago, my understanding has evolved and I would probably not write all the same now. In particular, the discussion at the end on the impossibility to apply a flash-type calculation [Chalony 2011, Kwong 2014, Kwong 2015] to describe off-axis superradiance has been proven wrong by the article [Kuraptsev 2017]. I will discuss this model in Section VI.4. Concerning subradiance, the question of having a ‘photon picture’ is still an open problem (see Section VI.5.3).

For completeness, even if I’m not involved, I should also mention that the understanding of the ‘cooperative’ Lamb shift problem [Scully 2010] also evolved significantly in the recent years, in particular thanks to the work done by the Palaiseau group in collaboration with the Durham group [Peyrot 2018].

V.2. Radiation pressure force?

After years of experiments on multiple scattering of light [Labeyrie 2008], the first experiment on ‘cooperative’ scattering in Nice was performed in 2008 by Simone Bux (visiting PhD student from the Tübingen group) and Eleonora Lucioni (Master student from Milan) in the context of a collaboration with Philippe Courteille and Nicola Piovella¹. By chance, as it was not the initial goal of the experiment, they observed an atom-number-dependent reduction of the residual radiation-pressure force on atoms trapped in a not-very-far-detuned dipole trap (Figs. 3-5 of [Bux 2010]). This was a new and unexpected collective effect. After some time it was suspected that it could be due to the new ‘single-photon superradiance’ proposed by Scully [Scully 2006]: if spontaneous emission is more directed in the forward direction, the net momentum transferred to the atoms is reduced.

Scully’s theory was then generalized to the case of driven atoms and the corresponding collective force was computed using the Timed-Dicke (TD) ansatz [Courteille 2010]. Then some cleaner and more systematic data was taken, with a plane wave for the driving beam, and a smaller detuning to have a stronger force. The data was consistent with the coupled-dipole (CD) model and was thus interpreted as due to the forward emission of the superradiant TD state [Bienaimé 2010]. Another experiment was performed in Tübingen on a much colder and smaller cloud: in that case there is a strong influence of diffraction and Mie scattering such that the collective radiation force can be larger than the single-atom one [Bender 2010].

Some time later, in 2011 or 2012, new data was taken closer to resonance, in a regime of large optical thickness. The opposite was expected, i.e. an increase of the collective force. Indeed, as shown in [Labeyrie 2004] and in Fig. IV.1(b), in the multiple scattering regime, light is more emitted in the backward direction (this is also shown in Fig. 1(b) of [Guerin 2017c] above). However, a collective *reduction* of the force was also observed, which was very puzzling.

Finally it was understood that another effect had been overlooked so far (although mentioned in Tom Bienaimé’s thesis [Bienaimé 2011a], p. 80), which is the ‘shadow effect’: the exponential attenuation of the driving field in the medium makes that, in average, atoms interact less with the field. Then a precise comparison between the emission diagrams computed with the CD model and an incoherent random walk (RW) model [Fig. V.1] showed that the only differences were a very narrow forward scattering cone, which does not contribute to the force, and the coherent backscattering cone, which has a negligible effect on the force [Chabé 2014].

¹ After Philippe Courteille moved to Brazil, the Nice-Milan-Tübingen-São Carlos groups formed the COSCALI (COLlective SCAttering of LIGHT) network, an International Research Staff Exchange Scheme funded by the EU, which initiated the series of COSCALI workshops.

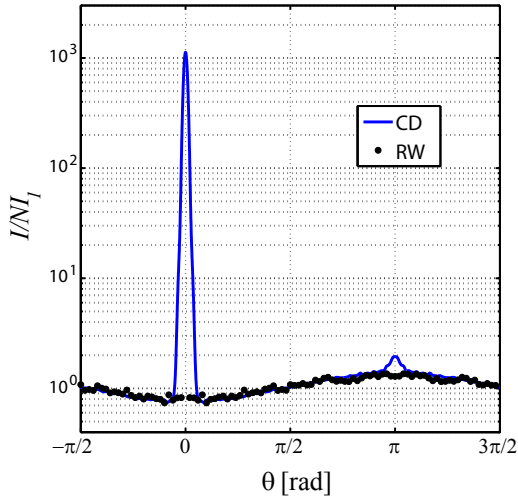



Figure V.1: Emission diagram computed with the coupled-dipole (CD) model and the random walk (RW) model, with a Gaussian cloud (rms size $\sigma = 20/k_0$) of resonant optical thickness $b_0 = 8$ illuminated by a resonant plane wave. Taken from [Chabé 2014].

This doesn't mean, of course, that the previous interpretation based on the TD state was wrong, it only means that there is another possible interpretation, which does not need the concept of cooperativity or superradiance, and might thus be considered simpler. Let us however insist on the fact that the agreement between the shadow effect and the TD ansatz is surprising, because the TD states is based on the fact that all dipoles have the same amplitudes, so it is, in principle, a good hypothesis only when the detuning is large enough such that the attenuation and the dephasing of the driving field inside the cloud is negligible. Although it was not the case of the data of [Bienaimé 2010], it still gave correct results.

I was not involved in all these studies. However I contributed to a final article on this subject, in which we study in detail the different effects contributing to the collective radiation-pressure force (shadow effect, diffraction, coherent backscattering) and discuss which effects are included in the different possible models (CD, RW, TD ansatz) [Bachelard 2016]. We show in particular that the TD ansatz, as a mean-field solution of the full CD problem, captures the first-order correction in b , the actual optical thickness, corresponding to the shadow effect for small b . The general conclusion of that paper, which I don't include here, is that the radiation-pressure force is not a good observable to put in evidence cooperative scattering effects because in all regimes of parameters, one can use other, simpler interpretations. Note, nevertheless, that the very first data taken with the dipole trap [Bux 2010] has not been yet fully explained...

V.3. Off-axis scattering?

Also at the PQE 2016 conference, Mark Havey presented a systematic experimental study of light scattering by an elongated and less dilute cloud of cold rubidium atoms. I suggested that I could provide RW simulations of the experiment in order to help interpret the results. I thus did it but I also found out that, by a proper normalization of the data, the shadow effect (i.e. Beer-Lambert law) could explain the experiment pretty well and RW simulations are actually not even needed. The resulting paper [Kemp 2020], which was published only recently, is reproduced below.

Optical-depth scaling of light scattering from a dense and cold atomic ^{87}Rb gasK. J. Kemp, S. J. Roof, and M. D. Havey *Department of Physics, Old Dominion University, Norfolk, Virginia 23529, USA*

I. M. Sokolov

*Department of Theoretical Physics, Peter the Great St.-Petersburg Polytechnic University, 195251 St.-Petersburg, Russia
and Institute for Analytical Instrumentation, Russian Academy of Sciences, 198103 St.-Petersburg, Russia*

D. V. Kupriyanov

*Center for Advanced Studies, Peter the Great St.-Petersburg Polytechnic University, 195251 St.-Petersburg, Russia
and Quantum Technologies Center, M.V. Lomonosov Moscow State University, Leninskiye Gory 1-35, 119991 Moscow, Russia*

W. Guerin

Université Côte d'Azur, CNRS, Institut de Physique de Nice, 06560 Valbonne, France

(Received 28 July 2018; accepted 24 February 2020; published 20 March 2020)

We report investigation of near-resonance light scattering from a cold and dense atomic gas of ^{87}Rb atoms. Measurements are made for probe frequencies tuned near the $F = 2 \rightarrow F' = 3$ nearly closed hyperfine transition, with particular attention paid to the dependence of the scattered light intensity on detuning from resonance, the number of atoms in the sample, and atomic sample size. We find that, over a wide range of experimental variables, the optical depth of the atomic sample serves as an effective single scaling parameter which describes well all the experimental data.

DOI: [10.1103/PhysRevA.101.033832](https://doi.org/10.1103/PhysRevA.101.033832)**I. INTRODUCTION**

Study of light interacting with cold and ultracold atomic gases is an active area of experimental and theoretical research [1,2]. The subject appears to be deceptively simple, corresponding in many cases to a single weak probe beam scattering from a small cloud of cold atoms. However, under most realistic situations, the atoms in such a sample interact not only with the incident radiation field, but also with the light scattered by all the other atoms in the sample. The ensembles may then be viewed as many-body physical systems, and can display emergent complexity. The optical response reveals a collective optical response that differs significantly from that of a dilute, optically thin atomic ensemble.

Over the past few years, there have been a large number of reports on collective or cooperative effects in light scattering by atoms. For instance, steady-state experiments have revealed collective effects, such as lensing [3], light diffusion [4,5], changes in the radiation pressure force [6–8], etc. Because of potentially important consequences for clock technology [9], the question of collective shifts of the resonance line, in particular, raised a lot of discussions [10–15] and experiments [16–23]. Even without any shift, changes in the line shape, collective broadening, and saturation of the amount of scattered light have been observed in several experiments with different parameters and geometries, and interpreted somewhat differently [4,21–26].

In many of these studies, collective changes in the atomic response are measured and displayed as a function of the

atomic density. The results are then attributed to dipole-dipole interactions and presented in the context of the coupled dipole model. This approach basically includes all the essential physics (attenuation, diffraction, refraction, multiple scattering, collective frequency shifts, etc.). In a typical cold-atom experiment, however, the atomic density cannot be readily changed independent of other parameters such as the sample size or the atom number. Then it may be difficult to find if the measured collective effect really depends on the density, on the optical thickness, the number of atoms, or on something else altogether. Then, even though excellent results are often obtained from the coupled-dipole model, other approaches such as the Beer-Lambert law or random walk simulations are valuable and can allow identification of which physical ingredients are really necessary to explain the data.

In this paper, we report measurements of the scattered light intensity from a cloud of cold ^{87}Rb atoms. By changing the number of atoms and the size of the sample, we have varied the optical depth through the center of the trap by about a factor of 10^3 . This range is large enough to encompass an optically thin sample on one hand, and emergence of the so-called shadow effect on the other. All measurements are found to be in good agreement with microscopic and fully quantum calculations of the light scattering processes. We find also that over the full and wide range of optical depths the experimental data are well described by a random walk simulation of light transport in the atomic medium; in this model the optical depth serves as an effective single scaling parameter which quantitatively agrees with all the data. A Beer-Lambert's law

argument similarly shows a single parameter scaling with the optical depth.

In the following sections we first describe the experimental arrangement and measurement scheme. This is followed by presentation of the experimental results and comparison with quantum microscopic calculations. We follow this by a description of our random walk simulations, Beer-Lambert law scaling, and comparison of the simulations with the peak optical depth dependence of the experimental data.

II. EXPERIMENTAL ARRANGEMENT

The basic experimental scheme has been described in detail elsewhere [27]; here we provide only an outline of details necessary to understand the experimental approach and results. In the basic approach, we follow a multistep process to produce cold atom samples confined by a far off resonance trap (FORT). Initially, ^{87}Rb atoms are loaded into a three-dimensional magneto-optical trap (MOT), with a density distribution that can be approximated as Gaussian. The MOT is characterized using methods similar to those in [27]. The physical size and temperature of the MOT are found by directly measuring the radius of a fluorescence image projected onto a CCD camera (pixel resolution of $24\ \mu\text{m} \times 24\ \mu\text{m}$). The number of atoms trapped in the MOT is measured through traditional absorption imaging. The number is independently measured by using an optical pumping approach, as described in [28]. We find that normally we have about 450 million atoms contained in the MOT. At this stage of sample preparation, the distribution of atoms among the $F = 2$ Zeeman states is not known. Most groups assume, however, that the atoms plausibly have the atoms equally distributed among the Zeeman states; we assume that here. This hypothesis leads to an effective light scattering cross section of $7/15(3\lambda^2/2\pi)$.

A small fraction of the MOT atoms is then loaded into a far-off-resonance trap (FORT). This trap consists of a single laser beam ($\lambda = 1064\ \text{nm}$) focused to a beam waist ω_* of about $20\ \mu\text{m}$. This quantity was measured in an auxiliary experiment using a scanning knife edge to determine the beam shape and size around the focus. The longitudinal scale is given by the Rayleigh range, defined as $z_r = \pi\omega_*^2/\lambda$, which is about $900\ \mu\text{m}$ in our case. The intensity gradient of the focused light, along with being far detuned from resonance, creates a potential well in the ground state in which the atoms can be trapped. During the loading process, the MOT trapping laser is detuned $\sim 10\gamma$ below resonance and the repumping laser is attenuated by $\sim 99\%$. This reduces the radiation pressure and creates a compressed MOT, which has a better spatial overlap with the FORT laser beam. Atoms excited with the MOT trapping laser tuned near the $F = 2 \rightarrow F' = 2$ transition undergo inelastic Raman transitions, resulting in loading into the lower $F = 1$ ground level. After a loading time of 70 ms, the trapping and repumping lasers are fully extinguished, along with the external magnetic field. Starting with an initial load of $1.3(2) \times 10^6$ atoms, the FORT laser is kept on for a minimum of 200 ms, until the sample is approximately thermalized with $7.8(1) \times 10^5$ atoms at a temperature on the order of $100(5)\ \mu\text{K}$. The FORT atomic density distribution ρ is approximated by a Gaussian distribution as $\rho =$

$\rho_0 \exp(-\frac{r^2}{2r_0^2} - \frac{y^2}{2y_0^2})$ with a radial size r_0 , longitudinal radius y_0 , and peak density ρ_0 . This frequently made estimate is based on the observation that the atom distribution is dominantly located spatially at small y , such that y is smaller than the Rayleigh length for the trap.

The peak density is determined from the definition $\rho_0 = N/(2\pi)^{3/2}r_0^2y_0$ and measurements of N , r_0 , and y_0 and the temperature T . We described in an earlier paragraph measurement of N by two methods. The longitudinal size $y_0 = 259\ \mu\text{m}$ is sufficiently large to be measured directly by fluorescence imaging using the CCD, which has a pixel resolution of $24\ \mu\text{m} \times 24\ \mu\text{m}$. The transverse size of $r_0 = 3.0\ \mu\text{m}$ is too small to be directly measured that way. Instead, we make measurements of the highest transverse parametric resonance frequency (as driven by weak amplitude modulation of the trap depth), which appears at twice the harmonic-oscillator frequency ω . Measurement of the FORT temperature and the transverse confinement allow determination of $r_0^2 = k_B T/m\omega^2$.

Once the atomic sample is thermalized, the FORT trapping laser is turned off. Initially the atoms are repumped into the $F = 2$ ground state to prepare for probing on the $F = 2 \rightarrow F' = 3$ transition. After an optical pumping phase of about $8\ \mu\text{s}$, nearly all of the atoms are transferred to the $F = 2$ level. After another $2\ \mu\text{s}$, a near-resonance low intensity ($0.1 I_{\text{sat}}$) probe laser is flashed for $1\ \mu\text{s}$. As shown in Fig. 1(b) the probe beam is linearly polarized, creating by optical excitation an axially symmetric atomic polarization (alignment) in the excited $F = 3$ level with reference to the probe electric-field symmetry axis. This in turn modifies the emission diagram, generating an anisotropic diagram of spatial fluorescence. This is a rather small effect, even for an optically thin atomic sample, and results in an intensity difference of 12%, relative to the isotropic case, on the equatorial plane, and 24% at the poles. For the fluorescence geometry of our experiment, this is a 7.9% effect for single scattering from the atomic cloud. For the case of multiple scattering, these are even smaller effects at least for ^{85}Rb , as reported earlier [29]. These two effects are steady state and are hidden in the global rescaling of the data. We thus ignore these small effects in further discussion of the data.

The probe is offset from resonance by a detuning $\Delta = f - f_0$, where f_0 is the bare atomic resonance frequency. As shown schematically in Fig. 1, the probe beam is spatially much larger than the atomic sample, with a e^{-2} radius of $4.5\ \text{mm}$, and as shown in Fig. 1(b) is incident upon the sample at an oblique angle. Fluorescence detection of the fluorescence is also made at an oblique angle (viewing down the x axis). Following an initial measurement, the sample is allowed to continue to expand and is probed again $40\ \mu\text{s}$ after the initial flash. This process continues for a total of 10 probe pulses up to a total expansion time of $370\ \mu\text{s}$. The sample expands from an initial volume with radii $r_0 = 3.0\ \mu\text{m}$ and $y_0 = 259\ \mu\text{m}$ to final radii of $r_0 = 33.4\ \mu\text{m}$ and $y_0 = 261\ \mu\text{m}$. The fluorescence from the sample is collected without regard to light polarization for all 10 pulses and focused into a multimode fiber connected to an infrared sensitive photomultiplier tube (PMT). The output of the PMT is directed without preamplification to a multichannel scaler having 40 ns time resolution.

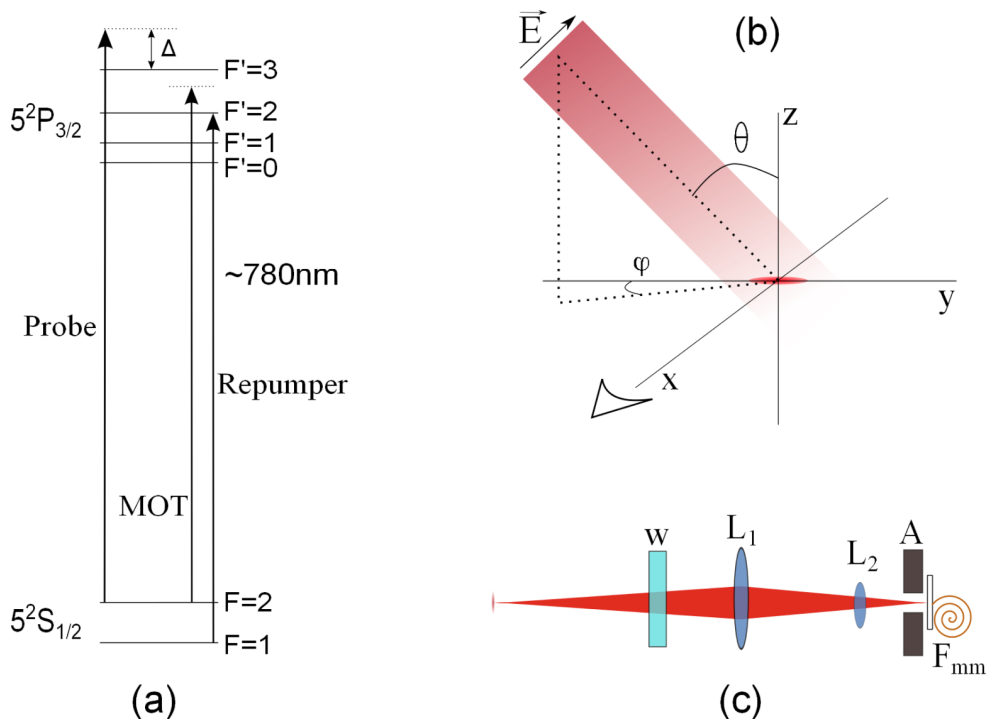


FIG. 1. Basic experimental scheme. (a) Relevant ^{87}Rb energy levels. (b) Geometry of probe optical excitation and fluorescence collection. The angles $\theta = 23^\circ$ and $\phi = 30^\circ$. (c) Fluorescence detection arm, viewing down the x axis. Light is detected in the far field through a window (w) and focused into a $600\ \mu\text{m}$ diameter multimode optical fiber F_{mm} with a pair of lenses L_1 and L_2 as shown.

For the results presented in this paper, this time signal was integrated over the duration of each individual pulse to show the total amount of fluorescence for each sample size, all while maintaining the same number of atoms.

In order to sample a broader range of atomic sizes and densities, the number of atoms can also be changed. The peak density of the sample depends on the holding time of the FORT; background gas collisions decrease the number of atoms within the sample. At the longest hold time used for these measurements (2.5 s), the number of atoms is reduced to $1.8(7) \times 10^5$. In Fig. 2, the peak density for each sample holding time as a function of expansion time is shown. Finally, we also studied the dependence of the scattered light intensity on probe detuning at the highest possible density for our thermalized sample. Using an acousto-optical modulator (AOM) in a double-pass setup, the frequency of the probe laser was tuned over a range of nearly 60 MHz while maintaining a constant probe optical power.

III. RESULTS AND DISCUSSION

In this section we present our experimental results and make side by side comparison of the measurements and fully quantum calculations of the measured quantities. These results and comparisons are followed by two subsections in which the data is globally analyzed and discussed in terms of attenuation of the propagating light beam and a random walk for the diffusing light.

The details of the microscopic calculational techniques are described in detail in several earlier papers [2,30,31] on the general subject of light scattering in a cold and dense gas. For

completeness, we include here a brief overview of this model. Our approach is one of the versions of the method known in the literature as the coupled dipoles (CD) model. This model has been heavily used in the context of cooperative scattering (see references in the Introduction and see also [32–36]). In our variant of the CD approach we solve the nonstationary Schrödinger equation for the wave function ψ of the joint system consisting of N motionless two-level atoms (ground state with the total angular momentum $J_g = 0$, and degenerate

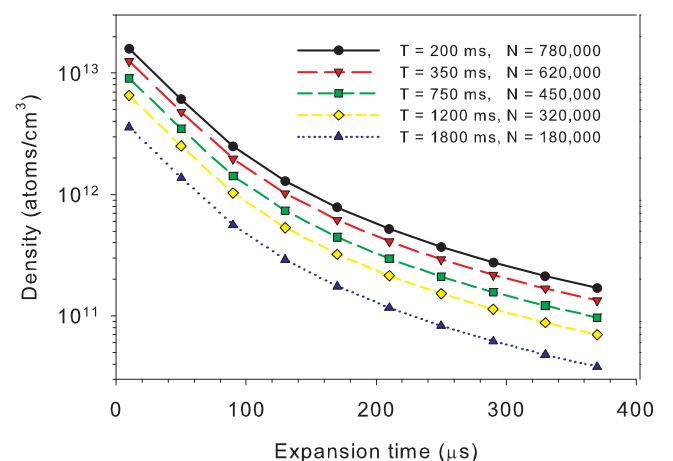


FIG. 2. Reduction of the number of atoms within the FORT over time due to ballistic expansion, thermalization, and background gas collisions. After various hold times T , there are N atoms in the trap (see legend). After the FORT trapping laser is extinguished, the sample expands, reducing the peak atomic density as shown.

excited state $J_e = 1$ with $m = J_z = 1, 0, -1$ and a weak electromagnetic field. A vacuum reservoir is also included in our considerations. We search for the wave function ψ as an expansion in a set of eigenfunctions of the Hamiltonian of the noninteracting atoms and field. For the considered case of weak excitation (linear optics regime), we account only for states with no more than one photon in the field. Tracing over the photon degrees of freedom we obtain a finite set of equations for the Fourier component of amplitudes of states with one excited atom, which are the basic equations of the CD model. This set of equations is solved numerically.

The resulting solution gives us the opportunity to find all the other amplitudes of the states taken in our consideration and consequently the approximate wave function of the studied joint physical system. Knowledge of the wave function allows us to describe the properties of the atomic ensemble as well as the properties of the secondary radiation. Particularly, we can calculate the intensity of the different polarization components of the light scattered in an arbitrary direction as a corresponding quantum-mechanical average (for more detail, see [31]). Possible atomic displacement caused by residual atomic motion is taken into account in our approach by averaging of calculated quantities over this random spatial distribution of the atoms. Theoretical results obtained in the framework of this procedure are scaled [37] to account for the fact that the measurements and theoretical calculations are made at very different numbers of atoms.

These results and comparisons are followed by two subsections in which the data is globally analyzed and discussed in terms of attenuation of the propagating light beam and a random walk for the diffusing light.

A. Experimental results and comparison with theory

We first point out that, in all cases, fluorescence measurements are made after the atoms in the FORT have essentially thermalized and the FORT has been turned off, so that the atoms are mainly in free space. There are two primary overlapping experimental protocols. In one, once the FORT has been extinguished, the expanding atomic sample is exposed to a series of ten $1 \mu\text{s}$ probe pulses temporally spaced to map out a factor of several hundred in peak atomic density. As the probe spatial profile is much larger than the atomic sample, the number of atoms probed remains essentially constant. In a second protocol, the atom sample is held in the trap for increasingly longer periods of time; background gas collisions reduce the number of atoms in the ensemble, while the sample size, as measured by the sample Gaussian radii, remains the same. Then the FORT is extinguished and a sequence of probe pulses is used to probe the sample. This dual approach allows mapping out of both the atomic sample size and atomic density dependence of the fluorescence signals.

As an initial result, we present in Fig. 3 the measured fluorescence signals from a $10 \mu\text{s}$ probe pulse and their dependence on the peak atomic density. We see in the figure that the signals increase with decreasing atomic density. The origin of this somewhat counterintuitive effect arises from the fact that, for the highest densities, and consequently the greatest optical depth, the probe beam is attenuated during its traversal through the sample. The scattering signals then should originate mainly from light scattered from the illumi-

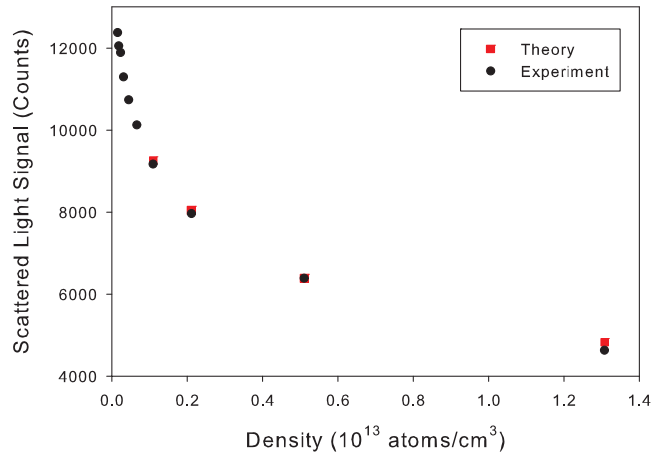


FIG. 3. On resonance variation of the scattered light signals with peak atomic density. Note the strong increase of the signal size with decreasing atomic density, for a fixed number of atoms in the sample.

nated outer regions of the sample surface, and the relatively fewer atoms compared to the sample as a whole. We will study in more detail this “shadow effect” in the next subsection. As the density is decreased, on the other hand, the sample becomes more optically thin; the sample ultimately scatters light as a collection of individual atoms. Comparison of the experimental results with calculations shows very good agreement. Note that the vertical (signal) scale is adjusted to match the experimental and theoretical responses.

We elaborated on this general effect by measuring the dependence of the scattering signals on atomic density and on detuning from atomic resonance. The overall experimental results for all positive blue detunings and densities are shown in Fig. 4(a). One striking feature of these results is that, for larger detunings, the sensitivity of the signals to density is significantly reduced, and for the largest detunings from resonance, there is, within the experimental uncertainty, no variation of the signal intensity with peak atomic density. This effect is due to the decreasing optical depth of the atomic sample with increasing detuning; for the smallest optical depth, all the atoms experience essentially the same probe intensity, and thus contribute to the scattering signals. The corresponding theoretical results are shown Fig. 4(b). These results are in very good qualitative agreement with the experimental ones. Red detuned measurements (not shown) are also in very good agreement with the simulations. The data are also quite symmetric about zero detuning; this is seen in the characteristic spectral response for two different densities, as shown in Fig. 5. There the solid lines represent Lorentzian spectral profiles; this line shape is a very good empirical fit to the measured profile.

Implicit in Figs. 3 and 4 is a dependence on the spectral width (viz. Fig. 5) and the ensemble response to changes in atomic density. This dependence is shown in Fig. 6, where we see a nonlinear increase of the spectral width with increasing density and an approach at low density to around 9 MHz, evidently larger than the 6.1 MHz expected for single scattering. This behavior should be compared to that reported by Pellegrino *et al.* [26] in a recent paper. In our case, the lower density limit is partly due to the technical

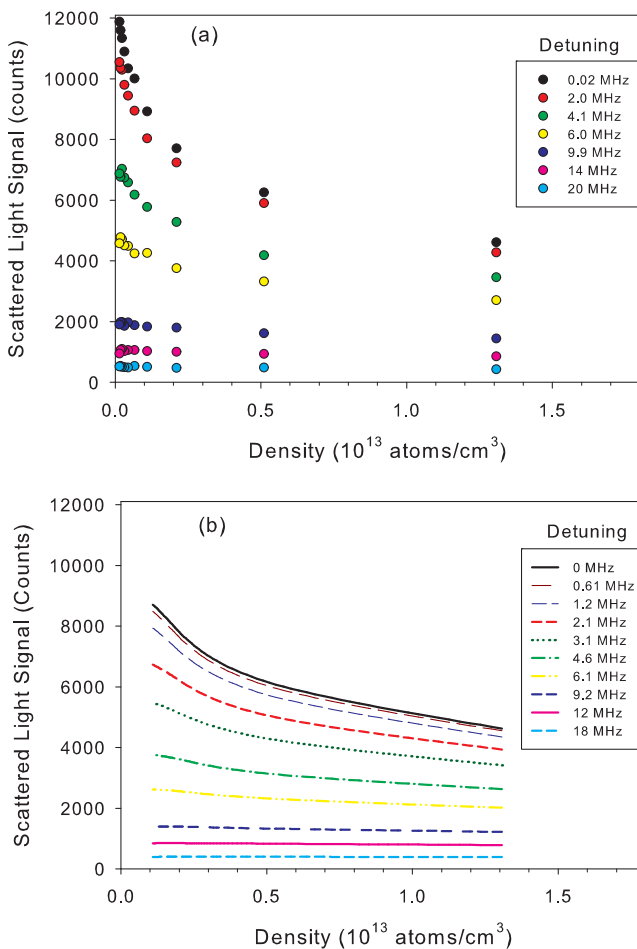


FIG. 4. Detuning and density dependence of the measured scattered light intensity. (a) Experimental results for positive (blue) detunings. (b) Theoretical results. The vertical scale has been adjusted to match the experimental data.

combination of the laser linewidth and the Doppler width of the transition. Further, this dependence is qualitatively due to the fact that major contributions to the signal arise from atoms near the outer regions of the atomic sample, the deeper atoms contributing less due to the shadow effect. For a large optical depth and a uniform density, this implies a roughly \sqrt{b} scaling of the width; here b is the peak optical depth through the center of the sample [37]. A fit to the data in Fig. 6 leads to a low density intercept of around 7(1) MHz, in reasonable agreement with expectations. We should point out that, realistically, our samples are strongly inhomogeneous, and there are contributions to the signals from a range of atomic densities. Such scaling should then be considered as only a qualitative feature of the measured spectral widths.

Finally, we have examined the dependence of the measured scattered light intensity with variations in the effective volume of the sample. We use as a measure of the sample volume the product of the atom sample Gaussian radii, viz. $(2\pi)^{3/2}y_0r_0^2$. In these measurements, this product is held fixed as the number of atoms in the sample is varied. Results are shown in Fig. 7. We see in Fig. 7 that, for each sample size

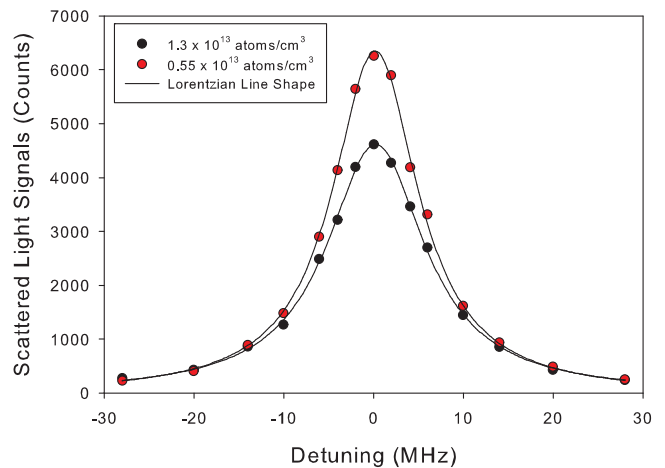


FIG. 5. Representative line shapes for the dependence of the measured signals on detuning from atomic resonance.

and within the experimental uncertainty, the signal increases monotonically with increasing number of atoms (or atomic density). However, the rate of increase is significantly different, depending on the sample size, and is strongly suppressed for the smallest sample sizes.

B. Rescaling according to the Beer-Lambert law

The good agreement between the data and the full microscopic theory is in itself satisfactory but it does not allow identifying the relevant physical ingredients at the origin of the specific behavior of the scattered light as a function of the different control parameters. This is because the microscopic theory naturally contains many effects: attenuation of the probe light, diffraction and refraction, multiple scattering, super and subradiance, collective shifts, etc. It is thus useful

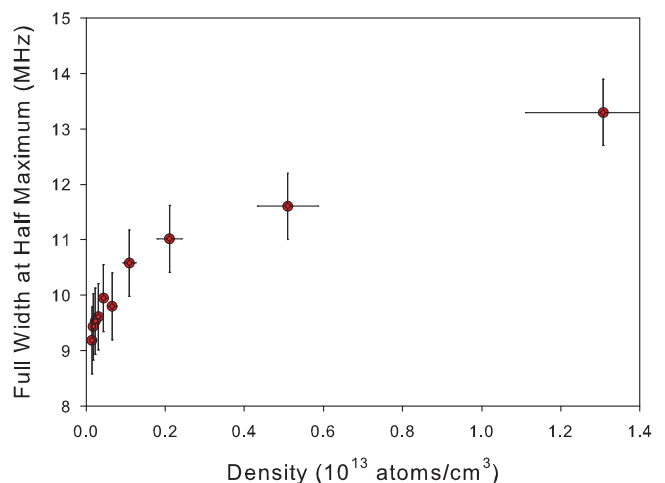


FIG. 6. Dependence of the full width at half maximum of the atomic resonance response as a function of atomic density. These measurements correspond to varying the density by changing the sample size while holding the number of atoms fixed.

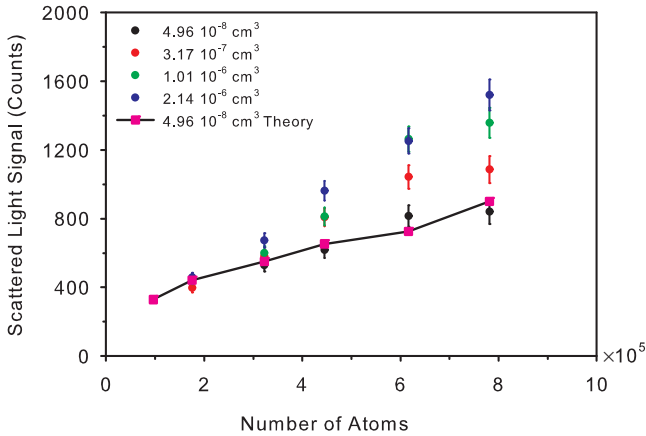


FIG. 7. Representative atom number dependence of the scattering signals as a function of the cold atom sample size. The data is labeled according to the volume of the sample, as described in the text.

to compare the data with a much simplified theory, including only some of these effects.

An effective approximation could be based on the ladder-type expansion of the light correlation function, which leads to a Bethe-Salpeter type equation. This can be numerically solved via a sequence of iterative steps (multiple scattering events); see [2]. Such an approach evidently ignores any cross interference in the process of multiple scattering, which seems a rather realistic assumption for a dilute and disordered atomic gas. The applicability of the Bethe-Salpeter approach has been successfully demonstrated for the theory of random lasing; see [38,39].

In this section, we show that taking into account only attenuation of the probe beam in the atomic sample, following the Beer-Lambert law, is enough to explain the data with rather good agreement. This shows that the main physical ingredient of the experiment is the so-called “shadow effect”: atoms at the back of the sample are less illuminated by the incident laser, which induces an effective reduction of the total scattering cross section compared to a collection of independent atoms illuminated by the same laser intensity. As explained in detail in [40], this effect also explains previous observations of a collective reduction of the radiation pressure force [6,8]. It could also explain the results of [26], although the very small sample sizes and high densities used in that work might induce some other effects.

From the Beer-Lambert law, one can easily show (see the Appendix A or Ref. [8]) that the total scattering cross section of a Gaussian cloud (containing N atoms and illuminated by a plane wave) is

$$\Sigma_{sc} = N\sigma_{sc} \times \frac{\text{Ein}(b)}{b}, \quad (1)$$

where Ein is the integer function [41]

$$\text{Ein}(b) = \int_0^b \frac{1 - e^{-x}}{x} dx = b \left[1 + \sum_{n=1}^{\infty} \frac{(-b)^n}{(n+1)(n+1)!} \right] \quad (2)$$

and σ_{sc} is the single-atom scattering cross section. Here b is the optical depth along the line of sight and the factor $\text{Ein}(b)/b$ in Eq. (1) corresponds to the deviation from single-atom physics induced by the shadow effect. In the limit of vanishing optical depth b , the value expected from single atom physics is recovered, $\Sigma_{sc} = N\sigma_{sc}$. For high optical depth, the cross section increases only logarithmically, which appears as a collective saturation of the scattered light.

Let us now use this result to rescale the experimental data. The measured scattered light is proportional to Σ_{sc} . For data taken with a fixed atom number and varying detuning (“protocol 1”), such as the data reported in Fig. 4(a) and Fig. 5, one should divide the signal by $\sigma_{sc} \propto 1/(1 + 4\Delta^2/\Gamma^2)$ and compare the results to $\text{Ein}(b)/b$. For data acquired at a fixed detuning and varying atom number (“protocol 2”), such as the data reported in Fig. 7, one should divide the signal by N and also compare to $\text{Ein}(b)/b$. In both cases one has to allow a global multiplicative factor to fit the data to the theoretical curve, since the signal is not calibrated in absolute value. In other words, the detection efficiency, which is the number of detected photons vs the number emitted in the detector direction, is not precisely known. The not-very-well-known factors include the detector solid angle, the absolute probe intensity, and the probe overlap with the sample spatial location, the transmission of the various optical elements in the detector arm of the apparatus, and the efficiency of the light detector to incoming photons. The relevant optical depth b is the one along the line of sight of the laser, given by

$$b = \frac{\sqrt{2\pi} \rho_0 \sigma_{sc} r_0}{\sqrt{\cos^2 \theta + \sin^2 \theta \sin^2 \phi + \eta^2 \sin^2 \theta \cos^2 \phi}}, \quad (3)$$

where $\eta = r_0/y_0$, r_0 , y_0 , ρ_0 vary during the expansion and the angles θ , ϕ are given by the geometry of the experiment as shown in Fig. 1 ($\theta = 23^\circ$ and $\phi = 30^\circ$).

We show the rescaled data in Fig. 8. The two panels correspond to the two different experimental protocols. The striking result is that, despite the different protocols and different orders of magnitude (almost three orders of magnitude in density and in optical depth), all data points collapse quite close to the curve $\text{Ein}(b)/b$ describing the shadow effect, demonstrating that it is indeed the main physical ingredient of the collective behavior of the scattered light intensity.

C. Impact of multiple scattering

The previous scaling based on the total scattering cross section supposes that the light is emitted isotropically from the atomic sample. This is not the case when the optical depth is large, as already studied in [4], although the anisotropy is much less pronounced when the cloud is illuminated by a wide beam (plane wave), as is the case here, compared to the case when a large cloud is illuminated by a narrow beam, as in [4].

To describe this effect one needs to take into account multiple scattering of light inside the sample. This is naturally included in the microscopic model, but it is also possible to use stochastic simulations based on a random walk algorithm for light. In such a model, cooperative and coherent effects such as super and subradiance, interference, and diffraction are neglected, but one can well describe diffuse light scattering with the true parameters of the experiments (also including

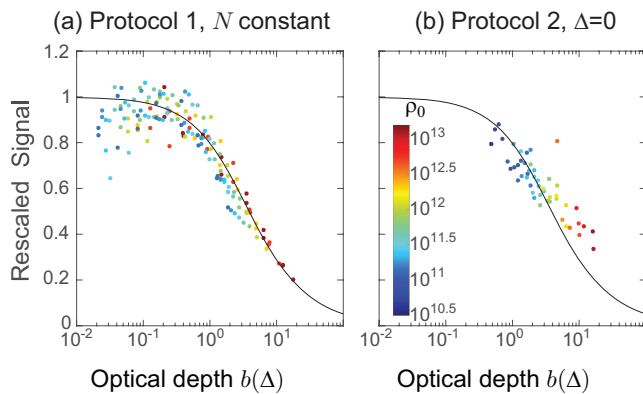


FIG. 8. Rescaled experimental data: the light scattering signal is plotted as a function of the detuning-dependent optical depth $b(\Delta)$ and the color code indicates the peak density ρ_0 in cm^{-3} (log scale). The solid line is the function $\text{Ein}(b)/b$, which describes the shadow effect from the Beer-Lambert law. The two panels correspond to the two different experimental protocols, the first one with a varying detuning and a constant atom number and the second one with the laser on resonance and a varying atom number. In both cases the sizes of the cloud also vary, and thus the volume and density. A global vertical scaling factor for each data set is the only free parameter.

subtle effects like the frequency redistribution due to Doppler broadening), if needed; see, e.g., Refs. [42–44].

We have performed such random walk simulations for varying optical depths. The simulations include the actual geometry of the laser beam (size and direction) and of the detection (direction), the anisotropy of the scattering diagram for the first scattering event, and the Gaussian density distribution of the cloud. We use the size y_0 of the cloud, which is almost constant for all data points, and the two extreme transverse sizes, corresponding to the shortest and longest time of flight. We do not take into account the Doppler-induced frequency redistribution during multiple scattering as it should be a tiny effect with the moderate temperature and optical depths explored here. The results are shown in Fig. 9.

The comparison between the random walk simulations and the simple Beer-Lambert prediction shows a small difference: the scattered light signal is always slightly larger in the random walk simulations. Several contributions explain this difference. First, the Gaussian beam profile has a stronger intensity at the center, where it interacts with the cloud, compared with a plane-wave illumination. Second, the small anisotropy of the scattering diagram of Rb (we suppose an equally populated mixture of Zeeman states) slightly favors the direction of detection. And third, at large optical depths, multiple scattering takes place and light has a higher probability to escape along the backward and transverse directions, which also favors the detection direction compared to an isotropic emission. Finally, at the precision of the numerical simulation, we do not see any significant difference between the two extreme aspect ratios of the cloud, showing that this parameter does not affect the results. In Fig. 9, the vertical scaling factor of each data set has been chosen to match the simulation results. With this as the only free parameter the simulations and the experimental points are in very good agreement.

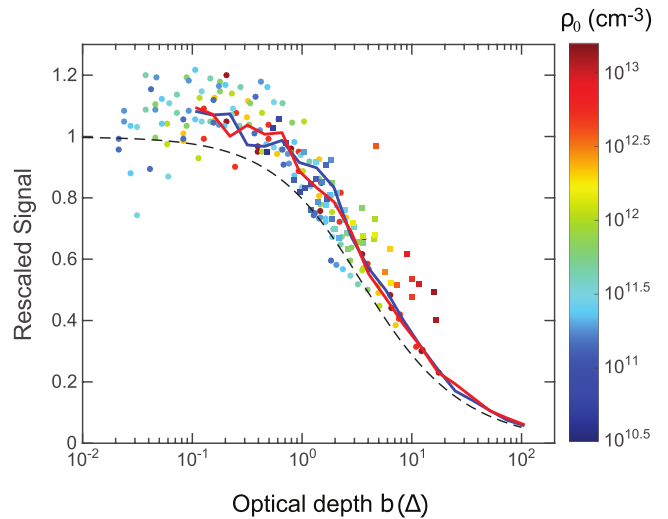


FIG. 9. Comparison between the experimental data and the random walk simulation. The data are rescaled like in Fig. 8, dots corresponds to the protocol 1, and squares to the protocol 2. The color code indicates the peak density ρ_0 in cm^{-3} (log scale). The solid lines are the results of the random walk simulations for the two extreme aspect ratios of the cloud, $\eta = r_0/y_0 \simeq 0.13$ (blue) and $\eta \simeq 0.013$ (red). The dashed line is the function $\text{Ein}(b)/b$ which describes the shadow effect from the Beer-Lambert law. The global vertical scaling factor for each data set has been adapted to match the random walk results.

IV. CONCLUSIONS

Using two different experimental protocols, we have made measurements of diffusive light scattering from a cold thermal gas of ^{87}Rb . Due to variations in the number of atoms in the sample, or the size of the sample at fixed number of atoms, the experiments extended over almost three orders of magnitude in density and in optical depth. The measured diffusive light spectra were found to be in very good agreement with fully quantum based calculations. A second and simpler analysis approach used stochastic simulations based on a random walk algorithm for the multiply scattered light. The simulations revealed that the optical depth of the atomic sample can serve as an effective single scaling parameter which describes very well all the experimental data. A final but important overall point, as mentioned earlier in the paper, is that a substantial portion of the scattered light undergoes multiple scattering. However, the multiple scattering only contributes a little to the emission diagram. With this, and the global scale factor needed to compare the data and Beer-Lambert law scaling, we can emphasize that the Beer-Lambert law works in spite of multiple scattering. This concluding point demonstrates the effectiveness of this rescaling.

ACKNOWLEDGMENTS

We appreciate financial support by the National Science Foundation (Grants No. NSF-PHY-1606743 and No. NSF-PHY-1939308), the Russian Foundation for Basic Research (Grant No. 18-02-00265), the Russian Science Foundation (Grants No. 18-72-10039 and No. 17-12-01085), and the French Agence Nationale pour la Recherche (project LOVE,

No. ANR-14-CE26-0032). The Foundation for the Advancement of Theoretical Physics and Mathematics ‘BASIS’ (Grant No. 18-1-1-48-1).

APPENDIX: PROOF OF EQ. (1) FOR THE SHADOW EFFECT

For simplicity, let us take an isotropic Gaussian cloud with density distribution $\rho = \rho_0 e^{-r^2/(2R^2)}$ and consider a plane wave (intensity I_0) propagating along z . The transmitted intensity has a transverse distribution

$$\begin{aligned} I_T(\mathbf{r}_\perp) &= I_0 \exp\left(-\rho_0 \sigma_{\text{sc}} \int e^{-r^2/(2R^2)} dz\right) \\ &= I_0 \exp(-b e^{-r_\perp^2/(2R^2)}), \end{aligned} \quad (\text{A1})$$

with $b = \sqrt{2\pi} \rho_0 \sigma_{\text{sc}} R$ and $\mathbf{r}_\perp = (x, y)$.

Moreover, what is scattered is what is not transmitted, so we have

$$\Sigma_{\text{sc}} = \frac{P_{\text{sc}}}{I_0} = \int [1 - \exp(-b e^{-r_\perp^2/(2R^2)})] d^2 \mathbf{r}_\perp. \quad (\text{A2})$$

Using $d^2 \mathbf{r}_\perp = 2\pi r_\perp dr_\perp$ and the change of variable $u = b e^{-r_\perp^2/(2R^2)}$ one obtains

$$\Sigma_{\text{sc}} = 2\pi R^2 \int_0^b \frac{1 - e^{-u}}{u} du = 2\pi R^2 \text{Ein}(b). \quad (\text{A3})$$

For single atom physics, the total cross section would be $N\sigma_{\text{sc}}$. Using $b = \sigma_{\text{sc}}/(2\pi) \times N/R^2$, it is thus physically meaningful to write

$$\Sigma_{\text{sc}} = N\sigma_{\text{sc}} \times \frac{\text{Ein}(b)}{b}, \quad (\text{A4})$$

which is Eq. (1).

-
- [1] W. Guerin, M. T. Rouabah, and R. Kaiser, *J. Mod. Opt.* **64**, 895 (2017).
- [2] D. V. Kupriyanov, I. M. Sokolov, and M. D. Havey, *Phys. Rep.* **671**, 1 (2017).
- [3] S. Roof, K. Kemp, M. D. Havey, I. M. Sokolov, and D. V. Kupriyanov, *Opt. Lett.* **40**, 1137 (2015).
- [4] G. Labeyrie, D. Delande, C. A. Müller, C. Miniatura, and R. Kaiser, *Opt. Commun.* **243**, 157 (2004).
- [5] R. Saint-Jalm, M. Aidelsburger, J. L. Ville, L. Corman, Z. Hadzibabic, D. Delande, S. Nascimbène, N. Cherroret, J. Dalibard, and J. Beugnon, *Phys. Rev. A* **97**, 061801 (2018).
- [6] T. Bienaimé, S. Bux, E. Lucioni, P. W. Courteille, N. Piovella, and R. Kaiser, *Phys. Rev. Lett.* **104**, 183602 (2010).
- [7] H. Bender, C. Stehle, S. Slama, R. Kaiser, N. Piovella, C. Zimmermann, and P. W. Courteille, *Phys. Rev. A* **82**, 011404(R) (2010).
- [8] J. Chabé, M. T. Rouabah, L. Bellando, T. Bienaimé, N. Piovella, R. Bachelard, and R. Kaiser, *Phys. Rev. A* **89**, 043833 (2014).
- [9] D. E. Chang, J. Ye, and M. D. Lukin, *Phys. Rev. A* **69**, 023810 (2004).
- [10] R. Friedberg, S. R. Hartmann, and J. T. Manassah, *Phys. Rep.* **7**, 101 (1973).
- [11] M. O. Scully, *Phys. Rev. Lett.* **102**, 143601 (2009).
- [12] M. O. Scully and A. A. Svidzinsky, *Science* **328**, 1239 (2010).
- [13] J. T. Manassah, *Adv. Opt. Photon.* **4**, 108 (2012).
- [14] J. Javanainen, J. Ruostekoski, Y. Li, and S.-M. Yoo, *Phys. Rev. Lett.* **112**, 113603 (2014).
- [15] J. Javanainen and J. Ruostekoski, *Opt. Express* **24**, 993 (2016).
- [16] R. Röhlsberger, K. Schlage, B. Sahoo, S. Couet, and R. Ruffer, *Science* **328**, 1248 (2010).
- [17] J. Keaveney, A. Sargsyan, U. Krohn, I. G. Hughes, D. Sarkisyan, and C. S. Adams, *Phys. Rev. Lett.* **108**, 173601 (2012).
- [18] S. Okaba, T. Takano, F. Benabid, T. Bradley, L. Vincetti, Z. Maizelis, V. Yampol'skii, F. Nori, and H. Katori, *Nat. Commun.* **5**, 4096 (2014).
- [19] Z. Meir, O. Schwartz, E. Shahmoon, D. Oron, and R. Ozeri, *Phys. Rev. Lett.* **113**, 193002 (2014).
- [20] S. L. Bromley, B. Zhu, M. Bishof, X. Zhang, T. Bothwell, J. Schachenmayer, T. L. Nicholson, R. Kaiser, S. F. Yelin, M. D. Lukin *et al.*, *Nat. Commun.* **7**, 11039 (2016).
- [21] S. Jennewein, M. Besbes, N. J. Schilder, S. D. Jenkins, C. Sauvan, J. Ruostekoski, J.-J. Greffet, Y. R. P. Sortais, and A. Browaeys, *Phys. Rev. Lett.* **116**, 233601 (2016).
- [22] S. J. Roof, K. J. Kemp, M. D. Havey, and I. M. Sokolov, *Phys. Rev. Lett.* **117**, 073003 (2016).
- [23] L. Corman, J. L. Ville, R. Saint-Jalm, M. Aidelsburger, T. Bienaimé, S. Nascimbène, J. Dalibard, and J. Beugnon, *Phys. Rev. A* **96**, 053629 (2017).
- [24] S. Balik, A. L. Win, M. D. Havey, I. M. Sokolov, and D. V. Kupriyanov, *Phys. Rev. A* **87**, 053817 (2013).
- [25] S. Balik, A. L. Win, M. D. Havey, A. S. Sheremet, I. M. Sokolov, and D. V. Kupriyanov, *J. Mod. Opt.* **61**, 77 (2014).
- [26] J. Pellegrino, R. Bourgain, S. Jennewein, Y. R. P. Sortais, A. Browaeys, S. D. Jenkins, and J. Ruostekoski, *Phys. Rev. Lett.* **113**, 133602 (2014).
- [27] R. G. Olave, A. L. Win, K. Kemp, S. J. Roof, S. Balik, M. D. Havey, I. M. Sokolov, and D. V. Kupriyanov, Optical manipulation of light scattering in cold atomic rubidium, in *From Atomic to Mesoscale: The Role of Quantum Coherence in Systems of Various Complexities* (World Scientific, Singapore, 2015), pp. 39–59.
- [28] Y.-C. Chen, Y.-A. Liao, L. Hsu, and I. A. Yu, *Phys. Rev. A* **64**, 031401(R) (2001).
- [29] S. Balik, R. Olave, C. I. Sukenik, M. D. Havey, V. M. Datsyuk, I. M. Sokolov, and D. V. Kupriyanov, *Phys. Rev. A* **72**, 051402(R) (2005).
- [30] I. M. Sokolov, M. D. Kupriyanova, D. V. Kupriyanov, and M. D. Havey, *Phys. Rev. A* **79**, 053405 (2009).
- [31] I. Sokolov, D. Kupriyanov, and M. Havey, *JETP* **112**, 246 (2011).
- [32] J. Ruostekoski and J. Javanainen, *Phys. Rev. A* **55**, 513 (1997).
- [33] A. A. Svidzinsky, J.-T. Chang, and M. O. Scully, *Phys. Rev. A* **81**, 053821 (2010).

- [34] A. S. Kuraptsev, I. M. Sokolov, and M. D. Havey, *Phys. Rev. A* **96**, 023830 (2017).
- [35] D. V. Kuznetsov, V. K. Roerich, and M. G. Gladush, *JETP* **113**, 647 (2011).
- [36] T. Bienaimé, R. Bachelard, P. W. Courteille, N. Piovella, and R. Kaiser, *Fortschr. Phys.* **61**, 377 (2013).
- [37] I. M. Sokolov, A. S. Kuraptsev, D. V. Kupriyanov, M. D. Havey, and S. Balik, *J. Mod. Opt.* **60**, 50 (2013).
- [38] L. V. Gerasimov, V. M. Ezhova, D. V. Kupriyanov, Q. Baudouin, W. Guerin, and R. Kaiser, *Phys. Rev. A* **90**, 013814 (2014).
- [39] L. Gerasimov, D. Kupriyanov, and M. Havey, *Opt. Spectrosc.* **119**, 403 (2015).
- [40] R. Bachelard, N. Piovella, W. Guerin, and R. Kaiser, *Phys. Rev. A* **94**, 033836 (2016).
- [41] E. W. Weisstein, Ein function, From MathWorld—A Wolfram Web Resource, <http://mathworld.wolfram.com/EinFunction.html>.
- [42] G. Labeyrie, E. Vaujour, C. A. Müller, D. Delande, C. Miniatura, D. Wilkowski, and R. Kaiser, *Phys. Rev. Lett.* **91**, 223904 (2003).
- [43] A. Eloy, Z. Yao, R. Bachelard, W. Guerin, M. Fouché, and R. Kaiser, *Phys. Rev. A* **97**, 013810 (2018).
- [44] P. Weiss, M. O. Araújo, R. Kaiser, and W. Guerin, *New J. Phys.* **20**, 063024 (2018).

Following this paper, a more systematic comparison between the complete CD model and the two levels of approximation that are the RW model and the shadow effect, has then been published by Igor Sokolov and myself [Sokolov 2019]. The message is that for moderate optical thickness (at least up to $b \sim 15$), i.e. even in the multiple scattering regime, although the shadow effect does not allow computing the proper emission diagram and thus the absolute quantity of scattered light in a given direction, the dependence with b still follows relatively well the scaling predicted by the shadow effect. It is thus a good starting hypothesis in a fairly large range of parameters in order to interpret light-scattering data.

Conclusion

We have seen that there are many different collective modifications of steady-state light scattering by cold and dilute ensembles of atoms: change of the emission diagram, of the scattering rate, of the spectrum, with different ways to probe them². They all can be described by the coupled-dipole model and thus attributed to collective modes induced by the dipole-dipole interaction. However, it is also possible to explain them by using simple ‘photon’/optical pictures, like attenuation, diffraction, or multiple scattering.

In the next chapter I will address collective effects that appear in the temporal dynamics at the switch-off (and at the switch-on) of the driving field.

² A recent paper reports a collective decrease of the hyperfine pumping, attributed to density-dependent dipole-dipole interaction [Machluf 2019], although the simulations show that it does not only depend on the density but also on the volume (Fig. 4b), concluding that the optical thickness also has an effect. It would be interesting to test if the shadow effect can explain these observations.

CHAPTER VI

Super- and subradiance in the linear-optics regime

Last but not least, this chapter is probably the most important one of this manuscript. It deals with our studies on the temporal dynamics of the scattered light, mainly at the switch-off of the driving field, but also at the switch-on (section VI.6). It contains the main results of Part Two and includes six articles, five of them with experimental results. The highlight is the first one, on the direct observation of subradiant decay [Guerin 2016a], which was a milestone for our team. This observation triggered several complementary studies, which are presented in the following of the chapter.

VI.1. Observation of subradiance

Just prior to my come-back in Nice, the team had published a proposal for the observation of subradiance in a dilute cold-atom cloud [Bienaimé 2012]. This was thus my first objective when I took in charge the experiment.

VI.1.1. Experimental requirements

The principle of the experiment is quite simple: we drive the atomic sample with a probe beam of detuning Δ for a few microseconds (enough to reach the steady state), switch it off abruptly, and monitor the decay of the scattered light. We use a beam much wider than the cloud such that it can be approximated by a plane wave. Moreover we want to use a large detuning to avoid radiation trapping [Labeyrie 2003] such that a slow decay can be unambiguously attributed to subradiance (I come back to this question in section VI.5).

There are, however, two technical difficulties to do so, a small one and a more challenging one.

The small technical difficulty is to get a fast extinction with a very good extinction ratio for the probe beam. How fast should it be? The timescale of the problem is given by the lifetime of the excited level $\tau_{\text{at}} = \Gamma_0^{-1} \simeq 26$ ns, so the switch-off duration should be very short compared to that if one wants to reach the limit of an infinitely fast switch-off. However it is not known how important this criterium is, and for subradiance we are interested in the slow decay visible at late time, so it should not be too critical. For simplicity we only used acousto-optical modulators (AOMs). After a very careful optimization I managed to get a switch-off duration of ~ 15 ns (defined as the fall time between the 90% and the 10% levels). To tell the truth, the ‘careful optimization’ is actually the empirical trying of many different optical combinations for focussing the beam in the AOM until one works well enough. Since the switch-off duration in AOMs is given by the sound velocity and the size of the beam,

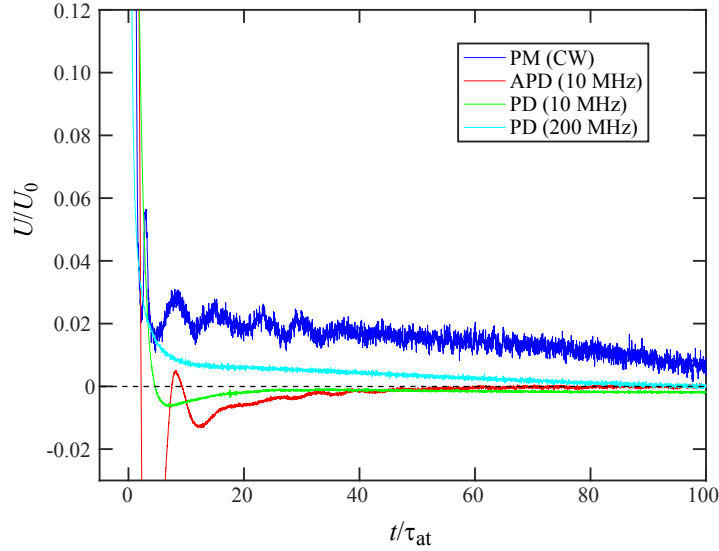


Figure VI.1: Test of several detectors: one photomultiplier (PM) working in the continuous regime (CW), one commercial avalanche photodiode (APD) with a bandwidth of 10 MHz, one home-made photodiode (PD) with a bandwidth of 10 MHz, and one commercial PD with a bandwidth of 200 MHz. Below $\sim 1\%$ of the steady-state voltage U_0 at the switch off, all detectors have a slow spurious response. Here there is no atom involved.

at first sight, one just has to focus stronger to switch off faster. However at some point the Rayleigh length becomes smaller than the crystal length and the size of the beam on the edges of the crystal matters. Moreover it becomes harder and harder to separate the diffraction orders because of the beam divergence, and we want to avoid any spurious light. A strong focussing also spoils the diffraction efficiency because of the associated angular distribution. As a consequence there is a delicate trade-off between the diffraction efficiency, the extinction ratio and the extinction duration. For the extinction ratio, there is always a bit of scattered light on the crystal surface that can enter the following optical path, even through a single-mode fiber, so we used a second AOM in series (actually set before the optimized AOM). The details of the whole setup are given in [Araújo 2018a]. The extinction ratio is better than 10^4 .

The challenging difficulty is to be able to *measure* a fast and good extinction. At first sight, one could think that any fast detector could do the job. Alas, this is not so simple. Even with a high-bandwidth, low-noise detector, the measured switch-off is fast until it reaches the level of typically $\sim 1 - 2\%$ of the initial steady-state level, and then there are some slow relaxation and/or spurious oscillations, which can last for a very long time¹ (see Fig. VI.1).

I initially thought that a solution to this problem would be to work in the photocounting regime because such slow electronic response would not exist. First, this is more demanding to work in the photocounting regime, because the detectors saturate at a much lower light level, and we have to attenuate the signal by a neutral density filter, which is a pity. The corresponding loss has to be compensated by a longer integration time. Moreover, to reconstruct the temporal trace one needs an extra device to detect the single-photon pulses and make a histogram of the arrival times. For that we use a ‘Multichannel scaler’ from the company FAST ComTech. Furthermore, and more importantly, this doesn’t even solve the problem of the slow spurious response, because of a phenomena called ‘afterpulsing’:

¹ In this chapter most temporal data are shown as a function of the normalized time t/τ_{at} and it may be useful to bear in mind that $40\tau_{\text{at}} \approx 1 \mu\text{s}$.

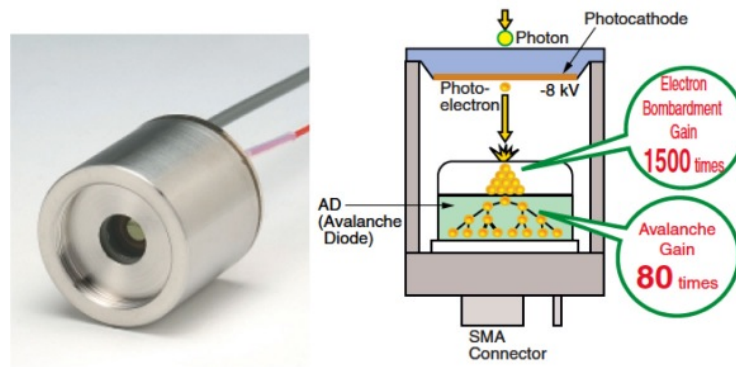


Figure VI.2: Picture and scheme of the hybrid photomultiplier. From Hamamatsu.

a detected photon has a small probability, on the order on 1%, to create a second, fake detection some time later. Although the physical mechanism is different for photomultipliers (PMs) and for avalanche photodiodes (APDs), it exists in both. Then the photons detected just before the switch-off create a fake response after the switch off, at the percent level and for as long as a few microseconds with the PM I tested.

The solution to this problem was the finding of a new detector, from the company Hamamatsu. Their so-called ‘hybrid photomultiplier’ (HPM) uses a hybrid technology with a first stage made of a photocathode and a high-voltage electron acceleration, like in a PM, and a second stage made of a semiconductor in which an avalanche process takes place, like in an APD (Fig. VI.2). Somehow, this detector doesn’t have any measurable afterpulsing, and is the only one with this remarkable property, to my knowledge, along with superconducting nanowire single-photon detectors, which are in a completely different category in term of price, size and complexity. Compared to APDs, it also has the advantage of having a large sensitive area, which is useful for collecting light from a MOT. Thanks to this detector we can measure a clean extinction down to at least 10^{-5} , the measurement being limited by the patience of the experimentalist...

Once those technical problems were solved, the observation of subradiance was ‘easy’, it just requires some patience because the necessary integration is quite long, on the order of 500 000 experimental cycles, corresponding to one full night of integration. So, acquiring a complete set of reliable data taken in the same conditions requires several weeks.

VI.1.2. First observation of subradiance

Although the prediction of subradiance in the dilute regime, based on the coupled-dipole (CD) model, was already made [Bienaimé 2012], there were still some unknowns. For instance, what about the temperature? Naively one could expect that the atomic motion, not negligible at the scale of the presumably long subradiant lifetime, could be detrimental, or at least should limit the measurable lifetime. Another open question was the role of the atomic Zeeman structure, which is known to be a source of decoherence for coherent backscattering [Labeyrie 1999, Jonckheere 2000, Bidet 2002]. No prediction was available for subradiance. Finally, the simulations done with the CD model can’t simulate the true parameters of the experiment (especially the atom number) and thus some scaling and extrapolation have to be made, the limit of which are not under control.

It was thus a good surprise that none of these effects were a problem. The paper [Guerin 2016a] was submitted in summer 2015 and is reproduced below.



Subradiance in a Large Cloud of Cold Atoms

William Guerin,^{1,*} Michelle O. Araújo,^{1,2} and Robin Kaiser¹

¹*Institut Non Linéaire de Nice, CNRS and Université Nice Sophia Antipolis, 1361 route des Lucioles, 06560 Valbonne, France*

²*CAPES Foundation, Ministry of Education of Brazil, Brasília DF 70040-020, Brazil*

(Received 8 September 2015; published 22 February 2016)

Since Dicke’s seminal paper on coherence in spontaneous radiation by atomic ensembles, superradiance has been extensively studied. Subradiance, on the contrary, has remained elusive, mainly because subradiant states are weakly coupled to the environment and are very sensitive to nonradiative decoherence processes. Here, we report the experimental observation of subradiance in an extended and dilute cold-atom sample containing a large number of particles. We use a far detuned laser to avoid multiple scattering and observe the temporal decay after a sudden switch-off of the laser beam. After the fast decay of most of the fluorescence, we detect a very slow decay, with time constants as long as 100 times the natural lifetime of the excited state of individual atoms. This subradiant time constant scales linearly with the cooperativity parameter, corresponding to the on-resonance optical depth of the sample, and is independent of the laser detuning, as expected from a coupled-dipole model.

DOI: 10.1103/PhysRevLett.116.083601

Despite its many applications, ranging from astrophysics [1] to mesoscopic physics [2,3] and quantum information technology [4], light interacting with a large ensemble of N scatterers still bears many surprising features and is at the focus of intense research. For $N = 2$ atoms placed close together, the in-phase oscillation of the induced dipoles produces a large, superradiant dipole, whereas the out-of-phase oscillation corresponds to a subradiant quadrupole. Generalizing for $N \gg 2$, Dicke has shown that, for samples of a small size compared to the wavelength of the atomic transition, the symmetric superposition of atomic states induces superradiant emission, scaling with the number of particles N , whereas the antisymmetric superpositions are decoupled from the environment, with vanishing emission rates, which corresponds to subradiance [5].

Dicke superradiance has been extensively studied in the 1970s [6–8] but the observation of its counterpart, subradiance, has been restricted to indirect evidence of modified decay rates in one particular direction [9] or in systems of two particles at very short distance [10–12]. One challenge for the observation of subradiance by a large number of particles is the fragile nature of these states, which require protection from any local nonradiative decay mechanism [13]. Furthermore, contrary to the two-atom case, for which the distance between atoms has to be small compared to the wavelength, for $N \gg 2$, the retarded, long-range resonant dipole-dipole interaction [14] gives rise to super- and subradiant effects (“cooperative scattering”) also in *dilute* samples, with interatomic distances much larger than the wavelength, and corresponding large system sizes. Since, for $N > 2$, the Hamiltonians for short and long-range interactions do not commute, the collective eigenstates due to the long-range interactions are suppressed by short-range interactions [8]. These short-range or near-field effects (or “van der Waals dephasing”) thus need to be

avoided in this case. As a consequence—and maybe counterintuitively—a large and dilute sample of interacting dipoles is the most appropriate system for the observation of N -body subradiance.

In this regime, and in the weak excitation limit (“single-photon superradiance”) [15–17], it has been shown that the superradiant enhancement of the emission rate scales as the cooperativity parameter N/M , where M is the number of available modes for the electromagnetic radiation [18–21]. For a spherical sample of radius R , $M \sim (k_0 R)^2$, where $k_0 = 2\pi/\lambda$, this cooperativity parameter is proportional to the peak on-resonant optical depth of the atomic cloud, given by $b_0 = 3N/(k_0 R)^2$ for a cold-atom cloud with a Gaussian density distribution of rms radius R . This number can be large even at low density. In a recent work [22], we used a coupled-dipole model to generalize this result to subradiance (see also the Supplemental Material [23]). In this Letter, we report the experimental observation of subradiance in this weak-excitation, dilute- and extended-sample limit.

In our experiment, we load $N \approx 10^9$ ^{87}Rb atoms from a background vapor into a magneto-optical trap (MOT) for 50 ms. A compressed MOT (30 ms) period allows for an increased and smooth spatial density with a Gaussian distribution of rms size $R \approx 1$ mm (typical density $\rho \approx 10^{11} \text{ cm}^{-3}$) and a reduced temperature $T \approx 50 \mu\text{K}$. We then switch off the MOT trapping beams and magnetic field gradient and allow for 3 ms of free expansion, used to optically pump all atoms into the upper hyperfine ground state $F = 2$. Next, we apply a series of 12 pulses of a weak probe beam (waist $w = 5.7$ mm), linearly polarized and detuned by $\delta = (\omega - \omega_0)/\Gamma$ from the closed atomic transition $F = 2 \rightarrow F' = 3$. Here, ω is the frequency of the laser, ω_0 the frequency of the atomic transition (of wavelength $\lambda = 2\pi c/\omega_0 = 780.24$ nm), and $\Gamma/2\pi = 6.07$ MHz

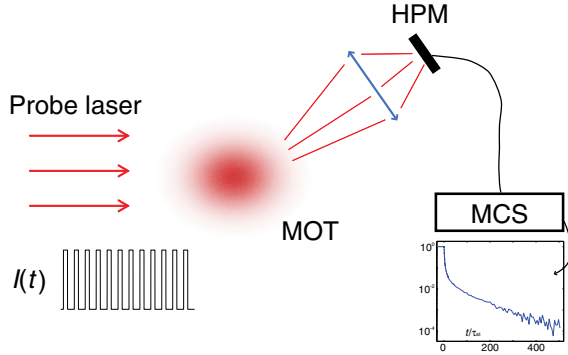


FIG. 1. Principle of the experiment. A large probe laser illuminates the atomic sample for $30 \mu\text{s}$ and is switched off rapidly. The fluorescence at $\sim 35^\circ$ is collected by a hybrid photomultiplier (HPM) and recorded on a multichannel scaler (MCS). The experiment is repeated 500 000 times. At each cycle, 12 pulses are recorded during the free expansion of the cloud, allowing the on-resonance optical depth to vary.

its linewidth. Note that when we varied the detuning, we also varied the laser intensity accordingly in order to keep the saturation parameter constant at $s \approx 4.5 \times 10^{-2}$. The pulses of duration $30 \mu\text{s}$ and separated by 1 ms are obtained by using two acousto-optical modulators in series to reach an extinction ratio better than 10^{-4} . The 90%–10% fall time at the switch-off is $\sim 15 \text{ ns}$, limiting the possibility of studying superradiance, but convenient for detecting subradiance. Between subsequent pulses of each series, the size of the cloud increases because of thermal expansion, and the atom number decreases due to off-resonant optical pumping into the $F = 1$ hyperfine state during each pulse. The corresponding change of the on-resonance optical depth b_0 allows us to conveniently measure the decay of the fluorescence as a function of b_0 and investigate whether b_0 is the relevant scaling parameter [23]. After this stage of

expansion and measurement, the MOT is switched on again and most of the atoms are recaptured. The complete cycle is thus short enough to allow the signal integration over a large number of cycles, typically $\sim 500\,000$ (complete acquisition time $\sim 14 \text{ h}$ per run). The scattering of the probe beam is collected by a lens with a solid angle of $\sim 5 \times 10^{-2} \text{ sr}$ at $\theta \approx 35^\circ$ from the incident direction of the laser beam (see Fig. 1). We use a hybrid photomultiplier (Hamamatsu HPM R10467U-50) in the photon-counting regime, without any measurable amount of afterpulsing, which would considerably mask signatures of subradiance. The signal is then recorded on a multichannel scaler (MCS6A by FAST ComTec) with a time bin of 1.6 ns , averaging over the cycles. The cooperativity parameter b_0 corresponding to each pulse is calibrated by an independent measurement of the atom number, cloud size, and temperature using absorption imaging [23].

Typical data are shown in Fig. 2. The signal is normalized to the steady-state fluorescence level and we focus on the switch-off period to highlight the slow fluorescence decay. In Fig. 2(a), the detuning δ of the probe beam is kept constant and the different decay curves correspond to different values of b_0 , obtained in a single run. On the contrary, Fig. 2(b) shows data taken with different detunings but for the same b_0 . In both cases, most of the fluorescence decays fast (note the logarithmic scale of the vertical axis), but a slow decay is clearly seen well above the noise floor (slightly below 10^{-4}). We stress that fluorescence can be detected at very large delays, as can be seen from the time axis, in units of $\tau_{\text{at}} = \Gamma^{-1} = 26 \text{ ns}$. We attribute this slow decay to subradiance in the single-photon (or weak excitation) regime, as predicted in Ref. [22].

A qualitative analysis of the two figures clearly shows different behaviors. As b_0 is varied, the slow decay rate changes, whereas its relative amplitude stays

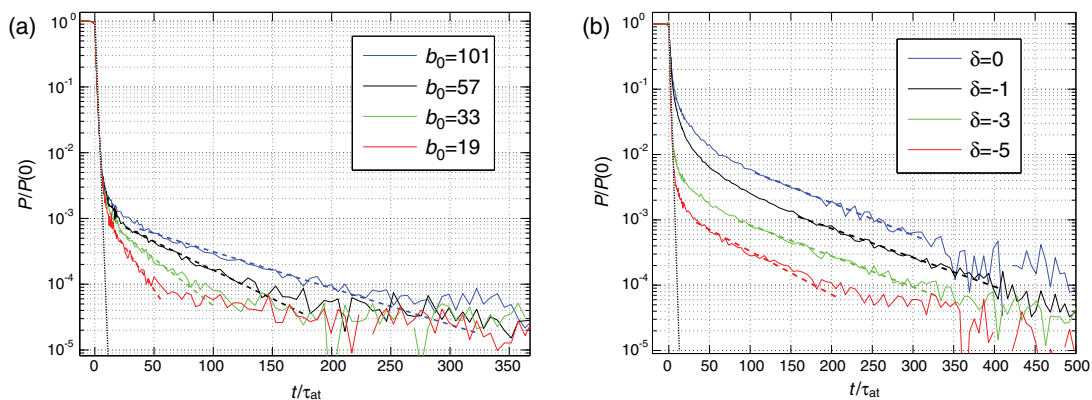


FIG. 2. Slow decay of the fluorescence after switching off the probe laser. The vertical scale is normalized by the steady-state detected power $P(0)$, and the time scale is normalized by the atomic lifetime of the excited state τ_{at} . Without any collective effect (single-atom physics), the decay would be given by $P(t) = P(0) \exp(-t/\tau_{\text{at}})$ (the black dotted line). (a) Several data are shown for different on-resonance optical depths b_0 and the same detuning $\delta = -6$ (in units of Γ). The time constant increases with b_0 . (b) Several data are shown for different detunings and the same $b_0 = 108 \pm 5$. The time constant remains unchanged, but the relative amplitude of the subradiant decay decreases as the detuning increases.

approximately the same. The exact opposite happens when we change the detuning, keeping b_0 fixed. For a quantitative analysis, we fit the slow tail at long delays by an exponential decay with two free parameters: the time constant τ_{sub} and its relative amplitude A_{sub} [23]. We systematically studied how these parameters depend on b_0 and δ . The result of this analysis is presented in Fig. 3. In Fig. 3(a) we plot the subradiant time constant as a function of b_0 for different detunings. The collapse of all points on the same curve clearly indicates that the slow decay rate does not depend on the detuning [see also Fig. 3(b)]. This demonstrates that this slow decay is not a multiple-scattering effect, such as previously observed radiation trapping [36], which depends on the optical depth at the laser frequency $b(\delta) \propto b_0/(1+4\delta^2)$, with a strong dependence with δ . The second feature in Fig. 3(a) is the linear increase of τ_{sub} with b_0 , up to time constants as long as $\tau_{\text{sub}} \sim 100\tau_{\text{at}}$. This is perfectly consistent with the predictions of the coupled-dipole model for subradiance [23]. We note that for large negative detunings, one has to take into account the variation of b_0 during the pulse series induced by the cloud expansion together with a significant contribution of atom losses by off-resonant hyperfine pumping. This allowed us to test different combinations of N and R as scaling parameters (see Fig. 2 of the Supplemental Material [23]). The comparison showed that the best collapse has been obtained with $N/R^2 \propto b_0$ as the scaling parameter, which demonstrates that b_0 is indeed the relevant cooperativity parameter in the regime of a

dilute and extended sample, as expected from the ratio of the number of atoms to the number of available electromagnetic modes radiating from the sample. Finally, we show in Fig. 3(c) the relative amplitude A_{sub} of the slow decay. As was already seen in Fig. 2(b), this amplitude is much larger near resonance, and it seems to reach a plateau for large detunings. We have checked that subradiant decay is still visible at a larger detuning, up to $\delta = -11$ [23]. This is in line with the coupled-dipole model, in which the weight of the long-lived modes are enhanced near resonance and the weight of all of the collective modes becomes independent of the detuning at large detuning.

As a long lifetime can also occur due to multiple scattering, when the optical depth $b(\delta) \gg 1$ [36], we investigated the decay time close to the atomic resonance to study how subradiance compares with radiation trapping. In the range of the accessible experimental values [Fig. 3(b)], no marked difference of the decay times around resonance is visible, even though a small difference was predicted in Ref. [22]. The interplay of radiation trapping and subradiance near resonance is still an open question and will be the subject of our further experiments.

We have also studied the effect of the probe intensity and checked that, at low saturation parameter, the observed subradiance is independent of the intensity (see Fig. 3 of the Supplemental Material [23]), which validates the use of the coupled-dipole model in the weak-excitation limit. We finally also excluded the possibility that residual

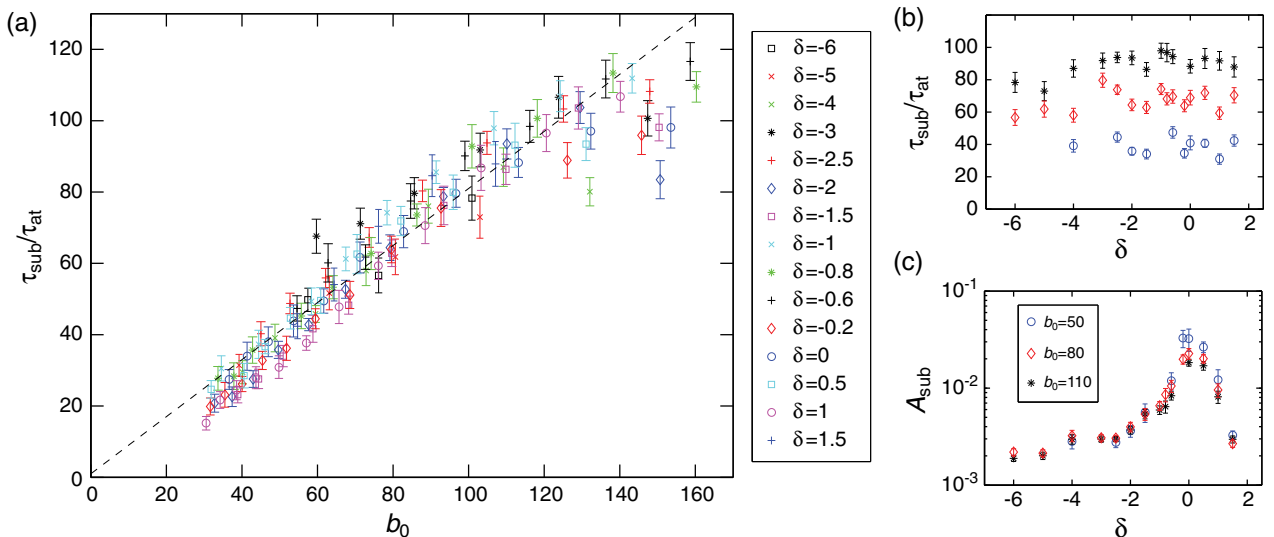


FIG. 3. Dependence of the subradiance time with the on-resonance optical depth b_0 and the laser detuning δ . (a) Subradiant time constant τ_{sub} (in units of τ_{at}) as a function of $b_0 = 3N/(k_0R)^2$ for different detunings of the probe laser. Almost all of the points collapse on a single curve, showing the linear scaling with b_0 . The dashed line is a linear fit $\tau_{\text{sub}}/\tau_{\text{at}} = 1 + \alpha b_0$, with the slope α as a free parameter. Excluding the data with $b_0 > 120$, we obtain $\alpha = 0.8$. (b) From the same data, τ_{sub} is plotted as a function of the detuning for three different values of b_0 , illustrating that τ_{sub} is independent of the detuning. (c) Similarly, the subradiant relative amplitude A_{sub} is plotted as a function of the detuning for the same three different values of b_0 . Subradiance is more important near resonance and decreases towards a plateau at large detuning.

near-resonant light might always be present and induce a slow decay due to radiation trapping, thus mimicking off-resonant subradiance [23].

To summarize, we have presented the first direct signatures of subradiance in a large system of resonant scatterers. We have shown that in the regime of dilute and extended samples, the subradiant decay rate is governed by a cooperativity parameter defined as the ratio of the number of scatterers and the sample size squared, which conveniently corresponds to the on-resonance optical depth. This observation of subradiance opens interesting questions, including the robustness of subradiance against decoherence mechanisms or the possibility of controlling the population of the subradiant modes by an appropriate temporal or spatial shaping of the driving laser or of the atomic levels. If the subradiant states can be manipulated with sufficient control [37], their isolation from the environment might be exploited as a resource for quantum information or quantum metrology [38]. As subradiance goes hand in hand with superradiance, simultaneous recording of fast and slow decays would be a beautiful illustration of the cooperative scattering envisioned by Dicke. By using a stronger laser drive, it would also be possible to access a larger subspace of the full Hilbert space, addressing the possibility of a photon-blockade effect [39].

In addition to quantum optics, our observation is also relevant to mesoscopic physics [40,41], a community less familiar with Dicke physics. One major challenge in this field is the observation of strong localization of light, the analogy for classical waves of Anderson localization of electrons [42]. Previous experimental observations of a decay of scattered light slower than predicted by the diffusion equation have been used as a signature of Anderson localization in dielectrics [43,44]. Our results show that it cannot always be the case with cold atoms. Similarly, recent numerical simulations considering point-dipole resonant scatterers study the collective modes of the effective Hamiltonian of the system and, in particular, their lifetimes [45–49]. Our work shows that Dicke subradiance can also be at the origin of very long lifetimes and that a careful analysis is required to distinguish subradiant from localized modes [49]. Finally, the combination of subradiance with disorder acting on the atomic transitions might provide an alternative route to strong localization of light, as was recently suggested [50].

We acknowledge fruitful discussions with Nicola Piovella, Tom Bienaimé, Romain Bachelard, Guillaume Labeyrie, and Dominique Delande and the technical help from Louis Bellando, Ivor Kresic, Loïc Lavenue, and Antoine Dussaux, and we thank Alain Aspect for his constructive comments on the manuscript. We also acknowledge financial support from the French Agence National pour la Recherche (project LOVE, Grant No. ANR-14-CE26-0032), the Brazilian Coordenação de Aperfeiçoamento de Pessoal de Nível Superior (CAPES), the Brazilian

Conselho Nacional de Desenvolvimento Científico e Tecnológico (project PVE, Grant No. 303426/2014-4), and the European Research Executive Agency (program COSCALI, Grant No. PIRSES-GA-2010-268717).

*william.guerin@inln.cnrs.fr

- [1] Q. Baudouin, W. Guerin, and R. Kaiser, in *Annual Review of Cold Atoms and Molecules*, Vol. 2, edited by K. Madison, K. Bongs, L. D. Carr, A. M. Rey, and H. Zhai (World Scientific, Singapore, 2014), p. 251.
- [2] G. Labeyrie, *Mod. Phys. Lett. B* **22**, 73 (2008).
- [3] R. Kaiser, *J. Mod. Opt.* **56**, 2082 (2009).
- [4] N. Sangouard, C. Simon, H. de Riedmatten, and N. Gisin, *Rev. Mod. Phys.* **83**, 33 (2011).
- [5] R. H. Dicke, *Phys. Rev.* **93**, 99 (1954).
- [6] N. Skribanowitz, I. P. Herman, J. C. MacGillivray, and M. S. Feld, *Phys. Rev. Lett.* **30**, 309 (1973).
- [7] R. Friedberg, S. R. Hartmann, and J. T. Manassah, *Phys. Rep.* **7**, 101 (1973).
- [8] M. Gross and S. Haroche, *Phys. Rep.* **93**, 301 (1982).
- [9] D. Pavolini, A. Crubellier, P. Pillet, L. Cabaret, and S. Liberman, *Phys. Rev. Lett.* **54**, 1917 (1985).
- [10] R. G. DeVoe and R. G. Brewer, *Phys. Rev. Lett.* **76**, 2049 (1996).
- [11] M. D. Barnes, P. S. Krstic, P. Kumar, A. Mehta, and J. C. Wells, *Phys. Rev. B* **71**, 241303(R) (2005).
- [12] D. H. McGuyer, M. McDonald, G. Z. Iwata, M. G. Tarallo, W. Skomorowski, R. Moszynski, and T. Zelevinsky, *Nat. Phys.* **11**, 32 (2015).
- [13] V. V. Temnov and U. Woggon, *Phys. Rev. Lett.* **95**, 243602 (2005).
- [14] M. J. Stephen, *J. Chem. Phys.* **40**, 669 (1964).
- [15] M. O. Scully, E. S. Fry, C. H. Raymond Ooi, and K. Wódkiewicz, *Phys. Rev. Lett.* **96**, 010501 (2006).
- [16] M. O. Scully and A. A. Svidzinsky, *Science* **325**, 1510 (2009).
- [17] R. Röhlsberger, K. Schlage, B. Sahoo, S. Couet, and R. Ruffer, *Science* **328**, 1248 (2010).
- [18] A. A. Svidzinsky, J.-T. Chang, and M. O. Scully, *Phys. Rev. Lett.* **100**, 160504 (2008).
- [19] A. Svidzinsky and J.-T. Chang, *Phys. Rev. A* **77**, 043833 (2008).
- [20] R. A. de Oliveira, M. S. Mendes, W. S. Martins, P. L. Saldanha, J. W. R. Tabosa, and D. Felinto, *Phys. Rev. A* **90**, 023848 (2014).
- [21] P. Longo, C. H. Keitel, and J. Evers, [arXiv:1503.04532](https://arxiv.org/abs/1503.04532).
- [22] T. Bienaimé, N. Piovella, and R. Kaiser, *Phys. Rev. Lett.* **108**, 123602 (2012).
- [23] See Supplemental Material at <http://link.aps.org/supplemental/10.1103/PhysRevLett.116.083601>, which includes Refs. [24–35], for the details of the calibration of the optical depth and data analysis, a brief presentation, and the main predictions of the coupled-dipole model, the test of different scaling parameters, the data taken for different probe intensities, and the analysis of the possible role of radiation trapping of near-resonant light.
- [24] P. W. Courteille, S. Bux, E. Lucioni, K. Lauber, T. Bienaimé, R. Kaiser, and N. Piovella, *Eur. Phys. J. D* **58**, 69 (2010).

- [25] A. A. Svidzinsky, J.-T. Chang, and M. O. Scully, *Phys. Rev. A* **81**, 053821 (2010).
- [26] T. Bienaimé, M. Petruzzo, D. Bigerni, N. Piovella, and R. Kaiser, *J. Mod. Opt.* **58**, 1942 (2011).
- [27] T. Bienaimé, R. Bachelard, P. W. Courteille, N. Piovella, and R. Kaiser, *Fortschr. Phys.* **61**, 377 (2013).
- [28] Y. Miroshnychenko, U. V. Poulsen, and K. Mølmer, *Phys. Rev. A* **87**, 023821 (2013).
- [29] W. Feng, Y. Li, and S.-Y. Zhu, *Phys. Rev. A* **89**, 013816 (2014).
- [30] G. Labeyrie, R. Kaiser, and D. Delande, *Appl. Phys. B* **81**, 1001 (2005).
- [31] C. Cohen-Tannoudji, J. Dupont-Roc, and G. Grynberg, *Atom-Photon Interactions: Basic Processes and Applications* (Wiley, New York, 1992).
- [32] B. R. Mollow, *Phys. Rev.* **188**, 1969 (1969).
- [33] See, e.g., T. Chanelière, Ph.D. thesis, Université Nice Sophia Antipolis, 2004, p. 40, <https://tel.archives-ouvertes.fr/tel-00007793>.
- [34] S. Kraft, A. Deninger, C. Trüch, J. Fortágh, F. Lison, and C. Zimmermann, *Laser Phys. Lett.* **2**, 71 (2005).
- [35] R. Pierrat, B. Grémaud, and D. Delande, *Phys. Rev. A* **80**, 013831 (2009).
- [36] G. Labeyrie, E. Vaujour, C. A. Müller, D. Delande, C. Miniatura, D. Wilkowski, and R. Kaiser, *Phys. Rev. Lett.* **91**, 223904 (2003).
- [37] M. O. Scully, *Phys. Rev. Lett.* **115**, 243602 (2015).
- [38] L. Ostermann, H. Ritsch, and C. Genes, *Phys. Rev. Lett.* **111**, 123601 (2013).
- [39] J. Pellegrino, R. Bourgain, S. Jennewein, Y. R. P. Sortais, A. Browaeys, S. D. Jenkins, and J. Ruostekoski, *Phys. Rev. Lett.* **113**, 133602 (2014).
- [40] M. C. W. van Rossum and T. M. Nieuwenhuizen, *Rev. Mod. Phys.* **71**, 313 (1999).
- [41] E. Akkermans and G. Montambaux, *Mesoscopic Physics of Electrons and Photons* (Cambridge University Press, Cambridge, England, 2007).
- [42] P. W. Anderson, *Phys. Rev.* **109**, 1492 (1958).
- [43] C. M. Aegerter, M. Störzer, and G. Maret, *Europhys. Lett.* **75**, 562 (2006).
- [44] F. Scheffold and D. Wiersma, *Nat. Photonics* **7**, 934 (2013).
- [45] E. Akkermans, A. Gero, and R. Kaiser, *Phys. Rev. Lett.* **101**, 103602 (2008).
- [46] S. E. Skipetrov and I. M. Sokolov, *Phys. Rev. Lett.* **112**, 023905 (2014).
- [47] L. Bellando, A. Gero, E. Akkermans, and R. Kaiser, *Phys. Rev. A* **90**, 063822 (2014).
- [48] S. E. Skipetrov and I. M. Sokolov, *Phys. Rev. Lett.* **114**, 053902 (2015).
- [49] C. E. Máximo, N. Piovella, P. W. Courteille, R. Kaiser, and R. Bachelard, *Phys. Rev. A* **92**, 062702 (2015).
- [50] A. Biella, F. Borgonovi, R. Kaiser, and G. L. Celardo, *Europhys. Lett.* **103**, 57009 (2013).

Subradiance in a large cloud of cold atoms: Supplemental Material

William Guerin,^{1,*} Michelle O. Araújo,^{1,2} and Robin Kaiser¹

¹*Institut Non Linéaire de Nice, CNRS and Université Nice Sophia-Antipolis,
1361 route des Lucioles, 06560 Valbonne, France*

²*CAPES Foundation, Ministry of Education of Brazil, Brasília - DF 70040-020, Brazil*

I. EXPERIMENTAL DETAILS

A. Calibration of b_0 .

As we cannot measure b_0 simultaneously to the data acquisition, the calibration is done in a separate time sequence, using absorption imaging, requiring a longer cycle without recapture of the atoms. We therefore increase the loading time of the MOT such that the fluorescence of the probe beam measured at large detuning is the same as in the measurement cycle, all other parameters being unchanged. The absorption images then provide the transverse profile of the probe transmission T , which is related to the optical depth by $T(x, y) = \exp[-b'(x, y)]$, where

$$b'(\delta) = C \frac{b_0}{1 + 4\delta^2}, \quad (1)$$

with δ the probe detuning and $C = 7/15$ is the average Clebsch-Gordan coefficient of the transition for a statistical mixture of the Zeeman substates. We use a Gaussian fit for $b'(x, y)$ and extract the r.m.s. size R directly from the fit, as well as b_0 from the amplitude of the Gaussian fit and the atom number N from its integral. This is done for different values for the time of flight of ballistic expansion, from which we extract the temperature, allowing us to know the size of the atomic cloud for the different pulses as well as the initial atom number.

During the pulse series, we need to take into account possible optical pumping by the probe beam into the other hyperfine ground state $F = 1$. This effect is almost negligible near resonance but becomes significant for the largest negative detunings used in this work. We therefore have precisely measured the pumping rate, from the fluorescence decay, at very large negative detuning ($\delta = -9$), and used this rate to calibrate the probe intensity, which is measured simultaneously to the data on a separate photodetector. Then we use this intensity to compute the atom losses induced by optical pumping and correct the atom number for each pulse.

Note that the uncertainty on the precise value C corresponding to the experimental conditions introduces a systematic uncertainty on N and b_0 , which is thus also affecting the precise value of the slope extracted from

the data of Fig. 3. Statistical uncertainties, estimated by the shot-to-shot fluctuations of b_0 , are of the order of 8% (standard deviation).

B. Analysis of the fluorescence decay.

The raw data are histograms of number of photons detected with a time bin of 1.6 ns. Our detection in the photon counting regime yields about 10^7 counts per second (cps) during the pulses, while between pulses, after the end of the subradiant decay, the ‘dark’ level is about 4000 cps, mainly due to stray light. For each pulse we subtract this dark level and normalize the signal to the steady state amplitude. Then we further bin the data to improve the signal to noise ratio. We use a variable binning, i.e., a larger bin size for later time, when the signal varies slowly, than for short times. We also implemented a systematic procedure to choose the range of data to be fitted by selecting data one decade above the noise floor. This allows us to fit the last measurable time constant. We found this procedure to give the most reliable and relevant fit. Finally, we compute the statistical coefficient of determination of the fit, which quantifies its relevance, and we keep only the points for which this coefficient is above 0.97 in Fig. 3 of the main paper.

The data gathered in this figure have been taken in exactly the same conditions (initial atom number, temperature, saturation parameter, experimental cycle), where the only changing parameters are the probe detuning and its intensity to keep the saturation parameter constant. We have also been able to observe subradiant decay for larger detunings, up to $\delta = -11$, but we have not included these data because we had to adapt other parameters. Indeed, because of the limited available power for the probe beam, the saturation parameter and the subsequent amount of fluorescence were lower, which we partially compensated by increasing the atom number via the loading time, which changed also the temperature and the cycle duration.

II. PREDICTIONS OF THE COUPLED-DIPOLE MODEL

We recall here the main ingredients of the coupled-dipole model, which has been widely used in the last years in the context of single-photon superradiance [1–10]. We consider N two-level atoms (positions \mathbf{r}_i , tran-

* william.guerin@inln.cnrs.fr

sition wavelength $\lambda = 2\pi/k_0$, excited state lifetime Γ^{-1}) driven by an incident laser (Rabi frequency Ω , detuning Δ , plane wave of wavevector \mathbf{k}_0). Restricting the Hilbert space to the subspace spanned by the ground state of the atoms $|G\rangle = |g \cdots g\rangle$ and the singly-excited states $|i\rangle = |g \cdots e_i \cdots g\rangle$ and tracing over the photon degrees of freedom, one obtains an effective Hamiltonian describing the time evolution of the atomic wave function $|\psi(t)\rangle$,

$$|\psi(t)\rangle = \alpha(t)|G\rangle + \sum_{i=1}^N \beta_i(t)|i\rangle. \quad (2)$$

Using standard approximations, the effective Hamiltonian can be written as

$$H_{\text{eff}} = \frac{\hbar\Omega}{2} \sum_i [e^{i\Delta t - i\mathbf{k}_0 \cdot \mathbf{r}_i} S_-^i + e^{-i\Delta t + i\mathbf{k}_0 \cdot \mathbf{r}_i} S_+^i] - \frac{i\hbar\Gamma}{2} \sum_i S_+^i S_-^i - \frac{\hbar\Gamma}{2} \sum_i \sum_{j \neq i} V_{ij} S_+^i S_-^j, \quad (3)$$

where S_{\pm}^i and S_z^i are the usual pseudospin operators for the kets g_i and e_i , respectively. The first term of H_{eff} describes the coupling to the laser field, the second accounts for the finite lifetime of the excited states and the third one describes the dipole-dipole interactions, with

$$V_{ij} = \frac{e^{ikr_{ij}}}{kr_{ij}}, \quad r_{ij} = |\mathbf{r}_i - \mathbf{r}_j|. \quad (4)$$

Here, we have considered a scalar model for light, which neglects polarization effects and near-field terms in the dipole-dipole interaction. It is known to be a good approximation for dilute clouds [11, 12], i.e., when the typical distance between atoms is much larger than the wavelength, which is the case in the experiment.

Considering the low intensity limit, when atoms are mainly in their ground states, i.e., $\alpha \simeq 1$, the problem amounts to determine the amplitudes β_i , which are then given by the linear system of coupled equations

$$\dot{\beta}_i = \left(i\Delta - \frac{\Gamma}{2}\right) \beta_i - \frac{i\Omega}{2} e^{i\mathbf{k}_0 \cdot \mathbf{r}_i} + \frac{i\Gamma}{2} \sum_{j \neq i} V_{ij} \beta_j. \quad (5)$$

These equations are the same as those describing N classical dipoles driven by an oscillating electric field [5], justifying the term ‘‘coupled-dipole model’’. The first term corresponds to the natural evolution of the dipoles (oscillation and damping), the second one to the driving by the external laser, the last term corresponds to the dipole-dipole interaction and is responsible for all collective effects, including dephasing and attenuation of the driving laser beam, as well as more subtle multiple scattering and cooperative effects (super- and sub-radiance). Note that even if the detuning does not appear explicitly in the dipole-dipole interaction term, it still strongly influences the collective behaviour of the system through the population of the eigenmodes that contribute to the

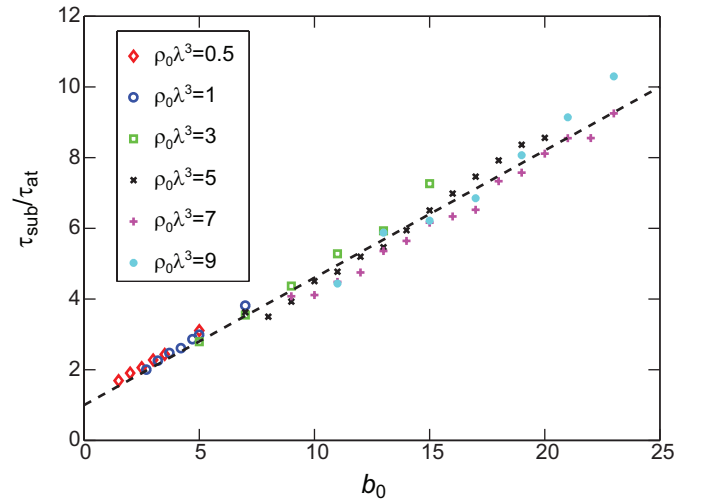


FIG. 1. Scaling of the the subradiant decay time constant as a function of b_0 in the coupled dipole model. We used different densities $\rho_0 \lambda^3 = \{0.5, 1, 3, 5, 7, 9\}$. The time constant is extracted from the exponential fit of the end of the decay of the total emitted power computed from Eqs. (5-6). The fit window is chosen for P (normalized to 1 at $t = 0$) to be between 10^{-4} and 10^{-6} .

system response to the driving field. At large detuning for instance, multiple scattering vanishes.

From the computed values of β_i , we can derive the intensity of the light radiated by the cloud as a function of time and of the angle [6]. The time dependence of the total radiated power P after switching off the laser is proportional to the derivative of the total excited state population,

$$P \propto -\frac{d}{dt} \sum_{j=1}^N |\beta_j(t)|^2. \quad (6)$$

We have used this model to study superradiance and subradiance decay in more detail than in the previous work [7]. The complete study will be published elsewhere [13]. Here, we only show the most important result for the subradiance experiment, which is the linear scaling of the decay time with the parameter $b_0 = 3N/(k_0 R)^2$, which also corresponds to the on-resonance optical depth through the center of the cloud. Here N is the atom number and R the r.m.s. radius of the atomic Gaussian density distribution, which are the two parameters of the simulation. However, in order to determine if b_0 is the scaling parameters, and not, e.g., the atomic density, we need to change b_0 while keeping the density $\rho \propto N/R^3$ constant, by changing simultaneously N and R . Since the atom number N is limited to a few thousands in our numerical simulations, quite large densities are required to reach large b_0 . It is then important to use an exclusion volume when drawing the random positions of the atoms in order to exclude close pairs of atoms [12]. We set our exclusion volume as $k_0 r_{ij} > 3$.

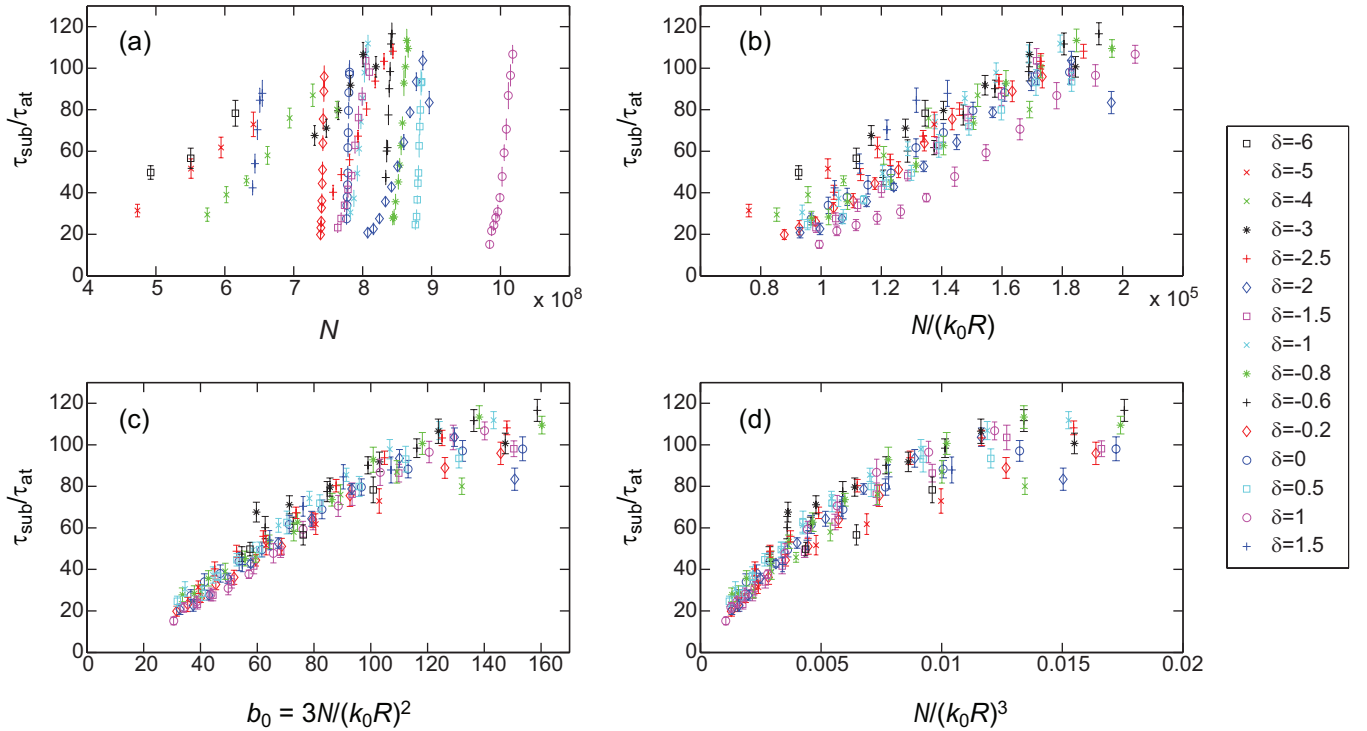


FIG. 2. Test of different scaling parameters. The subradiant decay time constant is plotted as a function of different combinations of N and R . The collapsing of all points on a single curve is best with b_0 as the scaling parameter.

In Fig. 1 we show the result of such simulations, for which we varied b_0 at constant density, for different values of $\rho_0 \lambda^3 = (2\pi)^{3/2} N / (k_0 R)^3$, where ρ_0 is the peak density (at the center of the Gaussian cloud). We clearly see that the different curves collapse on the same line, showing that the on-resonance optical depth is indeed the parameter that controls the subradiant decay. The slope of the line is 0.36. Note that we do not *a priori* expect this number to be in quantitative agreement with the experimental results, as polarization effects and the complex Zeeman structure of the rubidium atoms used in our experiment are neglected in the model.

III. TEST OF DIFFERENT SCALING PARAMETERS

During the series of pulses, two effects contribute to a change of b_0 . The most important one is the expansion of the cloud due to its thermal velocity distribution. Its r.m.s. size typically varies from 0.5 to 1.2 mm between the first and the last pulse. This variation is independent of the probe laser detuning. Another contribution to the change of b_0 between subsequent pulses is the loss of atoms due to optical pumping into the $F = 1$ ground state. Since we kept the same saturation parameter for all detuning, the number of scattered photons is always the same, about 25 per atom and per pulse. However, the probability that a scattering event transfers the

atom to the $F = 1$ state depends strongly on the detuning from the $F = 2 \rightarrow F' = 2$ transition, and thus it is much larger for large red detuning δ (defined from the $F = 2 \rightarrow F' = 3$ transition). For example, at $\delta = -6$, the number of atoms in the $F = 2$ ground state has decreased by 70% between the first and the last pulse, whereas on resonance it is almost constant for all pulses. Thus, for the different detunings the relative contributions of the variation of N and R are different.

We have exploited this fact to test which combination of N and R allows the different curves acquired with different detunings to collapse on a single curve. This is shown in Fig. 2, where it clearly appears that the combination $N/(k_0R)^2$ provides the best scaling parameter. This experimentally confirms that b_0 is indeed the parameter governing subradiance in dilute and extended samples, as predicted by the coupled-dipole model (Fig. 1).

IV. SUBRADIANCE AS A FUNCTION OF THE PROBE INTENSITY

In order to validate the weak excitation assumption, we have also studied the subradiance decay as a function of the probe intensity. In the linear optics regime, the probe intensity should not impact on the measured decay rates or normalized amplitudes. We have thus fixed the detuning δ and the optical depth and varied the intensity I . On Fig. 3 we plot the results for the subradiant

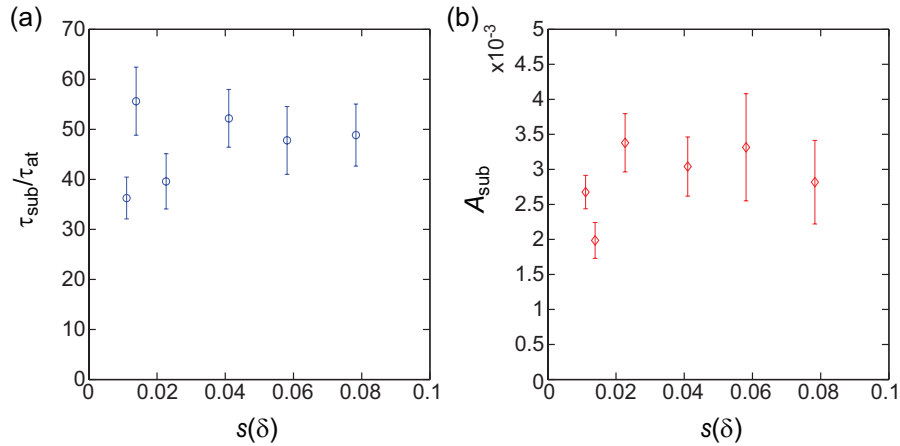


FIG. 3. Effect of the probe intensity. Subradiance time constant (a) and relative amplitude (b) as a function of the saturation parameter. The data have been taken with $b_0 = 110 \pm 8\%$ and $\delta = -5$.

time constant and relative amplitude as a function of the saturation parameter

$$s(\delta) = \frac{I/I_{\text{sat}}}{1 + 4\delta^2}, \quad (7)$$

where I_{sat} is the saturation intensity of the transition.

No significant dependence on the saturation parameter in the explored range ($10^{-2} < s(\delta) < 10^{-1}$) is observed, confirming that the other experimental data, for which $s(\delta) \simeq 0.05$, have been taken in the linear regime.

V. POSSIBLE ROLE OF RADIATION TRAPPING OF NEAR-RESONANT LIGHT

The very slow decays observed at large detuning cannot be simply interpreted as radiation trapping, as in the experiments by Labeyrie *et al.* [14, 15], since radiation trapping does not depend on b_0 only but depends on the optical depth ‘seen’ by the laser beam, i.e., $b'(\delta) \propto b_0/(1+4\delta^2)$, which is very small at large detuning.

However, since the amplitude of the subradiance decay is very small, we have to insure that it cannot be explained by radiation trapping of a small amount of light that would *always* be on resonance.

We have investigated two possible nonnegligible sources of near-resonant light: inelastic scattering due to the atomic saturation and the wings of the laser spectrum.

A. Inelastic scattering

The scattering rate Γ_{sc} of an atom driven by a laser is the sum of two contributions, elastic and inelastic scat-

tering, given by [16]

$$\Gamma_{\text{sc}} = \Gamma_{\text{el}} + \Gamma_{\text{inel}} = \frac{\Gamma}{2} \left(\frac{s}{(1+s)^2} + \frac{s^2}{(1+s)^2} \right) = \frac{\Gamma}{2} \frac{s}{1+s}, \quad (8)$$

where s is the saturation parameter defined above [Eq. (7)]. Usually, inelastic scattering is neglected when $s \ll 1$, which is the case in our experiment. However since subradiance is a small signal, special care is required. For $s \ll 1$, the *relative* weight of inelastic scattering compared to the total scattering is equal to s . The spectrum of this inelastic scattering is the well-known Mollow triplet [17], which is, in fact, a triplet only at large s . At large detuning and moderate intensity, it is a doublet constituted of two lines of equal weights, one of which is precisely on the atomic resonance [18]. Thus, we expect that after the first scattering event, a proportion $s/2$ of the light is shifted near resonance. Multiple scattering could then trap this light in the sample.

To estimate the weight of this inelastic component in the slow decay, we multiply this $s/2$ fraction by the relative amplitude of the slow decay for resonant photon, which is what we extract from our experiment when the laser is tuned to resonance ($A_{\text{sub}} \simeq 2 \times 10^{-2}$ for $b_0 = 110$, see Fig. 3c of the main paper). In this scenario, we would thus expect $A_{\text{sub}} \simeq s \times 10^{-2} \ll 10^{-2}$. On the contrary, we see on Fig. 3 (also with $b_0 = 110$) that A_{sub} is significantly larger and in any case not proportional to s . These data allow us to conclude that spurious resonant radiation trapping of one Mollow sideband is much smaller than the subradiance we observe.

Note that in this experiment, a laser beam larger than the atomic cloud has been used, leading to a significant proportion of single and low-order scattering events on the edges of the cloud, even on resonance, contrary to the previous experiments on radiation trapping [14, 15], where a small beam at the center of the atomic cloud was used. That is why the relative amplitude of the slow decay is low even on resonance.

B. Spectrum of the probe laser

In our experiment, we used a distributed-feedback (DFB) laser diode as probe. This laser is expected to have a spectral linewidth on the order of ~ 3 MHz [19] corresponding to 0.5Γ , which should not have any influence at large detuning. However, if the spectrum has slow-decaying wings (e.g., Lorentzian), the amount of light a few Γ 's from the central frequency might be not negligible in the experiment.

To characterize the spectrum of our probe laser, we performed a beat-note experiment with a commercial extended-cavity laser diode (Toptica DL pro), with a much narrower spectral width. It is thus a good (but slightly conservative) approximation to consider the power spectrum density of the beat-note signal, recorded with an electronic spectrum analyzer, as the optical spectrum of our probe laser. Such a measurement is shown in Fig. 4. The spectrum is composed of a central part, which can be well fitted by a Gaussian, superimposed on a small component with large wings, which is well fitted by a Lorentzian. The r.m.s. width of the Gaussian is 2.6 MHz (corresponding to a full width at half maximum of 1Γ , larger than expected) and the Lorentzian wings have a relative amplitude of 5.8×10^{-3} and a full width at half maximum $\gamma \approx 13.2$ MHz corresponding to 2.2Γ .

From the measured spectrum, we can numerically compute the amount of light near resonance (in a width Γ) given the detuning of the central frequency. For example, for $\delta = -6\Gamma$, corresponding to the largest detuning used in the measurements, this relative amount is $\approx 1.5 \times 10^{-4}$. We recall that even when the laser is set

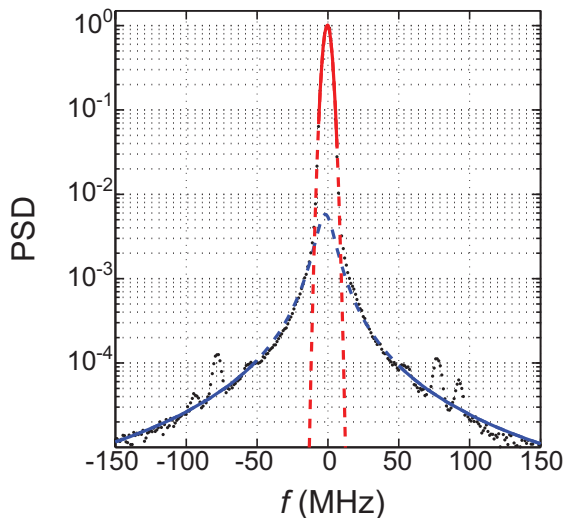


FIG. 4. Spectrum of the probe laser. The power spectrum density (PSD) of a beat-note signal with a reference laser has been averaged 100 times (scanning time ~ 1 s) and the central frequency (~ 1 GHz) has been shifted to zero (black dots). The result can be fitted by a Gaussian in the central part (red) and by a Lorentzian in the wings (blue).

on resonance, the relative amplitude of the slow decay is only $A_{\text{sub}} \simeq 2 \times 10^{-2}$ so that the two numbers should be multiplied to predict the relative amplitude of the slow decay induced by the small part of resonant light. This is thus much too small to be visible in the experiment.

C. Random walk model with frequency redistribution

One further spurious effect is frequency redistribution induced by the Doppler effect during the multiple scattering process, which is known to play an important role in radiation trapping experiments in cold atoms [14, 15, 20]. First, for light initially on-resonance, the light spectrum gets broader during the multiple scattering and the effective optical thickness decreases, breaking the $\tau \propto b^2$ scaling for high enough temperature. Second, light initially slightly detuned has a tendency to drift towards resonance (in addition to the broadening). It means that the previous evaluation considering a window of width Γ to define the resonant light may be not appropriate because frequency redistribution induces a broader ‘capture range’ of frequency.

To evaluate these effects, we performed numerical simulations considering the random walk of photons in a homogeneous spherical cloud of atoms, taking into account the Doppler effect and its associated frequency redistribution. We send photons one by one, we randomly draw their initial transverse positions and detuning taking into account the spatial shape and measured frequency spectrum of the probe laser, and we compute how many scattering events the photons undergo before escaping, which is converted to a time, using the fact that each scattering event takes in average τ_{at} [14]. We obtain thus a distribution of escape time, which is then convoluted by the duration of the pulse in order to simulate the fluorescence decay at the switch-off.

In Fig. 5(a), we show the fluorescence decay for a laser detuning centered at $\delta = -6$, a cloud with a temperature $T = 50 \mu\text{K}$ and an optical thickness $b'(0) = 53$, corresponding to $b_0 \simeq 110$ [Eq. (1)], for comparison with the data of Figs. 2-3 of the main paper. We see indeed that the small amount of light that is on resonance induces a slow decay, whose relative amplitude is $\sim 10^{-4}$. As anticipated, this is larger than expected from the previous simple evaluation, but it is still more than one order of magnitude smaller than the subradiance decay observed in the experiment. Moreover, the use of a homogeneous sphere instead of a Gaussian density distribution overestimates substantially this amplitude because for a given peak-optical thickness (as measured by the transmission of a small beam at the center of the cloud), the average optical thickness ‘seen’ by a large beam is larger with a homogeneous sphere than with a Gaussian cloud. We have also checked that if we consider an incident short pulse of duration similar to the switch-off of the probe beam, and its associated spectral broadening, the result-

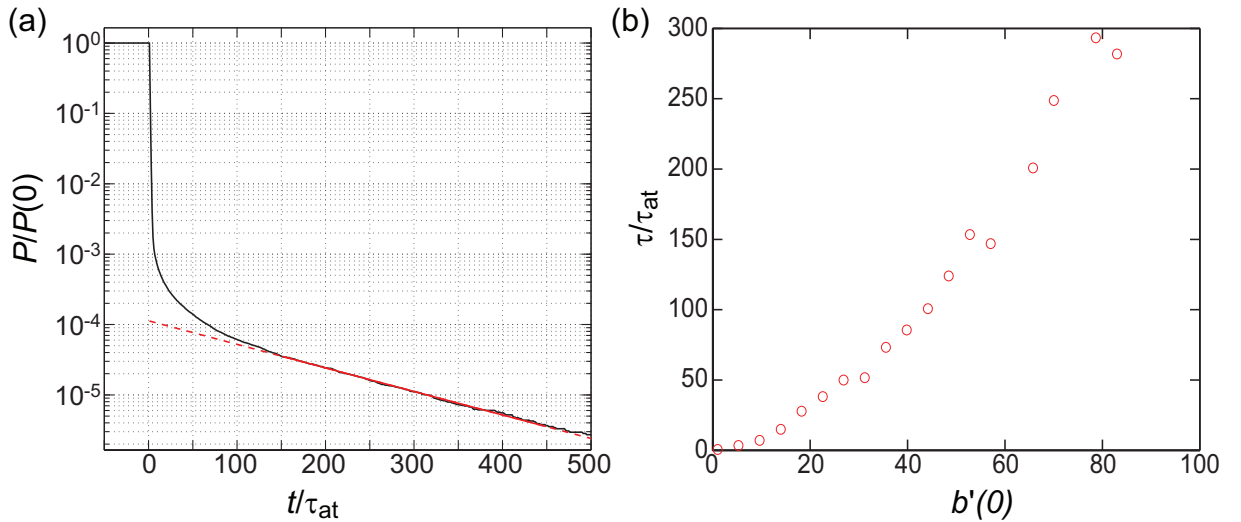


FIG. 5. Main results of a random walk model. (a) Temporal decay computed with $b'(0) = 53$ and $\delta = -6$. The relative amplitude of the slow part is 10^{-4} . (b) Fitted time constant of the slow tail as a function of the on-resonance optical thickness. The increase is clearly faster than linear.

ing slow decay also has a relative amplitude below 10^{-4} .

Finally, we show in Fig. 5(b) how the time constant associated with this small, slow decay, which can be fitted by a decaying exponential, evolves with the optical depth of the cloud. We can see that the increase with the

optical depth is much faster than linear in this regime of low temperature [20]. This provides another, qualitative difference between our subradiance data and what could be expected from spurious radiation trapping of near-resonant light.

-
- [1] M. O. Scully, E. S. Fry., H. R. Ooi, and K. Wódkiewicz, *Phys. Rev. Lett.* **96**, 010501 (2006).
- [2] A. A. Svidzinsky, J.-T. Chang, and M. O. Scully, *Phys. Rev. Lett.* **100**, 160504 (2008).
- [3] A. Svidzinsky and J.-T. Chang, *Phys. Rev. A* **77**, 043833 (2008).
- [4] P. W. Courteille, S. Bux, E. Lucioni, K. Lauber, T. Bienaimé, R. Kaiser, and N. Piovela, *Eur. Phys. J. D.* **58**, 69 (2010).
- [5] A. A. Svidzinsky, J.-T. Chang, and M. O. Scully, *Phys. Rev. A* **81**, 053821 (2010).
- [6] T. Bienaimé, M. Petruzzo, D. Bigerni, N. Piovela, and R. Kaiser, *J. Mod. Opt.* **58**, 1942 (2011).
- [7] T. Bienaimé, N. Piovela, and R. Kaiser, *Phys. Rev. Lett.* **108**, 123602 (2012).
- [8] T. Bienaimé, R. Bachelard, P. W. Courteille, N. Piovela, and R. Kaiser, *Fortschr. Phys.* **61**, 377 (2013).
- [9] Y. Miroshnychenko, U. V. Poulsen, and K. Mølmer, *Phys. Rev. A* **87**, 023821 (2013).
- [10] W. Feng, Y. Li, and S.-Y. Zhu, *Phys. Rev. A* **89**, 013816 (2014).
- [11] S. E. Skipetrov and I. M. Sokolov, *Phys. Rev. Lett.* **112**, 023905 (2014).
- [12] L. Bellando, A. Gero, E. Akkermans, and R. Kaiser, *Phys. Rev. A* **90**, 063822 (2014).
- [13] M. O. Araújo, W. Guerin, and R. Kaiser, in preparation.
- [14] G. Labeyrie, E. Vaujour, C. A. Müller, D. Delande, C. Miniatura, D. Wilkowski, and R. Kaiser, *Phys. Rev. Lett.* **91**, 223904 (2003).
- [15] G. Labeyrie, R. Kaiser, and D. Delande, *Appl. Phys. B* **81**, 1001 (2005).
- [16] C. Cohen-Tannoudji, J. Dupont-Roc, and G. Grynberg, *Atom-Photon Interactions: Basic Processes and Applications* (Wiley, New York, 1992).
- [17] B. R. Mollow, *Phys. Rev.* **188**, 1969 (1969).
- [18] See, e.g., T. Chanelière, PhD Thesis, Université Nice Sophia-Antipolis (2004), p. 40, available on <https://tel.archives-ouvertes.fr/tel-00007793>.
- [19] S. Kraft, A. Denning, C. Trück, J. Fortágh, F. Lison, and C. Zimmermann, *Laser Phys. Lett.* **2**, 71 (2005).
- [20] R. Pierrat, B. Grémaud, and D. Delande, *Phys. Rev. A* **80**, 013831 (2009).

As evidenced by the lengthy discussion in the Supplemental Material (section V), we took great care of excluding an alternative explanation based on incoherent radiation trapping as studied in [Labeyrie 2003] (see also section IV.1.2.2). In particular I developed random-walk (RW) simulations in order to study some spurious effects like the wings of the laser spectrum². Still, the fact that we didn't see any signature of radiation trapping near resonance was puzzling, which motivated the study of section VI.5.1.

VI.1.3. Influence of the temperature

Another puzzling observation was that, apparently and luckily, the temperature was not a problem. During the data acquisition of the first paper I had taken one data set at a higher temperature ($\approx 200\mu\text{K}$) without any significant change. This motivated a more systematic study, published recently and reproduced below [Weiss 2019], on the influence of thermal motion on subradiance. As anticipated it shows a nonintuitive robustness, confirmed by CD simulations. The numerics even allow exploring much higher temperature and suggest that subradiance might be visible even at room temperature.

²I thank Guillaume Labeyrie and Dominique Delande, whose skepticism encouraged me to develop those simulations, which I used on several occasions later.

Robustness of Dicke subradiance against thermal decoherenceP. Weiss,^{1,*} A. Cipris,¹ M. O. Araújo,^{1,2,†} R. Kaiser,¹ and W. Guerin¹¹*Université Côte d'Azur, CNRS, Institut de Physique de Nice, France*²*CAPES Foundation, Ministry of Education of Brazil, Brasília, DF 70040-020, Brazil*

(Received 5 June 2019; published 26 September 2019)

Subradiance is the cooperative inhibition of the radiation by several emitters coupled to the same electromagnetic modes. It was predicted by Dicke in 1954 and only recently observed in cold atomic vapors. Here we address the question to what extent this cooperative effect survives outside the limit of frozen two-level systems by studying the subradiant decay in an ensemble of cold atoms as a function of the temperature. Experimentally, we observe only a slight decrease of the subradiant decay time when increasing the temperature up to several millikelvins, and in particular we measure subradiant decay rates that are much smaller than the Doppler broadening. This demonstrates that subradiance is surprisingly robust against thermal decoherence. The numerical simulations are in good agreement and allow us to extrapolate the behavior of subradiance at higher temperatures.

DOI: [10.1103/PhysRevA.100.033833](https://doi.org/10.1103/PhysRevA.100.033833)**I. INTRODUCTION**

Understanding the influence of decoherence or dephasing processes in cooperative effects such as super- and subradiance [1–7] is not only interesting from a fundamental point of view, but it is also important for the possible developments of photonic device exploiting cooperativity in the classical or quantum regime [8–13]. This is especially true if one wants to use solid-state devices [14,15], which are subject to phonon-induced decoherence. Previous theoretical studies of various toy models in the framework of open quantum systems have predicted some robustness of superradiance to noise and dephasing [16–19].

In this article, we report an experimental study of thermal decoherence of subradiant Dicke states in a large ensemble of cold atoms [4]. Indeed, even if laser-cooled atoms are not coupled to phonons, they are not completely frozen. Atomic motion has been shown to be a source of decoherence for coherent backscattering [20] and to suppress the effect of recurrent scattering on the refractive index of dense atomic media [21,22]. Since subradiance is an interference effect involving very long time scales, it is expected to be particularly fragile. The lifetime of subradiant states τ_{sub} can exceed several hundred times the single atom lifetime τ_{at} . An intuitive guess how residual atomic motion due to finite temperature should limit this lifetime is given by the restriction that the atoms should not move during this lifetime farther than the wavelength $\lambda/2\pi$ to not change the interference condition. Taking the rms velocity of a Maxwell-Boltzmann distribution σ_v , subradiance would require $\Gamma_{\text{D}} \leq \Gamma_{\text{sub}}$, where $\Gamma_{\text{D}} = k\sigma_v$ is the Doppler width.

Contrary to that, and quite surprisingly, we show here that subradiance in the linear-optics regime is robust against thermal motion. We observe only a slight decrease of the subradiant decay time when increasing the temperature up to several millikelvins, and in particular we measure subradiant decay rates Γ_{sub} that are much smaller than the Doppler broadening Γ_{D} . We also perform numerical simulations showing that the breakdown of subradiance only occurs when the Doppler broadening is on the same order of magnitude as the natural lifetime of the atomic transition Γ_0 . In practice, this means that subradiance can be observed and used at any “cold-atom” temperature and even beyond.

II. EXPERIMENTAL SETUP

The experimental setup is based on a cloud of cold ⁸⁷Rb atoms prepared in a magneto-optical trap (MOT). After 60 ms of loading from the background vapor and a stage of compressed MOT (30 ms) we obtain a sample of $N \approx 3 \times 10^9$ atoms at a temperature $T \approx 100 \mu\text{K}$ with a Gaussian density distribution (peak densities $\rho_0 \sim 10^{11} \text{ cm}^{-3}$ and rms size $R \approx 1 \text{ mm}$). A more detailed description of the setup as well as the procedure to observe and analyze subradiance can be found in [4,23]. For this new series of experiments we now add an optical molasses in order to vary the temperature in a controlled manner. To do so, we varied the detuning of the cooling laser in a range between $-10\Gamma_0$ to the atomic resonance. We also use the molasses duration (1 ms to 10 ms) as a parameter to tune the final temperature, which is between 50 μK and 11 mK, corresponding to $\Gamma_{\text{D}}/\Gamma_0$ between 0.01 and 0.2.

After this preparation the cloud expands ballistically. During the expansion the atoms are first optically pumped to the hyperfine ground state $F = 2$ and then excited by a series of 12 weak laser pulses with a duration of 10 μs (Fig. 1). The pulses are separated by either 1 ms or 0.5 ms depending on the temperature. The time shaping of the pulses is done with

*patrizia.weiss@inphyni.cnrs.fr

†Present address: Departamento de Física, Universidade Federal de Pernambuco, 50670-901, Recife-PE, Brazil.

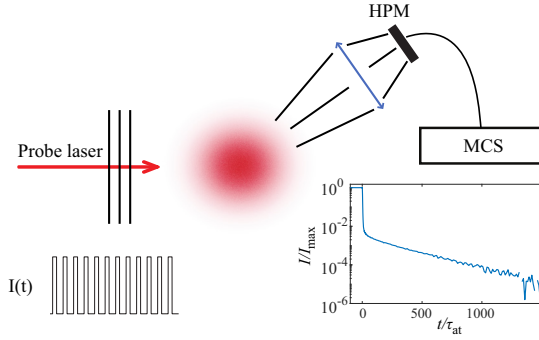


FIG. 1. Sketch of our setup based on an ensemble of atoms in a MOT. The cloud is excited with a time sequence of probe laser pulses. The switch-off dynamics of the scattered light is detected under an angle 35° to the probe beam axis with a hybrid photon multiplier (HPM) and averaged with a multichannel scaler (MCS).

two acousto-optical modulators, achieving a faster switch-off ($t_{\text{switch}} \approx 15$ ns) than the natural lifetime $\tau_{\text{at}} = \Gamma_0^{-1} = 26.24$ ns, and at the same time providing an extinction ratio better than 10^{-5} . The probe beam is large compared to the cloud size ($1/e^2$ radius 5.3 mm) to ensure a homogeneous driving and is linearly polarized. In previous experiments it has been shown that subradiance is independent of the detuning as long as multiple scattering is negligible [4,23]. As a consequence we have chosen here to work with a constant detuning $\delta = (\omega - \omega_0) = -4\Gamma_0$, with ω the laser frequency, ω_0 the frequency of the atomic transition $F = 2 \rightarrow F' = 3$, and $\Gamma_0/2\pi = 6.07$ MHz the natural linewidth. The intensity of the probe is chosen such that the saturation parameter is

$$s(\delta) = g \frac{I/I_{\text{sat}}}{1 + 4\delta^2/\Gamma_0^2} \approx 0.02, \quad (1)$$

well in the linear-optics regime, with $g = 7/15$ the degeneracy factor of the transition for equally populated Zeeman states and $I_{\text{sat}} = 1.6$ mW/cm² the saturation intensity. The scattered light is collected by a two-inch lens and detected with a hybrid photon multiplier under an angle of 35° to the probe beam (see Fig. 1). The signal is then sent to a multichannel scaler for averaging over typically more than 400 000 cycles with a time resolution of 1.6 ns.

Because of the ballistic expansion during the pulse series the cloud size increases and the cooperativity parameter that controls super- and subradiance effects [4,24], $b_0 = 3N/(kR)^2$, decreases (here $k = 2\pi/\lambda$ and $\lambda = 780$ nm is the wavelength of the transition). For simplicity, we call this parameter the on-resonance optical depth, although the actual optical depth is

$$b(\delta) = g \frac{b_0}{1 + 4\delta^2/\Gamma_0^2}, \quad (2)$$

which can be measured by absorption imaging. This measurement is interlaced with the data acquisition by changing one out of 750 cycles. For those special cycles, the measurement sequence with the pulse series is replaced by an absorption imaging procedure. The time of flight before imaging is varied over the data acquisition such that the temperature and the optical depth for each pulse are measured several times during an acquisition run. This improved calibration procedure gives us access to any drift that might occur during the data acquisition.

III. SUBRADIANT DECAY FOR DIFFERENT ENSEMBLE TEMPERATURES

We report in Fig. 2 the results of our systematic experimental study of the subradiant decay as a function of the temperature of the sample. In panel (a) we show the decay curves of the scattered light. The intensity is normalized to

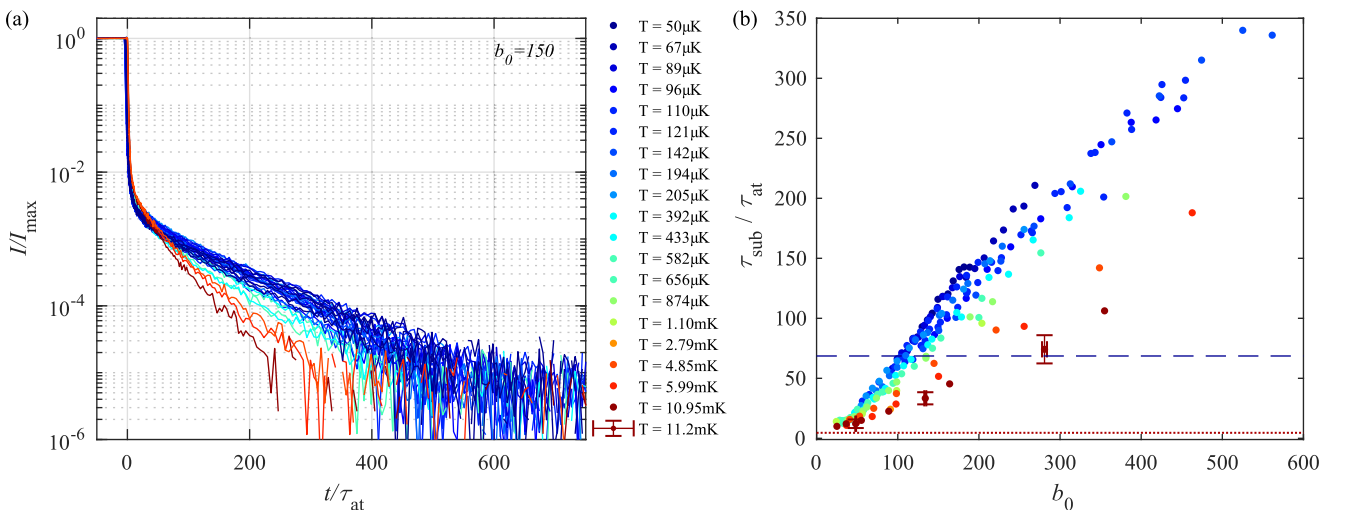


FIG. 2. (a) Experimental decay curves for several temperatures, all normalized to the pulse level at the switch-off time $t = 0$, with a resonant optical depth $b_0 = 150 \pm 8$. The temperature is encoded in the color scale. A smooth reduction of the subradiant decay with increasing temperature is well visible. (b) Subradiant decay times as a function of b_0 for different temperatures (same color code). For clarity only the last data set is shown with error bars. The horizontal blue dashed line shows the time scales Γ_D^{-1} corresponding to the Doppler width for the lowest temperature, 50 μK ($\Gamma_D^{-1} = 68.6\tau_{\text{at}}$), and the highest one, 11.2 mK ($\Gamma_D^{-1} = 4.58\tau_{\text{at}}$), red dotted line.

its steady-state value just before the switch-off at $t = 0$. All curves are recorded for an on-resonant optical depth $b_0 = 150 \pm 8$ and the temperature is encoded in the color scale, from 50 μK (dark blue) to 11.2 mK (dark red). The first observation is that subradiance is clearly visible in all curves, even in the mK range, which demonstrates its robustness against thermal motion. The second is that we do observe a reduction of the subradiant decay time when the temperature increases.

To study this effect more precisely we fit all decay curves by an exponential decay at late time (the fitting range is taken as one decade above the noise floor, to cover the longest-lived visible mode). The obtained subradiant time τ_{sub} is reported in Fig. 2(b) as a function of the on-resonance optical depth b_0 for each temperature (same color code). Note that the number of data points is reduced for the highest temperatures because of the fast ballistic expansion of the cloud. The linear scaling of τ_{sub} with b_0 , as previously reported [4,23], is observed at all temperatures; however, the slope is reduced when the temperature increases.

For each temperature T we fit this linear trend as $\tau_{\text{sub}}/\tau_{\text{at}} = 1 + \alpha_{\text{sub}} \cdot b_0$ to obtain the slope of the subradiant enhancement. In the inset of Fig. 4 we plot the slope α_{sub} as a function of the ratio between the Doppler broadening $\Gamma_{\text{D}} = k\sigma_v$, with $\sigma_v = (k_{\text{B}}T/m_{\text{Rb}})^{1/2}$ the rms width of the atomic velocity distribution (k_{B} is the Boltzmann constant and m_{Rb} the atomic mass), and the natural decay rate Γ_0 . Although the temperature is varied by more than two orders of magnitude, the slope only changes by a factor ~ 3 . Within this limited range the decrease fits best with a logarithmic function of $\Gamma_{\text{D}}/\Gamma_0$.

For almost all our data we have $\Gamma_{\text{sub}} < \Gamma_{\text{D}} < \Gamma_0$. The characteristic time corresponding to the Doppler width, Γ_{D}^{-1} , is shown in dashed lines in Fig. 2(b) for the lowest and highest temperatures. Since $\Gamma_{\text{sub}} < \Gamma_{\text{D}}$ it is not surprising that thermal motion affects subradiance, which is built up by the interference of light scattered by many atoms. However, it is a nonintuitive result that subradiant modes with lifetimes long compared to the typical atomic motion survive. A possible explanation for this apparent robustness is the large number of subradiant modes. As the atoms move and the eigenmodes of the system are modified, the excitation contained in a subradiant mode has a larger probability to stay in the subradiant manifold because, at large b_0 , there are much more subradiant modes than superradiant ones [25]. In the extreme case of the Dicke limit ($R \leq \lambda$), there is only one superradiant mode in the low excitation limit, while $N - 1$ subradiant modes are present.

IV. TEMPERATURE EFFECTS IN THE COUPLED-DIPOLE MODEL

To provide a comparable numerical study of the decay dynamics of the interacting atomic ensemble, as well as to explore the regimes of parameters that we cannot reach experimentally, i.e., $\Gamma_{\text{sub}} > \Gamma_{\text{D}}$ and $\Gamma_{\text{D}} > \Gamma_0$, we now turn to numerical simulations of an adapted version of the coupled-dipole (CD) model, which includes atomic motion [26,27].

The CD model provides a well-suited description in the context of cooperative effects, especially for super- and

subradiance in the linear optics regime [4–6,26,28–32]. The model consists of N two-level atoms randomly distributed in space at position \mathbf{r}_i . The atoms are driven with an incident laser field with a Rabi frequency $\Omega(\mathbf{r}_i)$ and a detuning δ . For the low excitation limit, which is considered here, the only relevant states are the ground state $|G\rangle = |g \cdots g\rangle$ and the single-excited states $|i\rangle = |g \cdots e_i \cdots g\rangle$. One can then obtain an effective Hamiltonian for the time evolution of the atomic wave function

$$|\psi(t)\rangle = \alpha(t)|G\rangle + \sum_{i=1}^N \beta_i(t)|i\rangle. \quad (3)$$

Since we are in the low excitation limit ($\alpha \simeq 1$) the time evolution of the system is described by the time evolution of the excitation probabilities

$$\dot{\beta}_i = \left(i\delta - \frac{\Gamma}{2} \right) \beta_i - \frac{i\Omega_i}{2} + \frac{i\Gamma}{2} \sum_{i \neq j} V_{ij} \beta_j. \quad (4)$$

The first term represents the single-atom decay dynamics, the second term the driving field for the excitation, and the last term the dipole-dipole interaction containing the cooperative effects. We use a scalar model to describe the dipole-dipole interaction, neglecting any polarization effect as well as near-field terms, which is a good approximation for a very dilute gas, as used in our experiment. In this case the dipole-dipole interaction term is

$$V_{ij} = \frac{e^{ikr_{ij}}}{kr_{ij}}, \quad \text{with } r_{ij} = |\mathbf{r}_i - \mathbf{r}_j|, \quad (5)$$

with r_{ij} the relative distances between the atoms. Since the $\beta_i(t)$ provide the time evolution of the excitation probability one can then calculate the emitted light intensity as a function of time. A more detailed description can be found in Refs. [31,32].

In order to include the effect of temperature, we include atomic motion by assigning to each atom a velocity v_i following a normal distribution of rms width $\sigma_v = (k_{\text{B}}T/m_{\text{Rb}})^{1/2}$ in each direction of space and let the space vector $\mathbf{r}_i(t)$ be time dependent. At low temperature we use a ballistic motion for each atom, as in the experiment. However, this turned out to be problematic with increasing temperatures, since it comes along with a non-negligible increase of size (and correspondingly a drop of the optical depth) of the sample during the subradiant decay time [33]. This effect is negligible in the experiment, where the spatial width of the distribution $\sigma_x \gg k\sigma_v\tau_{\text{sub}}$, but can become important in simulations, where one needs to use smaller values of σ_x to simulate large values of b_0 , as the number of atoms in the simulations is limited to a few 1000. To avoid this and keep a well-defined optical depth during the simulation, for temperatures larger than 500 μK , we simulate the atomic motion with a harmonic trapping. By choosing the oscillation frequency ω_{H} as the ratio between the rms widths of the velocity and space distributions, $\omega_{\text{H}} = \sigma_v/\sigma_x$, the sample keeps its Gaussian density distribution with a constant size. The initial position and velocity of each atom are drawn independently in their respective normal distributions. We have checked that the two ways of including atomic motion (ballistic or harmonic) give the same results

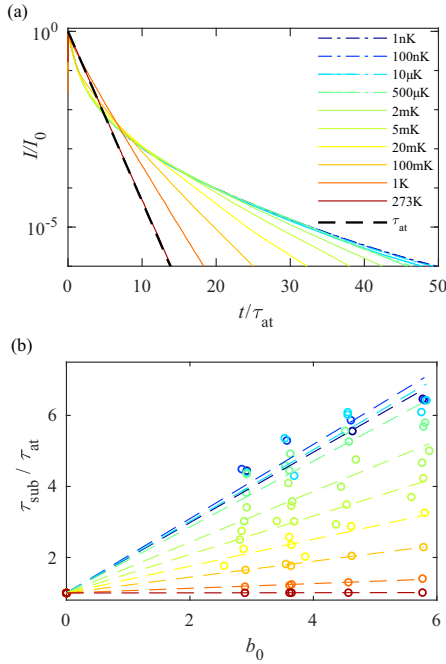


FIG. 3. (a) Numerical results of the decay curves for $N_{\text{at}} = 1500$ atoms. Subradiance starts to be significantly reduced in the mK range, but still shows decay time much longer than the single atom decay time τ_{at} . Only when reaching room temperature does the decay curve follow the one of the single-atom case (dashed black line). The dashed lines are obtained with a ballistic motion of the atoms, while the solid lines are with the harmonic oscillator model. For 10 μK and 500 μK both models are displayed but are hardly distinguishable. (b) Numerical results for the fitted subradiant decay times for different resonant optical depths b_0 . The temperatures are the same as in (a). For temperatures below 2 mK the decay times are almost the same, while increasing the temperature further leads to a smooth decrease of the decay times. The dashed lines are linear fits, whose slopes α_{sub} are reported in Fig. 4.

around 500 μK , the temperature beyond which we use the harmonic motion.

V. SCALING LAW OF THE TEMPERATURE DEPENDENCE

Solving Eqs. (4) for different temperatures ranging from 1 nK to 273 K with an atom number $N = 1500$ and computing the total scattered intensity, we obtain the decay curves shown in Fig. 3(a). The long-lived subradiant states decay faster when the temperature increases; however, it reaches the single-atom decay only close to room temperature ($\Gamma_{\text{D}}/\Gamma_0 \approx 100$). As in the experiment, we extract the subradiant decay time τ_{sub} by an exponential fit of the slow decay at late time and low level (we choose the fitting range between 10^{-6} and 5×10^{-5} for the relative intensity). The results are reported in Fig. 3(b) as a function of the on-resonance optical depth b_0 . The linear trend of τ_{sub} as a function of b_0 is well visible at all temperatures, which is consistent with the experimental observations.

Note that, at large temperature, the Doppler broadening becomes comparable to, or larger than, the detuning (we used $\delta = -4\Gamma$ in all simulations), such that the driving laser is

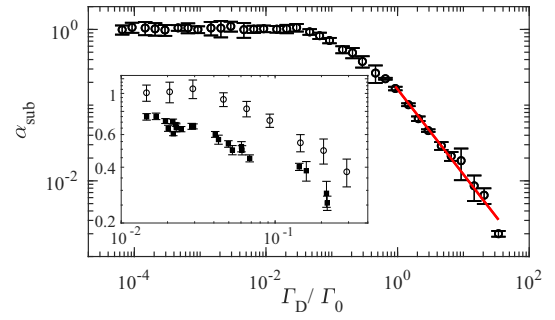


FIG. 4. Numerical results for the subradiant decay time slopes α_{sub} as a function of the Doppler width Γ_{D} in units of Γ_0 . After a plateau the decay time is reduced smoothly with increasing temperatures. When $\Gamma_{\text{D}}/\Gamma_0 > 1$, the decay is a power law (note the log-log scales). The fit (red solid line) gives an exponent compatible with -1 . Inset: direct comparison between the experimental (filled rectangles) and numerical (open circles) results for α_{sub} . The behaviors with the temperature are the same, which demonstrates the validity of our modeling of the atomic motion.

de facto on resonance, which may introduce radiation trapping [34]. However, as studied in detail in Ref. [23], radiation trapping dominates the slow decay only when the actual optical depth $b(\delta)$ is larger than ~ 10 at zero temperature, and is even less visible with Doppler-induced frequency redistribution. In our simulations, the Doppler-broadened optical depth is at most ~ 0.5 , such that the observed slow decays in Fig. 3 can be safely attributed to subradiance.

To provide a more quantitative study on the impact of temperature on the subradiant decay times, we show in Fig. 4 the slopes α_{sub} extracted from the linear fit of the data of Fig. 3(b), as a function of the Doppler width in units of the natural linewidth. For the lowest temperatures a plateau is visible, i.e., α_{sub} becomes independent of T for low enough temperature, the atoms are quasistatic. When the Doppler broadening becomes nonnegligible, α_{sub} starts to slowly decrease. This is the range we experimentally explore, as seen in the insets of Figs. 2(b) and 4. When the Doppler broadening reaches the single atom decay rate, $\Gamma_{\text{D}}/\Gamma_0 > 1$, the decrease of subradiance follows a power law. A power-law fit $\alpha_{\text{sub}} = \beta(\Gamma_{\text{D}}/\Gamma_0)^m$ gives $\beta \simeq 0.16$ and $m = -1.12 \pm 0.14$, compatible with $m = -1$. This exponent can be interpreted as follows. In the regime when $\Gamma_{\text{D}}/\Gamma_0 > 1$, the convolution of the scattering cross section with the Doppler broadening leads to a reduced center of line scattering cross-section scaling as $(\Gamma_{\text{D}}/\Gamma_0)^{-1}$ and, for a given atomic density and sample size, the optical depth is also proportional to $(\Gamma_{\text{D}}/\Gamma_0)^{-1}$. The observed scaling of the subradiant decay rates as shown in Fig. 4 is thus primarily consistent with a Doppler-broadened resonant optical depth in the limit of $\Gamma_{\text{D}} \gg \Gamma_0$. Note that a simple selection of slow atoms up to a certain cutoff velocity inside the Maxwell-Boltzmann distribution would lead to a different scaling, with a more drastic decrease as $(\Gamma_{\text{D}}/\Gamma_0)^{-3}$.

We finally show in the inset of Fig. 4 the direct comparison (without any free parameter) of the measured and computed slopes α_{sub} as a function of the temperature. Although we do not expect any quantitative agreement on the precise values of α_{sub} , even at zero temperature, because of the complex

level structure of rubidium that is not taken into account in the model, the behaviors of α_{sub} with T are in remarkable agreement. This validates *a posteriori* our way of introducing the atomic motion in the coupled-dipole model.

VI. CONCLUSION AND OUTLOOK

In summary, we have demonstrated that for a large temperature range of the atomic cloud the subradiant decay is robust against thermal decoherence. In particular, the time scale corresponding to the Doppler broadening, Γ_{D}^{-1} , does not directly introduce a limit for the subradiant lifetime, but merely provides a rescaling of the subradiant enhancement factor ($\alpha_{\text{sub}}b_0$) in the high temperature regime. This rescaling can be interpreted as a modification of the resonant optical depth, which is reduced by the Doppler broadening but remains the cooperativity parameter controlling subradiance.

These results open up the prospect of observing and using subradiance at room temperature or with hot atomic vapors. Indeed, an extrapolation of the scaling laws discovered in

this work predicts subradiance with $\tau_{\text{sub}}/\tau_{\text{at}} \sim 40$ with a 5-cm Rb cell at 100 °C (with these parameters, $b_0 \sim 10^4$ and $\Gamma_{\text{D}}/\Gamma_0 \sim 40$ [35]). Similar to room-temperature atomic quantum memories, which have already reached excellent performances [36,37], subradiance could be more broadly used for quantum-optics or quantum-metrology applications [8–13] at room temperature. This robustness may also be applied to other interference effects in light scattering, such as coherent backscattering [38].

ACKNOWLEDGMENTS

The authors thank Romain Bachelard for useful discussions and advice on the numerical simulations. This work was supported by the ANR (project LOVE, Grant No. ANR-14-CE26-0032), the European Training Network ColOpt (European Union Horizon 2020 program under the Marie Skłodowska-Curie action, Grant agreement No. 721465), the Brazilian Coordenação de Aperfeiçoamento de Pessoal de Nível Superior (CAPES), and the Deutsche Forschungsgemeinschaft (Grant No. WE 6356/1-1).

-
- [1] R. H. Dicke, Coherence in spontaneous radiation processes, *Phys. Rev.* **93**, 99 (1954).
 - [2] M. O. Scully and A. A. Svidzinsky, The super of superradiance, *Science* **325**, 1510 (2009).
 - [3] A. Goban, C.-L. Hung, J. D. Hood, S.-P. Yu, J. A. Muniz, O. Painter, and H. J. Kimble, Superradiance for Atoms Trapped Along a Photonic Crystal Waveguide, *Phys. Rev. Lett.* **115**, 063601 (2015).
 - [4] W. Guerin, M. O. Araújo, and R. Kaiser, Subradiance in a Large Cloud of Cold Atoms, *Phys. Rev. Lett.* **116**, 083601 (2016).
 - [5] M. O. Araújo, I. Krešić, R. Kaiser, and W. Guerin, Superradiance in a Large Cloud of Cold Atoms in the Linear-Optics Regime, *Phys. Rev. Lett.* **117**, 073002 (2016).
 - [6] S. J. Roof, K. J. Kemp, M. D. Havey, and I. M. Sokolov, Observation of Single-Photon Superradiance and the Cooperative Lamb Shift in an Extended Sample of Cold Atoms, *Phys. Rev. Lett.* **117**, 073003 (2016).
 - [7] P. Solano, P. Barberis-Blostein, F. K. Fatemi, L. A. Orozco, and S. L. Rolston, Super-radiance reveals infinite-range dipole interactions through a nanofiber, *Nat. Commun.* **8**, 1857 (2017).
 - [8] L. Ostermann, H. Ritsch, and C. Genes, Protected State Enhanced Quantum Metrology with Interacting Two-Level Ensembles, *Phys. Rev. Lett.* **111**, 123601 (2013).
 - [9] M. O. Scully, Single Photon Subradiance: Quantum Control of Spontaneous Emission and Ultrafast Readout, *Phys. Rev. Lett.* **115**, 243602 (2015).
 - [10] G. Facchinetti, S. D. Jenkins, and J. Ruostekoski, Storing Light with Subradiant Correlations in Arrays of Atoms, *Phys. Rev. Lett.* **117**, 243601 (2016).
 - [11] A. Asenjo-Garcia, M. Moreno-Cardoner, A. Albrecht, H. J. Kimble, and D. E. Chang, Exponential Improvement in Photon Storage Fidelities Using Subradiance and “Selective Radiance” in Atomic Arrays, *Phys. Rev. X* **7**, 031024 (2017).
 - [12] G. Facchinetti and J. Ruostekoski, Interaction of light with planar lattices of atoms: Reflection, transmission, and cooperative magnetometry, *Phys. Rev. A* **97**, 023833 (2018).
 - [13] P.-O. Guimond, A. Grankin, D. V. Vasilyev, B. Vermersch, and P. Zoller, Subradiant Bell States in Distant Atomic Arrays, *Phys. Rev. Lett.* **122**, 093601 (2019).
 - [14] J. A. Mlynek, A. A. Abdumalikov, C. Eichler, and A. Wallraff, Observation of Dicke superradiance for two artificial atoms in a cavity with high decay rate, *Nat. Commun.* **5**, 5186 (2014).
 - [15] S. D. Jenkins, J. Ruostekoski, N. Papisimakis, S. Savo, and N. I. Zheludev, Many-Body Subradiant Excitations in Metamaterial Arrays: Experiment and Theory, *Phys. Rev. Lett.* **119**, 053901 (2017).
 - [16] G. L. Celardo, G. G. Giusteri, and F. Borgonovi, Cooperative robustness to static disorder: Superradiance and localization in a nanoscale ring to model light-harvesting systems found in nature, *Phys. Rev. B* **90**, 075113 (2014).
 - [17] G. L. Celardo, P. Poli, L. Lussardi, and F. Borgonovi, Cooperative robustness to dephasing: Single-exciton superradiance in a nanoscale ring to model light-harvesting systems, *Phys. Rev. B* **90**, 085142 (2014).
 - [18] A. Tayebi, T. N. Hoatson, J. Wang, and V. Zelevinsky, Environment-protected solid-state-based distributed charge qubit, *Phys. Rev. B* **94**, 235150 (2016).
 - [19] F. Damanet, D. Braun, and J. Martin, Cooperative spontaneous emission from indistinguishable atoms in arbitrary motional quantum states, *Phys. Rev. A* **94**, 033838 (2016).
 - [20] G. Labeyrie, D. Delande, R. Kaiser, and C. Miniatura, Light Transport in Cold Atoms and Thermal Decoherence, *Phys. Rev. Lett.* **97**, 013004 (2006).
 - [21] J. Javanainen, J. Ruostekoski, Y. Li, and S.-M. Yoo, Shifts of a Resonance Line in a Dense Atomic Sample, *Phys. Rev. Lett.* **112**, 113603 (2014).
 - [22] S. D. Jenkins, J. Ruostekoski, J. Javanainen, R. Bourgain, S. Jennewein, Y. R. P. Sortais, and A. Browaeys, Optical Resonance Shifts in the Fluorescence of Thermal and Cold Atomic Gases, *Phys. Rev. Lett.* **116**, 183601 (2016).

- [23] P. Weiss, M. O. Araújo, R. Kaiser, and W. Guerin, Subradiance and radiation trapping in cold atoms, *New J. Phys.* **20**, 063024 (2018).
- [24] W. Guerin, M. T. Rouabah, and R. Kaiser, Light interacting with atomic ensembles: Collective, cooperative and mesoscopic effects, *J. Mod. Opt.* **64**, 895 (2017).
- [25] H. Ritsch, Workshop on “strongly disordered optical systems: from the white paint to cold atoms”, Cargèse, France, 2016 (unpublished).
- [26] T. Bienaimé, N. Piovella, and R. Kaiser, Controlled Dicke Subradiance from a Large Cloud of Two-Level Systems, *Phys. Rev. Lett.* **108**, 123602 (2012).
- [27] A. Eloy, Z. Yao, R. Bachelard, W. Guerin, M. Fouché, and R. Kaiser, Diffusive wave spectroscopy of cold atoms in ballistic motion, *Phys. Rev. A* **97**, 013810 (2018).
- [28] J. Javanainen, J. Ruostekoski, B. Vestergaard, and M. R. Francis, One-dimensional modeling of light propagation in dense and degenerate samples, *Phys. Rev. A* **59**, 649 (1999).
- [29] A. A. Svidzinsky, J.-T. Chang, and M. O. Scully, Cooperative spontaneous emission of N atoms: Many-body eigenstates, the effect of virtual Lamb shift processes, and analogy with radiation of N classical oscillators, *Phys. Rev. A* **81**, 053821 (2010).
- [30] Ph. W. Courteille, S. Bux, E. Lucioni, K. Lauber, T. Bienaimé, R. Kaiser, and N. Piovella, Modification of radiation pressure due to cooperative scattering of light, *Eur. Phys. J. D* **58**, 69 (2010).
- [31] T. Bienaimé, M. Petruzzo, D. Bigerni, N. Piovella, and R. Kaiser, Atom and photon measurement in cooperative scattering by cold atoms, *J. Mod. Opt.* **58**, 1942 (2011).
- [32] M. O. Araújo, W. Guerin, and R. Kaiser, Decay dynamics in the coupled-dipole model, *J. Mod. Opt.* **65**, 1345 (2018).
- [33] This problem affects the results presented in Fig. 3 of Ref. [26].
- [34] G. Labeyrie, E. Vaujour, C. A. Müller, D. Delande, C. Miniatura, D. Wilkowski, and R. Kaiser, Slow Diffusion of Light in a Cold Atomic Cloud, *Phys. Rev. Lett.* **91**, 223904 (2003).
- [35] Q. Baudouin, R. Pierrat, A. Eloy, E. J. Nunes-Pereira, P.-A. Cuniasse, N. Mercadier, and R. Kaiser, Signatures of Lévy flights with annealed disorder, *Phys. Rev. E* **90**, 052114 (2014).
- [36] O. Katz and O. Firstenberg, Light storage for one second in room-temperature alkali vapor, *Nat. Commun.* **9**, 2074 (2018).
- [37] J. Guo, X. Feng, P. Yang, Z. Yu, L. Q. Chen, C.-H. Yuan, and W. Zhang, High-performance Raman quantum memory with optimal control in room temperature atoms, *Nat. Commun.* **9**, 148 (2019).
- [38] N. Cherroret, M. Hemmerling, V. Nador, J. T. M. Walraven, and R. Kaiser, Robust Coherent Transport of Light in Multilevel Hot Atomic Vapors, *Phys. Rev. Lett.* **122**, 183203 (2019).

Note that another, complementary work has been performed by Kuraptsev & Sokolov on the effect of atomic motion on the long-lived state in the dense regime and probed near resonance. In that case, corresponding to radiation trapping and Anderson-localized modes, they find that atomic motion can be detrimental [Kuraptsev 2020].

VI.2. Observation of superradiance off axis

In the subradiance data we also looked at the decay at early time, just after the switch-off, and observed that the initial decay rate could be faster than Γ_0 . This was a bit surprising because in the recent literature about single-photon superradiance, the superradiant decay was always associated to the timed-Dicke (TD) state, whose emission diagram is mainly a forward lobe. Indeed, the decay rate of the TD state for a Gaussian cloud is [Courteille 2010]

$$\Gamma_{\text{TD}} = \left(1 + \frac{b_0}{8}\right) \Gamma_0, \quad (\text{VI.1})$$

where $b_0 = \sqrt{2\pi}\sigma_0\rho_0R$ is the resonant optical thickness at the center of the cloud (σ_0 is the resonant scattering cross-section³, ρ_0 is the peak density at the center and R is the rms width) and some authors attributed the b_0 enhancement term to the forward lobe and the 1 to the incoherent scattering off axis, which is never completely suppressed because of the finite size of the scattering medium.⁴

As shown numerically and experimentally in the following paper [Araújo 2016], this vision is not correct. On the contrary, when the driving field is detuned enough to fulfill the TD approximation, the decay rate off axis is even more superradiant than the one in the forward lobe.

In the subradiance data the superradiant decay was hardly visible because the switch-off was not fast enough. To acquire a new series of data devoted to superradiance, we changed our switch-off setup and replaced the ‘fast AOM’ by an electro-optical modulator (EOM) driven by a pulse generator. The setup is detailed in Michelle Araújo’s PhD thesis [Araújo 2018a]. We could reach a falltime of about 3 ns, and observed superradiant decay rates up to $\sim 6\Gamma_0$.

The paper [Araújo 2016] was published simultaneously to a complementary one by the group of Mark Havey, where they report the study of the superradiant decay rate in the forward lobe [Roof 2016]. These are, to my knowledge, the first experiments on superradiance in the linear-optics regime.

³ For a closed transition, $\sigma_0 = 3\lambda^2/(2\pi)$, which is the commonly-used value. However, in the *scalar* CD model, the scattering cross section is actually λ^2/π , which led to some confusion in the first papers of the group, in which the optical thickness was erroneously defined as $3N/(kR)^2$ instead of $2N/(kR)^2$ (correspondingly, the enhancement factor was given as $b_0/12$ instead of $b_0/8$) [Courteille 2010, Bienaimé 2010, Bienaimé 2011b, Bienaimé 2012, Bienaimé 2013]. This has been corrected in [Bienaimé 2014]. Moreover, in the experiment, we don’t have a closed transition because of the Zeeman degeneracy. The usual method is to suppose that all Zeeman states are equipopulated, which gives, in the case of the $|2\rangle \rightarrow |3'\rangle$ transition of ^{87}Rb , an extra factor $\mathcal{C} = 7/15$. Since the influence of the Zeeman degeneracy on super- and subradiance is not really known, by convention and for consistency with previous papers, we defined $b_0 = 3N/(kR)^2$ as the ‘cooperativity parameter’, noting that the true optical thickness was $\mathcal{C} \times b_0$ in the experiment and $2b_0/3$ in the CD simulations [Guerin 2016a, Araújo 2016, Weiss 2018, Weiss 2019].

⁴ I can’t find the reference any more but I’m pretty sure I’ve read that somewhere.

Superradiance in a Large and Dilute Cloud of Cold Atoms in the Linear-Optics Regime

Michelle O. Araújo,^{1,2} Ivor Krešić,³ Robin Kaiser,¹ and William Guerin^{1,*}

¹Université Côte d'Azur, CNRS, INLN, 06560 Valbonne, France

²CAPES Foundation, Ministry of Education of Brazil, Brasília, DF 70040-020, Brazil

³SUPA and Department of Physics, University of Strathclyde, Glasgow G4 0NG, Scotland, United Kingdom

(Received 22 March 2016; published 10 August 2016)

Superradiance has been extensively studied in the 1970s and 1980s in the regime of superfluorescence, where a large number of atoms are initially excited. Cooperative scattering in the linear-optics regime, or “single-photon superradiance,” has been investigated much more recently, and superradiant decay has also been predicted, even for a spherical sample of large extent and low density, where the distance between atoms is much larger than the wavelength. Here, we demonstrate this effect experimentally by directly measuring the decay rate of the off-axis fluorescence of a large and dilute cloud of cold rubidium atoms after the sudden switch off of a low-intensity laser driving the atomic transition. We show that, at large detuning, the decay rate increases with the on-resonance optical depth. In contrast to forward scattering, the superradiant decay of off-axis fluorescence is suppressed near resonance due to attenuation and multiple-scattering effects.

DOI: 10.1103/PhysRevLett.117.073002

In his classic paper on coherence in spontaneous radiation by atomic samples [1], Dicke showed that a collection of identical excited atoms could synchronize to emit light coherently. In the case initially envisioned by Dicke, an atomic sample of size small compared to the wavelength of the transition, superradiance can be interpreted as the spontaneous synchronization of the radiation by all atoms and can be understood by the buildup of a giant dipole corresponding to the symmetric superposition of atomic states. Since it is difficult to prepare such dense and small samples, and since near-field dipole-dipole interaction may in fact prevent superradiance at high density [2], experimental studies of superradiance in the 1970s and 1980s were realized with large-size samples (mainly pencil shaped) of low density [3,4]. In this regime, superradiance, more precisely called superfluorescence [5,6], is intrinsically a nonlinear optical process.

More recently, it has been pointed out that a single photon, first absorbed by one atom among N others in a sample of large size and low density, would be spontaneously emitted in the direction of the initial photon wave vector [7], in contrast with the simple picture of isotropic spontaneous emission. This coherent forward scattering, which has been observed very recently [8], can be explained by a phase-matching condition, and thus does not rely on dipole-dipole interactions. This extended-volume regime was already mentioned by Dicke [1] and was further developed by others [9,10].

A less obvious result, which does rely on the long-range, light-induced dipole-dipole interactions between atoms, is the decay rate Γ_N of the corresponding collective excited state, which has been computed by many authors [9–17],

$$\Gamma_N = C \frac{N}{(kR)^2} \Gamma, \quad (1)$$

where Γ^{-1} is the lifetime of the excited state of a single-atom in vacuum, N is the number of atoms, $k = 2\pi/\lambda$ is the wave vector associated with the optical transition, R is the radius of the sample, and C is a numerical factor on the order of unity, which depends on the precise geometry of the sample. If the number of atoms is sufficiently large, one can have $\Gamma_N \gg \Gamma$, corresponding to a superradiant decay, even at low spatial density, where the separation between atoms is much larger than the wavelength. This is in contrast with the case of two particles [18–20], for which the single-atom decay rate is recovered for an atomic separation larger than λ . This “single-photon superradiance” has attracted a lot of attention in the last years [21–23], but direct experimental evidence has been limited to special geometries involving cavities or waveguides [24,25] or to multilevel schemes [26,27]. Related phenomena are optical precursors [28,29] or “flash” [30–32], which can also have a temporal dynamic faster than Γ . Since these effects come from the interference between the scattered field and the driving field, they are only visible in the forward direction and can be explained by the transient response of the complex refractive index of the gas.

On the contrary, light emission at different angles (“off-axis scattering” or “fluorescence”) cannot be explained by a phase-matching condition imposed by the initial laser field or a continuous-medium description [33]. Recently, we have used off-axis scattering to observe subradiance [34,35]. In this Letter, we present the direct observation of the superradiant decay of the fluorescence emitted in free space by a large spherical sample of cold atoms, which is continuously driven by a low-intensity laser that is abruptly switched off.

A true single-photon source is indeed not necessary to observe single-photon superradiance. As stressed by Prasad

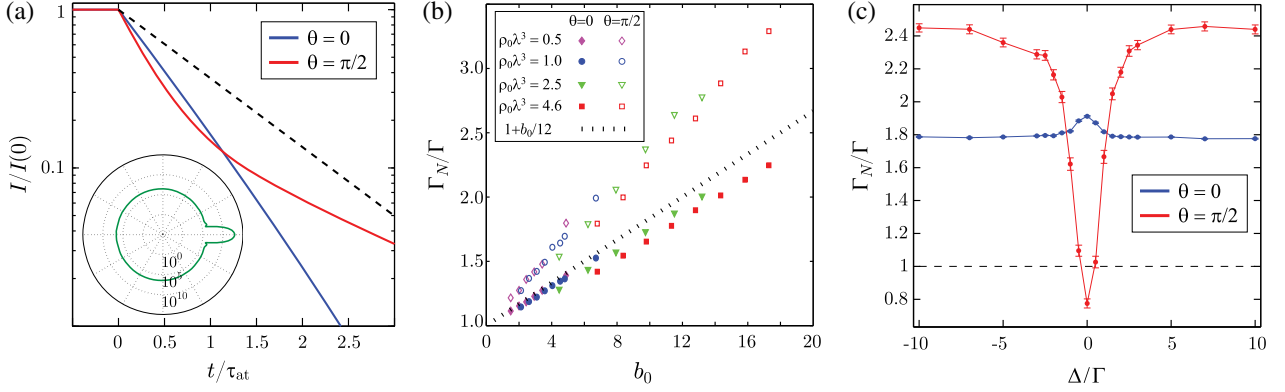


FIG. 1. Numerical study of the initial collective decay rate Γ_N . (a) Temporal evolution of the fluorescence after the switch off of the driving laser at $t = 0$, with $b_0 = 11.3$, $\rho_0\lambda^3 = 4.6$, $\Delta = 10\Gamma$, averaged over 50 configurations, for two different angles, in the forward direction $\theta = 0^\circ$ and at 90° ($\theta = \pi/2$). The amplitude is normalized to the steady-state amplitude, which is much larger for $\theta = 0^\circ$ as shown in the emission diagram (inset, in log scale). The time axis is normalized to the lifetime of the excited state $\tau_{\text{at}} = \Gamma^{-1} \approx 26$ ns. An exponential fit in the range $0 < t/\tau_{\text{at}} \leq 0.2$ allows us to extract the initial decay rate Γ_N . At late time, the decay becomes subradiant [34,35]. The dashed line shows the decay expected for a single atom (rate Γ). (b) Decay rate as a function of the resonant optical thickness $b_0 = 3N/(kR)^2$ for different densities (ρ_0 is the density at the center of the cloud). Filled symbols are for $\theta = 0^\circ$ and open symbols for $\theta = \pi/2$. The increase is mainly linear in b_0 . The slope of the linear increase slightly depends on the angle. The dotted line shows the expectation for the decay of the timed-Dicke state [Eq. (4)]. (c) Decay rate as a function of the detuning, for $b_0 = 17$, $\rho_0\lambda^3 = 4.6$, and detection angles $\theta = 0, \pi/2$. Off-axis superradiance is suppressed near resonance. The error bars shown in panel (c) and omitted in panel (b) for clarity correspond to the 95% confidence interval for the exponential fit of the decay rate.

and Glauber [16], it is the spatially extended initial coherence, not entanglement *per se*, that is fundamentally responsible for cooperative radiation processes such as superradiance and subradiance (see also Refs. [36–38]), so that continuous driving by a low-intensity laser (compared to the saturation intensity of the atomic transition) can also be used to study these effects [14,15]. Similarly, it has been shown that the full quantum problem is equivalent, in the linear-optics regime, to classical coupled dipoles [39,40].

Before turning to the experimental results, we use the coupled-dipole model to illustrate the qualitative differences between forward and off-axis scattering. We consider a sample of N motionless two-level atoms distributed over a 3D Gaussian atomic density distribution of rms radius R , illuminated along the z axis by a plane wave (wave vector $\mathbf{k}_0 = k\hat{z}$) with detuning $\Delta = \omega - \omega_0$ and Rabi frequency $\Omega \ll \Gamma$. In the low-intensity limit, using the Markov approximation, the linear response of this many-body system can be simulated by N coupled-dipole equations [14,38]

$$\dot{\beta}_i = \left(i\Delta - \frac{\Gamma}{2} \right) \beta_i - \frac{i\Omega}{2} e^{ik_0 r_i} + \frac{i\Gamma}{2} \sum_{i \neq j} V_{ij} \beta_j, \quad (2)$$

where β_i is the amplitude of the single-excited-atom state $|i\rangle = |g \cdots e_i \cdots g\rangle$ and

$$V_{ij} = \frac{e^{ikr_{ij}}}{kr_{ij}}, \quad r_{ij} = |\mathbf{r}_i - \mathbf{r}_j|, \quad (3)$$

describes the light-induced dipole-dipole interaction in the scalar approximation, neglecting near-field terms and

polarization effects, which is a good approximation for our dilute samples [41,42]. The first term of the rhs of Eq. (2) corresponds to the natural evolution of the dipoles (oscillation and damping), the second one corresponds to the driving by the external laser, and the last one, the dipole-dipole interaction term, is responsible for cooperative effects.

Numerically solving these equations allows us to compute the emission diagram [38] as well as the temporal decay after switching off the driving term [34,35]. By fitting the initial decay just after the switch off, we can study how the collective decay rate Γ_N depends on the emission direction, on the resonant optical depth $b_0 = 3N/(kR)^2$ [43], and on the detuning Δ . Note that the atom number is limited to a few thousands in the simulations and that the complex Zeeman structure of rubidium atoms is not taken into account, so that a quantitative agreement with the experiment is not expected.

The main results of the numerical study are reported in Fig. 1. At large detuning, the steady state reached before switch off tends to the “driven timed-Dicke state” [7,14,23], in which all atoms have the same excitation probability. As for a collection of independent atoms, the emission diagram is mainly forward directed for large b_0 [inset of Fig. 1(a)], but it also contains a non-negligible quasi-isotropic background, which is neglected in the continuous-medium approach used in Refs. [11–16]. It has also been shown in Ref. [38] that this collective state decays with an initial rate

$$\Gamma_N = \left(1 + \frac{b_0}{12} \right) \Gamma \quad (4)$$

for a Gaussian atomic distribution, which is consistent with the scaling of Eq. (1) for very large b_0 and with the single-atom limit for small b_0 . We observe this scaling in Fig. 1(b). The slope for the forward scattered light ($\theta = 0$) is very close to the one predicted by Eq. (4) because forward scattering is the most important contribution. Moreover, maybe surprisingly, the light scattered off axis exhibits superradiant decay as well [44], with a similar linear scaling with b_0 , the slope being slightly modified by the angle difference [Figs. 1(a) and 1(b)]. Superradiance is thus also visible, and even with a faster decay rate, in the off-axis scattering.

In an experiment, it is hard to use a very large detuning because it obviously decreases the amount of fluorescence. In practice, using a moderate detuning contributes to populate other states than the timed-Dicke state [23], essentially because of the exponential attenuation of the driving field inside the cloud. This contributes to populate longer-lived states, which can be interpreted as subradiant states at large or moderate detuning [35] or simply as radiation trapping due to multiple scattering near resonance [45]. We thus expect that the superradiant decay is suppressed near resonance. This is what we observe in the numerical results of Fig. 1(c) for off-axis scattering. The behavior of forward scattering is different because it is related to the transient response of the refractive index. As shown in Ref. [32], it is slightly faster on resonance. These qualitatively different behaviors of forward and off-axis scattering emphasize that the two are different physical mechanisms. Although this is almost never stated clearly, the forward lobe seen in Fig. 1(a) and discussed in many papers (see, e.g., Refs. [8,12,14,46]) should indeed be seen as diffracted and refracted light more than scattered light.

Let us now turn to our experimental observation of superradiance. In our experiment, we load $N \approx 10^9$ ^{87}Rb atoms from a background vapor into a magneto-optical trap (MOT) for 50 ms. A compressed MOT (30 ms) period allows for an increased and smooth spatial density with a Gaussian distribution of rms radius $R \approx 1$ mm (typical density $\rho \approx 10^{11}$ cm^{-3}) and a reduced temperature $T \approx 50$ μK . We then switch off the MOT trapping beams and magnetic field gradient and allow for 3 ms of free expansion, used to optically pump all atoms into the upper hyperfine ground state $F = 2$. Next, we apply a series of 12 pulses of a weak probe beam (waist $w = 5.7$ mm), linearly polarized and detuned by Δ from the closed atomic transition $F = 2 \rightarrow F' = 3$ ($\lambda = 780.24$ nm and $\Gamma/2\pi = 6.07$ MHz). When we varied the detuning, we also varied the laser intensity accordingly in order to keep the saturation parameter approximately constant at $s \approx (2.2 \pm 0.6) \times 10^{-2}$. The pulses of duration 30 μs and separated by 1 ms are obtained by an electro-optical modulator (EOM, fibered Mach-Zehnder intensity modulator by Eospace, Ref. AZ-0K5-10-PFU-SFU-780) with a 90%-10% falltime of about 3 ns (Fig. 2). It is driven by a

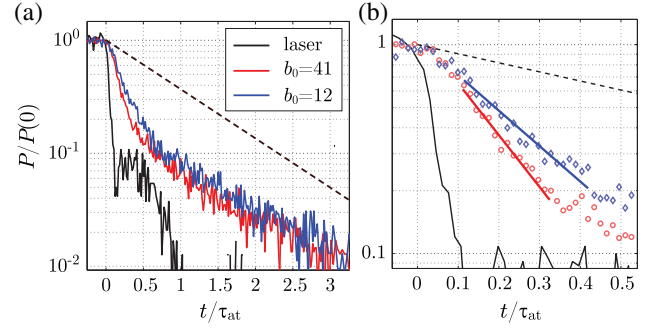


FIG. 2. (a) Decay of the measured fluorescence power P after switching off the probe laser for two different b_0 (red and blue solid lines) at a given detuning $\Delta = -6\Gamma$. The vertical axis is normalized to the steady-state fluorescence level. The dashed line shows the expected decay for a single atom, $e^{-t/\tau_{\text{at}}}$, and the black solid line is the switch off of the laser (the fast part with a poor extinction ratio is due to the EOM and the slower part is due to the AOM). (b) Same data at shorter time scales, with the exponential fit of the initial decay that allows us to measure Γ_N .

pulse generator (DG535 by SRS) and actively locked to avoid any drift of the working point. In order to improve the extinction ratio, we also use an acousto-optical modulator (AOM) in series with the EOM. Between subsequent pulses of each series, the size of the cloud increases because of thermal expansion, and the atom number decreases due to off resonant optical pumping into the $F = 1$ hyperfine state during each pulse, which allows us to realize different optical depths within one series of pulses. After this stage of expansion and measurement, the MOT is switched on again and most of the atoms are recaptured. The complete cycle is thus short enough to allow the signal integration over a large number of cycles, typically $\sim 500\,000$. The fluorescence is collected by a lens with a solid angle of $\sim 5 \times 10^{-2}$ sr at $\theta \approx 35^\circ$ from the incident direction of the laser beam and detected by a photomultiplier (Hamamatsu HPM R10467U-50). The signal is then recorded on a multichannel scaler (MCS6A by FAST ComTec) with a time bin of 0.4 ns, averaging over the cycles. The cooperativity parameter b_0 corresponding to each pulse is calibrated by an independent measurement of the atom number, cloud size, and temperature using absorption imaging (see the Supplemental Material of Ref. [35]).

We show in Fig. 2 examples of the measured fluorescence decay for different values of b_0 and a fixed detuning $\Delta = -6\Gamma$. We clearly see that the decay is much faster than the single-atom decay, in contrast to the behavior of collective incoherent scattering effects such as radiation trapping [45]. This fast decay rate increases with b_0 , in line with the expected superradiant behavior. From these data we can fit the initial decay by an exponential and extract the collective decay rate. The fitting procedure has been chosen as follows. The range of the fit starts at $t/\tau_{\text{at}} = 0.1$, when the probe laser intensity has decayed to 10% of its initial value. It ends when the measured signal arrives at 20% of

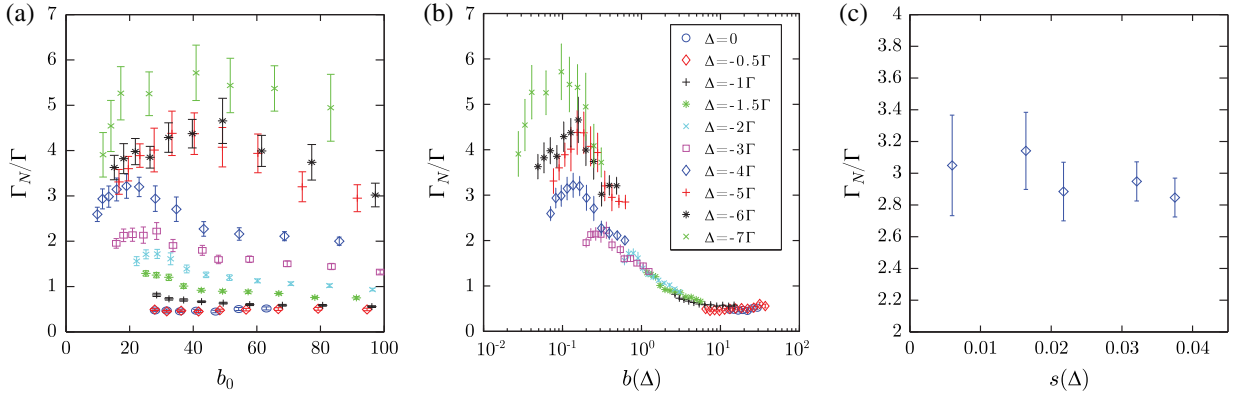


FIG. 3. Experimental study of the initial collective decay rate Γ_N . (a) Systematic analysis of Γ_N as a function of the resonance optical thickness b_0 and the detuning Δ . (b) Same data shown as a function of $b(\Delta)$. When $b(\Delta) \gtrsim 1$, it becomes the scaling parameter. (c) Γ_N as a function of the saturation parameter $s(\Delta)$, for $b_0 = 21 \pm 1$ and $\Delta = -4\Gamma$. In all panels, the error bars represent the 95% confidence interval of the fit.

its initial value or when the background light scattered from the hot Rb vapor in the vacuum chamber is at this level. This background light decays like $e^{-t/\tau_{\text{at}}}$ [well visible in Fig. 2 for $P/P(0) < 10^{-1}$] and has a relative weight that depends on the atom number and the detuning (it is negligible on resonance with the cold atoms and becomes important far from resonance) and which is independently calibrated for each measurement. Finally, when the number of points in the fitting range is less than 15, or when the statistical coefficient of determination of the fit R^2 is less than 0.85, the data are discarded.

The systematic study of the collective decay rate Γ_N as a function of the resonant optical thickness b_0 and the detuning Δ is presented in Fig. 3(a). The increase with b_0 is well visible, especially at large detuning, up to a maximum value $\Gamma_{\text{max}} \sim 5\Gamma - 6\Gamma$, well above the decay rate of independent atoms. We note that the curves acquired for different detunings do not collapse on a single curve, contrary to what has been observed for superradiance [35], showing the sensitivity of superradiance to the proximity of the resonance. Indeed, the decay rates measured for small detunings do not exhibit superradiance, and even at moderate detuning, the decay rate starts to decrease at high b_0 , when the actual optical thickness

$$b(\Delta) = g \frac{b_0}{1 + 4\Delta^2/\Gamma^2} \quad (5)$$

is on the order of 1 or higher (here $g = 7/15$ is the relative strength of the transition for a statistical mixture of Zeeman states). We show indeed in Fig. 3(b) that $b(\Delta)$ becomes the relevant parameter in this regime. These observations are perfectly consistent with the expectation of the coupled-dipole model [Fig. 1(c)] and with the intuition that collective superradiant states are less populated if the driving field is attenuated inside the sample [23].

Finally, we checked that the results are independent of the intensity (or the saturation parameter) to confirm that

the experiments have been done in the linear-optics regime. For this we varied the intensity I of the probe beam at fixed detuning and b_0 , and we report in Fig. 3(c) the decay rate as a function of the saturation parameter

$$s(\Delta) = g \frac{I/I_{\text{sat}}}{1 + 4\Delta^2/\Gamma^2} \quad (6)$$

with $I_{\text{sat}} = 1.6 \text{ mW/cm}^2$ the saturation intensity. We observe no significant variation of Γ_N with the saturation parameter in the explored range $s < 0.04$.

In summary, we have reported the first observation of superradiant decay in free space (without a cavity) in the low-intensity regime, using the fluorescence (off-axis scattering) of a cold-atom cloud. We have shown that at large detuning, the decay rate increases with the resonant optical depth, but it is suppressed near resonance. These observations are consistent with numerical solutions of coupled-dipole equations in the dilute limit. The shortening of the radiative lifetime due to cooperativity is potentially important to a number of areas, such as the diagnostics of ultracold gases [47,48], quantum memories [27,49], optical clocks [8,50,51], ultranarrow lasers [52], photon-pair sources [26], and light-harvesting systems [53,54].

To conclude, let us notice that in Dicke superfluorescence [3], in optical precursors (or flash) [32], as well as in the experiment reported here dealing with low-saturation fluorescence, the time scales associated with the transient regimes are always governed by the same cooperativity parameter, the resonant optical depth. These three phenomena can be related to stimulated emission, the refractive index, and spontaneous emission, respectively, and are thus different facets of light-atom interaction. It is interesting, and also beautiful, to see that they exhibit cooperativity in a similar way. On the other hand, other collective properties, such as the cw susceptibility (including the refractive index, the linear attenuation coefficient or gain coefficient for

inverted systems, the Lorentz-Lorenz shift [55], and beyond mean-field corrections [56,57]) and weak-localization corrections to diffusive transport [58], are governed by the atomic density. The fundamental difference is that the latter are properties of the bulk material, which can be defined for an infinite medium. Transient phenomena, on the contrary, involve light escaping from the sample, in which case the finite size of the medium and the finite number of atoms are necessarily key parameters [59].

We thank R. Bachelard and N. Piovella for fruitful discussions. We acknowledge financial support from the CNRS international program, the French Agence National pour la Recherche (Project LOVE, No. ANR-14-CE26-0032), the Brazilian Coordenação de Aperfeiçoamento de Pessoal de Nível Superior (CAPES), the Brazilian Conselho Nacional de Desenvolvimento Científico e Tecnológico (CNPq, Project PVE, No. 303426/2014-4), and the European Research Executive Agency (Program COSCALI, No. PIRSES-GA-2010-268717). I. K. was supported by a University Studentship of the University of Strathclyde and the Leverhulme Trust.

Note added.—Recently, we have learned of a complementary experiment on superradiance in the forward direction; see Ref. [60].

*william.guerin@inln.cnrs.fr

- [1] R. H. Dicke, *Phys. Rev.* **93**, 99 (1954).
- [2] R. Friedberg and S. R. Hartmann, *Phys. Rev. A* **10**, 1728 (1974).
- [3] M. S. Feld and J. C. MacGillivray, in *Coherent Nonlinear Optics. Recent Advances*, edited by M. S. Feld and V. S. Letokhov, Topics in Current Physics Vol. 21 (Springer, Berlin, 1980), pp. 7–57.
- [4] M. Gross and S. Haroche, *Phys. Rep.* **93**, 301 (1982).
- [5] R. Bonifacio and L. A. Lugiato, *Phys. Rev. A* **11**, 1507 (1975).
- [6] M. S. Malcuit, J. J. Maki, D. J. Simkin, and R. W. Boyd, *Phys. Rev. Lett.* **59**, 1189 (1987).
- [7] M. O. Scully, E. S. Fry, C. H. Raymond Ooi, and K. Wódkiewicz, *Phys. Rev. Lett.* **96**, 010501 (2006).
- [8] S. L. Bromley, B. Zhu, M. Bishof, X. Zhang, T. Bothwell, J. Schachenmayer, T. L. Nicholson, R. Kaiser, S. F. Yelin, M. D. Lukin, A. M. Rey, and J. Ye, *Nat. Commun.* **7**, 11039 (2016).
- [9] F. T. Arecchi and E. Courtens, *Phys. Rev. A* **2**, 1730 (1970).
- [10] N. E. Rehler and J. H. Eberly, *Phys. Rev. A* **3**, 1735 (1971).
- [11] I. E. Mazets and G. Kurizki, *J. Phys. B* **40**, F105 (2007).
- [12] A. A. Svidzinsky, J.-T. Chang, and M. O. Scully, *Phys. Rev. Lett.* **100**, 160504 (2008).
- [13] A. Svidzinsky and J.-T. Chang, *Phys. Rev. A* **77**, 043833 (2008).
- [14] P. W. Courteille, S. Bux, E. Lucioni, K. Lauber, T. Bienaimé, R. Kaiser, and N. Piovella, *Eur. Phys. J. D* **58**, 69 (2010).
- [15] R. Friedberg and J. T. Manassah, *Phys. Lett. A* **374**, 1648 (2010).
- [16] S. Prasad and R. J. Glauber, *Phys. Rev. A* **82**, 063805 (2010).
- [17] S. E. Skipetrov and A. Goetschy, *J. Phys. A* **44**, 065102 (2011).
- [18] R. G. DeVoe and R. G. Brewer, *Phys. Rev. Lett.* **76**, 2049 (1996).
- [19] M. D. Barnes, P. S. Krstic, P. Kumar, A. Mehta, and J. C. Wells, *Phys. Rev. B* **71**, 241303 (2005).
- [20] B. H. McGuyer, M. McDonald, G. Z. Iwata, M. G. Tarallo, W. Skomorowski, R. Moszynski, and T. Zelevinsky, *Nat. Phys.* **11**, 32 (2015).
- [21] M. O. Scully and A. A. Svidzinsky, *Science* **325**, 1510 (2009).
- [22] J. T. Manassah, *Adv. Opt. Photonics* **4**, 108 (2012).
- [23] T. Bienaimé, R. Bachelard, P. W. Courteille, N. Piovella, and R. Kaiser, *Fortschr. Phys.* **61**, 377 (2013).
- [24] R. Röhlsberger, K. Schlage, B. Sahoo, S. Couet, and R. Ruffer, *Science* **328**, 1248 (2010).
- [25] A. Goban, C.-L. Hung, J. D. Hood, S.-P. Yu, J. A. Muniz, O. Painter, and H. J. Kimble, *Phys. Rev. Lett.* **115**, 063601 (2015).
- [26] B. Srivathsan, G. K. Gulati, B. Chng, G. Maslennikov, D. Matsukevich, and C. Kurtsiefer, *Phys. Rev. Lett.* **111**, 123602 (2013).
- [27] R. A. de Oliveira, M. S. Mendes, W. S. Martins, P. L. Saldanha, J. W. R. Tabosa, and D. Felinto, *Phys. Rev. A* **90**, 023848 (2014).
- [28] H. Jeong, A. M. C. Dawes, and D. J. Gauthier, *Phys. Rev. Lett.* **96**, 143901 (2006).
- [29] J. F. Chen, S. Wang, D. Wei, M. M. T. Loy, G. K. L. Wong, and S. Du, *Phys. Rev. A* **81**, 033844 (2010).
- [30] M. Chalony, R. Pierrat, D. Delande, and D. Wilkowski, *Phys. Rev. A* **84**, 011401(R) (2011).
- [31] C. C. Kwong, T. Yang, M. S. Pramod, K. Pandey, D. Delande, R. Pierrat, and D. Wilkowski, *Phys. Rev. Lett.* **113**, 223601 (2014).
- [32] C. C. Kwong, T. Yang, D. Delande, R. Pierrat, and D. Wilkowski, *Phys. Rev. Lett.* **115**, 223601 (2015).
- [33] R. Bachelard, P. W. Courteille, R. Kaiser, and N. Piovella, *Europhys. Lett.* **97**, 14004 (2012).
- [34] T. Bienaimé, N. Piovella, and R. Kaiser, *Phys. Rev. Lett.* **108**, 123602 (2012).
- [35] W. Guerin, M. O. Araújo, and R. Kaiser, *Phys. Rev. Lett.* **116**, 083601 (2016).
- [36] J. H. Eberly, *J. Phys. B* **39**, S599 (2006).
- [37] R. Friedberg and J. T. Manassah, *Laser Phys. Lett.* **4**, 900 (2007).
- [38] T. Bienaimé, M. Petruzzo, D. Bigerni, N. Piovella, and R. Kaiser, *J. Mod. Opt.* **58**, 1942 (2011).
- [39] J. Javanainen, J. Ruostekoski, B. Vestergaard, and M. R. Francis, *Phys. Rev. A* **59**, 649 (1999).
- [40] A. A. Svidzinsky, J.-T. Chang, and M. O. Scully, *Phys. Rev. A* **81**, 053821 (2010).
- [41] S. E. Skipetrov and I. M. Sokolov, *Phys. Rev. Lett.* **112**, 023905 (2014).
- [42] L. Bellando, A. Gero, E. Akkermans, and R. Kaiser, *Phys. Rev. A* **90**, 063822 (2014).

- [43] We use here the definition of b_0 corresponding to a vectorial model for light, even if the actual optical thickness in the scalar model is given by $2N/(kR)^2 = 2b_0/3$.
- [44] A similar numerical observation has been recently reported in a slightly different configuration; see S. E. Skipetrov, I. M. Sokolov, and M. D. Havey, *Phys. Rev. A* **94**, 013825 (2016).
- [45] G. Labeyrie, E. Vaujour, C. A. Müller, D. Delande, C. Miniatura, D. Wilkowski, and R. Kaiser, *Phys. Rev. Lett.* **91**, 223904 (2003).
- [46] J. Chabé, M. T. Rouabah, L. Bellando, T. Bienaimé, N. Piovella, R. Bachelard, and R. Kaiser, *Phys. Rev. A* **89**, 043833 (2014).
- [47] L. Chomaz, L. Corman, T. Yefsah, R. Desbuquois, and J. Dalibard, *New J. Phys.* **14**, 055001 (2012).
- [48] P. C. Bons, R. de Haas, D. de Jong, A. Groot, and P. van der Straten, *Phys. Rev. Lett.* **116**, 173602 (2016).
- [49] A. Walther, A. Amari, S. Kröll, and A. Kalachev, *Phys. Rev. A* **80**, 012317 (2009).
- [50] D. E. Chang, J. Ye, and M. D. Lukin, *Phys. Rev. A* **69**, 023810 (2004).
- [51] S. Okaba, T. Takano, F. Benabid, T. Bradley, L. Vincetti, Z. Maizelis, V. Yampol'skii, F. Nori, and H. Katori, *Nat. Commun.* **5**, 4096 (2014).
- [52] J. G. Bohnet, Z. Chen, J. M. Weiner, D. Meiser, M. J. Holland, and J. K. Thompson, *Nature (London)* **484**, 78 (2012).
- [53] R. Monshouwer, M. Abrahamsson, F. van Mourik, and R. van Grondelle, *J. Phys. Chem. B* **101**, 7241 (1997).
- [54] G. L. Celardo, G. G. Giusteri, and F. Borgonovi, *Phys. Rev. B* **90**, 075113 (2014).
- [55] R. Friedberg, S. R. Hartmann, and J. T. Manassah, *Phys. Rep.* **7**, 101 (1973).
- [56] J. Javanainen and J. Ruostekoski, *Opt. Express* **24**, 993 (2016).
- [57] S. Jennewein, M. Besbes, N. J. Schilder, S. D. Jenkins, C. Sauvan, J. Ruostekoski, J.-J. Greffet, Y. R. P. Sortais, and A. Browaeys, *Phys. Rev. Lett.* **116**, 233601 (2016).
- [58] M. C. W. van Rossum and T. M. Nieuwenhuizen, *Rev. Mod. Phys.* **71**, 313 (1999).
- [59] W. Guerin, M. T. Rouabah, and R. Kaiser, *J. Mod. Opt.*, doi: 10.1080/09500340.2016.1215564 (2016).
- [60] S. J. Roof, K. J. Kemp, M. D. Havey, I. M. Sokolov, following Letter, *Phys. Rev. Lett.* **117**, 073003 (2016).

VI.3. Population of the collective modes

At this point some observations can seem puzzling. In [Guerin 2016a] we observed that subradiance is enhanced near resonance (the lifetime is the same but the relative amplitude of long-lived modes is higher), while on the contrary, in [Araújo 2016] we observed that superradiance off axis is suppressed. How to understand that?

More generally, how can we understand the role of the detuning? Actually, even before those observations, since I started to think about these subjects, I was puzzled by the ‘problem’ of the detuning, which is the following: in the CD equations (see one of the previous papers), the detuning is present in the driving term but not in the dipole-dipole interaction term, although this term is responsible for *all* collective effects, the trivial ones (attenuation and refractive index) and the nontrivial ones like multiple scattering and super/subradiance. Most of these effects obviously depend on the detuning. Even, the very existence of cooperative effects like super/subradiance at very large detuning is not intuitive. Moreover, many numerical studies of collective effects in light-atom interaction are based on the analysis of the eigenvalues and eigenvectors of an effective Hamiltonian (in particular for the problem of Anderson localization [Rusek 1996, Rusek 2000, Pinheiro 2004, Skipetrov 2014, Bellando 2014, Skipetrov 2015, Máximo 2015, Skipetrov 2016]), and the detuning does not appear in this approach (the effective Hamiltonian is our dipole-dipole interaction matrix). At the same time, collective modes, for instance long-lived ones, may be given different interpretations depending on the detuning used to drive the system: radiation trapping near resonance or subradiance far from resonance.

Clearly there is something missing. The missing ingredient is the *population* of the different collective modes, which depends on how the system is driven, in particular on the detuning. One can even find a simple analytical expression for this dependence and understand many things by examining the consequences of this relation [Guerin 2017b].

Maybe these results are obvious, but when I obtained them it was enlightening for me! Note that I actually did that in December 2014, such that I *predicted* that subradiance would be higher and superradiance suppressed near resonance. It was very satisfying when the experiment confirmed. I wrote the paper later. The paper [Guerin 2017b], reproduced below, also addresses the spatial properties of the collective modes and suggests a difference between the collective modes responsible for radiation trapping and the ones responsible for subradiance, the latter being more extended.

Population of collective modes in light scattering by many atoms

William Guerin* and Robin Kaiser

Université Côte d'Azur, CNRS, Institut de Physique de Nice, France

(Received 1 February 2017; published 26 May 2017)

The interaction of light with an atomic sample containing a large number of particles gives rise to many collective (or cooperative) effects, such as multiple scattering, superradiance, and subradiance, even if the atomic density is low and the incident optical intensity weak (linear optics regime). Tracing over the degrees of freedom of the light field, the system can be well described by an effective atomic Hamiltonian, which contains the light-mediated dipole-dipole interaction between atoms. This long-range interaction is at the origin of the various collective effects, or of collective excitation modes of the system. Even though an analysis of the eigenvalues and eigenfunctions of these collective modes does allow distinguishing superradiant modes, for instance, from other collective modes, this is not sufficient to understand the dynamics of a driven system, as not all collective modes are significantly populated. Here, we study how the excitation parameters, i.e., the driving field, determines the population of the collective modes. We investigate in particular the role of the laser detuning from the atomic transition, and demonstrate a simple relation between the detuning and the steady-state population of the modes. This relation allows understanding several properties of cooperative scattering, such as why superradiance and subradiance become independent of the detuning at large enough detuning without vanishing, and why superradiance, but not subradiance, is suppressed near resonance. We also show that the spatial properties of the collective modes allow distinguishing diffusive modes, responsible for radiation trapping, from subradiant modes.

DOI: [10.1103/PhysRevA.95.053865](https://doi.org/10.1103/PhysRevA.95.053865)

I. INTRODUCTION

Collective effects in light scattering by atomic ensembles are at the focus of intense research, both theoretically and experimentally [1]. Recently, the question of light localization in atomic media has been the subject of several studies based on an effective Hamiltonian approach [2–9]. From a total Hamiltonian describing a system of N atoms with at most one quantum of excitation (one photon), the degrees of freedom of the light field are traced over to get an effective non-Hermitian atomic Hamiltonian H_{eff} . In this approach, the eigenmodes and eigenvalues of H_{eff} are computed and analyzed. However, these quantities are not direct experimental observables, which makes the interpretation more difficult, in particular because the way the initial excitation entered the system is not specified. In a real experiment, the system is driven or excited by some external field and the outcome of the experiment depends on the parameters of this field.

Another, complementary approach has been used recently in the context of single-photon superradiance [10–13]: coupled-dipole equations (CDEs) [14,15]. This approach is based on the same effective Hamiltonian, but adding an external driving field is straightforward [16–18]. This describes the dynamics of the system in the low-intensity regime of excitation (linear optics) and allows computing experimental observables, such as the emission diagram [16,17], collective line shape and width [19–25], or the temporal dynamics of the scattered light [12,13,26–28].

The coupled-dipole equations including the external drive read

$$\dot{\beta}_i = \left(i\Delta - \frac{\Gamma_0}{2} \right) \beta_i - \frac{i\Omega(\mathbf{r})}{2} + \frac{i\Gamma_0}{2} \sum_{i \neq j} V_{ij}(r_{ij}) \beta_j, \quad (1)$$

where β_i is the amplitude of the single-excited-atom state $|i\rangle = |g \cdots e_i \cdots g\rangle$ with $|g\rangle$ ($|e\rangle$) denoting the ground (excited) state, Δ is the detuning of the driving field from the two-level atomic dipolar transition, $\Omega(\mathbf{r}) = -dE(\mathbf{r})/\hbar$ its complex Rabi frequency with $E(\mathbf{r})$ the driving electric field, Γ_0 the natural decay rate for a single excited atoms, and $V_{ij}(r_{ij})$ is the dipole-dipole interaction (DDI) between atoms i and j , which depends on their separation r_{ij} . For simplicity we will consider only the scalar model of the DDI, which is relevant at low density. We will also set $\Gamma_0 = 1$ and drop it in the following. The first term of Eq. (1) corresponds to the natural evolution of the dipoles (oscillation and damping), the second one to the driving by the external laser, and the last term corresponds to the DDI interaction.

In the CDEs, the detuning Δ of the driving field is taken into account, but all collective effects [1]—the trivial ones like the refractive index and the beam attenuation, as well as the nontrivial ones like multiple scattering and super- and subradiance—come from the DDI term, in which the detuning does not directly enter. Since many collective effects obviously depend on the detuning, this can seem puzzling. Moreover, the long-lived modes discussed in the effective Hamiltonian approach [5–8] may be given different interpretations depending on the detuning (e.g., radiation trapping near resonance [29], or subradiance far from resonance [27]), although the eigenmodes themselves do not depend on the detuning. Understanding the influence of the detuning is thus crucial to making the link between the CDE and the effective Hamiltonian approach.

In this paper, we study the influence of the detuning on the *populations* of the collective modes, a quantity that has been overlooked so far, except in very few works [30,31]. In Sec. II we derive a simple and intuitive analytical expression relating the steady-state mode populations and the detuning. Although the result [Eq. (9)] is well known, we show in Sec. III that it has interesting and nonobvious consequences. In

*william.guerin@inphyni.cnrs.fr

particular, it allows us to understand why cooperative effects such as super- and subradiance become independent of the detuning at large detuning and why superradiance vanishes near resonance but not subradiance. Those behaviors are not intuitive and have already been observed experimentally and numerically [12,26,27]. We also show that subradiance and radiation trapping [29] can be attributed to collective modes with different eigenvalues, an interpretation supported by an analysis of the spatial properties of the corresponding eigenmodes. Finally, in Sec. IV, we present a numerical analysis of the weighted average of the eigenvalues, which puts in evidence empirical scaling laws.

II. ANALYTICAL RESULT

Let us first write the CDEs [Eq. (1)] in a matrix form,

$$\dot{\mathbf{B}} = \mathbf{M} \times \mathbf{B} + \mathbf{\Omega}, \quad (2)$$

with $\mathbf{B} = [\beta_1, \dots, \beta_i, \dots, \beta_N]^T$, $\mathbf{\Omega} = -i/2 \times [\Omega(\mathbf{r}_1), \dots, \Omega(\mathbf{r}_i), \dots, \Omega(\mathbf{r}_N)]^T$, and

$$\mathbf{M} = \begin{bmatrix} -1/2 + i\Delta & \dots & V_{1,N} \\ V_{2,1} & \dots & V_{2,N} \\ \vdots & \ddots & \vdots \\ V_{N,1} & \dots & -1/2 + i\Delta \end{bmatrix}. \quad (3)$$

We note that the detuning Δ appears as a constant shift of the imaginary part of the diagonal elements of the coupling matrix \mathbf{M} . As a consequence, it corresponds to a constant shift of all eigenfrequencies and does not change the eigenvectors. That is the reason why its influence is not discussed in the effective Hamiltonian approach [2–9], in which $H_{\text{eff}} = i\hbar\mathbf{M}(\Delta = 0)$ is used, although the correct definition of H_{eff} should in principle include the detuning [32].

By definition, the eigenvalues λ_k and eigenvectors \mathbf{V}_k are such that $\mathbf{M} = \mathbf{D}\mathbf{V}\mathbf{V}^{-1}$ and $\mathbf{D} = \mathbf{V}^{-1}\mathbf{M}\mathbf{V}$, where $\mathbf{D} = \text{diag}(\lambda_1, \dots, \lambda_k, \dots, \lambda_N)$ and $\mathbf{V} = [\mathbf{V}_1, \dots, \mathbf{V}_k, \dots, \mathbf{V}_N]$.

Many experiments [12,27,29] consist of studying the dynamics of the system when it relaxes from the steady state to the ground state after the switch-off of the driving laser. This dynamics is then given by the natural evolution of each mode,

$$\mathbf{B}(t) = \sum_k \alpha_k \mathbf{V}_k e^{\lambda_k t}, \quad (4)$$

where the α_k are the complex coefficients of each mode, as given by the initial condition. In the case we consider here, the initial condition corresponds to the steady state reached when the driving laser is on. Let us call this steady state \mathbf{B}_0 . Obviously,

$$\mathbf{B}_0 = -\mathbf{M}^{-1}\mathbf{\Omega} = -(\mathbf{V}\mathbf{D}\mathbf{V}^{-1})^{-1}\mathbf{\Omega} = -\mathbf{V}\mathbf{D}^{-1}\mathbf{V}^{-1}\mathbf{\Omega}. \quad (5)$$

Let us also project the steady state \mathbf{B}_0 on the eigenmodes of the system, we have

$$\mathbf{B}_0 = \sum_k \alpha_k \mathbf{V}_k, \quad (6)$$

where the coefficients of the decomposition are

$$\boldsymbol{\alpha} = [\alpha_1, \dots, \alpha_k, \dots, \alpha_N]^T = \mathbf{V}^{-1}\mathbf{B}_0. \quad (7)$$

Using the expression (5) above for \mathbf{B}_0 , $\boldsymbol{\alpha} = -\mathbf{D}^{-1}\mathbf{V}^{-1}\mathbf{\Omega}$, and we obtain, using the fact that \mathbf{D} is diagonal,

$$\alpha_k = -\frac{(\mathbf{V}^{-1}\mathbf{\Omega})_k}{\lambda_k} = -\frac{P_k(\mathbf{\Omega})}{\lambda_k}, \quad (8)$$

where we note $P_k(\mathbf{\Omega})$ the k th coefficient of the decomposition of $\mathbf{\Omega}$ onto the basis made of all \mathbf{V}_k .

This relation is interesting because the weight of each eigenmode in the steady state appears as the product of two factors, one purely “geometrical,” $\mathbf{V}^{-1}\mathbf{\Omega}$, which is the projection of the driving field on the eigenmodes, independent of the detuning, and one purely “spectral,” the inverse of the corresponding eigenvalue, which does depend on the detuning. Defining the “population” $p_k = |\alpha_k|^2$ of the modes, and noting $\lambda_k = -\Gamma_k/2 + iE_k$, we have

$$p_k = \frac{|P_k(\mathbf{\Omega})|^2}{\Gamma_k^2/4 + (E_k^0 + \Delta)^2}, \quad (9)$$

where E_k^0 is the eigenfrequency for $\Delta = 0$ as in the H_{eff} approach. We recover an intuitive result, which describes a Lorentzian coupling efficiency to each mode. This Lorentzian depends on the width of the modes Γ_k and is shifted by the detuning Δ .

Note that this derivation and the result of Eqs. (8) and (9) is a simple example of the more general relations that exist between the effective Hamiltonian, its related scattering matrix, and decay rates, which are well known in the context of open quantum systems [see the reviews [32–35] and, for instance, Eq. (44) of [32]]. The similarities between cooperative scattering and the physics of open quantum systems has started to be discussed only recently [36,37]. Here, we just aim at discussing the consequences of this result on the decay of the steady state after the driving laser is switched off, and in particular the role of the initial detuning of the laser.

III. QUALITATIVE ANALYSIS

To fully understand the consequences of this result, let us turn to some graphical representations, where we plot the eigenvalue distribution of the coupling matrix in the complex plane. The main consequence of Eq. (9) is that the spectral factor $1/|\lambda_k|^2$ favors the modes located near the origin $E_k = \Gamma_k = 0$.

In the following, for simplicity, we will focus on the dilute limit, we thus do not discuss the localization problem [2–9], and we discard the near-field terms of the DDI, which are negligible in this limit. Our investigation is thus relevant, for example, to discuss the difference between subradiance [27] and radiation trapping [29], or the suppression of superradiance near resonance, as observed in a recent experiment [12].

In this dilute limit the DDI term is

$$V_{ij}(r_{ij}) = \frac{e^{ikr_{ij}}}{kr_{ij}}, \quad r_{ij} = |\mathbf{r}_i - \mathbf{r}_j|, \quad (10)$$

where $k = 2\pi/\lambda$ is the wave vector of the associated atomic transition.

Still for simplicity, we will also take the electric field $E(\mathbf{r})$ as a plane wave such that

$$\mathbf{\Omega} = -\frac{i\Omega}{2} [e^{ikz_1}, \dots, e^{ikz_i}, \dots, e^{ikz_N}]^T. \quad (11)$$

We draw N random positions for the atoms in a spherical Gaussian distribution (rms width R) such that the density varies smoothly, thus avoiding sharp edges responsible for internal reflection of light [38,39]. We also apply an exclusion volume $kr_{ij} > 3$ to avoid pairs of very close atoms responsible for subradiant and superradiant branches in the complex plane [3,6,40,41]. These two phenomena are interesting in themselves but complicate the interpretation, because they can produce long-lived modes that are related to neither the collective N -body subradiance nor the diffusion of light. Then we diagonalize the coupling matrix \mathbf{M} and compute the weight of the different modes using Eq. (9).

A. Influence of detuning

We show in Figs. 1 and 2 the outcome of such a computation, in which each panel shows the eigenvalue distribution in the complex plane for a single realization of the positions. Similar distributions have been studied before [2–9,40]. It is known that the eigenvalue distribution spreads from the single-atom limit $\{E_k = \Delta, \Gamma_k = 1\}$ as the on-resonance optical thickness $b_0 = 2N/(k_0R)^2$ increases, first forming a disk of radius $\propto \sqrt{b_0}$ for $b_0 \ll 1$, and then deforms at high b_0 with an accumulation of eigenvalues at small $\Gamma_k \ll 1$ and a corresponding spreading at high $\Gamma_k > 1$ [40]. This departure from single-atom physics exists at low density and is responsible for many collective effects in light scattering [1].

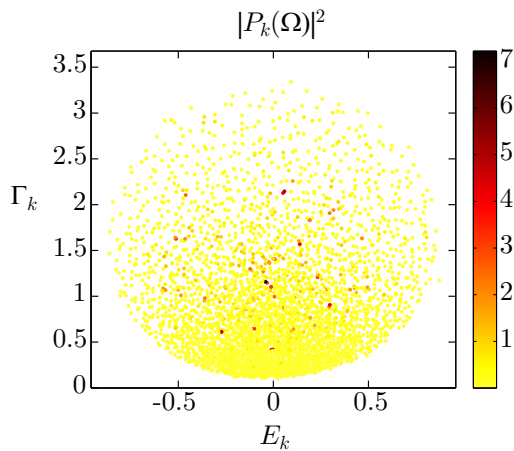


FIG. 1. Distribution of the eigenvalues $\lambda_k = -\Gamma_k/2 + iE_k$ in the complex plane (for $\Delta = 0$) with the geometrical factor $|P_k(\mathbf{\Omega})|^2$ represented in the color scale. The parameters of the atomic sample are $N = 3000$ and $kR \simeq 26.3$, yielding $b_0 \simeq 8.7$ and $\rho_0 k^{-3} \simeq 10^{-2}$.

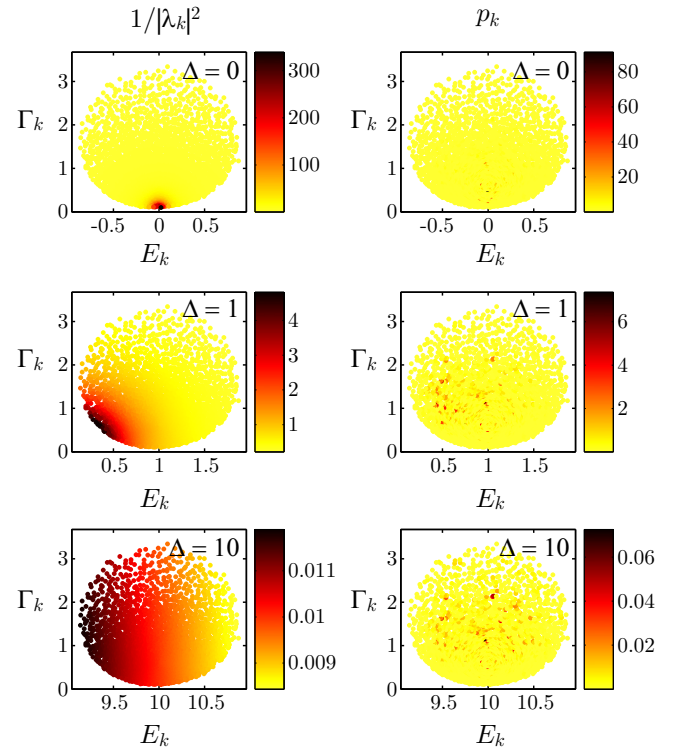


FIG. 2. Same as in Fig. 1 but the color scale now shows the spectral factor $1/|\lambda_k|^2$ (left column) and the populations p_k (right column). The different rows are for different detunings, from top to bottom $\Delta = 0, 1, 10$. Note the different color scale for each panel, showing that at large detuning, the spectral factor is almost uniform.

Here, we also show the geometrical factor $|P_k(\mathbf{\Omega})|^2$ (Fig. 1), the spectral factor $1/|\lambda_k|^2$ (Fig. 2, left column), and the population of the modes p_k (Fig. 2, right column) encoded in the color scale. The different rows of Fig. 2 are for different detunings, on resonance $\Delta = 0$ (first row), slightly detuned $\Delta = 1$ (second row), and far detuned $\Delta = 10$ (third row). The geometrical factor (Fig. 1) does not depend on the detuning. Here we have chosen a moderately large on-resonance optical thickness $b_0 \simeq 9$ and a low density $\rho_0 k^{-3} \simeq 10^{-2}$ (ρ_0 is the peak atomic density). Since the problem is linear, the value of Ω can be chosen at will and we have taken $\Omega = 2/\sqrt{N}$ such that $\mathbf{\Omega}$ is normalized to unity.

From these figures, several relevant observations can be made: (1) Only a few modes, mainly selected by the geometrical factor, have a non-negligible population and thus contribute to the dynamics of the system. Studying the whole eigenvalue distribution is thus not directly relevant to the experiment. In particular, the extreme modes, for example, the most superradiant ones, whose eigenvalues lie on the border of the distribution, are not significantly populated. (2) The geometrical factor favors the short-lived modes, i.e., the superradiant modes ($\Gamma_k > 1$). This was expected from the idea that superradiant modes are more coupled to the environment than subradiant modes. (3) Far from resonance, the spectral factor only induces an overall decrease of the populations and has a negligible effect on the mode selection. (4) It is very hard, if not impossible, to select any specific

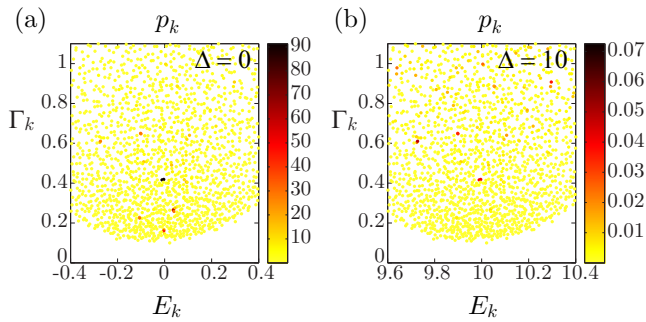


FIG. 3. Close-up of the populations of the long-lived modes, at resonance (a) and far from resonance (b). Same parameters as in Fig. 1.

mode by tuning the driving field frequency. For the $\Delta = 1$ case, for example, one might expect to selectively populate modes on the left border of the distribution, but that is actually not the case. The geometrical factor dominates over the spectral factor. Other strategies, based for instance on the spatial shaping of the driving field, are needed to selectively populate targeted modes [42]. (5) The spectral factor has an important effect only near resonance. It strongly favors the long-lived modes and thus decreases considerably the relative population of the superradiant modes. This demonstrates that superradiance disappears near resonance, as observed in previous experiments and numerical simulations [12,43].

A closer look on the populations of the long-lived modes is shown in Fig. 3(a) for the resonant case and in Fig. 3(b) for the far-detuned case. Even on resonance, only a few modes are strongly populated, showing that the geometrical factor still plays an important role. At large detuning, the long-lived modes that are populated are responsible for subradiance. These modes are still populated (and even more) near resonance, showing that the relative weight of subradiance increases near resonance, as seen experimentally [27]. Moreover, in addition to the modes strongly populated at large detuning, additional eigenmodes acquire noticeable population near resonance, with even longer lifetimes. These modes are responsible for radiation trapping due to multiple scattering [29]. This interpretation is validated by an analysis of the spatial properties of the modes, summarized in Fig. 4 and detailed in the next section.

At large detuning, the effect of the spectral factor on the relative population of the eigenmodes is negligible and completely vanishes for $\Delta \rightarrow \infty$, such that the relative populations are only given by the geometrical factor $|P_k(\Omega)|^2$, which actually means that the steady state \mathbf{B}_0 is proportional to Ω . This is precisely the timed-Dicke (TD) state approximation, introduced for single-photon excitation by Scully *et al.* [10] and further developed for continuous driving in Refs. [16–18]. Although this state is mainly superradiant, even though not the largest Γ_k of the distribution, it also contains subradiant components [Fig. 3(b)], as recently observed experimentally [27]. In other words, using a large detuning causes the driving field to couple weakly, but *equally*, to all modes having a good geometrical overlap with the driving field, and it thus reveals a part of the underlying mode structure, which is independent of the detuning. The consequence is that the collective dynamics

after switching off the driving field is still cooperative at very large detuning, with superradiant and subradiant decay rates becoming asymptotically independent of the detuning.

B. Spatial properties of the modes

It is also interesting to study the spatial properties of the collective modes in order to identify their physical meaning. Two quantities are useful to characterize the mode spatial properties: the rms size of the modes σ_k and the participation ratio (PR), defined as

$$\mathcal{R}_k^P = \frac{\sum_i |V_{ki}|^2}{\sum_i |V_{ki}|^4}, \quad (12)$$

which indicates the number of atoms participating significantly to the mode [5,44]. We represent in Figs. 4(a) and 4(b) these two quantities in the color scale of the eigenvalue distribution. We observe three distinctive areas: (i) Near the single-atom-physics case $\{E_k = 0, \Gamma_k = 1\}$, the modes have a larger rms size than the Gaussian atomic sample, $\sigma_k > R$, and a local minimum of the PR. This denotes modes delocalized at the boundary of the sample. Physically, this situation corresponds to single scattering (or low-order scattering) on the edges of the sample, as confirmed by the profile shown in Fig. 4(c). (ii) For the longest-lived modes ($\Gamma_k \ll 1$, at the border of the distribution), the size and the PR are both small, which means that the modes are not very extended. As seen in Fig. 4(d), they are located at the center of the sample. We attribute this behavior to diffusive modes due to multiple scattering. (iii) In the rest of the complex plane (most modes), the modes have approximately the same size as the

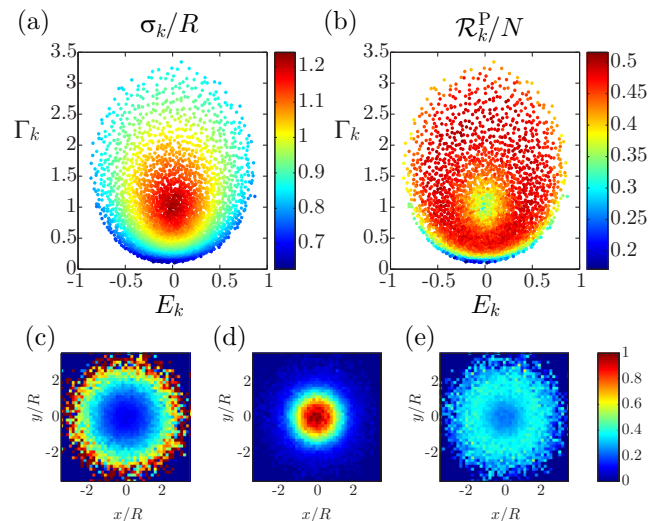


FIG. 4. Spatial properties of the collective modes. Same parameters are in Fig. 1, but the color scale now shows (a) the rms size σ_k of the modes (normalized by the sample size R), and (b) the participation ratio \mathcal{R}_k^P (normalized by the atom number N). We show in panels (c)–(e) the average over 120 realizations of the excitation probability (mode intensity divided by atomic density) for atoms located in a slice $|z| < R/5$, for each kind of mode, selected by the following conditions: (c) $0.9 < \Gamma_k < 1.1$ and $-0.1 < E_k < 0.1$; (d) $\Gamma_k < 0.2$; (e) $PR_k > 0.45$.

sample ($\sigma_k \sim R$) and a maximum PR (around $N/2$). They correspond to collective and extended modes, with almost uniform excitation probability across the sample Fig. 4(e). These modes can exhibit superradiant ($\Gamma_k > 1$) or subradiant ($\Gamma_k < 1$ or $\Gamma_k \ll 1$) behavior.

This analysis validates the interpretation given above on the different nature of the long-lived modes that are populated near resonance (diffusive modes responsible for radiation trapping [29]) compared to those excited far from resonance (subradiant modes).

IV. NUMERICAL STUDY

Many statistical quantities can in principle be computed and studied from the eigenvalue distribution [2–9,40]. Here we will focus on quantities that use the information contained in the populations p_k . These quantities, not studied before, are thus not only related to the properties of the effective Hamiltonian, but also to the way the system is excited. In particular, they will depend on the detuning Δ . They are thus less universal, but they are more related to experimental observables. One can thus expect to recover qualitative behaviors similar to what has been observed in experiments or in numerical simulations of the CDEs.

A. Behavior of the weighted averages

Let us now turn to a systematic analysis of the weighted averages of the eigenfrequencies (or eigenenergies) and decay rates (or linewidth), defined as

$$\langle E \rangle = \frac{\sum_k p_k E_k}{\sum_k p_k} \quad \text{and} \quad \langle \Gamma \rangle = \frac{\sum_k p_k \Gamma_k}{\sum_k p_k}. \quad (13)$$

We show in Fig. 5 a systematic study of these quantities as a function of the on-resonance optical thickness b_0 and on the detuning Δ . For each b_0 , 120 realizations of the disorder configuration have been used.

We observe that the average eigenenergy is slightly shifted from Δ and the shift $\langle E \rangle - \Delta$ displays a dispersion-like behavior, which becomes higher and broader as the optical thickness increases. On the contrary, the average decay rate $\langle \Gamma \rangle$ exhibits a negative resonance-like structure, which is also more important at larger b_0 . These behaviors are due to the spectral factor and can be qualitatively understood as follows.

First, on resonance ($\Delta = 0$), positive and negative values of E_k compensate so that $\langle E \rangle = 0$ after averaging over the disorder configurations (we remain here in the dilute limit such that the cooperative Lamb shift is negligible [20–24,45–51]). The same applies at very large detuning, for which the spectral factor plays a negligible role on the relative populations. At intermediate detuning, the spectral factor favors one side of the eigenvalue distribution, such that $\langle E \rangle$ departs from Δ to get slightly closer to zero [Fig. 2]. The difference $\langle E \rangle - \Delta$ has thus an opposite sign from Δ , which produces a dispersion behavior for the frequency shift, similar to an effective refractive index. This effect is more important as the eigenvalue distribution spreads for increasing b_0 .

Similarly for $\langle \Gamma \rangle$, at large detuning, the geometrical factor dominates and we have seen previously that it favors the superradiant modes, such that $\langle \Gamma \rangle > 1$, and superradiance is stronger as b_0 increases. We can actually compute $\langle \Gamma \rangle$ in the $\Delta \rightarrow \infty$ limit (TD approximation) by replacing the populations by the geometrical factor in the averaging Eq. (13). We clearly observe in Fig. 5(c) a linear scaling with b_0 :

$$\langle \Gamma \rangle_{\Delta \rightarrow \infty} = 1 + \frac{b_0}{24}. \quad (14)$$

We note that a similar linear scaling is expected for the superradiant decay rate of the TD state [12,13,16,52–56].

On resonance, however, the spectral factor favors the long-lived modes [Fig. 2] and thus $\langle \Gamma \rangle$ drops to values smaller than unity. Interestingly, we have found [Fig. 5(c)] that the data follow very closely the empirical relationship

$$\langle \Gamma \rangle_{\Delta=0} = 1 - \frac{1}{4}(1 - e^{-b_0/8}), \quad (15)$$

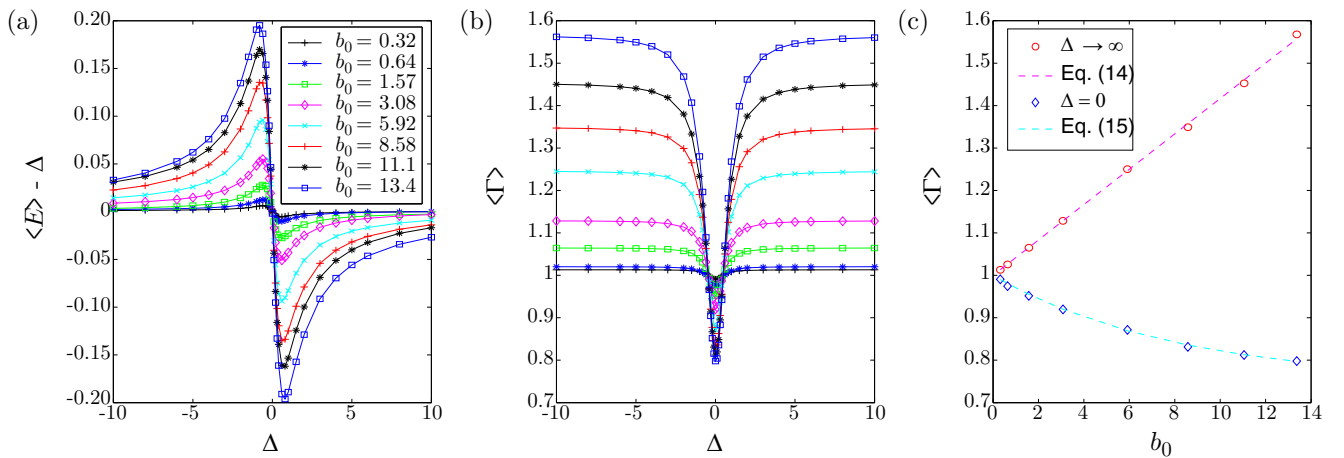


FIG. 5. Study of the weighted averages $\langle E \rangle$ and $\langle \Gamma \rangle$ [Eq. (13)] as a function of the detuning Δ and the on-resonance optical thickness b_0 . (a) The frequency shift $\langle E \rangle - \Delta$ is plotted as a function of Δ for different b_0 . (b) $\langle \Gamma \rangle$ is plotted as a function of Δ for different b_0 . (c) $\langle \Gamma \rangle$ is plotted as a function of b_0 for the two extreme cases, $\Delta \rightarrow \infty$ (red circles) and $\Delta = 0$ (blue diamonds). The dashed lines correspond to the empirical relations given in Eqs. (14) and (15).

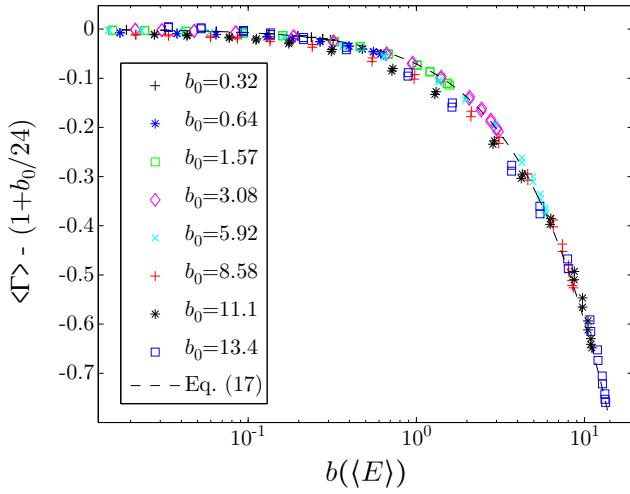


FIG. 6. Same numerical data as in Figs. 5(a) and 5(b) but $\langle \Gamma \rangle - (1 + b_0/24)$ is plotted as a function of $b(\langle E \rangle) = b_0/(1 + 4\langle E \rangle^2)$ (log scale). All points collapse on a single curve (dashed line), well described by Eq. (17).

which denotes an exponential decrease of $\langle \Gamma \rangle$ with the optical thickness, with a saturation effect. This is consistent with the idea that attenuation and multiple scattering suppress superradiance, as observed in Ref. [12] and in Fig. 2, but the plane-wave illumination ensures that there is always a large proportion of single scattering at the borders of the atomic cloud, and thus a large fraction of modes with $\Gamma_k \sim 1$, such that $\langle \Gamma \rangle_{\Delta=0}$ does not decrease to zero as b_0 increases.

Given the relatively simple behaviors of $\langle \Gamma \rangle$ and $\langle E \rangle$, one can wonder whether a more general relationship between $\langle \Gamma \rangle$, $\langle E \rangle$, and b_0 can be found. The limit cases [Eqs. (14) and (15)] suggest a route to a more refined scaling law. Plotting $\langle \Gamma \rangle - (1 + b_0/24)$ as a function of the detuning Δ exhibits a Lorentzian absorption profile whose depth and width depends on b_0 . It is thus natural to plot it as a function of $b(\Delta) = b_0/(1 + 4\Delta^2)$. The points then tend to collapse on a single curve, but with significant deviations. In fact, $b(\Delta)$ would be the actual optical thickness at the laser detuning without cooperativity. To take into account the spreading of the eigenvalue distribution, it makes sense to replace $b(\Delta)$ by

$$b(\langle E \rangle) = \frac{b_0}{1 + 4\langle E \rangle^2}. \quad (16)$$

In that case, all data points collapse almost perfectly on a single curve (Fig. 6). This curve is well described by

$$\langle \Gamma \rangle - \left(1 + \frac{b_0}{24}\right) \simeq -\frac{b(\langle E \rangle)}{24} - \frac{1}{4}(1 - e^{-b(\langle E \rangle)/8}), \quad (17)$$

or, in a more compact form, defining $b \equiv b(\langle E \rangle)$,

$$\langle \Gamma \rangle \simeq 1 + \frac{1}{4} \left[\frac{b_0 - b}{6} - (1 - e^{-b/8}) \right], \quad (18)$$

which contains the previous limiting cases. The quality of the collapse on such a universal curve as seen in Fig. 6 and expressed by Eq. (18) suggests that it should be possible to obtain analytical results describing the observed behaviors.

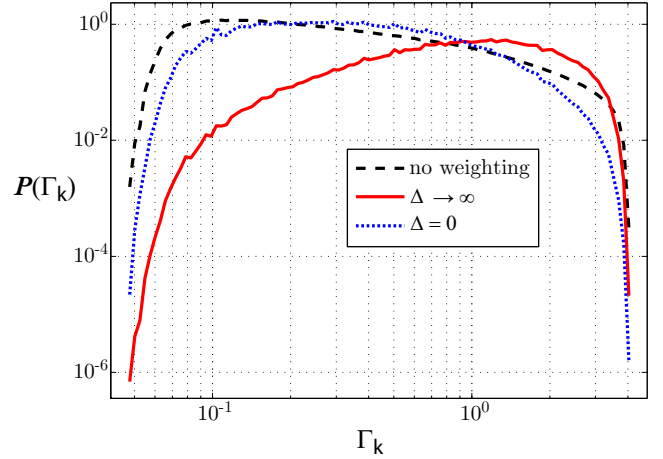


FIG. 7. Linewidth distribution $P(\Gamma_k)$ without weighting (dashed black line) and with weighting corresponding to the populations p_k computed far from resonance ($\Delta \rightarrow \infty$, solid red line) or at resonance ($\Delta = 0$, dotted blue line). The parameters of the atomic sample are $N = 5000$, $kR \simeq 27.3$ yielding $b_0 \simeq 13.4$, $\rho_0 k^{-3} \simeq 1.55 \times 10^{-2}$, and we used 120 realizations.

B. Linewidth distribution

Another interesting quantity is the distribution of the linewidths, $P(\Gamma_k)$. This distribution has been studied in several papers [4,6,57,58], but here we include p_k as a weighting factor of the Γ_k in the distribution $P(\Gamma_k)$, still computed over 120 realizations of the positions.

We show in Fig. 7 the comparison of the distribution $P(\Gamma_k)$ without weighting (and thus independent of Δ), with the ones computed with weighting corresponding to $\Delta \rightarrow \infty$ and $\Delta = 0$ (and excitation by a plane wave, as previously). As expected from the previous discussions, taking into account the weighting due to the population p_k increases the probability density of the short-lived (superradiant) modes far from resonance and of the long-lived modes near resonance. We note that this distribution $P(\Gamma_k)$ has a strong dependence on the detuning. This suggests that a characterization of the transport properties of light through resonant two-level systems needs to go beyond a mere eigenvalues analysis [4], since the transport properties obviously depend on the detuning. In general, the distribution $P(\Gamma_k)$ depends on the way the system is coupled to the environment [33,58].

We also note that the linewidth distribution does not allow us to extract any specific value for the long-lived modes effectively populated by an external drive, even when taking into account the weighting function of Eq. (9). Therefore, we cannot recover the scaling laws that can be observed in experiments on subradiance [27] or radiation trapping [29], indicating that the approach presented in this paper is not sufficient to recover experimentally observed scaling laws.

C. Discussion

We attribute this limitation to the fact that the quantities studied in this paper (such as the Γ_k) are not direct experimental observables. Indeed, when measuring the light escaping from

the atomic sample, for example, the total scattered power [41]

$$P \propto -\frac{d}{dt} \sum_{i=1}^N |\beta_i(t)|^2 = -\frac{d}{dt} \|\mathbf{B}(t)\| \\ = -\frac{d}{dt} \left\| \sum_k \alpha_k \mathbf{V}_k e^{\lambda_k t} \right\|, \quad (19)$$

the nonorthogonality of the eigenmodes \mathbf{V}_k (due to the non-Hermiticity of the effective Hamiltonian) are at the origin of oscillating terms [34], which may change the dynamics of the decay, even after configuration averaging. It is thus not surprising to find a quantitative difference in the decay rates. For example, the linear scaling of $\langle \Gamma \rangle$ with b_0 obtained at Eq. (14) does not have the same slope as what has been found by studying the decay of the scattered light in the coupled-dipole model [12,41]. Obtaining analytical results on experimental observables remains thus an open problem.

In the framework of the effective Hamiltonian approach, one can also study the spectrum of the Hermitian operator $\text{Im}(H_{\text{eff}})$ [59]. In that case, the eigenvalues are directly related to the probability of returning in the ground state, and thus correspond to the light escape rates from the sample [60,61]. However, this is only valid when the initial state contains one excitation but no coherence, and thus does not apply to driven systems.

V. CONCLUSION

Several properties of cooperative scattering, such as the enhancement of subradiance and suppression of superradiance

near resonance [12,27], and the very existence of cooperative decay at very large detuning, are highly nonintuitive. We have shown in this paper that they are consequences of the simple analytical relationship that exists between the population of the collective modes of the effective Hamiltonian and the detuning of the driving field [Eq. (9)]. We have also put in evidence an empirical scaling law on the weighted averages of the eigenvalues of the effective Hamiltonian, which suggests the possibility of further analytical results.

In general, statistical properties of the eigenvalues of the effective Hamiltonian can be efficiently studied using random matrix theory [40], whereas very few analytical results have been obtained from the coupled-dipole equation model [15,54]. The populations of the collective modes and their dependence on the parameters of the driving field is an important ingredient bridging the gap between the two approaches.

We also discussed the spatial properties of the modes and showed that we can distinguish two kinds of long-lived modes that can be associated with radiation trapping and subradiance. Extending this analysis to the high-density case could be useful to better understand the transition to Anderson localization [5,6].

ACKNOWLEDGMENTS

We thank Johannes Schachenmayer for careful reading of the manuscript. We acknowledge financial support from the ANR (Agence National pour la Recherche, project LOVE, No. ANR-14-CE26-0032).

-
- [1] W. Guerin, M. T. Rouabah, and R. Kaiser, Light interacting with atomic ensembles: Collective, cooperative and mesoscopic effects, *J. Mod. Opt.* **64**, 895 (2017).
- [2] M. Rusek, A. Orłowski, and J. Mostowski, Localization of light in three-dimensional random dielectric media, *Phys. Rev. E* **53**, 4122 (1996).
- [3] M. Rusek, J. Mostowski, and A. Orłowski, Random green matrices: From proximity resonances to Anderson localization, *Phys. Rev. A* **61**, 022704 (2000).
- [4] F. A. Pinheiro, M. Rusek, A. Orłowski, and B. A. van Tiggelen, Probing Anderson localization of light via decay rate statistics, *Phys. Rev. E* **69**, 026605 (2004).
- [5] S. E. Skipetrov and I. M. Sokolov, Absence of Anderson Localization of Light in a Random Ensemble of Point Scatterers, *Phys. Rev. Lett.* **112**, 023905 (2014).
- [6] L. Bellando, A. Gero, E. Akkermans, and R. Kaiser, Cooperative effects and disorder: A scaling analysis of the spectrum of the effective atomic Hamiltonian, *Phys. Rev. A* **90**, 063822 (2014).
- [7] S. E. Skipetrov and I. M. Sokolov, Magnetic-Field-Driven Localization of Light in a Cold-Atom Gas, *Phys. Rev. Lett.* **114**, 053902 (2015).
- [8] C. E. Máximo, N. Piovella, P. W. Courteille, R. Kaiser, and R. Bachelard, Spatial and temporal localization of light in two dimensions, *Phys. Rev. A* **92**, 062702 (2015).
- [9] S. E. Skipetrov, Finite-size scaling analysis of localization transition for scalar waves in a three-dimensional ensemble of resonant point scatterers, *Phys. Rev. B* **94**, 064202 (2016).
- [10] M. O. Scully, E. S. Fry, C. H. R. Ooi, and K. Wódkiewicz, Directed Spontaneous Emission from an Extended Ensemble of N Atoms: Timing is Everything, *Phys. Rev. Lett.* **96**, 010501 (2006).
- [11] M. O. Scully and A. A. Svidzinsky, The super of superradiance, *Science* **325**, 1510 (2009).
- [12] M. O. Araújo, I. Krešić, R. Kaiser, and W. Guerin, Superradiance in a Large Cloud of Cold Atoms in the Linear-Optics Regime, *Phys. Rev. Lett.* **117**, 073002 (2016).
- [13] S. J. Roof, K. J. Kemp, M. D. Havey, and I. M. Sokolov, Observation of Single-Photon Superradiance and the Cooperative Lamb Shift in an Extended Sample of Cold Atoms, *Phys. Rev. Lett.* **117**, 073003 (2016).
- [14] J. Javanainen, J. Ruostekoski, B. Vestergaard, and M. R. Francis, One-dimensional modeling of light propagation in dense and degenerate samples, *Phys. Rev. A* **59**, 649 (1999).
- [15] A. A. Svidzinsky, J.-T. Chang, and M. O. Scully, Cooperative spontaneous emission of N atoms: Many-body eigenstates, the effect of virtual Lamb shift processes, and analogy with radiation of N classical oscillators, *Phys. Rev. A* **81**, 053821 (2010).
- [16] Ph. W. Courteille, S. Bux, E. Lucioni, K. Lauber, T. Bienaimé, R. Kaiser, and N. Piovella, Modification of radiation pressure

- due to cooperative scattering of light, *Eur. Phys. J. D.* **58**, 69 (2010).
- [17] T. Bienaimé, M. Petruzzo, D. Bigerni, N. Piovella, and R. Kaiser, Atom and photon measurement in cooperative scattering by cold atoms, *J. Mod. Opt.* **58**, 1942 (2011).
- [18] T. Bienaimé, R. Bachelard, P. W. Courteille, N. Piovella, and R. Kaiser, Cooperativity in light scattering by cold atoms, *Fortschr. Phys.* **61**, 377 (2013).
- [19] L. Chomaz, L. Corman, T. Yefsah, R. Desbuquois, and J. Dalibard, Absorption imaging of a quasi-two-dimensional gas: A multiple scattering analysis, *New J. Phys.* **14**, 055001 (2012).
- [20] J. Javanainen, J. Ruostekoski, Y. Li, and S.-M. Yoo, Shifts of a Resonance Line in a Dense Atomic Sample, *Phys. Rev. Lett.* **112**, 113603 (2014).
- [21] Z. Meir, O. Schwartz, E. Shahmoon, D. Oron, and R. Ozeri, Cooperative Lamb Shift in a Mesoscopic Atomic Array, *Phys. Rev. Lett.* **113**, 193002 (2014).
- [22] S. L. Bromley, B. Zhu, M. Bishof, X. Zhang, T. Bothwell, J. Schachenmayer, T. L. Nicholson, R. Kaiser, S. F. Yelin, M. D. Lukin, A. M. Rey, and J. Ye, Collective atomic scattering and motional effects in a dense coherent medium, *Nat. Commun.* **7**, 11039 (2016).
- [23] S. Jennewein, M. Besbes, N. J. Schilder, S. D. Jenkins, C. Sauvan, J. Ruostekoski, J.-J. Greffet, Y. R. P. Sortais, and A. Browaeys, Coherent Scattering of Near-Resonant Light by a Dense Microscopic Cold Atomic Cloud, *Phys. Rev. Lett.* **116**, 233601 (2016).
- [24] B. Zhu, J. Cooper, J. Ye, and A. M. Rey, Light scattering from dense cold atomic media, *Phys. Rev. A* **94**, 023612 (2016).
- [25] R. T. Sutherland and F. Robicheaux, Coherent forward broadening in cold atom clouds, *Phys. Rev. A* **93**, 023407 (2016).
- [26] T. Bienaimé, N. Piovella, and R. Kaiser, Controlled Dicke Subradiance from a Large Cloud of two-Level Systems, *Phys. Rev. Lett.* **108**, 123602 (2012).
- [27] W. Guerin, M. O. Araújo, and R. Kaiser, Subradiance in a Large Cloud of Cold Atoms, *Phys. Rev. Lett.* **116**, 083601 (2016).
- [28] S. E. Skipetrov, I. M. Sokolov, and M. D. Havey, Control of light trapping in a large atomic system by a static magnetic field, *Phys. Rev. A* **94**, 013825 (2016).
- [29] G. Labeyrie, E. Vaujour, C. A. Müller, D. Delande, C. Miniatura, D. Wilkowski, and R. Kaiser, Slow Diffusion of Light in a Cold Atomic Cloud, *Phys. Rev. Lett.* **91**, 223904 (2003).
- [30] Y. Li, J. Evers, W. Feng, and S.-Y. Zhu, Spectrum of collective spontaneous emission beyond the rotating-wave approximation, *Phys. Rev. A* **87**, 053837 (2013).
- [31] W. Feng, Y. Li, and S.-Y. Zhu, Effect of atomic distribution on cooperative spontaneous emission, *Phys. Rev. A* **89**, 013816 (2014).
- [32] I. Rotter, A non-Hermitian Hamilton operator and the physics of open quantum systems, *J. Phys. A* **42**, 153001 (2009).
- [33] F.-M. Dittes, The decay of quantum systems with a small number of open channels, *Phys. Rep.* **339**, 215 (2000).
- [34] J. Okołowicz, M. Płoszajczak, and I. Rotter, Dynamics of quantum systems embedded in a continuum, *Phys. Rep.* **374**, 271 (2003).
- [35] U. Kuhl, O. Legrand, and F. Mortessagne, Microwave experiments using open chaotic cavities in the realm of the effective Hamiltonian formalism, *Fortschr. Phys.* **61**, 404 (2012).
- [36] *Special Issue: Quantum Physics with non-Hermitian Operators: Theory and Experiment*, edited by J. P. Bird, R. Kaiser, I. Rotter, and G. Wunner, *Fortschr. Phys.*, Vol. 61 (Wiley, Weinheim, 2012).
- [37] I. Rotter and J. P. Bird, A review of progress in the physics of open quantum systems: Theory and experiment, *Rep. Prog. Phys.* **78**, 114001 (2015).
- [38] R. Bachelard, P. W. Courteille, R. Kaiser, and N. Piovella, Resonances in Mie scattering by an inhomogeneous atomic cloud, *Europhys. Lett.* **97**, 14004 (2012).
- [39] N. J. Schilder, C. Sauvan, J.-P. Hugonin, S. Jennewein, Y. R. P. Sortais, A. Browaeys, and J.-J. Greffet, Role of polaritonic modes on light scattering from a dense cloud of atoms, *Phys. Rev. A* **93**, 063835 (2016).
- [40] S. E. Skipetrov and A. Goetschy, Eigenvalue distributions of large Euclidean random matrices for waves in random media, *J. Phys. A* **44**, 065102 (2011).
- [41] M. O. Araújo, W. Guerin, and R. Kaiser, Decay dynamics in the coupled-dipole model, [arXiv:1705.02190](https://arxiv.org/abs/1705.02190).
- [42] M. O. Scully, Single Photon Subradiance: Quantum Control of Spontaneous Emission and Ultrafast Readout, *Phys. Rev. Lett.* **115**, 243602 (2015).
- [43] This discussion does not apply to experiments using a pulsed excitation, as in Ref. [13], since we are dealing with the steady state obtained with a continuous monochromatic excitation. For a detailed study about the influence of the exciting pulse duration, see A. S. Kuraptsev, I. Sokolov, and M. D. Havey, Angular distribution of single photon superradiance in a dilute and cold atomic ensemble, [arXiv:1701.07503](https://arxiv.org/abs/1701.07503).
- [44] A. Biella, F. Borgonovi, R. Kaiser, and G. L. Celardo, Subradiant hybrid states in the open 3D Anderson-Dicke model, *Europhys. Lett.* **103**, 57009 (2013).
- [45] R. Friedberg, S. R. Hartmann, and J. T. Manassah, Frequency shifts in emission and absorption by resonant systems of two-level atoms, *Phys. Rep.* **7**, 101 (1973).
- [46] M. O. Scully, Collective Lamb Shift in Single Photon Dicke Superradiance, *Phys. Rev. Lett.* **102**, 143601 (2009).
- [47] R. Röhlsberger, K. Schlage, B. Sahoo, S. Couet, and R. Ruffer, Collective Lamb shift in single-photon superradiance, *Science* **328**, 1248 (2010).
- [48] J. Keaveney, A. Sargsyan, U. Krohn, I. G. Hughes, D. Sarkisyan, and C. S. Adams, Cooperative Lamb Shift in an Atomic Vapor Layer of Nanometer Thickness, *Phys. Rev. Lett.* **108**, 173601 (2012).
- [49] J. T. Manassah, Cooperative radiation from atoms in different geometries: Decay rate and frequency shift, *Adv. Opt. Photon.* **4**, 108 (2012).
- [50] S. D. Jenkins, J. Ruostekoski, J. Javanainen, R. Bourgain, S. Jennewein, Y. R. P. Sortais, and A. Browaeys, Optical Resonance Shifts in the Fluorescence of Thermal and Cold Atomic Gases, *Phys. Rev. Lett.* **116**, 183601 (2016).
- [51] J. Javanainen and J. Ruostekoski, Light propagation beyond the mean-field theory of standard optics, *Opt. Express* **24**, 993 (2016).
- [52] I. E. Mazets and G. Kurizki, Multiatom cooperative emission following single-photon absorption: Dicke-state dynamics, *J. Phys. B* **40**, F105 (2007).

- [53] A. A. Svidzinsky, J.-T. Chang, and M. O. Scully, Dynamical Evolution of Correlated Spontaneous Emission of a Single Photon from a Uniformly Excited Cloud of N Atoms, *Phys. Rev. Lett.* **100**, 160504 (2008).
- [54] A. A. Svidzinsky and J.-T. Chang, Cooperative spontaneous emission as a many-body eigenvalue problem, *Phys. Rev. A* **77**, 043833 (2008).
- [55] R. Friedberg and J. T. Manassah, Analytic expressions for the initial cooperative decay rate and cooperative Lamb shift for a spherical sample of two-level atoms, *Phys. Lett. A* **374**, 1648 (2010).
- [56] S. Prasad and R. J. Glauber, Coherent radiation by a spherical medium of resonant atoms, *Phys. Rev. A* **82**, 063805 (2010).
- [57] T. Kottos and M. Weiss, Statistics of Resonance and Delay Times: A Criterion for Metal-Insulator Transition, *Phys. Rev. Lett.* **89**, 056401 (2002).
- [58] M. Weiss, J. A. Méndez-Bermúdez, and T. Kottos, Resonance width distribution for high-dimensional random media, *Phys. Rev. B* **73**, 045103 (2006).
- [59] E. Akkermans, A. Gero, and R. Kaiser, Photon Localization and Dicke Superradiance in Atomic Gases, *Phys. Rev. Lett.* **101**, 103602 (2008).
- [60] V. Ernst and P. Stehle, Emission of radiation from a system of many excited atoms, *Phys. Rev.* **176**, 1456 (1968).
- [61] E. Ressayre and A. Tallet, Quantum theory for superradiance, *Phys. Rev. A* **15**, 2410 (1977).

VI.4. Superradiance as single scattering embedded in an effective medium

So far, our modeling and interpretation of super- and subradiance are based on the coupled-dipole model and the associated collective modes. In this picture the light provides an effective interaction between atoms, and we only consider the dynamics of the atoms, supposed to be classical dipoles. Alternatively, it should be possible to understand what happens by considering the light propagating and being scattered inside the disordered atomic medium. The complementarity and equivalence between the two approaches are discussed, for instance, in [Lax 1951, Legendijk 1996], although some phenomena may be easier to describe in one framework. It is, for example, easier and more efficient to describe incoherent multiple scattering (radiation trapping) by a radiative transfer approach, such as random walk simulations. On the contrary, super- and subradiance are well described by the CD model, and also easy to understand: coupled oscillators build collective modes...

In this section, I present a ‘photonic’ model of superradiance, which I didn’t find myself: it is used in [Kuraptsev 2017]. However, it may be not well known and I would like to promote it. Moreover it is also efficient for modeling what happens at the switch-on, which we studied recently (section VI.6). We called this model ‘linear-dispersion theory’.

Let us start from the result and explain its meaning. The intensity $I_{\mathbf{u}}(t)$ detected in the direction \mathbf{u} as a function of time is given by Eq. (3.4) of [Kuraptsev 2017], which I rewrite below, in the scalar approximation for simplicity, and with slightly simplified notations:

$$I_{\mathbf{u}}(t) \propto \int d^3\mathbf{r} \rho(r) \left| \int_{-\infty}^{\infty} d\omega E_0(\omega) e^{-i\omega t} \times \exp \left[i \frac{b_0(\mathbf{r}, \mathbf{u})}{2} \tilde{\alpha}(\omega) \right] \tilde{\alpha}(\omega) \exp \left[i \frac{b_0(\mathbf{r}, \mathbf{k})}{2} \tilde{\alpha}(\omega) \right] \right|^2. \quad (\text{VI.2})$$

In this equation, $\rho(\mathbf{r})$ is the density distribution, $E_0(\omega)$ is the Fourier transform of the incident field,

$$\tilde{\alpha}(\omega) = \frac{-1}{i + 2(\omega - \omega_{\text{at}})/\Gamma} = \frac{i - 2(\omega - \omega_{\text{at}})}{1 + 4(\omega - \omega_{\text{at}})^2/\Gamma^2} \quad (\text{VI.3})$$

is the dimensionless atomic polarizability (already defined in [Froufe-Pérez 2009]), and the b_0 terms denote the resonant optical thickness through a part of the cloud, from the position \mathbf{r} into the direction \mathbf{u} and from the incident direction \mathbf{k} to the position \mathbf{r} . In the case of a Gaussian cloud of rms size R , and taking the incident wavevector along the z axis and putting the center of coordinates at the center of the cloud, one can find:

$$b_0(\mathbf{r}, \mathbf{k}) = \frac{b_0}{2} \exp \left[-\frac{x^2 + y^2}{2R^2} \right] \left[1 + \operatorname{erf} \left(\frac{z}{\sqrt{2}R} \right) \right], \quad (\text{VI.4})$$

$$b_0(\mathbf{r}, \mathbf{u}) = \frac{b_0}{2} \exp \left[\frac{-r^2 + (\mathbf{r} \cdot \mathbf{u})^2}{2R^2} \right] \left[1 - \operatorname{erf} \left(\frac{\mathbf{r} \cdot \mathbf{u}}{\sqrt{2}R} \right) \right]. \quad (\text{VI.5})$$

The meaning of Eq. (VI.2) is clear: each Fourier component of the initial field (not monochromatic because of the switch-off) propagates through the cloud until the scattering position \mathbf{r} , propagation during which it undergoes attenuation and dephasing. Then it is scattered at position \mathbf{r} with some probability and associated dephasing given by the atomic polarizability, and finally it propagates until it escapes the sample. The whole process acts as a linear transfer function. The temporal dependence is recovered by a Fourier transform and the intensity is computed by taking the squared modulus. Then all possible scattering positions are averaged.

This equation is valid for single-scattering only, since there is only one scattering term. Note also that the average over the scattering positions is done *after* the squared modulus, i.e. on the intensity: the random phase associated to incoherent scattering and the associated speckle pattern are averaged out. Indeed, what is computed is formally a quantum-mechanical average⁵, i.e. an average over the disorder configurations. Still, it means that superradiance is not related to the interference between light scattered by different atoms, which was not obvious to me. It is actually related to the interference between the different Fourier components of the incident field scattered by the atoms and attenuated/dephased by the surrounding effective medium. It is thus mainly a *dispersion* effect. Of course, the complex refractive index of the effective medium can still be understood as an interference between light coherently scattered by all atoms...

This calculation is very similar to what is done to explain the transient effects observed in the coherently transmitted beam, the so-called optical precursors and flash effects [Jeong 2006, Chen 2010, Chalony 2011, Kwong 2014, Kwong 2015], except for the extra scattering term. In this case, though, this approach is more natural/intuitive because there is no random phase associated to any scattering.

In this approach, one can understand the occurrence of a superradiant decay rate by the spectral broadening of the transfer function induced by the larger value of b_0 : if the transfer function gets broader in Fourier space, the temporal response gets faster. This is the intuitive picture given for the flash, which can also have a decay rate faster than Γ_0 [Kwong 2015].

In Fig. VI.3 we compare the results of the decay rate fitted at very early time on temporal traces computed from the CD model and the linear-dispersion (LD) model (Eq. VI.2), at large detuning ($\Delta = -10\Gamma$). The agreement is excellent. Also shown is the analytical result in the $|\Delta| \rightarrow \infty$ limit, obtained from Eq. (VI.2) [Kuraptsev 2017],

$$\Gamma_{\text{sup}} = \left(1 + \frac{b_0}{4}\right) \Gamma_0. \quad (\text{VI.6})$$

Note that this does not depend on the observing direction, and that the model only contains superradiance off axis, i.e. with a true scattering event, it does not include the forward lobe of the TD state. As a consequence the decay rate is different, even in the forward direction, than Eq. (VI.1) for the TD state. The extra $\tilde{\alpha}(\omega)$ term (scattering) is responsible for a factor 2 in the superradiant enhancement factor. It emphasizes the different nature of the forward lobe, which is, in a photon picture, diffracted/refracted light by the effective medium without any true scattering.

A deviation from the analytical result can be seen for the largest b_0 's. This is the first sign of the suppression of superradiance as soon as $b(\Delta)$ is not negligible, as observed in [Araújo 2016]. Actually, while doing this comparison, we observed that the good agreement between the two models, as well as the deviation from Eq. (VI.6), was quite sensitive to the fitting range used for determining the decay rate. The reduction of the superradiant decay rate near resonance is less visible if the decay rate is measured closer to the switch-off time $t = 0$. It seems that there is, in fact, always a little bit of superradiance at $t = 0^+$, with an unchanged rate, but it is more and more limited in time as the detuning goes closer to resonance, and thus harder to see. This is consistent with a decrease of the superradiant population as discussed in the previous section [Guerin 2017b].

Of course, this approach is extremely efficient from a computing point of view. Moreover it is not limited in term of atom number or b_0 , and we can also include the Zeeman structure.

⁵ I thank Igor Sokolov for providing me the detailed derivation.

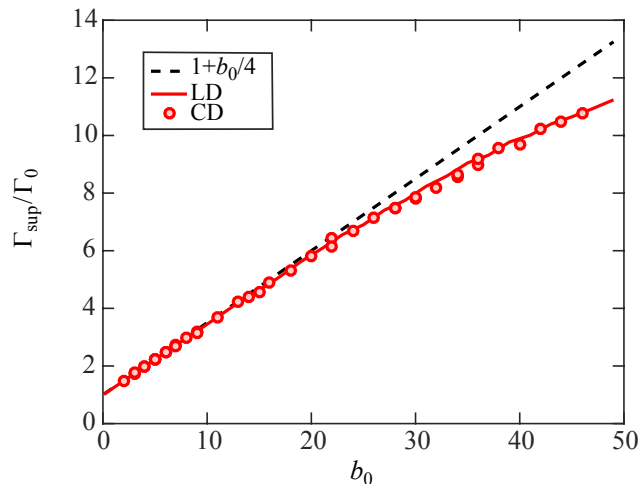


Figure VI.3: Comparison between the coupled-dipole (CD) model and the linear-dispersion (LD) theory for the superradiant decay rate Γ_{sup} . Also shown is the analytical results for the large detuning limit. The detuning is $\Delta = -10\Gamma_0$, the observation direction is $\theta = 45^\circ$. The fitting range is $0 < t/\tau_{\text{at}} < 0.02$. Note that several densities are used in the CD simulations, from $\rho_0\lambda^3 = 1.5$ to 25 (with an exclusion volume $k_0r_{ij} > 0.5$), while the density is not a parameter in the LD model.

It should thus be possible to make a direct comparison with experimental data without any free parameters. Another possible extension is to include the effect of atomic motion, which can be done by a simple Doppler broadening of the atomic polarizability. While the CD simulations with moving atoms are extremely time-demanding [Weiss 2019], the LD theory allows very fast computing. At the time of writing we have already advanced on those two applications and we are preparing an article in collaboration with Igor Sokolov.

VI.5. Subradiance and multiple scattering

Let's go back to subradiance. In this section I want to address the problem of the difference (or not) between subradiance and multiple scattering.

VI.5.1. Interplay of subradiance and radiation trapping

As briefly mentioned after the paper [Guerin 2016a], the fact that we don't observe any difference for the subradiant time constant near resonance was puzzling. We expected an increase, as predicted in [Bienaimé 2012], due to the occurrence of an even slower decay due to radiation trapping. Indeed, radiation trapping times scale as $b(\Delta)^2$ (see section IV.1.2.2), while subradiance times scale as b_0 . So, even with an unfavorable prefactor, near resonance, for high enough b_0 , radiation trapping should give the slowest decay and thus dominate at late time.

However, this is only true at zero temperature. With moving atoms, the frequency redistribution due to the Doppler effect breaks the $b(\Delta)^2$ scaling, which actually becomes almost linear at large temperature [Pierrat 2009]. Moreover, another important parameter is the relative amplitude of the slow decay that we are able to observe. If subradiance starts at a relative level of 10^{-2} and radiation trapping at 10^{-4} , then even if radiation trapping is slower and ultimately dominates at very late time, it will be hard to see experimentally.

Obviously, driving the system with a plane wave does not favor the observation of multiple scattering, because a large part of the light only interacts with the edges of the sample. That's

why, in the radiation trapping experiment of [Labeyrie 2003], a probe beam smaller than the cloud and a detection near the forward direction was used in order to select multiply-scattered light.

We have thus repeated this experiment but, now, with a measurement dynamics over four decades. We can thus observe simultaneously subradiance and radiation trapping, as shown in the following paper [Weiss 2018]. Because of the finite temperature, subradiance always dominates at late time, i.e. we don't reach the regime where radiation trapping is slower than subradiance.



PAPER

Subradiance and radiation trapping in cold atoms

OPEN ACCESS

RECEIVED
3 March 2018REVISED
3 May 2018ACCEPTED FOR PUBLICATION
17 May 2018PUBLISHED
15 June 2018Original content from this work may be used under the terms of the [Creative Commons Attribution 3.0 licence](https://creativecommons.org/licenses/by/4.0/).

Any further distribution of this work must maintain attribution to the author(s) and the title of the work, journal citation and DOI.

Patrizia Weiss¹, Michelle O Araújo^{1,2}, Robin Kaiser¹ and William Guerin¹¹ Université Côte d'Azur, CNRS, Institut de Physique de Nice, France² CAPES Foundation, Ministry of Education of Brazil, Brasília, DF 70040-020, BrazilE-mail: Patrizia.weiss@inphyni.cnrs.fr

Keywords: subradiance, radiation trapping, light diffusion, cold atoms, multiple scattering

Abstract

We experimentally and numerically study the temporal dynamics of light scattered by large clouds of cold atoms after the exciting laser is switched off, in the low intensity (linear-optics) regime. Radiation trapping due to multiple scattering as well as subradiance lead to decay much slower than the single atom fluorescence decay. These two effects have already been observed separately, but the interplay between them remained to be understood. Here, we show that with well chosen parameters of the driving field, the two effects can occur at the same time, but follow different scaling behaviors. The subradiant decay is observed at late time and its rate is independent of the detuning, while the radiation trapping decay is observed at intermediate time and depends on the detuning through the optical depth of the sample. Numerical simulations based on random walk process and coupled-dipole equations support our interpretations. Our study clarifies the different interpretations and physical mechanisms at the origin of slow temporal dynamics of light in cold atoms.

1. Introduction

Collective effects in light scattering by atomic ensembles have recently been the subject of intense research, both theoretically and experimentally [1, 2]. Even in the most simple situation, when the atomic system is driven by a low intensity laser (single-photon or linear-optics regime) and when the atomic cloud has a low density, various phenomena can occur [3–6]. For example, steady-state experiments about light diffusion [7, 8], coherent backscattering [9, 10] and the resonance line shape and shift [11–18] have been performed. Several recent experiments also studied the temporal dynamics of the light scattered by cold atoms at the switch-off of the driving field. A decay faster than the natural decay rate Γ has been observed at short time, a signature of superradiance [17, 19]. A decay rate much slower than Γ has also been detected at later time, a direct observation of subradiance [20]. It has been shown experimentally that the subradiant decay rate depends on the resonant optical depth b_0 , independently of the detuning $\Delta = \omega - \omega_0$ from the atomic resonance ω_0 , which has been confirmed by numerical simulations [20–22].

Interestingly, a slow decay can also be interpreted completely differently. Indeed, near resonance, when the actual optical depth $b(\Delta) \propto b_0 / (1 + 4\Delta^2/\Gamma^2)$ is large, light undergoes multiple scattering. This leads to a slowed transport velocity inside the diffusive medium [23] and ultimately to a slow decay when the incident light is switched off. This effect, called radiation trapping [24–26], has also been studied in cold atoms [27–32]. In particular, it has been shown that, at low enough temperature, the dynamics depends on the detuning only through the optical depth $b(\Delta)$, because this parameter controls the distribution of the number of scattering events that light undergoes before escaping, the average time between scattering events being remarkably independent of the detuning [28].

Radiation suppression can be obtained by different physical mechanisms, as already pointed out by Cummings [33] who noted that interference-based radiation suppression is ‘much more exotic and unexpected than the ordinary radiation trapping’, which can be explained by photon rescattering. As the different scalings [b_0 versus $b^2(\Delta)$] show, these two effects are not two different interpretations of the same phenomena, but are really due to two different physical mechanisms. This difference does not appear when one studies the

eigenvalues of the effective Hamiltonian describing the atoms interacting through the shared excitation [34–38], all long-lived collective atomic modes being often called ‘subradiant’, although differences in the shape of the eigenmodes have been discussed as a possible way to distinguish between modes associated to subradiance and to radiation trapping [39].

In this article, we experimentally study these two effects, showing in particular that, with well chosen parameters, both occur simultaneously. We find that when the atomic sample is driven by a plane wave, as in [20], subradiance is observed and radiation trapping is not clearly visible, even on resonance, mainly because the signal is dominated by single scattering occurring on the edges of the sample. The situation is different with an exciting beam much smaller than the cloud, as in [28], because single scattering is strongly reduced if light is detected near the forward direction. In this paper we show that with reduced single scattering near resonance, a slow decay due to radiation trapping is visible at intermediate time and, at later time, an even slower decay appears due to subradiance. Although at zero temperature and for large enough optical depth, radiation trapping could be slower than subradiance and dominate even at late time, the frequency redistribution due to Doppler broadening strongly reduces the number of scattering events that light can undergo before escaping, and we find that, at $T \sim 100 \mu\text{K}$, subradiant decay always dominates at late time.

The paper is organized as follows. In the next section we present the experimental setup and in the following the observation of subradiance for an excitation with a plane wave. In section 4 we present the data acquired with a narrow driving beam, showing the simultaneous observation of subradiance and radiation trapping. We study in detail how the corresponding decay times scale with the parameters. In section 5 we present numerical simulations which support our interpretations. In particular, the comparison between the simulations based on the coupled-dipole (CD) equations and on a random walk (RW) model performed at $T = 0$ allows us to discuss the physics in an ideal case. Moreover, the simulations based on the RW model including the effect of the temperature, laser spectrum and beam size are in fair agreement with our experimental data on radiation trapping. We finally conclude in section 6.

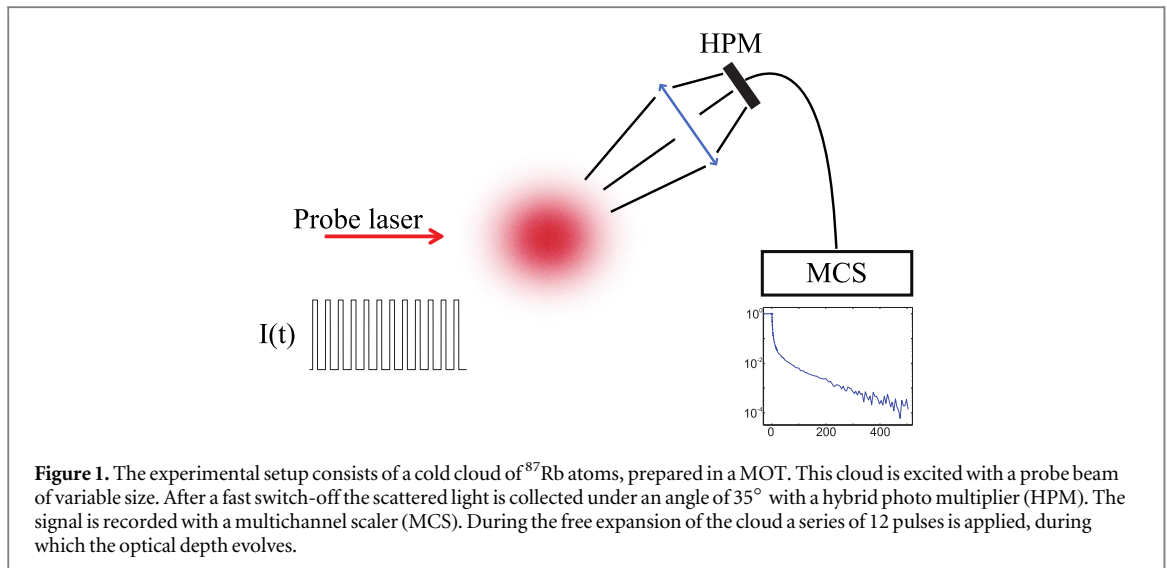
2. Experimental setup

In the experiment, we prepare a cloud of cold rubidium-87 atoms in a magneto-optical trap (MOT), which is loaded during 60 ms from the background vapor in the glass chamber. For further increase of the optical depth a compressed MOT stage follows for 30 ms, which additionally leads to a cleaner shape of the cloud (close to a Gaussian density distribution) and a reduced temperature. We obtain an ensemble of $N \approx 2.5 \times 10^9$ atoms at a temperature $T \approx 100 \mu\text{K}$. After switching off all MOT beams as well as the magnetic fields, the cloud is allowed to expand ballistically for a duration of 3 ms, during which the atoms are optically pumped to the upper hyperfine ground state $F = 2$. After this preparation stage the typical peak density is $\rho_0 \sim 10^{11} \text{ cm}^{-3}$ and the rms size is $R \approx 1 \text{ mm}$. To weakly excite the cloud a series of 12 pulses are applied, each of them with a duration of $10 \mu\text{s}$ and a separation of 1 ms. The probe beam is generated by a commercial external-cavity diode laser with a linewidth of $\text{FWHM} = 500 \text{ kHz}$ ³. The probe laser has a linear polarization and a normalized detuning to the atomic resonance of $\delta = (\omega - \omega_0)/\Gamma$, where ω is the laser frequency, ω_0 the atomic transition frequency of the $F = 2 \rightarrow F' = 3$ transition and $\Gamma/2\pi = 6.07 \text{ MHz}$ is the natural linewidth. We ensure that we stay in the weak excitation limit by adapting the probe intensity to the detuning δ , such that the saturation parameter

$$s(\delta) = g \frac{I/I_{\text{sat}}}{1 + 4\delta^2}, \quad (1)$$

remains small with $I_{\text{sat}} = 1.6 \text{ mW cm}^{-2}$ and $g = 7/15$ the degeneracy factor of the transition for equipopulated Zeeman states. The dynamic range for the light detection is mainly determined by the extinction ratio of the probe, which is achieved to a level of 10^{-4} by using two acousto-optical modulators in series and being satisfactory faster ($t_{\text{switch}} \approx 15 \text{ ns}$) than the natural lifetime of the excited state, $\tau_{\text{at}} = \Gamma^{-1} = 26 \text{ ns}$. Due to the free expansion of the cloud during the pulse series, the optical depth changes for every pulse. After the pulse series the MOT is turned on again and most of the atoms are recaptured. This leads to a total cycle duration below 150 ms and allows averaging over a large number of cycles ($\sim 500\,000$) for each measurement. As sketched in figure 1 the scattered light is collected via a two-inch lens under an angle of 35° and collected by a hybrid photo

³ Compared to our previous study of subradiance [20], we have changed the probe laser (Toptica DLpro) to have a much narrower spectrum. In order to validate the subradiance interpretation of the slow decays at large detuning, it is indeed very important to insure that no resonant photon could create unwanted radiation trapping. As detailed in the supplemental material of [20], the main source of spurious resonant photons was the wings of the laser spectrum. Moreover, a broad spectrum for the probe beam also affects radiation trapping experiments, as studied in detail in [29]. We have fully characterized the spectrum of our new laser and we have checked by RW simulations that the wings of the spectrum are negligible for all experiments presented here.



multiplier (HPM, ref. R10467U-50 from Hamamatsu). The signal is recorded via a multichannel scaler (MCS) with a time resolution of 1.6 ns while averaging over the cycles.

The optical depth during the pulse series is calibrated afterwards via absorption imaging⁴. In the following we will note b_0 the optical depth of the cloud on resonance assuming the Clebsch–Gordan coefficient of the transition is unity, which corresponds for a Gaussian cloud to $b_0 = 3N/(kR)^2$ with N the atom number and R the rms radius. The actual detuning-dependent optical depth is then given by

$$b(\delta) = g \frac{b_0}{1 + 4\delta^2}, \quad (2)$$

including the degeneracy factor $g = 7/15$ of the probed transition.

3. Observation of subradiance

The direct observation of subradiance for a large number of atoms N was accomplished in [20]. We present here similar measurements to confirm the results with the upgraded set-up (see footnote 3), as well as to serve as a reference for the following measurements.

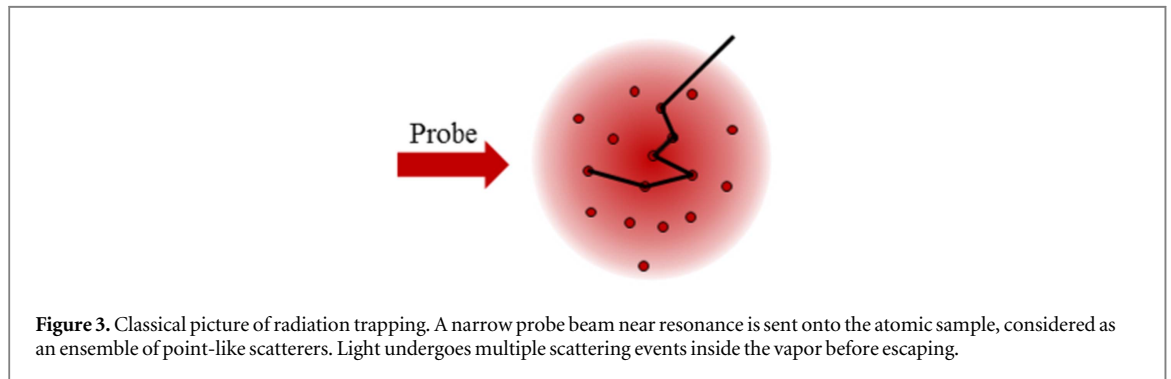
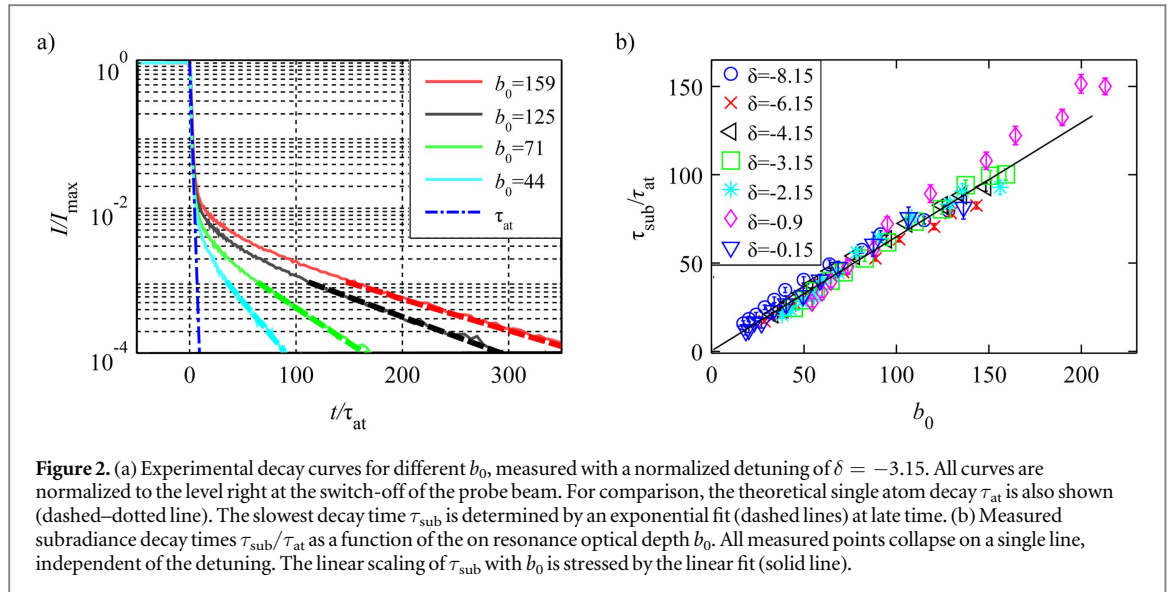
In this section, we use a driving beam which is much larger in diameter than the atomic cloud, with a waist ($1/e^2$ radius) $w = 5.7$ mm, creating a homogenous excitation of the cloud. The saturation parameter is set to $s(\delta) \approx 0.02$. In figure 2(a) an example of a data set acquired with a detuning of $\delta = -3.15$ is shown. Four decay curves are plotted, corresponding to different pulses and thus to different values for b_0 . After an initial fast decay down to an amplitude of $\sim 10^{-2}$ relative to the steady-state level (before switch-off), a very slow decay is well visible, with a time constant that clearly changes with b_0 . To characterize this time constant, we choose to fit the experimental decay curve by a single decaying exponential in a range defined as one decade above the noise floor. This procedure thus corresponds to the longest visible decay time.

We performed a series of measurements for different detunings δ . The measured time constants τ_{sub} , in unit of the single atom decay time τ_{at} are shown in figure 2(b) as a function of the on-resonant optical depth b_0 for the different detunings. All points collapse on a single curve, well fitted by a single line with $\tau_{\text{sub}}/\tau_{\text{at}} \approx 1 + 0.65 b_0$. This demonstrates that this longest decay time is independent of the detuning and scales linearly with b_0 , in perfect agreement with the expectations for subradiance [1, 20–22].

4. Simultaneous observation of radiation trapping and subradiance

As the data of figure 2(b) show, the decay rate at long time is independent of the detuning, even close to resonance. This fact might come surprising, since close to resonance, the actual optical depth $b(\delta)$ is large, which induces attenuation of the driving beam inside the sample and multiple scattering. It has been shown in previous studies that this indeed leads to a suppression of some cooperative effects close to resonance, i.e. the fast decaying modes of superradiance [19, 39]. Nevertheless, the slow-decaying modes remain visible and are even enhanced

⁴ See the supplemental material of [20] for the detailed calibration procedure.



on resonance [20, 39]. This raises the question of the interpretation of these slow-decaying modes near resonance: subradiance or radiation trapping due to multiple scattering?

4.1. Classical description of radiation trapping

To describe multiple scattering of light, the basic quantity is the mean-free path $\ell_{\text{sc}} = 1/(\rho\sigma_{\text{sc}})$, where ρ is the density of scatterers and σ_{sc} their scattering cross section. We suppose here that the scattering diagram is isotropic, which is a good approximation for multi-level Rb atoms, where all Zeeman-sublevels of the $F = 2$ ground state are equally populated [40].

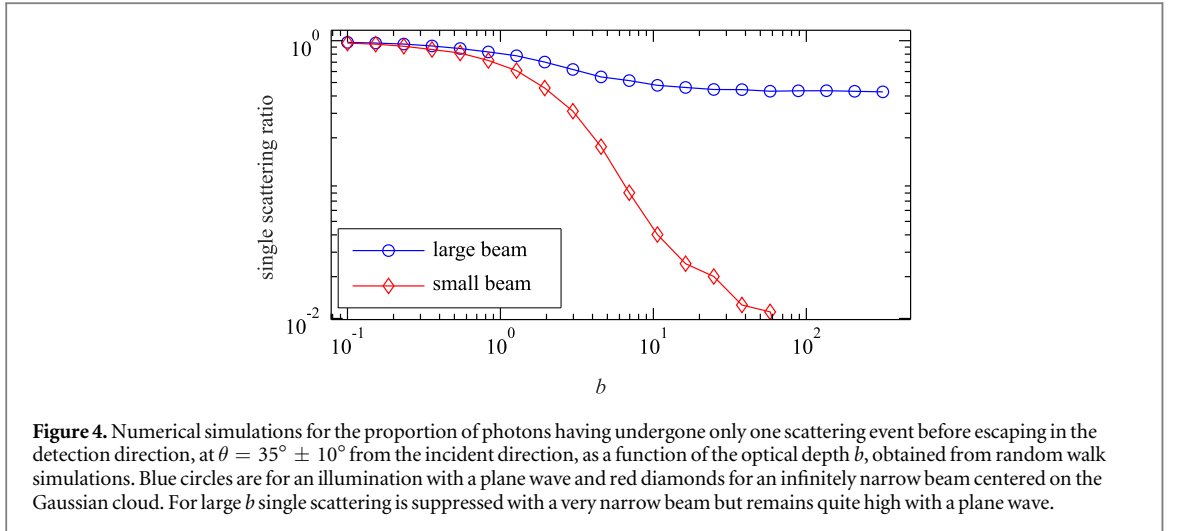
In a scattering medium of size much larger than the mean-free path (large optical depth), light is scattered many times before escaping (figure 3). In this case, many observables can be very well described by a diffusion equation for the electromagnetic energy density, at the condition to perform an average over the disorder configurations [41]. In three dimensions the spatial diffusion coefficient reads

$$D = \frac{v_E \ell_{\text{sc}}}{3} = \frac{\ell_{\text{sc}}^2}{3\tau_{\text{tr}}}, \quad (3)$$

where $v_E = \ell_{\text{sc}}/\tau_{\text{tr}}$ is the energy transport velocity inside the medium and τ_{tr} the transport time [42]. The transport time is the sum of the group delay between two scattering events and the delay associated with the elastic scattering process, called Wigner's delay time τ_{W} [23, 28]:

$$\tau_{\text{tr}} = \tau_{\text{W}} + \frac{\ell_{\text{sc}}}{v_g}, \quad (4)$$

where v_g is the group velocity. For near-resonant light, a remarkable property of cold atomic vapor is that $\tau_{\text{tr}} = \tau_{\text{at}}$, the lifetime of the excited state, independently of the detuning [23, 28] (see appendix A for discussion and full derivation of this property).



As a consequence, the temporal dynamics of the diffuse light is mainly governed by the number of scattering events $\langle N_{sc} \rangle$ that light undergoes before escaping the atomic cloud. This number can be evaluated from hand-waving arguments based on a diffusion process. In 3D, the energy density spreads as $\langle r^2 \rangle = 6Dt$. Then the average number of scattering events for escaping photons is the ratio between the time spent in the system and the scattering time τ_{at} ,

$$\langle N_{sc} \rangle = \frac{t}{\tau_{at}} = \frac{\langle r^2 \rangle}{6D\tau_{at}}. \quad (5)$$

The radiation can escape the system when $\sqrt{\langle r^2 \rangle} \sim R = b\ell_{sc}/2$. Using $D = \ell_{sc}^2/(3\tau_{at})$ leads to $\langle N_{sc} \rangle \sim b^2/8$. In the diffusive regime (large b), radiation trapping times are thus expected to scale as b^2 , with a precise numerical prefactor that depends on the geometry of the medium [28, 43].

Since radiation trapping scales as b^2 and subradiance as b_0 , one can expect that for large enough b , radiation trapping leads to a slower decay than subradiance and dominates the long time dynamics. As we will see in section 5.2, this is indeed what numerical simulations performed at zero temperature show.

However, frequency redistribution due to Doppler broadening breaks the b^2 scaling. Indeed, at each scattering event, light is Doppler shifted by only a small amount, but at large optical thickness the number of scattering events becomes large and a part of the light eventually gets out of resonance. This mechanism thus limits the number of scattering events, and consequently the characteristic time of radiation trapping [28, 29], which scales almost linearly with b [31]. There is however, to our knowledge, no analytical description of radiation trapping in this regime and one has to use numerical simulations including the frequency redistribution to describe the decay dynamics. Such simulations will be discussed in section 5.3.

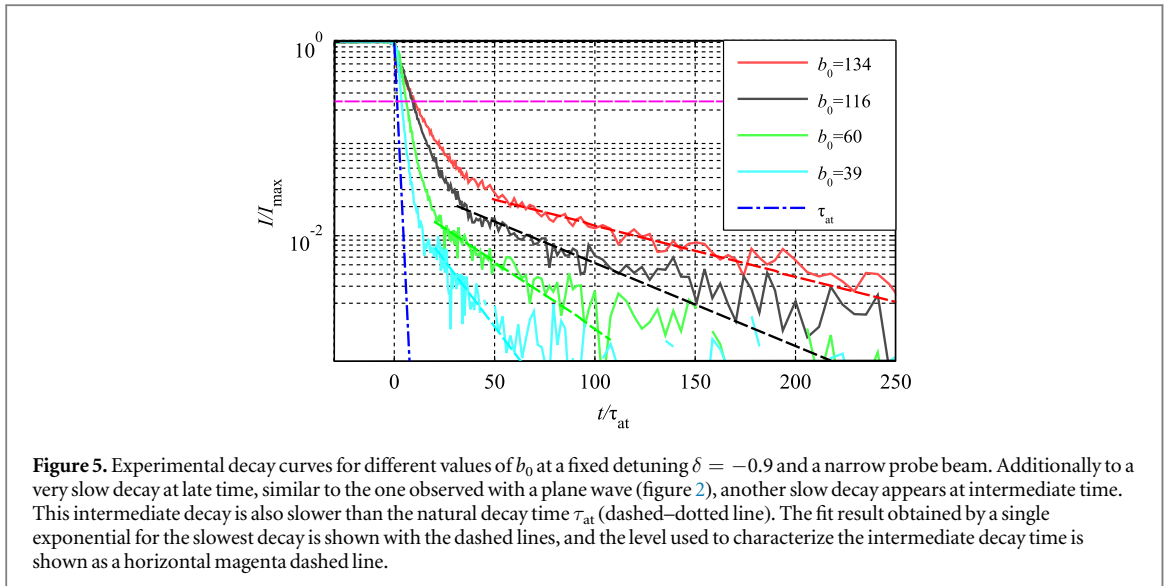
4.2. Impact of the probe beam size

Beside the time scale of radiation trapping, the relative amplitude of the slow-decaying part of the signal is of paramount importance to be able to observe radiation trapping. This is largely related to the relative proportion of multiply scattered light in the detected signal, which is itself related to the geometry of the experiment, especially the size of the exciting beam, the cloud shape and detection direction.

We illustrate this by showing in figure 4 the proportion of photons having undergone only one scattering event before escaping the sample in the detection direction, for excitation with a plane wave and with a beam sufficiently smaller than the cloud. It shows that for large optical depth, single scattering is suppressed with a very narrow beam, as is intuitively expected, and so the detected signal is almost exclusively due to multiply scattered light. This is very different for an illuminating beam larger than the cloud, like a plane wave, because a non-negligible proportion of the incoming light will probe the edges of the atomic cloud, where the optical depth is much lower, and slowly tends to zero with a Gaussian cloud. Therefore there is always a large proportion of single and low-order scattering, even for very large optical depth b (defined for light crossing the cloud along its center).

For the subradiance measurement presented in [20] and in section 2, the probe beam is much larger than the atomic cloud, which leads to a dominant contribution of single and low-order scattering, even on resonance. The slow decay that could be due to radiation trapping has thus a reduced relative amplitude, and subradiance dominates.

In order to study radiation trapping, it is thus necessary to use a driving beam significantly smaller than the size of the atomic sample, as in [28]. We will use in the following a beam with a waist $w = 200 \mu\text{m}$, well below the radius of the atomic cloud.



The strong reduction of the beam size comes along with several experimental difficulties. First, the intensity has to remain low enough in order to keep the saturation parameter still small, which for a narrow beam size corresponds to very low power, and thus a reduced detected signal. Second, because of multiple scattering, the amount of scattered light near the forward direction *decreases* when the optical depth increases [8], much more strongly than with a plane wave where light is transmitted near the edges. As a consequence we were not able to acquire data with a sufficient dynamics for detunings very close to resonance, and the dynamics of the recorded decay curves with a narrow beam is not as good as those recorded with a plane wave (more than 4 decades in figure 2). Nevertheless, we were able to obtain clear signatures of radiation trapping and subradiance, as detailed in the following.

4.3. Measurements and data analysis

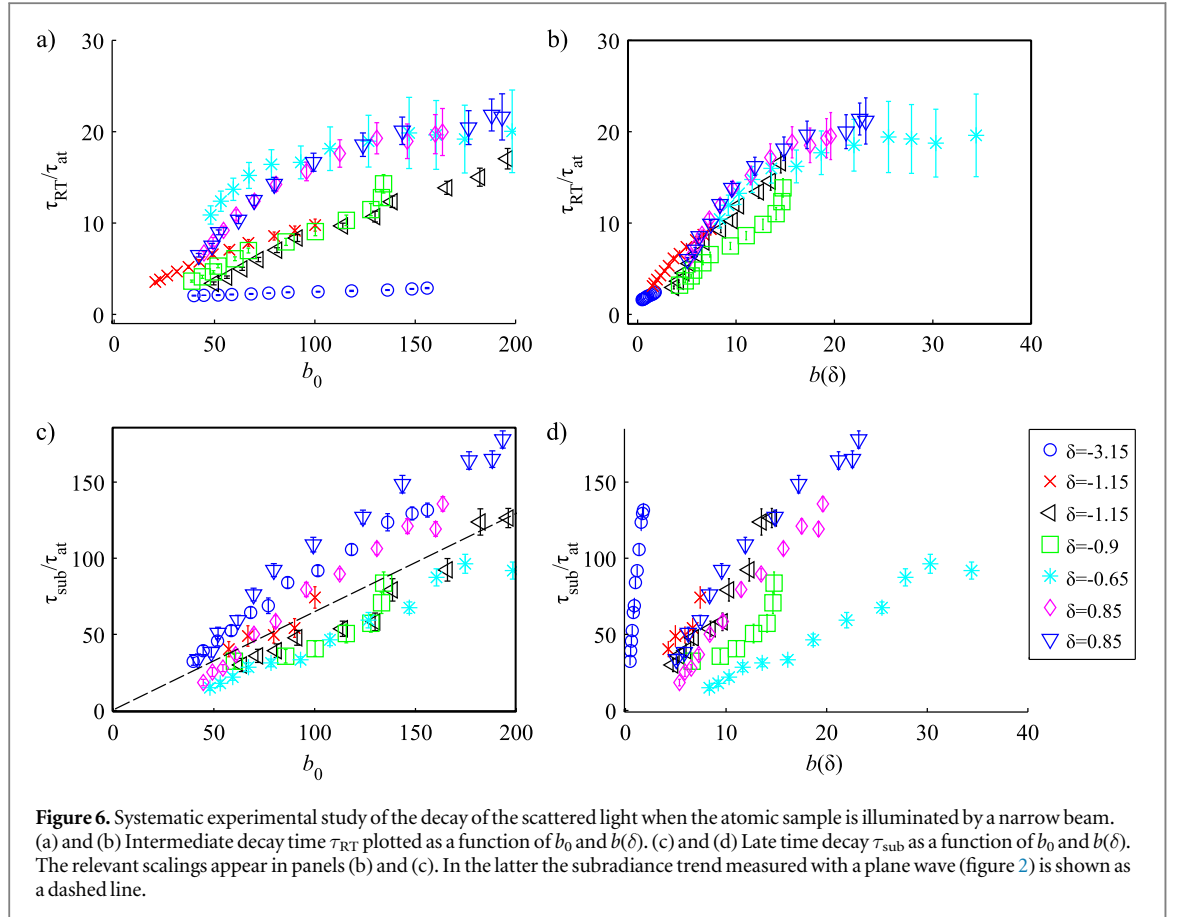
The experimental setup and procedure is the same as described in section 2, except the size of the probe beam, which now has a waist of $w = 200 \mu\text{m}$. Measurements with this narrow beam are shown in figure 5. The decay curves are averaged over 600 000 cycles and the different values for the optical depth are again due to the free expansion of the cloud during the pulse series. The curves are recorded for a detuning of $\delta = -0.9$, which is close enough to resonance to be in the multiple scattering regime ($b(\delta) \gg 1$). At long time, we clearly observe a very slow decay similar to the subradiant decay observed with a plane wave (figure 2). However, the decay at short and intermediate time is now much slower than in the plane wave case. The two parts of the decay curves evolve both with the optical depth.

In order to interpret these curves and identify the physical mechanisms at the origin of the two slow decays, we have performed systematic measurements for several b_0 and δ . We have kept the saturation parameter lower than 0.4 for all data and the lowest count rate in steady-state was 6×10^5 counts per seconds.

In order to characterize those decays by simple numbers, we have used the following procedure. For the late time decay we use a single exponential fit and we keep the same fitting range as for the previous measurements with a plane wave, i.e. one decade above the noise floor. The characterization of the intermediate decay is less straightforward since it is clearly not a single exponential decay. We have chosen to measure the time at which the normalized intensity reaches $e^{-1} = 36.8\%$ as an effective decay time. This level seemed a good trade-off between waiting long enough such that the fastest modes have decayed and not too long not to enter the late time decay. A reliable determination of this time has to take into account the non-negligible amount of detected light which does not come from the cold atoms but from the scattering off the glass windows and the background hot vapor, such that the 36.8% level is always defined respective to the steady-state level of the light scattered by the cold atoms. The corresponding level is shown in figure 5 as a dashed horizontal line.

The results of the measured decay times for several b_0 and δ are shown in figure 6. In the first row (panels (a) and (b)), we plot the effective decay time characterizing the intermediate decay, noted τ_{RT} , and in the second row (panels (c) and (d)) we plot the slowest decay time, noted τ_{sub} . Moreover, in order to identify the relevant scaling parameter for each decay time, we plot them as a function of b_0 (left panels (a) and (c)) and $b(\delta)$ (right panels (b) and (d)). One can see that b_0 is not the right parameter governing the intermediate decay (figure 6(a)) and $b(\delta)$ is not the right parameter governing the long time decay (figure 6(d)). The relevant scaling are those of figure 6(b), (c), highlighted by thick mirrored axes.

The measured values τ_{RT} for the intermediate decay plotted as a function of $b(\delta)$ all collapse quite well on a single curve, showing that the optical thickness governs this decay. We therefore associate this to radiation



trapping. Note that τ_{RT} does not scale as b^2 , which is partly due to the Doppler-induced frequency redistribution, as already explained, and also partly due to our empirical definition of τ_{RT} , which does not correspond to the lifetime of the longest-lived diffusive mode. The data is in fair agreement with the RW simulations shown in section 5.3, which demonstrates that classical multiple scattering is a sufficient ingredient to explain this part of the decay curve. However we note that the scaling with $b(\delta)$ has been obtained using an empirical frequency shift of $-0.15\Gamma \approx 0.9$ MHz for the probe detuning, which might be due to calibration errors or spurious magnetic fields. All data are presented with this shifted detuning.

The measured values τ_{sub} for the slowest decay time plotted as a function of b_0 are scattered around the trend of the subradiance decay measured with the plane wave (figure 2), shown by the dashed line. We do not observe any significant systematic effect with the detuning. The higher level of the noise floor compared to the plane wave data, due to the reduced probe power, explains the spreading of the data, but the trend shows unambiguously that this decay is similar to the one observed with the plane wave, and can thus be attributed to subradiance. As a consequence, we can conclude that with these parameters, in particular the temperature $T \approx 100$ μ K, the late time decay is dominated by subradiance, even with a narrow exciting beam, at least up to $b \sim 35$, which is the maximum we have been able to study in our experiment.

5. Numerical simulations

In order to provide further evidence of our interpretation to distinguish radiation trapping from subradiance, we now turn to numerical simulations. Numerical simulations allow us to discuss the physics of subradiance and radiation trapping in an idealized scenario, for example at zero temperature. It also allows comparing the data to a model including a number of experimental imperfections.

5.1. Description of the models

We use two very different models in the following: coupled dipole (CD) equations and random walk (RW) simulations.

The CD model has been widely used in the last years in the context of single-photon superradiance and subradiance [4, 17, 19–21, 44–48]. It considers N two-level atoms at random positions r_i driven by an incident laser (Rabi frequency $\Omega(r)$, detuning Δ). Restricting the Hilbert space to the subspace spanned by the ground state of the atoms $|G\rangle = |g \cdots g\rangle$ and the singly excited states $|i\rangle = |g \cdots e_i \cdots g\rangle$ and tracing over the photon

degrees of freedom, one obtains an effective Hamiltonian describing the time evolution of the atomic wave function $|\psi(t)\rangle$,

$$|\psi(t)\rangle = \alpha(t)|G\rangle + \sum_{i=1}^N \beta_i(t)|i\rangle. \quad (6)$$

Considering the low intensity limit, when atoms are mainly in their ground states, i.e. $\alpha \simeq 1$, the problem amounts to determine the amplitudes β_i , which are then given by the linear system of coupled equations

$$\dot{\beta}_i = \left(i\Delta - \frac{\Gamma}{2} \right) \beta_i - \frac{i\Omega_i}{2} + \frac{i\Gamma}{2} \sum_{i \neq j} V_{ij} \beta_j. \quad (7)$$

These equations are the same as those describing N classical dipoles driven by an oscillating electric field [46]. The first term on the left-hand side corresponds to the natural evolution of independent dipoles, the second one to the driving by the external laser, the last term corresponds to the dipole–dipole interaction and is responsible for all collective effects. In the scalar model for light, which neglects polarization effects and near-field terms in the dipole–dipole interaction, it reads

$$V_{ij} = \frac{e^{ik_0 r_{ij}}}{k_0 r_{ij}}, \text{ with } r_{ij} = |\mathbf{r}_i - \mathbf{r}_j|, \quad (8)$$

where $k_0 = \omega_0/c$ is the wavevector associated to the transition. Neglecting the near-field terms of the dipole–dipole interaction is a good approximation for dilute clouds, i.e. when the typical distance between atoms is much larger than the wavelength, which is the case in the experiment. The impact of the polarization of light on subradiance, as well as the Zeeman structure of the atoms, is still an open question and has been the subject of several recent theoretical works [49–51]. From the computed values of β_i , we can derive the intensity of the light radiated by the cloud as a function of time and of the angle [47]. Technical details on the simulations can be found in [22].

The second model is a RW model, where the atoms are treated as classical scatterers and photons as particles, neglecting wave aspects. Photons are sent one by one by randomly drawing their initial transverse position according to the exciting laser profile and their initial detuning according to the laser spectrum. The number of scattering events until the photon escapes the medium, as well as its escape direction, is computed from a stochastic algorithm based on the mean-free path [26]. By repeating this with many photons, we can build the distribution of the number of scattering events per photon for a given detection direction. By converting the number of scattering to a time using the transport time τ_{at} (see appendix A) and convoluting by the pulse duration, we obtain a decay curve for the scattered light at the switch-off.

The advantage of the CD model is that it includes interference and cooperative effects. One can also include temperature effects by using time dependent positions of the atoms [21, 52]. However, computing capabilities limit its use to a few thousand atoms and it is thus hard to explore large optical depths without introducing spurious high-density effects. The RW model does not suffer from this limitation and can be applied with the parameters of our experiment. It can also easily account for some experimental imperfections, like the finite linewidth of the laser spectrum. Doppler broadening can also be included ‘by hand’ by a probabilistic frequency shift at each scattering [52], also accounting for subtle effects like the correlation between the frequency shift and the initial detuning and the scattering angle (see, e.g., [53]). However, all coherent and interference effects are neglected. Therefore, comparing the results given by the two models helps identify the relevant physics.

5.2. Comparison between the CD and the RW models in the ideal case

In this section we consider motionless atoms ($T = 0$). In the CD equations, the driving beam profile $\Omega(\mathbf{r})$ is a truncated plane wave of radius $R/2$, where R is the rms radius of the atomic cloud. In the RW simulations, the excitation beam is infinitely narrow and centered on the cloud. In the two models the driving field is perfectly monochromatic.

Examples of decay curves for different optical depths b are shown in figure 7. Solid lines are computed from the CD equations and the dashed lines from RW simulations. Here, the resonant optical depth is fixed, $b_0 = 17$, and the optical depth is changed by varying the detuning. The data for the highest b corresponds to $\delta = 0$. The main observation is that the two models are in good agreement for the highest optical depth, showing that in this case, radiation trapping completely dominates the decay dynamics, and subradiance is not or hardly visible. As the detuning increases and the optical depth decreases accordingly, while b_0 remains large, radiation trapping becomes less and less important. It still dominates the early decay (superradiance is not visible above $b \sim 1$ [19]) but subradiance dominates afterwards.

A systematic comparison between the two models is performed in figure 8, in which we plot the late decay time determined by an exponential fit in the amplitude range $[10^{-3} - 10^{-4}]$. We also show the prediction of a diffusion model for multiple scattering,

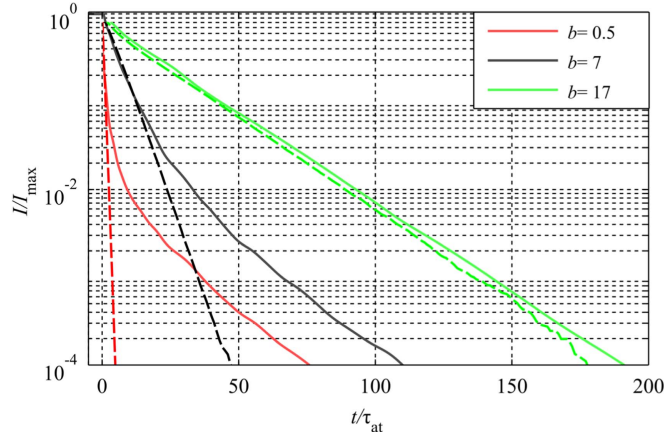


Figure 7. Numerical simulations of the decay for a fixed $b_0 = 17$ and different detunings $\delta = \{0, 0.6, 2.9\}$ in order to vary the optical depth (legend). The solid lines represent the calculations for the coupled-dipole model, the dashed lines show the result for the random walk model. The two models are in agreement at high b . For large b_0 and moderate b (slightly detuned excitation), radiation trapping dominates the decay at the beginning and subradiance dominates at the end. For very large detuning and very low b , superradiance at early times would be visible in the CD model [19].

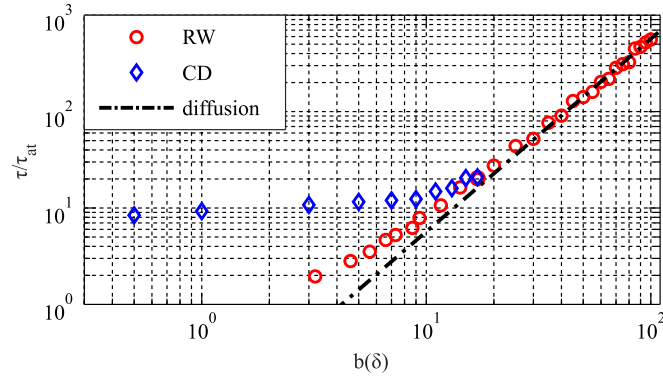


Figure 8. Comparison of the late decay time in different models. The optical depth $b(\delta)$ is changed by varying the detuning and keeping the on-resonant optical depth constant, $b_0 = 17$. Red circles correspond to random walk simulations, blue diamonds to the coupled-dipole model and the dashed-dotted line to the diffusion model (9).

$$\tau_{\text{diff}} = \frac{3b^2}{\alpha\pi^2} \tau_{\text{at}}, \quad (9)$$

with $\alpha \approx 5.35$ for a Gaussian density distribution [28].

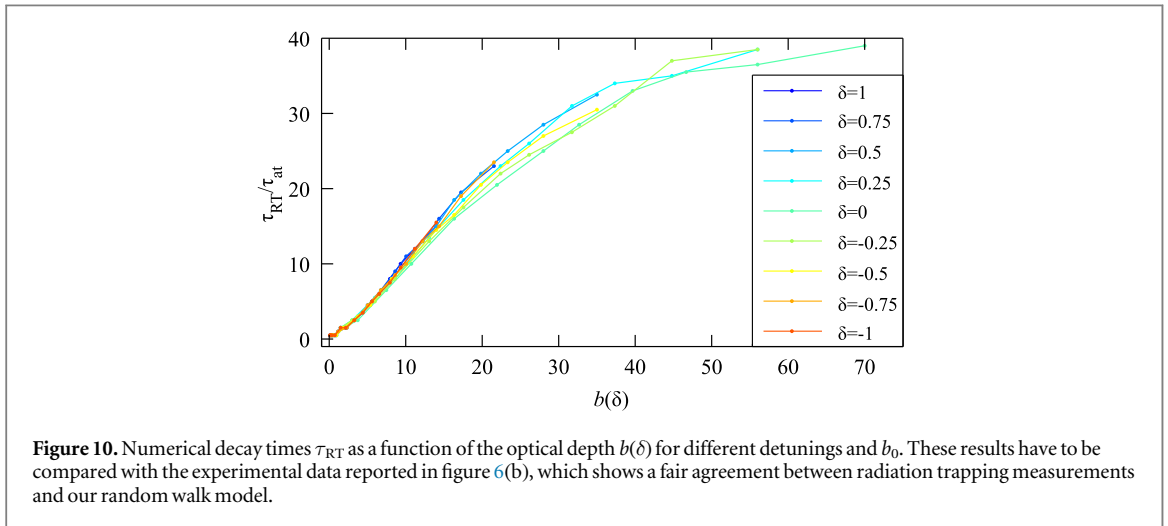
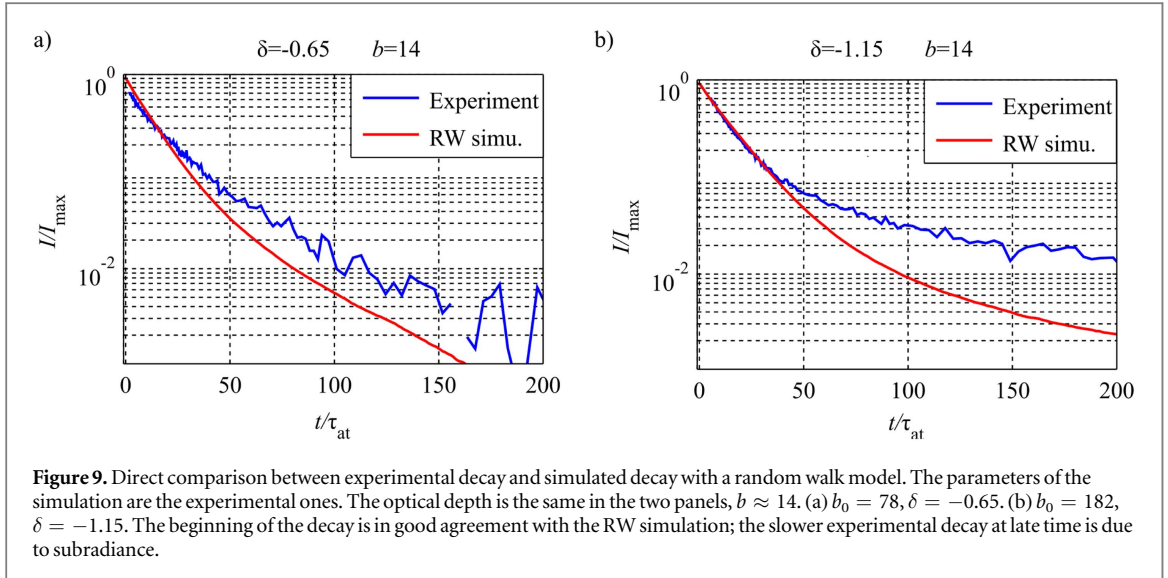
Figure 8 shows that the decay computed by the RW simulation tends toward the asymptotic behavior described by the diffusion equation, which is a good approximation for optical depth larger than $b \sim 20$. More interestingly, the CD model also starts to reach this asymptotic behavior and gives results very close to the RW model above $b \sim 10$. On the contrary, at low b (large δ), the CD model levels to a constant value for the decay time, which corresponds to subradiance, not included in the RW model.

Similar comparisons (not shown here) for resonant excitation and different b_0 show the same behavior: the two models are in agreement above $b \sim 10$ while for smaller b subradiance is visible in the CD model.

To conclude, in this idealized scenario (narrow exciting beam, $T = 0$), subradiance dominates the slow switch-off dynamics for small b and radiation trapping dominates for large b , as expected from the scaling behaviors, respectively linear in b_0 and quadratic in b . Moreover, although the deep multiple scattering regime is hard to explore, these results confirm that radiation trapping is well included in the CD model.

5.3. Comparison between experimental data and RW simulations

The situation is not so simple in the experiment because of a number of effects. As already discussed in [28, 29], the two most important effects are the temperature and the spectrum of the incident laser. First, frequency redistribution during multiple scattering due to Doppler broadening breaks the b^2 scaling law, and can even make it close to a linear scaling [31]. Second, the finite spectrum of the incident laser, with possibly broad wings, can be a source of resonant photons when a moderate detuning is chosen. By combining the two effects, spurious resonant photons could mimic subradiance. Fortunately, these two effects can be included in RW



simulations, which allows us to check that the slow decay due to this spurious radiation trapping is well below the measured slow decay that we attribute to subradiance. We have also checked that a number of other imperfections, such as a slight anisotropy of the cloud or a small misalignment of the beam from the cloud center, are indeed negligible with our parameters (see appendix B).

Figure 9 shows the direct comparison between normalized experimental data and RW simulations performed with the experimental parameters, for the same $b(\delta) \approx 14$ but different b_0 and δ . Since the optical depths are the same, in the ideal case the two RW simulations would give the same results. Their small difference is due to the temperature ($T = 100 \mu\text{K}$) and laser spectrum (FWHM = 500 kHz), which have different effects depending on b_0 and δ . The experimental data, however, have a much larger difference. They are very close to the simulations at early time, which confirms that the measured intermediate decay is well explained by radiation trapping. On the contrary, at long time, the experimental data are significantly above the simulations, a difference which increases with b_0 . This is well consistent with subradiance, absent in the RW model, which dominates at long time.

Moreover, the RW simulations allow the direct comparison with the measured intermediate decay time reported in figure 6(b). Using the same definition for extracting τ_{RT} from the simulated decay, we report in figure 10 the results of systematic simulations for different b_0 and δ , plotted as a function of $b(\delta)$. As previously, the simulations are performed with the parameters of the experiment including the effects of the temperature and laser spectrum. Therefore the decay times do not follow the quadratic behavior expected for the ideal case of zero temperature. With these effects the decay time increases almost linearly with the optical thickness and saturates for large optical thickness. It shows a fair agreement with the experimental data of figure 6(b), without any free parameter, although we observe a discrepancy for the largest optical thickness. Indeed above $b \approx 25$ the time τ_{RT} saturates faster in the experimental data than in the simulations. This could be due to a loss process for the light during multiple scattering, for instance inelastic scattering (Raman scattering, light-induced collisions, scattering by the hot vapor background, etc).

It is interesting to note that despite several experiments on radiation trapping in cold atoms, it is still challenging to observe a clear quadratic dependence of the radiation trapping time with the optical thickness. Indeed one needs at the same time a large cloud (such that the exciting beam can reasonably be smaller), a large optical thickness to be deep in the diffusive regime, and a very cold sample such that frequency redistribution is negligible. More precisely, one needs $bk_0v \ll \Gamma$, where v is the rms width of the velocity distribution [28, 29, 31]. This condition comes from the Doppler shift at each scattering event, which induces a RW of the light frequency of step k_0v , thus producing a broadening given by k_0v times the square root of the number of scattering events, i.e. b . Taking $b = 50$ and $bk_0v = 0.1\Gamma$ gives a temperature $T \approx 1 \mu\text{K}$.

6. Summary

In summary, we have demonstrated that with a large cold atomic cloud of ^{87}Rb driven by a weak laser near resonance, we can observe two different types of slow decay of the scattered light when the laser is switched off. Moreover, with appropriate parameters, the two slow decays appear simultaneously. At early and intermediate time, the decay is mainly due to radiation trapping, i.e. classical multiple scattering. It is well explained by a RW description. At late time, subradiance creates an even slower decay. We find that, at large enough optical depth and at zero temperature, radiation trapping could dominate the whole decay dynamics. However, temperature-induced frequency redistribution limits radiation trapping and in our experiment, subradiance always dominates at late time.

Following previous independent observations of radiation trapping [28, 29] and subradiance [20] as well as a theoretical analysis of the nature of collective long-lived modes of the effective atomic Hamiltonian [39], these new results significantly contribute to clarify the interplay between radiation trapping and subradiance, their dependence with experimental parameters, and more generally the physical interpretation of the slow decay at the switch-off. This is crucial for further use of this kind of experiments for probing more subtle phenomena, as it has been proposed, for instance, for the experimental observation of Anderson localization of light in cold atoms [54].

Acknowledgments

The authors would like to thank Guillaume Labeyrie for fruitful discussions and Ana Cipris for help in final calibration experiments. This work was supported by the ANR (project LOVE, Grant No. ANR-14-CE26-0032), the CAPES and the Deutsche Forschungsgemeinschaft (WE 6356/1-1).

Appendix A. Transport time of light in cold atoms

The transport time is the sum of the group delay between two scattering events and the delay corresponding to the elastic scattering process, called Wigner's delay time τ_W [23, 28]:

$$\tau_{\text{tr}} = \tau_W + \frac{\ell_{\text{sc}}}{v_g}, \quad (\text{A.1})$$

where ℓ_{sc} is the mean-free path and v_g the group velocity.

The fundamental ingredient to compute the different terms is the atomic polarizability,

$$\alpha(\omega) = \frac{6\pi}{k_0^3} \times \frac{-2(\omega - \omega_0)/\Gamma + i}{1 + 4(\omega - \omega_0)^2/\Gamma^2}, \quad (\text{A.2})$$

where $k_0 = \omega_0/c$ is the wavevector associated to the transition. Note that the prefactor $6\pi/k_0^3$ can also be written σ_0/k_0 with σ_0 the resonant scattering cross section. For simplicity, we will also use the notation $\mathcal{L}(\omega)$ for the Lorentzian function

$$\mathcal{L}(\omega) = \frac{1}{1 + 4(\omega - \omega_0)^2/\Gamma^2}. \quad (\text{A.3})$$

The Wigner delay time is given by the energy derivative of the dephasing acquired at the scattering [55, 56],

$$\tau_W = \frac{\partial \phi}{\partial \omega}. \quad (\text{A.4})$$

This phase is actually the argument of the polarizability,

$$\phi(\omega) = \arctan\left(\frac{-\Gamma/2}{\omega - \omega_0}\right), \quad (\text{A.5})$$

which gives

$$\tau_W = \frac{2}{\Gamma} \mathcal{L}(\omega). \quad (\text{A.6})$$

The mean-free path is related to the scattering cross section, proportional to the imaginary part of the polarizability,

$$\ell_{sc} = \frac{1}{\rho\sigma_{sc}} = \frac{1}{\rho\sigma_0 \mathcal{L}(\omega)}. \quad (\text{A.7})$$

Finally, the group velocity is defined by

$$v_g = \frac{\partial\omega}{\partial k}, \quad (\text{A.8})$$

with $k = n k_0$ and n the refractive index. It follows

$$\frac{1}{v_g} = \frac{n}{c} + k_0 \frac{\partial n}{\partial\omega}. \quad (\text{A.9})$$

The refractive index is given by the real part of the polarizability,

$$n - 1 = \frac{\rho}{2} \text{Re}(\alpha). \quad (\text{A.10})$$

Using

$$\text{Re}(\alpha) = \frac{\sigma_0}{k_0} \times -\frac{2(\omega - \omega_0)}{\Gamma} \mathcal{L}(\omega) \quad (\text{A.11})$$

and combining equations (A.7) and (A.9)–(A.11), we obtain

$$\frac{\ell_{sc}}{v_g} = \frac{n\ell_{sc}}{c} + \frac{1}{2\mathcal{L}(\omega)} \frac{\partial}{\partial\omega} \left(-\frac{2(\omega - \omega_0)}{\Gamma} \mathcal{L}(\omega) \right). \quad (\text{A.12})$$

At this stage we consider that the first term is negligible, which is true for sample of reasonable size because $R \ll c/\Gamma$. We thus obtain

$$\frac{\ell_{sc}}{v_g} = -\frac{1}{\Gamma} \left[1 + \frac{(\omega - \omega_0) \mathcal{L}'(\omega)}{\mathcal{L}(\omega)} \right], \quad (\text{A.13})$$

where $\mathcal{L}'(\omega)$ is the derivative of the Lorentzian function,

$$\mathcal{L}'(\omega) = -\frac{8(\omega - \omega_0)}{\Gamma^2} \mathcal{L}(\omega)^2. \quad (\text{A.14})$$

We obtain

$$\frac{\ell_{sc}}{v_g} = -\frac{1}{\Gamma} \left[1 - \frac{8(\omega - \omega_0)^2}{\Gamma^2} \mathcal{L}(\omega) \right]. \quad (\text{A.15})$$

Finally, combining equations (A.6) and (A.15) in equation (A.1) leads to

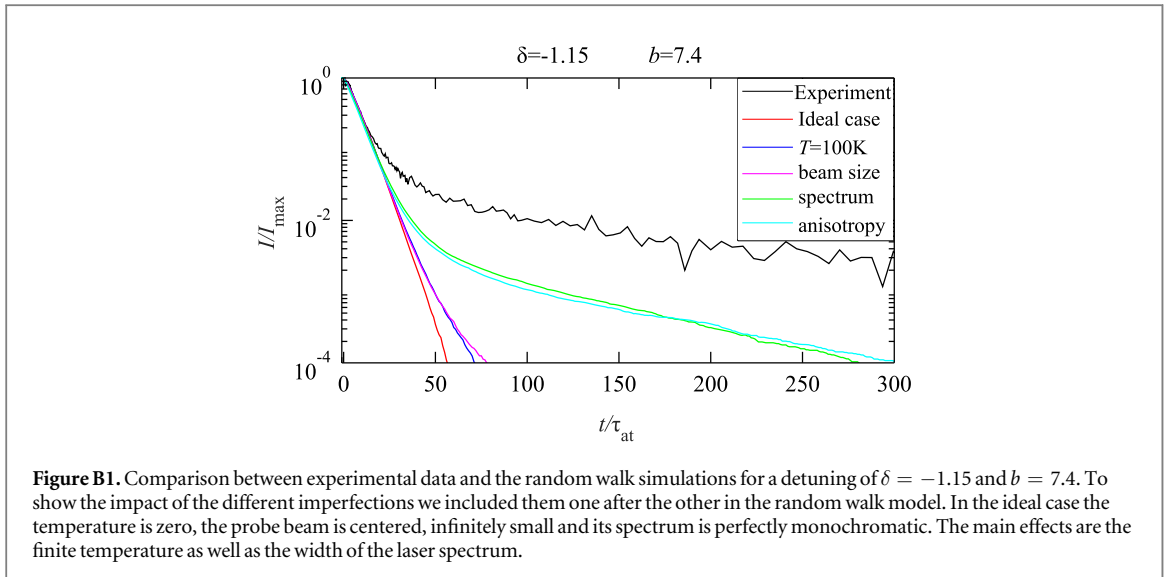
$$\tau_{tr} = \frac{1}{\Gamma} \left[2\mathcal{L}(\omega) - 1 + \frac{8(\omega - \omega_0)^2}{\Gamma^2} \mathcal{L}(\omega) \right] \quad (\text{A.16})$$

$$= \frac{1}{\Gamma} \left\{ 2\mathcal{L}(\omega) \left[1 + \frac{4(\omega - \omega_0)^2}{\Gamma^2} \right] - 1 \right\} \quad (\text{A.17})$$

$$= \tau_{at}. \quad (\text{A.18})$$

Although this result is well known, writing down its derivation allows one to notice that near resonance, the Wigner time is actually *larger* than the natural lifetime of the excited state, and this is compensated by a *negative* group velocity. This shows that the simple physical picture of photons bouncing between atoms with a well ordered sequence of events, with some duration for the scattering process and some duration for the propagation between atoms, is clearly a bad picture. Yet, it works surprisingly well in a great number of circumstances.

Another remark is that RW simulations are considered to neglect coherent and wave effects, which is true for diffraction, interference or cooperativity. But, as far as the temporal dynamics is concerned, a bit of wave physics enters with the use of equation (A.18), since it relies on wave quantities like the group velocity or the dephasing at the scattering process. Moreover it also relies on the refractive index, which is a coherent and collective quantity. In this respect, the RW model corresponds to a hybrid approach.



Appendix B. Influence of imperfections

To evaluate which experimental imperfections influence the radiation trapping decay we performed a systematic study by adding one effect after the other in the RW simulations. We also want to check that none of these imperfections is strong enough to create spurious photons on resonance, which would mimic subradiance. We thus used the parameters of the data taken off resonance, at $\delta = -1.15$.

The curves are shown in figure B1, starting from the ideal case of zero temperature, an infinitely narrow beam crossing the sample at its center, a spherical Gaussian atomic distribution and a perfectly monochromatic light. First, the finite temperature is added, which changes the slope of the late decay. Afterward the finite beam size is added, which does not affect the decay much since the beam is still much smaller than the cloud. Next the finite width of the probe spectrum (FWHM = 500 kHz), including its measured Lorentzian wings, is added, which leads to a significant change in the decay time as well as in the relative level of the slow decay. This is due to the resonant photons contained in the broad Lorentzian wings of the laser spectrum. Finally the slight anisotropy in the cloud shape is added, which only leads to a minor change. We also display the corresponding experimental data, which shows that the slow decay at late time, attributed to subradiance, is indeed well above the simulated radiation trapping decay.

References

- [1] Guerin W, Rouabah M T and Kaiser R 2017 Light interacting with atomic ensembles: collective, cooperative and mesoscopic effects *J. Mod. Opt.* **64** 895–907
- [2] Kupriyanov D V, Sokolov I M and Havey M D 2017 Mesoscopic coherence in light scattering from cold, optically dense and disordered atomic systems *Phys. Rep.* **671** 1–60
- [3] Ruostekoski J and Javanainen J 1997 Quantum field theory of cooperative atom response: low light intensity *Phys. Rev. A* **55** 513–26
- [4] Scully M O, Fry E S, Raymond Ooi C H and Wódkiewicz K 2006 Directed spontaneous emission from an extended ensemble of N atoms: timing is everything *Phys. Rev. Lett.* **96** 010501
- [5] Eberly J H 2006 Emission of one photon in an electric dipole transition of one among N atoms *J. Phys. B: At. Mol. Opt. Phys.* **39** S599–604
- [6] Scully M O 2009 Collective Lamb shift in single photon Dicke superradiance *Phys. Rev. Lett.* **102** 143601
- [7] Matsko A B, Novikova I, Scully M O and Welch G R 2001 Radiation trapping in coherent media *Phys. Rev. Lett.* **87** 133601
- [8] Labeyrie G, Delande D, Müller C A, Miniatura C and Kaiser R 2004 Multiple scattering of light in a resonant medium *Opt. Commun.* **243** 157–64
- [9] Labeyrie G, de Tomasi F, Bernard J-C, Müller C A, Miniatura C and Kaiser R 1999 Coherent backscattering of light by cold atoms *Phys. Rev. Lett.* **83** 5266–9
- [10] Bidely J, Klappauf B, Bernard J C, Delande D, Labeyrie G, Miniatura C, Wilkowski D and Kaiser R 2002 Coherent light transport in a cold strontium cloud *Phys. Rev. Lett.* **88** 203902
- [11] Röhlberger R, Schlage K, Sahoo B, Couet S and Ruffer R 2010 Collective Lamb shift in single-photon superradiance *Science* **328** 1248–51
- [12] Keaveney J, Sargsyan A, Krohn U, Hughes I G, Sarkisyan D and Adams C S 2012 Cooperative Lamb shift in an atomic vapor layer of nanometer thickness *Phys. Rev. Lett.* **108** 173601
- [13] Pellegrino J, Bourgain R, Jennewein S, Sortais Y R P, Browaeys A, Jenkins S D and Ruostekoski J 2014 Observation of suppression of light scattering induced by dipole–dipole interactions in a cold-atom ensemble *Phys. Rev. Lett.* **113** 133602
- [14] Okaba S, Takano T, Benabid F, Bradley T, Vincetti L, Maizelis Z, Yampol’skii V, Nori F and Katori H 2014 Lamb–Dicke spectroscopy of atoms in a hollow-core photonic crystal fibre *Nat. Commun.* **5** 4096
- [15] Bromley S L et al 2016 Collective atomic scattering and motional effects in a dense coherent medium *Nat. Commun.* **7** 11039
- [16] Jennewein S, Besbes M, Schilder N J, Jenkins S D, Sauvan C, Ruostekoski J, Greffet J-J, Sortais Y R P and Browaeys A 2016 Coherent scattering of near-resonant light by a dense microscopic cold atomic cloud *Phys. Rev. Lett.* **116** 233601

- [17] Roof S J, Kemp K J, Havey M D and Sokolov I M 2016 Observation of single-photon superradiance and the cooperative Lamb shift in an extended sample of cold atoms *Phys. Rev. Lett.* **117** 073003
- [18] Corman L, Ville J L, Saint-Jalm R, Aidelsburger M, Bienaimé T, Nascimbène S, Dalibard J and Beugnon J 2017 Transmission of near-resonant light through a dense slab of cold atoms *Phys. Rev. A* **96** 053629
- [19] Araújo M O, Krešić I, Kaiser R and Guerin W 2016 Superradiance in a large cloud of cold atoms in the linear-optics regime *Phys. Rev. Lett.* **117** 073002
- [20] Guerin W, Araújo M O and Kaiser R 2016 Subradiance in a large cloud of cold atoms *Phys. Rev. Lett.* **116** 083601
- [21] Bienaimé T, Piovella N and Kaiser R 2012 Controlled Dicke subradiance from a large cloud of two-level systems *Phys. Rev. Lett.* **108** 123602
- [22] Araújo M O, Guerin W and Kaiser R 2018 Decay dynamics in the coupled-dipole model *J. Mod. Opt.* **65** 1345–54
- [23] Legendijk A and van Tiggelen B A 1996 Resonant multiple scattering of light *Phys. Rep.* **270** 143–215
- [24] Carl Kenty 1932 On radiation diffusion and the rapidity of escape of resonance radiation from a gas *Phys. Rev.* **42** 823–42
- [25] Holstein T 1947 Imprisonment of resonance radiation in gases *Phys. Rev.* **72** 1212–33
- [26] Molisch A F and Oehry B P 1998 *Radiation Trapping in Atomic Vapours* (Oxford: Oxford University Press)
- [27] Fioretti A, Molisch A F, Mutter J H, Verkerk P and Allegrini M 1998 Observation of radiation trapping in a dense Cs magneto-optical trap *Opt. Commun.* **149** 415–22
- [28] Labeyrie G, Vaujour E, Müller C A, Delande D, Miniatura C, Wilkowski D and Kaiser R 2003 Slow diffusion of light in a cold atomic cloud *Phys. Rev. Lett.* **91** 223904
- [29] Labeyrie G, Kaiser R and Delande D 2005 Radiation trapping in a cold atomic gas *Appl. Phys. B* **81** 1001–8
- [30] Balik S, Olave R G, Sukenik C I, Havey M D, Datsyuk V M, Sokolov I M and Kupriyanov D V 2005 Alignment dynamics of slow light diffusion in ultracold atomic ^{85}Rb *Phys. Rev. A* **72** 051402
- [31] Pierrat R, Grémaud B and Delande D 2009 Enhancement of radiation trapping for quasiresonant scatterers at low temperature *Phys. Rev. A* **80** 013831
- [32] Balik S, Win A L, Havey M D, Sokolov I M and Kupriyanov D V 2013 Near-resonance light scattering from a high-density ultracold atomic ^{87}Rb gas *Phys. Rev. A* **87** 053817
- [33] Cummings F W 1986 Spontaneous emission from a single two-level atom in the presence of N initially unexcited identical atoms *Phys. Rev. A* **33** 1683–7
- [34] Rusek M, Orłowski A and Mostowski J 1996 Localization of light in three-dimensional random dielectric media *Phys. Rev. E* **53** 4122–30
- [35] Rusek M, Mostowski J and Orłowski A 2000 Random Green matrices: from proximity resonances to Anderson localization *Phys. Rev. A* **61** 022704
- [36] Pinheiro F A, Rusek M, Orłowski A and van Tiggelen B A 2004 Probing Anderson localization of light via decay rate statistics *Phys. Rev. E* **69** 026605
- [37] Skipetrov S E and Sokolov I M 2014 Absence of Anderson localization of light in a random ensemble of point scatterers *Phys. Rev. Lett.* **112** 023905
- [38] Bellando L, Gero A, Akkermans E and Kaiser R 2014 Cooperative effects and disorder: a scaling analysis of the spectrum of the effective atomic Hamiltonian *Phys. Rev. A* **90** 063822
- [39] Guerin W and Kaiser R 2017 Population of collective modes in light scattering by many atoms *Phys. Rev. A* **95** 053865
- [40] Greene C H and Zare R N 1982 Photofragment alignment and orientation *Annu. Rev. Phys. Chem.* **33** 119–50
- [41] Johnson P, Imhof A, Bret B P J, Rivas J G and Legendijk A 2003 Time-resolved pulse propagation in a strongly scattering material *Phys. Rev. E* **68** 016604
- [42] van Rossum M C W and Nieuwenhuizen T M 1999 Multiple scattering of classical waves: microscopy, mesoscopy, and diffusion *Rev. Mod. Phys.* **71** 313–71
- [43] Cao H 2003 Lasing in random media *Waves Random Media* **13** R1–39
- [44] Scully M O and Svidzinsky A A 2009 The super of superradiance *Science* **325** 1510–1
- [45] Courteille P W, Bux S, Lucioni E, Lauber K, Bienaimé T, Kaiser R and Piovella N 2010 Modification of radiation pressure due to cooperative scattering of light *Eur. Phys. J. D* **58** 69–73
- [46] Svidzinsky A A, Chang J-T and Scully M O 2010 Cooperative spontaneous emission of N atoms: many-body eigenstates, the effect of virtual Lamb shift processes, and analogy with radiation of N classical oscillators *Phys. Rev. A* **81** 053821
- [47] Bienaimé T, Petruzzo M, Bigerni D, Piovella N and Kaiser R 2011 Atom and photon measurement in cooperative scattering by cold atoms *J. Mod. Opt.* **58** 1942–50
- [48] Bienaimé T, Bachelard R, Courteille P W, Piovella N and Kaiser R 2013 Cooperativity in light scattering by cold atoms *Fortschr. Phys.* **61** 377–92
- [49] Lee M D, Jenkins S D and Ruostekoski J 2016 Stochastic methods for light propagation and recurrent scattering in saturated and nonsaturated atomic ensembles *Phys. Rev. A* **93** 063803
- [50] Hebenstreit M, Kraus B, Ostermann L and Ritsch H 2017 Subradiance via entanglement in atoms with several independent decay channels *Phys. Rev. Lett.* **118** 143602
- [51] Sutherland R T and Robicheaux F 2017 Degenerate Zeeman ground states in the single-excitation regime *Phys. Rev. A* **96** 053840
- [52] Eloy A, Yao Z, Bachelard R, Guerin W, Fouché M and Kaiser R 2018 Diffusive wave spectroscopy of cold atoms in ballistic motion *Phys. Rev. A* **97** 013810
- [53] Carvalho J C de A, Oriá M, Chevrollier M, de Souza Cavalcante H L D and Passerat de Silans T 2015 Redistribution of light frequency by multiple scattering in a resonant atomic vapor *Phys. Rev. A* **91** 053846
- [54] Skipetrov S E, Sokolov I M and Havey M D 2016 Control of light trapping in a large atomic system by a static magnetic field *Phys. Rev. A* **94** 013825
- [55] Wigner E P 1955 Lower limit for the energy derivative of the scattering phase shift *Phys. Rev.* **98** 145
- [56] Bourgain R, Pellegrino J, Jennewein S, Sortais Y R P and Browaeys A 2013 Direct measurement of the Wigner time delay for the scattering of light by a single atom *Opt. Lett.* **38** 1963–5

VI.5.2. Update with recent results

In the previous paper, and also in the Supplemental material of [Guerin 2016a], we made a dedicated effort to make sure that the quantity of spurious light near resonance was always small enough to be unable to explain the data with a random walk model. Although I still think that a random walk model is not able to explain the data, as discussed later in this section, recent findings now show that resonant light plays an important role on the observed long-lived modes.

First, we have recently performed a theoretical and experimental study of subradiance beyond the linear-optics regime, by using a higher saturation parameter s for the probe beam [article in preparation]. Of course we have to check that we recover the previous results in the limit of low saturation. In the linear-optics limit we expect the results to be independent of the saturation parameter. As shown in Fig. VI.4 representing the relative amplitude of subradiance as a function of the saturation parameter, even going down to $s \sim 3 \times 10^{-3}$ is not enough to reach a plateau. This seems to be in contradiction with Fig. 3(b) of the Supplemental Material of [Guerin 2016a], but the range of explored value of s was more limited, and we might have by chance only explored to top of the curve, where it is locally flat. As explained there, at large detuning and low intensity, the inelastic spectrum looks like a doublet, one being on resonance. The relative proportion of light scattered on resonance is thus $s/2$. The increase of the subradiant amplitude with s seems to show that the slow decay is due to resonant light.

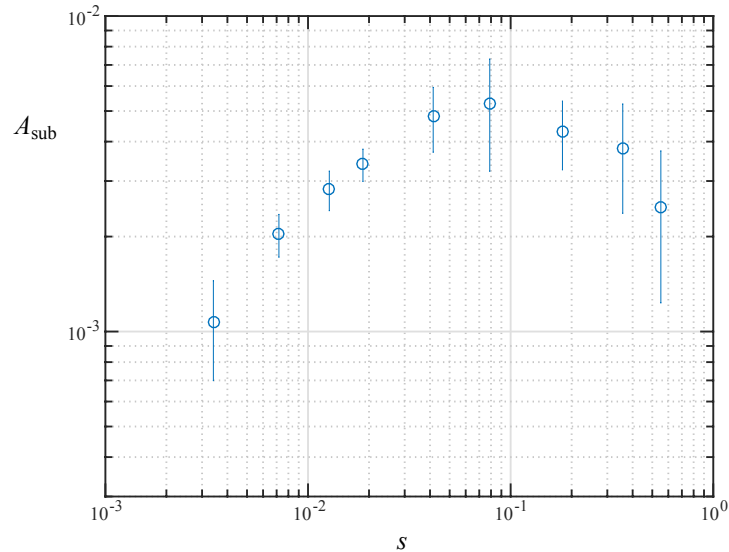


Figure VI.4: Experimental measurement of the relative subradiant amplitude as a function of the saturation parameter of the probe beam. We do not observe any plateau at low s , which means that the linear-optics limit is not reached. The parameters are $b_0 = 54$ and $\Delta = -4\Gamma$.

There is another effect that we overlooked so far, and we became aware of its importance during our work on the linear-dispersion theory: it is the broadening induced by the fast switch-off. This effect is not a spurious one but is fundamental and intrinsically related to the fact that we study the temporal dynamics: there is no such thing as a monochromatic field if the problem is not stationary. In particular, in the CD model at zero temperature, this is the only effect that can ‘generate’ light on resonance. To test its influence, one can compare the relative amplitude of the slow decay for different switch-off durations and switch-off profiles. This is done in Fig. VI.5. Here also, the result is unambiguous: the relative amplitude of subradiance seems related to the amount of resonant light. Indeed, at large detuning, an

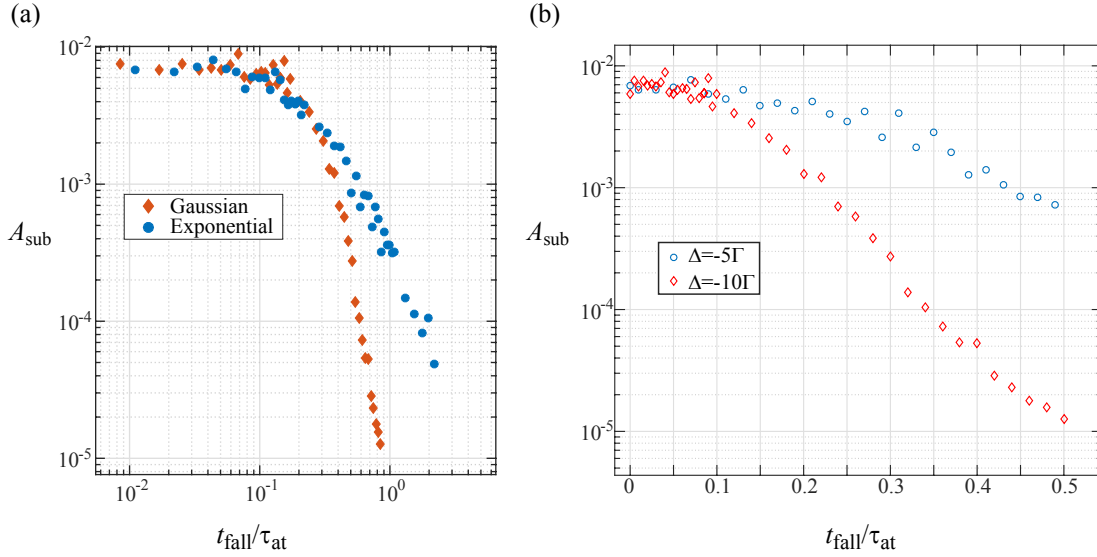


Figure VI.5: Influence of the switch-off profile and duration of the driving field on the relative amplitude of subradiance. (a) Comparison between an exponential and a Gaussian switch-off. The latter case induces less spectral broadening. The switch-off duration t_{fall} is defined as the 90% – 10% fall time. The parameters are $b_0 = 10$ and $\Delta = -10\Gamma_0$. (b) The switch-off duration (this time defined as the rms width of a Gaussian profile) is varied for two different detunings (same b_0).

exponential switch-off (inducing a heavy-tailed spectrum) leads to much more subradiance than a Gaussian switch-off (inducing a more compact spectrum), as can be seen in panel (a). In panel (b) we compare the effect of the switch-off duration for two different large detunings with a Gaussian switch-off: the decrease of the subradiant amplitude for slower switch-off is more pronounced at larger detuning, showing the role of the overlap of the incident spectrum with the atomic resonance. In all cases the time constant is not affected, only the relative amplitude is changed.

Note that the fact that the long-lived modes are enhanced by near resonant light doesn't tell us if they should be interpreted as radiation trapping or subradiance, since we have seen that both are favored near resonance [Guerin 2017b]. Moreover, let's remark that in the experiment, the switch-off is smooth and with a not-so-small fall time, so we don't expect the broadening effect to be significant.

Nevertheless it seems highly necessary to perform again a comparison between the CD and RW models, this time with the broadening effect included, to make sure that the slow decay observed in the CD model cannot be attributed to spurious radiation trapping. However including the switch-off-induced broadening in the RW simulations is not an easy task because we deal with a nonstationary situation: a simple Fourier transform is not enough (the spectrum during the long pulse is monochromatic and it is broadened only at the switch-off). Methods to tackle this kind of problems are presented in [Bozhokin 2018]. A simpler way is to consider a pulsed excitation, with a pulse duration much shorter than τ_{at} . Then the spectrum is well defined and can easily be taken into account in the RW model. Note that this is a worst-case scenario, with a very broad spectrum and thus a significant proportion of resonant light. We have performed this comparison in Fig. VI.6(a), where we show the decay curves computed using the two models. There is a slow decay in both but we do observe a significant difference. The slow decay of the RW model corresponds to the radiation trapping induced by near-resonant light, which is a significant contribution of the slow decay of the CD model. But in the latter, the late decay is even slower, showing that there is something more:

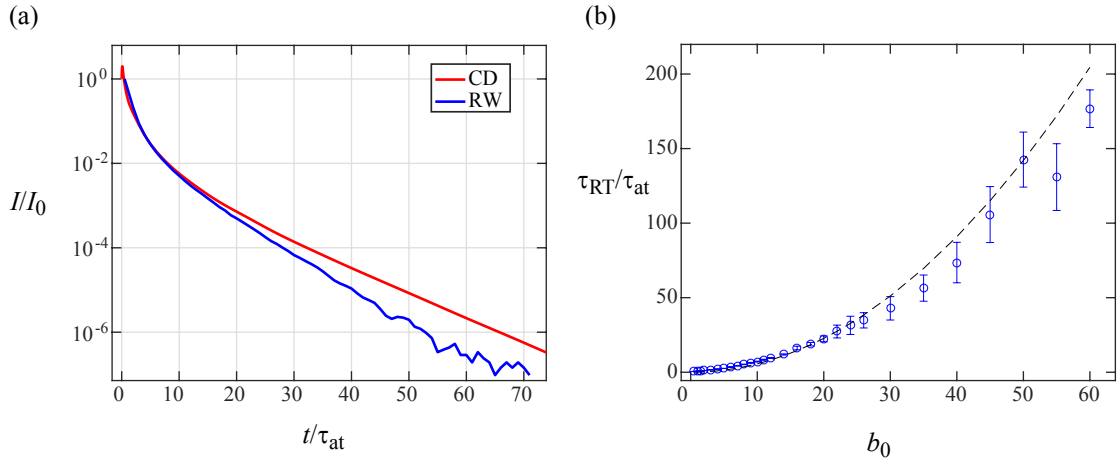


Figure VI.6: (a) Temporal traces of the slow decays following a pulsed excitation computed with the CD and the RW models. The parameters are $b_0 = 8$ and $\Delta = 10$ (central detuning). The pulse is a Gaussian of rms width $0.1\tau_{\text{at}}$, inducing a Gaussian spectral broadening of rms width $\sim 7\Gamma$. (b) Late time constant as a function of b_0 computed in the RW model (radiation trapping). The dashed line shows the analytical prediction in the diffusive regime.

subradiance. In panel (b) we show the scaling of the radiation trapping decay, which still scales quadratically with b_0 , demonstrating that, even with a broad spectrum illumination, spurious radiation trapping at zero temperature never gives linear scaling with b_0 , as observed for subradiance.

Finally, another proof that there is some coherence effects in the subradiance (and thus that it is different from radiation trapping) can be obtained from the CD model only and is already discussed in [Araújo 2018b] (not reproduced here): the *phase* profile of the driving field changes the relative amplitude of subradiance. For instance, applying a dephasing of π on half of the beam produces an increase by a factor ~ 2 , as shown on Fig. VI.7. The

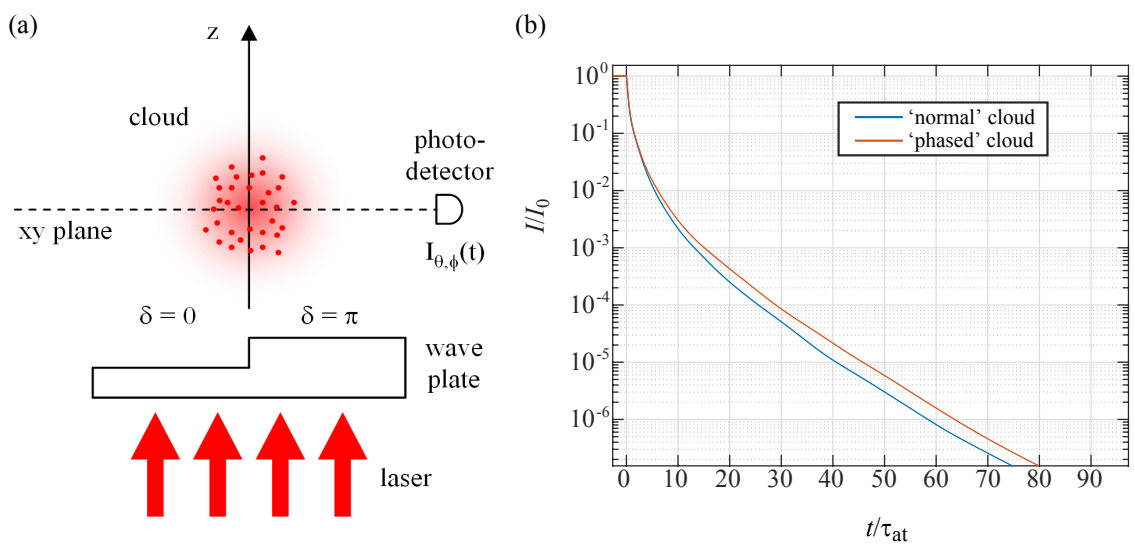


Figure VI.7: Influence of the phase profile of the driving field on the relative amplitude of subradiance. (a) Scheme of the experiment. Taken from [Araújo 2018b]. (b) Computed decay with and without the π dephasing. The parameters are $b_0 = 10$, $\rho_0\lambda^5 = 5$, $\Delta = -10\Gamma_0$ and the observation direction is $\theta = \pi/4$ (averaged of ϕ and over 30 realizations).

influence of the phase profile of the beam is an unambiguous signature of a phase-coherent effect. At the time of writing this experiment is being done in the lab.⁶

VI.5.3. Towards a ‘photonic’ picture of subradiance?

In this last subsection on subradiance I’d like to share some thoughts, which are not completely mature, and may thus change in the future!

As already mentioned there should be some equivalence between an atomic description and a light description of collective effects in light-matter interaction [Lax 1951, Lagendijk 1996], and we did find an optical description of superradiance (section VI.4). The case of long-lived states is however more complicated. In the framework of the atomic description (the CD model), it is straightforward to call all short-lived state ($\Gamma > \Gamma_0$) superradiant and all long-lived state ($\Gamma < \Gamma_0$) subradiant, and that’s what many authors do. Nevertheless, for people familiar with the field of multiple scattering, it is not very satisfactory, since we know that slow decays (i.e. long-lived states) can also be due to incoherent multiple scattering, which we call radiation trapping. As discussed in the previous section, we claim that subradiance is something else. Then what is it? What are those photons doing during all this time?

Note that many papers deal with super- and subradiant collective modes in mesoscopic ensembles of a small number of atoms, sometimes in 1D or 2D, often ordered. In these cases, of course, the atomic picture is much more adapted and an optical picture is probably not possible, or at least not relevant. I am concerned here with macroscopic disordered ensembles of atoms.

Since superradiance can be explained by a linear-dispersion theory, it is natural to wonder if it can also explain subradiance, like a kind of slow-light effect. A numerical study of Eq. (VI.2) shows that it is not the case: after the superradiant decay, the temporal trace quickly becomes a single exponential of decay rate Γ_0 . Subradiance can thus not be explained by a single scattering event embedded in a dispersive effective medium.⁷

Another, strong argument showing that subradiance and superradiance are due to different optical mechanisms can be found in the polarization. Using the vectorial version of the CD equations, based on a $J = 0 \rightarrow J = 1$ transition, one can compute the polarization of scattered light as a function of time. Fig. VI.8 shows the result of such a computation, with a circularly-polarized driving field and light detection at 90° : single scattering should produce a linear polarization. The result is unambiguous: at late time light is depolarized.

Note that in most of our computations (including the one of Fig. VI.8) we use an exclusion volume to avoid pairs or clusters of very close atoms, which might create strong super- and subradiant modes, because we think that such effects don’t occur in the experiment due to the low density and atomic motion. I am concerned here with dilute samples.

Let us then examine two different hypotheses for photonic/optical pictures of subradiance.

The case of *coherent* multiple scattering

The fact that resonant light plays an important role, as well as the depolarization effect, naturally hint towards a multiple scattering picture. Moreover the fact that the RW model doesn’t predict the same slow decay as the CD model (even with the broadening included) and

⁶ It has been actually interrupted by the Covid-19 crisis and will resume as soon as possible.

⁷ I have also tested to change the equation in order to average the field and then compute the intensity. Even without any mathematical justification, it is numerically easy to do. There is still no subradiance.

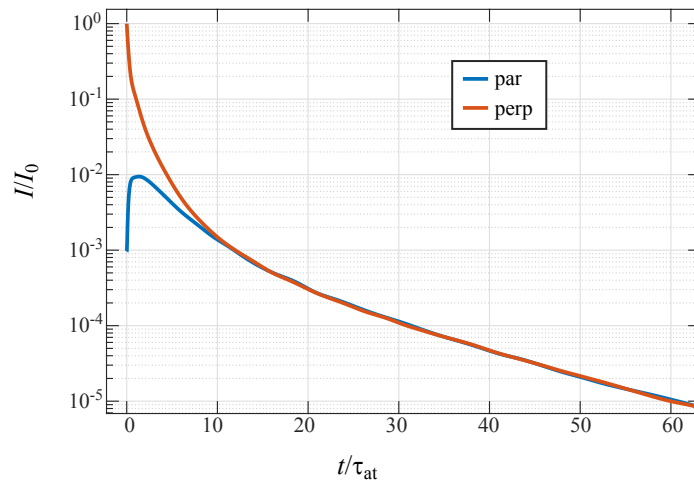


Figure VI.8: Results of CD simulations using the vectorial model. The probe beam has a circular polarization and we compute the light scattered at 90° , in two orthogonal linear polarization channels: orthogonal (perp) and parallel (par) to the scattering plane. One can see that the superradiant part of the decay is polarized whereas the subradiant part is depolarized. The parameters are $b_0 = 16$, $\rho_0\lambda^3 = 5$, $\Delta = -10\Gamma_0$. Computations done by Ana Cipris.

the phased-excitation enhancement show that incoherent multiple scattering is not enough and that some phase-coherent or interference effects are involved. Subradiance would thus be due to *coherent multiple scattering*. In other words, it would be a phase-coherent correction to the dynamical properties of multiple scattering, or, one may also say, it would be radiation trapping beyond the independent scattering approximation.

One flaw of this hypothesis is that it is absolutely not obvious, at least to me, within the multiple-scattering picture, to physically understand the observed robustness with the atomic motion [Weiss 2019] (subradiance seems less sensitive than radiation trapping) and how the phased excitation can favor the longest multiple-scattering paths.

Another flaw is that in the mesoscopy community, it is widely accepted that effects beyond the independent scattering approximation appear at high density only, more precisely when the parameter $1/k_0\ell$, where ℓ is the mean free path, is not completely negligible compared to one [Legendijk 1996, van Rossum 1999]. On the contrary we have shown that subradiance exists in the low-density regime.

As a consequence, we may have some confidence in this interpretation of subradiance only when the nature of the phase-coherent correction, and its modeling within a multiple-scattering approach, will be available.

The case of refractive long-lived modes

In a recent paper [Cottier 2018], my colleagues suggested that subradiance is present in a ‘mean-field model’ in which the atomic distribution is continuous: mathematically, all sums are replaced by integrals. This approach has been used by several authors [Prasad 2010, Svidzinsky 2010, Bachelard 2012, Schilder 2016], but mainly to discuss superradiance. Physically it means that disorder is absent, and there is no ‘scattering’ by the atoms, only by the whole cloud itself, which is represented by an effective dielectric medium. The long-lived modes can then appear due to boundary effects (Fabry-Perot modes or whispering-gallery modes) if the refractive index is high enough [Schilder 2016]. In [Cottier 2018] it is shown that short- and long-lived modes are also present with a smooth Gaussian density distribution, which is not

obvious. A physical picture is that the refractive-index profile of the medium somehow traps the light, similarly to the guiding of graded-index multimode fibers. One can also imagine that this trapped light is depolarized, like in fibers.

However, the refractive index is given by the density and, although some quantities may be given by b_0 (e.g. the dephasing accumulated along a trajectory), intuitively, I expect the density and the size to play an important role in this process via the refractive index gradient. Indeed, all numerical calculations presented in [Cottier 2018] have been done with rather high-density and/or small-size samples. For technical reasons no quantitative study of the subradiant modes could be performed, so we don't know if they depend on b_0 , on the density or on something else. As a consequence, more work is needed to know if those refractive long-lived modes survive in the low-density, large-sample case and if they can still be populated in a nonnegligible way.

Moreover, it is intuitively clear that in the light detected off axis, the relative proportion of diffracted/refracted light (which is what the mean-field model computes) compared to the scattered light strongly depends on the density/size of the medium. In that scenario, the relative weight of the long-lived modes should thus decrease a lot at low density, and in particular should be negligible in the experiment. This is not what we observed, even in the CD model: for instance, the Fig. 3(c) of [Guerin 2017c] shows that the whole decay curve, and therefore the relative amplitude of subradiance, is independent of the density.

One hypothesis to reconcile the refractive scenario with this observation is to add a single scattering event in the picture: this scattering event redirects light off axis and may even increase the coupling to the long-lived modes, in comparison with what would happen with an incoming plane wave. Indeed the long-lived modes are those with the less homogeneous phase/intensity profiles [Cottier 2018]. Therefore this scenario would be an extension of the superradiance one: single-scattering embedded in an effective dispersive graded-index medium.

It might be easier, in this scenario, to understand the robustness with the temperature (it only induces a broadening of the optical response, and no frequency drift of the light, since there is no scattering) and the phased-excitation enhancement (better coupling to inhomogeneous-phased modes). However it is not clear why resonant light would be good: near resonance there are more losses (in this picture the imaginary part of the refractive index is absorption).

Conclusion

Clearly, none of these two scenarios are convincing so far, and the question of a photonic picture of subradiance is still wide open.

Maybe it is a useless question and we should just be happy with the atomic picture of collective modes of coupled dipoles! I personally think it is important in order to get some realistic idea about what subradiance might be useful for.

VI.6. Excitation dynamics: collective Rabi oscillations

In this last section I now turn to a detailed study of the excitation dynamics. Indeed, in the superradiance data of [Araújo 2016], we also observed oscillations at the switch-on. After some analysis, initially motivated by discussions with Johannes Schachenmayer (Strasbourg), we found out that those oscillations clearly depend on the resonant optical thickness b_0 and

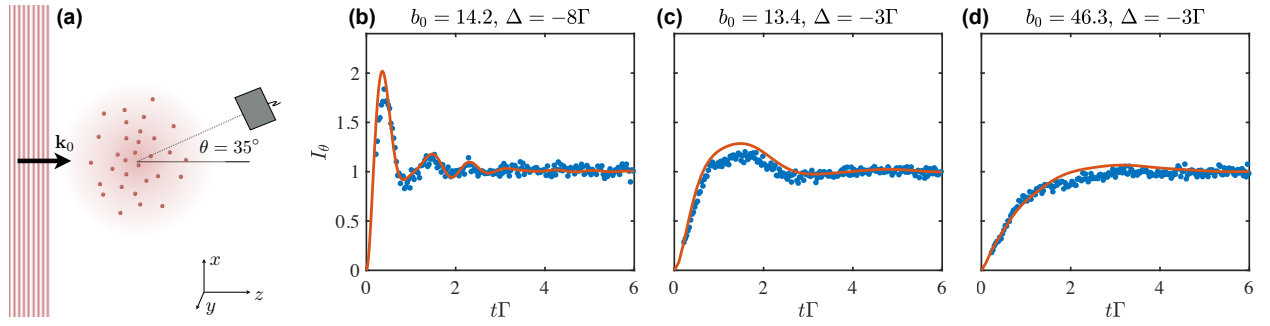


Figure VI.9: (a) Sketch of the experiment: a probe beam (plane wave) at a detuning Δ is suddenly switched on to illuminates a Gaussian cloud of cold atoms with resonant optical thickness b_0 . (b-d) Collective Rabi oscillations observed at the switch-on for different detunings. Blue dots are experimental data and the solid line is a simulation of the CD equations, without any free parameter. Near resonance the frequency is smaller and the oscillations becomes overdamped. Taken from [do Espirito Santo 2020].

the detuning Δ . Interestingly, the linear-dispersion (LD) theory presented and validated for superradiance (section VI.4), with the same Eq. (VI.2), can also be used to model this excitation dynamics. Using this LD approach allowed us to put in evidence an interesting analogy with the phenomenon of collective vacuum Rabi splitting, well known in the context of cavity quantum electrodynamics [Miller 2005].

For a single atom, the switch-on dynamics exhibits oscillations with a frequency given by the generalized Rabi frequency $\sqrt{\Omega_0^2 + \Delta^2}$ and a damping rate Γ_0 . At low saturation parameter, which is the case we consider here, $\Omega_0 \ll \Delta$ and the generalized Rabi frequency is dominated by the detuning Δ .

In the data, we observe for the collective oscillation frequency Ω_N a shift from Δ , and a collective damping rate Γ_N different from Γ_0 , both effects depending on b_0 and Δ . In Fig. VI.9 I show a few examples of temporal traces, along with coupled-dipole simulations, which agree very well.

In order to experimentally determine those parameters, an empirical fit with the function

$$I(t) = I_0 \left| 1 - e^{(i\Omega_N - \Gamma_N/2)t} \right|^2, \quad (\text{VI.7})$$

describing a single macroscopic damped oscillator, works remarkably well for most data, as shown in [do Espirito Santo 2020]. We will discuss in the following the behavior of Γ_N first, and then Ω_N .

VI.6.1. Superradiant damping

The damping rate Γ_N , determined by the empirical fit (VI.7), is reported in Fig. VI.10, for numerical simulations based on the CD (panel a) and for experimental data (panel b), plotted as a function of the optical thickness $b(\Delta)$.

The first observation is that the damping rate can be significantly larger than Γ_0 , i.e. it is superradiant. At large detuning Γ_N increases with the optical thickness and at lower detuning it decreases. Actually the behavior is completely similar to the superradiant decay rate measured at the switch-off, see Fig. 3(b) of [Araújo 2016] (section VI.2).

The measurements are in good qualitative agreement with CD simulations, although there is a small systematic quantitative discrepancy: the damping rate is slightly larger in the

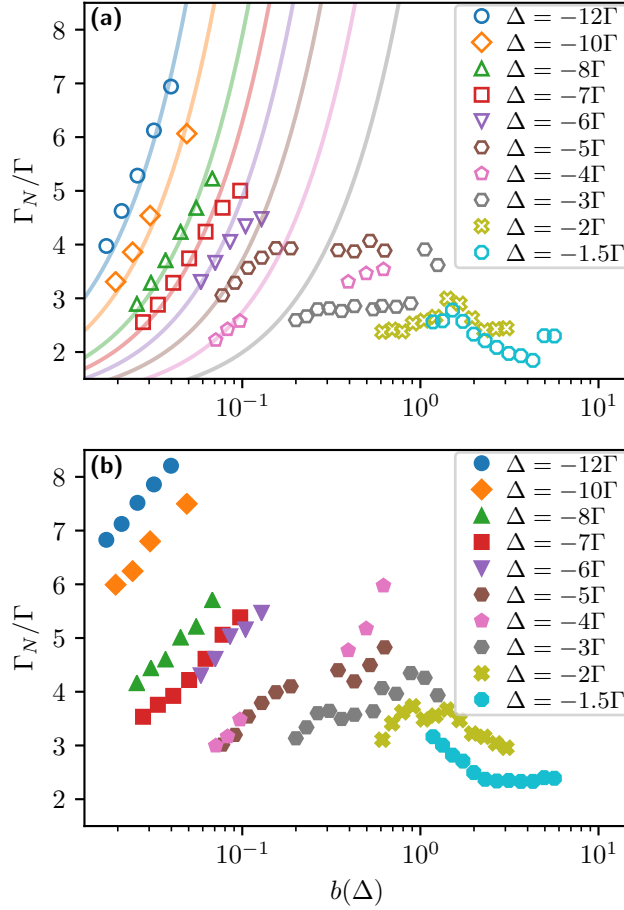


Figure VI.10: Damping rate of the collective Rabi oscillations observed at the switch-on, in the CD simulations (a) and in the experiment (b). The qualitative agreement is very good. The solid lines in panel (a) are the large detuning limit. Taken from [do Espirito Santo 2020].

experiment than in the simulations, which might be due to the finite rise time of the probe beam.

These results have been published in [do Espirito Santo 2020], which I don't include here. The paper also contains recent data taken at higher saturation parameter, i.e. going beyond the linear-optics regime. It is shown that a mean-field model, based on a product-state ansatz, describes the experiment well.

VI.6.2. Shift and splitting

For the collective oscillation frequency Ω_N extracted from the fit by Eq. (VI.7), we observed a shift from the single-atom frequency Δ , with what seemed to be a square-root behavior with b_0 ,

$$|\Omega_N| \sim |\Delta| - \frac{\sqrt{b_0}}{2}, \quad (\text{VI.8})$$

i.e. the oscillations get *slower*.

Following the analogy with a driven damped harmonic oscillator, the slowing down of the oscillations might be attributed to the effect of the damping: when the damping ratio increases, the oscillations cannot follow the driving frequency. However this analogy does not explain the $\sqrt{b_0}$ behavior.

The linear-dispersion theory provides a way to understand what happens. Let's look again at Eq. (VI.2) and consider what happens in frequency space. The input field $E_0(\omega)$ has a monochromatic component at ω_L , with $\Delta = \omega_L - \omega_{\text{at}}$, and broad slow-decaying wings

($\propto 1/|\omega - \omega_L|$) due to the instantaneous switch-on. This broad spectrum undergoes a response function that is the product of three terms, describing the propagation and the scattering. There is a competition between the propagation terms and the scattering term. Indeed the scattering term is a positive Lorentzian, with slow-decaying wings, while the propagation terms induce an attenuation, with an exponential of Lorentzian, which reads $\exp[-b(\Delta)]$ in squared modulus for a scattering position at the center of the cloud. The width of this attenuation term is proportional to $\sqrt{b_0}$. As a consequence only the frequency components on the wings of the attenuation spectrum are ‘transmitted’, which results in a double peak. One of this peak is much more pronounced because the system is driven on one side, given by Δ , and not by a white spectrum. Therefore, the most visible frequency component has a shift evolving like $\sqrt{b_0}$, and there is actually another frequency component, on the other side, corresponding to faster oscillations: this is not only a shift but a splitting.

By a deeper analysis of the experimental data we could indeed observe the predicted second frequency component, see Fig. 3a of the following article [[Guerin 2019](#)].

In this paper, an analogy is made with the vacuum Rabi splitting. The vacuum Rabi splitting corresponds to the shifting of the degeneracy when an atom is coupled to an optical cavity with the same resonance frequency (atom and cavity). It is an emblematic effect of cavity electrodynamics (see, e.g., [[Miller 2005](#)]), especially when it deals with a single atom. However, first observations of this effect were done with atomic ensembles, and it was found out later that a classical linear-dispersion theory could perfectly explain the observations [[Zhu 1990](#)]. In that case what happens is the following: the refractive index of the atomic cloud changes the resonance condition of the cavity and make two new resonances appear. The initial resonance, which coincides with the atomic resonance, is still there (since the refractive index is zero on resonance) but killed by the scattering/attenuation due to the atoms. Looking at the modes of the cavity selects, among all the possible eigenmodes of the atoms-cavity system, those with less scattering. In our case, looking at very short time after the switch-on also selects the modes with less scattering, because multiple scattering gives rise to slower time constants.

Collective Multimode Vacuum Rabi Splitting

W. Guerin¹, T. S. do Espirito Santo^{2,3}, P. Weiss,¹ A. Cipris,¹ J. Schachenmayer,³ R. Kaiser¹, and R. Bachelard^{4,1}

¹Université Côte d'Azur, CNRS, INPHYNI, F-06560 Valbonne, France

²Instituto de Física de São Carlos, Universidade de São Paulo, 13566-590 São Carlos, São Paulo, Brazil

³IPCMS (UMR 7504) and ISIS (UMR 7006), Université de Strasbourg, CNRS, 67000 Strasbourg, France

⁴Departamento de Física, Universidade Federal de São Carlos, Rodovia Washington Luís, km 235–SP-310, 13565-905 São Carlos, São Paulo, Brazil



(Received 13 September 2019; published 12 December 2019)

We report the experimental observation of collective multimode vacuum Rabi splitting in free space. In contrast to optical cavities, the atoms couple to a continuum of modes, and the optical thickness of the cloud provides a measure of this coupling. The splitting, also referred as normal mode splitting, is monitored through the Rabi oscillations in the scattered intensity, and the results are fully explained by a linear-dispersion theory.

DOI: 10.1103/PhysRevLett.123.243401

Light scattering encompasses a broad range of phenomena, and its elementary brick can be found in the interaction of a vacuum mode with a single atom. From a fundamental point of view, the vacuum mode and the atom are two oscillators, whose coupling leads to hybrid modes with specific energies. In case the two oscillators possess the same natural frequency, the interaction lifts the degeneracy, and the new eigenenergies split by an amount proportional to the coupling. In the context of optical cavities, where the single mode hypothesis is best achieved, the phenomenon has been coined vacuum Rabi splitting [1,2]. The effect has been successfully observed and utilized in a wide range of fields from cavity quantum electrodynamics in atomic physics [3,4] to solid-state systems and chemistry [5–15].

Interestingly, before the strong coupling regime could be achieved experimentally with single atoms, the splitting was noted to be accessible experimentally in larger-volume cavities: If an ensemble of N atoms are coupled to the cavity, the coupling strength to the vacuum mode is enhanced by a factor \sqrt{N} . This allowed for early observations in optical cavities [16–18], and it was later understood that a linear-dispersion theory could describe the phenomenon [19,20]. The fundamental difference between the single- and the many-atom case is that in the former case, the quantization of the electromagnetic mode becomes relevant [21] (see left part of Fig. 1).

In contrast with high-finesse optical cavities, our three-dimensional world presents a continuum of vacuum modes, both in space and in frequency. Nevertheless, this multimode characteristics does not prevent the building up of collective modes. The first brick of collective scattering was laid down by Dicke, when he showed that a collection of atoms, either in the small or the large volume limit, emit light at a “superradiant” rate [22]. At first discussed in

the quantum context of fully inverted atoms, superradiant decay was later predicted in the limit of a single excitation [23,24], as confirmed by linear-optics measurements [25,26]. In the field of cooperative scattering, subradiance [27], superflash [28] and collective frequency shifts [26,29–33] contribute to the rich variety of observed phenomena.

The continuum of vacuum modes calls for a different modeling of the light-atom interaction in free space: An interpretation in terms of dipole-dipole interactions, obtained by tracing over the light degrees of freedom, is in general favored, as it allows addressing only the atomic degrees of freedom [34]. Such a coupled-dipole approach was largely used to describe the cooperative phenomena described above. In particular, differently from optical

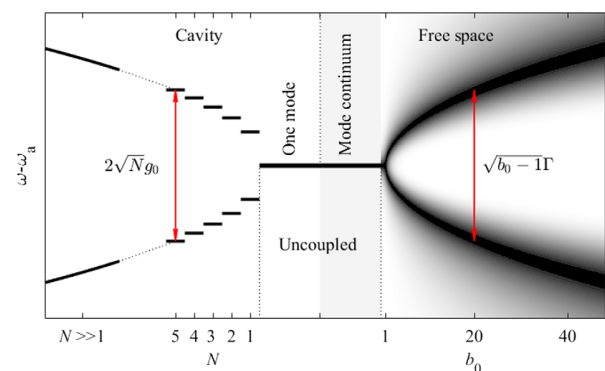


FIG. 1. Eigenenergies of an atomic cloud coupled to vacuum mode(s). Left: N atoms coupled to a resonant single mode cavity; the mode splitting scales as $\sqrt{N}g_0$, with g_0 the single-atom coupling to the mode. Right: A cloud with resonant optical thickness b_0 , coupled to the continuum of vacuum modes of free space; the mode splitting scales as $\sqrt{b_0} - \Gamma$, with Γ the single-atom decay rate in free space (see text for details).

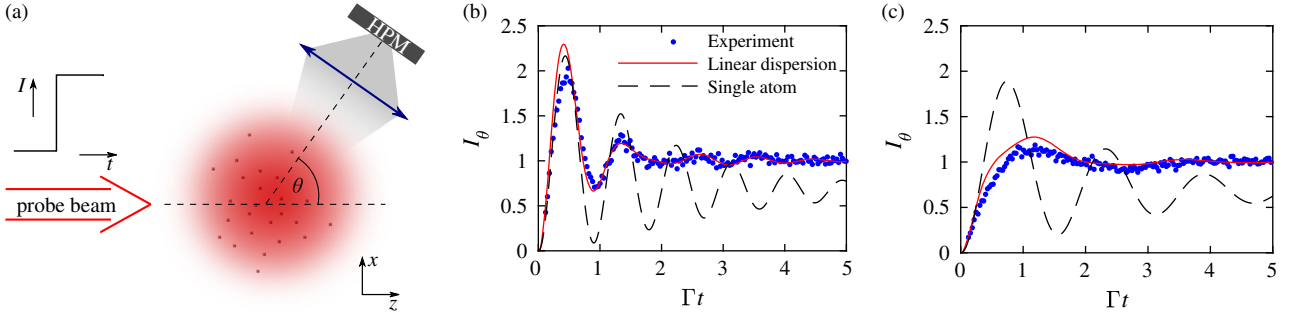


FIG. 2. (a) Sketch of the experiment: A monochromatic plane-wave laser suddenly illuminates a Gaussian cloud of two-level atoms, while the dynamics of the scattered intensity is measured at an angle of $\theta \approx 35^\circ$ from the axis of the incident beam by a hybrid photon detector (HPM). (b),(c) Experimentally recorded intensity (dots) after the laser switch-on, normalized to 1 in the long-time limit, for different values of the optical thickness of the cloud and laser detunings [(b) $b_0 \approx 8.1$ and $\Delta = -7\Gamma$; (c) $b_0 \approx 20.3$ and $\Delta = -4\Gamma$]. The plain lines are obtained by a numerical simulation of the linear-dispersion theory (see text), the dashed lines denote the single-atom response (not normalized, for visibility purposes).

cavities where the cooperativity parameter is N , the resonant optical thickness of the cloud was identified to play this role in free space for dilute clouds with a spatial extent larger than the optical wavelength [35].

In this Letter, we report on the experimental signatures of collective multimode vacuum Rabi oscillations in free space, where the optical thickness acts as a measure of the coupling between the atomic cloud and the light modes (see right part of Fig. 1). The splitting is monitored through the linear-optics Rabi oscillations of the cloud after an abrupt switch-on of the pump laser. Our measurements, realized over a set of driving frequencies and optical thicknesses, are in very good agreement with linear-dispersion theories for three-dimensional clouds.

Our experimental setup, which has been detailed in Ref. [25], is sketched in Fig. 2(a): A three-dimensional Gaussian cloud (rms width $R \approx 1$ mm) of $N \approx 10^9$ randomly distributed ^{87}Rb atoms is produced in a magneto-optical trap at a temperature $T \approx 100$ μK . After switching off the trap, the atoms are optically pumped to the $F = 2$ state, and driven on the $F = 2 \rightarrow F = 3$ transition (with wavelength $\lambda = 780.24$ nm and linewidth $\Gamma/2\pi = 6.07$ MHz). The cloud is homogeneously illuminated by a linearly polarized laser beam (waist $w \approx 5.7$ mm, detuning $\Delta = \omega_L - \omega_a$ from the atomic transition) propagating along the z axis. A series of pulses of duration 30 μs with 10%–90% rise time of about 6 ns, short compared to the lifetime of the excited state $\tau_{\text{at}} = \Gamma^{-1} = 26.2$ ns, are produced by acousto- and electro-optical modulators. During the series of pulses, the atomic cloud expands ballistically, which allows us to probe different on-resonance optical depths, defined as $b_0 = \sigma_0^{\text{Rb}} \int \rho(0, 0, z) dz$, with σ_0^{Rb} the resonant Rubidium atomic cross section. The light intensity is adjusted to keep a constant saturation parameter $s = 2\Omega_0^2/(\Gamma^2 + 4\Delta^2) \approx (2.2 \pm 0.6) \times 10^{-2}$, with Ω_0 the Rabi frequency of the laser. The time-dependent scattered light intensity is recorded by a

photon detector in the far field at an angle of $\theta \approx 35^\circ$ from the laser axis. The finite rise time of the laser field, as well as small spurious overshoots, are accounted for by first dividing the recorded signal by the switch-on temporal profile of the laser alone (recorded with the same cycle and same detector with light scattered on white paper), in order to focus on the atomic dynamics.

Typical examples of intensity signal from the experiment are presented in Figs. 2(b) and 2(c). The radiation emitted by the cloud of cold atoms exhibits Rabi oscillations, whose frequency is smaller than the single-atom one: For a single atom, one indeed expects an oscillation of the excited state population with the generalized Rabi frequency $\Omega_R = \sqrt{\Delta^2 + \Omega_0^2} \approx |\Delta|$ in the linear-optics regime considered here. As we shall now show, the deviation from this single-atom oscillation frequency finds its origin in the large resonant optical thickness of the cloud, which considerably enhances its dispersive features, and provides a direct measurement of the coupling strength between the cloud and the vacuum modes.

Differently from optical cavities, in free space the three-dimensional continuum of vacuum modes forces us to adopt a space-dependent theory in order to investigate the dispersion properties of the cloud. In our setup, let us first consider the propagation of a wave scattered off an atom at position \mathbf{r} . The wave of frequency ω moves from an initial position $\mathbf{r}_i = \mathbf{r} - w\hat{z}$ ($w \rightarrow \infty$) to the atom at \mathbf{r} where it is scattered, and then to the detector positioned at $\mathbf{r}_f = \mathbf{r} + w\hat{\theta}$, where \hat{z} and $\hat{\theta}$ denote the unit vectors of the z axis and the detector direction with respect to the atom, respectively. In the dilute regime with atoms being distributed in the cloud by a density distribution function $\rho(\mathbf{r})$ and being uniformly illuminated by the laser, this process can be described by the following transfer function for an atom in \mathbf{r} [36]:

$$t_{\mathbf{r},\theta}(\omega) = \frac{\exp\left(-\frac{1}{2} \frac{b_{\mathbf{r}-w\hat{\mathbf{z}}}^{\mathbf{r}} + b_{\mathbf{r}}^{\mathbf{r}+w\hat{\theta}}}{1-2i(\omega-\omega_a)/\Gamma}\right)}{1-2i(\omega-\omega_a)/\Gamma}. \quad (1)$$

Here, $b_{\mathbf{r}}^{\mathbf{r}'}$ = $\sigma_{\text{sc}} \int_{\mathbf{r}}^{\mathbf{r}'} d\mathbf{r} \rho(\mathbf{r})$ denotes the optical thickness for a light ray propagating from \mathbf{r} to \mathbf{r}' . The expression assumes $w \gg R$, which corresponds to a detector in the far-field. Although it neglects disorder in single experimental realizations, this approach captures well collective phenomena such as superradiance [36]. In Fig. 2(b), one can observe that it captures very well the damped oscillations (note the longer duration between the second and the third maxima) of the radiated intensity. More precisely, the radiated intensity presents irregular oscillations that result from the beating between the two split frequencies. Naturally absent from the single-atom response, this beating is well captured by the linear-dispersion approach.

In the simplified case of an infinite slab illuminated by a plane wave, the forward-scattering response ($\theta = 0$) is obtained by integrating the local response over the cloud, $t_0(\omega) = \int d\mathbf{r} \rho(\mathbf{r}) t_{\mathbf{r},\theta}(\omega)$, which leads to

$$t_0(\omega) \sim \frac{\exp\left[-\frac{b_0}{2} \left(1 - \frac{2i(\omega-\omega_a)}{\Gamma}\right)^{-1}\right]}{1-2i(\omega-\omega_a)/\Gamma}, \quad (2)$$

where b_0 is the resonant optical thickness of the slab. The square modulus of the response function $t_0(\omega)$ thus reads $|t_0|^2 = \exp(-b_0/(1+4\delta^2))/(1+4\delta^2)$, with $\delta = (\omega - \omega_a)/\Gamma$, and it transforms from a single-peak Lorentzian in the single-atom limit ($b_0 \rightarrow 0$) to a double-peaked function for larger b_0 , whose peaks are found at

$$\omega_{\pm} = \omega_a \pm \frac{\sqrt{b_0 - 1}}{2} \Gamma. \quad (3)$$

This behavior is illustrated in Fig. 3(c) (dash-dotted lines), and in the right part of Fig. 1: The role of the coupling strength between the cloud and the vacuum modes, quantified by the resonance splitting, is thus here assumed by the resonant optical thickness.

For our spherical Gaussian cloud, we call the observation angle $\hat{\theta}$ and normalize the distances as $\mathbf{r} \rightarrow \mathbf{r}/R$:

$$\begin{aligned} b_{\mathbf{r}-w\hat{\mathbf{z}}}^{\mathbf{r}} &= \frac{b_0}{2} e^{-\{[r^2 - (\mathbf{r}\cdot\hat{\mathbf{z}})^2]/2\}} \left[1 + \text{Erf}\left(\frac{\mathbf{r}\cdot\hat{\mathbf{z}}}{\sqrt{2}}\right)\right], \\ b_{\mathbf{r}}^{\mathbf{r}+w\hat{\theta}} &= \frac{b_0}{2} e^{-\{[r^2 - (\mathbf{r}\cdot\hat{\theta})^2]/2\}} \left[1 - \text{Erf}\left(\frac{\mathbf{r}\cdot\hat{\theta}}{\sqrt{2}}\right)\right], \end{aligned} \quad (4)$$

where the limit $w \rightarrow \infty$ is used. The cloud response for the Gaussian sphere is then computed numerically using Eq. (1), which in turn allows us to obtain the intensity dynamics in the temporal domain: After multiplying it by the Fourier transform of the pump beam temporal profile (a Heaviside function), the local frequency response of the

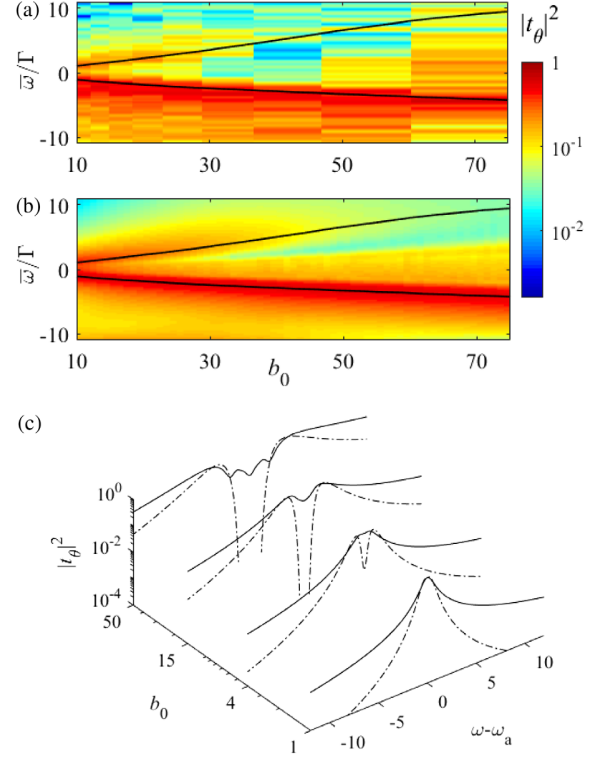


FIG. 3. Frequency response of the cloud to the switch-on of the laser, at an angle $\theta = 35^\circ$. $|t_{\theta}(\omega)|^2$ is computed from the Fourier transform of the intensity (a) from the experiment and (b) from the linear-dispersion theory. The black lines denote, in both figures, the maxima derived from the linear-dispersion approach. $\bar{\omega} = \omega_L - \omega_{\text{opt}}$, i.e., it corresponds to the difference between the laser frequency (here detuned by $\Delta = -12\Gamma$) and the optical frequency. (c) Frequency response of the cloud for increasing optical thicknesses, for a slab and in the forward direction (dash-dotted curves), and for a spherical cloud with a Gaussian density and for light at an angle $\theta = 35^\circ$ (plain lines).

atoms is converted into a temporal response by computing its inverse Fourier transform; the obtained intensity is then integrated over all the cloud [36,37]. The temporal curves presented in Fig. 2 were obtained this way. We have also checked that the microscopic coupled-dipole model discussed in the introduction [34,38] provides temporal signals in excellent agreement with the linear-dispersion approach (1) [39]. An important difference, though, is that these microscopic simulations are limited to thousands of particles, so they address much smaller systems.

The measurement of the splitting requires the oscillations to be faster than the decay rate [40]. Close to resonance, we observe that the oscillations vanish, see Fig. 2(c), which we attribute to occurrence of multiple scattering [$b(\Delta) = b_0/(1+4\Delta^2/\Gamma^2) > 1$] [25]. Out of resonance [such that $b(\Delta) < 1$], the detuning is chosen such that the single-atom generalized Rabi frequency $\Omega_R \approx |\Delta|$ be larger than the superradiant decay rate [25], which allows us to monitor the deviation from the single-atom

oscillations, see Fig. 2(b). Note that while the experimental curves are obtained from averaging the signal over thousands of runs (typically $\sim 10^5$, see Ref. [39] for details on fluctuations), the linear-dispersion effective-medium approach provides a signal that is naturally fluctuation free.

Let us now discuss in more detail the splitting in frequency space: In Figs. 3(a) and 3(b), the Fourier transform of the intensity signal is presented, for the experimental data and the linear-dispersion simulations. We first note that while the splitting is present, the lower branch ω_- is much more visible, especially at high b_0 . This is due to the fact that the system is probed with a negative detuning ($\Delta = -12\Gamma$ in this case), so the laser couples more strongly to this branch. The increasing optical thickness makes this lower branch even closer to the laser frequency, and the upper branch ω_+ even farther, which results in an increasing imbalance between the branches. A pumping at $\Delta \gg \omega_{\pm}$ would allow us to populate almost equally the two branches, yet at the price of a weaker radiated intensity. Finally, we have checked that the linear-dispersion theory predicts no change when changing the sign of the detuning (not shown here).

As discussed above [see Eq. (3)], the one-dimensional geometry of the slab provides a simple scaling $\Delta\omega \sim \sqrt{b_0 - 1}$ for the splitting, see Eq. (3) and Fig. 1. The three-dimensional Gaussian cloud used in our experiment, with an observation angle at $\theta = 35^\circ$ and a beam larger than the cloud, leads to the coupling of the atoms to a larger family of vacuum modes. This is illustrated in Fig. 3(c), where the difference of the splitting process for the slab and the Gaussian sphere is presented. The slab is characterized by a strong gap between the two resonances, whereas the Gaussian sphere presents a rather shallow dip, with even the emergence of secondary resonances at higher b_0 . Furthermore, the decay of the tails of the frequency response are much slower for the Gaussian sphere. One explanation for these differences is that in an ideal (i.e., infinite) slab, all incoming rays see the same optical thickness. Differently, in a Gaussian sphere rays outside the z axis go through the medium with a different optical thickness; the presence of this variety of optical thicknesses for a three-dimensional cloud (an effect reinforced by the observation angle $\theta > 0$) leads to a broadening of the cloud dispersive response. More generally, in a single-mode cavity, the system possesses only two modes (plus $N - 1$ degenerate dark states), and the large N limit makes the quantization of the photons irrelevant; but in free space, a single atom couples to a continuum of light modes, already leading to a broad response.

The shift of the dominant branch is then systematically deduced from the experimental data by fitting it to a single-dipole function $I_\theta(t) = |1 - \exp[(i(\Delta + \omega_- - \Gamma_{\text{SR}}/2)t]|^2$, with ω_- and Γ_{SR} as fitting parameters. This procedure yields fewer fluctuations than the Fourier transform. The results are presented in Fig. 4, for a set of detunings and

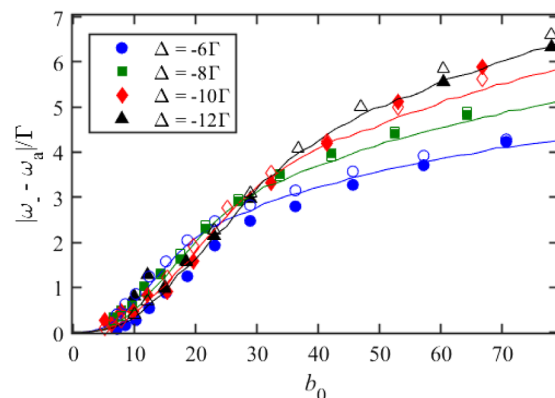


FIG. 4. Splitting amplitude extracted from the experiment (full symbols), from the coupled-dipole simulations (empty symbols) and from the linear-dispersion theory (lines), for different detunings and optical thicknesses.

resonant optical thicknesses. They are compared to the linear-dispersion theory results and to the coupled-dipole model using the same procedure. All three approaches present results in very good agreement. The different values of detuning used, as well as the different system sizes simulated (in particular for the coupled-dipole approach) highlight the role of the resonant optical thickness b_0 as a measure of the collective coupling of the atomic cloud to the vacuum modes in free space. We note that for larger values of b_0 , an increasing detuning $|\Delta|$ is necessary to obtain a splitting that does not depend on the detuning, an effect which we attribute to multiple scattering.

We stress that the collective splitting discussed here is fundamentally different from the “collective Lamb shift” (CLS) reported in atomic systems [26,29–33]. In the larger sample limit ($R \gg \lambda$), the CLS scales with the atomic density [41–43], whereas the present experiment was realized using dilute clouds ($\rho/k^3 \sim 0.01$). In particular, we point out that the splitting for the slab [see Eq. (3)] depends only on b_0 , and does not present any explicit dependence on the atomic density, which clearly differentiates it from the CLS. We note that the oscillations which emerge from the light-atom coupling, sometimes called “ringing,” has stimulated several experimental and theoretical works [40,44,45]. Here, within the context of free space linear optics, we propose a unified picture of the macroscopic coupling between an atomic cloud and vacuum modes.

As a final remark, it is interesting to note the connection between steady-state frequency-resolved spectroscopy and time-dependent spectroscopy. In cavity spectroscopy, a well-known technique called ring-down spectroscopy [46] has been developed, where a photon bullet picture, which neglects interference effects, can describe the observed phenomena, whereas cavity transmission experiments involve interference effects between multiple reflections inside the cavity. For our mirrorless configuration,

steady-state experiments sensitive to the frequency-dependent scattered intensity $T(\omega) = |t(\omega)|^2$ have been presented in Ref. [47]. In contrast, the data presented in this work have been obtained in time-dependent experiments and depend on the Fourier transform of $t(\omega)$. Similar to the situation of cavity spectroscopy, we expect the sensitivity to intensity and phase fluctuations to scale differently using these different protocols, a feature which might be exploited when considering fluctuations or dephasing mechanisms.

In conclusion, we have reported on the experimental observation of the collective multimode vacuum Rabi splitting in free space, by monitoring the linear-optics Rabi oscillations of the scattered intensity after an abrupt switch-on of the pump laser. The scaling of the splitting with the resonant optical thickness shows that the latter is a measure of the coupling between the atomic clouds and the three-dimensional continuum of vacuum modes in free space.

We thank Ivor Krešić and Michelle Araújo for their contribution in setting up the fast switch-on system and Luis Orozco for fruitful discussions. Part of this work was performed in the framework of the European Training Network ColOpt, which is funded by the European Union (EU) Horizon 2020 programme under the Marie Skłodowska-Curie action, grant agreement No. 721465. R. B. and T. S. E. S. benefited from Grants from São Paulo Research Foundation (FAPESP) (Grants No. 2018/01447-2, No. 2018/15554-5, No. 2018/12653-2, and No. 2019/02071-9) and from the National Council for Scientific and Technological Development (CNPq) Grants No. 302981/2017-9 and No. 409946/2018-4. R. B. and R. K. received support from project CAPES-COFECUB (Ph879-17/CAPES 88887.130197/2017-01). J. S. is supported by the French National Research Agency (ANR) through the Programme d'Investissement d'Avenir under Contract No. ANR-11-LABX-0058_NIE within the Investissement d'Avenir program ANR-10-IDEX-0002-02 and by QuantERA–Project “RouTe.” P. W. is supported by the Deutsche Forschungsgemeinschaft (Grant No. WE 6356/1-1). The Titan X Pascal used for this research was donated by the NVIDIA Corporation. Research carried out using the computational resources of the Center for Mathematical Sciences Applied to Industry (CeMEAI) funded by FAPESP (Grant No. 2013/07375-0).

-
- [1] J. J. Sanchez-Mondragon, N. B. Narozhny, and J. H. Eberly, *Phys. Rev. Lett.* **51**, 550 (1983).
 [2] H. J. Carmichael, *Phys. Rev. A* **33**, 3262 (1986).
 [3] R. J. Thompson, G. Rempe, and H. J. Kimble, *Phys. Rev. Lett.* **68**, 1132 (1992).
 [4] A. Boca, R. Miller, K. M. Birnbaum, A. D. Boozer, J. McKeever, and H. J. Kimble, *Phys. Rev. Lett.* **93**, 233603 (2004).

- [5] T. Yoshie, A. Scherer, J. Hendrickson, G. Khitrova, H. M. Gibbs, G. Rupper, C. Ell, O. B. Shchekin, and D. G. Deppe, *Nature (London)* **432**, 200 (2004).
 [6] J. P. Reithmaier, G. Sek, A. Löffler, C. Hofmann, S. Kuhn, S. Reitzenstein, L. V. Keldysh, V. D. Kulakovskii, T. L. Reinecke, and A. Forchel, *Nature (London)* **432**, 197 (2004).
 [7] E. Peter, P. Senellart, D. Martrou, A. Lemaître, J. Hours, J. M. Gérard, and J. Bloch, *Phys. Rev. Lett.* **95**, 067401 (2005).
 [8] K. Santhosh, O. Bitton, L. Chuntonov, and G. Haran, *Nat. Commun.* **7**, ncomms11823 (2016).
 [9] A. Ask, M. Ekström, P. Delsing, and G. Johansson, *Phys. Rev. A* **99**, 013840 (2019).
 [10] I. Pockrand, A. Brillante, and D. Möbius, *J. Chem. Phys.* **77**, 6289 (1982).
 [11] D. G. Lidzey, D. D. C. Bradley, M. S. Skolnick, T. Virgili, S. Walker, and D. M. Whittaker, *Nature (London)* **395**, 53 (1998).
 [12] J. A. Hutchison, T. Schwartz, C. Genet, E. Devaux, and T. W. Ebbesen, *Angew. Chem., Int. Ed. Engl.* **51**, 1592 (2012).
 [13] A. Shalabney, J. George, J. Hutchison, G. Pupillo, C. Genet, and T. W. Ebbesen, *Nat. Commun.* **6**, 5981 (2015).
 [14] V. M. Agranovich, Y. N. Gartstein, and M. Litinskaya, *Chem. Rev.* **111**, 5179 (2011).
 [15] Y. Colombe, T. Steinmetz, G. Dubois, F. Linke, D. Hunger, and J. Reichel, *Nature (London)* **450**, 272 (2007).
 [16] L. A. Orozco, M. G. Raizen, M. Xiao, R. J. Brecha, and H. J. Kimble, *J. Opt. Soc. Am. B* **4**, 1490 (1987).
 [17] M. G. Raizen, R. J. Thompson, R. J. Brecha, H. J. Kimble, and H. J. Carmichael, *Phys. Rev. Lett.* **63**, 240 (1989).
 [18] R. J. Brecha, L. A. Orozco, M. G. Raizen, M. Xiao, and H. J. Kimble, *J. Opt. Soc. Am. B* **12**, 2329 (1995).
 [19] Y. Zhu, D. J. Gauthier, S. E. Morin, Q. Wu, H. J. Carmichael, and T. W. Mossberg, *Phys. Rev. Lett.* **64**, 2499 (1990).
 [20] H. Yokoyama, *J. Mater. Sci. Eng. B* **48**, 39 (1997).
 [21] M. Brune, F. Schmidt-Kaler, A. Maali, J. Dreyer, E. Hagley, J. M. Raimond, and S. Haroche, *Phys. Rev. Lett.* **76**, 1800 (1996).
 [22] R. H. Dicke, *Phys. Rev.* **93**, 99 (1954).
 [23] M. O. Scully, E. S. Fry, C. H. R. Ooi, and K. Wódkiewicz, *Phys. Rev. Lett.* **96**, 010501 (2006).
 [24] A. A. Svidzinsky, J.-T. Chang, and M. O. Scully, *Phys. Rev. Lett.* **100**, 160504 (2008).
 [25] M. O. Araújo, I. Krešić, R. Kaiser, and W. Guerin, *Phys. Rev. Lett.* **117**, 073002 (2016).
 [26] S. J. Roof, K. J. Kemp, M. D. Havey, and I. M. Sokolov, *Phys. Rev. Lett.* **117**, 073003 (2016).
 [27] W. Guerin, M. O. Araújo, and R. Kaiser, *Phys. Rev. Lett.* **116**, 083601 (2016).
 [28] C. C. Kwong, T. Yang, M. S. Pramod, K. Pandey, D. Delande, R. Pierrat, and D. Wilkowski, *Phys. Rev. Lett.* **113**, 223601 (2014).
 [29] R. Rohlsberger, K. Schlage, B. Sahoo, S. Couet, and R. Ruffer, *Science* **328**, 1248 (2010).
 [30] J. Keaveney, A. Sargsyan, U. Krohn, I. G. Hughes, D. Sarkisyan, and C. S. Adams, *Phys. Rev. Lett.* **108**, 173601 (2012).

- [31] S. Okaba, T. Takano, F. Benabid, T. Bradley, L. Vincetti, Z. Maizelis, V. Yampolskii, F. Nori, and H. Katori, *Nat. Commun.* **5**, 4096 (2014).
- [32] Z. Meir, O. Schwartz, E. Shahmoon, D. Oron, and R. Ozeri, *Phys. Rev. Lett.* **113**, 193002 (2014).
- [33] T. Peyrot, Y. R. P. Sortais, A. Browaeys, A. Sargsyan, D. Sarkisyan, J. Keaveney, I. G. Hughes, and C. S. Adams, *Phys. Rev. Lett.* **120**, 243401 (2018).
- [34] R. H. Lehmburg, *Phys. Rev. A* **2**, 883 (1970).
- [35] W. Guerin, M. Rouabah, and R. Kaiser, *J. Mod. Opt.* **64**, 895 (2017).
- [36] A. S. Kuraptsev, I. M. Sokolov, and M. D. Havey, *Phys. Rev. A* **96**, 023830 (2017).
- [37] M. Chalony, R. Pierrat, D. Delande, and D. Wilkowski, *Phys. Rev. A* **84**, 011401(R) (2011).
- [38] A. A. Svidzinsky, J.-T. Chang, and M. O. Scully, *Phys. Rev. A* **81**, 053821 (2010).
- [39] T. S. do Espirito Santo, P. Weiss, A. Cipris, R. Kaiser, W. Guerin, R. Bachelard, and J. Schachenmayer, [arXiv:1910.06679](https://arxiv.org/abs/1910.06679).
- [40] Y. Kaluzny, P. Goy, M. Gross, J. M. Raimond, and S. Haroche, *Phys. Rev. Lett.* **51**, 1175 (1983).
- [41] R. Friedberg, S. R. Hartmann, and J. T. Manassah, *Phys. Rep.* **7**, 101 (1973).
- [42] R. Friedberg and J. T. Manassah, *Phys. Lett. A* **374**, 1648 (2010).
- [43] J. T. Manassah, *Adv. Opt. Photonics* **4**, 108 (2012).
- [44] D. Pavolini, A. Crubellier, P. Pillet, L. Cabaret, and S. Liberman, *Phys. Rev. Lett.* **54**, 1917 (1985).
- [45] F. W. Cummings, *Phys. Rev. A* **33**, 1683 (1986).
- [46] J. M. Herbelin, J. A. McKay, M. A. Kwok, R. H. Ueunten, D. S. Urevig, D. J. Spencer, and D. J. Benard, *Appl. Opt.* **19**, 144 (1980).
- [47] G. Labeyrie, D. Delande, C. Müller, C. Miniatura, and R. Kaiser, *Opt. Commun.* **243**, 157 (2004).

Conclusion on Part Two

The interaction of light with an atomic sample is at the heart of so many applications, from clocks to sensors, from quantum-information protocols to new types of photonic materials, that it has been studied a lot over decades, with several revivals triggered by new experimental possibilities or emerging concepts. This situation creates a very rich field, but it also creates the risk of reinventing the wheel, even more so when the problem can be tackled from different perspectives and by different communities. This sometimes gave me the feeling that the field was quite confused [Guerin 2017c].

Our group, like many others, might have added to the confusion sometimes. My own understanding evolved over the years and, for instance, I'm not convinced any more than we should distinguish 'cooperative' and 'collective' effects, as I claimed in [Guerin 2017c]. I now like very much the very simple definition given in a recent paper by Ketterle's group: "*Collective scattering occurs when it is impossible to determine which particle scattered a photon.*" [Dimitrova 2017].

Nevertheless, when the few remaining open questions are answered, hopefully soon, I will probably be able to pretend that I significantly contributed to the understanding of cooperative scattering in dilute and large samples, and in particular to the properties of the temporal dynamics. I hope it will be considered a nice achievement!

Complementary studies to be done

At short term, if the phased-excitation enhancement of subradiant states is successful with a simple π phase shift on half of the driving beam, the natural following is to increase the complexity of the phase profile: how much can we increase the subradiant population? At less short term, we can investigate dynamical protocols, such as in [He 2020], in order to selectively populate subradiant states.

Another question is in the continuity of our study about the influence of thermal motion and is about the influence of other kinds of decoherence mechanisms. Experimentally, we could try to break subradiance by adding, for instance, a noisy laser coupling the upper level to another excited state. This might emulate some kind of phonon dephasing. Another interesting possibility is to test if we can observe super and subradiance in room-temperature vapors, as we suggest in [Weiss 2019].

Finally, another open question is the influence of the Zeeman degeneracy on subradiance. Several theoretical works have investigated this problem within some approximations or toy models [Lee 2016, Hebenstreit 2017, Sutherland 2017, Munro 2018]. It would be interesting to confront those theories to the experiment. Our group is building an experiment with ytterbium atoms, which will soon give us the possibility to explore subradiance in a $J = 0 \rightarrow J = 1$ transition.

Long-term outlook

My future research will probably lie at the intersection of the different topics I explored so far and exposed in the two Parts of this document.

One first possible direction is cooperative scattering beyond the linear-optics regime. If atoms get significantly excited, their response become inelastic, and also some gain feature may appear, which makes an obvious link with my former work on gain and lasing. As also mentioned in the introduction of Part Two, there is a continuum between Dicke superradiance or superfluorescence (with many excited atoms) and amplified spontaneous emission.

The interest in going beyond the linear-optics regime is to explore quantum effects, which might be created by the correlations due to inelastic scattering or by the nonlinear atomic response. In both cases one should explore different signatures than the simple decay dynamics, for instance the light statistics. For that we will make use of the technique for measuring intensity correlations, developed in the context of our astronomical projects and already successfully applied to atomic physics experiments with hot vapors [Dussaux 2016] and cold atoms [Éloy 2018b, Ortiz-Gutiérrez 2019].

Another possible and different direction is cooperative scattering with *ordered or partially ordered samples*, which makes a link with my work on photonic band gaps (Section III.1). Many proposals have been made in this spirit in the last years: light transport in 1D chain [Chui 2015, Bettles 2016a, Needham 2019], atomic mirror from a 2D lattice [Bettles 2016b, Shahmoon 2017, Rui 2020], quantum memory with exponentially suppressed errors [Asenjo-Garcia 2017], lasing of subradiant modes [Holzinger 2020], etc. All this generally goes towards quantum metamaterials [Chang 2018], which is a very promising topic. Most of these proposals, however, are based on mesoscopic samples with a small number of atoms.

One original line of research would be to investigate the situation of large samples of ordered atoms. The order would only be very partial because, with 3D lattices for instance, the filling factor would be small. Therefore this would correspond to a situation of a disordered sample with strong long-range correlations. Back in the 1990s Bragg scattering experiments were performed on such samples [Birkel 1995, Weidemüller 1995]. One could now investigate the dynamical properties (super- and subradiance) in those samples, for instance. Is light emission superradiant in the Bragg directions and subradiant elsewhere? The emission from atoms in a 1D lattice has been recently discussed in terms of superradiant states [Chen 2018]. Another promising idea would be to engineer other kinds of correlation between the atomic positions. One could for example exploit the light-induced repulsive interaction between atoms in a MOT, which creates a kind of natural exclusion volume, analogous to the Debye length in nonneutral plasmas [Dubin 1999, Barré 2019]. More speculatively, could we somehow create hyperuniform densities [Torquato 2018] ?

Appendices

APPENDIX A

Detailed CV

Personal data

William GUERIN

Born November 1st, 1980 in Poissy (78), France

CNRS Associate researcher (*Chargé de recherche*), section 4

Institut de Physique de Nice (INPHYNI)

1361 route des lucioles, 06560 Valbonne, France

Email: william.guerin@inphyni.cnrs.fr

Web page: <https://inphyni.cnrs.fr/webpages/william-guerin>

Web of Science ResearcherID: E-2081-2012

ORCID: 0000-0001-8194-8351

Cursus

- 2007: PhD in physics, Université Paris-Sud (Orsay), supervisor: Alain Aspect
- 2003: Msc ‘Optics and photonics’, Université Paris-Sud
- 2003: Engineering degree, Institut d’Optique Graduate School (Palaiseau)
- 1998: Baccalauréat scientifique (High School degree, Science major)

Employment

- Since Oct. 2012: CNRS associate researcher at Institut de Physique de Nice (formerly Institut Non Linéaire de Nice, INLN), in the ‘Cold Atoms’ team supervised by Robin Kaiser
- Jan. 2010 – Aug. 2012: Post-doc researcher at Tübingen University (Germany) in the group of Claus Zimmermann; project leader, fellow of the Alexander von Humboldt Foundation
- June 2007 – Sept. 2009: Post-doc researcher at INLN in the team of Robin Kaiser
- Oct. 2003 – May 2007: Graduate student at Institut d’Optique in the team of Alain Aspect and Philippe Bouyer.

Grants

Personal or as PI

- 2018: Research grant from the Doebelin Federation: 4.5 k€
- 2017: Research grant from Université Côte d’Azur (Idex): 28 k€
- 2014: Research grant from Université Nice sophia-Antipolis (CSI): 5 k€
- 2012: Post-doc grant (declined) from the Carl Zeiss Foundation: 160 k€
- 2009: Post-doc grant from the Alexander von Humboldt Foundation: 2 years (2010–2011)
- 2003: PhD grant from the Délégation Générale à l’Armement (DGA): 3 years (2003 – 2006)

As everyone sadly knows, the success rate at the French national research funding agency (ANR) is incredibly low, which means that it involves a lot of luck. I’d like to mention here that I’ve got two projects that *almost* made it (they reached the waiting list): in 2012 (program ‘retour post-doc’) and in 2018 (collaborative project ‘Intensity Interferometry at Calern’). This didn’t bring me anything.

Other main funded projects in which I was/am/will be strongly involved

- 2020: Research grant from the QuantERA program: ~ 300 k€ for our team (PI: Robin Kaiser)
- 2019: Research grant from ANR: ~ 280 k€ for our team (PI: Mathilde Fouché)
- 2019: Research grant from ERC: ~ 2.4 M€ (PI: Robin Kaiser)
- 2019: Research grant from Région PACA: 80 k€ (PI: Robin Kaiser)
- 2018: Research grant from the FIRST-TF Labex network: 28.8 k€ (PI: Julien Chabé)
- 2016: European Training Network ColOpt: ~ 500 k€ for our team (Coordinator: Thorsten Ackemann; local PI: Robin Kaiser)
- 2014: Research grant from ANR: ~ 375 k€ for our team (PI: Sergey Skipetrov)

I also largely wrote the projects for Michelle Araújo’s PhD grant (2014, CAPES, Brazil) and Patrizia Weiss’s post-doc grant (2017, DFB, Germany).

Organization of workshops

- 2019: “Atoms and Photons Nice 2019”, Nice, 6–8 November (50 participants)
- 2016: “Strongly disordered optical systems: from the white paint to cold atoms”, Cargèse, 26–30 September (65 participants, but most of the work was done by Sergey Skipetrov)
- 2014: Annual meeting of the COSCALI network, Porquerolles, 7–11 September (25 participants)

Supervision activities

I am officially co-supervisor of Ana Cipris’s PhD thesis.
My other supervisees are listed in the following table:

Level	Name	Period	Publications	Share (with ...)
Post-doc	Patrizia Weiss	2016 – 2019	≥ 4	80% (RK)
Post-doc	Antoine Dussaux	2015 – 2016	2	20% (RK)
PhD	Antonin Siciak	2018 – now	≥ 2	25% (RK, JPR, MH)
PhD	Ana Cipris	2017 – now	≥ 4	80% (RK)
PhD	Michelle Araújo	2014 – 2018	5	80% (RK)
PhD	Aurélien Eloy	2015 – 2018	3	20% (MH, RK)
PhD	Samir Vartabi Kashanian	2013 – 2016	1	20% (RK, MH)
PhD	Alexander Schilke	2010 – 2012	3	80% (CZ)
PhD	Nicolas Mercadier	2008 – 2009	8	50% (RK)
M2	Adam Bellity	2019		100%
M2	Habibul Hasan	2016		80% (AD)
M2	Aurélien Eloy	2015	see above	30% (RK)
M2	T. Siva Pradyumna	2014		100%
M2	Djeylan Aktas	2013		30% (QB, RK)
M2	Davide Brivio	2008	2	80% (RK)
M2	Nicolas Mercadier	2008	see above	20% (RK)
M1	Pierre Menuge	2015		50% (AD)
L3	Louis Garbe	2014		100%
L3	Loïc Lavenu	2014		100%
L3	Wissam Fakhardji	2013		50%

The ‘Share’ column indicates what I subjectively evaluate as my participation to the supervision, which was often shared with other people: RK = Robin Kaiser, MH = Mathilde Hugbart, JPR = Jean-Pierre Rivet, CZ = Claus Zimmermann, AD = Antoine Dussaux, QB = Quentin Baudouin.

Teaching activities

In all contracts/status I had, I never had any teaching duty. All my teaching activities have thus been done on a voluntarily basis.

- 2017 & 2018: Exercises on ‘Cold Atoms’, M2 (9th semester), Nice University (10 h/yr)
- 2017: Tutorial lecture on ‘Light scattering by atoms’ for the Graduate students of the ITN ColOpt (2 h)
- 2016 & 2017: Lab courses on ‘Atoms and photons’, L3 (5th semester), Nice University (40 h/yr)
- 2013 & 2016: Tutored projects, L3 (6th semester), Nice University (15 d/yr)
- 2008: Exercises in Optics, L1 (1st semester), École Polytechnique Universitaire de Nice (12 h)
- 2003 – 2006: Lab courses in Optics, 1st year/L3 (5th semester), Institut d’Optique (50 h/yr)

Outreach activities

I haven’t done a lot of outreach activities but what I did with some success is to write press releases and/or short broad-audience summaries of my important results in order to attract

the attention of the specialized press, or even, sometimes, of the local general press:

- On the revival of intensity interferometry [[Guerin 2017a](#), [Guerin 2018](#), [Rivet 2018](#)]:
 - “**La microscopie spatiale est née**”, S. Brunier, *Sciences & Vie* n° 129, April 2019
- On the observation of subradiance [[Guerin 2016a](#)]:
 - “**Observation de la sous-radiance de Dicke dans un nuage d’atomes froids**”, *INP CNRS*, March 2016
 - “**Inibindo emissão espontânea de fótons em nuvem de átomos**”, *SFB (Brazilian physical Society)*, 25 Feb. 2016
 - “**Storing Light in the Dark**”, A. Carmele, *Physics* **9**, 20 (2016)
- On the random laser with cold atoms [[Baudouin 2013b](#)]:
 - “**D’un laser sans miroirs à certaines sources stellaires de lumière**”, *Science blog of ONISEP*, Feb. 2014
 - “**Lasers: Amplified by randomness**”, V. Vuletic, *Nature Physics* **9**, 325 (2013)
 - “**Nice: les physiciens de l’Institut Non Linéaire créent un nouveau laser**”, *Web Time Medias*, 21 May 2013
 - “**Cold-atom random laser simulates stellar clouds**”, *Physics World*, 9 May 2013
 - “**Physicists generate lasers inspired by space clouds**”, *Wired UK*, 8 Jan. 2013
 - “**Researchers Create The First Earth-Based Laser Built From A Cloud Of Gas**”, *Popular Science*, 7 Jan. 2013
 - “**Physicists Demonstrate First Laser Made From a Cloud of Gas**”, *MIT Technology Review*, 7 Jan. 2013
- On the DFB laser with cold atoms [[Schilke 2012a](#)]:
 - “**Light from the cold**”, *Laser Community* **2012:1**, 9 (2012)
 - “**Überraschung: Neuer Laser aus kaltem Gas**”, *Euro Laser*, March 2012
 - “**All-atom parametric oscillator**”, M. T. Rakher and K. Srinivasan, *Nature Photonics* **6**, 73 (2012)
 - “**Tübinger entwickeln neuen Laser aus kaltem Gas**”, *Reutlinger General-Anzeiger*, 20 Dec. 2011
 - “**Da waren Lichtblitze**”, *Schwäbisches Tagblatt*, 20 Dec. 2011
- On the Lévy flights of light [[Mercadier 2009](#), [Chevrollier 2010](#)]:
 - “**Anomalous photon diffusion in atomic vapor**”, *Europhysics News* **41**(4), 10 & *EPJD Highlights*, March 2010
 - “**Des photons attrapés au vol**”, *Le journal du CNRS* **242**, 12 (March 2010)
- On the the feasibility of a random laser with cold atoms [[Froufe-Pérez 2009](#)]:
 - “**Scientists are creating an unusual type of laser from a strange material**”, *Photonics Spectra*, Aug. 2009
 - “**Is random lasing possible with a cold atom cloud?**”, *PhysOrg.com*, 18 May 2009
 - “**The Laser Glow of an Atom Cloud**”, *Physical Review Focus* **23**, 14 (May 2009)
- On the guided atom laser [[Guerin 2006](#)]:
 - “**Guided atom laser**”, *Physics Today* **60**(2), 22 (Feb. 2007) & *AIP Physics News Update* **16**, 806 (Dec. 2006)
 - “**Horizontal lasing matters**”, *Nature Physics* **12**, 798 (Dec. 2006)
 - “**Guiding an atom laser**”, *PhysOrg.com*, 24 Nov. 2006
 - “**New atom laser could improve navigation system**”, *NewScientist.com*, 16 Nov. 2006

I have also written an article on my PhD thesis [[Guerin 2007](#)] for the review of the Institut d’Optique Alumni Association:

“**Le laser à atomes, source cohérente pour l’optique atomique**”, *Opto* **158**, 20 (2008).

Other activities

- Member of the INPHYNI advisory board (since 2017)
- Responsible of the INPHYNI weekly seminars (with Claire Michel, since 2017)
- Reviewer for several journals (Phys. Rev. Lett, Phys. Rev. A, Phys. Rev. X, New. J. Phys., Opt. Express, J. Opt., ...) and national competitive calls for funding (ANR, SIRTEQ, Labex, ...)
- In charge of the [Team web page](#)

APPENDIX B

List of publications and communications

B.1. Publications

Articles in peer-reviewed journals

Articles are in inverse chronological order. My name is underlined and the papers that are reproduced in this document have their numbers highlighted in bold with a link within the manuscript.

- [39] **Connecting field and intensity correlations: the Siegert relation and how to test it**
D. Ferreira, R. Bachelard, W. Guerin, R. Kaiser, and M. Fouché
American Journal of Physics, in press; preprint [arXiv:2002.05425](https://arxiv.org/abs/2002.05425)
- [38] **Intensity interferometry of P Cygni in the H α emission line: towards distance calibration of LBV supergiant stars**
J.-P. Rivet, A. Siciak, E. S. G. de Almeida, F. Vakili, A. Domiciano de Souza, M. Fouché, O. Lai, D. Vernet, R. Kaiser, and W. Guerin
Monthly Notices of the Royal Astronomical Society **494**, 218 (2020); preprint [arXiv:1910.08366](https://arxiv.org/abs/1910.08366)
- [37] **Optical-depth scaling of light scattering from a dense and cold atomic ^{87}Rb gas**
K. J. Kemp, S. J. Roof, M. D. Havey, I. M. Sokolov, D. V. Kupriyanov, and W. Guerin
Physical Review A **101**, 033832 (2020); preprint [arXiv:1807.10939](https://arxiv.org/abs/1807.10939)
- [36] **Collective excitation dynamics of a cold-atom cloud**
T. S. do Espirito Santo, P. Weiss, A. Cipris, R. Kaiser, W. Guerin, R. Bachelard, and J. Schachenmayer
Physical Review A **101**, 013617 (2020); preprint [arXiv:1910.06679](https://arxiv.org/abs/1910.06679)
- [35] **Collective multimode vacuum Rabi splitting**
W. Guerin, T. S. do Espirito Santo, P. Weiss, A. Cipris, J. Schachenmayer, R. Kaiser, and R. Bachelard
Physical Review Letters **123**, 243401 (2019); preprint [arXiv:1909.06454](https://arxiv.org/abs/1909.06454)
- [34] **Robustness of Dicke subradiance against thermal decoherence**
P. Weiss, A. Cipris, M. O. Araújo, R. Kaiser and W. Guerin
Physical Review A **100**, 033833 (2019); preprint [arXiv:1906.02918](https://arxiv.org/abs/1906.02918)
- [33] **Dressed dense atomic gases**
I. Lesanovsky, B. Olmos, W. Guerin, and R. Kaiser
Physical Review A **100**, 021401(R) (2019); preprint [arXiv:1902.02989](https://arxiv.org/abs/1902.02989)

- [32] **Comparison of three approaches to light scattering by dilute cold atomic ensembles**
I. M. Sokolov and W. Guerin
Journal of the Optical Society of America B **36**, 2030 (2019); preprint arXiv:1902.04289
- [31] **Optical long baseline intensity interferometry: prospects for stellar physics**
J.-P. Rivet, F. Vakili, O. Lai, D. Vernet, M. Fouché, W. Guerin, G. Labeyrie, and R. Kaiser
Experimental Astronomy **46**, 531 (2018); preprint arXiv:1805.06078
- [30] **Spatial intensity interferometry on three bright stars**
W. Guerin, J.-P. Rivet, M. Fouché, G. Labeyrie, D. Vernet, F. Vakili and R. Kaiser
Monthly Notices of the Royal Astronomical Society **480**, 245 (2018); preprint arXiv:1805.06653
- [29] **Subradiance and radiation trapping in cold atoms**
P. Weiss, M. O. Araújo, R. Kaiser, and W. Guerin
New Journal of Physics **20**, 063024 (2018); preprint arXiv:1803.01646
- [28] **Decay dynamics in the coupled-dipole model**
M. O. Araújo, W. Guerin, and R. Kaiser
Journal of Modern Optics **65**, 1345 (2018); preprint arXiv:1705.02190
- [27] **Diffusing-wave spectroscopy of cold atoms in ballistic motion**
A. Eloy, Z. Yao, R. Bachelard, W. Guerin, M. Fouché, and R. Kaiser
Physical Review A **97**, 013810 (2018); preprint arXiv:1710.03974
- [26] **Temporal intensity interferometry: photon bunching in three bright stars**
W. Guerin, A. Dussaux, M. Fouché, G. Labeyrie, J.-P. Rivet, D. Vernet, F. Vakili, and R. Kaiser
Monthly Notices of the Royal Astronomical Society **472**, 4126 (2017); preprint arXiv:1708.06119
- [25] **Population of collective modes in light scattering by many atoms**
W. Guerin and R. Kaiser
Physical Review A **5**, 053865 (2017); preprint arXiv:1702.01053
- [24] **Light interacting with atomic ensembles: collective, cooperative and mesoscopic effects**
W. Guerin, M. T. Rouabah, and R. Kaiser
Journal of Modern Optics **64**, 895-907 (2017); preprint arXiv:1605.02439
- [23] **Noise spectroscopy with large clouds of cold atoms**
S. Vartabi Kashanian, A. Eloy, W. Guerin, M. Lintz, M. Fouché, and R. Kaiser
Physical Review A **94**, 043622 (2016); preprint arXiv:1606.07658
- [22] **Collective effects in the radiation pressure force**
R. Bachelard, N. Piovella, W. Guerin, and R. Kaiser
Physical Review A **94**, 033838 (2016); preprint arXiv:1607.01157
- [21] **Diffusive to quasi-ballistic random laser: incoherent and coherent models**
W. Guerin, Y. D. Chong, Q. Baudouin, M. Liertz, S. Rotter, and R. Kaiser
Journal of the Optical Society of America B **33**, 1888 (2016); preprint arXiv:1606.03679
- [20] **Superradiance in a large and dilute cloud of cold atoms in the linear-optics regime**
M. O. Araújo, I. Krešić, R. Kaiser, and W. Guerin
Physical Review Letters **117**, 073002 (2016); preprint arXiv:1603.07204

-
- [19] **Temporal intensity correlation of light scattered by a hot atomic vapor**
A. Dussaux, T. Passerat de Silans, W. Guerin, O. Alibart, S. Tanzilli, F. Vakili, R. Kaiser
Physical Review A **93**, 043826 (2016); preprint arXiv:1601.00853
- [18] **Subradiance in a large cloud of cold atoms**
W. Guerin, M. O. Araújo, and R. Kaiser
Physical Review Letters **116**, 083601 (2016); preprint arXiv:1509.00227
- [17] **Raman process under condition of radiation trapping in a disordered atomic medium**
L. V. Gerasimov, V. M. Ezhova, D. V. Kupriyanov, Q. Baudouin, W. Guerin, and R. Kaiser
Physical Review A **90**, 013814 (2014); preprint arXiv:1401.6641
- [16] **Microscopic characterization of Lévy flights of light in atomic vapors**
N. Mercadier, M. Chevrollier, W. Guerin, and R. Kaiser
Physical Review A **87**, 063837 (2013); preprint arXiv:1305.1714
- [15] **A cold-atom random laser**
Q. Baudouin, N. Mercadier, V. Guarrera, W. Guerin, and R. Kaiser
Nature Physics **9**, 357 (2013); preprint arXiv:1301.0522
- [14] **Photonic properties of one-dimensionally-ordered cold atomic vapors under conditions of electromagnetically induced transparency**
A. Schilke, C. Zimmermann, and W. Guerin
Physical Review A **86**, 023809 (2012); preprint arXiv:1206.2622
- [13] **Optical parametric oscillation with distributed feedback in cold atoms**
A. Schilke, C. Zimmermann, Ph. W. Courteille, and W. Guerin
Nature Photonics **6**, 101 (2012); preprint arXiv:1109.6114
- [12] **Quasicontinuous horizontally guided atom laser: coupling spectrum and flux limits**
A. Bernard, W. Guerin, J. Billy, F. Jendrzejewski, P. Cheinet, A. Aspect, V. Josse, and P. Bouyer
New Journal of Physics **13**, 065015 (2011); preprint arXiv:1012.2971
- [11] **Photonic Band Gaps in One-Dimensionally Ordered Cold Atomic Vapors**
A. Schilke, C. Zimmermann, Ph. W. Courteille, and W. Guerin
Physical Review Letters **106**, 223903 (2011); preprint arXiv:1101.3469
- [10] **Anomalous photon diffusion in atomic vapors**
M. Chevrollier, N. Mercadier, W. Guerin, and R. Kaiser
European Physical Journal D **58**, 161 (2010); preprint arXiv:1001.0320
- [9] **Towards a random laser with cold atoms**
W. Guerin, N. Mercadier, F. Michaud, D. Brivio, L. S. Froufe-Pérez, R. Carminati, V. Ereemeev, A. Goetschy, S. E. Skipetrov, and R. Kaiser
Journal of Optics **12**, 024002 (2010); preprint arXiv:0906.0714
- [8] **Lévy flights of photons in hot atomic vapours**
N. Mercadier, W. Guerin, M. Chevrollier, and R. Kaiser
Nature Physics **5**, 602 (2009); preprint arXiv:0904.2454
- [7] **Threshold of a random laser based on Raman gain in cold atoms**
W. Guerin, N. Mercadier, D. Brivio, and R. Kaiser

Optics Express **17**, 11236 (2009); preprint arXiv:0903.5190

[6] **Threshold of a Random Laser with Cold Atoms**

L. S. Froufe-Pérez, W. Guerin, R. Carminati, and R. Kaiser

Physical Review Letters **102**, 173903 (2009); preprint arXiv:0812.0266

[5] **Mechanisms for Lasing with Cold Atoms as the Gain Medium**

W. Guerin, F. Michaud, and R. Kaiser

Physical Review Letters **101**, 093002 (2008); preprint arXiv:0804.0109

[4] **Theoretical tools for atom-laser-beam propagation**

J.-F. Riou, Y. Le Coq, F. Impens, W. Guerin, C. J. Bordé, A. Aspect, and P. Bouyer

Physical Review A **77**, 033630 (2008); preprint arXiv:0802.4039

[3] **Guided Quasicontinuous Atom Laser**

W. Guerin, J.-F. Riou, J. P. Gaebler, V. Josse, P. Bouyer, and A. Aspect

Physical Review Letters **97**, 200402 (2006); preprint arXiv:cond-mat/0607438

[2] **Beam Quality of a Nonideal Atom Laser**

J.-F. Riou, W. Guerin, Y. Le Coq, M. Fauquembergue, V. Josse, P. Bouyer, and A. Aspect

Physical Review Letters **96**, 070404 (2006); preprint arXiv:cond-mat/0509281

[1] **Partially ferromagnetic electromagnet for trapping and cooling neutral atoms to quantum degeneracy**

M. Fauquembergue, J.-F. Riou, W. Guerin, S. Rangwala, F. Moron, A. Villing, Y. Le Coq, P. Bouyer, A. Aspect, and M. Lécivain

Review of Scientific Instruments **76**, 103104 (2005); preprint arXiv:cond-mat/0507129

Proceedings

I have some documents that officially are proceedings but actually are only abstracts of conferences, I don't include them. The proceedings below really contain original material (data or ideas or discussions unpublished otherwise).

- **Intensity Interferometry revival on the Côte d'Azur**

O. Lai, W. Guerin, F. Vakili, R. Kaiser, J.-P. Rivet, M. Fouché, G. Labeyrie, J. Chabé, C. Courde, E. Samain, D. Vernet

Proceedings SPIE **10701**, *Optical and Infrared Interferometry and Imaging VI*, 1070121 (2018); preprint arXiv:1810.08023

- **Guided atom laser : a new tool for guided atom optics**

J. Billy, V. Josse, Z. Zuo, W. Guerin, A. Aspect and P. Bouyer

Annales de Physique (France) **32**, 17 (2007); preprint arXiv:0712.1482

Book chapter

- **Cold and hot atomic vapors: a testbed for astrophysics?**

Q. Baudouin, W. Guerin, and R. Kaiser

in *Annual Review of Cold Atoms and Molecules*, vol. 2, edited by K. Madison, K. Bongs, L. D. Carr, A. M. Rey, and H. Zhai, World Scientific (Singapore, 2014); preprint HAL-00968233

Patent

- **Guided coherent atom source and atomic interferometer**
P. Bouyer, V. Josse, W. Guerin J. Billy and A. Landragin
[EP2104406B1](#) – [US8288712B2](#) (2009)

Thesis

- **Source atomique cohérente dans des pièges optique et magnétique: réalisation d'un laser à atomes guidé**
W. Guerin (Supervisor: A. Aspect)
PhD thesis of Université Paris Sud 11 (2007)
Reprint: [TEL-00146375](#)

B.2. Communications

Of course I only list communications that I personally delivered.

In summary: 37 talks and 14 posters.

Invited talks at conferences

- **Direct observation of subradiance in cold atoms**
Winter Colloquium on the Physics of Quantum Electronics (PQE), Snowbird (Utah, USA), Jan. 2016
- **Optical Parametric Oscillation with Distributed Feedback in Cold Atoms**
International Quantum Electronics Conference (IQEC), Munich (Germany), May 2013
- **Towards a Random Laser with Cold Atoms**
Colloque sur les Lasers et l'Optique Quantique (COLOQ), Nice, Sept. 2009

Invited talks at workshops or symposia

- **Super- and sub-radiance in dilute atomic ensembles**
Annual Workshop of the 'GDR Complexe', Paris (France), April 2019
- **Super- and sub-radiance in optically dense atomic systems**
Mini-workshop on Multiple Scattering and Localization of Light, Grenoble, Nov. 2018
- **Intensity Correlations from Atoms to Stars**
Journées du Programme structurant UCA^{JEDI} 'Matière, Lumière, Interactions', Fréjus, Oct. 2018
- **Subradiance and superradiance in a dilute cloud of cold atoms**
Workshop on Collective Scattering of Light, Fernando de Noronha (Brazil), Aug. 2018
- **I2C: Intensity Interferometry at Calern**
Meeting of the CTA Intensity Interferometry Science Working Group, Barcelona (Spain), April 2018
- **Superradiance and subradiance in a large and dilute cold-atom sample**
Workshop on Strongly disordered optical systems: from the white paint to cold atoms, Cargèse, Sept. 2016

- **The laser which came from the cold**
Journée de la physique niçoise, Nice, Jan. 2015
- **Cooperative scattering of light in cold atoms**
Workshop on Long Range Interactions in Quantum Systems, Palaiseau, Sept. 2014
- **A random laser with cold atoms**
Workshop on Hanbury-Brown and Twiss Interferometry: Prospects for astrophysics and quantum optics, Nice, May 2014
- **A random laser with cold atoms**
Indo-French Physics Conference on Optics, Nano Sciences, Cold Atoms and Synchrotron facilities, Bangalore (India), March 2014
- **Photonic properties of one-dimensionally ordered cold atomic vapors**
Meeting of the COSCALI (COllective SCAttering of LIght) international network, Tübingen (Germany), July 2012
- **Towards a Random Laser with Cold Atoms**
ILLUMINYating Atoms and Molecules Symposium, Marseilles, Oct. 2008

Invited seminars

- **Intensity Interferometry for the 21st Century**
– Electronic Department, Politecnico di Milano, Milan (Italy), July 2018
- **Subradiance and superradiance in a dilute cloud of cold atoms**
– Instituto de Ciencias Fotónicas (ICFO), on-line seminar, May 2020
– Institut de Physique et Chimie des Matériaux de Strasbourg (IPCMS), Strasbourg, April 2017
– Laboratoire de Physique des Lasers (LPL), Villetaneuse, Oct. 2016
– Laboratoire de Physique de la Matière Condensée (LPMC), Nice, Nov. 2015
- **A random laser with cold atoms**
– Physikalisches Institut, Universität Tübingen (Germany), Feb. 2013
- **Photonic Properties of 1D Ordered Cold Atomic Vapors**
– Institut Non Linéaire de Nice (INLN), Sophia-Antipolis, Nov. 2011
– Laboratoire Ondes et Matière d'Aquitaine (LOMA), Bordeaux, Nov. 2011
– Laboratoire Charles Coulomb (L2C), Montpellier, October 2011
- **Towards a Random Laser with Cold Atoms**
– Laboratoire Collisions Agrégats Réactivité (LCAR), Toulouse, Nov. 2009
– Physikalisches Institut, Universität Tübingen (Germany), Jan. 2009
– Laboratoire des Collisions Atomiques et Moléculaires (LCAM), Orsay, Dec. 2008
- **Le laser à atomes, source cohérente pour l'optique atomique**
– Laboratoire de Physique des Lasers (LPL), Villetaneuse, March 2008
– Centre de Physique Moléculaire, Optique et Hertzienne (CPMOH), Bordeaux, Dec. 2007
– Laboratoire de Physique des Interactions Ioniques et Moléculaires (PIIM), Marseilles, Nov. 2007
– Institut Non Linéaire de Nice (INLN), Sophia-Antipolis, March 2007

Contributions to conferences

- **Photonic bunching with starlight** (poster)
International Conference on Laser Spectroscopy (ICOLS), Arcachon, July 2017

- **Subradiance and superradiance in a dilute cloud of cold atoms** (poster)
International Conference on Laser Spectroscopy (ICOLS), Arcachon, July 2017
- **Direct observation of subradiance in cold atoms** (talk)
Congrès général de la Société Française de Physique, Strasbourg, Aug. 2015
- **A random laser with cold atoms** (talk)
International Quantum Electronics Conference (IQEC), Munich (Germany), May 2013
- **Photonic Band Gaps and Distributed Feedback Lasing in Cold Atoms** (poster)
International Conference on Atomic Physics (ICAP), Palaiseau, July 2012
- **Photonic Band Gaps and Distributed Feedback Lasing with Cold Atoms** (poster)
International Conference on Laser Spectroscopy (ICOLS), Hameln (Germany), May 2011
- **Towards a Random Laser with Cold Atoms** (poster)
International Conference on Atomic Physics (ICAP), Storrs (Connecticut, USA), July 2008
- **A Guided Atom Laser** (talk)
European Optical Society Annual Meeting, Paris, Oct. 2006
- **A Guided Atom Laser** (poster)
International Conference on Atomic Physics (ICAP), Innsbruck (Austria), July 2006
- **Profil transverse d'un laser à atomes** (poster)
Colloque sur les Lasers et l'Optique Quantique (COLOQ), Dijon, Sept. 2005
- **Observation of the transverse mode of an atom laser** (talk)
Young Atom Opticians Conference (YAO), Hannover (Germany), Feb. 2005

Contributions to workshops or symposia

- **Intensity correlations with starlight** (poster)
WE Heraeus Seminar on Physics and Applications of Superconducting Nanowire Single Photon Detectors, Bad Honnef (Germany), Nov. 2018
- **Observation of subradiance in cold atoms** (poster)
Atomes froids: concepts fondamentaux et applications, Meeting of the 'GDR Atomes Froids', Paris, Nov. 2015
- **Subradiance in a dilute and extended atomic sample?** (talk)
Meeting of the COSCALI (Collective SCAttering of LIght) international network, Porquerolles, Sept. 2014
- **A cold-atom random laser** (poster)
Third Bonn Humboldt Award Winners' Forum 'Frontiers in Quantum Optics: Taming the World of Atoms and Photons - 100 Years after Niels Bohr', Bonn (Germany), Oct. 2013
- **A cold-atom random laser** (poster)
Atomes froids et ingénierie quantique, Meeting of the 'GDR Atomes Froids', Paris, May 2013
- **Photonic Band Gaps in Cold Atoms** (poster)
Network Meeting of the Alexander von Humboldt Foundation, Ulm (Germany), Oct. 2010
- **A Guided Atom Laser** (poster)
Atelier de l'Institut Francilien de Recherche sur les Atomes Froids (IFRAF), Paris, May 2006

- **Coherent atom optics: transverse mode of an atom laser and optical manipulation** (poster)
European Graduate College Workshop, Gif-sur-Yvette, June 2005
- **Manipulation of Bose-Einstein condensates with optical tweezers** (talk)
Russian-French Laser Physics Workshop for Young Scientists, Saint-Petersburg (Russia), July 2004

Bibliography

- [Abrams 1978] R. L. Abrams & R. C. Lind. *Degenerate four-wave mixing in absorbing media*. *Opt. Lett.* **2**, 94–96 (1978). Errata, *Opt. Lett.* **3**, 205 (1978).
- [Aktas 2013] D. Aktas. *Upgrade of a cold-atom experimental setup for the study of random lasers*. Master’s thesis, Université Nice Sophia-Antipolis (2013).
- [Anderson 1958] P. W. Anderson. *Absence of Diffusion in Certain Random Lattices*. *Phys. Rev.* **109**, 1492–1505 (1958).
- [Andreasen 2011] J. Andreasen, A. A. Asatryan, L. C. Botten, M. A. Byrne, H. Cao, L. Ge, L. Labonté, P. Sebbah, A. D. Stone, H. E. Türeci, & C. Vanneste. *Modes of random lasers*. *Adv. Opt. Photon.* **3**, 88–127 (2011).
- [Antezza 2009] M. Antezza & Y. Castin. *Fano-Hopfield model and photonic band gaps for an arbitrary atomic lattice*. *Phys. Rev. A* **80**, 013816 (2009).
- [Antezza 2013] M. Antezza & Y. Castin. *Photonic band gaps in an imperfect atomic diamond lattice: Penetration depth and effects of finite size and vacancies*. *Phys. Rev. A* **88**, 033844 (2013).
- [Araújo 2016] M. O. Araújo, I. Krešić, R. Kaiser, & W. Guerin. *Superradiance in a Large Cloud of Cold Atoms in the Linear-Optics Regime*. *Phys. Rev. Lett.* **117**, 073002 (2016).
- [Araújo 2018a] M. O. Araújo. *Super- et sous-radiance dans un nuage dilué d’atomes froids*. PhD thesis, Université Côte d’Azur (2018).
- [Araújo 2018b] M. O. Araújo, W. Guerin, & R. Kaiser. *Decay dynamics in the coupled-dipole model*. *J. Mod. Opt.* **65**, 1345–1354 (2018).
- [Arecchi 1970] F. T. Arecchi & E. Courtens. *Cooperative phenomena in resonant electromagnetic propagation*. *Phys. Rev. A* **2**, 1730–1737 (1970).
- [Asenjo-Garcia 2017] A. Asenjo-Garcia, M. Moreno-Cardoer, A. Albrecht, H. J. Kimble, & D. E. Chang. *Exponential improvement in photon storage fidelities using subradiance and “selective radiance” in atomic arrays*. *Phys. Rev. X* **7**, 031024 (2017).

- [Bachelard 2012] R. Bachelard, P. W. Courteille, R. Kaiser, & N. Piovella. *Resonances in Mie scattering by an inhomogeneous atomic cloud*. Europhys. Lett. **97**, 14004 (2012).
- [Bachelard 2016] R. Bachelard, N. Piovella, W. Guerin, & R. Kaiser. *Collective effects in the radiation pressure force*. Phys. Rev. A **94**, 033836 (2016).
- [Bar-Gill 2007] N. Bar-Gill, E. E. Rowen, & N. Davidson. *Spectroscopy of strong-pulse superradiance in a Bose-Einstein condensate*. Phys. Rev. A **76**, 043603 (2007).
- [Barré 2019] J. Barré, R. Kaiser, G. Labeyrie, B. Marcos, & D. Métivier. *Towards a measurement of the Debye length in very large magneto-optical traps*. Phys. Rev. A **100**, 013624 (2019).
- [Baudouin 2013a] Q. Baudouin. *Lumière dans des vapeurs atomiques opaques: piégeage radiatif, laser aléatoire et vols de Lévy*. PhD thesis, Université Nice Sophia-Antipolis (2013).
- [Baudouin 2013b] Q. Baudouin, N. Mercadier, V. Guarrera, W. Guerin, & R. Kaiser. *A cold-atom random laser*. Nature Phys. **9**, 357–360 (2013).
- [Baudouin 2013c] Q. Baudouin, N. Mercadier, & R. Kaiser. *Steady-state signatures of radiation trapping by cold multilevel atoms*. Phys. Rev. A **87**, 013412 (2013).
- [Baudouin 2014a] Q. Baudouin, W. Guerin, & R. Kaiser. *Cold and hot atomic vapors: a testbed for astrophysics?* vol. 2 of *Annual Review of Cold Atoms and Molecules* 251–311. World Scientific Singapore (2014).
- [Baudouin 2014b] Q. Baudouin, R. Pierrat, A. Eloy, E. J. Nunes-Pereira, P. Cuni-asse, N. Mercadier, & R. Kaiser. *Signatures of Lévy flights with annealed disorder*. Phys. Rev. E **90**, 052114 (2014).
- [Bellando 2013] L. Bellando. *Localisation de la lumière et effets coopératifs dans des nuages d’atomes froids*. PhD thesis, Université de Nice Sophia-Antipolis (2013).
- [Bellando 2014] L. Bellando, A. Gero, E. Akkermans, & R. Kaiser. *Cooperative effects and disorder: A scaling analysis of the spectrum of the effective atomic Hamiltonian*. Phys. Rev. A **90**, 063822 (2014).
- [Bender 2010] H. Bender, C. Stehle, S. Slama, R. Kaiser, N. Piovella, C. Zimmermann, & P. W. Courteille. *Observation of cooperative Mie scattering from an ultracold atomic cloud*. Phys. Rev. A **82**, 011404(R) (2010).
- [Berman 1999] P. R. Berman. *Comparison of recoil-induced resonances and the collective atomic recoil laser*. Phys. Rev. A **59**, 585–596 (1999).
- [Berman 2010] P. R. Berman. *Energy conservation in collective coherent emission by dipole oscillators*. Am. J. Phys. **79**, 1323–1330 (2010).
- [Bernard 2011] A. Bernard, W. Guerin, J. Billy, F. Jendrzejewski, P. Cheinet, A. Aspect, V. Josse, & P. Bouyer. *Quasicontinuous horizontally*

- guided atom laser: coupling spectrum and flux limits.* New J. Phys. **13**, 065015 (2011).
- [Bettles 2016a] R. J. Bettles, S. A. Gardiner, & C. S. Adams. *Cooperative eigenmodes and scattering in one-dimensional atomic arrays.* Phys. Rev. A **94**, 043844 (2016).
- [Bettles 2016b] R. J. Bettles, S. A. Gardiner, & C. S. Adams. *Enhanced Optical Cross Section via Collective Coupling of Atomic Dipoles in a 2D Array.* Phys. Rev. Lett. **116**, 103602 (2016).
- [Bidel 2002] Y. Bidel, B. Klappauf, J. C. Bernard, D. Delande, G. Labeyrie, C. Miniatura, D. Wilkowski, & R. Kaiser. *Coherent Light Transport in a Cold Strontium Cloud.* Phys. Rev. Lett. **88**, 203902 (2002).
- [Bienaimé 2010] T. Bienaimé, S. Bux, E. Lucioni, P. W. Courteille, N. Piovella, & R. Kaiser. *Observation of Cooperative Radiation Pressure in Presence of Disorder.* Phys. Rev. Lett. **104**, 183602 (2010).
- [Bienaimé 2011a] T. Bienaimé. *Effets coopératifs dans les nuages d'atomes froids.* PhD thesis, Université de Nice-Sophia Antipolis (2011).
- [Bienaimé 2011b] T. Bienaimé, M. Petruzzo, D. Bigerni, N. Piovella, & R. Kaiser. *Atom and photon measurement in cooperative scattering by cold atoms.* J. Mod. Opt. **58**, 1942–1950 (2011).
- [Bienaimé 2012] T. Bienaimé, N. Piovella, & R. Kaiser. *Controlled Dicke subradiance from a large cloud of two-level systems.* Phys. Rev. Lett. **108**, 123602 (2012).
- [Bienaimé 2013] T. Bienaimé, R. Bachelard, P. W. Courteille, N. Piovella, & R. Kaiser. *Cooperativity in light scattering by cold atoms.* Fortschr. Phys. **61**, 377–392 (2013).
- [Bienaimé 2014] T. Bienaimé, R. Bachelard, J. Chabé, M. Rouabah, L. Bellando, P. W. Courteille, N. Piovella, & R. Kaiser. *Interplay between radiation pressure force and scattered light intensity in the cooperative scattering by cold atoms.* J. Mod. Opt. **61**, 18 (2014).
- [Billy 2007] J. Billy, V. Josse, Z. Zuo, W. Guerin, A. Aspect, & P. Bouyer. *Guided atom laser : a new tool for guided atom optics.* Ann. Phys. (Fr.) **32**, 17 (2007).
- [Birkel 1995] G. Birkel, M. Gatzke, I. H. Deutsch, S. L. Rolston, & W. D. Phillips. *Bragg scattering from Atoms in optical Lattices.* Phys. Rev. Lett. **75**, 2823 (1995).
- [Bloch 1999] I. Bloch, T. W. Hänsch, & T. Esslinger. *Atom laser with a CW output coupler.* Phys. Rev. Lett. **82**, No. 15 3008 (1999).
- [Bohnet 2012] J. G. Bohnet, Z. Chen, J. M. Weiner, D. Meiser, M. J. Holland, & J. K. Thompson. *A steady-state superradiant laser with less than one intracavity photon.* Nature **484**, 78–81 (2012).

- [Bonifacio 1975] R. Bonifacio & L. A. Lugiato. *Cooperative radiation processes in two-level systems: Superfluorescence*. Phys. Rev. A **11**, 1507 – 1521 (1975).
- [Bonifacio 1994] R. Bonifacio & L. De Salvo. *Collective atomic recoil laser (CARL): optical gain without inversion by collective atomic recoil and self-bunching of two-level atoms*. Nucl. Instrum. Methods Phys. Res. Sect. A **341**, 360 – 362 (1994).
- [Boyd 1981] R. W. Boyd, M. G. Raymer, P. Narum, & D. J. Harter. *Four-wave parametric interactions in a strongly driven two-level system*. Phys. Rev. A **24**, 411–423 (1981).
- [Bozhokin 2018] S. V. Bozhokin & I. M. Sokolov. *Comparison of the wavelet and Gabor transforms in the spectral analysis of nonstationary signals*. Tech. Phys. **63**, 1711–1717 (2018).
- [Brivio 2008] D. Brivio. *Random laser with cold atoms: extracting information from atomic fluorescence*. Tesi di Laurea, Università di Milano (2008).
- [Brzozowski 2005] T. M. Brzozowski, M. Brzozowska, J. Zachorowski, M. Zawada, & W. Gawlik. *Probe spectroscopy in an operating magneto-optical trap: The role of Raman transitions between discrete and continuum atomic states*. Phys. Rev. A **71**, 013401 (2005).
- [Burin 2001] A. L. Burin, M. A. Ratner, H. Cao, & R. P. H. Chang. *Model for a Random Laser*. Phys. Rev. Lett. **87**, 215503 (2001).
- [Bux 2010] S. Bux, E. Lucioni, H. Bender, T. Bienaimé, K. Lauber, C. Stehle, C. Zimmermann, S. Slama, P. W. Courteille, N. Piovela, & R. Kaiser. *Cooperative Scattering by Cold Atoms*. J. Mod. Opt. **57**, 1841 (2010).
- [Bux 2011] S. Bux, C. Gnahn, R. A. W. Maier, C. Zimmermann, & P. W. Courteille. *Cavity-controlled collective scattering at the recoil limit*. Phys. Rev. Lett. **106**, 203601 (2011).
- [Cao 1998] H. Cao, Y. G. Zhao, H. C. Ong, S. T. Ho, J. Y. Dai, J. Y. Wu, & R. P. H. Chang. *Ultraviolet Lasing in Resonators Formed by Scattering in Semiconductor Polycrystalline Films*. Appl. Phys. Lett. **73**, 3656–3658 (1998).
- [Cao 1999] H. Cao, Y. G. Zhao, S. T. Ho, E. W. Seeling, Q. H. Wang, & R. P. H. Chang. *Random Laser Action in Semiconductor Powder*. Phys. Rev. Lett. **82**, 2278–2281 (1999).
- [Cao 2001] H. Cao, Y. Ling, J. Y. Xu, C. Q. Cao, & P. Kumar. *Photon statistics of random lasers with resonant feedback*. Phys. Rev. Lett. **86**, 4524 (2001).
- [Cao 2003] H. Cao. *Lasing in random media*. Waves Random Media **13**, R1–R39 (2003).

- [Cao 2005] H. Cao. *Review on latest developments in random lasers with coherent feedback*. J. Phys. A: Math. Gen. **38**, 10497–10535 (2005).
- [Cerjan 2015] A. Cerjan, Y. D. Chong, & A. D. Stone. *Steady-state ab initio laser theory for complex gain media*. Opt. Express **23**, 6455–6477 (2015).
- [Chabé 2014] J. Chabé, M. T. Rouabah, L. Bellando, T. Bienaimé, N. Piovella, R. Bachelard, & R. Kaiser. *Coherent and incoherent multiple scattering*. Phys. Rev. A **89**, 043833 (2014).
- [Chalony 2011] M. Chalony, R. Pierrat, D. Delande, & D. Wilkowski. *Coherent flash of light emitted by a cold atomic cloud*. Phys. Rev. A **84**, 011401(R) (2011).
- [Chang 2018] D. E. Chang, J. S. Douglas, A. Gonzáles-Tudela, C.-L. Hung, & H. J. Kimble. *Colloquium: Quantum matter built from nanoscopic lattices of atoms and photons*. Rev. Mod. Phys. **90**, 031002 (2018).
- [Chen 2010] J. F. Chen, S. Wang, D. Wei, M. M. T. Loy, G. K. L. Wong, & S. Du. *Optical coherent transients in cold atoms: From free-induction decay to optical precursors*. Phys. Rev. A **81**, 033844 (2010).
- [Chen 2018] L. Chen, P. Wang, Z. Meng, L. Huang, H. Cai, D.-W. Wang, S.-Y. Zhu, & J. Zhan. *Experimental observation of one-dimensional superradiance lattices in ultracold atoms*. Phys. Rev. Lett. **120**, 193601 (2018).
- [Chevrollier 2010] M. Chevrollier, N. Mercadier, W. Guerin, & R. Kaiser. *Anomalous photon diffusion in atomic vapors*. Eur. Phys. J. D **58**, 161 (2010).
- [Chevrollier 2012] M. Chevrollier. *Radiation trapping and Lévy flights in atomic vapours: an introductory review*. Contemp. Phys. **53**, 227–239 (2012).
- [Chui 2015] S.-T. Chui, S. Du, & G.-B. Jo. *Subwavelength transportation of light with atomic resonances*. Phys. Rev. A **92**, 053826 (2015).
- [Chung 1980] J. C. Chung, J. C. Huang, & N. B. Abraham. *Intensity fluctuations and spatial coherence of a single polarized component of a saturating amplified-spontaneous-emission source*. Phys. Rev. A **22**, 1018–1021 (1980).
- [Cohen-Tannoudji 1992] C. Cohen-Tannoudji, J. Dupont-Roc, & G. Grynberg. *Atom-Photon Interactions: Basic Processes and Applications*. Wiley New York (1992).
- [Compton 1922] K. T. Compton. *Theory of Ionization by Cumulative Action and the Low Voltage Arc*. Phys. Rev. **20**, 283–299 (1922).
- [Compton 1923] K. T. Compton. *Some properties of resonance radiation and excited atoms*. Philos. Mag. **45**, 752 (1923).

- [Conti 2008] C. Conti & A. Fratalocchi. *Dynamic light diffusion, three-dimensional Anderson localization and lasing in inverted opals*. Nature Phys. **4**, 794–798 (2008).
- [Cottier 2018] F. Cottier, R. Kaiser, & R. Bachelard. *Role of disorder in super- and subradiance of cold atomic clouds*. Phys. Rev. A **98**, 013622 (2018).
- [Courteille 2010] P. W. Courteille, S. Bux, E. Lucioni, K. Lauber, T. Bienaimé, R. Kaiser, & N. Piovella. *Modification of Radiation Pressure due to Cooperative Scattering of Light*. Eur. Phys. J. D. **58**, 69–73 (2010).
- [Courtois 1994] J.-Y. Courtois, G. Grynberg, B. Lounis, & P. Verkerk. *Recoil-induced resonances in cesium: An atomic analog to the free-electron laser*. Phys. Rev. Lett. **72**, 3017–3020 (1994).
- [Couvert 2008] A. Couvert, M. Jeppesen, T. Kawalec, G. Reinaudi, R. Mathevet, & D. Guéry-Odelin. *A quasi-monomode guided atom-laser from an all-optical Bose-Einstein condensate*. Europhys. Lett. **83**, 50001 (2008).
- [Crubellier 1980] A. Crubellier, S. Liberman, & P. Pillet. *Superradiance and subradiance in three-level systems*. Opt. Commun. **33**, 143–148 (1980).
- [Dall 2010] R. G. Dall, S. S. Hodgman, M. T. Johnsson, K. G. H. Baldwin, & A. G. Truscott. *Transverse mode imaging of guided matter waves*. Phys. Rev. A **81**, 011602 (2010).
- [de Vries 1998] P. de Vries, D. V. van Coevorden, & A. Lagendijk. *Point scatterers for classical waves*. Rev. Mod. Phys. **70**, 447–466 (1998).
- [Deutsch 1995] I. H. Deutsch, R. J. C. Spreeuw, S. L. Rolston, & W. D. Phillips. *Photonic band gaps in optical lattices*. Phys. Rev. A **52**, 1394 (1995).
- [DeVoe 1996] R. G. DeVoe & R. G. Brewer. *Observation of Superradiant and Subradiant Spontaneous Emission of Two Trapped Ions*. Phys. Rev. Lett. **76**, 2049–2052 (1996).
- [Dicke 1954] R. H. Dicke. *Coherence in Spontaneous Radiation Processes*. Phys. Rev. **93**, 99–110 (1954).
- [Dimitrova 2017] I. Dimitrova, W. Lunden, J. Amato-Grill, N. Jepsen, Y. Yu, M. Messer, T. Rigaldo, G. Puentes, D. Weld, & W. Ketterle. *Observation of two-beam collective scattering phenomena in a Bose-Einstein condensate*. Phys. Rev. A **96**, 051603(R) (2017).
- [do Espirito Santo 2020] T. S. do Espirito Santo, P. Weiss, A. Cipris, R. Kaiser, W. Guerin, R. Bachelard, & J. Schachenmayer. *Collective excitation dynamics of a cold-atom cloud*. Phys. Rev. A **101**, 013617 (2020).
- [Dravins 2008] D. Dravins. *High Time Resolution Astrophysics* vol. 351 of *Astrophysics and Space Science Library* Chapter: Photonic Astronomy and Quantum Optics, 95–132. Springer Netherland (2008).

- [Du 2007] S. Du, J. Wen, M. H. Rubin, & G. Y. Yin. *Four-Wave Mixing and Biphotons Generation in a Two-Level System*. Phys. Rev. Lett. **98**, 053601 (2007).
- [Dubin 1999] D. H. E. Dubin & T. M. O’Neil. *Trapped nonneutral plasmas, liquids, and crystals (the thermal equilibrium states)*. Rev. Mod. Phys. **71**, 87 (1999).
- [Dussaux 2016] A. Dussaux, T. Passerat de Silans, W. Guerin, O. Alibart, S. Tanzilli, F. Vakiki, & R. Kaiser. *Temporal intensity correlation of light scattered by a hot atomic vapor*. Phys. Rev. A **043826** (2016).
- [Eberly 2006] J. H. Eberly. *Emission of one photon in an electric dipole transition of one among N atoms*. J. Phys. B: At. Mol. Opt. Phys. **39**, S599–S604 (2006).
- [Elitzur 1982] M. Elitzur. *Physical characteristics of astronomical masers*. Rev. Mod. Phys. **54**, 1225–1260 (1982).
- [Éloy 2018a] A. Éloy. *Étude des fluctuations temporelles de la lumière diffusée par des atomes froids*. PhD thesis, Université Côte d’Azur (2018).
- [Éloy 2018b] A. Éloy, Z. Yao, R. Bachelard, W. Guerin, M. Fouché, & R. Kaiser. *Diffusive wave spectroscopy of cold atoms in ballistic motion*. Phys. Rev. A **97**, 013810 (2018).
- [Ernst 1968] V. Ernst & P. Stehle. *Emission of radiation from a system of many excited atoms*. Phys. Rev. **176**, 1456–1479 (1968).
- [Ernst 1969] V. Ernst. *Coherent emission of a photon by many atoms*. Z. Physik **218**, 111–128 (1969).
- [Faccio 2019] D. Faccio & E. M. Wright. *Superradiant Amplification of Acoustic Beams via Medium Rotation*. Phys. Rev. Lett. **123**, 044301 (2019).
- [Fallert 2009] J. Fallert, R. J. B. Dietz, J. Sartor, D. Schneider, C. Klingshirn, & H. Kalt. *Co-existence of strongly and weakly localized random laser modes*. Nature Photon. **3**, 279–282 (2009).
- [Fauquembergue 2005] M. Fauquembergue, J.-F. Riou, W. Guerin, S. Rangwala, F. Moron, A. Villing, Y. Le Coq, P. Bouyer, A. Aspect, & M. Lécrivain. *Partially ferromagnetic electromagnet for trapping and cooling neutral atoms to quantum degeneracy*. Rev. Sci. Instrum. **76**, 103104 (2005).
- [Feld 1980] M. S. Feld & J. C. MacGillivray. *Coherent Nonlinear Optics. Recent Advances* vol. 21 of *Topics in Current Physics* Chapter: Superradiance, 7–57. Springer Berlin (1980).
- [Filipp 2011] S. Filipp, A. F. van Loo, M. Baur, L. Steffen, & A. Wallraff. *Preparation of subradiant states using local qubit control in circuit QED*. Phys. Rev. A **84**, 061805 (2011).
- [Fioretti 1998] A. Fioretti, A. F. Molisch, J. H. Mutter, P. Verkerk, & M. Allegrini. *Observation of radiation trapping in a dense Cs magneto-optical trap*. Opt. Commun. **149**, 415–422 (1998).

- [Frank 2009] R. Frank, A. Lubatsch, & J. Kroha. *Light transport and localization in diffusive random lasers*. J. Opt. A: Pure Appl. Opt. **11**, 114012 (2009).
- [Freedhoff 1967] H. Freedhoff & J. Van Kranendonk. *Theory of coherent resonant absorption and emission at infrared and optical frequencies*. Can. J. Phys. **45**, 1833–1859 (1967).
- [Friedberg 1971] R. Friedberg & S. R. Hartmann. *Superradiant damping and absorption*. Phys. Lett. **37A**, 285–286 (1971).
- [Friedberg 1972] R. Friedberg, S. R. Hartmann, & J. T. Manassah. *Limited superradiant damping of small samples*. Phys. Lett. **40A**, 365–366 (1972).
- [Friedberg 1973] R. Friedberg, S. R. Hartmann, & J. T. Manassah. *Frequency shifts in emission and absorption by resonant systems of two-level atoms*. Phys. Rep. **7**, 101–179 (1973).
- [Friedberg 1976] R. Friedberg & S. R. Hartmann. *Superradiant lifetime: Its definitions and relation to absorption length*. Phys. Rev. A **13**, 495–496 (1976).
- [Friedberg 2010] R. Friedberg & J. T. Manassah. *Analytic expressions for the initial cooperative decay rate and cooperative Lamb shift for a spherical sample of two-level atoms*. Phys. Lett. A **374**, 1648–1659 (2010).
- [Froufe-Pérez 2009] L. S. Froufe-Pérez, W. Guerin, R. Carminati, & R. Kaiser. *Threshold of a Random Laser with Cold Atoms*. Phys. Rev. Lett. **102**, 173903 (2009).
- [Fröwis 2017] F. Fröwis, P. C. Strassmann, A. Tiranov, C. Gut, J. Lavoie, N. Brunner, F. Bussi eres, M. Afzelius, & N. Gisin. *Experimental certification of millions of genuinely entangled atoms in a solid*. Nature Commun. **8**, 907 (2017).
- [Gatti 2017] A. Gatti, T. Corti, & E. Brambilla. *Squeezing and Einstein-Podolsky-Rosen correlation in the mirrorless optical parametric oscillator*. Phys. Rev. A **96**, 013820 (2017).
- [Gattobigio 2006] G. Gattobigio, F. Michaud, J. Javaloyes, J. W. R. Tabosa, & R. Kaiser. *Bunching-induced asymmetry in degenerate four-wave mixing with cold-atoms*. Phys. Rev. A **74**, 043407 (2006).
- [Gattobigio 2008] G. Gattobigio. *Manipulation of a Large Magneto-Optical Trap: Application to Four-Wave Mixing*. PhD thesis, Ferrara University (2008).
- [Gattobigio 2009] G. L. Gattobigio, A. Couvert, M. Jeppesen, R. Mathevet, & D. Gu ery-Odelin. *Multimode-to-monomode guided-atom lasers: An entropic analysis*. Phys. Rev. A **80**, 041605(R) (2009).
- [Gattobigio 2011] G. L. Gattobigio, A. Couvert, B. Georgeot, & D. Gu ery-Odelin. *Exploring classically chaotic potentials with a matter wave quantum probe*. Phys. Rev. Lett **80**, 041605(R) (2011).

- [Gauthier 1992] D. J. Gauthier, Q. Wu, S. E. Morin, & T. W. Mossberg. *Realization of a continuous-wave, two-photon optical laser*. Phys. Rev. Lett. **68**, 464–467 (1992).
- [Ge 2010] L. Ge, Y. D. Chong, & A. D. Stone. *Steady-state ab initio laser theory: Generalizations and analytic results*. Phys. Rev. A **82**, 063824 (2010).
- [Gerasimov 2014] L. V. Gerasimov, V. M. Ezhova, D. V. Kupriyanov, Q. Baudouin, W. Guerin, & R. Kaiser. *Raman process under condition of radiation trapping in a disordered atomic medium*. Phys. Rev. A **90**, 013814 (2014).
- [Gibbs 1977] H. M. Gibbs, Q. H. F. Vrehen, & H. M. J. Hikspoors. *Single-pulse superfluorescence in cesium*. Phys. Rev. Lett. **39**, 547–550 (1977).
- [Goetschy 2011] A. Goetschy & S. E. Skipetrov. *Euclidean matrix theory of random lasing in a cloud of cold atoms*. Europhys. Lett. **96**, 34005 (2011).
- [Gothe 2019] H. Gothe, D. Sholokhov, A. Breunig, M. Steinel, & J. Eschner. *Continuous-wave virtual-state lasing from cold ytterbium atoms*. Phys. Rev. A **99**, 013415 (2019).
- [Gottardo 2008] S. Gottardo, R. Sapienza, P. D. García, A. Blanco, D. S. Wiersma, & C. López. *Resonance-driven random lasing*. Nature Photon. **2**, 429–432 (2008).
- [Gouedard 1993] C. Gouedard, D. Husson, D. Sauteret, F. Auzel, & A. Migus. *Generation of spatially incoherent short pulses in laser-pumped neodymium stoichiometric crystals and powders*. J. Opt. Soc. Am. B **10**, 2358–2362 (1993).
- [Grangier 1985] P. Grangier, A. Aspect, & J. Vigué. *Quantum Interference Effect for Two Atoms Radiating a Single Photon*. Phys. Rev. Lett. **54**, 418–421 (1985).
- [Greenberg 2012] J. A. Greenberg & D. J. Gauthier. *Steady-state, cavityless, multimode superradiance in a cold vapor*. Phys. Rev. A **86**, 013823 (2012).
- [Grison 1991] D. Grison, B. Lounis, C. Salomon, J.-Y. Courtois, & G. Grynberg. *Raman Spectroscopy of Cesium Atoms in a Laser Trap*. Europhys. Lett. **15**, 149–154 (1991).
- [Gross 1976] M. Gross, C. Fabre, P. Pillet, & S. Haroche. *Observation of near-infrared Dicke superradiance on cascading transitions in atomic sodium*. Phys. Rev. Lett. **36**, 1035–1038 (1976).
- [Gross 1982] M. Gross & S. Haroche. *Superradiance: an essay on the theory of collective spontaneous emission*. Phys. Rep. **93**, 301–396 (1982).
- [Grynberg 1988a] G. Grynberg. *Mirrorless four-wave mixing oscillation in atomic vapors*. Opt. Commun. **66**, 321 (1988).
- [Grynberg 1988b] G. Grynberg, E. Le Bihan, P. Verkerk, P. Simoneau, J. R. R. Leite, D. Bloch, S. Le Boiteux, & M. Ducloy. *Observation of*

- instabilities due to mirrorless four-wave mixing oscillation in sodium.* Opt. Commun. **67**, 363 (1988).
- [Grynberg 1993] G. Grynberg & C. Cohen-Tannoudji. *Central resonance of the Mollow absorption spectrum: physical origin of gain without population inversion.* Opt. Commun. **96**, 150–163 (1993).
- [Grynberg 2001] G. Grynberg & C. Robilliard. *Cold atoms in dissipative optical lattices.* Phys. Rep. **355**, 335–451 (2001).
- [Guerin 2006] W. Guerin, J.-F. Riou, J. P. Gaebler, V. Josse, P. Bouyer, & A. Aspect. *Guided Quasicontinuous Atom Laser.* Phys. Rev. Lett. **97**, 200402 (2006).
- [Guerin 2007] W. Guerin. *Source atomique cohérente dans des pièges optique et magnétique: réalisation d'un laser à atomes guidé.* PhD thesis, Université Paris-Sud (2007).
- [Guerin 2008] W. Guerin, F. Michaud, & R. Kaiser. *Mechanisms for Lasing with Cold Atoms as the Gain Medium.* Phys. Rev. Lett. **101**, 093002 (2008).
- [Guerin 2009] W. Guerin, N. Mercadier, D. Brivio, & R. Kaiser. *Threshold of a random laser based on Raman gain in cold atoms.* Opt. Express **17**, 11236 (2009).
- [Guerin 2010] W. Guerin, N. Mercadier, F. Michaud, D. Brivio, L. S. Froufe-Pérez, R. Carminati, V. Ereameev, A. Goetschy, S. E. Skipetrov, & R. Kaiser. *Towards a random laser with cold atoms.* J. Opt. **12**, 024002 (2010).
- [Guerin 2016a] W. Guerin, M. O. Araújo, & R. Kaiser. *Subradiance in a large cloud of cold atoms.* Phys. Rev. Lett. **116**, 083601 (2016).
- [Guerin 2016b] W. Guerin, Y. D. Chong, Q. Baudouin, M. Liertzer, S. Rotter, & R. Kaiser. *Diffusive to quasi-ballistic random laser: incoherent and coherent models.* J. Opt. Soc. Am. B **33**, 1888–1896 (2016).
- [Guerin 2017a] W. Guerin, A. Dussaux, M. Fouché, G. Labeyrie, J. Rivet, D. Vernet, F. Vakili, & R. Kaiser. *Temporal intensity interferometry: photon bunching on three bright stars.* MNRAS **472**, 4126 (2017).
- [Guerin 2017b] W. Guerin & R. Kaiser. *Population of collective modes in light scattering by many atoms.* Phys. Rev. A **95**, 053865 (2017).
- [Guerin 2017c] W. Guerin, M. T. Rouabah, & R. Kaiser. *Light interacting with atomic ensembles: collective, cooperative and mesoscopic effects.* J. Mod. Opt. **64**, 895–907 (2017).
- [Guerin 2018] W. Guerin, J.-P. Rivet, M. Fouché, G. Labeyrie, D. Vernet, F. Vakili, & R. Kaiser. *Spatial intensity interferometry on three bright stars.* MNRAS **480**, No. 4 245–250 (2018).
- [Guerin 2019] W. Guerin, T. S. do Espirito Santo, P. Weiss, A. Cipris, J. Schachenmayer, R. Kaiser, & R. Bachelard. *Collective Multi-mode Vacuum Rabi Splitting.* Phys. Rev. Lett. **123**, 243401 (2019).

- [Hammerer 2010] K. Hammerer, A. S. Sørensen, & E. S. Polzik. *Quantum interface between light and atomic ensembles*. Rev. Mod. Phys. **82**, 1041–1093 (2010).
- [Hanbury Brown 1956] R. Hanbury Brown & R. Q. Twiss. *A test of a new type of stellar interferometer on Sirius*. Nature **178**, 1046 (1956).
- [Hanbury Brown 1974] R. Hanbury Brown. *The intensity interferometer: its application to astronomy*. Taylor & Francis London (1974).
- [He 2020] Y. He, L. Ji, Y. Wang, L. Qiu, J. Zhao, Y. Ma, X. Huang, D. E. Chang, & S. Wu. *Geometric control of collective spontaneous emission*. arXiv:1910.02289v2 (2020).
- [Hebenstreit 2017] M. Hebenstreit, B. Kraus, L. Ostermann, & H. Ritsch. *Subradiance via entanglement in atoms with several independent decay channels*. Phys. Rev. Lett. **118**, 143602 (2017).
- [Hettich 2002] C. Hettich, C. Schmitt, J. Zitzmann, S. Kühn, I. Gerhardt, & V. Sandoghdar. *Nanometer resolution and coherent optical dipole coupling of two individual molecules*. Science **298**, 385–389 (2002).
- [Hilico 1992] L. Hilico, C. Fabre, & E. Giacobino. *Operation of a “Cold-Atom Laser” in a Magneto-Optical Trap*. Europhys. Lett. **18**, 685–688 (1992).
- [Hilliard 2008] A. Hilliard, F. Kaminski, R. le Targat, C. Olausson, E. S. Polzik, & J. H. Müller. *Rayleigh superradiance and dynamic Bragg gratings in an end-pumped Bose-Einstein condensate*. Phys. Rev. A **78**, 051403 (2008).
- [Hirota 2011] T. Hirota, M. Tsuboi, K. Fujisawa, M. Honma, N. Kawaguchi, M. K. Kim, H. Kobayashi, H. Imai, T. Omodaka, K. M. Shibata, T. Shimoikura, & Y. Yonekura. *Identification of bursting water maser features in Orion KL*. ApJ **739**, L59 (2011).
- [Holstein 1947] T. Holstein. *Imprisonment of Resonance Radiation in Gases*. Phys. Rev. **72**, 1212–1233 (1947).
- [Holzinger 2020] R. Holzinger, D. Plankensteiner, L. Ostermann, & H. Ritsch. *A nanoscale coherent light source*. arXiv:2002.07352 (2020).
- [Huang 2005] Y.-C. Huang. *Theory of backward distributed-feedback optical parametric amplifiers and oscillators*. J. Opt. Soc. Am. B **22**, 1244 (2005).
- [Inouye 1999] S. Inouye, A. P. Chikkatur, D. M. Stamper-Kurn, J. Stenger, D. E. Pritchard, & W. Ketterle. *Superradiant Rayleigh scattering from a Bose-Einstein condensate*. Science **285**, 571 (1999).
- [Inouye 2000] S. Inouye, R. F. Löw, S. Gupta, A. Görlitz, T. L. Gustavson, D. E. Pritchard, & W. Ketterle. *Amplification of light and atoms in a Bose-Einstein condensate*. Phys. Rev. Lett. **85**, 4225–4228 (2000).

- [Javanainen 1999] J. Javanainen, J. Ruostekoski, B. Vestergaard, & M. R. Francis. *One-dimensional modeling of light propagation in dense and degenerate samples*. Phys. Rev. A **59**, 649 – 666 (1999).
- [Jeong 2006] H. Jeong, A. M. C. Dawes, & D. J. Gauthier. *Direct observation of optical precursors in a region of anomalous dispersion*. Phys. Rev. Lett. **96**, 143901 (2006).
- [Jeppesen 2008] M. Jeppesen, J. Dugué, G. Dennis, M. T. Johnsson, C. Figl, N. P. Robins, & J. D. Close. *Multibeam atom laser: Coherent atom beam splitting from a single far-detuned laser*. Phys. Rev. A **77**, (2008).
- [Johansson 2004] S. Johansson & V. S. Letokhov. *Astrophysical lasers operating in optical Fe II lines in stellar ejecta of η Carinae*. A&A **428**, 497–509 (2004).
- [Johansson 2005] S. Johansson & V. S. Letokhov. *Astrophysical laser operating in the O I 8446-Å line in the Weigelt blobs of η Carinae*. Mon. Not. Roy. Astron. Soc. **364**, 731–737 (2005).
- [Johansson 2007] S. Johansson & V. S. Letokhov. *Astrophysical lasers and nonlinear optical effects in space*. New. Astron. Rev. **51**, 443–523 (2007).
- [Johnson 1976] M. A. Johnson, M. A. Betz, R. A. McLaren, E. C. Sutton, & C. H. Townes. *Nonthermal 10 micron CO₂ emission lines in the atmospheres of Mars and Venus*. ApJ **208**, L145–L148 (1976).
- [Jonckheere 2000] T. Jonckheere, C. A. Müller, R. Kaiser, C. Miniatura, & D. Delande. *Multiple scattering of light by atoms in the weak localization regime*. Phys. Rev. Lett. **85**, 4269 (2000).
- [Kaiser 2000] R. Kaiser. *Cold atoms and multiple scattering*. In R. Kaiser & J. Montaldi, editors, *Peyresq Lectures on Nonlinear Phenomena*. World Scientific Singapur (2000).
- [Kemp 2020] K. J. Kemp, S. J. Roof, M. D. Havey, I. M. Sokolov, D. V. Kupriyanov, & W. Guerin. *Optical-depth scaling of light scattering from a dense and cold atomic ⁸⁷Rb gas*. Phys. Rev. A **101**, 033832 (2020).
- [Kenty 1932] C. Kenty. *On Radiation Diffusion and the Rapidity of Escape of Resonance Radiation from a Gas*. Phys. Rev. **42**, 823–842 (1932).
- [Keßler 2014] H. Keßler, J. Klinder, M. Wolke, & A. Hemmerich. *Steering Matter Wave Superradiance with an Ultranarrow-Band Optical Cavity*. Phys. Rev. Lett. **113**, 070404 (2014).
- [Kitching 1999] J. Kitching & L. Hollberg. *Interference-induced optical gain without population inversion in cold, trapped atoms*. Phys. Rev. A **59**, 4685–4689 (1999).
- [Kleine Büning 2010] G. Kleine Büning, J. Will, W. Ertmer, C. Klempt, & J. Arlt. *A slow gravity compensated atom laser*. Appl. Phys. B **100**, No. 1 117–123 (2010).

- [Kleinmann 1985] B. Kleinmann, F. Trehin, M. Pinard, & G. Grynberg. *Degenerate four-wave mixing in sodium vapor in the Rabi regime*. J. Opt. Soc. Am. B **2**, 704–713 (1985).
- [Kogelnik 1971] H. Kogelnik & C. V. Shank. *Stimulated emission in a periodic structure*. Appl. Phys. Lett. **18**, 152 (1971).
- [Kogelnik 1972] H. Kogelnik & C. V. Shank. *Coupled-Wave Theory of Distributed Feedback Lasers*. J. Appl. Phys. **43**, 2327 (1972).
- [Kruse 2003] D. Kruse, C. von Cube, C. Zimmermann, & P. W. Courteille. *Observation of Lasing Mediated by Collective Atomic Recoil*. Phys. Rev. Lett. **91**, 183601 (2003).
- [Kumar 1985] P. Kumar & J. H. Shapiro. *Observation of Raman-shifted oscillation near the sodium D lines*. Opt. Lett. **10**, 226–228 (1985).
- [Kuraptsev 2017] A. S. Kuraptsev, I. Sokolov, & M. D. Havey. *Angular distribution of single photon superradiance in a dilute and cold atomic ensemble*. Phys. Rev. A **96**, 023830 (2017).
- [Kuraptsev 2020] A. S. Kuraptsev & I. M. Sokolov. *Influence of atomic motion on the collective effects in dense and cold atomic ensembles*. Phys. Rev. A **101**, 033602 (2020).
- [Kwong 2014] C. C. Kwong, T. Yang, M. S. Pramod, K. Pandey, D. Delande, R. Pierrat, & D. Wilkowski. *Cooperative Emission of a Coherent Superflash of Light*. Phys. Rev. Lett. **113**, 223601 (2014).
- [Kwong 2015] C. C. Kwong, T. Yang, , D. Delande, R. Pierrat, & D. Wilkowski. *Cooperative emission of a pulse train in an optically thick scattering medium*. Phys. Rev. Lett. **115**, 223601 (2015).
- [Labeyrie 1999] G. Labeyrie, F. de Tomasi, J.-C. Bernard, C. A. Müller, C. Miniatura, & R. Kaiser. *Coherent Backscattering of Light by Cold Atoms*. Phys. Rev. Lett. **83**, 5266–5269 (1999).
- [Labeyrie 2003] G. Labeyrie, E. Vaujour, C. A. Müller, D. Delande, C. Miniatura, D. Wilkowski, & R. Kaiser. *Slow Diffusion of Light in a Cold Atomic Cloud*. Phys. Rev. Lett. **91**, 223904 (2003).
- [Labeyrie 2004] G. Labeyrie, D. Delande, C. A. Müller, C. Miniatura, & R. Kaiser. *Multiple scattering of light in a resonant medium*. Opt. Commun. **243**, 157–164 (2004).
- [Labeyrie 2005] G. Labeyrie, R. Kaiser, & D. Delande. *Radiation trapping in a cold atomic gas*. Appl. Phys. B **81**, 1001–1008 (2005).
- [Labeyrie 2008] G. Labeyrie. *Coherent transport of light in cold atoms*. Mod. Phys. Lett. B **22**, 73–99 (2008).
- [Lagendijk 1996] A. Lagendijk & B. A. van Tiggelen. *Resonant multiple scattering of light*. Phys. Rep. **270**, 143–215 (1996).
- [Lagendijk 2009] A. Lagendijk, B. van Tiggelen, & D. S. Wiersma. *Fifty years of Anderson localization*. Phys. Today **62**, No. 8 24–29 (2009).

- [Lai 2018] O. Lai, W. Guerin, F. Vakili, R. Kaiser, J.-P. Rivet, M. Fouché, G. Labeyrie, J. Chabé, C. Courde, E. Samain, & D. Vernet. *Intensity Interferometry revival on the Côte d'Azur*. In Proc. SPIE vol. 10701 of *Optical and Infrared Interferometry and Imaging VI* 1070121 (2018).
- [Lavrinovich 1975] N. N. Lavrinovich & V. S. Letokhov. *The possibility of the laser effect in stellar atmospheres*. Sov. Phys. JETP **40**, 800–805 (1975).
- [Lawandy 1994] N. M. Lawandy, R. M. Balachandran, A. S. L. Gomes, & E. Sauvain. *Laser action in strongly scattering media*. Nature **368**, 436–438 (1994).
- [Lax 1951] M. Lax. *Multiple scattering of waves*. Rev. Mod. Phys. **23**, 287–310 (1951).
- [Le Coq 2001] Y. Le Coq, J. H. Thywissen, S. A. Rangawala, F. Gerbier, S. Richard, G. Delannoy, P. Bouyer, & A. Aspect. *Atom laser divergence*. Phys. Rev. Lett. **87**, No. 17 170403 (2001).
- [LeBohec 2006] S. LeBohec & J. Holder. *Optical intensity interferometry with atomospheric Cherenkov telescope arrays*. ApJ **649**, 399–405 (2006).
- [Lee 2016] M. D. Lee, S. D. Jenkins, & J. Ruostekoski. *Stochastic methods for light propagation and recurrent scattering in saturated and nonsaturated atomic ensembles*. Phys. Rev. A **93**, 063803 (2016).
- [Lehmberg 1970a] R. H. Lehmberg. *Radiation from an N -atom system. I. General formalism*. Phys. Rev. A **2**, 883–888 (1970).
- [Lehmberg 1970b] R. H. Lehmberg. *Radiation from an N -atom system. II. Spontaneous emission from a pair of atoms*. Phys. Rev. A **2**, 889–896 (1970).
- [Leite 1986] M. R. R. Leite, P. Simoneau, D. Bloch, S. Le Boiteux, & M. Ducloy. *Continuous-Wave Phase-Conjugate Self-Oscillation Induced by Na-Vapour Degenerate Four-Wave Mixing with Gain*. Europhys. Lett. **2**, 747–753 (1986).
- [Letokhov 1968] V. S. Letokhov. *Generation of light by a scattering medium with negative resonance absorption*. Sov. Phys. JETP **26**, 835–840 (1968).
- [Letokhov 1972] V. S. Letokhov. *Laser action in stellar atmospheres*. IEEE J. Quantum. Electron. **8**, 615 (1972).
- [Letokhov 2009] V. S. Letokhov & S. Johansson. *Astrophysical Lasers*. Oxford University Press (2009).
- [Lezama 2000] A. Lezama, G. C. Cardoso, & J. W. R. Tabosa. *Polarization dependence of four-wave mixing in a degenerate two-level system*. Phys. Rev. A **63**, 013805 (2000).
- [Lind 1981] R. C. Lind & D. G. Steel. *Demonstration of the longitudinal modes and aberration correction properties of a continuous-wave*

- dye laser with a phase-conjugate mirror*. Opt. Lett. **6**, 554–556 (1981).
- [Litvak 1966] M. M. Litvak, A. L. McWhorter, M. L. Meeks, & H. J. Zeiger. *Maser Model for Interstellar OH Microwave Emission*. Phys. Rev. Lett. **17**, 821–826 (1966).
- [Lopez 2019] J. P. Lopez, A. M. G. de Melo, D. Felinto, & J. W. R. Tabosa. *Observation of giant gain and coupled parametric oscillations between four optical channels in cascaded four-wave mixing*. Phys. Rev. A **100**, 023839 (2019).
- [MacGillivray 1976] J. C. MacGillivray & M. S. Feld. *Theory of superradiance in an extended, optically thick medium*. Phys. Rev. A **14**, 1169–1189 (1976).
- [Machluf 2019] S. Machluf, J. B. Naber, M. L. Soudijn, J. Ruostekoski, & R. J. C. Spreeuw. *Collective suppression of optical hyperfine pumping in dense clouds of atoms in microtraps*. Phys. Rev. A **100**, 051801(R) (2019).
- [Mahler 2010] L. Mahler, A. Tredicucci, F. Beltram, C. Walther, J. Faist, H. E. Beere, D. A. Ritchie, & D. S. Wiersma. *Quasi-periodic distributed feedback laser*. Nature Photon. **4**, 165–169 (2010).
- [Malcuit 1987] M. S. Malcuit, J. J. Maki, D. J. Simkin, & R. W. Boyd. *Transition from superfluorescence to amplified spontaneous emission*. Phys. Rev. Lett. **59**, No. 11 1189–1192 (1987).
- [Markushev 1986] V. M. Markushev, V. F. Zolin, & C. M. Briskina. *Luminescence and stimulated emission of neodymium in sodium lanthanum molybdate powders*. Sov. J. Quantum Electron. **16**, 281–282 (1986).
- [Máximo 2015] C. E. Máximo, N. Piovella, P. W. Courteille, R. Kaiser, & R. Bachelard. *Spatial and temporal localization of light in two dimensions*. Phys. Rev. A **92**, 062702 (2015).
- [Mazets 2007] I. E. Mazets & G. Kurizki. *Multiatom cooperative emission following single-photon absorption: Dicke-state dynamics*. J. Phys. B: At. Mol. Opt. Phys. **40**, F105–F112 (2007).
- [McGuyer 2015] B. H. McGuyer, M. McDonald, G. Z. Iwata, M. G. Tarallo, W. Skomorowski, R. Moszynski, & T. Zelevinsky. *Precise study of asymptotic physics with subradiant ultracold molecules*. Nature Phys. **11**, 32–36 (2015).
- [McKeever 2003] J. McKeever, A. Boca, A. D. Boozer, J. R. Buck, & H. J. Kimble. *Experimental realization of a one-atom laser in the regime of strong coupling*. Nature **425**, 268–271 (2003).
- [Megyeri 2018] B. Megyeri, G. Harvie, A. Lampis, & J. Goldwin. *Directional Bistability and Nonreciprocal Lasing with Cold Atoms in a Ring Cavity*. Phys. Rev. Lett. **121**, 163603 (2018).

- [Mei 2017] Y. Mei, X. Guo, L. Zhao, & S. Du. *Mirrorless Optical Parametric Oscillation with Tunable Threshold in Cold Atoms*. *Phys. Rev. Lett.* **119**, 150406 (2017).
- [Mercadier 2009] N. Mercadier, W. Guerin, M. Chevrollier, & R. Kaiser. *Lévy flights of photons in hot atomic vapors*. *Nature Phys.* **5**, 602 (2009).
- [Mercadier 2011] N. Mercadier. *Diffusion résonante de la lumière: laser aléatoire à atomes et vols de Lévy des photons*. PhD thesis, Université Nice Sophia Antipolis (2011).
- [Mercadier 2013] N. Mercadier, M. Chevrollier, W. Guerin, & R. Kaiser. *Microscopic characterization of Lévy flights of light in atomic vapors*. *Phys. Rev. A* **87**, 063837 (2013).
- [Merrill 1956] P. W. Merrill. *Lines of the Chemical Elements in Astronomical Spectra*. Carnegie Institution of Washington (1956).
- [Messenger 2010] S. J. Messenger & V. Strel'nitski. *On the 1.7 μm Fe II and other natural lasers*. *Mon. Not. Roy. Astron. Soc.* **404**, 1545–1550 (2010).
- [Michaud 2007] F. Michaud, G.-L. Gattobigio, J. W. R. Tabosa, & R. Kaiser. *Interference between Raman gain and four-wave mixing in cold atoms*. *J. Opt. Soc. Am. B* **24**, A40–A47 (2007).
- [Michaud 2008] F. Michaud. *Diffusion multiple de la lumière en présence de gain dans un nuage d'atomes froids: vers un laser aléatoire*. PhD thesis, Université de Nice Sophia-Antipolis (2008).
- [Miller 2005] R. Miller, T. E. Northup, K. M. Birnbaum, A. Boca, A. D. Boozer, & H. J. Kimble. *Trapped atoms in cavity QED: coupling quantized light and matter*. *J. Phys. B: At. Mol. Opt. Phys.* **38**, S551–S565 (2005).
- [Milonni 1974] P. W. Milonni & P. L. Knight. *Retardation in the resonant interaction of two identical atoms*. *Phys. Rev. A* **10**, 1096–1108 (1974).
- [Molisch 1998] A. Molisch & B. Oehry. *Radiation Trapping in Atomic Vapours*. Oxford University Press Oxford (1998).
- [Mollow 1969] B. R. Mollow. *Power Spectrum of Light Scattered by Two-Level Systems*. *Phys. Rev.* **188**, 1969–1975 (1969).
- [Mollow 1972] B. R. Mollow. *Stimulated Emission and Absorption near Resonance for Driven Systems*. *Phys. Rev. A* **5**, 2217–2222 (1972).
- [Mompart 2000] J. Mompart & R. Corbalán. *Lasing without inversion*. *J. Opt. B: Quantum Semiclass. Opt.* **2**, R7–R24 (2000).
- [Mumma 1981] M. J. Mumma, D. Buhl, G. Chin, D. Deming, F. Espenak, T. Kostiuk, & D. Zipoy. *Discovery of natural gain amplification in the 10-micrometer carbon dioxide laser bands on Mars: a natural laser*. *Science* **212**, 45–49 (1981).

- [Munro 2018] E. Munro, A. Asenjo-Garcia, Y. Lin, L. C. Kwek, C. A. Regal, & D. E. Chang. *Population mixing due to dipole-dipole interactions in a one-dimensional array of multilevel atoms*. Phys. Rev. A **98**, (2018).
- [Needham 2019] J. A. Needham, I. Lesanovsky, & B. Olmos. *Subradiance-protected excitation transport*. New J. Phys. **21**, 073061 (2019).
- [Nilsen 1979] J. Nilsen & A. Yariv. *Nearly degenerate four-wave mixing applied to optical filters*. Appl. Opt. **18**, 143–145 (1979).
- [Noda 2010] S. Noda. *Photonic crystal lasers – ultimate nanolasers and broad-area coherent lasers*. J. Opt. Soc. Am. B **27**, B1 (2010).
- [Noh 2011] H. Noh, J.-K. Yang, S. F. Liew, M. J. Rooks, G. S. Solomon, & H. Cao. *Control of Lasing in Biomimetic Structures with Short-Range Order*. Phys. Rev. Lett. **106**, 183901 (2011).
- [Norcia 2016] M. A. Norcia & J. K. Thompson. *Cold-Strontium Laser in the Superradiant Crossover Regime*. Phys. Rev. X **6**, 011025 (2016).
- [Ortiz-Gutiérrez 2019] L. Ortiz-Gutiérrez, R. Celistrino Teixeira, A. Eloy, D. Ferreira da Silva, R. Kaiser, R. Bachelard, & M. Fouché. *Mollow triplet in cold atoms*. New J. Phys. **21**, 093019 (2019).
- [Ott 2013] J. R. Ott, M. Wubs, P. Lodahl, N. A. Mortensen, & R. Kaiser. *Cooperative Fluorescence from a Strongly Driven Dilute Cloud of Atoms*. Phys. Rev. A **87**, 061801(R) (2013).
- [Padmabandu 1996] G. G. Padmabandu, G. R. Welch, I. N. Shubin, E. S. Fry, D. E. Nikonov, M. D. Lukin, & M. O. Scully. *Laser Oscillation without Population Inversion in a Sodium Atomic Beam*. Phys. Rev. Lett. **76**, 2053–2056 (1996).
- [Pavolini 1985] D. Pavolini, A. Crubellier, P. Pillet, L. Cabaret, & S. Liberman. *Experimental Evidence for Subradiance*. Phys. Rev. Lett. **54**, 1917–1920 (1985).
- [Pereira 2004] E. Pereira, J. M. G. Martinho, & M. N. Berberan-Santos. *Photon Trajectories in Incoherent Atomic Radiation Trapping as Lévy Flights*. Phys. Rev. Lett. **93**, 120201 (2004).
- [Petrosyan 2007] D. Petrosyan. *Tunable photonic band gaps with coherently driven atoms in optical lattices*. Phys. Rev. A **76**, 053823 (2007).
- [Peyrot 2018] T. Peyrot, Y. R. P. Sortais, A. Browaeys, A. Sargsyan, D. Sarkisyan, J. Keaveney, I. G. Hughes, & C. S. Adams. *Collective Lamb shift of a nanoscale atomic vapour layer within a sapphire cavity*. Phys. Rev. Lett. **120**, 243401 (2018).
- [Pierrat 2007] R. Pierrat & R. Carminati. *Threshold of random laser in the incoherent transport regime*. Phys. Rev. A **76**, 023821 (2007).
- [Pierrat 2009] R. Pierrat, B. Grémaud, & D. Delande. *Enhancement of radiation trapping for quasidegenerate scatterers at low temperature*. Phys. Rev. A **80**, 013831 (2009).

- [Pinard 1986] M. Pinard, D. Grandclement, & G. Grynberg. *Continuous-Wave Self-Oscillation Using Pair Production of Photons in Four-Wave Mixing in Sodium*. *Europhys. Lett.* **2**, 755–760 (1986).
- [Pinheiro 2004] F. A. Pinheiro, M. Rusek, A. Orłowski, & B. A. van Tiggelen. *Probing Anderson localization of light via decay rate statistics*. *Phys. Rev. E* **69**, 026605 (2004).
- [Polson 2004] R. C. Polson & Z. Vally Vardeny. *Random lasing in human tissues*. *Appl. Phys. Lett.* **85**, 1289 (2004).
- [Prasad 2010] S. Prasad & R. J. Glauber. *Coherent radiation by a spherical medium of resonant atoms*. *Phys. Rev. A* **82**, 063805 (2010).
- [Pucci 2017] L. Pucci, A. Roy, T. Santiago do Espirito Santo, R. Kaiser, M. Kastner, & R. Bachelard. *Quantum effects in the cooperative scattering of light by cold atomic clouds*. *Phys. Rev. A* **95**, 053625 (2017).
- [Rakher 2012] M. T. Rakher & K. Srinivasan. *All-atom parametric oscillator*. *Nature. Photon.* **6**, (2012).
- [Redding 2012] B. Redding, M. A. Choma, & H. Cao. *Speckle-free laser imaging using random laser illumination*. *Nature Photon.* **6**, 355–359 (2012).
- [Rehler 1971] N. E. Rehler & J. H. Eberly. *Superradiance*. *Phys. Rev. A* **3**, 1735–1751 (1971).
- [Reid 1981] M. J. Reid & J. M. Moran. *Masers*. *Ann. Rev. Astron. Astrophys.* **19**, 231–276 (1981).
- [Ressayre 1976] E. Ressayre & A. Tallet. *Basic properties for cooperative emission of radiation*. *Phys. Rev. Lett.* **37**, 424–427 (1976).
- [Ressayre 1977] E. Ressayre & A. Tallet. *Quantum theory for superradiance*. *Phys. Rev. A* **15**, 2410–2423 (1977).
- [Riou 2006] J.-F. Riou, W. Guerin, Y. Le Coq, M. Fauquembergue, V. Josse, P. Bouyer, & A. Aspect. *Beam Quality of a Nonideal Atom Laser*. *Phys. Rev. Lett.* **96**, 070404 (2006).
- [Riou 2008] J.-F. Riou, Y. Le Coq, F. Impens, W. Guerin, C. J. Bordé, & A. A. et P. Bouyer. *Theoretical tools for atom-laser-beam propagation*. *Phys. Rev. A* **77**, 033630 (2008).
- [Rivet 2018] J.-P. Rivet, F. Vakili, O. Lai, D. Vernet, M. Fouché, W. Guerin, G. Labeyrie, & R. Kaiser. *Optical long baseline intensity interferometry: prospects for stellar physics*. *Exp. Astron.* **46**, 531–542 (2018).
- [Rivet 2020] J.-P. Rivet, A. Siciak, E. S. G. de Almeida, F. Vakili, A. Domiciano de Souza, M. Fouché, O. Lai, D. Vernet, R. Kaiser, & W. Guerin. *Intensity interferometry of P Cygni in the H α emission line: towards distance calibration of LBV supergiant stars*. *MNRAS* **494**, 218–227 (2020).

- [Roof 2016] S. J. Roof, K. J. Kemp, M. D. Havey, & I. M. Sokolov. *Observation of single-photon superradiance and the cooperative Lamb shift in an extended sample of cold atoms*. Phys. Rev. Lett. **117**, 073003 (2016).
- [Rouabah 2015] M. T. Rouabah. *Effets de cohérence en diffusion multiple de la lumière et intrication des états cohérents*. PhD thesis, Université Nice Sophia-Antipolis (2015).
- [Rui 2020] J. Rui, D. Wei, A. Rubio-Abadal, S. Hollerith, J. Zeiher, D. M. Stamper-Kurn, C. Gross, & I. Bloch. *A subradiant optical mirror formed by a single structured atomic layer*. arXiv:2001.00795 (2020).
- [Ruostekoski 1997] J. Ruostekoski & J. Javanainen. *Quantum field theory of cooperative atom response: low light intensity*. Phys. Rev. A **55**, 513 – 526 (1997).
- [Rusek 1996] M. Rusek, A. Orłowski, & J. Mostowski. *Localization of light in three-dimensional random dielectric media*. Phys. Rev. E **53**, 4122–4130 (1996).
- [Rusek 2000] M. Rusek, J. Mostowski, & A. Orłowski. *Random Green matrices: From proximity resonances to Anderson localization*. Phys. Rev. A **61**, 022704 (2000).
- [Sangouard 2011] N. Sangouard, C. Simon, H. de Riedmatten, & N. Gisin. *Quantum repeaters based on atomic ensembles and linear optics*. Rev. Mod. Phys. **83**, 33–80 (2011).
- [Saunders 1973a] R. Saunders & R. K. Bullough. *Perturbation theory of superradiance I. Super-radiant emission*. J. Phys. A: Math., Nucl. Gen. **6**, 1348–1359 (1973).
- [Saunders 1973b] R. Saunders & R. K. Bullough. *Perturbation theory of superradiance II. Cooperative and non-cooperative level shifts*. J. Phys. A: Math., Nucl. Gen. **6**, 1360–1374 (1973).
- [Sawant 2017] R. Sawant & S. A. Rangwala. *Lasing by driven atoms-cavity system in collective strong coupling regime*. Scientific Rep. **7**, 11432 (2017).
- [Schilder 2016] N. J. Schilder, C. Sauvan, J.-P. Hugonin, S. Jennewein, Y. R. P. Sortais, A. Browaeys, & J.-J. Greffet. *Role of polaritonic modes on light scattering from a dense cloud of atoms*. Phys. Rev. A **93**, 063835 (2016).
- [Schilke 2011] A. Schilke, C. Zimmermann, P. W. Courteille, & W. Guerin. *Photonic Band gaps in One-Dimensionally Ordered Cold Atomic Vapors*. Phys. Rev. Lett. **106**, 223903 (2011).
- [Schilke 2012a] A. Schilke, C. Zimmermann, P. W. Courteille, & W. Guerin. *Optical parametric oscillation with distributed feedback in cold atoms*. Nature Photon. **6**, 101 (2012).

- [Schilke 2012b] A. Schilke, C. Zimmermann, & W. Guerin. *Photonic properties of one-dimensionally ordered cold atomic vapors under conditions of electromagnetically-induced transparency*. Phys. Rev. A **86**, 023809 (2012).
- [Schilke 2013] A. Schilke. *Photonische Eigenschaften eines eindimensionalen geordneten atomaren Mediums*. PhD thesis, Universität Tübingen (2013).
- [Schneble 2003] D. Schneble, Y. Torii, M. Boyd, E. W. Streed, D. E. Pritchard, & W. Ketterle. *The onset of matter-wave amplification in a superradiant Bose-Einstein Condensate*. Science **300**, 475–478 (2003).
- [Schneble 2004] D. Schneble, G. K. Campbell, E. W. Streed, M. Boyd, D. E. Pritchard, & W. Ketterle. *Raman amplification of matter waves*. Phys. Rev. A **69**, 041601(R) (2004).
- [Schuurmans 1979] M. F. H. Schuurmans & D. Polder. *Superfluorescence and amplified spontaneous emission: a unified theory*. Phys. Lett. **72A**, 306–308 (1979).
- [Scully 1994] M. O. Scully & M. Fleischhauer. *Lasers Without Inversion*. Science **263**, 337–338 (1994).
- [Scully 2006] M. O. Scully, E. S. Fry., C. H. Raymond Ooi, & K. Wódkiewicz. *Directed Spontaneous Emission from an Extended Ensemble of N Atoms: Timing Is Everything*. Phys. Rev. Lett. **96**, 010501 (2006).
- [Scully 2007] M. O. Scully. *Correlated spontaneous emission on the Volga*. Laser Phys. **17**, 635–646 (2007).
- [Scully 2009a] M. O. Scully. *Collective Lamb shift in Single Photon Dicke Superradiance*. Phys. Rev. Lett. **102**, 143601 (2009).
- [Scully 2009b] M. O. Scully & A. A. Svidzinsky. *The super of superradiance*. Science **325**, 1510–1511 (2009).
- [Scully 2010] M. O. Scully & A. A. Svidzinsky. *The Lamb shift – Yesterday, Today, and Tomorrow*. Science **328**, 1239–1241 (2010).
- [Seufert 2008] J. Seufert, M. Fischer, M. Legge, K. Roessner, R. Werner, J. Hildenbrand, J. Herbst, A. Lambrecht, & J. Koeth. *DFB laser diodes and quantum cascade lasers for sensors in safeguard applications*. In Proc. SPIE vol. 7114 71140K (2008).
- [Shahmoon 2017] E. Shahmoon, D. S. Wild, M. D. Lukin, & S. Yelin. *Cooperative Resonances in Light Scattering from Two-Dimensional Atomic Arrays*. Phys. Rev. Lett. **118**, 113601 (2017).
- [Shimoikura 2005] T. Shimoikura, H. Kobayashi, T. Omodaka, P. J. Diamond, L. I. Matveyenko, & K. Fujisawa. *VLBA observations of a bursting water maser in Orion KL*. ApJ. **634**, 459–467 (2005).

- [Skipetrov 2014] S. E. Skipetrov & I. M. Sokolov. *Absence of Anderson localization of light in a random ensemble of point scatterers*. Phys. Rev. Lett. **112**, 023905 (2014).
- [Skipetrov 2015] S. E. Skipetrov & I. M. Sokolov. *Magnetic-Field-Driven Localization of Light in a Cold-Atom Gas*. Phys. Rev. Lett. **114**, 053902 (2015).
- [Skipetrov 2016] S. E. Skipetrov. *Finite-size scaling analysis of localization transition for scalar waves in a three-dimensional ensemble of resonant point scatterers*. Phys. Rev. B **94**, 064202 (2016).
- [Skribanowitz 1973] N. Skribanowitz, I. P. Herman, J. C. MacGillivray, & M. S. Feld. *Observation of Dicke Superradiance in Optically Pumped HF Gas*. Phys. Rev. Lett. **30**, 309–312 (1973).
- [Slama 2005a] S. Slama, C. von Cube, A. Ludewig, M. Kohler, C. Zimmermann, & P. Courteille. *Dimensional crossover in Bragg scattering from an optical lattice*. Phys. Rev. A **72**, 031402(R) (2005).
- [Slama 2005b] S. Slama, C. von Cube, B. Deh, A. Ludewig, C. Zimmermann, & P. Courteille. *Phase-Sensitive Detection of Bragg Scattering at 1D Optical Lattices*. Phys. Rev. Lett. **94**, 193901 (2005).
- [Slama 2006] S. Slama, C. von Cube, M. Kohler, C. Zimmermann, & P. Courteille. *Multiple reflections and diffuse scattering in Bragg scattering at optical lattice*. Phys. Rev. A **73**, 023424 (2006).
- [Slama 2007] S. Slama, S. Bux, G. Krenz, C. Zimmermann, & P. W. Courteille. *Superradiant Rayleigh scattering and collective atomic recoil lasing in a ring cavity*. Phys. Rev. Lett. **98**, 053603 (2007).
- [Sokolov 2019] I. M. Sokolov & W. Guerin. *Comparison of three approaches to light scattering by dilute cold atomic ensembles*. J. Opt. Soc. Am. B **36**, 2030–2037 (2019).
- [Stephen 1964] M. J. Stephen. *First order dispersion forces*. J. Chem. Phys. **40**, 669 (1964).
- [Strangi 2006] G. Strangi, S. Ferjani, V. Barna, A. D. Luca, C. Versace, N. Scaramuzza, & R. Bartolino. *Random lasing and weak localization of light in dye-doped nematic liquid crystals*. Opt. Express **14**, 7737–7744 (2006).
- [Strelmitski 1996] V. S. Strelmitski, M. R. Haas, H. A. Smith, E. F. Erickson, S. W. J. Colgan, & D. J. Hallenbach. *Far-infrared hydrogen lasers in the peculiar star MWC 349A*. Science **272**, 1459–1461 (1996).
- [Stroud 1972] C. R. J. Stroud, J. H. Eberly, W. L. Lama, & L. Mandel. *Superradiant effects in systems of two-level atoms*. Phys. Rev. A **5**, 1094–1104 (1972).
- [Sutherland 2017] R. T. Sutherland & F. Robicheaux. *Degenerated Zeeman ground states in the single-excitation regime*. Phys. Rev. A **96**, 053840 (2017).

- [Svidzinsky 2008] A. A. Svidzinsky, J.-T. Chang, & M. O. Scully. *Dynamical Evolution of Correlated Spontaneous Emission of a Single Photon from a Uniformly Excited Cloud of N Atoms*. Phys. Rev. Lett. **100**, 160504 (2008).
- [Svidzinsky 2010] A. A. Svidzinsky, J. Chang, & M. O. Scully. *Cooperative spontaneous emission of N atoms: Many-body eigenstates, the effect of virtual Lamb shift processes, and analogy with radiation of N classical oscillators*. Phys. Rev. A **81**, 053821 (2010).
- [Tabosa 1991] J. W. R. Tabosa, G. Chen, Z. Hu, R. B. Lee, & H. J. Kimble. *Nonlinear Spectroscopy of Cold Atoms in a Spontaneous-Force Optical Trap*. Phys. Rev. Lett. **66**, 3245–3248 (1991).
- [Thackeray 1935] A. D. Thackeray. *The emission line $\lambda 4511$ in late-type variables*. ApJ. **81**, 467–473 (1935).
- [Torquato 2018] S. Torquato. *Hyperuniform states of matter*. Phys. Rep. **745**, 1–95 (2018).
- [Truitt 2000] P. Truitt & V. Strelitski. *Transition to oscillation regime in flaring water vapour masers*. Bull. Am. Astron. Soc. **32**, 1484 (2000).
- [Türeci 2008] H. E. Türeci, L. Ge, S. Rotter, & A. D. Stone. *Strong Interactions in Multimode Random Lasers*. Science **320**, 643–646 (2008).
- [Turitsyn 2010] S. K. Turitsyn, S. A. Babin, A. E. El-Taher, P. Harper, D. V. Churkin, S. I. Kablukov, J. D. Ania-Castañón, V. Karalekas, & E. V. Podivilov. *Random distributed feedback fibre laser*. Nat. Photon. **4**, 231–235 (2010).
- [Turitsyn 2014] S. K. Turitsyn, S. A. Babin, D. V. Churkin, I. D. Vatnik, M. Nikulin, & E. V. Podivilov. *Random distributed feedback fiber lasers*. Phys. Rep. **542**, (2014).
- [Vallet 1990] M. Vallet, M. Pinard, & G. Grynberg. *Generation of Twin Photon Beams in a Ring Four-Wave Mixing Oscillator*. Europhys. Lett. **11**, 739–744 (1990).
- [van Rossum 1999] M. C. W. van Rossum & T. M. Nieuwenhuizen. *Multiple scattering of classical waves: microscopy, mesoscopy, and diffusion*. Rev. Mod. Phys. **71**, 313–371 (1999).
- [Vanneste 2007] C. Vanneste, P. Sebbah, & H. Cao. *Lasing with Resonant Feedback in Weakly Scattering Random Systems*. Phys. Rev. Lett. **98**, 143902 (2007).
- [Vartabi Kashanian 2016a] S. Vartabi Kashanian. *Noise spectroscopy with large clouds of cold atoms*. PhD thesis, Université de Nice Sophia-Antipolis (2016).
- [Vartabi Kashanian 2016b] S. Vartabi Kashanian, A. Eloy, W. Guerin, M. Lintz, M. Fouché, & R. Kaiser. *Noise spectroscopy with large clouds of cold atoms*. Phys. Rev. A **94**, 043622 (2016).
- [Vengalattore 2005] M. Vengalattore & M. Prentiss. *Recoil-induced resonances in the high-gain regime*. Phys. Rev. A **72**, 021401 (2005).

- [Vrijsen 2011] G. Vrijsen, O. Hosten, J. Lee, S. Bernon, & M. A. Kasevich. *Raman Lasing with a Cold Atom Gain Medium in a High-Finesse Optical Cavity*. Phys. Rev. Lett. **107**, 063904 (2011).
- [Weaver 1965] H. Weaver, D. R. W. Williams, N. H. Dieter, & W. T. Lum. *Observations of a strong unidentified microwave line and of emission from the OH molecule*. Nature **208**, 29–31 (1965).
- [Weidemüller 1995] M. Weidemüller, A. Hemmerich, A. Görlitz, T. Esslinger, & T. W. Hänsch. *Bragg Diffraction in an Atomic Lattices Bound by Light*. Phys. Rev. Lett. **75**, 4583 (1995).
- [Weiss 2018] P. Weiss, M. O. Araújo, R. Kaiser, & W. Guerin. *Subradiance and radiation trapping in cold atoms*. New. J. Phys. **20**, 063024 (2018).
- [Weiss 2019] P. Weiss, A. Cipris, M. O. Araújo, R. Kaiser, & W. Guerin. *Robustness of Dicke subradiance against thermal decoherence*. Phys. Rev. A **100**, 033833 (2019).
- [Wiersma 1996] D. S. Wiersma & A. Lagendijk. *Light diffusion with gain and random lasers*. Phys. Rev. E **54**, 4256–4265 (1996).
- [Wiersma 2000] D. Wiersma. *The smallest random laser*. Nature **406**, 133–135 (2000).
- [Wiersma 2001] D. S. Wiersma & S. Cavalier. *Light emission: A temperature-tunable random laser*. Nature **414**, 708–709 (2001).
- [Wiersma 2008] D. S. Wiersma. *The physics and applications of random lasers*. Nature Phys. **4**, 359–367 (2008).
- [Wiersma 2010] D. S. Wiersma & M. A. Noginov, editeurs. *Special issue: Nano and random Laser* vol. 12(2) of *J. Opt.* (2010).
- [Wiersma 2013] D. S. Wiersma. *Disordered photonics*. Nature Photon. **7**, 188–196 (2013).
- [Wolf 2018] P. Wolf, S. C. Schuster, D. Schmidt, S. Slama, & C. Zimmermann. *Observation of Subradiant Atomic Momentum States with Bose-Einstein Condensates in a Recoil Resolving Optical Ring Resonator*. Phys. Rev. Lett. **121**, 173602 (2018).
- [Wu 1977] F. Y. Wu, S. Ezekiel, M. Ducloy, & B. R. Mollow. *Observation of Amplification in a Strongly Driven Two-Level Atomic System at Optical Frequencies*. Phys. Rev. Lett. **38**, 1077–1080 (1977).
- [Yariv 1977] A. Yariv & D. M. Pepper. *Amplified reflection, phase conjugation, and oscillation in degenerate four-wave mixing*. Opt. Lett. **1**, 16–18 (1977).
- [Yariv 1988] A. Yariv. *Quantum Electronics*. Wiley New York 3rd edition (1988).
- [Yoshikawa 2004] Y. Yoshikawa, T. Sugiura, Y. Torii, & T. Kuga. *Observation of superradiant Raman scattering in a Bose-Einstein condensate*. Phys. Rev. A **69**, 041603 (2004).

- [Yu 2011] D. Yu. *Photonic band structure of the three-dimensional ^{88}Sr atomic lattice*. Phys. Rev. A **84**, 043833 (2011).
- [Zakrzewski 1992] J. Zakrzewski. *Theoretical explanation of the first experimentally observed laser without inversion in a two-level scheme*. Phys. Rev. A **46**, 6010–6014 (1992).
- [Zemansky 1927] M. W. Zemansky. *The Diffusion of Imprisoned Resonance Radiation in Mercury Vapor*. Phys. Rev. **29**, 513–523 (1927).
- [Zhu 1990] Y. Zhu, D. J. Gauthier, S. E. Morin, Q. Wu, H. J. Carmichael, & T. W. Mossberg. *Vacuum Rabi splitting as a feature of linear-dispersion theory: Analysis and experimental observations*. Phys. Rev. Lett. **64**, 2499 (1990).
- [Zibrov 1995] A. S. Zibrov, M. D. Lukin, D. E. Nikonov, L. Hollberg, M. O. Scully, V. L. Velichansky, & H. G. Robinson. *Experimental Demonstration of Laser Oscillation without Population Inversion via Quantum Interference in Rb*. Phys. Rev. Lett. **75**, 1499–1502 (1995).

Mirrorless lasing and cooperative scattering with cold atoms

Abstract:

This manuscript reports several studies on collective effects in light-atom interactions, divided into two topics.

The first one is mirrorless lasing with cold atoms. A traditional laser is made of an amplifying material and an optical cavity, whose primary role is to induce feedback, i.e., a kind of trapping effect for the light. In a mirrorless laser the trapping effect can be provided by multiple scattering in the gain medium (random laser) or by the periodicity of the medium (photonic-crystal laser or distributed-feedback laser in 1D). We have produced and studied such mirrorless lasers using cold atoms as the gain medium and for providing the feedback. More precisely, we have realized a random laser and a distributed-feedback optical parametric oscillator.

The second topic is about cooperative scattering or, more precisely, about superradiance and subradiance in dilute atomic samples in the linear-optics regime. After discussing the interpretation of some experiments realized on steady-state light scattering, we present our results on the temporal dynamics of the light scattered by cold atoms when the driving laser is switched off or on. We report the first direct observation of subradiance (slowed-down decay) and of superradiance (accelerated decay) in the linear-optics regime and we study their properties, in particular the dependence on the detuning of the driving field and on the temperature of the sample. We also study the collective Rabi oscillations at the switch-on.

Laser sans miroir et diffusion coopérative avec des atomes froids

Résumé:

Ce manuscrit décrit plusieurs études sur des effets collectifs dans l'interaction lumière-atomes, réparties en deux thèmes.

Le premier concerne les lasers sans miroirs. Un laser traditionnel est constitué d'un milieu à gain et d'une cavité optique, dont le rôle premier est d'induire une rétroaction, c'est-à-dire un effet de piégeage de la lumière. Dans un laser sans miroir l'effet de piégeage est produit soit par de la diffusion multiple dans le milieu à gain (laser aléatoire), soit par la périodicité du milieu (laser à cristal photonique ou laser à rétroaction distribuée pour le cas 1D). Nous avons réalisé de tels lasers en utilisant des atomes froids comme milieu à gain et pour produire la rétroaction. Plus précisément, nous avons réalisé un laser aléatoire et un oscillateur paramétrique optique à rétroaction distribuée.

Le deuxième thème porte sur la diffusion coopérative ou, plus précisément, sur la superradiance et la sous-radiance dans des échantillons atomiques dilués dans le régime de l'optique linéaire. Après avoir discuté l'interprétation de certaines expériences sur la diffusion de la lumière à l'état stationnaire, nous présentons nos résultats sur la dynamique temporelle de la lumière diffusée par des atomes froids lors de l'extinction ou de l'allumage du faisceau excitateur. Nous décrivons la première observation directe de la sous-radiance (décroissance ralentie) et de la super-radiance (décroissance accélérée) en régime de l'optique linéaire et nous étudions leurs propriétés, en particulier leur dépendance au désaccord du faisceau excitateur et à la température de l'échantillon. Nous avons également étudié les oscillations de Rabi collectives à l'allumage.